High recovery rate solar driven reverse osmosis and membrane distillation plants for brackish groundwater desalination in Egypt

Author:
Nashed, Amir Samy Wahib

Publication Date:
2015

DOI:
https://doi.org/10.26190/unsworks/18114

High recovery rate solar driven reverse osmosis and membrane distillation plants for brackish groundwater desalination in Egypt

By

Amir Nashed

School of Photovoltaic and Renewable Energy Engineering
Faculty of Engineering
University of New South Wales
Sydney, Australia

A thesis submitted in fulfilment of the requirements for the degree of

Doctor of Philosophy

August 2014

THE UNIVERSITY OF NEW SOUTH WALES

Thesis/Dissertation Sheet

Surname or Family name: **Nashed**

First name: **Amir Samy Wahib**

Other name/s:

Abbreviation for degree as given in the University calendar: **PhD**

School: **Photovoltaic and Renewable Energy Engineering**

Faculty: **Engineering**

Title: **High recovery rate solar driven reverse osmosis and membrane distillation plants for brackish groundwater desalination in Egypt**

Abstract 350 words maximum:

This thesis explores the feasibility of extracting and desalinating brackish groundwater in Egypt using solar driven high recovery rate reverse osmosis and membrane distillation desalination plants to help establishing decentralised agricultural communities.

Groundwater properties and potential for sustainable development from seven main hydro-geological systems in Egypt were investigated. It was found that approximately 55% of Egypt's area has access to brackish groundwater, 47% of which has access to aquifers with moderate to high potential for development.

The feasibility of high recovery rate photovoltaic driven reverse osmosis desalination plants was investigated. Using commercial simulation tools, it was found that the plant can operate at recovery rates of 75 to 90% with unit water costs of 0.7 to 1.65 USD/m^3 with the typical brackish groundwater composition and depths found in Egypt. Moreover, it was shown that such plants are cost competitive with similar plants driven by diesel generators if the subsidies on diesel are removed.

The feasibility of replacing standard photovoltaic modules with photovoltaic/thermal collectors to reduce the energy consumption of the reverse osmosis plant by heating the water was explored. The annual performance of the photovoltaic/thermal collectors was analysed using TRNSYS. It was concluded that for such application, photovoltaic/thermal collectors have no economic advantage.

The feasibility of using hybrid reverse osmosis/membrane distillation plants to increase the recovery rate was also investigated. A mathematical model was built using MATLAB to simulate the performance of a commercial full scale spiral wound permeate gap membrane distillation module. The model gave good agreement with experimental results available in the literature. A TRNSYS model was built to analyse the annual performance of the solar driven membrane distillation plant. It was found that evaporation losses from the cooling tower greatly limited the recovery rate where no more than 10% enhancement was feasible. Such small enhancement in the recovery rate resulted in a 1.9 to 3.6 fold increase in the unit water costs. It was concluded that higher recovery rates are possible with high recovery rate membrane distillation modules that have low cooling requirements; and that solar driven hybrid plants can be economically feasible if a source of waste heat from a renewable energy source is available to drive the membrane distillation process, the specific heat consumption of the process is reduced by 4 folds and the module costs drop by at least 3.5 folds.

COPYRIGHT STATEMENT

'I hereby grant the University of New South Wales or its agents the right to archive and to make available my thesis or dissertation in whole or part in the University libraries in all forms of media, now or here after known, subject to the provisions of the Copyright Act 1968. I retain all proprietary rights, such as patent rights. I also retain the right to use in future works (such as articles or books) all or part of this thesis or dissertation.

I also authorise University Microfilms to use the 350 word abstract of my thesis in Dissertation Abstract International (this is applicable to doctoral theses only).
I have either used no substantial portions of copyright material in my thesis or I have obtained permission to use copyright material; where permission has not been granted I have applied/will apply for a partial restriction of the digital copy of my thesis or dissertation.'

Signed ……………………………………………..........................
Date ……………………………………………..........................

AUTHENTICITY STATEMENT

'I certify that the Library deposit digital copy is a direct equivalent of the final officially approved version of my thesis. No emendation of content has occurred and if there are any minor variations in formatting, they are the result of the conversion to digital format.'

Signed ……………………………………………..........................
Date ……………………………………………..........................

ORIGINALITY STATEMENT

‘I hereby declare that this submission is my own work and to the best of my knowledge it contains no materials previously published or written by another person, or substantial proportions of material which have been accepted for the award of any other degree or diploma at UNSW or any other educational institution, except where due acknowledgement is made in the thesis. Any contribution made to the research by others, with whom I have worked at UNSW or elsewhere, is explicitly acknowledged in the thesis. I also declare that the intellectual content of this thesis is the product of my own work, except to the extent that assistance from others in the project's design and conception or in style, presentation and linguistic expression is acknowledged.’

Signed …………………………………………….............

Date ……………………………………………..............

Abstract

This thesis explores the feasibility of extracting and desalinating brackish groundwater in Egypt using solar driven high recovery rate reverse osmosis and membrane distillation desalination plants to help establishing decentralised agricultural communities.

Groundwater properties and potential for sustainable development from seven main hydro-geological systems in Egypt were investigated. It was found that approximately 55% of Egypt's area has access to brackish groundwater, 47% of which has access to aquifers with moderate to high potential for development.

The feasibility of high recovery rate photovoltaic driven reverse osmosis desalination plants was investigated. Using commercial simulation tools, it was found that the plant can operate at recovery rates of 75 to 90% with unit water costs of 0.7 to 1.65 USD/m^3 with the typical brackish groundwater composition and depths found in most of Egypt.

The feasibility of replacing standard photovoltaic modules with photovoltaic/thermal collectors to reduce the energy consumption of the reverse osmosis plant by heating the water was explored. The annual performance of the photovoltaic/thermal collectors was analysed using TRNSYS. It was concluded that for such application, photovoltaic/thermal collectors have no economic advantage over standard photovoltaic modules.

The feasibility of using hybrid reverse osmosis/membrane distillation plants to increase the recovery rate was also investigated. A mathematical model was built using MATLAB to simulate the performance of a commercial full scale spiral wound permeate gap membrane distillation module. The model gave good agreement with experimental results available in the literature. A TRNSYS model was built to analyse the annual performance of the solar driven membrane distillation plant. It was found that evaporation losses from the cooling tower greatly limited the recovery rate where no more than 10% enhancement was feasible with a hybrid plant. Such small enhancement in the recovery rate resulted in a 1.9 to 3.6 fold increase in the unit water costs over those of a plant only using reverse osmosis. Finally, it was concluded that

higher recovery rates are possible with high recovery rate membrane distillation modules with low cooling requirements; and that solar driven hybrid plants can be economically feasible if a source of waste heat from a renewable energy source is available to drive the membrane distillation process, the specific heat consumption of the process is reduced by 4 folds and the module costs drop by at least 3.5 folds.

Acknowledgments

I would like first to thank God for His leadership and guidance during my studies. I would like to thank my supervisor, Associate Professor Alistair Sproul, for all his support, time and effort during my studies. He has been an inspiration to me in his enthusiasm and passion about research; and my co-supervisor Professor Greg Leslie for his technical advice and valuable feedback on my work.

Special thanks to the Fraunhofer institute team including: Joachim Went, Daniel Winter and Rebecca Schwantes for their technical advice as well as giving me the opportunity to come to the Fraunhofer institute and learn about their work on solar desalination. Thanks also to Professor Hugh Outhred for his support and valuable insights at the start of my PhD work, and Dr Jose Bilbao for his help with the TRNSYS mathematical modelling carried out in this thesis.

I would like to acknowledge the financial support of the University of New South Wales by granting me the University International Postgraduate Award scholarship without which I would have not been able to pursue my PhD degree.

Finally, I am extremely grateful to my parents for giving me the opportunity to pursue postgraduate studies in the University of New South Wales and their continuous emotional support. Thanks also to Bassem Younan for his continuous support and motivation.

Table of Contents

1. Introduction **1**

1.1 Energy Status in Egypt **1**

1.2 Water Status in Egypt **2**

1.2.1 Nile water 2

1.2.2 Nile water reuse 6

1.2.3 Groundwater extraction 7

1.2.4 Seawater desalination 8

1.2.5 Water availability 8

1.3 Poverty in Egypt **9**

1.4 Decentralized Communities: A Solution **10**

1.5 Suitable Water and Energy Sources for Decentralized Communities **11**

1.5.1 Groundwater extraction 12

1.5.2 Solar energy 13

1.6 Motivation and Area of Research **14**

1.7 Thesis Outline **16**

2. Literature Review **18**

2.1 Aspects for Successful Implementation of Solar Driven Groundwater Extraction and Desalination Plants in Rural Areas **18**

2.2 Solar Energy Technology Comparison and Selection **18**

2.2.1 Electricity generating solar technologies 19

2.2.2 Process heating solar technologies 22

2.2.3 Conclusion 23

2.3 Desalination Processes **24**

2.3.1 Desalination processes comparison and selection 24

2.3.2 Summary and conclusion 34

2.4 Background Information **41**

2.4.1 RO plants 41

2.4.2 MD process 49

2.5 Research Gaps and Novelty 52

2.5.1 Solar driven RO desalination plants in Egypt 52

2.5.2 General application of brackish water PV-RO plants 55

2.5.3 Hybrid RO/MD plants 60

2.5.4 MD process modelling 67

2.5.5 PVT driven RO plants 70

2.5.6 Brackish GW potential in Egypt 70

2.6 Summary and Conclusion 71

3. Brackish Groundwater Potential in Egypt 72

3.1 Salinity Definition 72

3.2 Targeted Water for Treatment 73

3.3 Review of Groundwater in Egypt 74

3.3.1 Nubian sandstone aquifer 75

3.3.2 Fissured carbonate aquifer 77

3.3.3 Quaternary aquifer 80

3.3.4 Coastal aquifers 84

3.3.5 Basement fissured hard rock aquifer 87

3.3.6 Al-Moghra aquifer 88

3.4 Constraints Limiting Groundwater Development 89

3.5 Classification of Brackish Water Aquifers: Methodology 90

3.6 Classification of Brackish Water Aquifers: Results and Discussion 92

3.6.1 The Western Desert 94

3.6.2 The Eastern Desert 97

3.6.3 The Sinai Peninsula 99

3.6.4 Nile valley and delta 102

3.6.5 Mediterranean North West and Red Sea coastal Areas 103

3.7 Groundwater Suitability for Agriculture Use 104

3.8 Conclusion 106

4. Feasibility Study of PV Driven Brackish Water RO Plants 108

4.1 Methodology 109
4.1.1 General design considerations 109
4.1.2 System configuration 116
4.1.3 RO plant modelling and design 117
4.1.4 Photovoltaic system design 121
4.1.5 Cost analysis 125
4.2 Results and Discussion 139
4.2.1 RO plant maximum recovery rate 139
4.2.2 Effect of water temperature on RO plant energy consumption 140
4.2.3 Economic feasibility of PV-RO plants 141
4.2.4 Cost and energy consumption of brackish groundwater extraction and desalination versus seawater desalination 147
4.2.5 Unit water costs comparison with current water prices in Egypt 148
4.2.6 Sensitivity analysis 149
4.2.7 Impact of battery bank cost, interest rate and diesel prices on the feasibility of PV-RO plants 151
4.3 Conclusion 153
5. Feasibility Study of PVT Driven RO Plants 156
5.1 Methodology 156
5.1.1 PVT-RO plant configuration 156
5.1.2 RO plant design 157
5.1.3 PVT system modelling and design 158
5.1.4 PVT system costs 160
5.2 Results and Discussion 161
5.2.1 Conditions for coupling PVT collectors with RO plants 161
5.2.2 Glazed versus unglazed PVT collectors 163
5.2.3 Energy performance of unglazed PVT-RO plant 166
5.2.4 PVT driven RO plant economic analysis 170
5.3 Conclusion 172
6. Membrane Distillation Process Modelling 174
6.1 MD Module Description 174

6.2 Methodology 176
6.2.1 PGMD module mathematical representation 176
6.2.2 Mass transfer 180
6.2.3 Heat transfer 184
6.2.4 Mass and energy balance equations 190
6.2.5 Effect of spacer on convective heat transfer coefficients 191
6.2.6 Convective heat transfer coefficients 194
6.2.7 Modelling technique for a spiral wound module 196
6.2.8 Effect of salinity and temperature on water properties 199
6.3 Results 201
6.4 Discussion 203
6.4.1 Model accuracy 203
6.4.2 Optimal value for the membrane tortuosity 206
6.4.3 Heat transfer modelling in the permeate channel 207
6.4.4 Heat transfer modelling in the evaporator and cooling channels 209
6.5 Further Notes 211
6.6 Summary 213
7. Feasibility Study of Solar Driven Hybrid RO/MD Plants 214
7.1 Methodology 215
7.1.1 Hybrid plant configuration 215
7.1.2 MD plant capacity 216
7.1.3 MD module performance 218
7.1.4 MD module operating conditions 218
7.1.5 Solar heat supply system 220
7.1.6 Cost analysis 228
7.2 Results and Discussion 231
7.2.1 Scaling effect on the RO/MD plant maximum recovery rate 231
7.2.2 Effect of cooling tower water losses on the RO/MD plant maximum recovery rate 232
7.2.3 Enhanced MD configurations for higher RO/MD plant recovery rates 237
7.2.4 Solar driven MD plant performance 238

7.2.5 Sensitivity analysis 248
7.2.6 Possibilities to reduce the LCOW of the MD plant 249

7.3 Conclusion 252

8. Conclusion 254

8.1 Original Contributions 258

8.2 Future Work Recommendations 260

9. Bibliography 263

Appendix A: Groundwater Extraction and Estimated Reserves in Egypt 297

Appendix B: Review of Solar Energy Systems 299

Appendix C: Review of Desalination Processes 312

Appendix D: Guidelines for Irrigation Water 323

Appendix E: Groundwater Depth Data in Several Locations in Egypt 330

Appendix F: RO Plant Design Example 331

Appendix G: RO Plant Rosa Designs 333

Appendix H: Correlations to Estimate the Effect of Salinity and Temperature on Water Properties 338

Appendix I: Model "A" Flowchart 342

Appendix J: Model "B" Flowchart 346

Appendix K: Estimating the Cooling Channel Exit Temperature from Experimental Data 350

List of Figures

Figure 1-1: Egypt total oil production and consumption from 2000 to 2012 1
Figure 1-2: Annual average daily global irradiation in Egypt 13
Figure 2-1: Osmosis and reverse osmosis process 42
Figure 2-2: Schematic showing the main components of an RO desalination plant 43
Figure 2-3: Schematic showing the basic concept of an MD process 50
Figure 2-4: A rough estimate of the SEC of RO plants at different feed water salinities and RR's 57
Figure 3-1: Hydro-geological map of Egypt 79
Figure 3-2: Aquifers potential for brackish GW extraction 98
Figure 3-3: Aquifers potential for brackish GW extraction in the Sinai Peninsula 100
Figure 4-1: Schematic diagram of a DG driven RO plant 117
Figure 4-2: Schematic diagram of a PV driven RO plant 117
Figure 4-3: Simplified schematic diagram of the PV energy supply 121
Figure 4-4: Comparison between the maximum scaling limited RR's achieved with simple pre-treatment for different GW compositions and those limited by the RO plant design at the expected GW temperature range in Egypt 140
Figure 4-5: Comparison of the SEC of an RO plant designed to operate within the manufacture's recommended parameters at 20, 30 and 40°C at different water salinities and with low scaling potential GW 140
Figure 4-6: LCOW comparison between a DG and a PV driven RO plant in the HSI zone and designed to operate (a) during daytime only and (b) for 24 hours; and in the LSI zone and designed to operate (c) during daytime only and (d) for 24 hours when GW with low scaling potential is extracted from an unconfined aquifer with 50 m depth to water table 142
Figure 4-7: Percentage increase in the LCOW of a PV-RO plant located in the HSI zone designed to operate only during daytime over that of a plant designed to operate for 24 hours 143
Figure 4-8: Percentage increase in the LCOW of a PV-RO plant located in the LSI zone designed to operate only during daytime over that of a plant designed to operate for 24 hours 143

Figure 4-9: LCOE comparison between a DG and a PV energy supply located in the LSI zone ... 144
Figure 4-10: The estimated LCOW of a PV-RO plant extracting and desalinating GW with typical composition from different locations in Egypt ... 145
Figure 4-11: Percentage increase in the LCOW of extracting and desalinating GW after replacing the DG running with unsubsidized fuel with a PV system ... 146
Figure 4-12: Comparison of the SEC of extracting and desalinating brackish GW with typical composition from different locations in Egypt with those of SW RO plants ... 148
Figure 4-13: Impact of a 20% reduction in the main parameters used in determining the cost of the PV plant on the (a) LCOE and (b) LCOW of a PV-RO plant extracting and desalinating 2,000 mg/l GW from the Nubian aquifer in Eastern Desert or Western Desert (20 m depth to water table) ... 150
Figure 4-14: Variation in the LCOW of PV and DG driven RO plants by reducing the nominal interest rate from 13 to 9% for the case where the plant is extracting and desalinating GW from the Nubian aquifer in Eastern Desert or Western Desert (20 m depth to water table) ... 151
Figure 4-15: Effect of the battery bank specific cost on the percentage increase of the LCOW of a PV-RO over that of a DG-RO plant when the GW salinity is (a) 2,000 mg/l and (b) 10,000 mg/l ... 152
Figure 4-16: Effect of the price of unsubsidized diesel on the percentage increase of the LCOW of a PV-RO over that of a DG-RO plant when the GW salinity is (a) 2,000 mg/l and (b) 10,000 mg/l ... 153
Figure 5-1: Schematic diagram of a PVT driven RO plant ... 156
Figure 5-2: Percentage reduction in the RO plant power consumption after increasing the feed water temperature to 40°C for the cases where (a) typical composition GW and (b) low scaling potential GW are desalinated ... 162
Figure 5-3: Annual net energy saving by replacing standard PV modules with PVT collectors to drive an RO plant located in the LSI zone and desalinating GW extracted from an unconfined aquifer with 50 m depth to water table ... 164
Figure 5-4: Energy performance comparison between PV-RO, glazed PVT-RO and unglazed PVT-RO Plants ... 165

Figure 5-5: Net annual energy saving by partially and fully replacing PV modules by glazed PVT collectors in the HSI zone when the GW is extracted from the confined Nubian aquifer with 20 m depth to water table 165
Figure 5-6: Percentage increase in the annual energy yield by replacing the standard PV modules by unglazed PVT collectors 166
Figure 5-7: PV cell temperature profile in a PV-RO and a PVT-RO plant treating 2,000 mg/l GW extracted from an unconfined aquifer in the (a) HSI zone and (b) LSI zone on a typical summer day 167
Figure 5-8: PV cell temperature profile in a PVT-RO and a PV-RO plant treating 2,000 mg/l GW extracted from the Nubian aquifer in the Sinai Peninsula on a typical summer day 167
Figure 5-9: Percentage reduction in the RO plant annual energy consumption by replacing the PV modules by unglazed PVT collectors 168
Figure 5-10: Comparison of the temperature profiles of the water exiting the PVT collectors for PVT-RO plants treating 2,000 mg/l GW 169
Figure 5-11: Comparison of the array size and LCOW between a PV and a PVT driven RO plant 171
Figure 6-1: PGMD spiral wound module manufactured by SolarSpring 175
Figure 6-2: A schematic plan view of the PGMD spiral wound module 175
Figure 6-3: Approximated shape of the modelled PGMD spiral wound module 177
Figure 6-4: Electrical analogy of mass transfer resistances in the DGM model 181
Figure 6-5: Heat and mass transfer through a differential element of the MD membrane unit 190
Figure 6-6: Schematic showing a sample of the spacer of the PGMD module and its unit cell 193
Figure 6-7: Schematic showing the first two turns of the PGMD module membrane unit 198
Figure 6-8: Comparison between the experimental and calculated values of (a) the permeate flow rate and (b) the SHC of the PGMD module at different feed water salinities and cooling channel inlet temperatures, and at a constant evaporator channel inlet water temperature of 80°C using equation (6-51) with 0.40 correction factor 202
Figure 6-9: Comparison between the experimental and calculated values of the (a) permeate flow rate and (b) the SHC of the PGMD module at different feed water flow

rates at constant evaporator and cooling channel inlet water temperatures of 80°C and 25°C respectively using equation (6-51) with 0.40 correction factor 202
Figure 6-10: Comparison between the calculated cooling channel inlet temperature estimated using equations 6-50 and 6-51 in model “A” at different PGMD feed flow rates and water salinities 209
Figure 6-11: Heat transfer resistances within the evaporator channel 210
Figure 6-12: Approximated shape of the modelled PGMD module after adjusting the diameter of the inner tubes...212
Figure 6-13: Comparison between the calculated SHC of the PGMD module at different cooling channel inlet temperatures and feed water salinities, and a feed flow rate of 500 kg/h before and after the modification in the geometry of the module.........................213
Figure 7-1: Schematic diagram of a PV-RO/FPC-MD hybrid desalination plant 215
Figure 7-2: The variation of the SHC of the PGMD module with the feed flow rate at an evaporator channel and cooling inlet temperatures of 80°C and 25°C respectively with pure water as the feed water..219
Figure 7-3: The effect of water salinity and feed flow rate on the SHC of the PGMD module at an evaporator and a cooling channel inlet temperatures of 80°C and 20°C respectively 219
Figure 7-4: Schematic diagram of the solar driven MD Plant 220
Figure 7-5: Comparison between the maximum scaling limited RR’s that can be attained with simple pre-treatment with different GW compositions at the expected operating temperatures of the MD process and those limited by the RO plant design.232
Figure 7-6: Comparison of the maximum attainable RR of the hybrid RO/MD plant before and after accounting for the effect of 2.2% evaporation losses from the cooling tower when the RO plant is designed to operate only during daytime and when the PGMD module is operating at 20°C cooling channel inlet temperature and 500 kg/h feed flow rate...234
Figure 7-7: Effect of cooling tower evaporation losses on the available brine mass and salinity at an overall hybrid RO/MD plant RR of 82%, when the PGMD module is operating at 20°C cooling channel inlet temperature and 500 kg/h feed flow rate and when the RO plant is designed to operate only during daytime with 20,000 mg/l GW salinity...234

Figure 7-8: Comparison between the maximum attainable RR by the hybrid RO/MD plant when the PGMD module is operating at 20°C cooling channel inlet temperature and 500 kg/h feed flow rate and under the assumption that the brine can be concentrated to 250 g/kg 235
Figure 7-9: MD brine tank salinity profile comparison when the RO plant is designed to operate during daytime only and for 24 hours at 79% hybrid plant RR, 20,000 GW salinity and 20°C MD cooling channel inlet temperature 236
Figure 7-10: Comparison of the maximum attainable RR between a hybrid RO/MD plant using the PGMD module and another using the memsys module with 2.2% water losses from the cooling tower, 20°C MD cooling channel inlet temperature, 500 kg/h feed flow rate and when the RO plant is designed to operate only during daytime 238
Figure 7-11: The performance of the MD plant during a sunny day 240
Figure 7-12: Effect of the FPC area on the annual permeate production and LCOW of the MD plant with the initially estimated number of modules (NMD=63) and when GW with 2,000 mg/l salinity is desalinated by the hybrid plant.. 240
Figure 7-13: Effect of increasing the number of PGMD modules on the annual permeate production of the MD plant when GW with 2,000 mg/l salinity is desalinated by the hybrid plant and when the RO plant is designed to operate during daytime only and (b) when GW with 10,000 mg/l salinity is desalinated by the hybrid plant and when the RO plant is designed to operate 24 hours 242
Figure 7-14: Effect of increasing the number of PGMD modules on the LCOW of the MD plant when GW with 2,000 mg/l salinity is desalinated by the hybrid plant and when the RO plant is designed to operate during daytime only and (b) when GW with 10,000 mg/l salinity is desalinated by the hybrid plant and when the RO plant is designed to operate 24 hours.. 243
Figure 7-15: LCOW of the solar driven hybrid RO/MD plant with the typical GW depths in the HSI zone when the RO plant is designed to operate (a) during daytime only and (b) for 24 hours.. 245
Figure 7-16: Percentage increase in the LCOW after using an MD process to enhance the RR above the design limited values of the RO plant with the typical GW depths in the HSI zone and when the RO plant is designed to operate for 24 hours.................... 246

Figure 7-17: Effect of the feed flow rate of the PGMD module on the LCOW of the solar driven MD plant, the required number of modules, and its thermal efficiency when 2,000 GW is desalinated by the hybrid plant 247
Figure 7-18: Impact of a 20% reduction in the equipment and indirect costs of the solar driven MD plant on its LCOW when the plant is used to desalinate the brine of an RO plant designed to operate for 24 hours and desalinating 10,000 mg/l GW 248
Figure 7-19: Capital cost breakdown of a solar driven MD plant used to desalinate the brine of an RO plant designed to operate for 24 hours and desalinating 10,000 mg/l GW 249
Figure 7-20: LCOW of the hybrid RO/MD plant under different scenarios when the RO plant is designed to operate for 24 hours 251
Figure 7-21: Percentage increase in the LCOW after using an MD process under the "O" scenario to enhance the RR above the design limited values of the RO plant with the typical GW depths in the HSI zone and when the RO plant is designed to operate for 24 hours 252

List of Tables

Table 1-1: Summary of water resources availability and usage in Egypt......................... 3

Table 2-1: LCOE estimates of different CSP technologies in May 2012 21

Table 2-2: Specific energy consumption of major desalination processes 26

Table 2-3: Unit water and specific capital costs reported for conventional desalination plants 28

Table 2-4: Summary of the main advantages and disadvantages of the reviewed desalination processes 38

Table 2-5: Solar driven desalination plants in Egypt 53

Table 2-6: Summary of some of the BW PV-RO plants reported in the literature 61

Table 2-7: Flux and SHC of currently available full scale commercial MD modules 63

Table 2-8: Different module configurations and membrane types modelled in the literature 69

Table 3-1: Weights and ranks of factors used to assess the aquifers' potential for brackish GW extraction.. 91

Table 3-2: Classes of the aquifers and their associated productivity, renewability and GW depths classes in addition to the area covered by each aquifer class 93

Table 4-1: Solar irradiation and ambient temperatures data for several cities in Egypt 111

Table 4-2: Depth to water table and the corresponding assumed GW temperatures in the LSI and HSI zones 113

Table 4-3: Chemical composition of GW with low, typical and high scaling potential 115

Table 4-4: Recommended operating limits for the DOW FILMTEC 8 inch RO Modules 118

Table 4-5: Parameters used in designing the PV energy supply 124

Table 4-6: Optimal operating hours of the RO plant when designed to operate only during daytime 125

Table 4-7: PV system capital and operating costs available in the literature and the actual values selected for the cost estimation 129

Table 4-8: DG system capital and operating costs available in the literature and the actual values selected for the cost estimation 132

Table 4-9: Capital and operating costs of the RO plant available in the literature and the actual values selected for the cost estimation 136
Table 4-10: RO plant maximum RR without the limiting effect of scaling........ 139
Table 5-1: Thermal and optical characteristics of the PVT collector modelled in this study 159
Table 5-2: Deviation from the recommended RO module operating limits when 40°C typical composition GW is treated with RO plants designed to operate with feed water temperatures of 20 and 30°C........ 163
Table 6-1: Properties of the PGMD spiral wound module 175
Table 6-2: Comparison of the standard SW composition and the average major ions composition of brackish GW in some wells in Egypt........ 200
Table 6-3: Summary of the modelling studies in the literature and the accuracy of the models 204
Table 6-4: Model deviation from experimental values under different heat transfer mechanisms and thermal conductivity models in the permeate channel, and different convective heat transfer correlations for the main channels 208
Table 7-1: Summary of the solar driven MD plant control algorithm 222
Table 7-2: EURO C20 AR-M FPC specifications 223
Table 7-3: Solar driven MD plant capital and operating costs available in the literature and the actual values selected for the cost estimation........ 229
Table 7-4: Suggested scenarios to reduce the LCOW of the solar driven hybrid RO/MD plant........ 250

List of Acronyms

AGMD	Air Gap Membrane Distillation
AUD	Australian Dollars
bcm	Billion cubic meter
BGL	Below Ground Level
BW	Brackish Water
CF	Concentration Factor
CP	Concentration Polarization
CPC	Compound Parabolic Collector
CPV	Concentrated Photovoltaic
CSP	Concentrated Solar Power
DCMD	Direct Contact Membrane Distillation
DE	Differential Element
DGM	Dusty Gas Model
DOD	Depth of Discharge
e.coli	Escherichia coli
EC	Electro-conductivity
ED	Electro-Dialysis
EGP	Egyptian Pound
ERD	Energy Recovery Device
ETC	Evacuated Tube Collector
FAO	Food and Agriculture Organization
FPC	Flat Plate Collector
GDP	Gross Domestic Product
GHI	Global Horizontal Irradiation

GOE	Government of Egypt
GRD	Grand Renaissance Dam
GW	Groundwater
HDH	Humidification-Dehumidification
HPP	High Pressure Pump
HSI	High Solar Irradiation
HVLWC	High Value Low Water Consuming
IAM	Incidence angle modifier
IDA	International Desalination Association
LCC	Life Cycle Cost
LCOE	Levelized Cost of Electricity
LCOW	Levelized Cost of Water
LFR	Linear Fresnel Reflectors
LSI	Low Solar Irradiation
MD	Membrane Distillation
MED	Multi-Effect Distillation
MEH	Multi-Effect Humidification
MPPT	Maximum Power Point Tracker
MSF	Multi-Stage Flash Distillation
MTC	Mass Transfer Coefficient
MVC	Mechanical Vapour Compression
MWRI	Ministry of Water Resources and Irrigation
NF	Nano-Filtration
NREL	National Renewable Energy Laboratory
PGMD	Permeate Gap Membrane Distillation
PR	Performance Ratio

PTC	Parabolic Trough Collector
PV	Photovoltaic
PVT	Photovoltaic/Thermal
PWF	Present Worth Factor
RIGW	Research Institute for Groundwater
RO	Reverse Osmosis
ROSA	Reverse Osmosis System Analysis
RR	Recovery Rate
SAR	Sodium Adsorption Ratio
SDI	Silt Density Index
SEC	Specific Electrical Energy Consumption
SGMD	Sweeping Gas Membrane Distillation
SHC	Specific Heat Consumption
SOC	State of Charge
SW	Seawater
SWERA	Solar and Wind Energy Resource Assessment
TDS	Total Dissolved Solids
TVC	Thermal Vapour Compression
UXO	Unexploded Ordnance
USD	United States Dollars
VC	Vapour Compression
VMD	Vacuum Membrane Distillation
WHO	World Health Organization
Wp	Watt Peak

Nomenclature

Symbol	**Description**	**Units**
A	Area	m^2
b	Height	m
CC	Capital Cost	USD
Cp	Specific heat capacity at constant pressure	J/kg.K
CrF	Correction Factor	-
CSA	Cross Sectional Area	m^2
C	Solute molar concentration	mol/l
D	Diffusion Coefficient	m^2/s
d	Diameter	m
f	Inflation Rate	-
H	Enthalpy	J/kg
h	Convective heat transfer coefficient	$W/m^2.K$
IAM	Incidence Angle Modifier	-
J	Flux	$kg/m^2.s$
IR	Interest Rate	-
K_M	MD Membrane Mass Transfer Coefficient	$Kg/m^2.s.Pa$
Ksp	Spacer Correction factor	-
k	Thermal Conductivity	W/m.K
L	Length	m
LCC	Life Cycle Cost	USD
$Loss$	Cooling tower evaporation losses	-
LP	Life Cycle Evaluation Period	years
LT	Equipment Lifetime	years
M	Molar Mass	kg/mol
$\dot{m}$	Mass Flow Rate	kg/s
N	Number of Turns	-
n	Number of Differential Elements	-
NMD	Number of Modules	-
Nu	Nusselt Number	-
OC	Operating Cost	USD
P	Total Pressure	Pa[a]
p	Partial Pressure	Pa

Symbol	Description	Units
Pr	Prandlt Number	-
PWF	Present Worth Factor	-
Q	Heat Requirements	J
$Q^{\cdot}$	Heat Transfer Rate	W or kW
$q^{\cdot}$	Heat Transfer Rate Per Unit Area	W/m^2
R	Ideal Gas Constant	J/mol.K[a]
r	radius	m
RC	Replacement Cost	USD
Re	Reynolds' Number	-
ΣRMSE	Sum of the root mean square error	-
RR	Recovery Rate	-
S	Water Salinity	g/kg[a]
Sp	Spiral Spacing	m
Sv	Specific Volume	m^{-1}
Sw	Wetted Surface Area	m^2
T	Temperature	K[a]
$\bar{T}$	Mean Temperature	K
t	Operating Hours	Hours
V	Volume	m^3
$V^{\cdot}$	Volumetric Flow Rate	m^3/s[a]
v	Velocity	m/s

<u>Greek Letters</u>

ΔH	Latent heat of Vaporization	J/kg
β	Module Tilt Angle	°
δ	Thickness	m
ε	Membrane Porosity	-
θ	Spacer Hydrodynamic Angle	°
λ	Mean Free Path	m
μ	Dynamic Viscosity	kg/m.s
ρ	Water Density	kg/m^3
σ	Collision Diameter	m
ϕ	Spiral Angle	°
χ	Membrane Tortuosity	-

Subscripts

Symbol	**Description**
$_0$	Initial
a	Air
b	Bulk
c	Cooling Channel
cf	Condenser Foil
ch	Channel
$cond$	Conductive
$conv$	Convective
e	Evaporator Channel
eff	Effective
f	Filament
fl	Large Filament
fs	Small Filament
GW	Groundwater
h	Hydraulic
hyb	Hybrid
in	Inlet
J	Mass Transfer
L	Latent Heat
l	Liquid
m	Membrane
MD	Membrane Distillation
ml	Long Side of the unit cell mesh
Mod	Module
ms	Short Side of the unit cell mesh
msh	mesh
n	nominal
o	Outlet
p	Permeate
r	real
RO	Reverse Osmosis
s	Solid, i.e. Membrane Material
sp	Spacer

Symbol	**Description**
tot	Total
uc	Unit Cell
v	Vapour
w	Water

1. Introduction

Fresh water and energy, the most important resources for human survival and development, are getting scarcer every day. An expanding population in Egypt is increasing the pressure on its fresh water and fossil fuel resources.

In this chapter, the motivation and aims of this thesis are presented. Firstly, energy and water availability in Egypt is reviewed. Secondly, the research problem and aims are discussed, followed by the thesis outline.

1.1 Energy Status in Egypt

Egypt mainly relies on oil and natural gas which in 2010 covered 87% of Egypt's energy demand (U.S. Energy Information Administration, 2013). While Egypt used to have a surplus of oil for exports, an increasing oil demand with a concurrent drop in oil production resulted in a current oil production that barely meets the demand *(Figure 1-1)*[1].

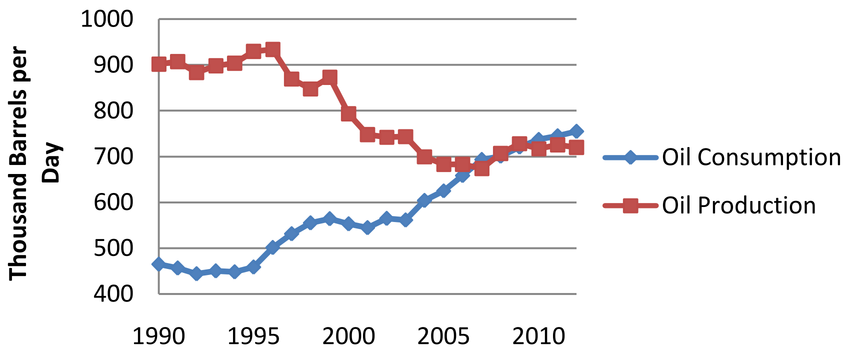

Figure 1-1: Egypt total oil production and consumption from 2000 to 2012
Source: (U.S. Energy Information Administration, 2013)

While Egypt has large natural gas reserves and has a surplus for exports, natural gas supplies is consumed at a rate[2] that will exhaust its 2013 proven 2,180 billion m^3 (bcm) reserves by 2028 (U.S. Energy Information Administration, 2013).

[1] It should be noted that the amounts shown in *Figure 1-1* are the overall oil production and consumption which include other liquid fossil fuels particularly natural gas liquids and Egypt is actually exporting a portion of its crude oil where in 2012, 18% of its production was exported.
[2] Based on the consumption growth rate from 2010 to 2011

Furthermore, in 2012 Egypt experienced intermittent shortages in transport fuel supplies and butane gas canisters used by most of the population in cooking and water heating (Sabry, 2012). These shortages were mainly due to the lack of resources given that Egypt imports about 40% and 50% of its diesel and butane needs respectively (Abo Alabass, 2012, Hussein, 2013), and also due to problems in distribution. Moreover, Egypt experienced severe shortages in electricity during summer peak hours in 2010 and 2012 due to continuous growth in demand, aging infrastructure and poor long term planning. The electricity shortage was also blamed on the lack of fuel supplies which decreased the generation capacity of the power plants particularly in 2012. (OMAR, 2010, El-Behary, 2012, Leila, 2012)

1.2 Water Status in Egypt

Egypt is an arid country (Hefny et al., 1992) with limited water resources. The main supply of fresh water in Egypt is the Nile River. Water supplies are augmented by groundwater (GW) extraction and seawater (SW) desalination. In addition, water from the Nile is reused to improve overall Nile water utilisation. A summary of water resources availability and use in Egypt is presented in *Table 1-1*.

1.2.1 Nile water

In 2000, extraction of Nile water accounted for 74% of Egypt's overall water demand, and with subsequent reuse, its utility extended to meet 98% of the demand (Allam and Allam, 2007). However, the steady increase in water demand driven by population growth has resulted in full allocation of Egypt's quota of the Nile water that is capped at 55.5 bcm/year by the 1959 agreement with Sudan[3] (El-Kady and El-Shibini, 2001, Hamza and Mason, 2004, Dawoud et al., 2005).

Moreover, Egypt's quota could be reduced if any of the other Nile basin countries, including Congo, Kenya, Rwanda, Burundi, Tanzania, Uganda, Eritrea, Ethiopia and South Sudan[4], that were not included in the 1959 agreement, construct dams to impound flow.

[3] Sudan was one country at the time of the agreement

[4] Now that South Sudan is a separate country, it is likely that the 1959 agreement only includes the Republic of Sudan

Table 1-1: Summary of water resources availability and usage in Egypt

Water Source	Current Water availability (bcm/year)	Water used (bcm/year)	Notes
Nile Water	55.5[a]	55.5	• Nile water share could increase to 65.1[b] bcm/year through projects aiming to decrease evaporation losses in the Nile basin countries and assuming that the GRD will be used only for hydro-electricity generation. Conversely, if Ethiopia used the stored water from the dam in irrigation and the aforementioned projects are not carried out, Nile water share may decrease to an amount ranging from 45.1 to 52.9 bcm/year.
Nile water evaporation losses	-2[c] to -3[d]	-2 to -3	
Nile flow needed for navigation	-0.3[c]	-0.3[c],-4[e]	• 0.3 bcm/year is the minimum flow needed for navigation after implementing proper measures to control Nile flow[c]. It is not clear however whether such measures are already implemented or not.
Rainfall (Including GW recharge)	1.8[e,f]	> 0.165[g]	• Average precipitation in Egypt amounts to 51 bcm/year[e]. The available amount of usable rainfall could therefore increase if measures are taken to improve rainfall utilization such as the use of dams, storage tanks, ponds and cisterns[h]
Reuse of Nile water through GW extraction	7.5[i,j]	7 (2009)[k]	• The maximum amount may decrease as Nile water is being diverted to Toshka and Al-Salam canals
Reuse of Nile water directly flowing back to the river, canals and drains	13.5[l]	13[m] (2010)	• Water Treatment and/or pollution control is required to fully use the available amount. The available amount may also decrease as Nile water is being diverted to Toshka and Al-Salam canals
Directly used treated waste water	0.7[n] (2000) – 1.3[o]	0.7 (2000) – 1.3	• Increasing treated waste water will not necessarily increase the water supply as most waste water flows back to the Nile river and drains and is counted as part of the reused Nile water
Desalinated SW	0.275 (2013)[p]	0.275 (2013)[p]	• Essentially indefinite potential. • Economical Limits • Seawater desalination capacity to increase to 0.32 bcm/year by 2016[p]
Fossil GW	2.7[d] to >4.16[q]	>1.6[q,r]	• Further studies required to estimate the available GW reserves especially in the Sinai

			Peninsula and the Eastern Desert.
Total	78.7 to >81.7	71.2 to >76.5	

a] (Swain, 1997) b] Refer to footnote 5. Value includes evaporation losses from the GRD reservoir c] (Abu Zeid, 1992) d] (Allam and Allam, 2007) e] (FAO AQUASTAT, 2005) f] Value includes 1.3 bcm/year recharging the aquifers and 0.5 bcm/year recharging surface waters g] (Hefny and Shata, 2004, Abdallah, 2006). It was also assumed that approximately all GW extracted from the Sinai Peninsula and the Eastern Desert is rainfall renewed GW h] (Sonbol, 2009) i] (Mostafa et al., 2004) j] Possible overlap with available Nile water (55.5 bcm/year) as the Nile basin aquifer is also directly recharged by Nile water seepage in some locations k] (MWRI, 2010) l] (Abdel-Shafy and Aly, 2007) m] (MWRI,2012, pers. comm., 23 Aug.) n] (Khalifa, 2011b) o] (Egypt State Information Service, n.d.) p] (IDA, 2013) q] (Nour and Khattab, 1998, Hefny and Shata, 2004) r] Value only includes fossil GW extracted from the Western Desert

As a matter of fact, Ethiopia have recently initiated the “Grand Renaissance Dam” (GRD) project on the Blue Nile River, where approximately 85% of the Nile water originates (Abu Zeid, 1992, Whittington and McClelland, 1992), which aims to generate 6,000 MW of hydropower (Ethiopian Electric Power Corporation, 2013). The GRD dam will have a short term and a long term impact on surface water supplies in Egypt and the Republic of Sudan. In the short term, there will be a reduction in water flow reaching Egypt as the Blue Nile water is diverted to fill the reservoir. The reservoir capacity is reported to be 74 bcm (Ethiopian Electric Power Corporation, 2013) and Ethiopian officials are aiming to fill the reservoir within five to six years (Davison, 2013). Therefore, a 10.5 to 12.6 bcm/year[5] reduction in the water flow reaching Egypt is expected which is equivalent to approximately 12.5 to 15%[6] decrease in Egypt’s annual Nile water share. In the long term, a permanent reduction in Nile water share is expected due to evaporation losses from the reservoir. At present, to author’s knowledge, there are no detailed estimation of the evaporation losses, but figures of 1.7 (Yirgu, 2012), 2.5 (Gleick, 2013) and 3 (Yousif, 2012) bcm/year have been reported without any indication of the methodology used in the estimation process. Using the simplified correlation derived by Linacre (1977) combined with climate data from the Solar and Wind Energy Resource Assessment (SWERA) website (2013), the annual

[5] Taking into account that the Blue Nile River contributes by 85% to the overall Nile water reaching the Aswan dam

[6] Assuming the same distribution of the Nile water as in the 1959 agreement where 66.1% of the Nile water flow was allocated to Egypt and 22% for Sudan and the rest accounts for evaporation losses.

evaporation losses from the reservoir's 1,680 km^2 (Ethiopian Electric Power Corporation, 2013) surface area could be as high as 4.1 bcm/year. This means that Egypt's Nile water share could permanently decrease by approximately 2.3 bcm/year[5,6].

Further reduction in the annual Nile flow is also expected if water from the GRD reservoir will be used by Ethiopia for land reclamation which is likely to occur for the following reasons: firstly, according to Mason (2004) Ethiopia has large development plans to meet its increasing demand of food especially that its irrigation is currently relying on rainfall which is irregular and unreliable; and secondly, the initial proposal by the United States Bureau of Reclamation for building several dams in Ethiopia to control the Blue Nile water included the use of the stored water for irrigating 434,000 hectares of land (Whittington and McClelland, 1992).

The United States Bureau of Reclamation concluded that the development of such irrigation projects would decrease the annual flow to Egypt and Sudan[7] by 4 bcm/year including evaporation losses from the reservoirs formed by the dams. However, these values could be underestimated given that the evaporation losses from the GRD reservoir alone could exceed 4 bcm/year. Moreover, based on the approximated method to determine the amount of water needed for irrigation discussed in Brouwer et al. (1992), irrigating 434,000 hectares of land with Ethiopia's climate conditions[8] would typically require 14.4 bcm/year assuming the use of water efficient sprinkler irrigation method and lined canals to transport the water which have 75%[9] and 95%[10] efficiency respectively (Brouwer et al., 1989). In this case, Egypt's Nile water share could decrease by approximately 19%[5,6] including the evaporation losses.

Droughts in watershed areas may also decrease Egypt's Nile water share which happened during 1976 to 1987 and resulted in approximately 6.9 bcm/year reduction in the amount of Nile water discharged from the Aswan dam (Abu Zeid, 1992).

---

[7] Sudan was one country at the time of the study

[8] An irrigation water need of 0.75 l/s/ha was used which is an average value between that required during a monsoon climate dry season and a monsoon climate wet season (Brouwer et al., 1982)

[9] The efficiency reflects the amount of water that percolates deep in the soil away from the plant roots or lost as surface runoff and is also referred to as the field application efficiency season (Brouwer et al., 1989)

[10] 5% water losses due to evaporation and seepage to the ground

There are few projects, however, that could increase Egypt's annual share of Nile water, mainly the Jonglei canal, Bahr-El-Ghazal and Machar swamps projects. These projects aim to increase the amount of water reaching the Nile River mainly through reducing evaporation losses in South Sudan. The expected increase in the Nile flow by these projects is estimated to be 18 bcm/year to be shared between Sudan[7] and Egypt (Abu Zeid, 1992). However, according to Allam and Allam (2007), these projects are unlikely to be carried out in the near future due to political, ecological and socio-economic issues which are discussed in detail in the literature (Whittington and McClelland, 1992, Swain, 1997).

1.2.2 Nile water reuse

Due to the full exploitation of Nile water, Egypt has relied on Nile water reuse as it is considered to be the most economical and efficient way to increase water availability (Mason, 2004). Nile water reuse consists of reusing excess irrigation water along the Nile flood plain which flows back to the Nile River, irrigation canals and drains[11]. This amount of water is estimated to be 21.5 bcm/year, out of which 16.5 bcm/year is found in the drains in the delta area (Abdel-Azim and Allam, 2004). The remaining 5 bcm/year directly flows back to the Nile River in the Nile valley area (Allam and Allam, 2007).

The reusable amount of water from the drains in the delta area is, however, limited to 8.5 bcm/year. This is because a minimum amount of about 8 bcm/year should be discharged into the Mediterranean Sea to avoid sea water back flow into the Nile River's branches and canals and to keep low salinity levels in the northern lakes which are used as fisheries (Abdel-Azim and Allam, 2004). The available reusable amount of Nile water is therefore 13.5 bcm/year out of which 13 bcm/year was used in 2010 (MWRI[12] 2012, pers. comm., 23 Aug.).

The available quantity of reused Nile water that is suitable for drinking and irrigation is also decreasing due to pollution caused by domestic and industrial effluents discharged into the Nile River, described as the main recipient of sewage water in Egypt, and drains in the delta (Wahaab and Badawy, 2004, United Nations Country Team, 2005, Abdel-

---

[11] Water from the drains are either reused directly in irrigation or after mixing with Nile water to improve its quality

[12] Ministry of Water Resources and Irrigation

Shafy and Aly, 2007). For example, in 2011/2012 about only half of the discharged waste water was treated (Khalifa, 2011a, Egypt State Information Service, n.d., Abdel-Wahaab, 2012). For the same reason, domestic and industrial waste water is not included in the water budget presented in *Table 1-1* and is assumed[13] to be a part of the available water in the Nile River and drains in the delta. This is except the treated waste water that has been reported to be directly used in irrigation in the reclaimed lands in desert areas as it is unlikely to be recycled back to the Nile River.

The maximum available amount of Nile water that could be reused could also decrease due to possible reduction in Nile water flow as water is being diverted to the Toshka project and Al-Salam Canal to reclaim desert land in southern Egypt and the Sinai Peninsula respectively (Abdel-Azim and Allam, 2004, Allam and Allam, 2007). This reduction is because the excess irrigation water cannot return to the Nile River. However, this reduction may have only a small effect on the overall water availability in Egypt because the excess irrigation water will still recharge the underlying aquifers in those areas and therefore can be reused. The excess irrigation water in desert areas is also minimized as the use of the water efficient sprinkler and drip irrigation is mandatory (FAO AQUASTAT, 2005).

1.2.3 Groundwater extraction

Excess irrigation water, in addition to seeping water from irrigation canals and drains, recharge the underlying Nile Basin aquifer (Hefny et al., 1992). Therefore, this water is reused indirectly through GW extraction from the aquifer.

In 2009, 7 bcm/year was extracted from the Nile basin aquifer (MWRI, 2010) while the maximum renewable amount of GW in the aquifer is estimated to be 7.5 bcm/year (Mostafa et al., 2004).

The available amount that is suitable for drinking and irrigation is also decreasing due to pollution caused by the excessive use of fertilizers in irrigation, leakage from old sewage networks in urban areas, and direct sewage dumping to the ground in rural

[13] The assumption is because part of the waste water has been reported to be also discharged in northern lakes or in open pits hence cannot be recycled, however the amount is likely to be small.

areas[14], that in addition to salinisation of GW in the delta area caused by SW intrusion (Sherif and Singh, 2002, Wahaab and Badawy, 2004, Abdalla et al., 2009).

Extracting fossil and rainfall renewed GW is another important source of water especially in border cities (United Nations Country Team, 2005). The overall extracted fossil and rainfall renewed GW has been estimated to be at least 1.8 bcm/year while the estimated exploitable GW reserves could exceed 5.46 bcm/year (Nour and Khattab, 1998, Hefny and Shata, 2004, FAO AQUASTAT, 2005)[15]. Therefore, while fossil and rainfall renewed GW represents a small percentage of the currently available water in Egypt, it is a highly underutilized water resource hence can play a larger role in meeting Egypt's water demand.

1.2.4 Seawater desalination

Seawater desalination is the remaining option for Egypt to indefinitely increase its water resources. Seawater desalination is an abundant and a secure source of water as it is independent of climatic conditions (Ghaffour et al., 2013). However, SW desalination currently accounts for only 0.35% of Egypt's available water resources (IDA, 2013) as it is a process constrained by costs and therefore its application is limited to installations that are insensitive to high prices. This is observed from the data obtained from the International Desalination Association (IDA) inventory (IDA, 2013) which shows that 58.5% of SW desalination plants are located in tourist areas on the Red Sea and Suez Gulf.

1.2.5 Water availability

Based on the estimated water availability shown in *Table 1-1* and the 2013 population (Central Agency for Public Mobilization & Statistics, 2013), the per capita water availability in Egypt is estimated to be from 919 to 954 m^3/year. This value is below the level associated with countries with chronic water shortages, i.e. 1,000 m^3/capita/year (Mason, 2004). Moreover, even in the best case scenario where the Nile projects discussed in section *1.2.1* were carried out, the increase in Nile water share would be

[14] Only 20% of these areas have access to a sewage system (MWRI, 2010)
[15] See Appendix A for more details on GW extraction and reserves

offset by the population growth[16] and the per capita water share would still be less than 1,000 m^3/year.

Accordingly, Egypt is forced to adopt strict water saving measures including water recycling, switching to drip and sprinkler irrigation methods[17], and growing less water intensive and high value crops such as fruits and vegetables while importing water intensive crops (United Nations Country Team, 2005).

It should be also noted that while Egypt imports most of its food where in 2008 it had between 30 to 60% self-sufficiency of its mainly used alimentary crops[18] (Central Agency for Public Mobilization & Statistics, 2010), its hopes of agricultural expansion to decrease its food import bill[19] are hampered by limited fresh water supplies. Moreover, the lack of fresh water forced many farmers in several locations to use of untreated waste water, and the heavily polluted and saline water from canals and drains in irrigation as well as illegally using water meant for drinking purposes (Amin, 2010, Viney, 2012). The use of such low quality water in irrigation affected the productivity of the soil and in some cases the soil became unsuitable for irrigation, which is likely due to the accumulation of salts, heavy metals and nutrients in the soil (Mohammad Rusan et al., 2007).

1.3 Poverty in Egypt

Poverty levels in Egypt are steadily increasing where the percentage of poor, defined as individuals who are unable to meet their basic needs of food, shelter and clothes as well as education, health and transportation services, increased from 16.7% in 1999/2000 to 25.2% in 2010/11 and 4.8% of the population were in absolute poverty not being able to meet their minimum food requirements (Central Agency for Public Mobilization & Statistics, 2011). While Egypt experienced high rates of economic growth during this period, only lower Egypt seemed to benefit from such growth with significant poverty

---

[16] Based on the 2014 population growth rate (The World Fact Book, 2014)

[17] Switching from flood to sprinkler or drip irrigation in the Nile valley and delta may not result in substantial water savings as the excess irrigation water is anyway recycled as previously discussed. It is also mandatory to use drip and sprinkler irrigation in areas far from Nile valley and delta which are at risk of water shortage (FAO AQUASTAT, 2005).

[18] Wheat, maize and beans

[19] In 2009, the crops import bill reached 5 billion USD, third of which was for importing wheat, while the income from exporting crops consisted less than quarter of this value (MWRI, 2010).

reduction, while it increased in upper Egypt (United Nations Country Team, 2005). This could be observed in food deficits reported in Upper Egypt manifested in higher rates of all kinds of malnutrition (United Nations Country Team, 2005).

While the government of Egypt (GOE) heavily subsidies fuel and food commodities with amounts reaching 10% of its gross domestic product (GDP) to ensure that the large poor segment of the population will have access to these commodities, a reduction in the subsidies is expected as a result of declining export income and government revenues that in addition to the devaluation in the national currency which will increase the price of imported goods (Bradley, 2012, Coleman, 2012). A reduction in subsidies, on which most of the population rely due to their low purchase power, will have the greatest impact on rural areas that are home to 57% of the population and approximately 70% of those who live at or below the poverty line (Rural Poverty Portal, 2010).

1.4 Decentralized Communities: A Solution

Schumacher (1974) considered uncontrolled urbanisation, heavy capital investments and centralized development as unsustainable and promoting inequity especially that most development efforts are directed to urban places; which, as discussed in the previous section, is already happening in Egypt. Accordingly, Schumacher (1974) argued that the development of decentralized communities increases the resiliency of the population particularly when the workplace is in the area where people are living and where local skills could be exploited.

Therefore, the development of decentralized agricultural communities could harness the skills of one third of Egypt’s workforce which are in the agriculture sector (FAO AQUASTAT, 2005) and mostly concentrated in rural areas (Shalaby et al., 2011) where poverty rates are the highest. In other words, creating such communities will create jobs for a large sector of the population who are mostly poor and thus raising their income especially when growing high value crops.

Increasing the cultivated land area will also decrease the trade deficit in agricultural products. Moreover, decentralized communities with a degree of autonomy, in terms of having a local decentralized access to water and energy, will increase the resiliency of their dwellers. The dwellers will rely less on subsidized and unreliable energy supplies (section *1.1*) from the government while a fresh and a reliable source of water will prevent farmers from resorting to using low quality water (section *1.2.5*).

Creating decentralized communities away from the Nile valley and delta area will also prevent further degradation of arable lands mainly caused by urban encroachment into agricultural areas (Lenney et al., 1996); especially that 85% of the cultivated lands and 97% of the population are concentrated in this area (FAO AQUASTAT, 2005). Creating such communities will result in a redistribution of the population and will improve land use. El-Kady and El Shibini (2001) even considered creating communities with local autonomy as the only way to relieve population pressure along the Nile valley and delta and to avoid further pollution and degradation of arable land.

Furthermore, decentralized communities require decentralized small scale infrastructure which could be easily financed, instead of investing a large amount of capital in building large scale infrastructure.

Moreover, small cultivated lands in a decentralized community could be more beneficial than large scale mechanized commercial agriculture. For the same investment, labour intensive small land holdings can potentially have more yield and better energy ratios[20] (Leach, 1975). Furthermore, according to Fraenkel and Thake (2006), small land holdings double the labour requirements per hectare of land creating more job opportunities and income for landless labourers. It should be noted, however, that an excessive fragmentation of the cultivated area will compromise the farmers' income (Allam and Allam, 2007).

1.5 Suitable Water and Energy Sources for Decentralized Communities

In the previous section, it was concluded that creating decentralized agricultural communities away from the Nile valley and delta area could reduce poverty rates and increase the resiliency of the low income segment of the population living in rural areas as well as preventing further degradation in arable land. The development of such resilient communities is, however, contingent upon access to reliable supplies of potable water and energy.

[20] Defined as the ratio between the energy stored in the crop and the energy required to produce it

1.5.1 Groundwater extraction

In section *1.2*, it was shown that Nile water quota is fully used and could be significantly reduced if Ethiopia carried on with constructing the GRD and used the water in irrigation. Moreover, the potential increase in Nile water share depends on projects outside Egypt's borders that are unlikely to be achieved in the near future. It was also shown that quantity of Nile water that could be reused is almost fully exploited. Therefore, it is concluded that SW desalination and the highly underutilized fossil and rainfall renewed GW resources will be the main remaining options to increase water availability.

While GW is a limited resource compared to the essentially unlimited SW, it is an ideal water resource for decentralized communities as it exists all over Egypt allowing the use of decentralized water supply systems which are suitable for areas with lack of infrastructure (Rommel et al., 2007), i.e. areas away from the Nile valley and delta. On the contrary, SW is confined to coastal areas necessitating large scale centralized desalination plants to meet the water demand of all inland areas. They also need to be located in major cities with sufficient infrastructure such as power grid, water distribution network and roads (Lattemann and Höpner, 2008). Furthermore, additional costs associated with pipes, pumps and energy demand will be required to convey the desalinated SW to deep inland areas and areas located at high elevations.

Decentralized applications also offer the most sustainable use of GW resources as the small water demand would prevent GW over extraction which could result in large drops in GW levels within a short duration to the point where the cost of extracting GW could outweigh the economic return (Hefny et al., 1992). Finally, it should be noted that GW is a limited resource especially when compared to Egypt's overall water demand (*Table 1-1*). Therefore, GW extraction is only proposed to be used to establish decentralized agricultural communities away from the Nile valley and delta that are growing high value low water consuming (HVLWC) crops using water efficient irrigation methods such as drip and sprinkler irrigation which can increase the income of the farmers.

1.5.2 Solar energy

As Egypt has limited and unreliable supplies of fossil fuel products whose prices are expected to increase with the reduction or removal of the subsidies (sections *1.1* and *1.3*), the use of solar energy will guarantee a long term and reliable supply of energy, and a minimal susceptibility to global market prices compared to the volatile fossil fuel prices (International Renewable Energy Agency, 2012). Many studies such as those of Abdelrassoul (1998), García-Rodríguez et al. (2002), Fiorenza et al. (2003), Garcı et al. (2003) and Kalogirou (2005) regarded solar energy as the most appropriate and promising renewable energy source in remote arid areas.

Solar energy is a locally and a highly available energy resource, a main requirement for establishing resilient and sustainable communities (Rheinländer, 2007). The annual average global irradiation in Egypt mostly falls in the 6 to 6.5 kWh/m^2/day range (*Figure 1-2*) which is one of the highest in the world based on NASA solar world map (NREL, 2013). Solar energy also has a low environmental impact in terms of greenhouse gas emissions (Richards and Schafer, 2003).

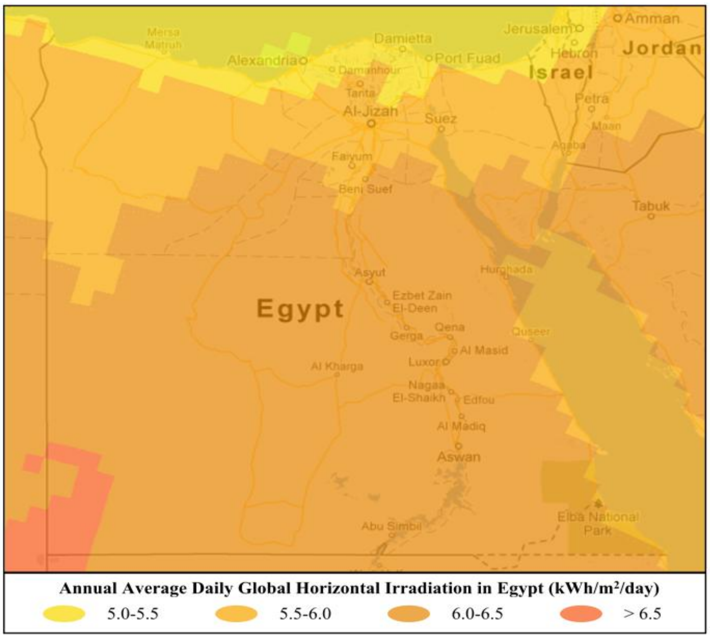

Figure 1-2: Annual average daily global irradiation in Egypt
Source: NREL Map modified after (NREL, 2013)

Solar energy plants are also suitable for decentralized small scale applications due to the modularity of most solar technologies[21]. Moreover, the introduction of a new

[21] More details are discussed in Chapter 2

decentralized technology can improve the economic status of rural communities through creating new jobs related to the production, operation and market distribution of the equipment (Kalogirou, 2004).

Furthermore, solar energy resources are evenly spread over Egypt (*Figure 1-2*) compared to other renewable energy sources such as wind energy which is site specific (Abu-Arabi, 2007, Eltawil et al., 2009). The wind energy atlas shows that only the eastern shore of the Suez Gulf in addition to small areas west of the Nile bank near El-Minya city and in the Sinai Peninsula along the Suez and Aqaba gulf, have enough wind resources that could be economically exploited (Elsobki et al., 2009). However, due to their low electricity cost (Kost et al., 2012), on shore wind energy systems should be considered as a better alternative only in these limited areas.

1.6 Motivation and Area of Research

This chapter has examined energy and water resources in Egypt. It was shown that Egypt has limited supplies of fossil fuels and the current supply of electricity is unreliable. It has also been shown that Egypt has a limited supply of fresh water where the Nile water is fully utilized and the available quantity could potentially decrease, and other measures such as Nile water reuse is almost fully exploited. Therefore, it was concluded that SW desalination and GW extraction will be the best options to increase Egypt's water supply. The latter option, however, was shown to suit decentralized applications and could potentially be more economical than SW desalination.

For this reason, GW extraction could help establishing decentralized agricultural communities growing HVLWC crops which can: increase the income and the resiliency of a large segment of the population working in the agriculture sector mainly concentrated in rural areas where poverty rates are the highest; reduce the trade deficit in agricultural product; and redistribute the population away from the heavily populated Nile valley and delta. It is worth mentioning that redistributing the population, improving land use, creating new jobs and establishing new agricultural communities away from Nile valley and delta area are amongst the development goals of the GOE (Gheith and Sultan, 2002). Furthermore, due to Egypt's vast solar resources, solar energy would provide a sustainable and clean energy supply for these communities.

Accordingly, this thesis explores the feasibility of solar driven small scale plants for brackish GW extraction and desalination. Egypt could potentially have more brackish GW accessibility and reserves than fresh GW. This is especially that brackish GW is considered by many studies, (Ahmad and Schmid, 2002, Allam et al., 2003, Talaat et al., 2003, El-Sadek, 2010) to be an important source to meet Egypt's growing water demands.

Moreover, while brackish GW requires the use of a desalination process to reduce its salt content to be suitable for drinking and in some cases for irrigation[22], its desalination costs are 3 to 5 times lower than SW desalination (Al-Karaghouli et al., 2010). This is due to its much lower salinity than SW which reduces the energy needed for desalination and also due to its lower pre-treatment requirements (Watson et al., 2003, Younos, 2005).

However, the main limitation with brackish GW extraction, and GW extraction in general, is its limited supplies as well as the environmental and extra costs associated with brine disposal which has a high salt concentration and filled with different feed water pre-treatment chemicals (Eltawil et al., 2009).

For this reason, this thesis particularly explores the feasibility of high recovery rate (RR) photovoltaic (PV) driven reverse osmosis (RO) plants for brackish GW desalination. Given that PV systems could be still regarded as an expensive energy supply (Milow and Zarza, 1997, García-Rodríguez, 2002, Kalogirou, 2005) for decision makers in Egypt, the economic feasibility of using PV instead of diesel generators (DG's), which is likely to be the only alternative decentralized energy supply in remote areas in Egypt, to drive the RO plant is explored.

Moreover, to further enhance the RR achieved by the RO process, the use of a membrane distillation (MD) process driven by flat plate collectors (FPC's) to treat the brine from the PV-RO plant is investigated in this thesis. Membrane distillation is a thermally driven process and therefore its maximum attainable RR is not limited by the water salinity as opposed to the RO process where the RR is limited by the osmotic pressure.

[22] More details on water quality needed for drinking and irrigation are discussed in Chapter 3

Furthermore, in an attempt to reduce the costs of a PV-RO plant, the feasibility of replacing the standard PV modules with photovoltaic/thermal (PVT) collectors is explored. In addition to the increase in the electricity yield of the PV system by using PVT collectors, they could potentially reduce the RO plant energy consumption through heating the water fed to the RO plant.

1.7 Thesis Outline

This thesis examines the feasibility of extracting and desalinating brackish GW in Egypt using solar driven high RR RO and MD desalination plants to help establishing decentralised agricultural communities.

In Chapter 2, different solar technologies and desalination processes are compared to justify the selection of PV, FPC, RO and MD as the most suitable for decentralized applications. The chapter will also provide background information on both the RO and MD processes. Different work carried out on brackish water (BW) PV-RO and hybrid RO/MD plants, and MD process modelling is then reviewed.

In Chapter 3, GW properties in the seven main hydro-geological systems across six regions in Egypt are investigated to identify aquifers with access to brackish GW. These aquifers are then investigated for their potential for sustainable development.

In Chapter 4, the feasibility of high RR PV-RO plants for brackish GW desalination is investigated. Using commercially available simulation tools, PV-RO plants are designed for the range of brackish GW salinities and depths, and solar irradiances encountered in Egypt. The plants will be designed to operate at the maximum possible RR which will be also examined for the range of GW compositions found in Egypt. The LCOW of the PV-RO plants is then estimated and compared to a similar plant driven by DG's. The chapter also investigates the effect of the PV-RO plant operating hours on its economic feasibility by considering two cases: a case where the RO plant operates only during the daytime; and a case where the RO plant is operating for 24 hours.

In Chapter 5, the feasibility of replacing standard PV modules with PVT collectors to drive the RO plant is assessed. The annual performance of the PVT-RO plants, in terms of the expected increase in the annual electricity yield of the PV system and the reduction in the RO plant energy consumption by heating the feed water, is examined using TRNSYS. The analysis will also compare the performance of glazed and unglazed PVT collectors. The LCOW of a PVT-RO plant is then estimated and compared to that of a PV-RO plant.

Chapter 7 presents a mathematical MATLAB model developed to simulate a full scale permeate gap MD (PGMD) module. The validity of the model is also examined by comparing the results with experimental data available in the literature. The results of the model will be used in Chapter 8 which examines the feasibility of using hybrid RO/MD plants to increase the overall RR. The chapter will investigate the maximum RR enhancement that could be attained by using an MD process to desalinate the RO plant brine. The annual performance of a solar driven hybrid RO/MD plant is assessed using TRNSYS. The LCOW of the plant is then estimated and compared to that of the plant using an RO process only.

Finally, Chapter 8 summarizes the main results and conclusions of this thesis and outlines future work recommendations.

2. Literature Review

Small scale solar driven systems for brackish GW extraction and desalination were proposed to establish decentralized agricultural communities in Egypt.

This chapter is divided into two parts. In the first part different solar energy systems and desalination processes are reviewed and compared to justify using RO and MD to desalinate the GW, and PV and FPC's to drive the desalination plants. This part will also provide background information on the RO and MD processes.

In the second part, different work carried out on BW PV-RO plants and the application of such plants in Egypt, hybrid RO/MD plants, and MD process modelling, is reviewed. The research gaps are then identified demonstrating the novelty of this research.

2.1 Aspects for Successful Implementation of Solar Driven Groundwater Extraction and Desalination Plants in Rural Areas

Decentralized agriculture communities are mainly targeting rural areas which have poor access to materials and high skills. For this reason, according to Koschikowski et al. (2003), Richards and Schafer (2003), Rheinländer (2007), Banat and Qiblawey (2007) and Retnanestri (2007), for a successful and a sustainable application and operation of the proposed solar driven GW extraction and desalination systems in rural areas the following aspects should be fulfilled: robustness, high reliability and low maintenance requirements; simple design that could be operated and maintained by locals; modularity to adapt with growth/variation in demand; and low capital and unit water costs. Accordingly, choosing the most suitable desalination and solar system technologies will be based on the aforementioned aspects.

2.2 Solar Energy Technology Comparison and Selection

In this section, different solar energy systems that can be coupled with desalination processes are compared. Solar energy systems are divided into PV based technologies which convert solar energy directly into electricity; and solar thermal collectors which convert solar energy to heat. This heat can be used directly in a heating process or can be used to generate electricity via a steam turbine, a Rankine cycle engine, or a Stirling heat engine (Morrison and Rosengarten, 2012).

Photovoltaic based technology comprises non-concentrating PV[23], PVT and concentrated PV (CPV) systems. Solar thermal collector technologies consists of Stationary and non-stationary collectors in addition to solar ponds. Stationary collectors mainly include FPC’s, and evacuated tube collectors (ETC’s). Non-stationary collectors are usually concentrating collectors which include parabolic trough collectors (PTC’s), central receiver power towers, parabolic dishes, and linear Fresnel reflectors (LFR’s). With concentrating collectors high operating temperatures, i.e. up to 1,500 °C, could be achieved (Morrison and Rosengarten, 2012). These high levels of temperature are mainly used for electricity generation and therefore these systems are usually referred to as concentrated solar power (CSP) systems. A brief description of each technology is shown in Appendix B.

For this reason, FPC’s are only compared to ETC’s in addition to solar ponds as they are usually used for process heating[24], while solar thermal concentrating collectors are compared with PV based technologies as both supply electricity.

2.2.1 Electricity generating solar technologies

Non-concentrating PV is a well-established and reliable technology and could be easily accessed in the market. Non-concentrating PV systems have also simple operation and low maintenance (Ahmad and Schmid, 2002, Richards and Schafer, 2002, Tzen et al., 2004), especially that there are no moving parts as solar tracking in not necessary. The aforementioned aspects are necessary for a successful implementation and operation in rural/remote areas (Rheinländer, 2007). Retnanestri (2007) described non-concentrating PV as a “democratic” technology as it can be installed and operated by the locals once they have sufficient training. Retnanestri (2007) also considered it as an important technology to promote the sustainability of remote communities. Non-concentrating PV

[23] In other parts of the thesis non-concentrating PV modules are directly referred to as PV modules, but in this part it is referred to as non-concentrating PV to differentiate it from CPV’s

[24] Solar ponds can be also used to generate electricity through a low temperature organic vapour Rankine cycle engine (Morrison and Rosengarten, 2012)

systems are also modular and therefore are suitable for decentralized applications. Moreover, while non-concentrating PV used to be regarded as an expensive technology (Milow and Zarza, 1997, García-Rodríguez, 2002, Kalogirou, 2005), a dramatic drop in module prices took place since 2009 due to market overcapacity and high competition between manufacturers (Kost et al., 2012). The average price of PV modules in November 2009 was 4.34 USD per Watt peak (Wp) (Ab Kadir et al., 2010) but it dropped to 0.67 USD/Wp in November 2013 (EnergyTrend, 2013), a 6.5 fold reduction in just 4 years.

Simplicity and low maintenance also apply for PVT collectors which have high solar radiation conversion efficiency. These systems, however, cannot operate at high temperatures because the module output electrical power will be highly reduced. For this reason, PVT cannot be used to supply the heat required for desalination processes. The PVT collectors would be ideal for desalination processes where preheating the feed water may reduce the desalination energy required.

While CSP systems have slightly better conversion efficiencies reaching up to 31.4% (U.S. Department of Energy, 2011), than non-concentrating PV, their capital and electricity costs are higher, and they also require precise tracking which increases their complexity and maintenance requirements. In particular, the levelized cost of electricity (LCOE) of a large scale (> 1 MW) ground mounted PV system is on average 0.147 USD/kWh[25] under Spain's weather conditions[26]. Conversely, the LCOE of a CSP system (100 MW) under the same weather conditions ranges from approximately 0.252 to 0.358 USD/kWh[27] depending on the CSP technology used (*Table 2-1*). Moreover, according to Kost et al. (2012), based on the learning curve rates of both technologies, the LCOE of CSP systems is forecasted to be still higher than large scale PV systems by 2030 and with almost the same ratio as in 2012 due to their weak market growth and lower learning curve.

---

[25] Based on 1.35 conversion rate from Euro and USD

[26] 2,000 kWh/m^2 average direct normal irradiation (DNI). The average DNI in Egypt ranges from about 1800 to 2750 kWh/m^2 respectively based on NREL solar irradiation data and therefore the reported LCOE values may also apply for systems installed in Egypt

[27] The indicated CSP LCOE values do not include parabolic dish systems, however according to Ab Kadir et al. (2010), the latter's electricity costs are higher than other CSP systems

Table 2-1: LCOE estimates of different CSP technologies in May 2012

Solar System Technology	Average LCOE (USD/kWh)
Utility Scale Ground Mounted PV Systems (>1 MW)	0.147
Small Scale PV Systems (< 10 kW)	0.169
Parabolic Trough with thermal storage (100MW)	0.252
Concentrated PV	0.27
Fresnel Collectors (100MW)	0.308
Power Tower with thermal storage (100MW)	0.312
Parabolic Trough without thermal storage (100MW)	0.358

Source: (Kost et al., 2012)

It should be noted, however, that CSP's might be an attractive option for dual generation, where the excess heat from the power generation system could be used to drive a thermal desalination process which would increase the overall utilization of solar energy similar to PVT collectors. Parabolic trough collectors in particular are suitable for such application as they are designed such that a working fluid flows into the receiver and therefore heat can be easily recuperated from the fluid (Appendix B). Parabolic trough collectors are also suitable for rural/remote areas as the systems are reliable and are the most mature (U.S. Department of Energy, 2011) and have the lowest LCOE compared to other CSP systems (*Table 2-1*). However, PTC's are best suited for large scale applications (Morrison and Rosengarten, 2012), similar to power towers. The only CSP system suitable for small scale applications is the parabolic dish system with Stirling engines. However such systems are not suitable for dual generation because the heat is converted to electricity in the dish, and the excess heat is vented to the atmosphere (Kalogirou, 2004).

Regarding CPV system, their electricity costs are generally lower than that of CSP's and are expected to be even lower than non-concentrating PV systems in the near future (Willis, 2012). For instance, CPV systems manufactured by SolarSystems are expected by the company to have an LCOE of 0.06 USD/kWh in the upcoming few years which will be less than that of non-concentrating PV systems (Parkinson, 2012). For existing CPV plants, little data have been found in the literature as there are currently very few CPV installations. However, in a 2010 summary report on CPV industry by Extance (2010), an average LCOE of 0.27 USD/kWh was reported and was forecasted to drop to 0.08 USD/kWh by 2015. While the LCOE of CPV systems is higher than that of a PTC CSP, the former systems are modular and suitable for small scale applications. For example, one parabolic dish such as the CS500 (SolarSystems, 2011) have a peak power of 35 kW. Concentrating PV systems can be also considered for dual generation of heat and electricity. Similar to PVT systems, the feed water could be used to cool the PV cells while gaining enough heat to be used in a thermal desalination process hence increasing the overall system efficiency. Due to the high temperatures generated, cooling is necessary in CPV systems to avoid component failure or a decrease in cell efficiency. Dual generation could be particularly suitable for the CPV configuration using Fresnel refractors as it has a large flat area and the PV cells are located on the back of the CPV panels. Therefore it would be easier to circulate water behind the CPV modules compared to configurations using parabolic dishes where, similar to parabolic dishes CSP's, it will be complex to circulate the working fluid through the receiver of each dish especially in terms of piping layout (Kalogirou, 2004).

2.2.2 Process heating solar technologies

Flat plate collectors have low costs and simple designs (Stine and Geyer, 2001). They also share the same modularity as PV modules and are expected to also have low maintenance requirement as they have no moving parts. Furthermore, while their operating temperatures are relatively low, i.e. operating temperatures up to 90°C (Morrison and Rosengarten, 2012), they are enough to drive most of thermal based desalination processes which mostly operate at temperatures less than 100 °C (Appendix B). Moreover, FPC's are locally available as they are manufactured in Egypt (Nafey et al., 2006) which increases the resiliency of the communities using them as there will be no need to import the systems and spare parts will be easily accessible in the market.

The main competitor of FPC's to supply process heating are ETC's which are more efficient especially when higher working fluid operating temperatures are required (Morrison and Rosengarten, 2012). The ETC's are also described as a mature and well proven technology (Belessiotis and Delyannis, 2001). However, ETC's are on average 2.6 times more expensive than FPC's (Belessiotis and Delyannis, 2001, Banat and Qiblawey, 2007). Therefore, ETC's are usually favourable for cold weathers, cloudy and windy locations (Kalogirou, 2004) where excessive heat losses would be otherwise expected with FPC's. Therefore, ETC's may not be needed under Egyptian warm to hot weather conditions. Moreover, while according to Belessiotis and Delyannis (2001), ETC’s are more suitable for conventional thermal based desalination processes, their use is likely to be superfluous given that most desalination processes operate at temperatures less than 100°C.

Finally, solar ponds have the advantage of thermal storage provided by the water mass (García-Rodríguez et al., 2002) and therefore the heat from the pond could be used for extended times without further costs. Moreover, solar ponds can make use of the otherwise waste brine from desalination processes (Abu-Arabi, 2007) to establish the required salinity gradient. However, due to the continuous loss of water by surface evaporation which needs to be continuously replaced, solar ponds are not suitable for a water scarce place like Egypt. They might be considered, however, in areas near the coast (Kalogirou, 2005) where SW could be used to replenish the water in the upper zone while the brine from the desalination process is used in the lower zone. Moreover, solar ponds may not be suitable for small scale applications as they tend to be more economical for large scale applications due to their high construction costs, which decreases with an increased pond size (Duffie and Beckman, 2006), and the long time required to reach the desired temperature gradient which may take up to a year (Porteous, 1984). Larger ponds are also preferred to smaller ponds as the transparency of water in the former is less affected by dirt and dust particles which otherwise reduce the amount of solar radiation absorbed in the bottom of the pond. Larger ponds are also more efficient because their large area to perimeter ratio reduces the heat losses which are mainly from the edges of the pond (Duffie and Beckman, 2006).

2.2.3 Conclusion

Based on the review carried out in this section, it has been concluded that non-concentrating PV modules and FPC’s will be the most suitable to drive the proposed decentralized GW extraction and desalination systems due to their simplicity, low maintenance, low cost and wide spread use. Photovoltaic/thermal collectors may also show some economic advantage when coupled with a desalination process that can make use of preheating the feed water to reduce desalination energy consumption. Finally, CPV is a promising technology with expected electricity costs to be less than that of a non-concentrating PV system, and their current costs could be substantially reduced if the CPV systems are used for dual generation of heat and electricity.

2.3 Desalination Processes

Desalination, also referred to as desalting or desalinization, is the process of turning brackish or saline water into fresh water that is suitable for drinking as well as agricultural use by mainly separating dissolved inorganic substances (Water Quality Association, 2012, U.S. Geological Survey, 2014).

Desalination processes are mainly divided into thermal processes, that mimic the natural water cycle where water is evaporated leaving behind non-volatile substances and then is condensed to obtain pure water, and membrane based processes which do not involve phase change. The main commercial thermal desalination processes are multi-stage flash distillation (MSF), multi-effect distillation (MED) and vapour compression (VC). The main commercial membrane desalination processes are RO and electro-dialysis (ED). Each of these conventional processes, in addition to other minor desalination processes which are either under research and development or in the early commercialization phase, will be compared. The comparison is based on a review carried out on each of these desalination processes which is shown in Appendix C.

2.3.1 Desalination processes comparison and selection

All thermal processes such as MSF and MED require heat energy to operate in addition to electrical energy for the auxiliary equipment particularly to run the pumps. This is except single effect passive solar stills and mechanical vapour compression (MVC) process which only require heat energy and electrical (or mechanical) energy respectively. Conversely, all membrane based technologies such as RO and ED only require electrical energy whether to drive pumps or to apply an electrical potential difference. The MD process is, however, an exception as it is a membrane process that requires both heat and electricity.

For this reason, thermal based technologies are usually coupled with solar thermal collectors while RO, ED and MVC are usually coupled with PV systems (Fiorenza et al., 2003, Abu-Arabi, 2007, Banat and Qiblawey, 2007, Zejli and Elmidaoui, 2007). Concentrating solar power plants may be also used to run RO, ED and MVC, however as discussed in section *2.2.1*, they are more expensive than PV systems and most of them are not suitable for small scale applications.

2.3.1.1 Major desalination processes

Multi-stage flash desalination is a very reliable and mature process where the plants exceed their expected life time and also do not show any performance degradation in terms of water production and energy consumption over their lifetime. The process is also easy to operate as it works similarly to power plants hence the skills required for plant operation and maintenance could be easily procured. (The National Reserach Council, 2004, Borsani and Rebagliati, 2005, Reddy and Ghaffour, 2007)

The MSF process has, however, high energy consumption (Wade, 2001, Abu-Arabi, 2007) as it is a thermodynamically inefficient process (Reddy and Ghaffour, 2007). The process's electricity consumption alone is close to that of the RO process (*Table 2-2*). The large electricity consumption is because the process requires a large amount of feed water to produce the desired distilled water as only small amounts of vapour are produced in each stage (Howe, 1974, Wade, 2001). For the same reason, MSF SW desalination plants usually operate at low RR's ranging from 10 to 20% (Watson et al., 2003). Moreover, while it started to gain a large market in small scale applications, the MSF process is only economical for large scale applications (Wade, 2001) due to the economies of scale (Assimacopoulos, 2001). For the aforementioned reasons, the MSF process is best suited for dual generation plants, i.e. combining large scale MSF plants with power stations, where the excess heat from the power generating cycle is used to run the desalination process (Watson et al., 2003, Borsani and Rebagliati, 2005).

Furthermore, a typical[28] MSF process is not suitable to be coupled with solar energy, i.e. intermittent operation, because the process requires transient time to stabilize and reach normal operating conditions (Kalogirou, 2005). Moreover, due to its low performance ratio (PR), the MSF process is better to operate at higher temperatures which will require the use of the more expensive ETC's or Compound parabolic collectors (CPC's)[29].

The MED process is more thermodynamically efficient than MSF and requires small amounts of feed water (Howe, 1974) to produce the same amount of distillate due to its

---

[28] One company, however, developed a special MSF configuration, called "Autoflash" to regulate the top brine temperature based on the available energy and overcome operation instability problems (García-Rodríguez, 2002, Ali et al., 2011).

[29] See Appendix B

Table 2-2: Specific energy consumption of major desalination processes

	Brackish Water	Seawater	
	Electricity kWh/m^3	**Electricity kWh/m^3**	**Heat kWh/m^3**
ED	0.5 to 10 [a][1] ≈ 0.5 for every 1 g/l of salts removed [b]	-	-
RO	1 to 3 [a] 0.5 to 3 [b] 2 to 3 [c] 0.5 to 2.5 [d]	10 to 15[2] (No ERD) [a] 9.5 (No ERD) [e] 2 to 5 (with ERD) [a] 2.5 to 7[3] (with ERD) [b] 3 to 4 (with ERD) [d] 2.3 to 3 (with ERD) [f] 3 to 5.5 (with ERD) [g][4]	None
MED[13]	-	MED/TVC 1.5 to 2.5 [b],[g] [5] 3.3 [h][6] 2.7 to 2.9 [e] 3.3-5 [l][7] MED only 3.5 [j][8] (MED only) 1.5 to 2.5 [g][9]	MED/TVC 40 to 108 [b],[g][5] 76.1 [h][6] 53.8 to 80.7 [e] 57.5-70.4[7] MED only 84.9[8] [j] 63.9 to 108 [g][9]
MSF[13]	-	3.6 [a] 3 to 5 [b][10] 3.9 [e] 4 to 6 [g] 4 [h][6],[i] 2.5 to 5 [j]	80.5 [a] 69.4 to 91.7 [b][10] 80.7 [e] 52.8 to 108 [g] 76.1 [h][6] 92.5 [i] 52.8 to 78.3 [j]
MVC	-	8.5 to 16 [a] 8 to 15 [b][11] 7 to 12 [g][12]	None
TVC	-	2 [k][13]	108.5 [k][13]

a] (Abu-Arabi, 2007) b] (National Research Council, 2008) c] (Miller, 2003) d] (Ghaffour et al., 2013) e] (Wade, 1993) f] (Desalination.com, 2008) g] (The Encyclopedia of Desalination and Water Resources, 2013) h] (Borsani and Rebagliati, 2005) i] (Raluy et al., 2005) j] (Al-Karaghouli and Kazmerski, 2013) k] (Darwish and Al-Najem, 1987) l] (Ali et al., 2011)

1] Specific electrical energy consumption (SEC) values depend on feed water salinity 2] The higher SEC value is for small scale plants 3] SEC for desalination plants with capacities less than 20,000 m^3/d 4] SEC values for a typical desalination plants with 24,000 m^3/d capacity 5] Specific energy consumption values for desalination plants with capacities from 10,000 to 35,000 m^3/d 6] Specific energy consumption values for desalination plants with 205,000 m^3/d capacity 7] Specific energy consumption values for MSF and MED include the actual energy needed by the process and do not include the energy reduction from using waste heat from turbines in cogeneration plants. 8] Specific energy consumption values for desalination plants with 180,000 m^3/d capacity 9] Specific energy consumption values for typical desalination plants with capacities from 5,000 to 15,000 m^3/d 10] Specific energy consumption values for desalination plants with capacities less than 76,000 m^3/d 11] SEC values for desalination plants with capacities less than 3,000 m^3/d 12] SEC values for desalination plants with capacities from 100 to 2,500 m^3/d 13] Specific energy consumption values for a desalination plant with 1,500 m^3/d capacity high heat transfer rates which also reduces its electrical energy consumption. For the same reason, MED desalination plants can operate at higher RR's than MSF plants with values ranging from 20 to 67% (Watson et al., 2003). The low energy consumption and high PR of the MED process are the main reasons for its lower capital and unit water costs which can be observed from cost analysis studies by Wade (2001), Borsani and Rebagliati (2005), and Reddy and Ghaffour (2007) (*Table 2-3*). It should be noted that while Borsani and Rebagliati (2005) reported higher specific capital costs for the MED process compared to MSF, this is not consistent with the other cost analysis studies, and other studies such as Watson et al. (2003) clearly indicated that the MED process has lower capital costs. The MED process is also suitable for intermittent operation (Garcia-Rodriguez, 2003) especially the multi stack effect configuration, discussed in Kalogirou (2005), which is the most suitable for solar energy and has a stable operation at partial load. Furthermore, the process's ability to operate at low temperatures is likely to make it suitable to be coupled with cheaper FPC's.

However, evaporating a thin film of feed water flowing over the surface of the heat exchanger, instead of bulk boiling as in the MSF process, increases the risk of scaling. This requires more frequent acid cleaning to remove scaling from the heat transfer surfaces which could not be cleaned using simpler and faster methods such as the use of sponge rubber balls[30] in MSF. This cleansing method does not require a plant shut-down, because the evaporation occurs on the outer surface of heat exchange tubes and not the inside. (Wade, 2001)

Vapour compression is described by several studies (Buros, 2000, García-Rodríguez, 2002, Eltawil et al., 2009) as a simple and reliable process especially for small scale applications. Higher RR's could be also obtained from the VC process compared to MSF with values reaching up to 50% for SW desalination plants (Watson et al., 2003). The VC process is carried out either through mechanical compression, i.e. MVC process, or through thermal compression, referred to as a thermal vapour compression (TVC) process (Appendix C).

The TVC process is usually combined with an MED process where it is more "convenient" to use due to economic reasons (Kalogirou, 2005) and is typically used in

[30] Sponge rubber balls are balls with a diameter larger than that of the heat exchanger tubes which are inserted inside the tubes to remove any deposits on their surface

Table 2-3: Unit water and specific capital costs reported for conventional desalination plants

Reference	Costs	MSF	MED	RO	Notes
(Borsani and Rebagliati, 2005)	Unit Water Cost USD/m^3	0.52	0.52	0.45	● Based on the average values of contracted plants in the middle east in the early 2000's and for a plant with 205,000 m^3/d capacity ● Values for MSF and MED are for a cogeneration plant
	Specific Capital Cost USD/m^3/d	880	950	830	
(Reddy and Ghaffour, 2007)	Unit Water Cost USD/m^3	Close to 1	0.55 to 0.7	0.5	● Values for recent MED Plants ● Capital cost values for RO are the usual value for plants built after 1995
	Specific Capital Cost USD/m^3/d	-	850	500 to 1000	
(Wade, 2001)	Unit Water Cost USD/m^3	1.04	0.95	0.8	● Values for a desalination plant with 31,822 m^3/d capacity ● Values for MSF and MED are for a cogeneration plant
	Specific Capital Cost USD/m^3/d	1615	1518	1330	
(Fiorenza et al., 2003)*	Unit Water Cost USD/m^3	1.1	0.8	0.7	● Values for a typical MSF plant with 25,000 m^3/d average capacity ● Values for a typical MED plant with 10,000 m^3/d average capacity ● Values for a typical RO plant with 6,000 m^3/d average capacity
	Specific Capital Cost USD/m^3/d	1300	1200	1300	

* Values combined from other studies

medium and large scale applications. Conversely, the MVC process is usually used by itself and is suitable for small scale applications. Moreover, the MVC process is able to cope with the intermittence of power supply (Garcia-Rodriguez, 2003, Abu-Arabi, 2007). Nevertheless, the MVC process has very high electrical energy consumption (*Table 2-2*). Moreover, Rayan et al (2001) reported that VC desalination units in Egypt showed maintenance problems and their production were less than their designed capacity.

The RO process is the most dominant process for water desalination worldwide where approximately 65% of the overall worldwide desalinated water in 2013 was produced from RO plants (IDA, 2013). This dominance of the RO process could be attributed to the following factors: the process's low energy consumption which is reported in many studies (Wade, 1993, Garcia-Rodriguez, 2003, Beccali et al., 2007, Elimelech and

Phillip, 2011) which can be also observed from *Table 2-2*; the process only requires electrical energy compared to the thermal processes which usually require both heat and electrical energy which increases the complexity of the plant and the costs; and its low unit water costs and capital costs compared to other major desalination processes which is reported in several cost analysis studies (Milow and Zarza, 1997, Wade, 2001, Borsani and Rebagliati, 2005, Reddy and Ghaffour, 2007) and can be also observed from *Table 2-3*. The low energy consumption of the RO process is because it does not involve phase change hence there is no need to supply the latent heat of evaporation (Porteous, 1984). Its low investment cost compared to thermal processes is also because the latter have larger footprint and require more expensive material compared to an RO plant with the same capacity (Ghaffour et al., 2013). The cost and energy advantages of RO over MED, MSF and thermal based desalination processes in general become more obvious when desalinating BW (*Table 2-2*). For this reason, the RO process, as well as ED, are recommended for BW desalination (Belessiotis and Delyannis, 2001, Abu-Arabi, 2007) and are considered to be the most economical processes for such application (Al-Karaghouli and Kazmerski, 2013) with reported desalination costs that are 3 to 5 times lower than SW desalination (Al-Karaghouli et al., 2010). The RO process is also modular and therefore can flexibly accommodate any future increase in water demand by simply adding more membrane modules (Richards and Schafer, 2002).

However, the RO process produces water with lower quality than distillation processes as it does not have 100% salt rejection. For example, product water with of 400 mg/l salinity could be obtained from SW RO plants (Wade, 1993) compared to less than 25 mg/l for MED and MSF processes (Abu-Arabi, 2007). The RO process also has high operating cost associated with its high pre-treatment and cleaning requirements in addition to membrane replacement (Wade, 2001). Pre-treatment requirements, according to Ghaffour et al. (2013), could increase the RO water costs “significantly” depending on feed water type especially if the water has high scaling and fouling potential[31]. For membrane replacement, an average membrane lifetime ranging from 3 (El-Kady and El-Shibini, 2001, DOW Chemical Company, 2013c) to 6 years (P Roginson 2013, pers. Comm., 27 Jul.) is expected. In a cost analysis study carried out

[31] Fouling and scaling in RO are discussed in more details in section *2.4.1.2*

by Borsani and Rebagliati (2005) to compare an RO,MED and an MSF large scale SW desalination plants, the operation cost of the RO process excluding energy costs was about 2.5 times more than that of MED and MSF. Furthermore, RO plants require highly trained operators (García-Rodríguez, 2002, Garcia-Rodriguez, 2003, Abu-Arabi, 2007, Banat and Qiblawey, 2007, Müller-Holst, 2007) especially that the process is “less tolerant than distillation to errors in operation” (Wade, 1993) and some small scale RO plants actually failed due to improper maintenance (Müller-Holst, 2007). Moreover, the RO process cannot cope with the intermittence of power supply which can damage the RO membranes or shorten their lifetime and for this reason energy storage, e.g. battery banks, is needed to ensure a constant supply of electricity (Garcia-Rodriguez, 2003, Abu-Arabi, 2007, Riffel and Carvalho, 2009). The use of a battery bank will, however, increase the costs and the maintenance required as well as decreasing the reliability of the plant (Forstmeier et al., 2008). Finally, because the feed pressure required in the RO process is proportional to the feed salinity, there is a limitation on the level of water salinity that can be desalinated as only a certain maximum pressure could be applied without damaging the RO membranes (DOW Chemical Company, 2011).

The ED process shares many advantages with RO such as low energy consumption and modularity. The ED process is, however, better than RO in terms of the durability of the membranes which could exceed 10 years (Watson et al., 2003). Furthermore, the ED process has low pre-treatment requirements which is further reduced when the EDR process is used, and is therefore more capable to treat waters with high fouling and scaling potential than RO (Buros, 2000, Watson et al., 2003). The ED/EDR membranes are also easy to maintain (Garcia-Rodriguez, 2003) where the membrane stack can be disassembled and the membranes can be then hand cleaned (Reahl, 2006) which is not possible with commercial RO membranes used for desalination. Moreover, the ED/EDR is able to cope with the intermittence of power supply (Garcia-Rodriguez, 2003, Banat and Qiblawey, 2007) and therefore could be easily coupled with solar energy without the need of batteries. Garcı et al. (2003) and Kalogirou (2005) also described the ED process to have a more robust and simpler operation compared to the RO process.

However, the ED/EDR process has a higher capital cost than the RO process especially that one stage of ED has a limited salt removal of 50% and therefore the higher the feed salinity and the more ED stages, i.e. series ED units, are required which significantly increases the costs (Howe, 1974). For this reason, the ED process is more suitable, to treat BW with salinities less than 5,000 mg/l (Fiorenza et al., 2003) beyond which it "becomes significantly more expensive" than RO (Banat and Qiblawey, 2007) which will impose a limitation on the maximum attainable RR's. Moreover, the ED process cannot be used to obtain high purity water as in this case the electrical resistance of the water will be very high necessitating higher voltage levels to be applied. For this reason the ED process is usually controlled to obtain product water with 300 to 500 mg/l salinity (Howe, 1974). The process also cannot separate non-charged particles such as pathogens in water which will necessitate the use of UF to remove them which will further increase the costs. The ED/EDR process is also less tolerant to high Iron and Magnesium contents in feed water compared to RO, which when oxidized become highly insoluble causing membrane fouling (Watson et al., 2003).

2.3.1.2 Minor desalination processes

The freezing process while has a low potential for scaling and corrosion problems, it is limited by the difficulties in moving and processing the bulky frozen water (Buros, 2000). The process also seems to have a high SEC where a solar driven freezing desalination plant installed in Saudi Arabia had a SEC of 103 kWh/m^3 and was eventually shut down as it was not economical to operate (Ali et al., 2011). The freezing process in general found little success in market and only few freezing desalination plants have been built since the concept was developed in the 1950's (Buros, 2000, Garcia-Rodriguez, 2003, Miller, 2003). Moreover, none of the currently operating or under construction desalination plants in the IDA inventory (2013) is using this process.

The humidification-dehumidification (HDH) process, regardless of the configuration used (Appendix C), is mainly endorsed over conventional desalination processes for its construction simplicity, ease of operation and low maintenance requirements (El-Kady and El-Shibini, 2001, Fiorenza et al., 2003, Parekh et al., 2004, Kalogirou, 2005, Aybar, 2007, Müller-Holst, 2007, Wang et al., 2012). Moreover, the process is mainly designed to be driven by solar energy especially that it only requires a low grade source of heat. Furthermore, Müller-Holst (2007) claimed that the multi-effect humidification (MEH) process[32] process in particular does not need chemical pre-treatment especially that the unit they discussed had all surfaces in contact with the brine made of corrosion resistant materials. However, pre-treatment is still likely to be required to avoid scaling issues and biological growth. Nevertheless, the process is expected to have low pre-treatment requirements given its low operating temperatures and simple design which should allow easy cleaning of the heat transfer surfaces. The HDH process is also robust and have long lifetime that could reach 20 years (Buros, 2000, Goosen et al., 2000).

The HDH process, however, has low productivity due to its low efficiency regardless of the configuration used. The HDH process therefore has a large footprint and for this reason its application is usually limited to very small scale applications. For example, early all of the solar HDH plants discussed in the literature (Parekh et al., 2004, Müller-Holst, 2007, Li et al., 2013) had capacities ranging from few tens of litres to 10 m^3 per day. The HDH process also has high energy consumption where specific heat consumption (SHC) values ranging from 150 to 180 kWh/m^3 have been reported for several solar MEH plants built in the Canary Islands in Spain (Müller-Holst et al., 1998). Müller-Holst (2007), however, reported that the MEH plant can have a SHC of less than 120 kWh/m^3. In all cases, the aforementioned values are much higher than that of conventional desalination processes shown in *Table 2-2*. The HDH process's electrical energy consumption may also increase for high RR operation as the feed water will need to be recirculated several times given the low productivity of the process. Furthermore, the HDH process has high unit water costs where a recent review by Li et al. (2013) on solar driven desalination plants showed that the costs of solar driven MEH process, which has the highest productivity and potentially the most thermally efficient amongst other HDH processes, was mostly higher than any other solar driven process. The review by Li et al. also showed that solar stills are more competitive with PV driven RO plants especially for capacities in the range of 10 m^3 per day given their cheap capital costs with reported specific capital cost[33] almost half of that of RO plants (Kalogirou, 2005). However, this should be taken with scepticism because of the low productivity of solar stills and their large space requirements which are expected to increase the capital costs (Fath et al., 2006). This is especially that

---

[32] Multi-effect humidification is another configuration of the HDH process. See Appendix C for more details

[33] Capital cost per m^3 of desalinated water capacity

studies such as those of Harrison et al. (1996) and Herold et al. (1998) clearly reported that solar stills have high costs as well as high maintenance.

The MD process has several advantages which were outlined in the literature (Fane et al., 1987, Gostoli and Sarti, 1989, Lawson and Lloyd, 1997, Banat and Simandl, 1998, Curcio and Drioli, 2005, Wieghaus et al., 2008, Koschikowski et al., 2009b, Khayet and Matsuura, 2011a, Winter et al., 2011). The MD process requires lower operating temperatures, i.e. 60 to 90°C, and therefore the process only requires a low grade source of heat which can be easily supplied by FPC's similar to MED and solar HDH processes. The low operating temperatures also give the possibility of using plastic equipment to overcome corrosion problems. Membrane distillation is also a compact process requiring low footprint and shares the same modularity advantage of RO. Moreover, compared to RO, the MD process operates at low pressure, e.g. atmospheric pressure, which reduces the cost of equipment and increases the safety of the process which also translates in cost saving, e.g. less sensors will be required to monitor the process. The MD process also can cope with the intermittent nature of solar energy due to the large heat capacity of water which impedes the change in temperature and also because there is no risk of membrane damage if the MD module run out dry compared to RO modules (Koschikowski et al., 2003). Furthermore, while the MD membrane is also exposed to fouling and scaling[34] similar to RO, their effect is likely to be less significant than with RO (El-Bourawi et al., 2006). A solar driven MD system discussed by Schwantes et al. (2013) was even designed to operate without chemical pre-treatment. Finally, the MD process is described by Koschikowski et al. (2003) as a robust technology that is easy to use which makes it a very compatible for standalone applications especially in rural/remote areas.

Nevertheless, the MD process has limited productivity (El-Bourawi et al., 2006, Banat and Qiblawey, 2007, Cheng et al., 2008) and high SHC similar to the HDH process. For example two solar driven MD commercial systems built by SolarSpring one without and the other with thermal storage have productivities of up to 21.5 and 28.5 l/d/m^2 of collector area respectively. The SHC of the MD process, obtained from Winter et al. (2011) on the same MD module used in the SolarSpring systems, was at least 145 kWh/m^3 when brackish/saline feed water, i.e. 13,000 mg/l, was desalinated and

[34] Fouling and scaling occurrence in MD are covered in more details in section *2.4.1.2*

increased to 180 kWh/m^3 for SW desalination. Furthermore, MD is an expensive process which is the main reason that limits its commercialization (Banat and Simandl, 1998, El-Bourawi et al., 2006). For example, Wieghaus et al. (2008) reported that the unit water costs for a solar driven system without thermal storage is approximately 34 USD/m^3, but could drop to 13.5 to 20[35] USD/m^3 after further improvement in the MD module performance and reduction in costs. Unit water costs ranging from 30 to 36 USD/m^3 were also estimated by Banat and Jwaied (2008) for a solar driven MD system with 0.1 and 0.5 m^3/d capacity where the latter plant had thermal storage.

Finally, forward osmosis is (FO) a promising technology which shares the main advantages of the RO process in terms of modularity and suitability for small scale applications but it is also prospected to have a lower fouling potential and energy consumption than the latter (Zhao et al., 2012). Moreover, as the process does not need high pressure, it is safer than RO and allows the use of simple (Cath et al., 2006) and cheaper equipment. Furthermore, the FO process should be able to cope with the intermittence of the solar energy compared to RO, because solar energy is only needed for circulating the water and in some cases separating the draw agent and is not needed for the desalination process itself. The FO process application is, however, limited by the low performance of the currently available FO membranes as well as the difficulties in separating the draw agent and finding a draw solution that can generate an osmotic pressure high enough to obtain higher RR's (Cath et al., 2006, Chung et al., 2012).

2.3.2 Summary and conclusion

In spite of its reliability and technological maturity, the large energy requirements, high unit water and capital costs, and high operating temperatures would be a main barrier to using MSF in solar driven small scale applications. Conversely, due to its lower costs and energy consumption, suitability for small scale applications, low operating temperatures, and ability to cope with the intermittence of power supply, the MED process is more suitable than MSF for decentralized solar driven applications in rural/remote areas.

Reverse osmosis has, however, lower capital and unit water costs as well as lower energy consumption than MED especially for BW applications. It should be also noted

[35] Original values given in Euro and were converted to USD using a factor of 1.35

that even when MED and MSF are used in a cogeneration setting, which is the most economical case for such processes, the unit water costs of the RO were still lower and therefore the cost advantage of the RO process is expected to be more evident for standalone solar driven desalination plants. Moreover, El-Kady and El-Shibini (2001) reported that some private companies are assembling and producing RO systems in Egypt which can further reduce the membrane cost and also increase its availability. Furthermore, the process's high chemical requirements and membrane replacement costs are offset by its low capital cost and low energy consumption. The costs associated with the chemical requirements are also expected to be low with GW applications which have low fouling potential (Watson et al., 2003). The clear cost advantages of the RO process over other conventional processes are reflected from the former's dominance in the global desalination market whose share will also increase by 1.7% after the completion of the currently constructed plants mostly on the expense of the MSF, MED and ED processes whose shares will drop by about 1.65%, 0.37% and 0.38% respectively (IDA, 2013). The RO process is also more suitable for decentralized small scale applications due to its modularity. Furthermore, the high maintenance requirements, need for skilled operators and the difficulty to cope with intermittent power supplies do not appear to be a significant barrier to RO application in rural areas for the following reasons: RO is the most dominant process in Egypt used in 89% of the desalination plants (IDA, 2013), therefore skilled operators should be easily found; and in practice the RO process is dominating decentralized applications in remote areas (Fiorenza et al., 2003) and based on the review carried out by Ali et al. (2011), almost half of 82 solar[36] driven desalination plants that were installed worldwide from 1977 to 2009 used an RO process. Finally, while the RO process produces water with less quality than distillation processes, this should not be a problem when water is used for drinking or irrigation given that water with salinities ranging from 500 to 1,000 mg/l is suitable for both purposes (Ayers and Westcot, 1994, WHO, 2011). Higher quality product water is only needed for industrial purposes and power plants. As a matter of fact, very low salinity water needs re-mineralization to prevent corrosion problems[37] and it may also be unsuitable for irrigation affecting the soil water infiltration rate[38]. Nevertheless, care should be taken with some dissolved solids that are not well rejected

[36] Including hybrid PV-wind energy and solar pond driven systems
[37] More details on water post-treatment are discussed in section *2.4.1.3*
[38] More details on the effect of water salinity on the soil are discussed in Appendix D

by the RO process and may cause health issues especially Boron (Choi et al., 2010, WHO, 2011).

In spite of its low pre-treatment requirements, membrane durability, ease of operation, low maintenance and the ability to cope with the intermittent nature of solar energy which makes the ED/EDR process more suitable for solar driven applications in rural areas than RO, the high capital cost and limited salt removal per stage are main barriers to its application. This can be clearly observed from the low global desalination market share of the ED process, i.e. 3% of the global installed capacity, in comparison with other desalination technologies (IDA, 2013). Moreover, the review carried out by Ali et al. (2011) showed that only 9% of 82 solar[39] driven desalination plants that were installed worldwide from 1977 to 2009 used an ED process while the statistical analysis on the worldwide renewable energy driven desalination plants carried out by Tzen (2005) showed that only 6% of the plants used ED. Finally, the ED process is not suitable for high RR operations as it is only economical when desalinating low salinity water as discussed in section *2.3.1.1*.

For the MVC process, while it is suitable for solar driven small scale applications, and only needs one source of energy similar to RO, its high energy requirements is a main limitation for its application. García-Rodríguez (2002), Garcı et al. (2003) and Fiorenza et al. (2003), however, argued that the MVC process could be still a better alternative for remote areas than RO despite its higher energy consumption due to its robustness, ease of operation and lower operational cost given that the process needs less chemical requirements and because no membrane replacement is needed. However, this conclusion is questionable given that in practice despite its technological maturity, the MVC process has a negligible global market share (IDA, 2013). Even amongst renewable energy driven desalination plants, which are usually small scale plants (Kalogirou, 2005) used in remote/rural areas, only 5% used an MVC process (Tzen, 2005). Moreover, as discussed in section *2.3.1.1,* MVC plants were reported to have poorer performance than RO plants in Egypt.

Minor desalination processes are mainly still under research and development or are in their early commercialization phase and with their current state they cannot compete

[39] Including hybrid PV-wind energy and solar pond driven systems

with conventional desalination processes mainly due to their low productivity and high unit water costs such as with the HDH and MD processes, or technical difficulties such as with the freezing and FO processes. While solar stills are more established, due to its very low productivity it is only ideal for household size applications in remote/rural areas (Fiorenza et al., 2003) due to their simplicity and low capital costs.

Nevertheless, the MD process is suitable for decentralized applications especially due to its modularity and simple operation. Even with its current high costs and low productivity, the MD process could be ideal when combined with RO to treat its brine to increase the overall RR which is important in the context of extracting GW in a water scarce country like Egypt as discussed in Chapter 1. Thermal processes in general are more suitable to desalinate high salinity water (Abu-Arabi, 2007), as long as scaling occurrence could be managed with chemicals, compared to the RO process where the membranes have pressure limitations (DOW Chemical Company, 2011).

To conclude with, based on the review carried out in this section, RO seems to be the most suitable process for small scale solar driven BW desalination plants in remote/rural areas mainly due to its low costs, low energy consumption, modularity, technological maturity and widespread use especially in Egypt. The low cost factor in particular is the most important factor where it is described by Banat and Jwaied (2008) as “the ultimate measure of the feasibility of the stand-alone system”. Finally, in spite of its low productivity and current high unit water costs, the MD process could be attractive to be used to treat the RO brine and increase the RR.

A summary of each process’s advantages and disadvantages please is shown in *Table 2-4*

Table 2-4: Summary of the main advantages and disadvantages of the reviewed desalination processes

	Advantages	Disadvantages	Notes
	Major Desalination Processes		
MSF	● A very reliable and well established process ● Maintenance and operator personnel could be easily found due to similarity with power plants	● High heat and electrical energy consumption ●Large solar collector area required ●High temperature operation is required due to the process's low PR ● Not economical for small scale applications ● Both heat and electrical energy required increasing the system components and complexity ● Standard MSF processes cannot cope with the intermittence of solar energy ● High capital and unit water costs compared to other desalination processes ● Large amount of brine recirculation required to obtain high RR's	● The MSF process should be mainly used for large scale applications in cogeneration plants
MED	● Lower capital and unit water costs than MSF ● Low operating temperatures which could be met by FPC's ●Suitable for small scale applications ● Ability to cope with the intermittence of solar energy ● Higher water RR's could be obtained without the need for large amount of brine to be re-circulated	● More frequent chemical cleaning is required. ●Cleaning requires plant shutdown ●High overall energy consumption ● Both heat and electrical energy required increasing the system components and complexity	● The process is suitable for small scale solar driven applications. However, cheaper desalination processes are available particularly RO, especially for BW desalination

VC	● Simple, robust and reliable process ● Designed for small scale applications ● One energy source needed in the MVC process ● Ability to cope with the intermittence of solar energy ● Higher water RR's could be obtained without the need for large amount of brine to be re-circulated	● Very high electrical energy consumption ●M VC units operating in Egypt showed maintenance problems and less production than designed value ● Insignificant desalination market share	● The MVC process is suitable for small scale solar driven applications. However, cheaper desalination processes are available particularly RO, especially for BW desalination ●TVC process is only suitable when combined with an MED process
RO	●Low energy consumption/Ideal for BW desalination ●Low capital cost and unit water costs ●Modularity ● Suitable for small scale applications ●High RR's especially with BW ●Well established process with a large market in Egypt ●One energy source needed	●High pre-treatment requirements ● High membrane replacement costs ●Difficulty to cope with the intermittence of solar energy ●Skilled operators needed ●Low salt rejection for some salts such as Boron that may cause health issues when water is used for drinking ● Can only desalinate water with certain levels of salinity due to pressure limitations	●Despite the large need of chemicals and complex operation, the process's low cost makes it the most dominant process whether for conventional or RE driven plants
ED/EDR	● Low energy consumption/Ideal for BW desalination ●Modularity ●Low pre-treatment requirements ●Ability to treat water with high scaling potential ●Membrane durability ●Robust and easy to maintain and operate ●Ability to cope with the intermittence of solar energy	●High capital costs ● Only suitable to treat feed water with salinities less than 5,000 mg/l. ● Not economical for high RR applications ●Low desalination market share ● Cannot remove silica and pathogens and therefore UF is a necessity for pre-treatment which will further increase the costs	● Solar driven ED/EDR process could be more suitable option than RO for treating BW with low salinity (i.e. < 1,500 mg/l) and with high scaling potential in rural/remote areas.

Minor Desalination Process			
Freezing Process	● Low risk of scaling and corrosion problems	●complex and bulky operation ●High energy consumption and costs	● In spite of its old concept, process has little success in market ●The freezing process with its current state is not attractive for desalination use.
HDH	● Simple operation and low maintenance ●Ability to cope with the intermittence of solar energy ● Low pre-treatment requirements ●Robust with long lifetime ●Ability to treat highly concentrated brines	●Large footprint ●Low productivity ●High specific energy consumption ●High capital and unit costs ●Application limited to very small capacities ● Both heat and electrical energy required in most configurations increasing the system components and complexity	● The HDH process with its current state could be useful when used for RO brine treatment to increase the RR.
MD	● Robust and simple operation ●Modularity ●Compact/small footprint ●Ability to cope with the intermittence of solar energy ● Low pre-treatment requirements ●Ability to treat highly concentrated brines	●Low productivity ●High specific energy consumption ●High unit water costs ●Risk of membrane fouling and wetting ● Both heat and electrical energy required increasing the system components and complexity	● The MD process with its current state could be useful should when used for RO brine treatment to increase the RR. ●The process has large development potential due to its potential higher productivities and cheap manufacturing materials
FO	● Potentially lower energy consumption than RO ● Potentially lower risk of fouling than RO ●Modularity ●Compact/small footprint ●Ability to cope with the intermittence of solar energy	● Membranes with higher performance are required ● Difficulties in separating the draw agent	● The FO process has the potential to be a better alternative than RO. However, it is still under research and development

2.4 Background Information

2.4.1 RO plants

Reverse osmosis is a relatively new process, compared to other well-established desalination processes such as MSF and MED, that started to be commercialized in 1969 and then increasingly gained market share (Reahl, 2006) to become the most dominant water desalination technology. The RO process covers all the spectrum of desalination plant scales with capacities as low as 1 m^3 per day to values up to 600,000 m^3 per day (IDA, 2013).

The following background information on the RO process is obtained from the literature (Howe, 1974, Porteous, 1984, Buros, 2000, Pinnekamp and Friedrich, 2006).The osmotic phenomenon is the natural tendency for a solution with less solute concentration to diffuse through a semi-permeable membrane, i.e. a membrane that is mainly highly permeable to water molecules to pass while non-permeable or has low permeability to other molecules, and dilute a solution with a higher solute concentration located on the other side of the membrane. In this case, under the setting shown in *Figure 2-1,* the height of the column of the more concentrated solution will keep increasing as more solution from the low concentrated side crosses the membrane until equilibrium is reached. At this point the rise in pressure in the higher concentrated solution is referred to as the osmotic pressure. Therefore, to force the salty water, i.e. the high concentration solution, to permeate through a semi-permeable membrane and becomes filtered, i.e. low concentration solution, the aforementioned process needs to be reversed and thus an external pressure needs to be applied on the salty water to overcome the osmotic pressure. The higher the water salinity, the higher is the osmotic pressure.

Reverse osmosis is therefore a pressure driven process where a membrane is used to block most of the dissolved solids as well as other undesired substances in the feed water. The separation mechanism in RO is complex but can be described by three mechanisms. The first mechanism is based on the electrostatic repulsion where the RO membrane surface negative polarity repels the anions in water while cations usually follow the anions to maintain the electro-neutrality of the feed solution.

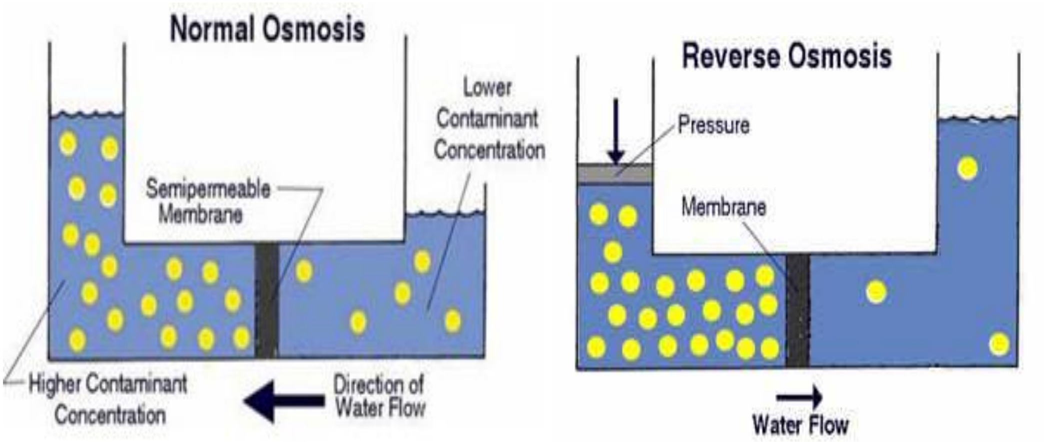

Figure 2-1: Osmosis and reverse osmosis process
Source:(Water Quality Association, 2005)

The higher the ion valence is the more effective is its rejection. For example, divalent ions such as calcium and magnesium are better rejected than monovalent ions such as sodium. The other mechanism is a sieving effect as the RO membrane pore size is very narrow, i.e. 0.1 to 1 ηm, and is therefore less than most of the particles in the water. Accordingly, RO membranes reject all non-charged substances such as bacteria, viruses and most of the dissolved organic matter in water. The last mechanism is solubility and diffusion where the polarity of water molecules and their small molecular size increases their solubility in the membrane material and diffusivity through it increasing their passage compared to solute molecules. More details on the RO separation mechanisms and models that describe the transport of water and solute molecules through the membrane could be found in Crittenden et al. (2012d).

2.4.1.1 RO plant design and operation description

The following data on RO plant design and operation is obtained from the DOW Chemical Company website (2013f). An RO desalination plant consists of four main parts: pre-treatment system; high pressure pump(s) (HPP); the RO stage(s); and the post treatment system.

The feed water first passes through the pre-treatment system which prevents fouling, scaling and chemical attacks from reducing the performance of the RO modules, reduces the cleaning requirements hence the RO plant downtime, and prolongs the membrane lifetime.

As the feed water needs to be pressurized to overcome the osmotic pressure and obtain the desired permeate flow, HPP's are used in conjunction with a valve installed at the concentrate side of the last RO plant stage to control the feed pressure. The feed water then enters the RO modules and is pressurized against the membrane where part of it crosses the membrane leaving most of the salts behind and is referred to as the permeate water. The remaining feed water therefore becomes more concentrated and is referred to as the concentrate or the brine[40]. Increasing the amount of permeate water for a given feed water flow rate, i.e. increasing the RR, increases the feed pressure due to an increase in the concentrate salinity as more salts are left behind which increases the osmotic pressure (Crittenden et al., 2012e).

The RO plant can include one or more stage, each composed of one or several pressure vessels connected in parallel (*Figure 2-2*). The pressure vessels are where the RO modules are housed and each vessel typically accommodates up to six modules connected in series such that the concentrate of one module is the feed of the following module.

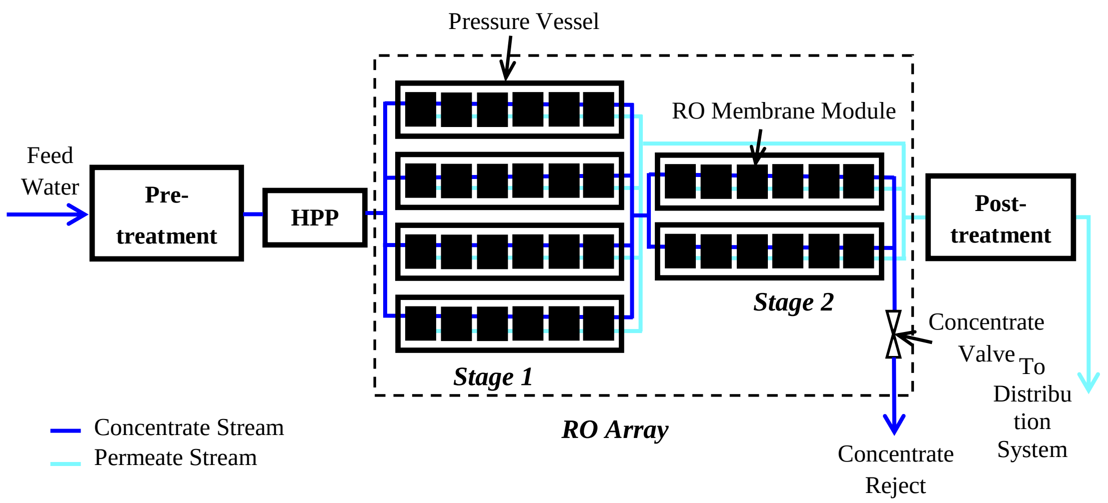

Figure 2-2: Schematic showing the main components of an RO desalination plant

The number of RO modules in series, which is determined by the number of modules in the pressure vessels and the number of stages in the RO plants, determines the RR of the plant. The more modules in series the higher the RR obtained as the concentrate is treated several times. The number of pressure vessels in each stage is determined by the amount feed flow. The higher the feed flow the more pressure vessels are needed in

[40] Both terminologies are used interchangeably in this study

parallel to ensure that the maximum feed flow in each RO module is not exceeded. The number of pressure vessels used in the second stage is less than the first stage to ensure that enough concentrate is flowing in each RO module in the former and therefore ensuring enough tangential flow to reduce the membrane's fouling potential and concentration polarization (CP). Concentration polarization refers to the local concentration of salts at the membrane surface as the water crosses the membrane leaving salts behind. This high concentration at the membrane surface increases the osmotic pressure and therefore for the same feed pressure the permeate flux[41] is decreased (Howe, 1974). For this reason a suitable tangential flow, or a minimum concentrate flow, is required to rapidly remove the accumulating salts away from the membrane surface.

The permeate flow of each pressure vessel is collected and further treated to be suitable for drinking and to be non-corrosive, a step referred to as post-treatment.

It should be noted that most of SW desalination plants use energy recovery devices (ERD's) which recover the pressure energy of the exiting concentrate. The existing concentrate is usually about only one to four bars less than the feed pressure (Buros, 2000) and is otherwise wasted by friction in the concentrate valve (Banat and Qiblawey, 2007). The pressure energy of the concentrate is then reused to pressurize the feed water such that only an amount equal to the RO plant permeate flow will need to be pressurized by the HPP. The use of ERD's is the main reason behind the currently reported low SEC of SW desalination plants. Several types of ERD's are used such as Pelton wheels, positive displacement pumps and isobaric pressure exchangers. However, ERD's devices are likely to be uneconomical with BW desalination as the RR's are higher than SW plants and therefore concentrate pressure energy that could be recovered may not be significant to justify the high costs of the ERD's. Moreover, most PV-RO plants for BW desalination reported in the literature (Alawaji et al., 1995, Al Suleimani and Nair, 2000, Joyce et al., 2001, Weiner et al., 2001, de Carvalho et al., 2004, Schafer and Richards, 2005, Schafer and Richards, 2007, Hrayshat, 2008, Richards et al., 2008, De Munari et al., 2009) while mostly operated at low RR's, none of them used ERD's. In contrast, almost all SW PV-RO units or conceptual designs reported in the literature (Mohamed and Papadakis, 2004, Thomson and Infield, 2003a,

---

[41] The permeate flow rate per unit area of membrane surface

Kershman et al., 2005), used an ERD. Only Richards and Schafer (2003) discussed the possibility of adding an ERD to their experimental BW RO-PV unit, but it was not eventually used with their experimental unit.

2.4.1.2 Pre-treatment

Fouling, scaling and chemical attacks are a major limitation to the RO process which can reduce the performance, shorten the lifetime or damage the RO membrane (Porteous, 1984).

Membrane fouling is the accumulation of solids on the membrane surface and/or within its pores clogging them or reducing their effective area resulting in a reduction of the permeate flow[42]. Fouling also increases the pressure drop along the membrane feed/concentrate channel which, at excessive levels, would mechanically damage the membrane (DOW Chemical Company, 2014a)[43].There are four main types of fouling: fouling caused by suspended solids and colloids[44] in water, referred to as particle or colloidal fouling; fouling caused by the precipitation of inorganic dissolved solids, referred to as scaling; fouling caused by the adsorption of organic matter to the membrane surface, referred to as organic fouling; fouling by metal oxides; and fouling caused by microorganism in water referred to as bio-fouling (Crittenden et al., 2012c).

Cartridge, sand and media filters in addition to clarification in conjunction with coagulation and flocculation are typically used to remove large particles and suspended solids including organic matter in the feed water (Kucera, 2010d, Crittenden et al., 2012e). Particulate and suspended solids fouling potential is usually assessed by the Silt Density Index (SDI) (AWWA Research Foundation Staff et al., 1996). The SDI measures the rate at which a fixed amount of the tested feed water will plug a 0.45 μm filter at a fixed pressure; the higher the SDI the more is the colloidal fouling potential of the feed water (Crittenden et al., 2012e). The Dow Chemical Company, one of the major companies supplying water treatment systems (Miller, 2003), recommends SDI's less than five for their RO spiral wound membranes (DOW Chemical Company, 2014d). It should be noted that, in contrast with surface water which has high colloidal fouling

---

[42] In practice RO plants operate at constant permeate flow by adjusting the feed pressure. Accordingly membrane fouling will lead to an increase in feed pressure and therefore the energy consumption.
[43] Membrane telescoping
[44] Colloids are a smaller type of suspended solids that are distributed evenly in the water due to their surface charge and therefore are harder to precipitate and cause water turbidity (Crittenden et al., 2012b)

potential as it contains high amount of suspended solids (Watson et al., 2003) and natural organic matter[45] (Liu et al., 2001), GW has usually a low SDI (<3) because the ground itself acts as a filter (Thomson and Infield, 2003b), and for this reason media filters, clarification, coagulation and flocculation are usually not required[46]. Nevertheless, as a precautionary measure, 5 μm cartridge filters are typically used for GW applications (DOW Chemical Company, 2013b).

Bio-fouling is controlled by disinfecting the water using oxidants such as chlorine, referred to as pre-chlorination, and non-oxidants biocides to inactivate bacteria and other microorganisms (Kucera, 2010e). Groundwater has also low bio-fouling potential (DOW Chemical Company, 2014a) compared with surface waters and for this reason disinfecting the water may not be needed as observed in some existing GW RO desalination plants discussed in AWWA Research Foundation Staff et al. (1996).

Regarding metal oxides fouling, when the feedwater has high concentrations of dissolved iron and manganese, which is typical for GW with low dissolved oxygen, and is exposed to air, these metals can oxidize and precipitate (Crittenden et al., 2012f). The precipitated metal oxides then accumulate on the membrane surface causing fouling problems. Fouling caused by iron and manganese oxides is prevented by deliberately oxidizing both metals so they can be easily filtered. For this reason, filters with a manganese dioxide media are typically used, and are referred to as iron filters, and with some types[47] additional oxidizing chemicals[48] such as chlorine and potassium permanganate are required to help with the oxidation process (Kucera, 2010d). The use of oxidizing chemicals in conjunction with MF is another method to remove iron oxides (Al-Sayed et al., 2012) that in addition to lime softening in conjunction with settling tanks particularly to remove iron (P. Roginson, 2014, pers. Comm., 5 Feb.), and the use of an ion exchange process (DOW Chemical Company, 2014c).

It should be noted that pressure driven processes such as MF and UF (Appendix C) can be also used to replace conventional pre-treatment methods. The advantages of using such membranes are their higher ability to produce higher feed quality for the RO plant

[45] Organic matter from natural sources
[46] RO membranes manufacturers usually recommend a feed water with SDI less than five to meet the warranty requirements
[47] i.e. manganese greensand media filter
[48] E.g. chlorine, chlorine dioxide, potassium permanganate, and ozone

in terms of removing the suspended solids as well as microorganisms preventing the RO modules from excessive fouling hence reducing their cleaning requirements (Wang et al., 2010, Schafer et al., 2005) and increasing their reliability (Drioli et al., 2002). Microfiltration in particular is also reliable in pre-treating water with iron content in contrast with cartridge filters which cannot be used in this case as they will be fouled quickly and may need to be replaced every day (P. Roginson, 2014, pers. Comm., 5 Feb.) which is not economical.

Scaling is the precipitation of salts as they exceed their solubility limit in water which takes place on the membrane surface where the salt concentration is the highest due to CP (Kucera, 2010a). In addition to fouling the membrane and increasing the pressure drop, scaling increases the salt passage through the membrane because the high concentration of salts on the membrane surface causes more salts to diffuse reducing the permeate quality (Crittenden et al., 2012e). The most common types of scales are calcium carbonate, reactive silica, magnesium hydroxide and calcium sulphate (Watson et al., 2003, DOW Chemical Company, 2013g) which all have a low solubility in pure water (Howe, 1974); that in addition to the less common barium sulphate, calcium phosphate, and strontium sulphate scales. Calcium carbonate, magnesium hydroxide, and calcium phosphate scaling can be controlled by lowering the pH of water, usually to values from 5.5 to 6.2 (Porteous, 1984, Gabelich et al., 2007, Crittenden et al., 2012e), by adding acids such as sulphuric or hydrochloric acids to increase their solubility. Calcium sulphate, reactive silica, barium sulphate and strontium sulphate scaling is more difficult to control and require the use of scale-inhibitors which prevent crystals from forming and growing (Crittenden et al., 2012e). Reactive silica, in particular may limit the RR that could be attained by the RO plant (Kucera, 2010e). Scaling could be also controlled through the use of an ion exchange process which is more effective than using chemicals as it removes most of the ions causing scaling (DOW Chemical Company, 2013g) or through lime softening to precipitate calcium and magnesium ions as well as silica, barium and strontium before going to the RO modules by adding chemicals such as lime and caustic soda to one or more clarifier tanks where the precipitation occurs (Crittenden et al., 2012d). However, the ion exchange process is expensive due to the high costs of the regeneration process (Miller, 2003) and is not economically feasible to treat high salinity BW (Dow Chemical Company, 2013, pers. Comm., 8 Jun.); while lime softening requires additional components such as clarifier tanks and re-carbonation reactors where carbon dioxide is added to the water to decrease its pH (Crittenden et al., 2012d).

Chemical attack refers to the degradation of the membrane active layer[49], particularly with the more widely used polyamide membranes (Nicolaisen, 2003), due to the presence of oxidizing agents (Micale et al., 2009) in water such as chlorine that are used during pre-treatment. Oxidizing agents reduce the membrane's salt rejection and therefore the permeate water quality. For this reason, all oxidizing agents need to be removed before reached the RO membrane through adding a reducing agent, such as sodium metabisulphite, to the water right before entering the RO membrane or through using activated carbon filters (DOW Chemical Company, 2014a).

It should be noted that in addition to pre-treatment, the RO membranes require periodic cleaning where the number of cleanings per year will vary according to the manufacturer and the feed water type. DOW Chemical Company for example recommends four cleanings per year as long as the RO membranes operate within the company's specified guidelines (DOW Chemical Company, 2013c). The cleaning involves the use of acid to remove scaling from the membranes surface then exposing the membrane to a high pH solution (pH>12), e.g. by using caustic soda, which acts as a biocide (Thomson et al., 2009) removing microorganisms while organic material dissolve in the water at this high pH.

2.4.1.3 Post treatment

Post treatment is required to ensure that the RO permeate water is suitable for drinking and that it is non-corrosive. It has been already discussed that acids are added to the feed water to prevent calcium carbonate and magnesium hydroxide scaling. Accordingly, the pH of the permeate water needs to be increased to prevent corrosion typically to values ranging from 6.5 to 8.5 (Wang et al., 2010). This is achieved by using degassers to remove carbon dioxide[50] which is formed from the reaction of the added acid with calcium bicarbonate (Porteous, 1984), and would otherwise redissolve in water forming carbonic acid further reducing the pH; and by re-mineralizing the water by increasing the carbonate and bicarbonate content, e.g. adding sodium

---

[49] The active layer is a very thin layer which is responsible for retaining the undesired substances in water.

[50] Carbon dioxide is not rejected by the RO membrane

bicarbonate, in the water (Watson et al., 2003, Al-Sayed et al., 2012). Re-mineralizing the water could be also achieved by blending the raw BW with the permeate water (Watson et al., 2003). Degasifiers are also used to remove hydrogen sulphide gases which may occasionally exist in GW (Crittenden et al., 2012a). Hydrogen sulphide produces offensive odour that reduces the acceptability of water and increase the corrosiveness of water, and if oxidized it can increase the turbidity of the water (Crittenden et al., 2012a).

The last step of post treatment is disinfection, usually through chlorination but there are also other methods such as the use of ozone and UV radiation which are discussed in (Crittenden et al., 2012d), to ensure that the water is free from viruses and germs in the permeate tank and the distribution system (Micale et al., 2009). In this case, a residual chlorine of 0.5 mg/l is commonly used (DOW Chemical Company, 2014a).

2.4.2 MD process

Membrane distillation is a thermally driven process that is similar to the HDH process where only surface evaporation occurs. The concept of MD was first developed in the early 1960’s then interest in this process weakened due to its lower production especially when compared to the RO process. However, since the 1980’s the interest in this process was renewed due to the advancement in the membrane manufacturing technology with an increasing amount of published papers on the MD process especially in the last couple of years (Khayet and Matsuura, 2011a). The increasing interest in MD was particularly for small scale applications due to the simplicity of the process simplicity and its ability to be coupled with low grade sources of heat (Cipollina et al., 2009).

In an MD process a micro-porous membrane is used to sustain a vapour-liquid interface and does not contribute to the separation process through selectivity as in other types of membrane filtration such as RO. To sustain such liquid-vapour interface, the membrane is composed of a hydrophobic material, e.g. polytetrafluoroethylene (PTFE) and polypropylene (PP), which does not allow water in liquid phase to enter the membrane pores due to the surface tension forces, and only water vapour molecules are allowed to pass. The feed water is heated then enters into the evaporator channel of the membrane where the water in contact with the membrane surface evaporates and the water vapour permeates, either by diffusion or convection, through the membrane pores (*Figure 2-3*). The trans-membrane pressure difference is the main driving force for water vapour mass transfer in the MD process. The crossing water vapour then condenses in the permeate side of the membrane which is kept at a lower temperature, or is collected outside the membrane to condense in a separate condensation chamber. (Gostoli et al., 1987, Schofield et al., 1987, Kurokawa et al., 1990, Lawson and Lloyd, 1997, Gryta and Tomaszewska, 1998, Khayet et al., 2001)

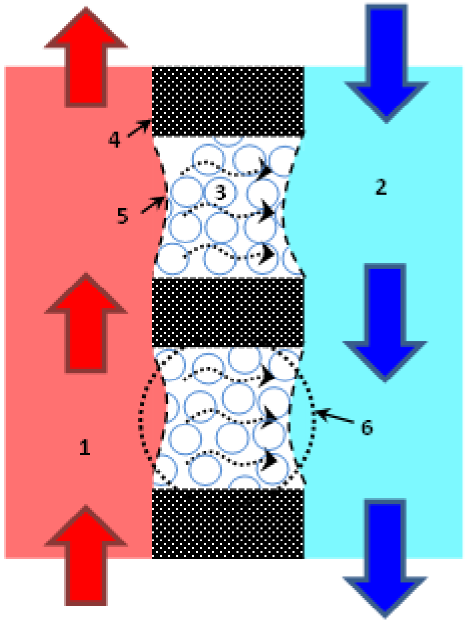

Figure 2-3: Schematic showing the basic concept of an MD process

1- Hot feed water flow	2- Cold water flow mixed with distillate
3- Water vapour molecules	4- Hydrophobic membrane material
5- Vapour-Liquid Interface	6- Membrane Pore

There are several MD configurations that differ in their operation which mainly are: direct contact membrane distillation (DCMD); air gap membrane distillation (AGMD); vacuum membrane distillation (VMD); and sweeping gas membrane distillation (SGMD). Direct contact membrane distillation is the most widely used configuration in water desalination (Phattaranawik and Jiraratananon, 2001, Khayet and Matsuura, 2011d) which is due to its simple operation and low cost as it requires the least number of equipment. In DCMD, the feed water and the distilled water are in direct contact with the membrane surface. The heated feed water evaporates at the membrane surface then diffuses through a stagnant film of air trapped in the membrane pores. The transferred vapour then condenses as it becomes in contact with the cool water flowing in the other side of the membrane. The pressure gradient between the evaporation and condensation surfaces is therefore maintained by the temperature difference across the membrane. The AGMD process similarly to DCMD, however an air gap is introduced on the condensation side of the membrane to increase the thermal efficiency of the process by limiting conductive heat transfer through the membrane material (Gostoli and Sarti, 1989, Khayet and Matsuura, 2011a). Conductive heat transfer through the membrane is a heat loss mechanism as it does not contribute to the mass transfer and leads to a decrease in the temperature difference between the evaporation and condensation surfaces decreasing the pressure gradient hence the flux (Banat and Simandl, 1998). The other advantage of this process is that there are separate cooling and permeate channels. Therefore, other liquids than the permeate could be used for cooling including the feed water itself which can then recuperate the latent heat of condensation and gets pre-heated, i.e. internal heat recovery, increasing the thermal efficiency of the process. The extra air gap, however, increases the water vapour diffusion length hence the resistance to mass transfer which reduces the flux. For this reason, AGMD has low productivities compared to other MD configurations (El-Bourawi et al., 2006). In the VMD configuration, the pressure gradient is mainly achieved by lowering the pressure on the permeate side below the vapour saturation pressure using vacuum pumps. The water vapour is then extracted and condensed outside the membrane. In the SGMD configuration, a cold inert gas is forced to flow in the permeate channel transporting vapour molecules outside the membrane where the vapour is eventually condensed in a separate device. The SGMD and the VMD configurations are more thermally efficient than DCMD as the gas barrier and the vacuum respectively, reduce the conductive heat losses. Moreover, both configurations have a lower mass transfer resistance than AGMD resulting in higher productivities (Lawson and Lloyd, 1997). However, both processes require extra equipment such as a separate condensation device and vacuum pumps which make them more complex and costly (Khayet and Matsuura, 2011e). For this reason, despite its lower productivity, DCMD is more suitable for desalination than SGMD and VMD due to its simplicity (Lawson and Lloyd, 1997). Different MD configurations are discussed in more details in the literature (Gostoli and Sarti, 1989, Lawson, 1995, Khayet and Matsuura, 2011f).

Finally, similar to RO membranes, MD membranes experience flux decay and an increase in pressure drop along the channels due to particulate fouling, bio-fouling (and scaling which clogs membrane pores (Lawson and Lloyd, 1997, Curcio and Drioli, 2005). The effect of scaling in particular on MD performance was investigated in several studies such as (Tun et al., 2005, Yun et al., 2006, Martinetti et al., 2009), and all the studies reported a sharp decline in MD flux when the feed water solute concentration is near or reached saturation due to the rapid growth of salt crystals deposits particularly at the membrane surface where the solute concentration is higher due to the effect of CP. Scaling also causes membrane pore wetting which causes the feed flow to cross the membrane contaminating the permeate water (Lawson and Lloyd, 1997, Tun et al., 2005). For this reason feed water pre-treatment using the same measures discussed in section *2.4.1.2* is required.

It should be noted however, MD membranes are reported be less affected by fouling and scaling (El-Bourawi et al., 2006, Khayet and Matsuura, 2011b) especially due to the relatively large size of the pores which reduces the risk of clogging (Lawson and Lloyd, 1997). Nevertheless, fouling and scaling effect on MD performance is not well studied (Tun et al., 2005, Khayet and Matsuura, 2011b).

2.5 Research Gaps and Novelty

In this section, a review is carried out on different work concerning: the application of PV-RO for BW desalination in Egypt; PV-RO plants for BW desalination in general with an emphasis on the RO plant design and operating conditions; the feasibility of hybrid RO/MD plants; and MD process modelling. This section will also demonstrate the novelty of this thesis with respect to the reviewed literature.

2.5.1 Solar driven RO desalination plants in Egypt

Despite its large solar resources, few studies concerning the application of solar, and RE in general, driven desalination plants in Egypt and their feasibility are found in the literature. Moreover, only few solar driven desalination units, including PV-RO plants for BW desalination, are reported to be installed in Egypt (*Table 2-5*).

Only one PV-RO plant was reported in Garci et al. (2003) which was used for BW desalination. The plant had a 50 m^3/d[51] capacity and was installed along the Red Sea

[51] In another study by Lamei et al. (2008), the same plant was reported to have a capacity of 240 m^3/d. However, the original studies cited by Garci et al. (2003) and Lamei et al. (2008) could not be found to verify the actual value.

Table 2-5: Solar driven desalination plants in Egypt

Reference	Solar system	Desalination process	Type of plant	Feed water	Fresh water productivity
(Libert and Maurel, 1981)	FPC driving a heat engine	RO	Demonstration	Brackish	54 m^3/d
(Garcia-Rodriguez, 2003)	PV	RO	Demonstration	Brackish	50 m^3/d
(Nafey et al., 2006)	FPC	MSF	Lab Scale	Seawater	< 12 l/d
(Fath et al., 2006, Wieghaus et al., 2008)	FPC+PV	MD	Demonstration	Seawater	Up to 64 l/d
(Abdel-Rehim and Lasheen, 2007)	- PTC	Solar Still	Lab Scale	-	< 2.5 l/d
(Vetter et al., 2010)	CPV	Not mentioned	Demonstration	Brackish	-
(Ali et al., 2011)	PV-Wind-diesel	RO	-	Brackish	30 m^3/d

coast and commissioned in 1986; it is not clear though if the plant is still running. There is also a CPV[52] demonstration plant installed in Wadi-Al-Natrun[53] that was discussed in Vetter et al. (2010) and is part of the NACIR project funded by the European union. The CPV 30 kWp plant is used to supply electricity for a GW submersible pump, a desalination unit, an irrigation pump, and an air conditioning system to cool the battery room. No details, however, were given on the desalination system as the study mainly focused on developing a control algorithm for load side management to maximize water production.

Regarding feasibility studies of PV-RO application in Egypt, Lamei et al. (2008) developed a correlation to estimate the unit water costs of PV-RO plants as a function of their capacity, SEC and electricity prices, using the data from 21 existing conventional[54] RO plants in the Mediterranean and Red Sea regions. The study concluded that battery-less PV-RO plants in Egypt could start to compete with conventional fossil fuel driven RO plants if the price of the PV modules was 1 USD/Wp. Lamei et al. (2008), however,

[52] The CPV trackers are supplied by SOITEC which use Fresnel refractor lenses
[53] Located on the western borders of Beheira governorate
[54] Either connected to the grid or driven by diesel generators

estimated that in this case the PV electricity cost would be 0.06 USD/kWh over a period of 25 years. This is an underestimated value given that, as previously reported in section *2.2.1*, the mid 2012 LCOE for PV systems with similar solar irradiation[55] and array size to that used in their study, was 0.147 USD/kWh at an average module price of about 1.11 USD/Wp[56] (pvXchange, 2013). This underestimation is due to an overestimation of the energy produced by the PV array as the energy losses, referred to as de-rating factors, were likely to be ignored in their study which otherwise could decrease the energy output from the PV array by 30% or more. Moreover, Lamei et al. (2008) used a value of 2,000 kWh as the annual energy produced from 1 kWp of PV array with Egyptian solar conditions while, using PVWATTS calculator developed by NREL (2012), 1 kWp would typically produce approximately 1,500 kWh/year if located in Aswan city[57], which receives one of the highest solar irradiation in Egypt, after including the de-rating factors. Furthermore, the accuracy of the correlation developed to estimate the RO unit water costs is questionable given that the unit water costs were estimated at an assumed RO plant SEC of 5[58] kWh/m^3. However, in practice this value would greatly vary based on the operating conditions such as the feed salinity and the RR. The variation in RO plants SEC and unit water costs is even more significant for small scale plants which could be observed from the reviews carried out by Ali et al. (2011) and Li et al. (2013). Therefore it is difficult to use such correlation to estimate the unit water costs without expecting significant errors. Furthermore, as the system is designed to operate without batteries, the SEC will vary according to the RO operating point which will vary with the available solar radiation. Finally, the correlation was based on SW RO plants and therefore may overestimate the costs for brackish GW RO plants given that they requires less pre-treatment as discussed in section *2.4.1.2*.

Finally, Ahmad and Schmid (2002) investigated the feasibility of PV-RO plants for BW desalination in Egypt. The authors designed a PV-RO system for BW desalination with 1 m^3/d capacity and using battery storage for power conditioning. The study showed that the unit water costs from such system under Cairo's solar irradiation could be 3.73

[55] 2000 kWh/m^2/year
[56] Original values in Euro converted to USD using a conversion factor of 1.35
[57] Tilted at an angle equal to the latitude
[58] Lamei et al. (2008) reported in the graph showing the PV-RO unit water costs that the costs are based on SEC of 3 kWh/m^3, however when the correlation was examined, it has been concluded that a SEC of 5 kWh/m^3 was used.

USD/m^3. Ahmad and Schmid (2002), however, only considered feed waters with salinities less than 2,000 mg/l and a low RO RR of only 50%. The study also used rough analysis in their design, for example the PV system was sized based on average yearly peak sun hours. Moreover, the method of estimating the RO power consumption and design was not clarified in the study.

From the review carried out in this section, it can be concluded from the review that there is a lack of studies concerning the economic feasibility of BW PV-RO in Egypt and the existing studies are not reliable and/or do not consider the different operating conditions of the RO plant.

Therefore, in this study the energy consumption and the economic feasibility of high RR BW PV-RO plants in Egypt will be analysed considering a wide range of feed salinities a at the expected range of solar irradiances. The analysis will give a new and a more accurate insight on the feasibility of PV-RO plants in Egypt compared to conventional RO plants driven by diesel generators that are commonly used in remote areas. The analysis will also include the costs associated with GW extraction for the range of water depths encountered in Egypt which to the author's knowledge has not been done before.

2.5.2 General application of brackish water PV-RO plants

Alawaji et al. (1995) described a brackish GW PV-RO plant with 15 m^3/d capacity with battery storage for whole day operation, that was installed in Saudi Arabia in late 1994. However, the performance of the plant was not evaluated and no specific details on the design of the RO system were given.

Al-Suleimani and Nair (2000) discussed the design of a brackish GW PV-RO plant with 6.5 m^3/d average productivity that was commissioned in 1995 in a remote desert area in the Nejd area in Oman. The plant desalinated water with 1,100 mg/l salinity and operated at relatively high RR‘s ranging from 65-70%. However, the SEC of the RO plant was not reported and no details on the RO plant performance design were given. Nevertheless, it is likely that the RO modules operated outside their recommended window given that one pressure vessel was used in each stage. This is would probably increase the scaling potential in the modules housed in the last pressure vessel due to the expected low tangential flow as discussed in section *2.4.1.1*. Al-Suleimani and Nair

(2000) also carried out an economic analysis to compare the water costs between the PV-RO plant and a similar RO plant driven by conventional diesel generators. The study showed that over a 20 years period, the unit water costs of the PV-RO was 25% lower than that driven by a DG. However, no details were given on the specific costs assigned to each component of the PV-RO plant.

Weiner et al. (2001) discussed the design of a 3 m^3/d brackish GW PV-RO experimental unit with wind energy as back up and using batteries for power conditioning, that was installed in Israel. The plant was used to desalinate water with 4,000 mg/l salinity and operated at a 50% RR. However, the RO system's SEC and its design were not reported.

Joyce et al. (2001) conducted experimental work on a battery-less brackish GW PV-RO pilot unit. The unit had a capacity of 20 l/d and was tested at different feed water salinities and two different PV array sizes of 100 and 150 Wp. The unit's SEC was very high ranging from 25.5 to 32.4 kWh/m^3 with feed water salinities ranging from approximately 1,820 to 2,870 mg/l[59] for the case using the larger size array[60]. The high SEC is because the unit operated at low feed pressures resulting in very low RR's of less than 2.4%. *Figure 2-4* shows a rough estimate of the SEC of RO plants as a function of the RR at different feed water salinities indicating that at a very low and very high RR's, the SEC starts to exponentially increase as it is proportional to the inverse of the product of the RR and 1-RR.

An experimental PV-RO unit installed in White Cliffs, Australia was discussed in Richards and Schafer (2003). The study investigated the effect of varying the feed pressure and flow rate on the SEC and the permeate flow rate. The unit was tested with three types of feed waters: dam water with 150 mg/l salinity; 2,000 mg/l sodium chloride water solution; and GW with 3,500 mg/l salinity. The SEC of the RO unit was approximately 2 to 2.25 and at least 8 kWh/m^3 for the sodium chloride solution and the GW cases, respectively. The aforementioned values are, however, questionable given their significant increase with respect to the modest increase in the feed water salinity while it is clear from the Van't Hoff equation that the osmotic pressure is directly proportional to the feed water salinity and therefore a significant increase in energy

[59] A conversion factor of 640 used to convert original value given in dS/m to mg/l
[60] An even higher SEC's were obtained from the RO unit connected to the smaller size PV array

consumption would be expected. In this case, other factors could be affecting the SEC particularly scaling issues especially that the sodium chloride solution does not cause scaling problems in contrast with GW which typically has high hardness and sulphate content which increases scaling potential.

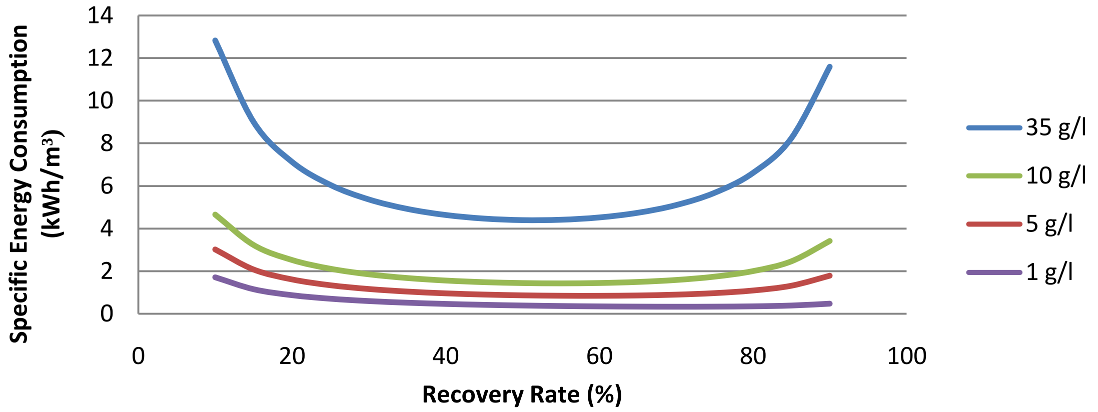

Figure 2-4: A rough estimate of the SEC of RO plants at different feed water salinities and RR's[61]

De Carvalho et al. (2004) described a PV-RO demonstration unit with 250 l/h capacity using batteries installed in Brazil. The SEC of the plant was reported to be 3.03 kWh/m^3 which is very high for the desalinated 1,200 mg/l feed water. The high SEC could be mainly attributed to the low operating RR of the plant i.e. 27%. The authors also conducted a cost analysis study and showed that the unit water cost of such plant was 12.75 USD/m^3.

Schafer and Richards (2005) tested an experimental PV-RO unit desalinating brackish GW with approximately 4,000 mg/l[62] salinity. The study investigated the effect of the intermittent nature of solar energy on the membrane performance in a directly coupled PV-RO plant. In their study it was particularly observed that the RO membrane was tested outside its recommended operating window by the manufacturer. For example,

[61] The SEC in the figure above was roughly estimated based on the following assumptions:
1- Water only contains sodium chloride salts for simplicity
2- The osmotic pressure was approximately calculated using Van't Hoff equation, $P_{osm} = 2\ C\ R\ T$ which assumes that the dissolved solids in water move in random motion (Howe, 1974) and that the solution is infinitely diluted (Crittenden et al., 2012d). C is the molar concentration (mol/m^3), R is the ideal gas constant (m^3 bar K^{-1} mol^{-1}) and T is the water temperature (K). The "2" factor in the equation is because each mole of sodium chloride dissolves into sodium and chloride ions and each ion contributes to the osmotic pressure and in this case a complete dissolution of sodium chloride is assumed.
3- An additional pressure of 4 bars was assumed to be required to obtain the desired permeate flow.

[62] The exact salinity is not mentioned, but based on the chemical composition shown in the study, it has been estimated that the salinity would be in the range of 4,000 mg/l

the concentrate flow in the study ranged from 258 to 437 l/h[63] which is much lower than the minimum recommended concentrate flow, i.e. 700 l/h, for the RO module model used[64] (DOW Chemical Company, 2013c). Moreover, the maximum recommended RR for this RO membrane is 19% while it was tested at RR's of up to 45%. Exceeding the maximum recommended RR and operating at concentrate flows less than the minimum recommended value would greatly increase CP[65] and scaling potential which will increase the SEC. The RO membrane also operated at fluxes of less than 21 $l/m^2/h$ while the manufacturer recommends an operating flux of 30 $l/m^2/h$ (DOW Chemical Company, 2013c). Operating at low fluxes reduces the SEC values but more RO modules would be required to obtain the desired permeate flow which will increase the costs.

Similar operation outside the manufactures operating windows was also observed in the studies by Schafer et al. (2007), Richards et al. (2008) and De Munari et al. (2009) which also investigated the effect of the intermittent nature of solar energy on the membrane performance in a directly coupled PV-RO plant.

Schafer et al. (2007) particularly investigated the operating window at which each membrane can produce good quality permeate water as well as determining the operating conditions at which the SEC is minimal. The SEC of the RO membrane varied from approximately 2.1 kWh/m^3 at a RR of 21%, dipping to 1.8 kWh/m^3 at a RR of 35%, than increasing again to 2 kWh/m^3 at a RR of 45% for the low feed flow case (300 l/h). In their study, the concentrate flow was less than the minimum recommended value[66]. Operating at low concentrate flow will result in an increase in the CP and therefore the scaling potential which could be the reason behind the increase in the SEC when the RR exceeded 35% while it is expected to keep decreasing at this low RR range.

---

[63] Assuming that the feed pump is operating at its rated capacity of 470 l/h
[64] FILMTEC BW30 4 inch membrane
[65] Concentration polarization refers to the local concentration of salts at the membrane surface as the water crosses the membrane leaving salts behind. A high concentration polarization factor increases then osmotic pressure and therefore the feed pressure required to obtain the same permeate flow. It also increases the amount of salts diffusing to the permeate reducing its quality
[66] The maximum operating feed flow, i.e. 500 l/h, which is already lower than the minimum recommended concentrate flow

In Richards et al. (2008), the RO unit desalinated water with 5,300 mg/l salinity and had an average SEC of 2.3 kWh/m^3 at an average RR and flux of 28% and 17 l/m^2/h respectively. In De Munari et al. (2009), the feed salinity was about 4,700 mg/l and the unit operated at an average RR and flux of 20% and 10 l/m^2/h at which the average SEC was 3.2 kWh/m^3. While the same PV-RO rig was used in both studies, it is observed that the SEC reported in De Munari et al. (2009) was higher than that reported in Richards et al. (2008) despite the lower feed salinity, flux and RR. This is likely due to improper pre-treatment and cleaning which would lead to the build-up of scales on the membrane surface and/or membrane fouling as the authors noted. This should be particularly expected given that in both studies the FILMTEC BW30 RO membrane was operating outside the manufacturer recommended guidelines (DOW Chemical Company, 2013c) particularly in terms of the minimum concentrate flow. Therefore, if De Munari et al. (2009) used the same RO membrane used in Richards et al. (2008), it is likely that it must have been already in a bad condition. It should be also noted that in both studies, the membrane operated a low fluxes than the recommended value.

Finally, Hrayshat (2008) investigated the feasibility of applying PV-RO brackish GW desalination plants in several regions in Jordan through computer modelling at different feed water salinities. The study did not discuss the RO plant operating conditions, e.g. the RR and daily operating hours. The exact method used in modelling the performance of the RO plant is also not clear but it seems that the author assumed that the RO plant productivity is proportional to the available solar energy. In this case, the RO plant productivity significantly varied from periods of low solar irradiance and those of high solar irradiance. Accordingly, it is likely that for an actual plant, the RO modules will be operating outside their recommended specifications. With such large variation in the productivity it is even expected that the modules will be damaged in periods of high solar irradiance due to the high feed pressure applied. The effect of the battery bank on the plant performance which was expected to make the productivity curve more uniform than that shown in the study is also not clear.

From the review carried out in this section, it is observed that almost all the brackish PV-RO plants were operating at low RR’s, i.e. less than 50%, while RR’s of up to 90% could be obtained from RO plants (DOW Chemical Company, 2013f) depending on the water salinity and its scaling potential, to reduce the wasted water. Low RR operation of

PV-RO plant was also observed from the review carried out in de Carvalho et al. (2004) concerning PV-RO plants. Moreover, as discussed in section *2.5.2*, low RR operation will result in a significant increase in the SEC of the plant.

Furthermore, it is observed that all of the BW PV-RO plants were designed in an ad-hoc manner or the design and the operating conditions were not reported. Accordingly, the membranes were either not or there was no indication that they are operating at optimal conditions. Working outside the membrane's optimal operating specifications can increase its SEC as well as the risk of fouling. Moreover, almost none of the reviewed studies on the economic feasibility of PV-RO plant considered the effect of the PV-RO plant operating hours on its LCOW. This is except the study by Al Suleimani and Nair (2000) which concluded that increasing the operating hours of the PV-RO plant would make it less economically competitive with a DG-RO plant. However, their study was only limited to an RO plant desalinating 1,100 mg/l and it is not clear whether the same conclusion applies for other feed water salinities as well as other RR's.

For this reason, the RO plants in this study will be designed to operate within their optimal operating window as recommended by the manufacturer, which will minimize cleaning requirements hence the costs and the impact on the environment (Kucera, 2010d), and increase the lifetime of the RO membranes and give more realistic SEC and costs values. The effect of scaling on the maximum attainable RR of the RO plant will be also investigated for the range of GW chemical compositions found in Egypt.

2.5.3 Hybrid RO/MD plants

The concept of integrating RO with an MD process to increase the RR is already being investigated in the literature.

Drioli et al. (1999) carried out an experiment where an MD process was used to treat the brine from an SW RO plant (45 g/l feed water salinity). The RO brine was concentrated to saturation (approximately 320 g/l salinity) and the RR increased from approximately 40% for the RO only plant to 86% for the hybrid plant. The study also showed that the unit water cost of a hybrid plant with 26,000 m^3/d capacity could be similar to that of an RO only plant with the same capacity, estimated to be 1.25 USD/m^3, if the MD plant installation costs were 116 USD/m^2.

Table 2-6: Summary of some of the BW PV-RO plants reported in the literature

Reference	Plant Capacity m^3/d	Feed Water Salinity g/l	SEC kWh/m^3	RR	Unit Water Costs USD/m^3	Energy Storage	Other details
(Alawaji et al., 1995)	15	Brackish unspecified	-	-	-	Battery Bank 5.5 days autonomy	GW pumping systems is separate from the RO plant.
(Al Suleimani and Nair, 2000)	6.5*	1.1	Approx. 1.08	65-70%	6.52^	Battery Bank for Power Conditioning	Evaporation pond used for brine discharge
(Joyce et al., 2001)	0.02	1.3 to 3.2** Lab prepared water	25.5 to 32.4	< 2.4%	-	Direct Coupling	Lab scale unit
(Weiner et al., 2001)	3	4	-	50%	-	Battery Bank for Power Conditioning	Wind energy as backup
(Richards and Schafer, 2003)	0.1	2	2 to 2.25	-	-	Direct Coupling via a MPPT[67]	Experimental unit
		3.2	8				
(de Carvalho et al., 2004)	250 l/h	1.2	3.03	27%	12.76^	Battery bank	-
(Schafer et al., 2005)	1	-	3	45%	-	Simulated PV supply through a constant power source	Experimental unit
(Schafer et al., 2007)	1	5.3	1.8	35%	-	Simulated PV supply through a constant power source	Experimental unit
(Richards et al., 2008)	1	5.3	2.3	28%	-	Direct Coupling via a MPPT	Experimental unit
(De Munari et al., 2009)	1	4.7	3.2	15 to 20%	-	Direct Coupling via a MPPT	Experimental unit

*Average productivity

^ Based on operating costs only

**using a factor of 0.64 to convert from µS/cm to mg/

[67] Maximum Power Point Tracker

While the study does not give much detail on the experiment carried out or the methodology used for the cost analysis, the reported hybrid plant RR and its unit water costs were based on experimental MD fluxes ranging from 2.4 to 1.4 kg/m^2/h at feed water salinities of 75 and 320 g/l, respectively, and at a feed water temperature of 35°C.These values seem to be high and questionable for the following reasons:

1- The flux values reported were attained after heating the feed water from 25°C to only 35°C which is questionable given that high fluxes can be usually attained at higher temperatures. For example, the manufactures typically report the nominal flux values of commercial MD modules at temperatures ranging from 75 to 80°C (*Table 2-7*), knowing that the MD flux increases exponentially with the increase in the feed water temperature due to an exponential increase in the water vapour pressure (Banat and Simandl, 1998, El-Bourawi et al., 2006).
2- The analysis in Drioli et al. (1999) was based on a lab scale MD module which, under the same operating conditions, is expected to have higher fluxes than full scale modules, on the expense of high SHC. This is due to the short length of the channel in a lab scale module which causes the average water temperature in the evaporator channel to be nearly equal to that at the evaporator inlet resulting in a maximization of the vapour pressure hence the flux. In contrast, with full scale MD modules the water temperature in the evaporator channel keeps decreasing along the channel as heat is being transferred to the cooling channel[68] lowering the average flux of the module. For the same reason, high temperature gradient can be achieved across the membrane in lab scale modules which will also increase the flux.
3- The flux reported at 320 g/l, i.e. 1.7 kg/m^2/h, is very high for such salinity and is likely to be unsustainable given that studies on concentrating sodium chloride solutions using an MD process such as those of Tun et al. (2005) and Yun et al. (2006) reported a sharp decline in the MD flux to eventually reach zero when the

[68] For example, for the PGMD module discussed in Winter et al. (2011), the temperature of the feed water exiting the evaporator channel could be more than 50°C lower than its value at the inlet of the channel.

solution concentration reached 260 g/l[69] due to the rapid growth of crystals deposits on the membrane surface.

Table 2-7: Flux and SHC of currently available full scale commercial MD modules

Brand/ Manufacturer	**Description**	**Flux**	**SHC**	**Notes**	**Reference**
SolarSpring	Spiral wound PGMD	1-2.5 $l/m^2/h$ (depending on the feed flow rate and the cooling water temperature)	127-207 kWh/m^3 (depending on the feed flow rate)	Flux and SHC are obtained with tap water as the feed water and an evaporator inlet temperature of 80°C	(Winter et al., 2011)
MEMSYS	6 effects vacuum multi-effect MD	6 $l/m^2/h$	158 kWh/m^3	Flux and SHC are obtained with tap water as the feed water and a steam raiser water temperature ranging from 75 to 80°C	(memsys, 2015)
Aquaver	Vacuum multi-effect MD	8.5 $l/m^2/h$	180 kWh/m^3	The operating conditions at which the flux and SHC values are obtained are not indicated	(Aquaver, 2015)
MEMSTILL/ Keppel Seghers	Multi-Stage AGMD	2.5-3 $l/m^2/h$ reported for 2 pilot MEMSYS plants in the Netherlands	SHC as low as 55.5 kWh/m^3 reported for a MEMSYS pilot plant in Singapore[70]	The 2 plants in the Netherlands desalinated BW while that in Singapore desalinated SW. Other operating conditions at which the flux and SHC values are obtained are not indicated.	(Dotremont et al., 2010, Jansen et al., 2010, Tarnacki et al., 2012)

[69] Yun et al. (2006) observed that the sharp decline in the flux occurred near saturation (NaCl concentration of 260 g/l) due to the effect of concentration polarization where the NaCl solution was already saturated at the membrane surface

[70] SHC values as low as 22 kWh/m^3 were also reported for the MEMSTILL module on the expense of using more modules (Jansen et al., 2010), however such low SHC was not obtained with real test data (Cipollina et al., 2012). A SHC value of approximately 278 kWh/m^3 and 550 278 kWh/m^3 was also reported for the same plant in Dotremont et al. (2010) and Nijskens et al., (2011), cited in (Cipollina et al., 2012), respectively

Criscuoli and Drioli (1999) also investigated the feasibility of integrating an SW RO plant (39 g/l feed water salinity) with an MD process for a large scale plant (approximately 24,000 m^3/d[71]) to enhance the RR. The hybrid RO/MD plant performance in their study was based on the study of Drioli et al. (1999) where the RR increased from 40% for the RO only plant to approximately 86% for the hybrid plant. The additionally required thermal energy to drive the MD process increased the specific energy consumption (heat and electricity) from 4.85 kWh/m^3 for the RO only plant to 15 kWh/m^3 for the hybrid plant. The study also concluded that the hybrid plant would be ideal when waste heat is available from another process to drive the MD process. However, based on the data reported in their study, the MD plant SHC was estimated to be approximately 13 kWh/m^3 for a feed water with an average[72] salinity of approximately 175 g/l, which seems to be a highly underestimated value for the following reasons:

1- As discussed above, the analysis in their study was based on the performance of the lab scale MD module discussed in Drioli et al. (1999). While the SHC of a lab scale module is expected to be higher than that of a full scale module because the larger the area of the membrane the lower is the SHC similar to heat exchangers (Cheng et al., 2008, Winter et al., 2011), it can be clearly observed from *Table 2-7* that the lowest SHC obtained from commercial full scale modules is much higher than the 13 kWh/m^3 value calculated from Criscuoli and Drioli (1999). That in addition that the values shown in *Table 2-7* are for either tap water or seawater, while the average feed water salinity in Criscuoli and Drioli (1999) was approximately 175 g/l which should further increase the SHC.
2- The latent heat of the condensed vapour in the MD process was not recovered in Criscuoli and Drioli (1999) study which is expected to significantly increase the SHC.

Drioli et al. (2006) and Macedonio et al. (2007) investigated the combination of an MD, as well as an MCr process[73] to recover the salts, with an RO and an Nano-Filtartion

[71] Assuming 24 hours operation
[72] The average salinity between the MD feed and concentrate salinities
[73] The MCr process consists of an MD process combined with a crystallization tank[73] (Curcio et al., 2001, Tun et al., 2005)

(NF)[74] processes[75] in a large scale plant. Both studies showed that the unit water costs of the hybrid plant become more competitive when waste heat is available to drive the MD and the MCr processes. However, similar to the study by Criscuoli and Drioli (1999), the SHC of the MD was also underestimated compared to current commercial MD modules with a value of approximately 45.5 kWh/m^3. Moreover, both studies based their analysis on the MD plant performance reported in Drioli et al. (1999), which is questionable given that the MD plant in both studies operated at a feed water temperature of 50°C compared to 35°C in the latter. It should be also noted that the higher feed water temperature used in Drioli et al. (2006) and Macedonio et al. (2007) with the same flux values obtained in Drioli et al. (1999) explains the higher SHC than the value estimated from Criscuoli and Drioli (1999). Finally, it is worth mentioning that while both studies concluded that the annual profit from selling the salts recovered from the MCr process in a hybrid plant using NF, RO, MD and MCr, offset its life cycle costs[76], the underestimated SHC, the likely overestimated flux, and the low specific cost assigned to the MD modules[77], are expected to significantly increase the LCC of the MD plant and therefore likely to result in a positive life cycle unit water costs.

Martinetti et al. (2009) considered the effect of scaling on the maximum attainable RR for a hybrid RO/MD plant which was not considered in any of the previously reviewed studies. In particular, Martinetti et al. (2009) investigated the use of a vacuum enhanced DCMD process, where the cooling water flows under vacuum conditions, to treat the brine from a brackish GW RO desalination plant. The experiments conducted with actual BW and using a bench scale MD unit, showed that, as expected, the presence of silica and calcium sulphate was a major RR limiting factor that caused a sharp decline in MD fluxes due to scale formation on the membrane surface that clogged its pores. Nevertheless, the study showed that an overall RR of up to 98% can be obtained from the hybrid plant after proper pre-treatment of the RO brine.

---

[74] NF membranes are similar to RO membranes but have larger pores which increases their permeate flux and RR compared to RO membranes operating at the same pressure; and therefore have lower SEC but on the expense of water quality

[75] The MD process was used to treat the brine of the NF process where the latter was used to pre-treat the feed water before going to the RO plant. The MCr process was used to treat the brine of the RO process

[76] i.e. negative life cycle unit water costs

[77] For example, the MD membrane specific cost in Drioli et al. (2006) and Macedonio et al. (2007) was 4 times lower than the full scale commercial MD module discussed in Winter et al. (2011)

Other studies, such as Karakulski et al. (2002) and Macedonio and Drioli (2008), considered using the MD process for RO permeate polishing. Macedonio and Drioli (2008) specifically investigated the use of the MD process to improve the rejection of Boron and Arsenic which otherwise have negative impact on crops and potentially human health, especially Arsenic. The study verified through experimental work that because the MD is a phase change process, the permeate flow was completely free from Arsenic and Boron. Macedonio and Drioli (2008) concluded that in this case, only a fraction of the RO permeate would need to be treated by the MD process to obtain Arsenic and Boron content that is within the World Health Organization (WHO) guidelines instead of using a second RO stage to treat the entire permeate of the first RO stage.

Based on the review carried out in this section, it is observed that all feasibility studies in the literature carried out on hybrid RO/MD plants were based on the fluxes reported in Drioli et al. (1999). The fluxes reported in Drioli et al. (1999) were obtained from a laboratory scale MD module and therefore may not be achieved with full scale modules under the same operating conditions. Moreover, Drioli et al. (1999) reported high flux values at feed water salinities near saturation which are likely to be unsustainable due to the effect of scaling. Furthermore, it was shown that in all studies where the economic feasibility of the hybrid plant was investigated, the SHC of MD plant was significantly underestimated. It was also shown that these studies ignored the effect of the operating conditions on the MD process performance where the same flux values reported in Drioli et al. (1999) were used with a different feed water temperature which raises questions on the accuracy of these analyses.

On top of that, most studies on hybrid RO/MD plants were used with SW applications except that of Martinetti et al. (2009) which investigated the use a hybrid plant with BW. However, the latter only focused on investigating the limiting effect of scaling on the RR, but neither carried out a cost analysis nor discussed the energy performance of the MD process.

For the aforementioned reasons, it has been concluded that the existing feasibility studies on hybrid RO/PMD plants are not reliable and a new feasibility study based on the more realistic performance of a full scale commercial MD module is required, which will be carried out in this thesis. The hybrid RO/MD plant will be also designed to operate with solar energy which, to the author's knowledge, has not been investigated in the literature. Finally, similar to the work of Martinetti et al. (2009), the effect of scaling on the maximum attainable RR of a hybrid RO/MD plant will be also considered as it was not considered in any of the studies concerned with investigating the techno-economic feasibility of hybrid RO/MD plants.

2.5.4 MD process modelling

In the previous section it was concluded that a new feasibility study on hybrid RO/MD plants based on the performance of a full scale commercial module will be carried out in this thesis.

The MD plant performance will be particularly based on the spiral wound PGMD module developed by the Fraunhofer Institute for Solar Energy Systems (ISE) and manufactured by SolarSpring[78]. While there are other available commercial full scale MD modules (*Table 2-7*), this particular module was selected due to the availability of experimental data in the literature that can be used in modelling validation as well as having access to more detailed information on the module geometry and dimensions from the Fraunhofer ISE solar desalination team.

Permeate gap MD is a special configuration of DCMD (Khayet and Matsuura, 2011a) where, similar to the latter, the permeate channel is in direct contact with the membrane surface. However, in PGMD the water vapour condenses in a separate channel from the cooling channel[79] similar to the AGMD configuration but without the extra air gap. Accordingly, this configuration allows for internal heat recovery by using the feed flow as the cooling fluid to recuperate the latent heat from the permeate channel hence increasing the thermal efficiency of the process without an additional mass transfer resistance from the air molecules[80].

However, due to the lack of commercial simulation tools for the MD process, a mathematical model is required to simulate the performance of the MD module at different operating conditions.

[78] http://www.solarspring.de/
[79] A condenser foil is added to separate the permeate and the cooling channels
[80] Mass transfer in an MD process is discussed in more details in Chapter 6

Numerous studies[81] on MD modelling are found in the literature. In all of the modelling studies a mathematical model is discussed and usually validated through experimental data. The modelling studies have, however, different emphasises and could be classified as follows: studies concerned about mass transfer in an MD process investigating the mechanism by which mass transfer occurs through experimental work then developing semi-empirical or theoretical equations, or assessing the validity of existing theoretical equations to predict the MD mass transfer coefficient (MTC) and/or the flux, for example (Kimura et al., 1987, Schofield et al., 1987, Schofield et al., 1990a, Ding et al., 2003, Martínez et al., 2002, Fernández-Pineda et al., 2002, Imdakm and Matsuura, 2004, Srisurichan et al., 2006); studies with an emphasis on the heat transfer in an MD process investigating the suitability of existing semi-empirical equations from the literature, that are initially developed for heat exchangers, to estimate the convective heat transfer coefficient through the boundary layers in the MD channels by comparing the predicted MD flux values from the model to that obtained experimentally, for example (Gryta et al., 1997, Gryta and Tomaszewska, 1998, Phattaranawik et al., 2003, Qtaishat et al., 2008); and studies using existing semi-empirical equations to estimate the convective heat transfer coefficient, and existing theoretical or semi-empirical equations to estimate the MD MTC to build a mathematical model and validate it through experimental work where the model is either used for optimization work, to perform a parametric study, or simply to build a model to predict the MD process flux at different operating conditions that those tested experimentally, for example (Fane et al., 1987, Gostoli and Sarti, 1989, Schofield et al., 1990b, Martínez-Díez and Vázquez-Gonzàlez, 1999, Banat and Simandl, 1998, Martínez-Díez and Florido-Díaz, 2001, Yun et al., 2006).

From the review carried out, it was observed that all of the available models in the literature were based on laboratory scale MD modules and mostly using flat sheet membranes (*Table 2-8*). Accordingly, in almost all of the reviewed studies a simple model using the average bulk water temperatures of the evaporator and cooling channels

[81] It should be noted that the review carried out on MD modelling studies mainly focused on studies using AGMD and DCMD module configurations due to their resemblance to that of PGMD as the pressure gradient, the main driving force, is maintained by a temperature difference between the evaporator and the cooling channels which is further discussed in Chapter 6.

was typically used to calculate the flux given the short length of the channel/membrane. In contrast, in a spiral wound full scale (e.g. area=10 m^2) module, a finite element series analysis, such as that carried out by Fane et al. (1987) and Cheng et al.(2008) for a hollow fibre DCMD module, is necessary to predict the module performance given the large length of the channel which in the module modelled in this study is 7 m.

Table 2-8: Different module configurations and membrane types modelled in the literature

Reference	Module Configuration	Membrane Type	Membrane Scale/Area	Channel/ Fibre Length
(Kimura et al., 1987)	AGMD	Flat Sheet	Lab scale/100 cm^2	15 cm
(Fane et al., 1987)	DCMD	Hollow Fibre	Lab scale/1 m^2	40 cm
(Gostoli and Sarti, 1989)	AGMD	Flat Sheet	Lab Scale/-	-
(Kurokawa et al., 1990)	AGMD	Flat Sheet	Lab Scale/142 cm^2	24 cm
(Schofield et al., 1990b)	DCMD	Flat Sheet	Lab scale/28 cm^2	11.4 cm
(Gryta et al., 1997)	DCMD	Flat Sheet	Lab scale/28 cm^2	66 cm
(Banat and Simandl, 1998)	AGMD	Flat Sheet	Lab scale/160 cm^2	21.5 cm
(Gryta and Tomaszewska, 1998)	DCMD	Capillary	Lab Scale/-	-
(Martínez-Díez and Vázquez-Gonzàlez, 1999)	DCMD	Flat Sheet	Lab scale/33.7 cm^2	5.5 cm
(Martínez-Díez and Florido-Díaz, 2001)	DCMD	Flat Sheet	Lab scale	5.5 cm
(Fernández-Pineda et al., 2002)	DCMD	Flat Sheet	Lab scale/260 cm^2	17.7 cm
(Ding et al., 2003)	DCMD	Flat Sheet	Lab scale/40 cm^2	-
(Srisurichan et al., 2006)	DCMD	Flat Sheet	Lab scale/47 cm^2	-
(Yun et al., 2006)	DCMD	Flat Sheet	Lab scale/40 cm^2	10 cm
(Qtaishat et al., 2008)	DCMD	Flat Sheet	Lab scale/236 cm^2	8 cm (maximum value)

While Koschikowski (2011) modelled the full scale PGMD module developed by the Fraunhofer ISE, the author assumed a simplified flat geometry for the spiral wound module (J. Koschikowski 2015, pers. Comm., 16 Jan.). In this thesis, however, the model will account for the spiral wound geometry of the module considering the complex heat transfer interactions between the different membrane layers. This is in contrast with flat sheet geometries where there is only one membrane layer which greatly simplifies the models discussed in the literature including those carried out for lab scale modules.

2.5.5 PVT driven RO plants

Increasing the feed water temperature increases the RO permeate flux (Porteous, 1984) due to the reduction in the water viscosity hence the water molecules can flow more easily through the membrane (Kucera, 2010b). For example, according to Al-Karaghouli et al. (2010) preheating the feed water could increase the permeate flux by 20 to 30%. As the aforementioned increase in permeate flux occurs at the same feed pressure, the SEC is reduced. Accordingly, heating the feed water could potentially reduce energy related costs. Moreover, Thomson and Infield (2003a) showed, through simulation work, that an RO system with feed water preheated from 15 to 35°C by a solar water heater could increase the permeate flux by 60% and concluded that the extra costs of equipment to preheat the water could be justified. It should be noted, however, that Thomson and Infield (2003a) neither discussed the methodology used in their model nor gave detailed results of the model.

For this reason, the economic feasibility of pre-heating the feed water through PVT systems to decrease the RO process’s SEC will be examined in this thesis. The annual performance of coupling both glazed and unglazed PVT collectors with RO plants is also considered. While the concept of preheating the feed water to reduce the RO energy requirements is already exploited, to the author’s knowledge, no studies using PVT with RO plants could be found in the literature.

2.5.6 Brackish GW potential in Egypt

In Chapter 1, it was concluded that GW extraction will be more suitable to establish decentralized communities in Egypt. Brackish GW extraction and desalination was particularly suggested as Egypt could potentially have more brackish GW accessibility and reserves than fresh GW.

Accordingly, in this thesis, GW properties in the seven main hydro-geological systems across six regions in Egypt are investigated to identify aquifers with access to brackish GW. These aquifers are then investigated for their potential for sustainable development. A similar work was carried out by Salim (2011) to assess the site appropriateness for solar driven brackish GW extraction in Egypt considering factors such as GW depth, GW salinity, distance from the Nile valley and delta and solar resources. The study carried out in this thesis extends on that of Salim (2011) with a greater focus on the potential of sustainable extraction of brackish GW in terms of productivity and renewability.

2.6 Summary and Conclusion

In this chapter, different desalination processes were reviewed and compared. It was concluded that PV driven RO desalination plants are the most suitable for small scale applications in rural areas in Egypt. Membrane distillation driven by FPC's was also proposed to be combined with the RO process to increase the overall RR.

Different work carried out on BW PV-RO plants and the application of such plants in Egypt, hybrid RO/MD plants, and MD process modelling, was reviewed. It was shown that existing economic feasibility studies on solar driven RO plants in Egypt were unreliable and considered narrow operating conditions. Moreover, it was shown that most PV-RO plants in the literature are not operating within their optimal window and were mostly operating at low RR. Furthermore, the existing feasibility studies on hybrid RO/MD plants are unreliable and based on laboratory scale membranes and therefore new feasibility studies based on the more realistic performance of a full scale commercial MD module is required.

Accordingly, in this thesis the feasibility of PV-RO plants for a wide range of brackish GW salinities is examined. The plants will be designed to operate at the maximum attainable RR to decrease the amount of wasted GW. The designs will be also carried out according to the manufacturer's recommended specifications to give more realistic results. The feasibility of the PV-RO plant will be also investigated for two cases: a case where the RO plant operates only during day time such that the PV system costs are minimized; and a case where the RO plant is operating for 24 hours to increase its capacity factor.

Investigating the use of FPC driven MD to increase the RR of the PV-RO system will be investigated using full scale commercial MD membranes considering the effect of scaling to guarantee more realistic results. Finally, the economic feasibility of using PVT to preheat the feed water going to the RO system to reduce the latter's energy consumption will be also investigate.

3. Brackish Groundwater Potential in Egypt

In Chapter 1, it was shown that GW extraction could help establishing decentralized agricultural communities in areas away from the Nile valley and delta in Egypt. Brackish GW extraction in particular was suggested as Egypt could potentially have more brackish GW accessibility and reserves than fresh GW. Therefore, in this chapter the potential for brackish GW to be the main water resource for the proposed decentralized communities is assessed.

Firstly, the seven main hydro-geological systems across six regions in Egypt are reviewed in terms of their GW properties, productivity and the amount of surface recharge. Secondly, the methodology used in classifying the brackish GW aquifers based on their potential for sustainable water extraction is presented. Locations with the highest priority for establishing decentralized agricultural communities based on brackish GW extraction and desalination are then identified. Finally, the suitability of BW for drinking and agricultural use is assessed.

3.1 Salinity Definition

The term salinity used in this thesis needs to be clarified to avoid any ambiguity. There are several definitions of water salinity discussed in Pawlowicz and Feistel (2012). First, there is the solution salinity which is the summation of the measured dissolved constituents in the water and is usually estimated by only summing the major anions and cations in addition to nitrate and silica. There is also the ionic salinity which is similar to the solution salinity but only sums the ions in the water. The water salinity is also estimated through electro-conductivity (EC) measurements which only accounts for the ionic content in the water. Finally, the total dissolved solids (TDS) is an American term (Hömig, 1978) often used in the literature to indicate the water salinity and is similar to the solution salinity accounting for both the dissolved inorganic and organic constituents in the water (WHO, 2011). The TDS is usually estimated by measuring the

EC of the water then multiplying it by an empirical factor based on the chemical composition of water.

Therefore, in this study the TDS is used when available and is referred to directly as the water salinity. Otherwise when only the GW chemical composition is available, the solution salinity is estimated by adding the concentrations of major ions in addition to nitrate and silica if included in the analysis. The solution salinity is assumed to be equal to the TDS and will be also referred to as the water salinity. When EC's are reported, the general conversion factors indicated by the Food and Agriculture Organization (FAO) (Rhoades et al., 1992) are used to convert the value to TDS.

3.2 Targeted Water for Treatment

Brackish water, defined as water with salinities exceeding 1,000 mg/l (Carter et al., 2005, Water Quality Association, 2012), is according to the WHO guidelines (WHO, 2011) not suitable for drinking, mainly due to taste considerations[82].

Conversely, the suitability of water for agriculture purposes depends on its salinity and specific elements concentrations in addition to the type of crops and animal species (Ayers and Westcot, 1994)[83]. In this study, the suitability of brackish GW for irrigation and livestock use is therefore investigated, based on the FAO guidelines (Ayers and Westcot, 1994)[84], in locations where GW chemical analyses are available in the literature to determine if desalination is required. The suitability of water for irrigation will be particularly investigated for HVLWC crops that are recommended to be grown in Egypt by El-Sherif (1997), Abdin and Gaafar (2009), Gad and Ramadan Ali (2009), the International Fund for Agricultural Development (2008, 2009), and Fahim et al. (2011). While cotton is a water intensive crop (Gad and Ramadan Ali, 2009), it is also

[82] According to the WHO guidelines, water with salinities exceeding 1,000 mg/l, though may not necessarily affect human health as long as specific chemical substance do not exceed the guideline limits, becomes increasingly unacceptable for drinking.
[83] Appendix D

suggested to be cultivated as it one of Egypt's traditional crops most important export crops[85] (El-Sherif, 1997).

3.3 Review of Groundwater in Egypt

Groundwater in Egypt is found in seven main hydro-geological systems: the Nubian sandstone aquifer, the fissured carbonate aquifer, the basement fissured hard rock aquifer, the Al-Moghra aquifer and the Quaternary aquifer which includes the Nile basin aquifer, the alluvial deposits aquifers and most of the coastal aquifers. *Figure 3-1* shows the main aquifers in Egypt and is based on the hydro-geological map from the Research Institute for Groundwater (RIGW) (1988) in addition to the studies by Gheith and Sultan (2002) and Sultan et al. (2008) which were used to identify the alluvial deposits Quaternary aquifer in the main wadis[86] in the Eastern Desert.

Brackish water is defined by the U.S Geological Survey Organization (Carter et al., 2005) and the Water Quality Association (2012) as those with salinities ranging from 1,000 to 10,000 mg/l and 1,000 to 15,000 mg/l respectively. In this study, the definition by the U.S Geological Survey Organization is used especially that most salinity maps in the literature do not indicate the 15,000 mg/l iso-salinity line.

Aquifer productivity and the amount of surface recharge were mainly based on the qualitative data compiled by RIGW (1988). The data was complemented by more recent quantitative and qualitative data available in literature. To relate quantitative and qualitative data, qualitative descriptions are compared to available well productivities and rainfall recharge estimates reported in the literature for the same region to get a rough estimate on the equivalent range related to each description. For example, well yields less than 5 m^3/h are reported in areas described to have low productivity while areas described to highly productive have well yields with average values exceeding 150 m^3/h, accordingly quantitative values could be roughly assigned to each description.

[85] Cotton is also a drought resistant and a salt tolerant crop which makes it ideal for areas away from the Nile valley and delta where brackish GW is used.
[86] Drainage Basins

3.3.1 Nubian sandstone aquifer

The Nubian sandstone aquifer is the most important source of GW in areas away from the Nile valley and delta (Hefny and Shata, 2004) and stretches over the Western Desert, Eastern Desert and the Sinai Peninsula and also to neighbouring Libya, Chad, Saudi Arabia and the Republic of Sudan. Groundwater reserves in the Nubian aquifer in Egypt are estimated to be at least 200,000 bcm and are mainly non-renewable. However, as the GW in the Nubian aquifer is shared with other countries, there could be a limit imposed on the amount of GW that could be annually extracted by each country.(Shata, 1982, Hefny et al., 1992, Hassan et al., 2004)

In the Western Desert, the Nubian aquifer stretches over the entire desert and is mainly unconfined south of 25° latitude where the aquifer outcrops, then it becomes confined northward where it is overlain by the fissured carbonate aquifer (*Figure 3-1*) (Nour, 1996, Sultan et al., 2007). According to Shata (1982) and Nour and Khattab (1998), the Nubian aquifer contains brackish GW (1,000 to 10,000 mg/l) within a narrow belt stretching along the Al-Qattara depression north of latitude 29° then southward along the Nile River western bank. In the north of the Al-Qattara Depression and El-Minya city, GW becomes saline and hyper saline. South of latitude 29°, the Nubian GW is fresh (<1,000 mg/l) and is mainly exploited from the New Valley oases (Hefny et al., 1992). Shata (1982) and Nour and Khattab (1998) also show that the Nubian aquifer is a deep aquifer system where well depths in the oases area range from 250 to 1,000 m below ground level (BGL) while at the Al-Qattara depression area, the GW is found at even larger depths that could exceed 2 km. However, as the aquifer is mainly confined, GW in most wells is flowing above ground level while in the unconfined area the depth to water table in the BW zone ranges from 30 to 110[87] m BGL. The Nubian aquifer in the Western Desert is a highly productive aquifer with reported average well yields exceeding 150 m^3/h in the oases area (Nour and Khattab, 1998) and therefore, assuming similar aquifer properties as the fresh GW zone, the brackish GW zone is likely to be as highly productive. Moreover, the aquifer has a high development potential where for example in the New Valley oases, one of the most important sites from which GW is extracted, approximately half of the estimated amount that could be economically

[87] Actual depth data are with respect to mean sea level therefore the depths with respect to ground level were approximately estimated based on ground elevation.

exploited was reported to be extracted (Hefny and Shata, 2004) while the brackish GW zone is likely to be unexploited as no wells in this zone were reported in the literature.

In the Eastern Desert, the Nubian aquifer outcrops in the southern parts but further north near Qena city the aquifer is overlain by the fissured carbonate aquifer (*Figure 3-1*). While the aquifer is mainly non-renewable, it receives some recharge by occasional infiltrating rainfall particularly where the aquifer outcrops (Abdel-Moneim, 2005). The Nubian aquifer in the Eastern Desert mainly contains BW (1,000 to 10,000 mg/l) (Hefny et al., 1992) except north of El-Minya city where the GW is mainly saline based on the aquifer's fresh /saline GW boundary line shown in Sultan et al. (2007). The depth to water table was only reported in the main wadis north of Aswan city where the aquifer is confined and it ranges from 20 to 50 m BGL while the depth to top aquifer is only reported in Qena area and ranges from 100 to 250 m BGL (Hefny and Shata, 2004). However, based on schematic cross sectional maps and well depth data from Sultan et al. (2000, 2007), the depth to the top of the Nubian aquifer is likely to exceed 1 km BGL north of Qena city except near the areas where the aquifer outcrops. Regarding the aquifer's productivity, while the Nubian aquifer in the Eastern Desert is described by RIGW (1988) to be moderately to highly productive similar to its counterpart in the Western Desert, test wells in wadi Qena and wadi Hammamat have well yields ranging from 2.7 to 83 m^3/h (Idris and Nour, 1990) which are much lower than those in the Western Desert. The Nubian aquifer in the Eastern Desert in general is likely to have lower GW reserves than in the Western Desert. For example in the East Oweinat area located south of the Western Desert and occupying an area of 16,000 km^2 (Nour and Khattab, 1998), it is estimated that an amount of 2.35 bcm per year could be economically extracted from the Nubian aquifer compared to less[88] than 0.07 bcm/year from wadi Qena and wadi Hammamat in the Eastern Desert (Hefny and Shata, 2004) which stretch over a larger area of about 23,500 km^2 (Gheith and Sultan, 2002). Nevertheless, the Nubian aquifer in the Eastern Desert has high development potential given that the absolute maximum GW that could be extracted from the Nubian aquifer

[88] 0.07 bcm/year is the maximum recharge rate for the Nubian aquifer which if extracted will lead to a drop in GW levels beyond economical limits therefore the amount that could be economically extracted is expected to be lower

underlying main wadis north of Aswan city is estimated to be 0.21[89] bcm/year while GW extracted from the whole Eastern Desert including the coastal aquifer was reported to be only 0.05 bcm/year (Hefny and Shata, 2004).

The Nubian aquifer also covers the Sinai Peninsula stretching from the southern parts of the peninsula, north of the outcropping basement fissured hard rock aquifer, to the northern parts at the Gabal-El- Maghara and Gabal-El-Halal zones (Abd-El-Rahman, 2001) located near the towns of Gifgaga and El-Quseima (*Figure 3-1*). The aquifer is recharged by infiltrating rainwater especially in the south where the aquifer outcrops (Abd-El-Samie and Sadek, 2001), however the recharge amount is small estimated to be about 33 million m^3/year (Nour and Khattab, 1998). The following data on the GW properties have been obtained from RIGW (1988), Mills and Shata (1989), and Nour and Khattab (1998). The Nubian aquifer's GW in the Sinai Peninsula is mainly brackish except in the south where the sandstone aquifer outcrops the GW is fresh (< 1,000 mg/l). The GW salinity then increases gradually northward to values exceeding 10,000 mg/l north of Gifgafa and also westward along the Suez Gulf coast where the GW is mainly saline or hyper saline with salinities as high as 220,000 mg/l (except the Ayun-Musa area where the GW is brackish). Groundwater in the Nubian aquifer in the Sinai Peninsula is found at large depths where the depth to top aquifer ranges from 500 to 1,100 m BGL and the depth to water table ranges from 100 to 400 m BGL (except for Ayun-Musa where the water flows above ground level). The Nubian aquifer in the Sinai Peninsula is not as productive as its counterpart in the Western Desert with reported well yields ranging from 20 to 80 m^3/h. Nevertheless, the aquifer has large GW reserves with an estimated amount of 1,100 bcm out of which at least 117 bcm is available for extraction (Hefny and Shata, 2004). Moreover, the aquifer has the highest development potential compared to other aquifers in the Sinai Peninsula (Nour and Khattab, 1998).

3.3.2 Fissured carbonate aquifer

The fissured carbonate aquifer covers almost half of Egypt's area (Hefny et al., 1992) and stretches over the central and northern parts of the Eastern Desert, Western Desert and the Sinai Peninsula (*Figure 3-1*). The aquifer is recharged by leaked water from the underlying Nubian aquifer through deep fractures and fissures in addition to occasional

[89] The maximum recharge rate for the Nubian aquifer which if extracted will lead to a drop in GW levels beyond economical limits

surface recharge from flash floods mainly occurring in the Eastern Desert and the Sinai Peninsula. However, the aquifer is composed of massive impervious rocks with low infiltration capacity reducing the aquifer's recharge potential except in areas that are highly fractured allowing water to percolate and recharge the aquifer (Shata, 1982, Gheith and Sultan, 2002, Abdel-Moneim, 2005). While RIGW (1988) described the fissured carbonate aquifer all over Egypt to have moderate productivities, wells tapping the aquifer in most areas were reported to have low productivities. Allam et al. (2003) also indicated that low amounts of GW reserves could be exploited from the carbonate aquifer, especially when compared to the large area covered by the aquifer. The aquifer is, however, not well studied (Nour and Khattab, 1998, Hefny and Shata, 2004) and little data on its GW potential and other GW properties were found in literature.

In the Western Desert, the fissured carbonate aquifer's water bearing horizons are the Upper Cretaceous and Eocene formation in addition to the Middle Miocene formation in the northern parts of the Western Desert (RIGW, 1988). Data on GW properties in the fissured carbonate aquifer were mainly reported in Nour and Khattab (1998). Brackish GW exists in the Upper Cretaceous and Eocene aquifers in the Al-Qattara depression area with salinities ranging from 2,000 to 5,000 mg/l and reaching up to 10,000 mg/l northeast near the Mediterranean coast. The entire Middle Miocene aquifer contains BW with salinities ranging from 1,600 to 2,800 mg/l in the Siwa oasis area then increasing further north reaching 10,000 mg/l near the Mediterranean coast. No data about GW depths were found in literature except for the Middle Miocene aquifer in the Siwa depression area where GW is found at relatively shallow depths ranging from 20 to 150 m BGL with mostly flowing GW above ground level. The Upper Cretaceous and Eocene aquifers have low well yields, i.e. <5 m^3/h, while the Middle Miocene aquifer have higher yields ranging from 10 to 35 m^3/h in the Siwa depression area. It is not clear however whether other areas in the Middle Miocene aquifer have similar moderate productivities to that of the Siwa depression area or low productivities as the Upper Cretaceous and Eocene aquifers, and no data were found in literature on other wells tapping the aquifer in other locations.

Figure 3-1: Hydro-geological map of Egypt

Base map of Egypt modified after: © 2007 World Trade Press All Rights Reserved

In the Eastern Desert, scarce data were found on the fissured carbonate aquifer. The GW salinities range from 1,000 to 9,000 mg/l but could reach 12,000 mg/l in some areas such as Wadi-Araba[90]. Groundwater in the fissured carbonate aquifer in the Eastern Desert is reported to be accessed in different locations at ground surface either from springs or flowing artesian wells and the depth to top aquifer is generally shallow with values up to 100 m BGL reported in the Wadi-Araba area. Springs tapping the aquifer are also reported to have limited productivities. (Hefny et al., 1992, Abdel-Moneim, 2005)

In the Sinai Peninsula, the fissured carbonate aquifer consists of the Upper Cretaceous and Eocene aquifers and their GW properties are reported in Mills and Shata (1989) and Nour and Khattab (1998). Groundwater in both aquifers is mainly brackish where the average salinity in the Eocene aquifer is estimated to be about 5,150 mg/l while the Upper Cretaceous aquifer has lower average salinity of about 2,750 mg/l. Saline and hyper saline GW is also reported in the Eocene aquifer in the area between Ras-Sudr and Hammam-Faraon, and the area north of Al-Quseima. No data were found in literature regarding GW depths in the Eocene aquifer while few wells tapping the Upper Cretaceous aquifer in different parts of the Sinai Peninsula have drilling depth and depth to water table ranging from 189 to 980 m BGL and 21 to 220 m BGL respectively. The Upper Cretaceous aquifer has one of the lowest productivities compared to other aquifers in the Sinai Peninsula and is considered as an aquifer with very poor productivity hence not recommended for future exploitation. Conversely, the Eocene aquifer is reported to have a moderate productivity with values close to that of the Nubian aquifer in this area. However there is an uncertainty about the Eocene aquifer’s productivity as scarce data were found in the literature on wells tapping this aquifer.

3.3.3 Quaternary aquifer

The Quaternary aquifer is divided into several hydro-geological systems that are different in lithology, recharge resources and productivity (RIGW, 1988). The Quaternary aquifer includes the Nile basin aquifer and the alluvial deposits aquifer which mainly exists in the Eastern Desert and the Sinai Peninsula. The Quaternary aquifer is also part of the Red Sea and Suez gulf coastal aquifers which are discussed separately.

---

[90] South of Ain-Sokhna

3.3.3.1 Nile basin aquifer

The Nile basin aquifer covers all the area along the Nile River basin underlying the cultivated lands (Idris and Nour, 1990). The aquifer mainly consists of the Quaternary Pleistocene epoch sand and gravel aquifer. The Pleistocene aquifer is overlain by a silt and clay cap belonging to the Holocene epoch which acts as a semi confining layer. The silt and clay cap disappears in the desert fringes where the aquifer becomes unconfined (Idris and Nour, 1990, Abdalla et al., 2009). The Nile basin aquifer is continuously recharged by water leaking from irrigation canals and drains as well as water leaching from excess irrigation water (Idris and Nour, 1990). Therefore, the aquifer is a renewable source of GW and is considered by RIGW (1988) as the most productive aquifer in Egypt except in the northern areas where the large thickness of the impervious clay lenses reduces the aquifer's productivity. Infiltrating rainfall also recharges the aquifer in the Nile Delta area mainly in the unconfined zone particularly in winter where rainfall ranges from 25 mm in the south to 200 mm per year in the north near the Mediterranean Sea (Geirnaert and Laeven, 1992). The aquifer is separated into the Nile Delta aquifer and the Nile Valley aquifer as the thickness of the Nile basin aquifer decreases from south to north near Cairo where it becomes very thin, then increases again further north, forming the Nile Delta aquifer (Hefny et al., 1992).

The Nile Valley aquifer stretches in the vicinity of the Nile River from Cairo in the north to Aswan southward (*Figure 3-1)*. Its GW is mainly fresh with an average salinity of 800 mg/l (Hefny et al., 1992) although brackish GW might be found at the fringes of the Nile valley where some wells analysed by Abdalla et al. (2009) in Qena area have GW salinities with values up to 3,000 mg/l. The fresh GW zone in the Nile basin aquifer is, however, polluted and will require treatment to be suitable for drinking. According to Abdel-Lah and Shamrukh (2001), Abdalla et al. (2009), Abdel-Latif and El-Kashouty (2010) and Ahmed and Ali (2011), *e.coli* bacteria and high levels of nitrate and iron were detected in many wells due to leaking sewage systems and septic tanks, mainly used in rural areas, and the excessive use of fertilizers.

The Nile Delta aquifer stretches east to the Suez Canal, north to the Mediterranean Sea and south to Cairo. Westward, the aquifer is bordered by the Al-Moghra and the fissured carbonate aquifers. Its GW is fresh in the southern and central parts of the delta but the GW salinity increases eastward and northward to become brackish and saline due to salt water intrusion from the Mediterranean Sea and the northern saline lakes. Groundwater salinity also increases westward due to its contact with the Al-Moghra aquifer (Hefny et al., 1992, Sharaky et al., 2007). The area containing brackish GW was identified based on the study by Sherif et al. (2012). The GW salinity maps in the study, which were based on simulation work and field observations, included the variation of salinity within a depth ranging from zero to 400 m below mean sea level. However, only the data for depths of zero and 100 m below mean sea level is included as this is where brackish GW mainly exists. It should be noted that in the transition areas between fresh/brackish and brackish/saline GW, fresh and brackish GW respectively might be only found at very shallow depths and within a very thin zone in the range of few meters and therefore the available GW quantities could be small. The GW salinity data were complemented from the iso-salinity map by Geirnaert and Laeven (1992) for the western fringes although the study did not consider the variation of salinity with depth. However, the fresh/brackish and the brackish/saline iso-salinity boundary lines agree well with those of Sherif et al. (2012) for the rest of the Nile Delta aquifer. It should be noted that while the study by Sherif et al. (2012) showed that all of the northern parts of the Nile Delta aquifer contains saline water, a study by Ebraheem et al. (1997) to determine the fresh/brackish/saline zone location and thickness showed that brackish GW also exists in the middle part of the northern delta but with a small thickness of about 60 m and is underlain by saline GW. Hefny and Shata (2004) also mentioned the presence of brackish GW in the northern delta at depths less than 100 m. However, based on field observations it is likely that only small volumes of brackish, as well as fresh, GW exist in this area (M. Sherif, 2013, pers. comm., 28 Nov.); accordingly it is concluded that the whole northern delta contains saline water. The study by Ebraheem et al. (1997) also showed that a thin zone, around 20 m in thickness, of brackish GW overlies the fresh GW zone in the middle area south of the 1,000 mg/l iso-salinity line, whose presence is attributed to salt leaching from irrigation water return. Regarding GW depths, the depth to top aquifer in the confined area of the Nile Delta aquifer is very shallow ranging from zero to 30 m BGL and the depth to water table ranges from zero (flowing wells) to few meters (<5 m) (RIGW, 1988, Dawoud et al., 2005, Sherif et al., 2012). In the unconfined areas in the western delta, the depth to water table and well depths are also shallow ranging from 35 to 60 m BGL and 40 to 80 m BGL respectively (Sharaky et al., 2007).

3.3.3.2 Quaternary alluvial deposits aquifer

The Quaternary alluvial deposits aquifer mainly covers wadi floors in the Eastern Desert and the Sinai Peninsula. The aquifer is renewable and has a high storage capacity and infiltration rates which increases its surface recharge potential (Gheith and Sultan, 2002, Abdel-Moneim, 2005).

In the Western Desert, the Quaternary alluvial deposits only exist in some areas along the Nile River's desert fringes and in the Siwa oasis area. Scarce data were found in the literature on the alluvial deposits aquifer in the former, but Hefny et al. (1992) reported that the aquifer in the fringes of the Western Desert and Eastern Desert in general has GW salinities ranging from 500 to 3,000 mg/l. In the Siwa oasis area, the Quaternary alluvial deposits aquifer is recharged from return irrigation water and from the uncontrolled flow of GW from wells tapping the Middle Miocene aquifer in addition to upward leakage of GW from the underlying carbonate aquifer. Groundwater salinities in the Quaternary aquifer in this area are high ranging from 5,000 up to 40,000 mg/l near the salt lakes while the depth to water table is very shallow ranging from 1 to 5 m BGL (Nour and Khattab, 1998).

In the Eastern Desert, the Quaternary alluvial deposits aquifer is the most important shallow GW supply in this area (Abdel-Moneim, 2005) and also has good potential for sustainable extraction (Sultan et al., 2000, 2002). Several wells analysed by Sultan et al. (2000) and Sturchio et al. (2005) in different wadis in the Eastern Desert showed that the GW is mainly brackish with salinities reaching up to around 5,500 mg/l but some wells contain fresh GW. The depth to water table ranges from 31 to 65 m BGL (Sultan et al., 2007). The aquifer is renewable and mainly recharged by flash floods surface runoff, where rainwater over the Red sea hills is channelled through the wadis towards the Nile valley, with an amount estimated to be from 2.9 to 54.1 million m^3/year (Milewski et al., 2009). The aquifer in this area is reported by RIGW (1988) to have lower productivities than other rainfall recharged aquifers such as the Mediterranean coastal aquifer. Nevertheless, Sultan et.al (2007) showed that the thick alluvium Quaternary aquifer in wadi Asyuti is recharged by ascending Nubian GW through deep seated faults which increases its potential for GW extraction (Sturchio et al., 2005) and its productivity. Sultan et.al (2007) reported that wells in this area have moderate to high well yields ranging from 50 to 100 m^3/h. The authors also identified other localities within the Nile flood plain and along the Suez Gulf and Red sea coast that are potentially recharged by ascending Nubian GW and therefore are also likely to have moderate to high productivities.

The Quaternary alluvial deposits aquifer in the Sinai Peninsula is recharged by flash floods surface runoff channelled through main wadis draining towards the Mediterranean Sea and both the Al-Aqaba and Suez gulfs (Gheith and Sultan, 2001). Scarce data were found in the literature regarding GW salinities, but according to Mills and Shata (1989) the Quaternary aquifer in the coastal areas and main wadis mainly contains brackish GW with an average salinity of 2,300 mg/l. The depth to the water table is shallow ranging from 3.5 to 45 m BGL (El-Fiky, 2010, Elewa and Qaddah, 2011). The aquifer receives much higher rainfall recharge than its counterpart in the Eastern Desert. According to Milewski et al. (2009), the alluvial deposits aquifer in wadi Al-Arish watershed, which stretches from Al-Arish city to the central parts of the Sinai Peninsula and encompasses most of alluvial deposits aquifers in the Sinai Peninsula, is annually recharged by an estimated amount of 381.6 million m^3/year. Assuming that, based on the geological map by Milewski et al. (2009), roughly 50% of the wadi Al-Arish watershed is covered by alluvial deposits, the amount of rainfall recharge per unit area is at least 2.5 times higher than the alluvial deposits aquifers in the main wadis in the Eastern Desert. Therefore, while RIGW (1988) described the alluvial deposits aquifer in the Sinai Peninsula to be low to moderately productive and receiving insignificant rainfall recharge similar to its counterpart in the Eastern Desert, it is concluded that the Quaternary alluvial deposits in the Sinai Peninsula is likely to be more productive.

3.3.4 Coastal aquifers

The coastal aquifers cover coastal areas along the Mediterranean Sea and the Red Sea in addition to the Suez gulf and the Suez Canal (*Figure 3-1).* The coastal aquifer along the Mediterranean coast includes the North Sinai coastal area, the North West Mediterranean coastal area and the northern delta area which is part of the previously discussed Nile Delta aquifer.

The North West Mediterranean coastal aquifer stretches from Alexandria city to Egypt's western borders. According to Hefny and Shata (2004) and Atta et al. (2005), the aquifer belongs to the Quaternary age and is recharged by: rainfall which could reach 200 mm/year; lateral seepage from the Nile Delta aquifer; excess irrigation water especially in the Maryut area where a large area is cultivated; and seepage from irrigation canals transporting Nile water to west Alexandria. The coastal aquifer in the North West Mediterranean area mainly contains BW with salinities ranging from 1,000 to 6,000 mg/l and the GW is found at shallow depths where the depth to water table is 15 m BGL on average. The aquifer in this area receives a high amount of rainfall recharge and is described as a moderately to highly productive aquifer (RIGW, 1988). The aquifer in this area is also heavily underutilized where only 10% of its estimated 50 million m^3/year of exploitable GW is extracted (Hefny and Shata, 2004).

The Red Sea coastal aquifer mainly consists of the Miocene sandstone aquifer and the Quaternary alluvial deposits aquifer where the latter exists in the deltaic areas of the main wadis in the coastal plains (Abdel-Moneim, 2005). The Nubian aquifer is also found along the Red Sea coast but it mainly exists at large depths reaching 3 km BGL (Sultan et al., 2007) while in the area where the aquifer outcrops the GW is likely to be saline based on the aquifer’s fresh /saline GW boundary line. The Quaternary and the Miocene aquifers are recharged by infiltrating surface runoff water from flash floods. However, according to RIGW (1988) they receive an insignificant amount of surface recharge compared to the Mediterranean coastal aquifer and therefore are considered to have a lower productivity except in the extreme southern parts where the aquifers receive higher amount of surface recharge and have a moderate to high productivity, which is because the amount of precipitation in this area is high (Abdel-Moneim, 2005). Nevertheless, while RIGW (1988) described the coastal aquifers’ productivity and surface recharge in the extreme southern parts of the Red Sea to be similar to that of the Mediterranean coast, they are expected to be lower as the amount of precipitation in the former is in the range of 33 to 60 mm/year compared to at least 75 mm/year in the latter based on the precipitation map shown in (Milewski et al., 2009).The precipitation map also shows that the Red Sea coastal area at Suez city has a high precipitation rate similar to that of the extreme southern parts and therefore the coastal aquifer in this area is likely to have similar productivities. Moreover, the area extending from Hurghada to Ras-Ghareb city was identified by Sultan et al. (2007) to be a potential discharge area for the Nubian aquifer and therefore the Quaternary aquifer could have higher productivities. Regarding GW properties, water salinity data in the Quaternary aquifer could be only found in the Al-Quseir/Safaga area where the salinities range from 1,500 to 9,500 mg/l (Awad et al., 1996). In general, the Quaternary alluvial deposits aquifer contains brackish GW and with relatively higher salinities than its counterpart near the Nile valley which is attributed to SW intrusion (Abdel-Moneim, 2005). Groundwater in the Miocene aquifer is also brackish with salinities ranging from 2,000 to 2,500 mg/l (Hefny et al., 1992). Hefny et al. (1992) also reported that GW in the Quaternary aquifer is shallow where the alluvial deposits are found at depths ranging from 1 to 15 m. For the Miocene aquifer, scarce data were found regarding GW depths, however it is likely to be shallow as the aquifer outcrops in many locations and also the depth to water table of two artesian wells analysed by Awad et al. (1996) in the Al-Quseir/Safaga area is only 12 m BGL in both wells while the drilling depths are 12 and 78 m BGL. The Red Sea coastal aquifer has a high development potential as out of the estimated 31 million m^3/year of GW that is available for extraction from the aquifer, only 5 million m^3/year was reported to be extracted from the entire Eastern Desert which includes other aquifers (Hefny and Shata, 2004).

The coastal aquifer in the Sinai Peninsula consists of the Quaternary and Miocene sandstone aquifers. Both aquifers are recharged by local rainfall in the northern coastal area, which could reach values as high as 300 mm/year at Rafah city (Abd-El-Samie and Sadek, 2001), and flash floods over the Sinai hills channelled towards main wadis and draining towards the Mediterranean Sea and the Al-Aqaba and Suez gulfs (Gheith and Sultan, 2001, Allam et al., 2003). The Quaternary aquifer in the Northern coastal area is also recharged from return imported Nile water (Abdallah, 2006). According to RIGW (1988), the Quaternary aquifer is moderately to highly productive along the Mediterranean coast and most of the Al-Qaa plain along the Suez gulf which is supported by well yield data reported in Mills and Shata (1989) with values up to 65 and 115 m^3/h in the Al-Arish area and the Al-Qaa plain respectively. The Miocene sandstone and the Quaternary aquifer in other areas along the Suez gulf is described by RIGW (1988) to have low to moderate productivities and to be limitedly recharged by rainfall similar to its counterpart in the Eastern Desert. Nevertheless, as the Sinai Peninsula receives higher rainfall than the Eastern Desert and according to Mills and Shata (1989) wells tapping the Miocene and the Quaternary aquifer in general have the highest productivities in the Sinai Peninsula, it is concluded that the coastal aquifer in the Sinai Peninsula is likely to be more productive than its counterpart in the Eastern Desert. The Suez gulf coastal aquifer has also high development potential as the GW is heavily underutilized where only 10% of the Suez gulf coastal aquifer's annual rainfall recharge rate is extracted (Hefny and Shata, 2004). The following data on GW properties have been obtained from RIGW (1988), Mills and Shata (1989), Hefny and Shata (2004), Abdallah (2006), and Elewa and Qaddah (2011). Groundwater in the Quaternary coastal aquifer is mainly brackish (1,000 to 10,000 mg/l) but fresh GW exists in some areas in the Al-Qaa plain and Rafah area while saline GW is reported south of the Al-Bardaweel Lake and the western corner of the North Sinai coastal aquifer. The Miocene aquifer's GW is also mainly brackish but more saline than the Quaternary aquifer with an average salinity of 5,500 mg/l. Saline and hyper saline GW with salinities ranging from 27,200 to 84,700 mg/l are also reported in the Miocene aquifer in the area between Ras-Sudr and Hammam-Faraon. The depth to water table in the Quaternary aquifer in northern Sinai is less than 15 m BGL while it can reach 70 m in the Al-Qaa plain and it ranges from 16 to 45 m BGL in the Miocene sandstone aquifer.

3.3.5 Basement fissured hard rock aquifer

The basement fissured hard rock aquifer belongs to the Pre-Cambrian Supereon and mainly outcrops in the mountainous area of the Eastern Desert and south of the Sinai Peninsula. Groundwater in this aquifer is limited to areas where the rocks contain cracks and fractures acting as a water bearing zone where rainfall is the only source of recharge (Sturchio et al., 2005). In the Eastern Desert, GW in the Pre-Cambrian aquifer varies from fresh to brackish with salinities up to 3,500 mg/l (Abdel-Moneim, 2005). The depth to water table and the drilling depth of some wells, reported in the literature (Awad et al., 1997, Sultan et al., 2007) range from 3 to 30 m BGL and 6.4 to 38.2 m BGL respectively. In the Sinai Peninsula, the Pre-Cambrian GW also exists at shallow depth (<50 m) and has low salinities ranging from 1,000 to 2,000 mg/l (RIGW, 1988) although GW with salinities up to 5,123 mg/l are reported (Hefny and Shata, 2004). The aquifer also contains fresh GW (<1,000 mg/l) especially in the Saint Catherine area (Tantawi et al., 1998). According to Hefny and Shata (2004), the aquifer has very limited potential for sustainable GW extraction because it is limitedly recharged by the occasional rainstorms over mountainous areas due to its hard rock composition which has negligible porosity increasing surface run off potential. The authors have also reported that most springs tapping the aquifer have very limited productivity.

3.3.6 Al-Moghra aquifer

The Al-Moghra aquifer belongs to the Lower Miocene age and is located in the Western Desert stretching from west of the Nile delta to, and encompassing most of, the Al-Qattara depression in the west covering an area of 50,000 Km^2 (Dawoud et al., 2005). The aquifer contains fossil water, which came from an old Nile delta that existed in this location millions of years ago (Allam et al., 2003). The following data on the aquifer's sources of recharge and GW properties were obtained from Rizk and Davis (1991), Hefny et al. (1992), Nour and Khattab (1998) and Hefny and Shata (2004). The Al-Moghra aquifer is recharged from several sources: lateral seepage from the Nile Delta aquifer in the east with an estimated amount of 50 to 100 million m^3/year; direct rainfall on the aquifer's outcrops with an estimated amount of 100 million m^3/year; leaking water from the underlying Nubian aquifer through cracks particularly in its southern parts by an amount preliminary estimated to be 1 bcm/year; seepage from the overlying Middle Miocene aquifer in the west; and Mediterranean SW from the north. The Al-Moghra aquifer's GW is mainly brackish (1,000 to 10,000 mg/l) except some areas in the east close to the recharge areas from the Nile delta where the aquifer contains fresh GW with salinities as low as 350 mg/l. Salinities as high as 15,000 mg/l are also reported in the northern parts of the aquifer near the Mediterranean coast. Groundwater in the Al-Moghra aquifer is shallow to moderately deep where the depth to top aquifer ranges from zero to 200 m BGL and based on piezometric contour map of the aquifer[10], the depth to water table ranges from zero, especially in the central areas of the aquifer and up to 290 m and 350 m BGL in some locations in the north western and south eastern parts respectively. The aquifer could have a promising potential for GW extraction due to its large GW stored volume that could reach 10,000 bcm (Hefny and Shata, 2004) and because the aquifer partially receives renewable water. However according to Allam et.al (2003) there is no estimation of the exploitable GW from the aquifer. No data regarding well yields were found in the literature but the aquifer is generally described by RIGW (1988) as a low to moderately productive aquifer.

The Pliocene epoch aquifer is another important aquifer that is sometimes associated with the Al-Moghra aquifer (Allam et al., 2003). The aquifer is recharged through lateral seepage from the Nile Delta aquifer, upward leakage from the Al-Moghra aquifer and drainage water from the Al-Nubareya reclamation project in the western delta (Hamza et al., 1984, El-Kashouty and El-Sabbagh, 2011). The Pliocene aquifer is described by RIGW (1988) to be a moderately to highly productive aquifer which is likely due to its closeness to the recharge areas in the Nile delta. The aquifer mainly contains brackish GW with salinities up to 5,000 mg/l (Ammar, 2010) but also contains fresh GW especially in the southern and eastern parts close to the recharge area from the Nile Delta aquifer (Sharaky et al., 2007). Groundwater depth in the Pliocene aquifer is mainly shallow where the drilling depths of several wells tapping the aquifer are reported to range from 23 to 119 m BGL (Idris and Nour, 1990).

3.4 Constraints Limiting Groundwater Development

There are several hazards that may limit brackish GW development and the establishment of decentralized communities away from the Nile valley and delta area. Sand drift is reported to constrain the development of cultivated lands and to cause damage to infrastructure such as houses, roads, irrigation canals and drains (Philip et al., 2004, El-Gammal and El-Gammal, 2010, Hereher, 2010). Sand drift hazard can however be combated by preserving natural vegetation, planting drought resistant trees and shrubs to break wind force, and mechanical stabilization of sands either through chemicals or through mulching[91] (Misak and Draz, 1997).

Flash floods is another constraint and is mainly affecting the Eastern Desert and the Sinai Peninsula causing damages to roads and residential areas (El-Fiky, 2010). For example, in 2010 flash floods affecting both areas caused the death of few as well as injuring and displacing hundreds of people in addition to roads and infrastructure damage (International Federation of Red Cross and Red Crescent Societies 2010).

For this reason, in the study by Salim (2011) to assess different sites' appropriateness for solar driven GW extraction, most flash floods prone areas were excluded. However, flash flood prone areas offer an opportunity to exploit this otherwise wasted water

[91] Covering sand dunes by sheets made of synthetic and dry plant materials

through the use of small dams across flood ways, settling tanks and trenches to recharge the underlying aquifers, as discussed in Sonbol (2009) and Masoud (2011), hence increasing their potential for sustainable extraction.

The presence of landmines in addition to unexploded ordnances (UXO) is another hazard that may limit GW extraction and development in Egypt because of the extra costs required for their clearance. The presence of landmines and UXO, mainly from the second world war, has affected and impeded the development of agricultural, touristic and irrigation projects (Trevelyan, 2001, Abdel-Kader and Yacoub, 2005, Hoelzgen, 2008, International Campaign to Ban Landmines, 2010, Egypt State Information Service, 2011).

3.5 Classification of Brackish Water Aquifers: Methodology

Brackish water aquifers in Egypt are classified for their potential for sustainable GW extraction based on their productivity, amount of surface recharge, GW depth and development potential. A multi-criteria analysis is used to rank the aquifers in the six main regions in Egypt and those having similar scores are assigned a similar rank.

The aquifer’s productivity determines the size of the supported decentralized community which is important as the established decentralized community should produce enough revenue exceeding the costs of extracting GW (Hefny and Shata, 2004), therefore it was given the highest weight (*Table 3-1*). The productivity factor is divided into five classes ranging from low to high. The highest rank is assigned to aquifers described by RIGW (1988) to have very high productivity as well as aquifers with reported well yields exceeding 150 m^3/h.

The amount of surface recharge reflects the potential for long term GW extraction hence the potential for sustainable development. Sustainability is important to justify the high cost of the infrastructure required to establish decentralized communities (Lamoreaux et al., 1985). Extracting non-renewable GW will result in a continuing decrease in GW levels which increases water lifting costs and compromises the sustainability of the community relying on GW. Large drops in water levels have been already reported in the oases area in the Western Desert where many wells tapping the Nubian aquifer ceased to flow naturally due to heavy extraction and digging closely spaced wells (Shata, 1982, Sultan et al., 2007). On the contrary, extracting GW from a renewable aquifer should not result in a drop in water levels as long as GW extraction rates do not exceed the surface recharge rates. A renewability factor is therefore used to differentiate between renewable and non-renewable aquifers and is given a weight of 10%. The renewability factor is divided into three classes: renewable aquifers which are mainly recharged from surface water; partially renewable aquifers which contain fossil water and are also renewed by surface water; and non-renewable aquifers which mainly contain fossil water with insignificant surface recharge.

Table 3-1: Weights and ranks of factors used to assess the aquifers' potential for brackish GW extraction

Factor	Weight	Class	Average Rank
Productivity	75%	High	90
		Moderate to High	70
		Moderate	50
		Low to Moderate	30
		Low	10
Renewability	10%	Renewable	100
		Partially Renewable	50
		Non Renewable	0
Groundwater Depth	15%	Shallow	90
		Shallow to moderate	70
		Moderate	50
		Moderate to Deep	30
		Deep	10

Groundwater depth determines the water lifting and drilling costs. The GW depth factor is divided into five main classes ranging from shallow to deep. Aquifers with depths to water table and depths to GW[92] less than 100 m BGL are classified as shallow aquifers; while aquifers with depth to water table and depth to GW exceeding 200 m and 500 m respectively are classified as deep aquifers. Confined aquifers with shallow water tables and deep depth to GW are assigned to the moderate GW depth class. It should be noted that all aquifers existing at depths larger than 1 km BGL are not considered for brackish GW extraction due to the high cost of extracting water.

[92] Depth to GW is the depth at which GW is found and reflects the drilling depth required. The depth to GW is determined either from well depth or depth to top aquifer data available in the literature. The depth to water table represents the actual water level in the well casing which determines the dynamic head required for water lifting and may differ from the depth to GW in confined aquifers

Aquifers where further GW extraction is not recommended because the maximum amount of exploitable GW is either reached or exceeded are considered to have low development potential and are assigned to the lowest potential class regardless of their productivity, renewability and depth to GW.

Each area's potential for brackish GW extraction is then determined based on the highest class aquifer as more than one aquifer may exist in the same area at different depths. It should be noted, however, that shallow/outcropping aquifers that have lower potential compared to the underlying aquifer could still be attractive for brackish GW extraction due to fewer costs of drilling wells and water lifting provided that sufficient GW is available to sustainably meet the demand of the decentralized community.

Finally, the locations of sand dunes and other Aeolian forms, hence area exposed to sand drift hazards, are identified from the study by Misak and Draz (1997). Furthermore, the whole Eastern Desert and the Sinai Peninsula is considered to be exposed to flash flood hazards based on the study by Abdel-Moneim (2005) and Salim (2011). Moreover, the studies by Trevelyan (2001), Said (2003) and Abdel-Kader and Yacoub (2005) are used to identify areas affected by landmines and UXO. It should be noted, however, that the available minefields records and maps are reported to be limited, lost, inaccurate or incomplete and the existence of UXO is usually not covered as it extends over a large area (Trevelyan, 2001, Said, 2003, Abdel-Kader and Yacoub, 2005, Megahed et al., 2010). In addition, as all available maps are before 2000 while land landmines and UXO clearance activities had been carried out until at least 2009 (Megahed et al., 2010, Abdel-Mohsen, 2012) the identified locations are likely to be overestimated. Therefore, while some areas that are already developed have been excluded, the locations identified will only be indicative of areas that are potentially affected.

3.6 Classification of Brackish Water Aquifers: Results and Discussion

The results of the classification are presented in *Table 3-2, Figure 3-2* and *Figure 3-3* and are discussed separately for each of the six main regions in Egypt which are: the Western Desert, the Eastern Desert, Nile valley and delta, the Sinai Peninsula, the Mediterranean and the Red Sea coastal areas.

Table 3-2: Classes of the aquifers and their associated productivity, renewability and GW depths classes in addition to the area covered by each aquifer class

Aquifers Ranking	Productivity	Renewability	Groundwater depth	Percentage of Egypt's Area
Class I (Highest Potential)	High	Renewable	Shallow	0.8% (Approx. Area: 7,500 km^2)
II	Moderate to High	Renewable	Shallow	16.6% (Approx. Area: 164,300 km^2)
	High	Non Renewable	Moderate to deep drilling depth & shallow depth to water table	
	Moderate to High	Partially Renewable	Shallow	
III	Moderate	Renewable	Shallow	8.3% (Approx. Area: 82,100 km^2)
	Moderately to High	Non Renewable	Moderate to Deep drilling depth with shallow depth to water table	
	Moderate	Non Renewable	Shallow	
IV	Moderate to High	Non Renewable	Deep	7.9% (Approx. Area: 78,600 km^2)
	Low	Renewable	Shallow	
	Low to Moderate	Partially Renewable	Shallow to Moderate	
V	Low	Non Renewable	Shallow	14.7% (Approx. Area: 145,400 km^2)
		Partially Renewable or Renewable	Shallow	
		Partially Renewable or Renewable	Deep	
	Very Low	Renewable	Shallow	
	Class V also includes aquifers where further extraction is not recommended as the maximum amount of exploitable GW is either reached or exceeded			

V-III/Lack of Data	Low or Moderate productivity. Uncertainty due to lack of data in the literature	Non Renewable in the Western Desert Partially renewable or renewable in the Eastern Desert and the Sinai Peninsula.	Shallow except in the Sinai Peninsula where depths are Moderate to deep	6.6% (Approx. Area: 65,500 km^2)
Saline GW	Aquifers mainly containing GW with salinities > 10,000 mg/l			1.1% (Approx. Area: 11,200 km^2)
No GW	Includes all aquicludes where there are no available data on the underlying aquifer in addition to aquifers which are likely to contain no GW due to absence of recharge resources.			1.3% (13,400 km^2)
Fresh GW	Groundwater with salinities < 1,000 mg/l not exposed to pollution			40.3% (Approx. Area: 399,900 km^2)
Fresh Polluted GW	Groundwater with salinities < 1,000 mg/l which are polluted with pathogens, nutrients and trace elements caused by anthropological activities			2.5% (Approx. Area: 24,500 km^2)

3.6.1 The Western Desert

The Western Desert occupies approximately 69% of Egypt's area (approx. 684,100 km^2) and has a great potential for brackish GW extraction. One fifth of the Western Desert's area has access to brackish GW from the Nubian aquifer which has large GW reserves and was considered as a class II aquifer due to its high productivity and high development potential in this region. In addition, while the Nubian aquifer is a deep aquifer system which increases drilling costs, GW in most wells is flowing to the surface which decreases water lifting costs.

Nearly 60% of the Western Desert's area, however, contains fresh GW found in the Nubian aquifer (*Figure 3-2*) and therefore the priority for establishing decentralized communities based on GW extraction should be given to this area as only simple GW treatment will be required. Groundwater treatment is required in the fresh GW zone of the Western Desert due to high concentrations of iron and manganese (Gossel et al., 2010, Hamza et al., 2000, El Tahlawi et al., 2008) exceeding the WHO guidelines (WHO, 2011). In this case, instead of desalination, an oxidization process is sufficient which is achieved through aeration[93] or oxidizing chemicals[94] to make iron and manganese insoluble hence can be easily removed[95] with media filters (National Drinking Water Clearinghouse, 1998, Colter and Mahler, 2006).

Nevertheless, given that the brackish GW zone in the Western Desert mainly occurs along the Nile River, establishing decentralized communities in this area would be more attractive due to its closeness to the Nile valley and therefore less investment will be required for providing the infrastructure needed to attract new immigrants (Lamoreaux et al., 1985) such as healthcare and educational services. For example, according to Lonergan and Wolf (2001), developing fresh water resources in areas close to major populated areas in Egypt, such as the Al-Nubareya canal, was more successful in attracting new families as opposed to isolated projects in the deserts such the Toshka project in the New Valley area in the Western Desert where farmers temporarily move to work without settling due to lack of infrastructure. The brackish GW zone is also less exposed to sand drift hazards opposed to the fresh GW zone where around 83% of sand dunes in the Western Desert are concentrated. Furthermore, most of the brackish GW zone along the Nile River has high potential for brackish GW extraction (Class II) as it has access to the Nubian aquifer in addition to the shallow Quaternary aquifer which in some areas has high potential for GW extraction as it is likely to be a discharge area of the Nubian aquifer.

In the northern parts of the Western Desert, the Nubian aquifer exists at large depths (>1 km BGL) and is mostly saline and therefore is not economical for extraction. Brackish GW could be extracted from the lower potential Middle Miocene and the Al-Moghra aquifers which outcrop in this area. Nevertheless, the northern part of the Western Desert may not be suitable for establishing decentralized communities due to its remoteness. Moreover, the northern area east of the Al-Qattara depression is exposed to sand drift hazard and many areas near the Mediterranean coast are likely to be affected by landmines and UXO. Furthermore, according to Masoud and Koike (2006), as Al-Qattara is a depression area with extremely arid climate, irrigation water demand as well

---

[93] Water is oxidized using Oxygen available in the air. Aeration is less efficient than using oxidizing chemicals

[94] E.g. chlorine, chlorine dioxide, potassium permanganate, and ozone

[95] Note that the type of treatments depends on the type of iron present in GW such as whether it is Ferrous, Ferric iron or Iron Bacteria.

as soil salinisation will increase due to high evaporation rates which will constrain the development of agricultural communities. Brackish GW extraction and desalination would be, however, ideal to supply water for the oil and gas exploration companies concentrated in this remote area (Oil&Gas, 2012), instead of transporting fresh GW with trucks which could be expensive.

The Siwa depression is another important area for brackish GW extraction. The area is an important site for agricultural development, the main activity in this area (Masoud and Koike, 2006, EI-Naggar, 2010), and due to its remoteness, water demand is met through GW extracted from the brackish Middle Miocene aquifer and the fresh Nubian aquifer. While the priority for GW extraction should be given to the Nubian aquifer as it contains fresh water, most agricultural water demand in the past was met through brackish GW from the Middle Miocene aquifer (Nour and Khattab, 1998) as its water is naturally discharged in springs or exists at shallow depths hence can be accessed through cheaply hand dug wells. While there are no recent data in the literature regarding GW extracted from each aquifer, it is likely that agricultural water demand is still and will continue to be mainly met from the Middle Miocene aquifer due to its shallowness, while GW extracted from the Nubian aquifer is likely to be reserved for domestic purposes. It should be noted that the cultivated zone of the Siwa depression area is reported to suffer from soil salinisation caused by water logging due to improper drainage systems, overuse of water in irrigation and the uncontrollable discharge of the natural flowing wells (Masoud and Koike, 2006, EI-Naggar, 2010), therefore further use of brackish GW directly in irrigation will exacerbate soil salinisation. Accordingly, desalinating the naturally flowing brackish GW from the Middle Miocene aquifer might be a necessity to avoid further soil salinisation and also to make use of this wasted resource which is otherwise causing water logging problems. Extracting brackish GW from the Quaternary aquifer is also recommended to lower the water table in this area hence avoiding further soil salinisation problems.

Finally, as all aquifers in the Western Desert are non-renewable, studies are required to determine the maximum withdrawal rate and the duration at which extracting GW would still be economical despite of increasing water lifting costs.

3.6.2 The Eastern Desert

The Eastern Desert occupies 19% of Egypt's area and is an important area for brackish GW extraction as 98.7% of the area has access to brackish GW. However, the Eastern Desert has a lower potential for brackish GW extraction compared to the Western Desert as approximately 60% of the area is covered by the low productive Pre-Cambrian and carbonate aquifers (*Figure 3-2*). Nevertheless, the Eastern Desert receives relatively high amounts of rainfall which mainly recharges the shallow Quaternary aquifer increasing its potential for sustainable extraction compared to the Western Desert whose GW is mainly non-renewable. Furthermore, the Eastern Desert is bordered by the populated areas all over the Nile valley and the reasonably populated Red sea coastal cities, such as Suez, which allows a gradual expansion of decentralized communities.

The Quaternary aquifer in wadi Qena, Hammamat and Asyuti, has the highest potential for brackish GW extraction (Class II) in the Eastern Desert as the aquifer is recharged by rainfall and is also likely to be recharged by ascending Nubian GW hence the GW could be produced sustainably and with high productivities. Therefore, priority for brackish GW extraction and establishing decentralized communities should be given to the shallow Quaternary aquifer in those wadis due to their high brackish GW potential and also their closeness to populated areas. Wadi Asyuti in particular is an important area for brackish GW extraction especially that the area is planned to be a major agricultural site relying on GW(Sultan et al., 2007).

The second priority should be given to the Nubian aquifer which covers one third of the Eastern Desert and has similar productivities as the Class II shallow Quaternary aquifers in the Eastern Desert. However due to its non-renewability and higher depths to GW, the aquifer was considered to have a lower potential (class III) for brackish GW extraction. Both areas where the Quaternary and the Nubian aquifer are accessed are also relatively plain compared to the rigorous mountainous area of the Pre Cambrian basement complex and therefore are more suitable for establishing new communities.

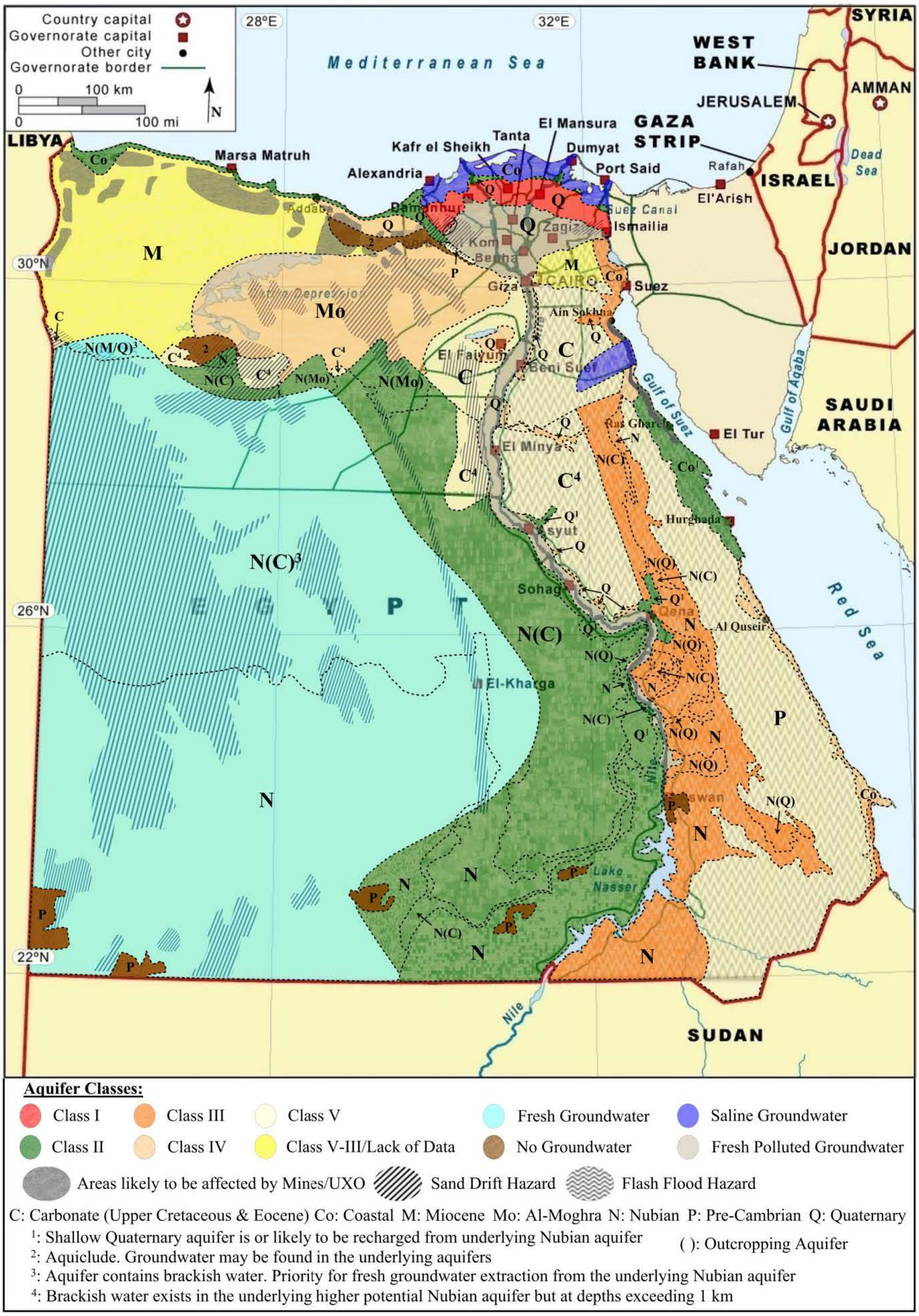

Figure 3-2: Aquifers potential for brackish GW extraction

The entire Eastern Desert is, however, exposed to flash floods hazard given that most of the Eastern Desert is covered by impervious limestone rocks which have low infiltration capacity. Abdel-Moneim (2005) classified the main wadis in the Eastern Desert based on their infiltration capacity and most of the wadis were shown to have poor recharge potential and therefore high probability of experiencing flash floods. Nevertheless, with proper measures flash floods offers an opportunity to increase shallow aquifers' recharge hence their potential for GW extraction.

3.6.3 The Sinai Peninsula

The Sinai Peninsula occupies approximately 6% of Egypt's area and is experiencing water shortages (Rayan et al., 2001) that hinders development efforts especially that the area has a high potential for tourism, agricultural, industrial and mining activities (Abd-El-Samie and Sadek, 2001). According to Rayan et al. (2001) and Elewa and Qaddah (2011), the current water demand in the Sinai Peninsula is met by SW desalination and GW extraction mainly in the north eastern Mediterranean coastal area. Drinking water is also transported by trucks in areas that are not connected to the water distribution network. The Al-Salam Canal which transports Nile water to be used in irrigation is another main source of water in the Sinai Peninsula. However, it has an unreliable water supply with reported water shortages in the canal and high salinity of the transported water (Abdallah, 2012). Therefore, given that approximately 85% of the Sinai Peninsula area has access to brackish GW aquifers, decentralized brackish GW extraction and desalination could be more economical and reliable to meet the water demand in this area. A local water supply would also save in costs associated with transporting water by trucks. Moreover, as previously discussed in Chapter 1 and 2, BW desalination is a better alternative than SW desalination due to the former's low energy consumption and pre-treatment requirements which decrease the costs especially when compared to the Red Sea water which has high fouling potential requiring expensive pre-treatment (Hafez and El-Manharawy, 2003).

Approximately 68% of the Sinai Peninsula has access to aquifers with moderate to high potential for brackish GW extraction (Class IV to II) (*Figure 3-3*).

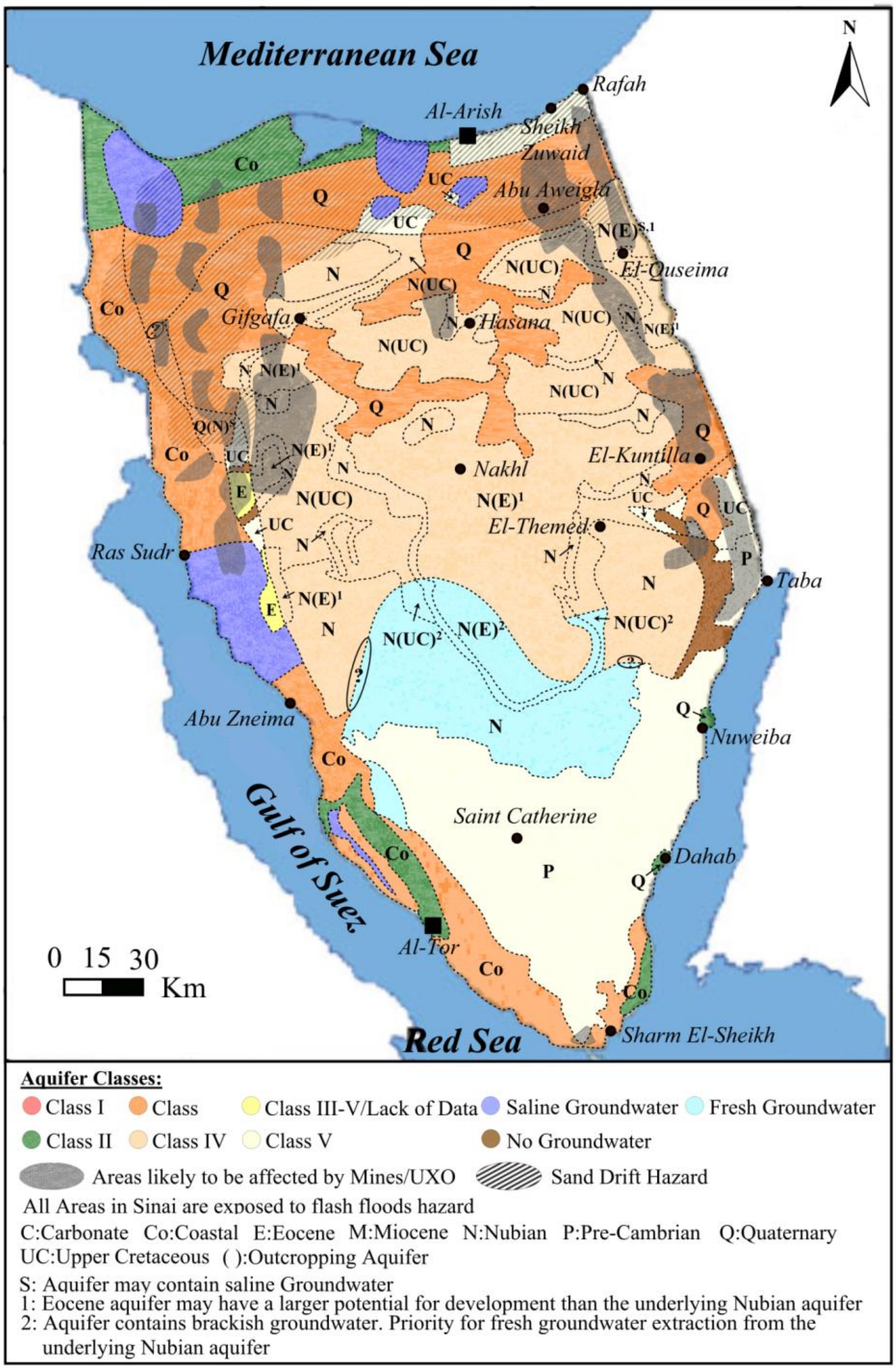

Figure 3-3: Aquifers potential for brackish GW extraction in the Sinai Peninsula
Base map modified after (Elewa and Qaddah, 2011)

The coastal and the alluvial deposits Quaternary aquifers have the highest potential due to the high amounts of rainfall in the Sinai Peninsula that recharges the aquifers especially the areas along the Mediterranean coast and in the Al-Qaa plain. However, some areas in North Sinai with access to the Quaternary aquifer are exposed to sand drift hazard and many parts are likely to contain landmines and UXO which will constrain the development of new communities. Therefore, priority for establishing decentralized communities based on brackish GW extraction and desalination should be given to the area accessing the Quaternary aquifer in the central parts of the peninsula. Further brackish GW extraction is also not possible from the Quaternary aquifer in the north eastern Mediterranean coastal area as GW extraction has already exceeded the annual rainfall recharge (Hefny and Shata, 2004) as it is heavily used to meet domestic and agricultural water needs. It should be noted, however, that brackish GW desalination is strongly required in this area as the GW is mostly brackish and, based on the chemical analysis carried by El-Alfy (2012), is heavily polluted and therefore is not suitable for human consumption and is, according to Kaiser and Greish (2007), associated with the widespread of diseases such as diarrhoea and kidney diseases in the area. Groundwater over extraction is also continually increasing the salinity of the water due to mixing with the higher saline GW from the underlying Miocene aquifer in addition to SW intrusion (Abdallah, 2006, Shawki, 2011).

The Nubian aquifer is also an important aquifer for brackish GW extraction and has the highest development potential in the peninsula. The Nubian aquifer in this area has large GW reserves and it contains brackish GW within a significant area of the peninsula (27%) particularly in the central parts. However, the main limitation for GW extraction from the aquifer is the large depths at which GW is found, which is the largest in Egypt in terms of drilling depths and depth to water table. Therefore, areas accessing the Nubian aquifer should have the second priority for brackish GW development. It should be noted that the Eocene aquifer which overlies the Nubian aquifer in many locations in the Sinai Peninsula may have more potential than the latter as it was reported to have a similar productivity but with shallower GW depths and therefore would be more attractive for brackish GW extraction; however little data on the aquifer’s productivity were found in the literature to confirm its high productivity.

Finally, the Sinai Peninsula is exposed to flash flood hazard which will require additional costs to adopt proper measures to reduce the damages caused by such events but it also offers an opportunity to recharge the aquifers hence increasing their potential for GW extraction.

3.6.4 Nile valley and delta

The Nile valley and delta is an important agricultural site where most of the cultivated lands are concentrated (FAO AQUASTAT, 2005). Groundwater in this highly populated area is already being used as a secondary source of water to meet domestic and irrigation water demand especially in the desert fringes (Hefny et al., 1992, Dawoud, 2004, Ahmed and Ali, 2011). Therefore, while the area is not suitable for establishing decentralized communities as it is already heavily populated, the availability of water that is suitable for irrigation is essential to keep lands cultivated hence keeping the jobs of a large segment of the population who are working in agriculture.

Approximately 62% of the Nile valley and delta area has access to fresh GW from the Nile basin aquifer. However, approximately 35% of the Nile delta's area has access to brackish GW. The Nile Delta aquifer has the highest potential (Class I and II) for GW extraction in Egypt due to its high productivity and continuous recharge by excess irrigation water. Brackish GW extraction from this area will also reduce the water table especially in the northern parts where continuous soil salinisation is reported due to the presence of brackish GW at very shallow depths (Franken, 2005, Elewa and El Nahry, 2009). Seawater intrusion is, however, a main limitation for further GW extraction from the Nile Delta aquifer (Idris and Nour, 1990, Sherif and Singh, 1996) as it will increase GW salinity with continuous extraction. Therefore studies to estimate the maximum amount of brackish GW that could be extracted while minimizing SW intrusion are required, similar to the study carried out by Sherif and Singh (2002) which investigated the maximum amount of fresh GW extraction from the Nile Delta aquifer. It should be also noted that while brackish GW may exist in the fresh GW zone due salt leaching from irrigation water return, the priority should be for fresh GW extraction to reduce treatment costs.

Wadi-Al-Natrun is a depression area of around 500 km^2 (Idris and Nour, 1990) located on the western borders of Beheira governorate and is considered as part of the Nile delta area. Groundwater extraction, which is mainly brackish, is important in this area as it is, according to El-Kashouty and El-Sabbagh (2011), the main water source for the reclamation projects and the development of new communities in this area that started since the 1960's. However, further extraction from the Pliocene aquifer, the main aquifer in this area, is not recommended as over extraction was already reported by Hamza et al. (1984) and El-Kashouty and El-Sabbag (2011) causing a drop in piezometric heads and salt water intrusion from deeper aquifers. Brackish GW desalination is however required because most of the extracted GW is brackish and is not suitable for drinking. In some cases, the GW was also not suitable for irrigation as some wells, based on the study by Sharaky et al. (2007), have high levels of chloride, sodium and bicarbonate in addition to high levels of nickel exceeding the limits recommended by the FAO guidelines (Ayers and Westcot, 1994) for most of the major crops cultivated in Egypt.

3.6.5 Mediterranean North West and Red Sea coastal Areas

The Mediterranean North West and Red Sea coastal areas are important touristic sites where water demand is mainly met through SW desalination and transported Nile water (RIGW, 1988). Transported Nile water, however, may not be a reliable source of water because, as discussed in Chapter 1, the Nile water is fully utilized and therefore would not be sufficient to meet additional water demand. For example, in 2012 a drop in the water level has been reported in the Al-Hammam Canal, which transports Nile water to the north west of the Mediterranean coast, due to unofficial use of the water in irrigation by the farmers, which led to severe water shortages in Marsa-Matruh city and required military interference to stop unofficial use of the water (Abd-Allah, 2012, Mashaly, 2012, Saleh, 2012). Moreover, while there are already three pipelines transporting Nile water to the Red Sea coast, the construction of additional pipelines is hampered by the high costs given that the area is separated from the Nile River by rigorous mountainous area (Hafez and El-Manharawy, 2003). For this reason, decentralized brackish GW extraction could be a more reliable alternative for both coastal areas. Moreover, as previously discussed in Chapter 1 and 2, BW desalination is a better alternative than SW desalination due to the former’s low energy consumption and pre-treatment requirements which decrease the costs especially when compared to the Red Sea water which has high fouling potential requiring expensive pre-treatment (Hafez and El-Manharawy, 2003). Coastal areas are also suitable for establishing decentralized communities due to their closeness to infrastructure found in main coastal cities such as Alexandria, Marsa-Matruh, Suez and Hurghada.

Groundwater in the coastal aquifers is a heavily underutilized resource and the aquifers have a great potential for future development. The Mediterranean North West coastal aquifer, covering an area of approximately 4,070 km^2, has high potential (Class II) for brackish GW extraction and therefore the area is very suitable for establishing decentralized communities. The Red Sea coastal aquifer, covering an area of approximately 15,200 km^2, has lower potential than the Mediterranean coastal as approximately half of its area has access to aquifers in the III to IV class range due to lower rainfall rates. However, in the area stretching between Hurghada and Ras-Ghareb cities, the Quaternary aquifer has high potential for brackish GW extraction (Class II) because it is likely to be a discharge area of the Nubian aquifer and therefore should have the priority for establishing decentralized communities along the Red Sea coast.

The main limitation for GW extraction from coastal aquifers, however, is SW intrusion which will require further studies to assess the maximum extractable amount of GW that will limit SW intrusion. The Red Sea coastal aquifer is also exposed to flash flood hazards and some areas are or likely to be affected by mines and UXO.

Brackish GW is favoured over fresh GW extraction because while the latter essentially needs no or little treatment to be suitable for consumption, it was found to be only confined to the overpopulated Nile delta and valley area and the Western Desert. Conversely, aquifers containing brackish GW cover more than half of Egypt’s area. In addition, areas like the Eastern Desert have access to only brackish GW therefore brackish GW extraction and desalination will be a necessity to establish decentralized communities in this area. Brackish GW is regarded by many studies, such as (Ahmad and Schmid, 2002, Allam et al., 2003, Talaat et al., 2003, El-Sadek, 2010), as an important source to meet Egypt’s growing water demands.

3.7 Groundwater Suitability for Agriculture Use

Detailed water chemical analyses are found for wells in the following areas: the Siwa oasis in the Western Desert (Abdel-Shafy et al., 1992); Wadi Asyuti and Qena area, which includes Wadi Qena and Wadi Hammamat, in the Eastern Desert (Sturchio et al., 2005); Central Sinai area (Abd El Samie and Sadek, 2001), Al-Qaa plain (Gorski and Ghodeif, 2000 cited in Sultan et al., 2009) and the vicinity of Al-Arish city (El Alfy,

2012) in the Sinai Peninsula; Wadi-Al-Natrun and the delta area (Sharaky et al., 2007); and Alexandria (Atta et al., 2005). Using FAO guidelines (Appendix D), the following have been observed: sprinkler irrigation may not be suitable to be used with the water in most of the reviewed wells due to high concentrations of sodium and chloride; water in most wells is likely to cause severe clogging issues with drip irrigation equipment due to high salinity in addition to high pH in some locations such as Siwa oasis, the delta area and Alexandria; and water in some areas may not be suitable for irrigation due to high concentrations of trace elements exceeding FAO guidelines such as fluoride, selenium, and manganese and nickel found in all of the analysed wells in the Al-Qaa plain and the vicinity of Al-Arish city and most of the analysed wells in Wadi-Al-Natrun respectively. The high concentrations of selenium and manganese found in most wells and all the wells in the vicinity of Al-Arish city and Wadi-Al-Natrun respectively will also make the water unsuitable for livestock use.

Moreover, based on the FAO guidelines (Ayers and Westcot, 1994), water salinities exceeding 1,220 mg/l are expected to cause more than 25% losses in the yield of sensitive crops and accordingly BW in general is not suitable for such crops. This also applies for moderately salt sensitive crops, which encompasses most of the HVLWC considered in this study, given that the average salinity of the reviewed wells in most of the aforementioned locations exceeded 2,500 mg/l which is expected to cause more than 25% losses to such crops. Furthermore, water may not be suitable at all for irrigation and livestock use in some areas such as the extreme northern parts of Central Sinai and of the BW zone in the delta area.

Therefore, it can be safely concluded that BW in Egypt will need to be desalinated to be suitable for irrigation and in some case livestock use. Using fresh water (< 1,000 mg/l) in irrigation also offers additional advantages:

1- Any crop could be cultivated without yield losses
2- Less leaching requirements, i.e. less leaching factor, reducing the water needed for irrigation to just what is needed by the crop. This is especially important when using a limited resource such as GW
3- Prevent long term soil salinisation problems as fewer salts would be accumulating in the soil. Experiments using RO and UF for irrigation are

already carried to desalinate the water to drinking quality to prevent soil salinisation such as the ones carried out by Oron et al. (2006, 2008).

4- Irrigating with drinking quality water may increase the yield and enhance crop development. For example, Oron et al. (2006, 2008) showed that irrigating corn and watermelon crops with RO permeate achieved better crop development, in terms of height and diameter size, and yield compared to using lower quality water.

Finally, it should be noted, that water quality is not enough to assess land suitability for cultivation as there are other important factors to be considered, for example soil texture, depth and salinity, terrain slope and drainage conditions (Arnous and Hassan, 2006).

3.8 Conclusion

Reviewing GW in the main seven hydro-geological systems in Egypt showed that the country has a great potential for brackish GW exploitation. More than half of Egypt’s area was found to have access to BW aquifers with whole regions such as the Eastern Desert and the Sinai Peninsula mostly having access to only BW. Conversely, fresh GW was found to be only confined to the overpopulated Nile delta and valley area in addition to the western and south western parts of the Western Desert which are exposed to sand drift hazard and are not attractive to establish communities due to its remoteness. The study also showed that 47% of BW aquifers have moderate to high potential for sustainable extraction. Five main areas were identified to have priority for establishing decentralized agricultural communities based on brackish GW extraction and desalination: areas along the Nile River in the Western Desert and the Eastern Desert having access to the Nubian aquifer and the shallow Quaternary aquifer; the central parts of the Sinai peninsula tapping the Quaternary and the Nubian aquifer; the coastal area along both shores of the Suez gulf; and the Mediterranean North West coastal area. Brackish GW extraction and/or desalination could be also required in: the northern parts of the Western Desert to supply water for oil and gas companies; in the Siwa depression area and the Nile delta to lower the water table and prevent soil salinisation; and in the north east coastal area of the Sinai Peninsula as brackish or polluted GW was reported to be used for drinking causing diseases. Finally, it was shown that brackish GW desalination will be required for water to be suitable for human consumption as well as agricultural use.

4. Feasibility Study of PV Driven Brackish Water RO Plants

As concluded from Chapter 1 and 2, PV driven high RR RO plants are suggested to establish decentralized communities in remote/rural areas. A PV system, and solar energy in general, is a sustainable and an ideal energy source for a place with high solar resources like Egypt. Moreover, the RO process is currently the cheapest and most suitable process for BW desalination. High RR operation is also suggested due to the limited GW resources in Egypt where GW is mostly non-renewable, that in addition to reducing the environmental impact and additional costs associated with brine disposal in inland areas.

It was shown that most BW PV-RO plants reported in the literature are not operating within their optimal window and were mostly operating at low RR. This will result in a significant increase in the SEC and will also compromise the performance of the RO modules by increasing the risk of scaling occurrence. Moreover, almost none of the reviewed studies on the economic feasibility of PV-RO plant considered the effect of the PV-RO plant operating hours on its LCOW or the effect was only considered for a specific operating condition. Furthermore, there is a lack of studies concerning the economic feasibility of BW PV-RO particularly in Egypt and the existing studies are not reliable and/or do not consider the different operating conditions of the RO plant.

For this reason, in this chapter the feasibility of BW PV-RO plants operating at the maximum attainable RR is investigated in terms of their energy performance and life cycle unit water costs. The designs will be carried out according to the manufacturer's recommended specifications using a commercially available simulation tool. The feasibility of the PV-RO plant will be also investigated for two cases: a case where the RO plant operates only during day time; and a case where the RO plant is operating for 24 hours.

Firstly the methodology used for estimating the maximum attainable RR of the RO plant, designing and modelling the RO plant and the PV energy supply, and determining the life cycle costs (LCC's) of the plant is presented. Secondly, the maximum attainable RR of the RO plant and its main limiting factors are then discussed; followed by the economic feasibility of PV driven RO plants in comparison with a similar plant driven by a DG.

4.1 Methodology

4.1.1 General design considerations

In this section, the general design methodology which applies for all the configurations considered in this chapter is discussed.

4.1.1.1 Desalination plant size selection

As discussed in Chapter 1, this thesis focuses on small scale decentralized desalination plants. In the literature the capacity associated with small scale plants significantly varies. Small scale plants have been defined as plants with capacities up to 50 m^3/day (Tzen et al., 2008, Eltawil et al., 2009), less than 10 m^3/day (Fiorenza et al., 2003), less than 1000 m^3/day (Sagie et al., 2001, IDA, 2013) and 0.5 to 100 m^3/day (Müller-Holst, 2007), and other studies, such as Ayoub et al. (1996), defined the scale according to the number of persons the water plant supplies.

In this study, the desalination plants are designed to have a production capacity of 500 m^3/day to 1,500 m^3/day depending on the number of operating hours of the plant (see section *4.1.4.2*). The former is a conservative value enough to irrigate 2.9 hectares of land; an area, based on data from Allam and Allam (2007), enough to produce a revenue exceeding the minimum annual wage in Egypt, i.e. 14,400 EGP[96] (Ahram Online, 2013), when high value crops are cultivated. The aforementioned capacity range could be also met by most wells in Egypt as they have average yields ranging from approximately 400 to 3900 m^3/day[97].

4.1.1.2 Product water target salinity

While water with salinities up to 1,000 mg/l is suitable for drinking (WHO, 2011), in this study the product water salinity is targeted to be in the range 500 mg/l to increase

[96] Egyptian Pounds
[97] Based on the GW review carried out in Chapter 3

the water acceptability by the population[98]. Moreover, water with 500 mg/l salinity is suitable for irrigating almost all crops without yield losses (Appendix D). The 500 mg/l limit is also used in numerous desalination studies and existing brackish GW RO plants (Herold et al., 1998, Soltan, 1998, Richards and Schafer, 2002, Martinetti et al., 2009, Riffel and Carvalho, 2009).

4.1.1.3 Groundwater blending

To reduce the energy consumption in addition to reducing, if not eliminating, the need to re-mineralize the permeate water (Watson et al., 2003), some of the GW is directly blended with the desalinated water such that the overall salinity stays in the range of 500 mg/l.

4.1.1.4 Solar irradiation

Solar irradiation is expected to play a major role in the PV system sizing. For this reason the different solar driven desalination plant configurations considered in this study are investigated with two extreme climate conditions: the low solar irradiation (LSI) zone which applies for areas along the Mediterranean coast and the Delta area and is represented in this study by the city of Alexandria; and the high solar irradiation (HSI) zone which applies for the central and southern parts of Egypt as well as the southern parts of the Sinai Peninsula and is represented in this study by the city of Aswan. *Table 4-1* shows the solar resources of few cities in Egypt and it is clear that cities in the LSI and the HSI zones have almost similar solar resources.

4.1.1.5 Groundwater temperature

In this study, the temperature of the feed water to the desalination plant is assumed to be the same as that of the GW. This is safe to assume as the desalination plants will be designed to treat the extracted GW within the same day. Therefore the water is expected to have a low settling time hence its temperature is less affected by the ambient. Moreover, given the small scale capacity of the RO plant and its decentralized nature, the water conveyance distance from the well to the RO plant is expected to be small for its temperature to be affected by the ambient.

---

[98] The WHO (2011) considers water with salinities less than 600 mg/l to have good palatability

Table 4-1: Solar irradiation and ambient temperatures data for several cities in Egypt

	Latitude and Longitude	**Annual Average Air Temperature (°C)**	**Annual Average Latitude Tilt Daily Global Irradiation ($kWh/m^2/day$)**
		Low Solar Irradiation Zone	
Marsa-Matruh	31.35-27.2	20.9	3.8-6.95 (av. 5.65)
Alexandria	31.2-29.95	20.7	3.75-6.6 (5.5)
Al-Arish	31.15-33.8	19.8	4.4-6.85 (5.9)
		High Solar Irradiation Zone	
Siwa	29.2-25.5	22.3	5.15-7.25 (6.55)
El-Tor	28.25-33.6	20.9	5.8-7.45 (6.8)
Asyut	27.2-31.2	22.8	5.65-7.4 (6.8)
Hurghada	27.2-33.8	23.1	5.7-7.35 (6.7)
Qena	26.15-32.7	23.6	5.9-7.3 (6.8)
Aswan	24.1-32.9	25.3	6.0-7.2 (6.75)

Data are obtained from the SWERA website (NREL, 2013)

Groundwater in the LSI zone is found in the shallow Mediterranean coastal aquifer in addition to the delta aquifer where the depths to water table range from 0 to 85 meters (Appendix E). For this reason the GW temperature could be assumed to be constant and close to that of the annual average air temperature (Kasenow, 2001, Popiel et al., 2001) which in this study is taken to be approximately 20°C.

In the HSI zone, GW is found at larger depths as it is mainly accessed from the deep Nubian aquifer where the depth to GW ranges from 100 to 1100 meters (Appendix E). In this case, the GW temperature will depend on its depth (Hamza et al., 2000). Based on the thermal gradients reported in the literature (Hamza et al., 2000, Swanberg et al., 1983, Nour, 1996) and a GW surface temperature equal to the mean annual ground temperature in Egypt (Swanberg et al., 1983), it is expected that for the reported GW depths in the Nubian aquifer, GW temperature should not exceed 40°C. In this study, GW temperature extracted from the HSI zone is assumed to range from 30°C to 40°C (*Table 4-2*) where the latter value applies only for GW extracted from the Nubian aquifer in the Sinai Peninsula where the depth to GW ranges from 500 to 1100 m (Nour and Khattab, 1998). It should be noted that if GW is extracted from larger depths or the thermal gradient is high, GW temperatures may exceed 45 °C[99] and therefore cooling towers will be necessary to prevent damaging the RO membrane (Sobhani et al., 2012).

4.1.1.6 Groundwater salinity and chemical composition

Groundwater salinity affects the energy requirements of the RO plant where, as observed from the Van't Hoff equation (Crittenden et al., 2012d), the osmotic pressure is directly proportionate to the number of moles of solutes in the water. For this reason, the RO plant designs are carried out for the expected salinity range of BW, i.e. 1,000 to 10,000 mg/l.

Furthermore, it is observed that in contrast with SW, which is mainly composed of sodium and chloride (Hömig, 1978), treating BW as a sodium chloride solution is found by the author to cause an inaccurate estimation of the osmotic pressure hence the energy consumption. For example, using the Reverse Osmosis System Analysis (ROSA) software (DOW Chemical Company, 2013e), the average osmotic pressure[100] and the RO plant SEC when the feed water has a salinity of approximately 4,000 mg/l and a chemical composition similar to that of a well tapping the Mediterranean costal aquifer, obtained from Atta et al. (2005), is found to be 25% and 7.6% respectively lower than that of a sodium chloride solution with the same salinity. The permeate salinity when treating the GW as a sodium chloride solution is also found to be 20% higher than the case where the actual chemical composition is used. The reduction in the osmotic pressure is because for the same water salinity GW typically contains a higher percentage of the heavier, i.e. higher molar mass, bicarbonate and sulphate ions. Accordingly, lower number of moles is present in the GW compared to a sodium chloride solution with the same salinity. Moreover, the RO membrane higher rejection to multivalent ions (Crittenden et al., 2012e) resulted in a lower permeate salinity when the actual composition of GW is used.

For this reason, the actual GW composition is needed for an accurate estimation of the SEC. However, as the GW composition varies from one well to another even within the same area (Sultan, 1999 cited in Masoud et al. 2003), in this study three GW compositions are considered: typical GW composition, represented by a well in the Al-

[99] As the Nubian aquifer is a deep aquifer, GW temperatures ranging from 30 to up to 60°C are reported in the literature (Morgan and Swanberg, 1978, El Tahlawi et al., 2008, Gad, 2009, Gossel et al., 2010).
[100] Osmotic pressure based on the average salinity between the feed water and the RO concentrate

Arish area tapping the Quaternary aquifer, which has a percentage composition of major ions close to the average of that of other wells in several locations in Egypt; GW with dominating sodium and chloride ion composition represented by a well in the Al-Quseir/Safaga area tapping the Red Sea coastal aquifer; and GW with dominating multivalent ion composition, i.e. calcium, sulphate and bicarbonate ions, represented by a well in Wadi Al-Tarfa tapping the Quaternary aquifer. The percentage major ions composition in each case is then applied at the different water salinities considered in this study.

4.1.1.7 Groundwater extraction power consumption

The power associated with GW extraction is included in sizing the energy supply. The power is calculated based on the expected depth to water table. Based on the data reported in several locations in the LSI and HSI zones (Appendix E), few values were chosen to represent the depth to water table expected in both zones and are shown in *Table 4-2*.

Table 4-2: Depth to water table and the corresponding assumed GW temperatures in the LSI and HSI zones

	Depth to water table	**Areas where the depth to water table applies**	**GW Temperature**
LSI	10 m	GW extracted from the coastal aquifer in Alexandria, and the confined delta aquifer	20°C
	50 m	GW extracted from the coastal aquifer in the Al-Arish and the unconfined delta aquifer	
HSI	20 m	GW extracted from the confined Nubian aquifer in the eastern and western deserts	30°C
	50 m	GW extracted from the unconfined Nubian aquifer in the eastern and western deserts or the Quaternary aquifer from any location in the HSI zone	
	200 m	GW extracted from the confined Nubian aquifer in the Sinai Peninsula	30°C,40°C

4.1.1.8 Recovery rates

As discussed in Chapter 1 and 2, this study mainly focuses on high RR operation. The RR for the RO plant is limited by the scaling potential of the desalinated water in addition to the maximum pressure that the RO membranes can withstand.

A) Feed pressure limited recovery rate

The RO modules used in this study are the FILMTEC modules manufactured by the DOW Chemical Company. These modules are not recommended to concentrate water to salinities beyond 70 g/l of sodium chloride in order not to exceed the maximum feed pressure of the company's highest salt rejection RO membranes and to maintain a reasonable amount of permeate flow production (DOW Chemical Company, 2011). This imposes a limit on the concentration factor (CF), i.e. the ratio between the concentrate salinity and the feed water salinity, hence the maximum attainable RR.

It should be noted however that, as discussed in section *4.1.1.6*, for the same water salinity the osmotic pressure of GW is usually lower than that of a sodium chloride solution. Accordingly, the RO membrane should be able to concentrate GW to salinities higher than 70 g/kg. Nevertheless, as the RO plant design can get very complex at high CF's, in this study the maximum salt concentration is taken to be 70 g/l. In this case, the maximum attainable feed pressure limited RR of the RO plant is calculated using equations *(4-1)* and *(4-2)*.

$$RR = 1 - \frac{1}{CF} \qquad \textbf{(4-1)}$$

$$CF = S_{max} / S_{feed\,,RO} \qquad \textbf{(4-2)}$$

where S_{max} is the maximum is concentrate salinity limit, i.e. 70 g/kg, and $S_{RO,feed}$ is the RO feed water salinity.

B) Scaling limited recovery rate

The presence of reactive silica, calcium carbonate and calcium sulphate in addition to barium and strontium sulphates limits the maximum attainable RR of the RO plant as they have a low solubility in pure water forming precipitates that clog the membrane pores and other issues as discussed in Chapter 2 (section *2.4.1.2*).

The three GW compositions discussed in section *4.1.1.6* are particularly chosen as they represent GW with low, typical and high scaling potential. Using the GW chemical analyses data of several wells in different areas in Egypt (Abdel-Shafy et al., 1992, Abd-El-Samie and Sadek, 2001, Masoud et al., 2003, Atta et al., 2005, Sturchio et al., 2005, Sharaky et al., 2007, Abdalla et al., 2009, Elewa and El Nahry, 2009, El Alfy, 2012), wells with water containing the lowest, average, and highest percentage of calcium, sulphate and bicarbonate ions are selected to represent each type of GW respectively[101] (*Table 4-3*).

Table 4-3: Chemical composition of GW with low, typical and high scaling potential

Major Ions	Low scaling potential GW composition	Typical scaling potential GW composition	High scaling potential GW composition
Na	21%	16.8%	14.1%
Ca	7.4%	11.9%	13.8%
Mg	5.5%	5.4%	2.8%
K	0.45%	0.4%	0.9%
Cl	63.7%	38.9%	17.9%
SO_4	1.1%	20.1%	46.3%
HCO_3	0.8%	6.5%	4.2%
SiO_2	1 mg/l	20.2 mg/l	50 mg/l
PO_4	0 mg/l	0.1 mg/l	3 mg/l
Sr	1 mg/l	6.5 mg/l	22.5 mg/l

Notes: The percentages given are with respect to the sum of major ions only.

It should be noted however, that because silica, strontium and phosphate content is not reported in most wells, the maximum, average, and minimum concentration of each element in the reviewed wells are assigned to the high, typical and the low scaling potential GW respectively.

A chemical simulation software is then used to determine the maximum attainable RR that could be attained without scaling issues after the use of scale inhibitors and acid dosing. Given that the solubility limit of different ions in water varies with temperature, the maximum attainable RR is examined at the expected water temperature range i.e. 20 to 40°C for the RO plant. For simplicity, the pH of water for all the considered GW compositions is initially assumed to be 7.7, the average value of the reviewed wells, and is reduced to 6.0[102] through sulphuric acid[103] dosing to limit scaling issues.

[101] Magnesium content is not considered in the high scaling potential case as the main limiting scalant is found to be calcium sulphate and calcium carbonate. For low scaling potential GW, only calcium content is considered as none of the most common scales would occur unless calcium is present in water regardless of sulphate and bicarbonate content, while barium and strontium contents, which can form scales with sulphate ions, are assumed to be negligible.

[102] Lower pH values may cause pipe corrosion (DOW Chemical Company 2013, pers. Comm., 8 Jun.)

Finally, it should be noted that while iron and manganese in addition to barium, whose concentration is not reported in all of the reviewed wells, could cause major fouling issues with the RO membranes, they are not considered in this study to be a RR limiting factor. This is because iron and manganese are typically removed during the pre-treatment phase as discussed in Chapter 2 (section *2.4.1.2*). Conversely, because barium sulphate is the most insoluble sulphate scale in water (DOW Chemical Company, 2014b), it is found, using the chemical simulation software, that even with scale inhibitors small concentrations of Barium significantly reduced the maximum attainable RR and therefore it is better to be removed during pre-treatment either through lime softening or ion exchange (DOW Chemical Company, 2013g).

4.1.2 System configuration

4.1.2.1 Diesel generator driven RO plant

In remote areas away from the grid, DG's are typically used in Egypt which could be particularly observed in most of the oil fields located in the desert areas[104]. This is especially true given that diesel is heavily subsidized by the GOE (section *4.1.5.2*). For this reason, in this study an RO plant driven by a DG represents the base case as the latter is suitable for decentralized applications away from the Nile valley and delta.

The system configuration is shown in *Figure 4-1*. The brackish GW is extracted from the well then mostly goes to the RO plant where the water is desalinated and stored in the permeate tank. The remaining portion of the extracted water is mixed with the RO plant permeate water in the permeate tank. The RO concentrate is discharged to a deep injection well. The DG supplies the electricity necessary for GW extraction and the RO plant.

[103] While hydrochloric acid (HCl) might be a better option to lower pH compared to sulphuric acid as it does not add sulphate ions to the water, the latter is more readily available and easier to handle (Prihasto et al., 2009, DOW Chemical Company, 2013g) and therefore suits remote area applications (Kucera, 2010d).

[104] Personal observation by the author from his previous work experience in oil industry

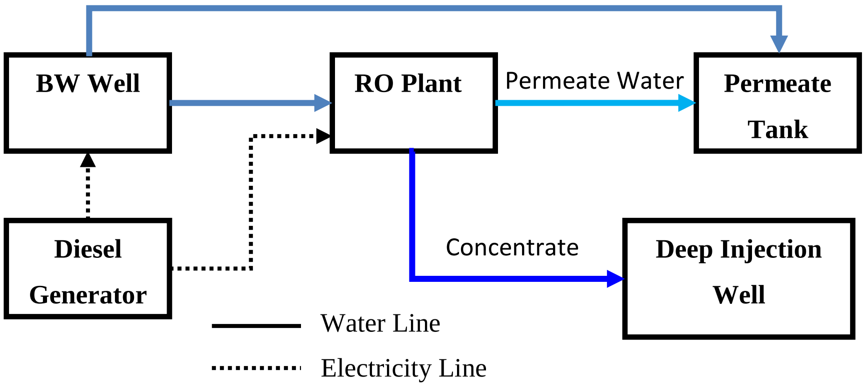

Figure 4-1: Schematic diagram of a DG driven RO plant

4.1.2.2 PV driven RO plant

The PV driven RO plant is similar to the base case, however the DG is replaced by a PV system with battery storage as shown in *Figure 4-2*.

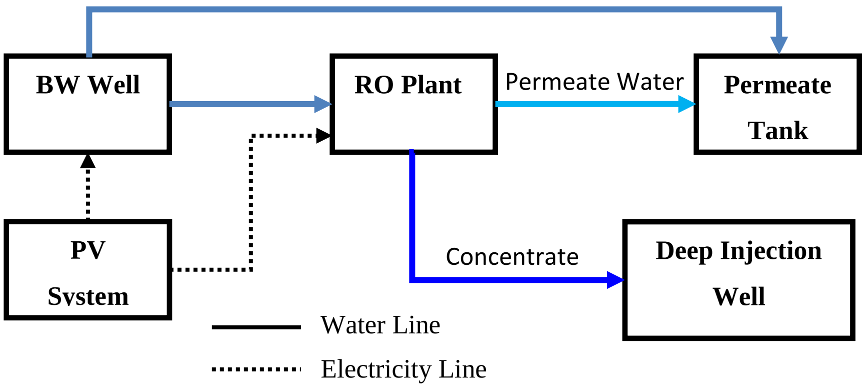

Figure 4-2: Schematic diagram of a PV driven RO plant

4.1.3 RO plant modelling and design

In this study, the RO plant is modelled using the ROSA software (DOW Chemical Company, 2013e). Using this existing commercial modelling software is preferred to building a new model because, while the latter gives more flexibility, ROSA is a mature commercial tool where calculations are based on the manufacturer's field experience which guarantees more accurate results.

The RO plant is designed to operate within the recommended operating specifications of the manufacturer which ensures a stable performance and minimizes the fouling potential where no more than 4 cleanings a year are likely to be needed (DOW Chemical Company, 2013d). The guidelines recommend the operating limits shown in

Table 4-4 when GW with SDI less than 3 is used with different types of the 8 inch RO DOW FILMTEC modules used in this study.

Table 4-4: Recommended operating limits for the DOW FILMTEC 8 inch RO Modules

Max. Permeate Flow Rate	1.58 m^3/h	**Min. Concentrate Flow Rate**	2.95 m^3/h
Average RO System Flux	27.2-34 $l/m^2/h$	**Max. Module RR**	19%
Max Feed Flow Rate	17.03 m^3/h for BW 440 ft^2 modules	**Max. Feed Pressure**	41.37 bar for BW modules
	17.99 m^3/h for SW 440 ft^2 modules		82.74 bar for SW modules

To ensure that the designed RO plant will not operate beyond the recommended limit, a safety factor of 5% is used for the maximum permeate flow and feed pressure and 10% for the RR and the minimum concentrate flow.

In all designs booster pumps are used to uniformly distribute, as much as possible, the permeate flow over the RO modules in the plant which helps to attain the highest possible RR without exceeding the recommended operating specifications. It should be noted that high RR operation could be also achieved through recirculating the concentrate flow; however such measure may not be practical due to the difficulties in determining the required dose of scale inhibitors (P. Roginson, 2013, pers. Comm., 27 Jul.).

Given that the RO plants are designed for a range of feed water salinities and temperatures, the designs must be consistent to ensure that they can be fairly compared. For example, operating the RO plant at a small flux reduces the SEC on the expense of using larger number of modules which increases the costs, and vice versa. Moreover, using RO modules with high salt rejection would improve the permeate quality on the expense of increasing the SEC, and vice versa.

For this reason the RO plants are designed based on the following criteria:

- The number of RO modules is selected such that the flux is in the range of 30 $l/m^2/h$ for all designs
- Uniformly distributing the permeate flow over every RO module in the plant as much as possible using booster pumps

- The RO module type, i.e. degree of salt rejection, and the RO array configuration, i.e. number of modules in series and pressure vessels in each stage, are chosen to minimize the SEC
- The RO module type and the RO array configuration are also determined such that the maximum permeate flow produced by each module is close as possible to, but not exceeding 1.5 m^3/h which is 95% of the maximum recommended permeate flow rate limit
- The RO module types are also chosen such that the permeate water salinity does not exceed 100 mg/l

Accordingly, for each design various configurations of RO module types and configurations are considered until the aforementioned criteria are satisfied. An example of an RO design is shown in Appendix F.

4.1.3.1 Recovery rate

The initial RO RR is set to be the lowest of that calculated based on the maximum recommended concentrate salinity and that limited by scaling. If it is not possible to obtain a design satisfying the criteria discussed in the previous section and operating within the manufacture’s operating specifications, then the plants are re-designed to operate at a 5% lower RR.

4.1.3.2 Flow factor

The flow factor considers the long term reduction in the nominal permeate water flow rate due to reversible and irreversible fouling in addition to membrane aging (DOW Chemical Company, 2012). Based on the DOW guidelines, the RO plant should be designed to operate within the recommended specifications at both a flow factor of 1 and 0.75. The former value applies for a newly operated RO plant where there is a great risk of exceeding the maximum recommended permeate flow, while the latter value accounts for the reduction in permeate water flow after 3 years of operation due to membrane fouling where a larger feed pressure would be required to obtain the desired permeate water flow.

The RO plant power requirements used in sizing the energy supply are those estimated at a flow factor of 0.75 to ensure that the designed permeate flow can be obtained throughout the RO module lifetime.

4.1.3.3 Flow rates

The extracted GW, blended GW and the RO plant feed flow rates are determined based on the operating RR, the required water production, and the feed water salinity by simultaneously solving the following equations:

$$\dot{V}_{blend} = \dot{V}_{feed,GW} - \dot{V}_{feed,RO} \tag{4-3}$$

$$\dot{V}_{prod\_tot} = \dot{V}_{blend} + \dot{V}_{feed,RO} * RR_{RO} \tag{4-4}$$

$$S_{prod,max} = 0.5 = \frac{\dot{V}_{blend} * S_{GW} + \dot{V}_{feed,RO} * RR_{RO} * S_{RO,p}}{\dot{V}_{blend} + \dot{V}_{feed,RO} * RR_{RO}} \tag{4-5}$$

RR_{RO} is the RO plant RR which is determined as discussed in section *4.1.3.1*. S_{GW}, $S_{prod,max}$ and $S_{RO,p}$ are the GW, overall produced water, and RO permeate salinities respectively. While the RO permeate salinity will vary according to the RO plant design, e.g. the type of module and the feed water temperature, for simplicity the extracted GW, the blended GW and RO plant feed volumetric flow rates, $\dot{V}_{feed,GW}$, $\dot{V}_{blend}$, and $\dot{V}_{feed,RO}$ respectively, are estimated based on a constant permeate salinity of 50 mg/l. As discussed in section *4.1.1.2*, the overall produced water salinity should not exceed 500 mg/l and therefore $S_{prod,max}$ is set to be equal to 500 mg/l. $\dot{V}_{prod\_tot}$ is the overall produced water volumetric flow rate of the desalination plant and as discussed in section *4.1.1.1*, should be at least 500 m^3/d.

4.1.3.4 High pressure pump efficiency

Finally, while within the expected operating conditions, motor-pump efficiencies ranging from 85 to 95% could be attained commercially, e.g. with the DANFOS APP axial piston pumps (Danfoss, 2014), a conservative value of 70% is used in this study to account for the worst case where lower quality pumps might be only available in the local market.

4.1.4 Photovoltaic system design

The PV energy supply consists of the PV modules, the battery bank, the solar inverter and the interactive inverter which acts as a battery charge controller and also supplies to AC signal required for the solar inverter to operate (*Figure 4-3*).

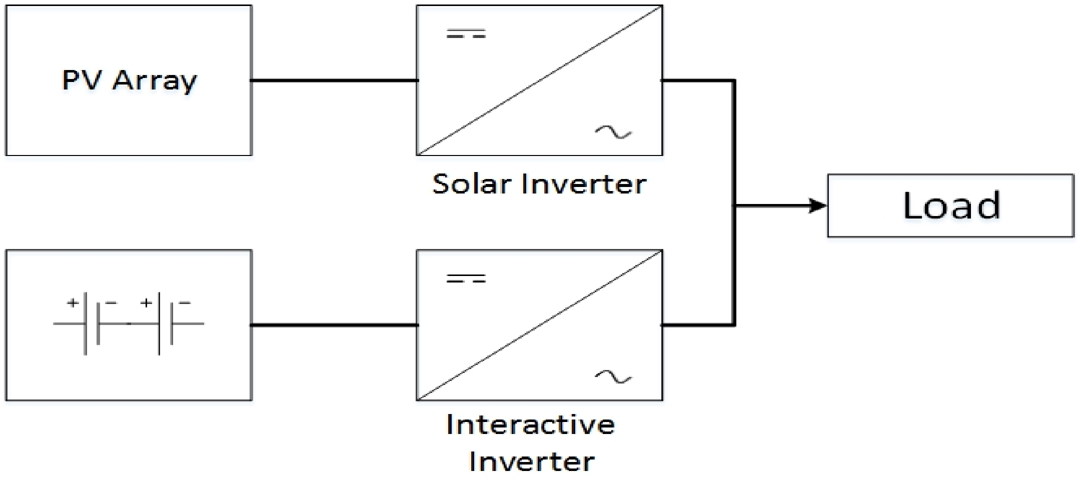

Figure 4-3: Simplified schematic diagram of the PV energy supply

The diagram is modified after the AS/NZS 4509.2 Australian standards (Committee EL-042, 2010)

In this study, PVSYST simulation tool is used to design and model the PV energy supply. PVSYST performs yearly simulations using hourly weather data which are more accurate over manual calculations using average monthly or yearly irradiation data. PVSYST also performs detailed analysis on the performance of the battery bank particularly in terms of the battery state of charge (SOC), which helps in obtaining more accurate battery sizing.

4.1.4.1 Weather data

Instead of using the default weather data in PVSYST, weather data from the weather library in TRNSYS is used. TRNSYS is a simulation tool that will be used to model the PVT collectors and the solar driven MD plant discussed in Chapter 5 and 7. Therefore, the same weather data is used such that there will be consistency in the results between the different desalination plants configurations considered in this study.

It should be noted that the default weather data in PVSYST for example is found to give a yearly global horizontal irradiation (GHI) 8.3% lower than that based on the TRNSYS weather data.

4.1.4.2 Operating hours

In this study the feasibility of a PV driven RO plant is investigated under daytime only operation, and 24 hours operation. In the first case, the PV-RO plant operates only during daytime and for 8 hours on average to match the typical irrigation practices in Egypt (Sultan et al., 2007). In this case, the battery bank is only used for power conditioning to ensure that the RO modules keep operating within their recommended operating specifications as discussed in Chapter 2. Accordingly, the battery bank and the array sizes are minimized which reduces the system costs and its maintenance requirements; that in addition to reducing the environmental hazards associated with battery disposal. However, the RO plant in this case has a low capacity factor[105] which is expected to increase the life cycle unit water costs.

In the second case, the PV-RO plant operates the whole day, i.e. 24 hours, which increases the capacity factor of the plant but on the expense of requiring a larger battery bank and array size.

4.1.4.3 Battery sizing

The battery bank capacity for both the day only and 24 hours operation cases is designed such that the maximum depth of discharge (DOD) does not exceed the typical recommended value of 70% (GSES, 2009).

While for standalone designs, 4 to 5 days of autonomy are usually recommended for PV driven loads (Committee EL-042, 2010), as the battery bank in the daytime only operation case is only used for power conditioning, it is designed to cover only 40%[106]of the daily energy requirements of the RO plant. For the day and night operation, the battery bank is selected to provide one day of autonomy assuming that it will be more economical to store water needed for urgent uses, i.e. domestic purposes, in cloudy days rather than over sizing the battery bank. With such smaller battery sizes, the number of hours at which the battery bank will not be able to supply the load due to

---

[105] The ratio between the actual water/electricity produced and the maximum water/electricity that could be produced if the plant is operating continuously during the same period (The U.S. Nuclear Regulatory Commission, 2014)

[106] This value was particularly chosen as it is found to give the minimum battery bank and array size that satisfies the maximum DOD considered in this study

low SOC, particularly during cloudy days, is expected to increase which will be examined during the analysis.

4.1.4.4 Array sizing

The PV array is designed based on the module specifications of the SUNTEC STP305 module (*Table 4-5*). The U-value used to calculate the thermal losses, hence the array temperature, is assumed to be constant at 29 $W/m^2.K$ based on PVSYST recommendation for free standing arrays which is based on the assumption of a constant wind velocity due to the lack of reliable data on the coefficient of wind velocity[107] (PVSYST, 2013a). As Egypt is mostly a desert area, a soiling de-rating factor of 10% is assumed to account for the losses caused by the expected dust accumulation on the module cover.

To maximize the battery life time, the array size is chosen such that the monthly average daily SOC does not go below 80% (GSES, 2009). Finally, to account for the module performance degradation over its lifetime, the array is oversized by 10%. It should be also noted that another 5% safety factor was applied on the overall power demand by the RO plant and by the GW pump.

4.1.4.5 Module orientation and operating hours

The module orientation and the exact operating time of the RO plant[108] are chosen such that the incident solar irradiation in each month matches the load energy requirements as much as possible to minimize the required battery bank capacity and array size. In this case, the system operates more efficiently particularly in terms of minimizing the wasted PV array energy when the batteries are fully charged and the number of hours when the PV system cannot meet the load energy requirements.

In this case, using PVSYST, several module orientations and operating hours are examined. For the day only operation case, it is found that tilt angles of 18 and 38° for Aswan and Marsa-Matruh respectively give the best match between the available solar irradiation and the load energy requirements.

[107] The coefficient used to estimate the wind heat losses as a function of the wind velocity
[108] Applies only when the RO plant is designed to operate only during daytime

Table 4-5: Parameters used in designing the PV energy supply

	PV Module Specifications[109]	
Vmpp (STC)	36.2 V	Module specifications based on the Suntech STP305-24/Ve commercial PV module
Impp (STC)	8.43 A	
Voc (STC)	44.7 V	
Isc (STC)	8.89 A	
Isc Temperature Coefficient (STC)	5.956 mA/°C	
Voc Temperature Coefficient (STC)	-168.5 mV/°C	
Max. Power Temperature Coefficient (STC)	-0.43%/°C	
Module Efficiency (STC)	15.7%	
Packing factor	0.9	
U_L	29 W/m^2.K	(PVSYST, 2013a)
Module Cover Transmittance	0.92	(Bilbao and Sproul, 2012a)
Module Absorption Coefficient	0.9	(PVSYST, 2013a)
Battery Specifications		
Battery Voltage	2 V/Cell[110]	Specifications are based on the Excide OPzS Solar 4600 battery[111]
Battery capacity	3450 Ah	
DOD Max	70%	(GSES, 2009)
Max Monthly Average Daily DOD	20%	
	Array De-rating Factors	
Mismatch Losses	2%	-
Manufacturer Tolerance	3%	-
Cable Losses	2%	-
Annual Soil Losses	10%	-
	Equipment Efficiencies	
Inverter Efficiency	95%	(Jacobson et al., 2013)
Battery Energy Efficiency	80%	(Tzen et al., 1998, GSES, 2009, Rehman and Al-Hadhrami, 2010, Jacobson et al., 2013)
Battery Columbic Efficiency	90%	(GSES, 2009)

[109] Module specifications are based on the Suntech STP305-24/Ve commercial PV module which, according to the manufacturer, is designed for open space systems. Data sheet can be accessed at http://file4.fanyacdn.com/imglibs/files/STP305_Ve(H4_305_300_295).pdf

[110] The battery is sold in one cell units and the batteries are then connected in series to attain higher voltages

[111] Battery model details could be found at http://www.exide.com/Media/files/Downloads/IndustEuro/Classic%20Solar.pdf

The suitable operating hours for each season and each city are shown in *Table 4-6* which as expected increase in seasons with high solar irradiation and therefore matches the expected increase in water consumption caused by the high ambient temperature[112]. It should be noted that the operating hours are varied such that their daily average is always 8 hours. For the 24 hours operation case, the optimal module orientation is found to be 52 and 26° for Marsa-Matruh and Aswan respectively.

Table 4-6: Optimal operating hours of the RO plant when designed to operate only during daytime

Season	Operating Time	Total Hours
Aswan (HSI Zone)		
Summer & Spring	7:30 to 16:00	8.5
Autumn & Winter	8:00 to 15:30	7.5
Marsa-Matruh (LSI Zone)		
Winter	7:30 to 14:00	6.5
Spring & Summer	7:30 to 16:30	9
Autumn	7:30 to 15:00	7.5

4.1.5 Cost analysis

In this study, the levelized cost of water (LCOW) is used to assess the feasibility of the different desalination plant configurations considered in this study. The LCOW is the cost necessary such that the present value of the income obtained from selling the water covers the system capital and operating costs during the lifetime of the project (National Energy Technology Laboratory et al., 2013) and is calculated as follows (Kolhe et al., 2002, Ghosh et al., 2003, Al-Hallaj et al., 2006, Branker et al., 2011, Kost et al., 2013):

$$LCOW = \frac{LCC}{\sum_{j=1}^{LP} \frac{\dot{V}_{p,tot}}{(1+IR_r)^j}} = \frac{CC_{tot} + RC_{tot} + \sum_{j=1}^{LP} \frac{OC_{tot}}{(1+IR)^j}}{\sum_{j=1}^{LP} \frac{\dot{V}_{prod\_tot}}{(1+IR_r)^j}} \qquad \textbf{(4-6)}$$

where LCC is the life cycle cost, LP is the evaluation period which is taken to be the lifetime of the PV modules, CC_{tot} and RC_{tot} are the total capital and replacement costs of the equipment respectively, OC_{tot} is the total yearly maintenance and operation cost, $\dot{V}_{prod}$ is the overall annual water production of the desalination plant, and IR_r is

[112] Water evaporation losses are expected to increase in warmer seasons

the real interest rate and is calculated using equation *(4-7)* obtained from Koner et al. (2000).

$$IR_r = \frac{IR_n - f}{1 + f} \qquad \textbf{(4-7)}$$

where IR_n is the nominal interest rate and f is the inflation rate. The inflation is obtained from the central bank of Egypt website[113] (f=8.87%). For the interest rate, while the base value indicated in the central bank of Egypt website is 9.25%, a more conservative value of 13% is used. It should be noted that for calculating the fuel costs of the DG, the diesel prices escalation costs should be used instead of the inflation rate (Kolhe et al., 2002, Ghosh et al., 2003), but in this study it is assumed to be the same as the inflation rate.

The annual operation and maintenance cost as well as the annual water production are assumed to be constant. In this case the LCOW is calculated as follows:

$$LCOW = \frac{CC_{tot} + RC_{tot} + PWF * OC_{tot}}{PWF * \dot{V}_{prod}} \qquad \textbf{(4-8)}$$

where PWF is the present worth factor and is calculated as follows:

$$PWF = \frac{1}{IR_r} * \left[1 - \frac{1}{(1 + IR_r)^{LP}}\right] \qquad \textbf{(4-9)}$$

The capital cost is divided into direct and indirect costs. Direct costs are the costs associated with all the components of the system including construction and land costs. Indirect costs include, among others, construction overhead, contingency, engineering, insurance and administration costs as well as import duties, and are often estimated as a percentage of the direct capital costs (El-Dessouky and Ettouney, 2002, Ghaffour et al., 2013).

In this study, the cost of the land is assumed to be zero (Banat and Jwaied, 2008) as the analysed desalination systems are aimed for remote desert areas in Egypt. Furthermore, when no data is available, the indirect costs are assumed to be 30% of the direct capital

---

[113] http://www.cbe.org.eg/English/

costs which falls within the typical values reported in the literature (Wade, 2001, El-Dessouky and Ettouney, 2002, Drioli et al., 2006, Ghaffour et al., 2013).

The replacement cost of each asset RC_i is calculated as follows (Bhuiyan et al., 2000, Kolhe et al., 2002):

$$RC_i = CC_i \sum_{j=1}^{Y_i = \frac{LP}{LT_i} - 1} \frac{1}{(1+IR_r)^{j*LT_i}} \qquad \textbf{(4-10)}$$

where Y_i is the number of times the ith asset will be replaced during the lifetime of the project and LT_i is the lifetime of the ith asset.

4.1.5.1 PV system costs

The PV system consists of the PV modules, the mounting supports, the battery bank, the solar inverter and the interactive inverter[114] that in addition to the balance of system (BOS) which includes the wiring, instrumentation, and other electrical equipment such as switches and fuses.

In this study, the average market spot price of the PV module (*Table 4-7*), obtained from (PV Insights, 2013), is used after increasing it by 40% to estimate the retail price (The International Renewable Energy Agency, 2012).

For the solar inverter and the interactive inverter, the retail prices of commercially available inverters are used. A scaling factor is applied for the solar inverter based on the retail price of a 250 kW and 500 kW size inverters. Conversely, no scaling factor is used with the interactive inverter as it seems that this type of inverter, e.g. SUNNY ISLAND, is only available at small sizes and therefore several inverters need to be connected in parallel to meet the desired load. For the same reason, a slightly higher price per kW is used to account for the interconnection costs between the interactive inverters[115] and communication devices between the PV and the interactive inverter. The size of the PV inverter and the combined size of the interactive inverters are chosen to be 140% of the power required by the load after assuming a load power factor of 0.8

[114] Acts as a charge regulator

[115] For example the manufacturer supplies a multi-cluster box to interconnect several SUNNY ISLAND inverters with an overall capacity up to 180 kW

and 10% safety factor based on the AS/NZS 4509.2 standard design guideline (Committee EL-042, 2010).

Regarding the battery bank, numerous cost values are used in the literature ranging from 89 to 278 USD/kWh as shown in *Table 4-7*. While the retail price of the actual battery used in the modelling is 265 USD/kWh, a value of 200 USD/kWh is used in this study as a cheaper alternative is likely to be available locally without compromising the battery lifetime; especially that the battery bank is operating under a favourable condition in terms of the DOD with an average monthly value lower than 20%. Regarding the battery lifetime, while a typical lifetime of 10 years is expected (GSES, 2009) especially if the DOD is lower than 20% (The International Renewable Energy Agency, 2012), a conservative value of 5 years is used to account for the effect of high temperature in Egypt which is expected to reduce the battery lifetime by 50% (PVSYST, 2013b)[116].

For the operation and maintenance costs, including labour costs, different figures used in the literature (*Table 4-7*) are found to give similar annual costs except that of Dufo-López and Bernal-Agustín (2005) which gives much lower operating costs and is also independent of the system size. In this study, the annual operation cost is assumed to be 1.5% of the direct costs which give annual cost values close to the average of those calculated using the figure by Muselli et al. (1999), Koner et al. (2000) and Jacobson et al. (2013).

Finally, for the BOS and the site preparation and mounting costs, the figure by the International Renewable Energy Agency (2012) (*Table 4-7*) give a 4 to 5 times higher estimation than those estimated using the figures by Koner et al. (2000) and Mahmoud and Ibrik (2006). The figure by the International Renewable Energy Agency (2012) is estimated based on data compiled from existing PV systems in the United States where higher labour costs and materials are expected hence the figure is likely to overestimate the BOS costs for a PV system installed in Egypt. Conversely, the figure by Koner et al. (2000) seems to underestimate the costs given that the construction costs alone could reach 25% of the module costs (Muselli et al., 1999).

[116] A 50% reduction in the lifetime of the battery is expected for every 10°C increase in ambient temperature above 20°C

Therefore, in this study the BOS cost including construction costs is assumed to be 35% of the total equipment costs which gives a cost estimation that falls between those calculated using the figure by the International Renewable Energy Agency (2012) and that of Mahmoud and Ibrik (2006).

Table 4-7: PV system capital and operating costs available in the literature and the actual values selected for the cost estimation

	Cost/Lifetime	**Reference**	**Value Used**
	Capital Costs		
Polycrystalline Silicon Module	0.66 USD/Wp	(PV Insights, 2013)	0.924 USD/Wp
Solar Inverter	300 USD/kVA[117] (250 kW size) & 260 USD/kVA[117] (500 kW size)	(EnergyBay, 2014a)	300 USD/kVA Scaling factor=0.8 Base Capacity=250 kVA
	570 USD/kW (10 kW size) & 230 USD/kW (100 kW size)	(The International Renewable Energy Agency, 2012)	
Interactive Inverter	830 USD/kVA[117] (5 kW capacity)	(EnergyBay, 2014b)	900 USD/kVA
Batteries	89 USD/kWh (Lead Acid)	(Arun et al., 2008)	200 USD/kWh
	82 USD/kWh[118] (battery type not specified)	(Kolhe et al., 2002)	
	150 USD/kWh (Battery type not clear but likely to be lead acid)	(The International Renewable Energy Agency, 2012)	
	124 USD/kWh (battery type not specified)	(Bhuiyan et al., 2000)	
	130 to 217 USD/kWh (battery type not specified)	(Muselli et al., 1999)	
	113 to 256 USD/kWh[119] (battery type not specified)	McLennan Magasanik and Associates (2009) cited in (Jacobson et al., 2013)	
	1329 USD[120]/524 Ah 12V Battery (211 USD/kWh) (Battery type not clear but likely to be lead acid)	(Dufo-López and Bernal-Agustín, 2005)	
	265 USD/kWh (2443.5 USD/unit)[121] (Lead Acid)	(MERKASOL, 2014)	
	278 USD[122]/kWh (Battery type not clear but likely to be lead acid)	(Tzen et al., 1998)	

117 The commercial inverter has a power factor of 1 hence the real power=apparent power
118 Original cost given in Indian Rupees and is converted to USD based on the 2002 exchange rate
119 Original cost given in AUD and is converted to USD based on the 2009 exchange rate
120 Original cost given in Euros and is converted to USD based on the 2005 exchange rate
121 Original cost in Euros converted to USD using 1.387 conversion rate
122 Original cost given in Euros and is converted to USD based on the 1999 exchange rate

Balance of System including construction costs	5-10% of the PV array cost	(Koner et al., 2000)	35% of the equipment cost
	0.25 USD/Wp (25kWp system)	(Mahmoud and Ibrik, 2006)	
	1.35 USD/Wp for ground mounted systems	(The International Renewable Energy Agency, 2012)	
Operating Costs			
Maintenance Costs	63 USD/year[123] for battery bank size ranging from 13.8 to 346 kWh + 50 USD/year for PV array size ranging from 5.6 to 17.6 kWp	(Dufo-López and Bernal-Agustín, 2005)	1.5% of the direct cost for the PV system
	926 USD/year & 1,482 USD/year for a battery bank with 50 & 100 battery units respectively. 3,162 USD/year &15,808 USD/year for a 100 & 500 kWp PV array respectively	(Jacobson et al., 2013)	
	0.5-2.4% of the PV system direct cost	(Koner et al., 2000)	
	2% of the PV system direct cost	(Muselli et al., 1999)	
	10 USD/Battery/year 50 USD/kW/year for the PV system	(Rehman and Al-Hadhrami, 2010)	
Insurance Annual Costs	0.5 % of the total capital cost	(Drioli et al., 2006)	0.5% of the total capital costs
Equipment Lifetime			
Battery	5 years	(Arun et al., 2008, Ahmad and Schmid, 2002, Muselli et al., 1999, Rehman and Al-Hadhrami, 2010)	5 years
	6 years	(U.S. Department of Energy, 2011)	
	5 to 8 years	(Richards and Schafer, 2002)	
	7 years	(Tzen et al., 1998)	
	10 years	(Jacobson et al., 2013)	
	15 years	Lifetime of the Enersol OPzS battery used in this study (MERKASOL, 2014)	
Inverter	10 years	(Arun et al., 2008, GSES, 2009, U.S. Department of Energy, 2011)	-

[123] Original cost in Euros then converted to USD using 2005 exchange rate then value converted to today's USD value

PV Module	20 years	(Tzen et al., 1998, Al Suleimani and Nair, 2000, de Carvalho et al., 2004, Laborde et al., 2001, De Munari et al., 2009)	-

4.1.5.2 Diesel generator costs

A wide range of values is reported in the literature (*Table 4-8*) for the capital costs of the DG. The correlation by developed by Muselli et al. (1999) to estimate the specific cost of the DG was found to significantly underestimate the cost for large generator sizes (i.e. 200 kW). Conversely, the specific costs used by Jacobson et al. (2013) seem to be exaggerated especially when compared to typical online retail prices. In this study, the values indicated by the Australian Greenhouse Office (1999) cited in (Jacobson et al., 2013) are used as they seem to be more consistent with online retail prices[124]. Moreover, as a conservative approach, the BOS is assumed to be included with the generator purchase cost. The generator size, i.e. real power, is chosen to be 110% of the load.

The diesel prices in Egypt are currently heavily subsidized where the selling price is approximately 6 times lower than the actual price (Ministry of Petroleum of Egypt, 2014, pers. Comm., 7 May). The subsidized and unsubsidized fuel costs are considered in this study. In both cases, as the diesel prices are expected to be higher in rural/remote areas due to the transportation costs (Lau et al., 2010)[125], in this study the prices are increased by 20%.

The fuel consumption of the DG is estimated based on the calculations used in TRNSYS. The calculations uses fuel efficiency curves based on the average of 5 generator sets and incorporates a correction factor based on actual fuel consumption measurements of several generator systems with average power ranging from 5 to 186 kW[126].

[124] Online retail prices could not be used as they show wide variations and some prices are for used DG's or low quality ones.
[125] Lau et al. (2010) reported that the diesel costs in a remote inland area in Malaysia is 4 times higher than in urban areas
[126] The value calculated using TRNSYS approach was tested and gave a similar value to that indicated by a commercial DG

Regarding the annual maintenance cost, the figures used by Jacobson et al. (2013) seem to exaggerate the costs which is likely because it was used for DG systems in Australia where high labour costs are expected. Conversely, the value used by Rehman and Al-Hadhrami (2010) gives an unrealistically low annual O&M cost. The figures used by Lau et al. (2010) and Biermann et al. (1995) cited in (Ghosh et al., 2003), and the correlation developed by Muselli et al. (1999) give close annual maintenance cost. In this study the correlation developed by Muselli et al. (1999) is used to estimate the annual maintenance cost as it takes into account the effect of the generator size on the costs.

Regarding the DG lifetime, a wide variation in the values is also reported in the literature (*Table 4-8*). It should be noted that the lifetime of the generator depends on its type, where low speed generators (1,500-1,800 RPM) last more due to slower wear of its components (Muselli et al., 1999). In this study, conservative values of 10 and 7 years are used for daytime only, and 24 hours operation cases respectively.

Table 4-8: DG system capital and operating costs available in the literature and the actual values selected for the cost estimation

	Cost/Lifetime	Reference	Value Used
	Capital Costs		
DG Capital Cost	199 USD/kW & 133 USD/kW for generator capacities of 100 & 500 kW respectively	Australian Greenhouse Office (1999) cited in (Jacobson et al., 2013)	199 USD/kW Scaling factor=0.75 Base Capacity=100 kW
	593 USD/kW & 494 USD/kW for a capacity of 50 & 100 kW respectively.	(Jacobson et al., 2013)	
	3362.2 (Prated)$^{-0.7184}$ USD/kW (1,500 RPM DG)	(Muselli et al., 1999)	
BOS including transportation	Included with the generator costs		
	Operating Costs		
Fuel Cost	0.157 USD/l after incentives 0.935 USD/l before incentives	(Ministry of Petroleum of Egypt, 2014, pers. Comm., 7 May)	0.157 USD/l after incentives 0.935 USD/l before incentives +20% for transporting the diesel
Operation & Maintenance Cost	4.7 USD/h & 8.9 USD/h for a 50 &100 kW generator size	(Jacobson et al., 2013)	Using the correlation developed by Muselli et al. (1999)
	0.025 USD/h/kW (50 kW generator)	(Lau et al., 2010)	

	5 to 20% of the total capital cost	(Biermann et al., 1995) cited in (Ghosh et al., 2003)	
	$\frac{[0.242 + 0.3505 * P_{DG}] * 15.2}{600}$ USD/h	(Muselli et al., 1999)	
	0.012 USD/h (150 to 2500 kW rated power)	(Rehman and Al-Hadhrami, 2010)	
Insurance Annual Costs	0.5 % of the total capital cost	(Drioli et al., 2006)	0.5% of the total capital costs
	Equipment Lifetime		
DG Lifetime	7,000 hours	(Dufo-López and Bernal-Agustín, 2005)	10 years for day operation case 7 years for 24 hours operation case
	10,000 hours (1500 RPM DG)	(Muselli et al., 1999)	
	6 years	(Kolhe et al., 2002)	
	20,000 hours (DG unspecified)	(Rehman and Al-Hadhrami, 2010)	
	5 to 10 years	(Al Suleimani and Nair, 2000)	
	30,000 hours	(Saengprajak, 2007)	
	13 years	(Mahmoud and Ibrik, 2006)	
	60,000 hours	(Jacobson et al., 2013)	

4.1.5.3 RO plant costs

The RO plant capital costs include the RO process equipment (e.g. RO modules, pressure vessels and pumps), the pre-treatment and post treatment equipment, and construction costs (El-Dessouky and Ettouney, 2002), that in addition to the indirect costs.

Unless detailed cost breakdown is available, the capital cost of the RO plant is usually determined using specific costs with respect to the plant capacity. Miller (2003) used a value of 1 USD per gallon per day (approximately 264 USD per 1 m^3/d), obtained from Pittner et al. (1993), to estimate the RO process equipment costs for a BW RO plant. For the pre-treatment and post-treatment equipment, and construction costs, they were estimated to be 30% and 30-50% of the RO process equipment costs, and 30% of the total equipment costs, respectively. It is not clear, however, whether the aforementioned values include the indirect capital and brine discharge costs. Fiorenza et al. (2003) used a figure of 1000 USD per 1 m^3/d to estimate the total capital cost (direct and indirect costs) for a SW RO plant with 10,000 m^3 capacity and used a scale factor of 0.9 to estimate the costs for other plant capacities. The authors, however, did not clarify the method by which the aforementioned figure was estimated. Hafez and El-Manharawy (2003) listed a detailed cost breakdown of an actual 500 m^3/d SW RO plant in Egypt and estimated its specific capital cost to be 2095 USD per 1 m^3/d of plant capacity.

In this study the costs indicated by Hafez and El-Manharawy (2003) are used for the following reasons: the cost figures are for an actual RO plant located in Egypt which guarantees more realistic costs; the plant has an almost similar capacity to that analysed in this study hence the costs can be used directly without applying scaling factors; and the costs include all of the equipment related to the RO plant including the deep injection well used for brine discharge.

It should be also noted that in the author's opinion, it is not accurate to directly use the specific RO plant costs reported in the literature as they are given with respect to the plant production capacity while RO plants even those with similar capacities operate at different RR's, and in this study even at different operating hours, which affects the size of the process equipment. For example, a 500 m^3/d capacity RO plant operating at 40% RR would require larger pumps, more pre-treatment equipment (e.g. more cartridge filters or MF modules) and more RO modules than an RO plant with the same capacity but operating at 70% RR. Therefore, great caution should be taken when using the specific cost figures commonly used in the literature particularly with BW RO plants where the RR would significantly vary depending on the feed water salinity. In this case, the RR of the plant discussed in Hafez and El-Manharawy (2003) is known and accordingly the actual process equipment size could be estimated more accurately as follows: the specific costs of the pre-treatment process equipment and pumps, infrastructure and indirect costs are calculated with respect to the feed water flow rate; the specific cost of the post-treatment process equipment is calculated with respect to the plant capacity, i.e. permeate water; and the specific cost of the brine discharge process is calculated with respect to the concentrate flow rate. The cost of the RO modules and pressure vessels is calculated separately using the current retail prices (*Table 4-9*).

It should be noted that some process equipment included in the cost breakdown in Hafez and El-Manharawy (2003) such as the settling equipment, media filtration and

ERD’s are not included as they are not needed when brackish GW is the feed water as discussed in Chapter 2 (section *2.4.1.2*). The cost of well construction is also calculated separately using the figure indicated by El-Dessouky and Ettouney (2002), i.e. 650 USD/m, which is for a well with 20.8 m^3/h capacity. A scaling factor of 0.9 is then used to estimate the cost at different capacities. The well depth is roughly assumed to be 1.5 times[127] that of the depths to GW in the LSI zone where the aquifers are mainly unconfined based on the data shown in Appendix E. In the HSI zone, average well depths of 250 m and 750 m are assumed when the GW is accessed from the Nubian aquifer in the eastern and western desserts, and the Sinai Peninsula, respectively. For the areas where the Nubian aquifer is unconfined or could be tapped from the Quaternary aquifer such as in Wadi Asyuti, the well depth is assumed to be 1.5 the depth to the water table.

The operating costs include that of labour, RO module replacement, chemicals, and maintenance and spare parts costs (Porteous, 1984, Ghaffour et al., 2013). The labour costs for the 500 m^3/d capacity SW RO plant discussed in Hafez and El-Manharawy (2003) is used in this study as the plant is in Egypt hence the labour costs are more realistic and there is no need to apply a scale factor[128].

For maintenance and spare parts (excluding RO module replacement costs), the annual costs shown in Hafez and El-Manharawy (2003) for the 500 m^3/d capacity SW RO plant were approximately 7.5% of the plant total capital costs. In other studies, such as (El-Dessouky and Ettouney, 2002, Fiorenza et al., 2003), a figure of 2% is used. In this study, a conservative value of 5% of the total capital cost is used rather than 7.5% as it is expected that the maintenance and spare part costs for a BW RO plant to be lower than those of a SW RO plant as it has less equipment particularly for pre-treatment.

Regarding the pre-treatment chemical costs, as the GW has variable composition in contrast with SW, in this study the costs are will depend on the considered GW composition where the dosage is determine using a chemical simulation software. It

[127] Roughly estimated from the GW depth data reviewed in Chapter 2

[128] The significance of the effect of scale on the labour costs can be observed from the specific daily labour costs used by Drioli et al. (2006) and El-Dessouky and Ettouney (2002) for SW RO plants with capacities of 12,423 and 94,625 m^3/d respectively which are 4 to 6.5 folds lower than that shown in Hafez and El-Manharawy (2003).

should be noted that it is assumed that pre-chlorination (hence de-chlorination) is not needed due to the low bio-fouling potential of the GW.

Other equipment cost and lifetime and operating costs used in this study are shown in *Table 4-9*.

Finally, in this study the RO plant availability is assumed to be 95% for the daytime only operation case as a conservative value to account for the times of low solar irradiance when the battery bank SOC goes below 30%. For the 24 hours operation case lower plant availability of 90% is used to account for the downtime needed for chemical cleaning of the RO modules.

Table 4-9: Capital and operating costs of the RO plant available in the literature and the actual values selected for the cost estimation

Component	Cost/Lifetime	Reference	Value Used
Equipment Capital Costs			
RO Module Cost	30 USD/m^2 (i.e. 1226 USD/440 ft^2 RO module)	(Ettouney et al. 2002) cited in (Macedonio et al., 2007)	630 USD/unit for BW module type 820 USD/unit for SW module type
	575-630 USD/Unit BW Module Type 685-820 USD/Unit SW Module Type	Online retailers[129]	
	700 to 900 USD/module	(Hafez and El-Manharawy, 2003)	
	500 to 1000 USD/module	(El-Dessouky and Ettouney, 2002)	
Pressure Vessel	1529, 1739 and 2539 USD for a 6 module PV with maximum pressure of 31, 41 and 69 bar respectively	Online retailers[130]	1.2*1529 USD/PV (max pressure 31 bar) 1.2*1739 USD/PV (max pressure 41 bar) 1.2*2539 USD/PV (max pressure 69 bar)[131]

[129] http://www.thefind.com/appliances/info-filmtec-seawater-membrane
http://www.bigbrandwater.com/
http://www.shop.discountedwaterfilters.com/main.sc
http://www.thepurchaseadvantage.com/
http://www.kfswater.com/membranes/membranes.asp
http://americanro.com/1772776.html
[130] http://www.thepurchaseadvantage.com/page/tpa/CTGY/codeline_side_entry_ro_pressure_vessels

Pre-treatment Equipment Cost	666 USD per 1 m^3/h of feed water	(Hafez and El-Manharawy, 2003)	-
Post-treatment Equipment Cost	141 USD per 1 m^3/h of produced water		-
RO Equipment Cost excluding RO modules and vessels	1847 USD per 1 m^3/h of feed flow		-
Brine Discharge Capital Cost	905 USD per 1 m^3/h of concentrate flow		-
Infrastructure Costs	3793 USD per 1 m^3/h of feed water		-
Indirect Costs	934 USD per 1 m^3/h of feed water		-
Well Costs	650 USD/m (20.8 m^3/h capacity	(El-Dessouky and Ettouney, 2002)	650 USD/m Scaling factor=0.9 Base Capacity=20.8 m^3/h
Operating Costs			
Maintenance & Spare parts (not including RO module replacement)	0.033 USD/m^3 of plant capacity	(Drioli et al., 2006)	5% of the total capital costs
	2% of the total plant capital cost	(El-Dessouky and Ettouney, 2002, Fiorenza et al., 2003)	
	Approximately 7.5 % of the total plant capital cost	(Hafez and El-Manharawy, 2003)	
Labor	0.03 USD/m^3 of RO produced water per day[132] (plant capacity 12,423 m^3/d)[133]	(Drioli et al., 2006, Macedonio et al., 2007)	0.2 USD/m^3 per day
	0.05 USD/m^3 of RO produced water per day[132] (RO plant capacity 94,625 m^3/d)[133]	(El-Dessouky and Ettouney, 2002)	
	0.2 USD/m^3 of RO produced water per day[132] (plant capacity 500 m^3/d)[133]	(Hafez and El-Manharawy, 2003)	
Post-treatment Chemicals	0.091 USD/m^3 of RO produced water per day (500 m^3/d plant)[133]	(Hafez and El-Manharawy, 2003)	0.091 USD/m^3 of total[134] produced water per day

[131] The pressure vessel price is increased by 20% as it seems the original prices include special discounts that may not be normally available. The prices indicated are also for 6 modules pressure vessels and for simplicity will be used for all pressure vessels regardless of its number of modules

[132] To get the annual costs, the specific cost is multiplied by the annual produced water

[133] Calculated assuming a plant availability of 0.9

Brine Disposal operating costs	0.0142 USD/m^3 of brine per day[133]	(Hafez and El-Manharawy, 2003)	-
Insurance Annual Costs	0.5 % of the total capital cost	(Drioli et al., 2006)	0.5% of the total capital costs
Pre-treatment chemicals Costs			
Scale Inhibitors	1.9 USD/kg	(El-Dessouky and Ettouney, 2002)	6.6 USD/kg
	6.6 USD/kg	(pers.Comm., ROB GOODLETT, 21 Jan. 2014)	
	8.8 USD/kg	(Kucera, 2010c)	
Acid	0.504 USD/kg	(El-Dessouky and Ettouney, 2002)	0.6 USD/kg
	0.6 USD/kg	(Kucera, 2010c)	
Equipment Lifetime			
Pressure Vessel Lifetime	Replaced after 3 to 4 RO module changes	(BCC Research, 2009)	4 module changes (i.e. 20 years)
RO Module Lifetime	2 to 5 years	(Thiesen, 2007)	4 years
	3 year	(El-Kady and El-Shibini, 2001, Laborde et al., 2001, Drioli et al., 2002, Miller, 2003)	
	> 3 years	(DOW Chemical Company, 2013c)	
	5 years	(Wade, 1993, AWWA Research Foundation Staff et al., 1996, Ahmad and Schmid, 2002, Drioli et al., 2002)	
Pump Lifetime	15 to 20 years	(Hydraulic Institute et al., 2001)	20 years
	20 years	(Richards and Schafer, 2003)	

[134] Total produced water includes that obtained by blending GW

4.2 Results and Discussion

4.2.1 RO plant maximum recovery rate

Without considering the limiting effect of scaling, it is found that the system design is the main RR limiting factor for an RO plant rather than the concentrate salinity particularly at low feed water salinities (*Table 4-10*). This is because achieving high RR's, i.e. > 90%, requires more RO modules in series on the expense of reducing the number of modules in the first two stages which made it impossible to keep the permeate flow of the RO modules in these stages within the recommended limits.

The highest RR at 40°C is also slightly lower than that attained at lower temperatures due to the increase in the permeate flow which made it extremely difficult to get a design within the recommended limits using the same number of RO modules.

Table 4-10: RO plant maximum RR without the limiting effect of scaling

Feed Water Salinity (mg/l)	2,000	4,000	6,000	8,000	10,000
Max. RO RR at Maximum Recommended Concentrate Salinity	97%	94%	91.5%	88.5%	85.5%
Design Limited Max. RO RR at 20-30°C	90%	90%	90%	85%	85%
Design Limited Max. RO RR at 40°C	90%	90%	85%	80%	80%

Figure 4-4 shows the maximum attainable RR for the three different types of GW considered in this study at the expected GW temperature range, i.e. 20 to 40°C[135] when the effect of scaling is considered. It is found that after using acid dosing and scale inhibitors, the RO plant maximum attainable RR's with the typical GW compositions found in Egypt are slightly limited by scaling where RR's slightly lower than those limited by the plant design were obtained. Conversely, with low scaling potential GW, the RO plant maximum attainable RR's are limited by the plant design and not scaling.

With high scaling potential GW, the maximum attainable RR is significantly reduced and therefore, in addition to the increased costs of pre-treatment chemicals, such water type is not recommended for extraction and will not be considered in the modelling work carried out in this thesis.

[135] The maximum attainable RR varies slightly at the considered temperature range and only the lowest value is considered

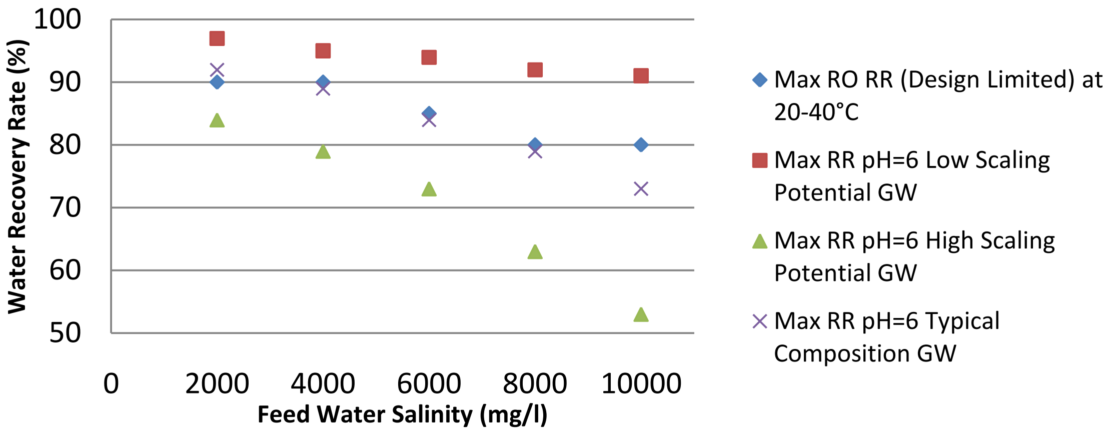

Figure 4-4: Comparison between the maximum scaling limited RR's achieved with simple pre-treatment for different GW compositions and those limited by the RO plant design at the expected GW temperature range in Egypt

4.2.2 Effect of water temperature on RO plant energy consumption

Figure 4-5 shows the SEC of the RO plants designed to operate with 20, 30 and 40°C feed water temperatures, i.e. the expected GW temperatures in the LSI and HSI zones[136].

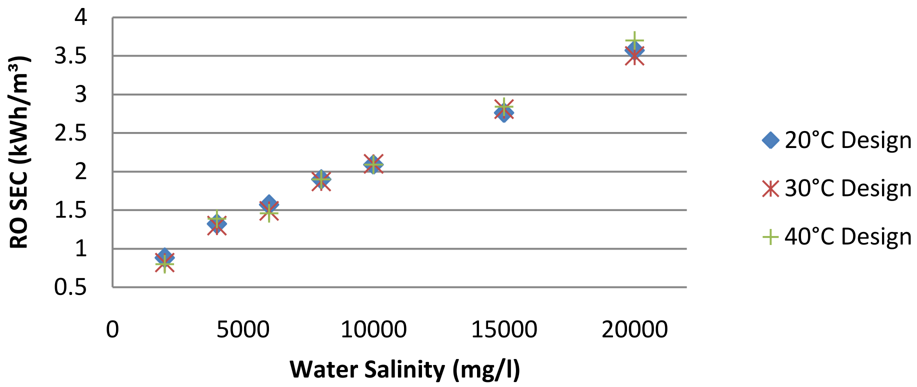

Figure 4-5: Comparison of the SEC of an RO plant designed to operate within the manufacture's recommended parameters at 20, 30 and 40°C at different water salinities and with low scaling potential GW [137]

It is observed from *Figure 4-5* that while the increase in the feed water temperatures is expected to reduce the RO SEC, the values are almost similar for the considered temperature range. This is explained by the increase in the permeate flow rate associated with the increase in the feed water temperature which required the use of higher salt

---

136 More details on the RO plant designs with low scaling potential GW are found in Appendix G

137 It should be noted that given that the maximum attainable RR's for the 20 and 30°C RO plant designs are slightly higher than those of the 40°C designs (*Table 4-10*), the SEC values shown in *Figure 4-5* are estimated at the maximum attainable RR's of the latter because they are the lowest to ensure a fair comparison.

rejection RO modules to keep the permeate flow rate within the recommended limits. Accordingly, it is concluded that the variation in GW temperatures from one location to another will have a negligible effect on the RO plant power consumption.

4.2.3 Economic feasibility of PV-RO plants

4.2.3.1 Day only versus 24 hours plant operation

As discussed in section *4.1.4.2*, the feasibility of PV-RO plant is assessed for two cases: day only operation; and 24 hours operation. *Figure 4-6* shows the LCOW for both cases for the PV and the DG driven RO plants operating at the maximum attainable RR's when GW with low scaling potential is desalinated.

It is clear that as long as the diesel is subsidized in Egypt, PV-RO plant becomes a significantly more costly alternative. Conversely, when the subsidies are removed, a PV-RO plant operating during daytime only is slightly more economical than a DG-RO especially in the HSI zone.

Nevertheless, the LCOW of day only operating RO plant is found to be 7 to 36% higher than that operating for 24 hours when brackish GW extracted. This is attributed to the low capacity factor of the RO plant when it is operating during daytime only and its higher LCC with respect to that of the PV system.

However, when the RO plant operates for 24 hours, its LCOW becomes clearly higher, i.e. 9 to 22% higher, than that of a DG-RO plant even when the subsidies are removed. In this case, a PV-RO plant can be only described as cost competitive particularly at low feed water salinities. This is because in this case due to the low capacity factor of the PV system, i.e. sun shines only during the day, a much larger battery bank and array size was used to provide the energy required during night operation. Accordingly, the LCOE of the PV energy supply increased from an average of 0.33 USD/kWh when the RO plant is only operating during the day to 0.44 USD/kWh when the RO plant is operating 24 hours. The decrease in economical competiveness of PV-RO with DG-RO when the operating hours are increased was also reported in Al Suleimani and Nair (2000). Al Suleimani and Nair (2000) also showed that the PV-RO plant investigated in their study which was designed to operate during daytime only for an average of 5 hours had a lower LCOW than that driven by a DG.

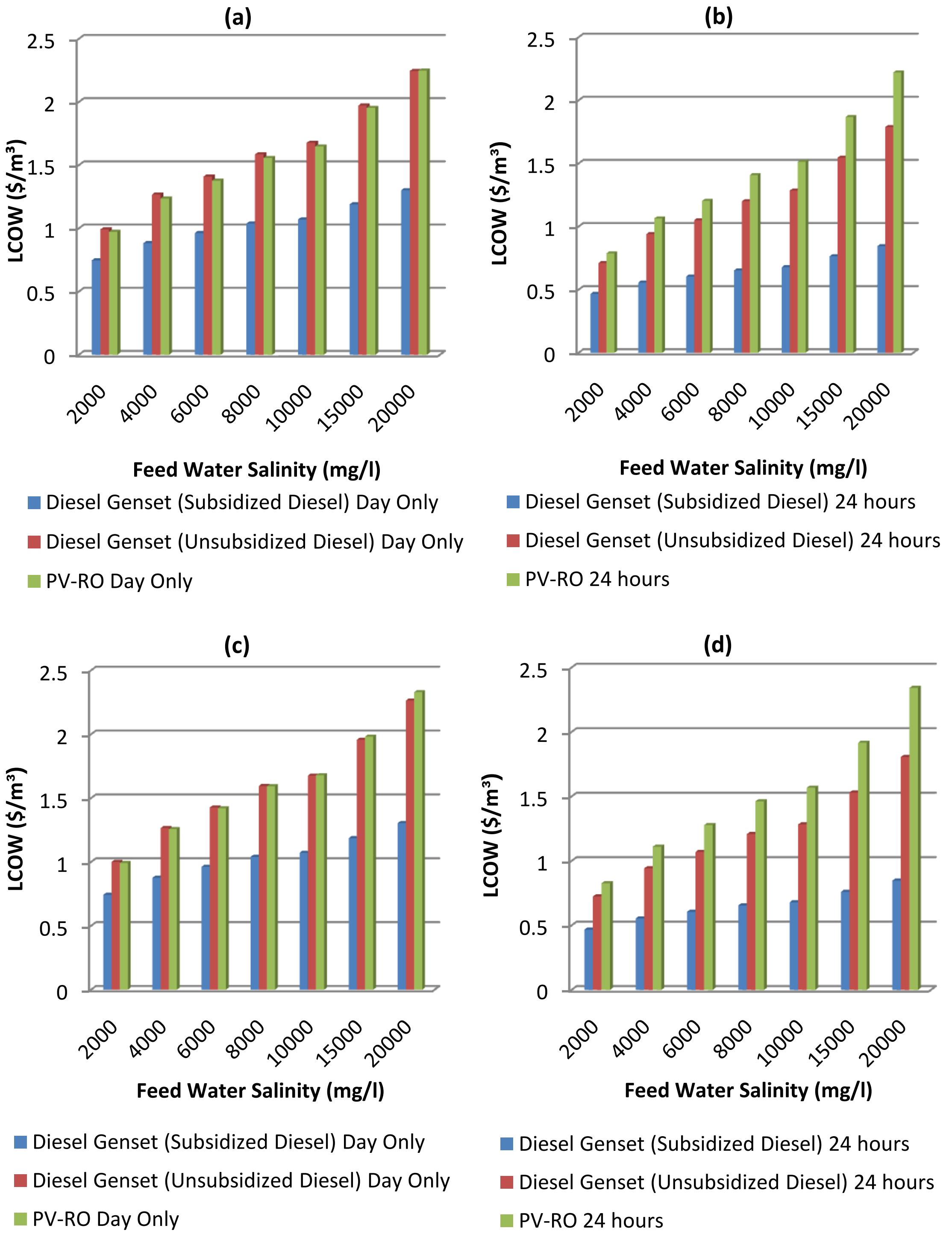

Figure 4-6: LCOW comparison between a DG and a PV driven RO plant in the HSI zone and designed to operate (a) during daytime only and (b) for 24 hours; and in the LSI zone and designed to operate (c) during daytime only and (d) for 24 hours when GW with low scaling potential is extracted from an unconfined aquifer with 50 m depth to water table[138]

[138] It should be noted that for the 24 hours operation case, it is found that to keep the monthly average daily SOC below 80% requires a significantly large array size which decreases the PV system efficiency and therefore a value of 60% is chosen instead. Accordingly, the battery lifetime in this case is assumed to be 4 instead of 5 years

It should be also noted that at feed water salinities larger than 15,000 mg/l, the LCOW of a day only operating RO plant was almost the same as that of a plant operating for 24 hours. This is because at such high water salinity, the power requirements are very high and therefore the LCC of the PV system dominates over that of the RO plant and therefore the effect of operating the latter at low capacity factor becomes less significant. This, however, does not apply for the case when GW is extracted from the confined Nubian aquifer either in the eastern and western deserts or the in the Sinai Peninsula as shown in *Figure 4-7* and *Figure 4-8*. This is because in this case, despite the large energy requirements for GW extraction especially in the Sinai Peninsula, the high costs associated with well construction made significantly increased the LCC of the RO plant.

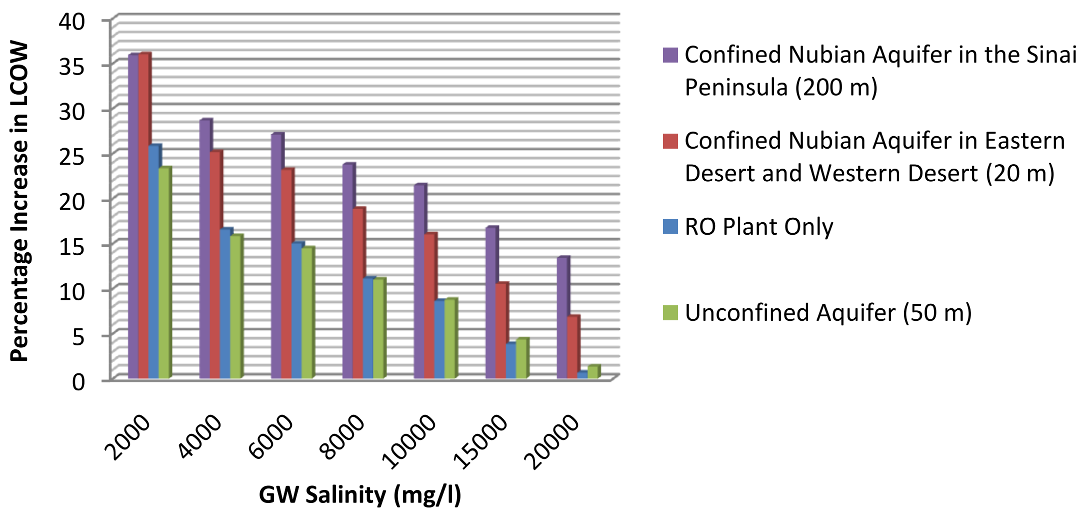

Figure 4-7: Percentage increase in the LCOW of a PV-RO plant located in the HSI zone designed to operate only during daytime over that of a plant designed to operate for 24 hours

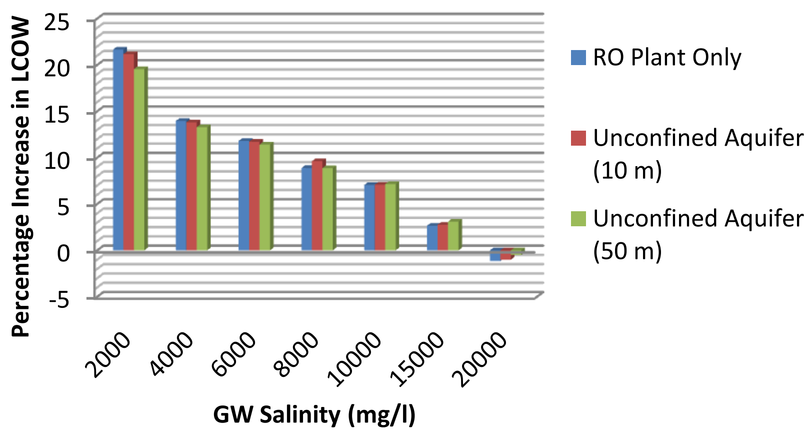

Figure 4-8: Percentage increase in the LCOW of a PV-RO plant located in the LSI zone designed to operate only during daytime over that of a plant designed to operate for 24 hours

It is also observed from *Figure 4-6* that the higher the feed water salinity, the less economically competitive the PV-RO plant becomes with a DG-RO plant. In other words, a PV-RO plant becomes less economically competitive at larger loads, a trend that was also reported in Jacobson et al. (2013). This could be explained by the decrease in the LCOE of the DG as the load increases in contrast with that of the PV which remained nearly constant for all designs (*Figure 4-9*). This is caused by two factors: a scaling factor is used for the DG case which decreases its capital cost in contrast with the PV modules and the batteries whose costs are assumed to be constant due to their modularity; and the slight improvement in the DG efficiency as its capacity increases based on the equations used to estimate its annual fuel consumption.

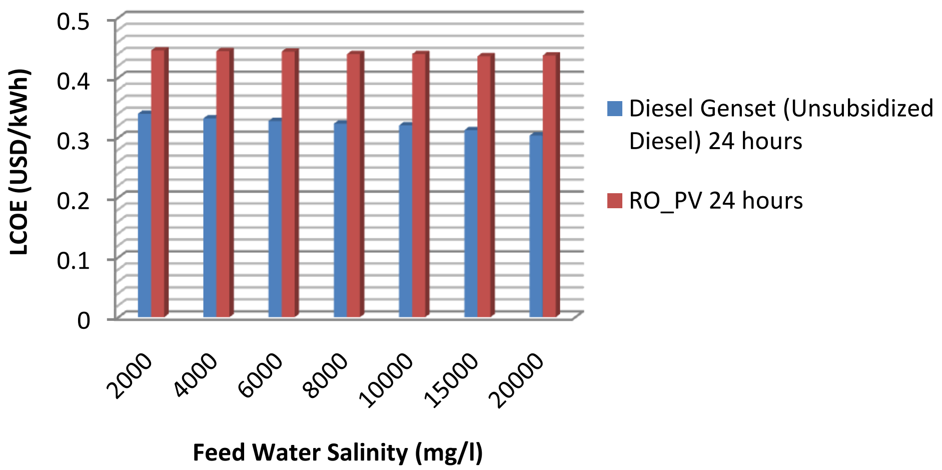

Figure 4-9: LCOE comparison between a DG and a PV energy supply located in the LSI zone

Finally, it should be noted that for all the considered designs the number of hours at which the PV system will not be able to supply the energy requited by the RO plants was zero for systems applied in Aswan where the average daily total sky cover[139] for a typical year is less than 5% based on the TRNSYS weather file. Conversely, in Marsa-Matruh the number of hours ranged from an average of approximately 20 to 75 for the day only and 24 hours operation respectively due to the higher number of cloudy days where for 20% of year the total cloud cover is more than 50%. Nevertheless, the aforementioned hours where the RO plant cannot operate represent less than 1% of the total yearly operating hours for both the day and 24 hours operation cases and should not affect the estimated LCOW knowing that it has been already assumed a plant availability of 95% and 90% for each case respectively.

[139] Defined as the amount of sky dome covered by clouds or obscuring phenomena at a certain hour

4.2.3.2 Expected LCOW of a PV-RO plant

As it is found that the LCOW of a PV-RO plant treating BW is lower when the plant is operating 24 hours, the expected LCOW of such plant when treating typical composition GW accessed from aquifers in different locations in Egypt is determined (*Figure 4-10*) for this case[140].

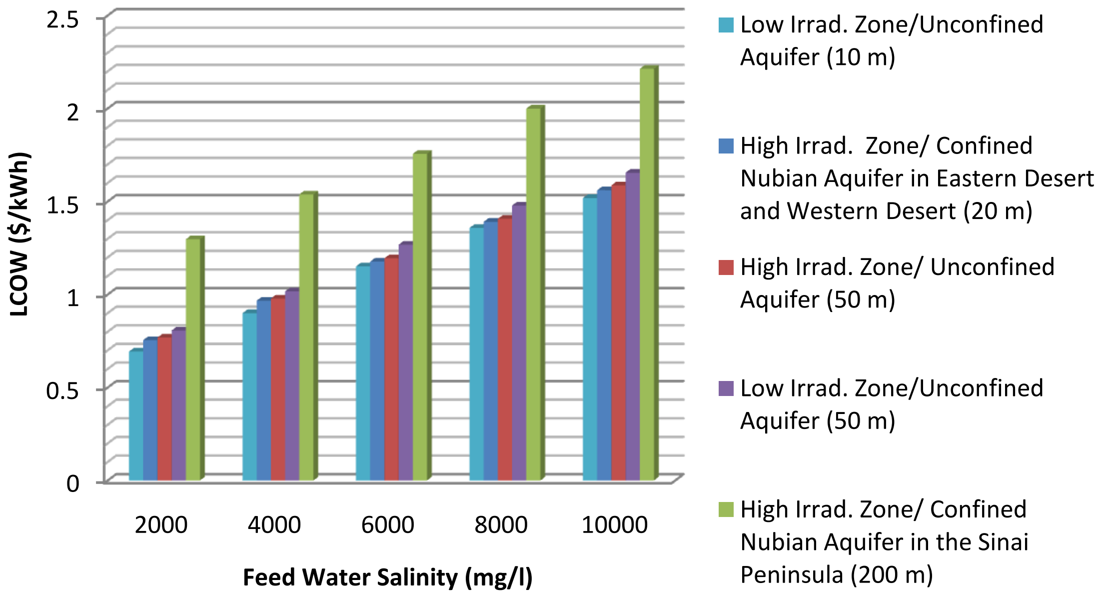

Figure 4-10: The estimated LCOW of a PV-RO plant extracting and desalinating GW with typical composition from different locations in Egypt

The LCOW ranges from 0.7 USD/m^3 to 1.65 USD/m^3 at 2,000 and 10,000 feed water salinity respectively in most locations in Egypt. Higher LCOW's ranging from 1.3 to 2.2 USD/m^3 at 2,000 and 10,000 feed water salinity respectively is encountered in the Sinai Peninsula due to the large well depths and depths to water table.

In spite of the lower solar resources, the lowest LCOW for a PV-RO plant is obtained when GW is extracted from the unconfined aquifers in the LSI zone due to the low cost of well construction and the low depth to water table. In contrast, the highest LCOW is when GW is extracted from the Nubian aquifer in the Sinai Peninsula. It is also observed that when GW is extracted from the unconfined aquifers with same depth to water table in the LSI and HSI zones, the low solar resources in the former did not result in a significant increase in the LCOW where the maximum increase in the LCOW did not exceed 6% for the considered waters salinity range.

[140] More details on the RO plant designs with typical GW composition are found in Appendix G

Moreover, as shown in *Figure 4-11*, it is clear that the PV-RO plant is cost competitive with an RO plant driven by a DG with unsubsidized fuel where its percentage increase in LCOW over the latter did not exceed 16.4%.

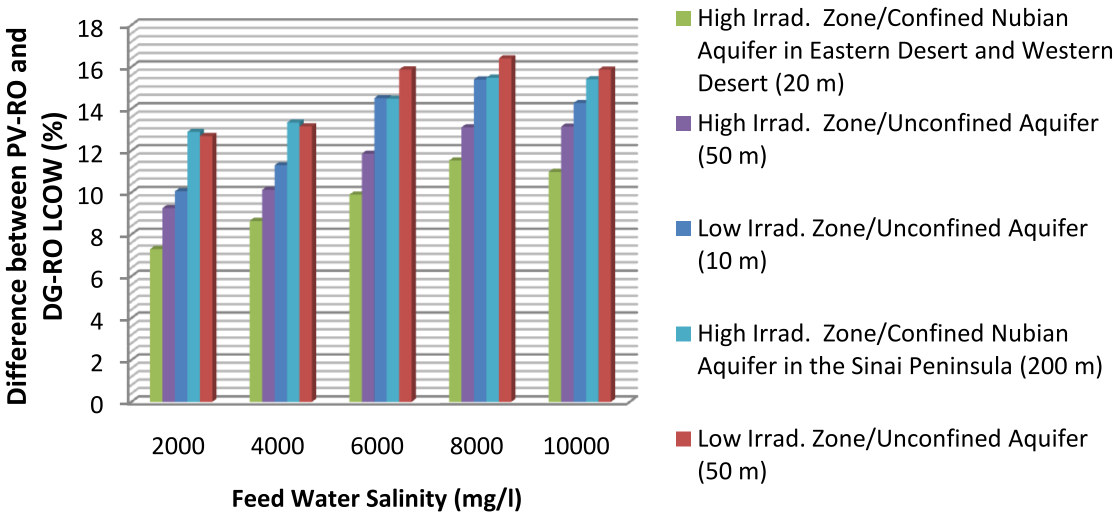

Figure 4-11: Percentage increase in the LCOW of extracting and desalinating GW after replacing the DG running with unsubsidized fuel with a PV system[141]

It can be also observed that a PV-RO was more cost competitive with a DG-RO in the HSI zone when GW is extracted from the confined Nubian aquifer in the Eastern and Western deserts. This is simply due to the high solar irradiance in these areas in addition to the low energy consumption required in this case as the depth to water table is small. Low energy consumption translates into a smaller PV system size and, as discussed in section *4.2.3.1*, a PV-RO plant becomes more economically competitive at smaller loads.

While it is impossible to compare the LCOW's estimated in this study and those reported in the literature due to the different operating conditions particularly in terms of the RO plant design[142], operating hours and RR, and the GW salinity, it is observed that the values estimated in this study are much lower than those reported in the literature which ranged from 3.6 to 14.9 USD/m^3 (Al Suleimani and Nair, 2000, Ahmad and Schmid, 2002, de Carvalho et al., 2004, Karagiannis and Soldatos, 2008, Al-Karaghouli et al., 2010).

[141] It should be noted that while the power required at 10,000 mg/l is more than that required at 8,000 mg/l, the percentage increase in the LCOW is lower or similar. This is because the RO plant at 10,000 mg/l feed water salinity operates at a lower RR (75%) due to scaling limitations hence the increase in power consumption from the 8,000 mg/l case is not significant.

[142] That is the design flux which determines the number of RO module used hence the SEC

In this study, the average estimated LCOE of the PV system, i.e. 0.44 USD/kWh, is consistent with the LCOE range, reported in The International Renewable Energy Agency (2012) which ranged from 0.36 to 0.71 USD/kWh for PV systems with battery storage. Conversely, the RO plant costs were based on those of an actual plant in Egypt. Moreover, the estimated RO plant SEC in this study falls between the typical values for BW RO plants reported in the literature (Chapter 2 *Table 2-2*). For this reason, it is likely that the LCOW reported in the literature to be overestimated especially that all of these studies were carried out before mid 2000's where the PV module costs were more than 3 USD/Wp, i.e. at least 4.5 times higher than the current module cost, and where the non-module costs were still high (Feldman et al., 2012). Moreover, it was shown in Chapter 2 (section *2.5.2*) that most of the brackish PV-RO plants operated at very low RR's which would significantly increase their SEC. Finally, some studies such as that of Al Suleimani and Nair (2000) and de Carvalho et al. (2004) ignored the effect on inflation which will result in a overestimated LCOW.

4.2.4 Cost and energy consumption of brackish groundwater extraction and desalination versus seawater desalination

While the RO plants considered in this study are designed to operate at high RR's and in spite of the additional energy requirements for GW extraction, the overall SEC of the brackish GW RO plant ranged from 0.6 to 2.8 kWh/m^3 at the expected GW depths in Egypt. This SEC range is lower than that of SW RO plants using ERD reported in the literature, i.e. 2 to 7 kWh/m^3 (Chapter 2 *Table 2-2*), as shown in *Figure 4-12*. Moreover, the overall SEC of SW RO plants built to supply water to inland areas is expected to be higher after including the additional energy requirements for water conveyance.

Regarding the unit water costs of PV driven SW RO plants, a wide range of values was reported in the literature. In a recent study, Li et al. (2013) compiled data reported in the literature on the unit water costs of such plants, whether those of existing plants or those estimated through modelling. For capacities[143] similar to those modelled in this study, the unit water costs ranged from 2 to 3 USD/m^3 which is higher than those of PV driven BW RO plants estimated in this study.

[143] Only cost data for plants with capacities ranging from 300 to 5,000 m^3/d were taken from Li et al. (2013)

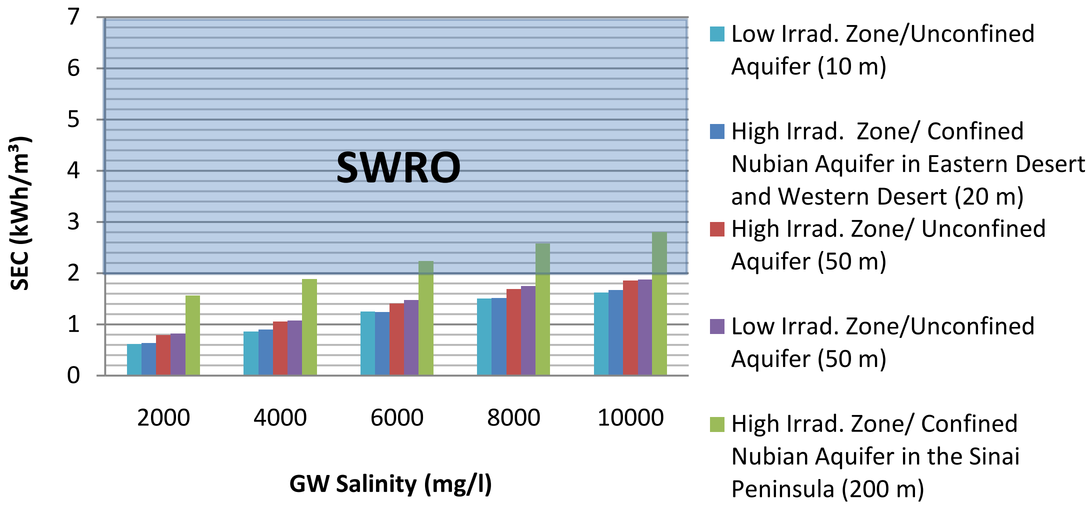

Figure 4-12: Comparison of the SEC of extracting and desalinating brackish GW with typical composition from different locations in Egypt with those of SW RO plants

It should be noted, however, that the LCOW values of the SW PV-RO plants reported in the literature are not based on recent studies, i.e. most recent study was conducted in 2008, and therefore it is expected that the current LCOW will be lower due to the dramatic drop in PV module prices after 2009 as discussed in section *2.2.1*.

Nevertheless, the lower SEC of extracting and desalinating BW, in addition to the lower pre-treatment requirements, are likely to still make a PV driven BW RO plant in inland areas more economical than a PV driven SW RO plant; not to mention that the unit water costs of the latter are expected to be even higher after considering the costs associated with conveying the treated SW to inland areas.

4.2.5 Unit water costs comparison with current water prices in Egypt

As discussed in section *4.2.3.2*, the LCOW of the BW PV-RO plant was estimated to range from approximately 0.7 USD/m^3 to 1.65 USD/m^3 when GW with salinity ranging from 2,000 to 10,000 mg/l is extracted and treated from most aquifers in Egypt; but reaching up to 2.2 USD/m^3 when the GW is extracted from the Nubian aquifer in the Sinai Peninsula due to the high costs associated with GW extraction and well construction.

Conversely, the current drinking water prices[144] in Egypt were generally reported to range from 0.03 to 0.1 USD/m^3 for the domestic sector and reaching up to 0.34 USD/m^3

[144] The word price is used here as the value indicated is what the consumer actually pays for

for the industrial sector (Ahram Online, 2014). The domestic water prices in border governorates, however, seem to be higher where prices ranging from 0.09 to 0.22 USD[145]/m^3 are reported in Matruh governorate (Abd-Allah, 2015). Regarding the water used in irrigation, farmers do not pay for the water use, however, they pay taxes which cover a portion of the irrigation system costs including the cost of water (Gersfelt, 2007). The actual cost of irrigation water is therefore not clear. However, in a study by the Irrigation Support Project for Asia and the Near East (1993), the unit cost of water used in irrigation, which includes the administrative, maintenance, replacement and upgrading costs of the irrigation network, was estimated to range from 0.016 to 0.03 USD/m^3; a similar value was also estimated by Allam et al. (1994).

In all cases, it is clear that the LCOW of the PV-RO plant, including the cost of extracting the GW, is at least 3 times higher than current domestic water prices and almost 20 times higher than the cost of water used in irrigation. However, the aforementioned domestic water prices and irrigation water costs are based on the available and cheap fresh Nile water; and as discussed in Chapter 1, the Nile water is fully utilized and even the available quantity could potentially decrease if the other Nile basin countries construct dams to impound flow. It was also discussed that the lack of fresh water forced many farmers in several locations to use of untreated waste water, and the heavily polluted and saline water from canals and drains in irrigation as well as illegally using water meant for drinking purposes. Accordingly, it was concluded in Chapter 1 that Egypt will need to resort to SW desalination and GW extraction to increase its water supply. Therefore, it is not adequate to compare the costs of extracting and desalinating brackish GW with the current water prices as using Nile water is not an option anymore.

4.2.6 Sensitivity analysis

A sensitivity analysis was carried out to assess the impact of the nominal interest rate, and costs of the battery bank, PV system BOS, and module costs in addition to the indirect costs. The focus was mainly on the PV plant as the cost of its components is likely to have more uncertainty than the more established RO technology; this is

[145] 1 USD=7 EGP

especially true given that the cost of the RO plant in this study was based on data from an actual plant in Egypt.

Each of the aforementioned parameters was reduced by 20% and the corresponding percentage decrease in the LCOW of the PV-RO plant was examined. It can be clearly observed *Figure 4-13* that the nominal interest rate and the battery bank specific cost have the biggest impact on the LCOW of the PV-RO plant.

It can be also observed that while the battery bank cost had the biggest impact on the LCOE of the PV-RO plant, the nominal interest rate had a bigger impact on its LCOW. This is because the battery specific costs only affects the LCC of the PV plant, which as discussed in section *4.2.3.1*, was found to be relatively smaller than that of the RO plant; conversely, the change in the nominal interest rate, hence the PWF, mainly affects the denominator in equation *(4-8)*, by which the LCC of the PV and the RO plants is divided to estimate the LCOW.

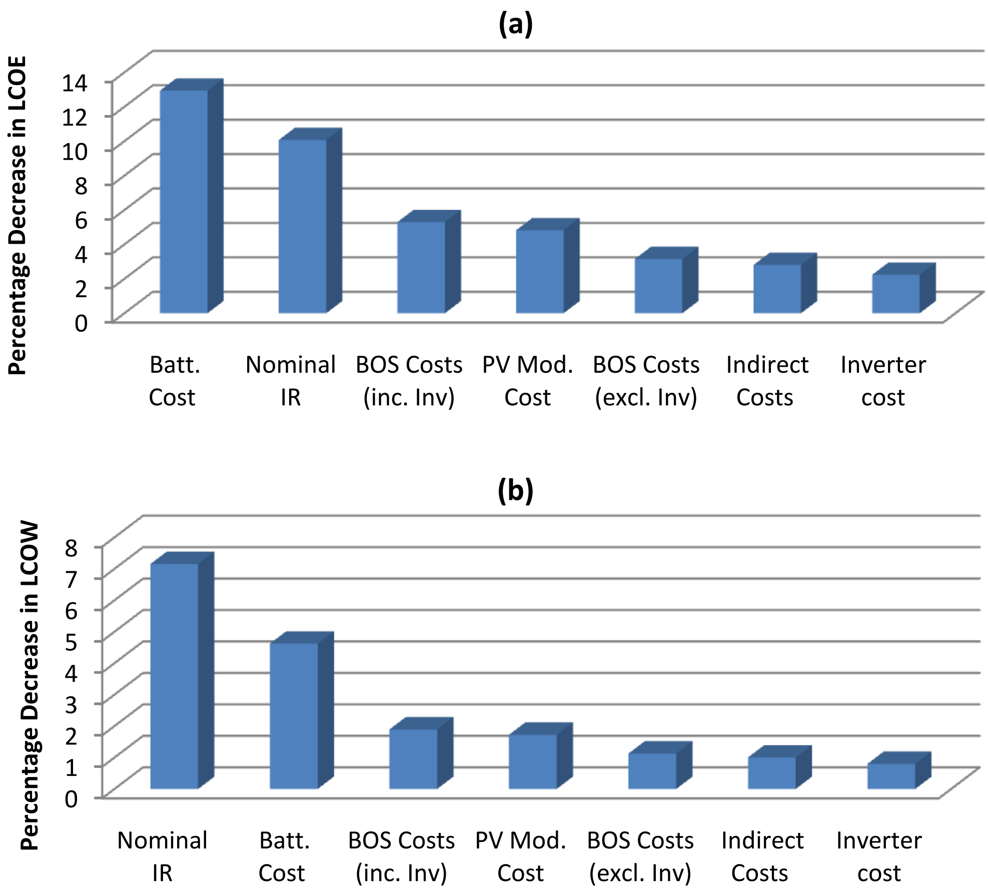

Figure 4-13: Impact of a 20% reduction in the main parameters used in determining the cost of the PV plant on the (a) LCOE and (b) LCOW of a PV-RO plant extracting and desalinating 2,000 mg/l GW from the Nubian aquifer in Eastern Desert or Western Desert (20 m depth to water table)

4.2.7 Impact of battery bank cost, interest rate and diesel prices on the feasibility of PV-RO plants

In the previous section, it was concluded that the impact of the battery bank specific cost and the nominal interest rate on the LCOW of the PV-RO plant was the biggest. Accordingly, the effect of both parameters on the economic feasibility of using PV instead of DG's to drive the RO plant was investigated.

As shown in *Figure 4-14*, decreasing the interest rate works in favour of PV driven RO plants rather than those driven by a DG which experienced the higher percentage decrease in the LCOW, a trend that was also reported in Jacobson et al. (2013). To explain this further, the decrease in the nominal interest rate results in an increase in the PWF. While the increase in the PWF increases the LCC of the plant, it resulted in a higher increase in the denominator of equation *(4-8)* and therefore lowering the LCOW. For the same reason, decreasing the nominal interest rate was more beneficial to PV-RO plants because the PV plant had lower operational costs than that of the DG and therefore its LCC was least affected by the increase in the PWF.

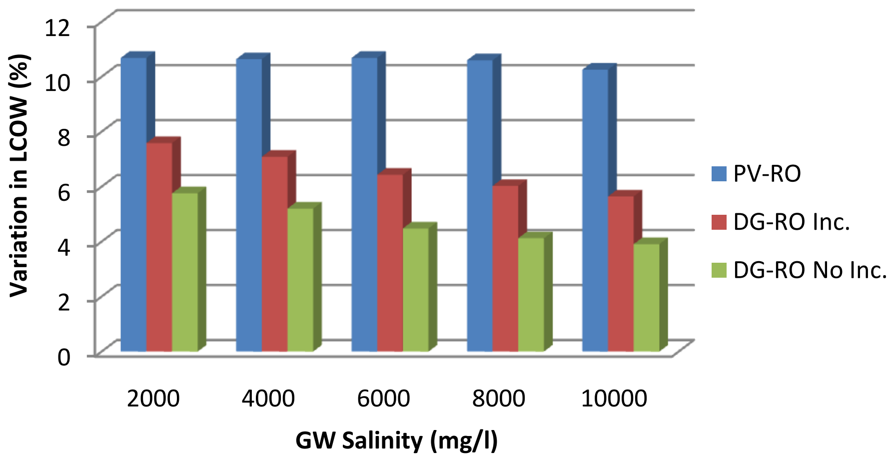

Figure 4-14: Variation in the LCOW of PV and DG driven RO plants by reducing the nominal interest rate from 13 to 9% for the case where the plant is extracting and desalinating GW from the Nubian aquifer in Eastern Desert or Western Desert (20 m depth to water table)

Accordingly, reducing the nominal interest rate resulted in making the PV-RO plant more cost competitive with a similar plant driven by a DG. In particular, the percentage increase in the LCOW by replacing the DG with a PV plant after reducing the nominal interest rate from 13% to 9%, a value almost equal to the inflation rate, dropped from approximately 7 to 16% (section *4.2.3.2*) to 2 to 5% when brackish GW is desalinated with the typical composition, and expected range of GW depths and solar irradiance found in Egypt.

Regarding the battery bank costs, it was found that if the battery specific costs dropped from 200 to 100 USD/kWh then, as shown in *Figure 4-15*, a PV-RO plant will be more economical than a similar plant driven by a DG. This figure is likely to be already achievable especially that similar specific battery costs was previously used in the literature such as in Kolhe et al. (2002) and Arun et al. (2008).

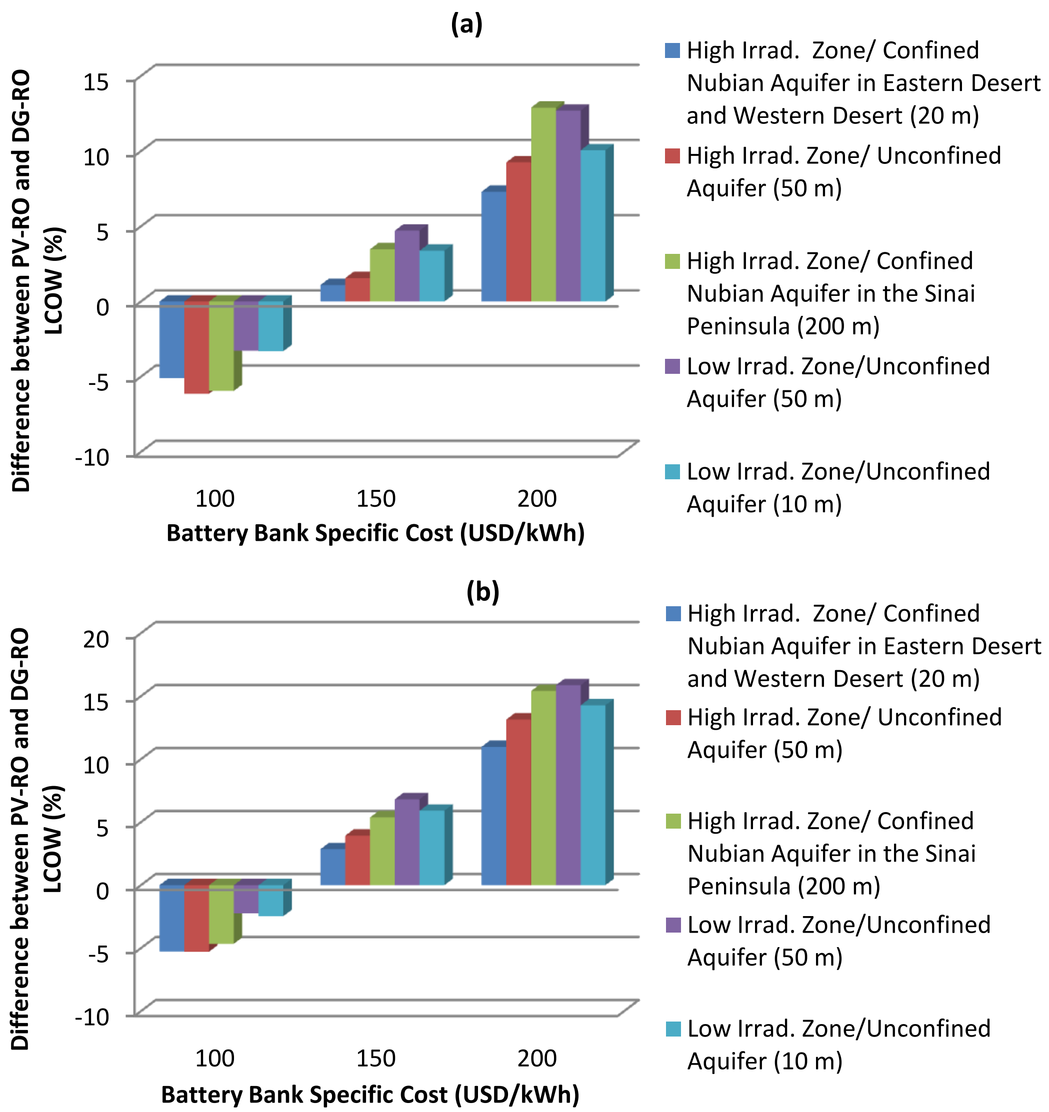

Figure 4-15: Effect of the battery bank specific cost on the percentage increase of the LCOW of a PV-RO over that of a DG-RO plant when the GW salinity is (a) 2,000 mg/l and (b) 10,000 mg/l

Finally, the effect of increasing the diesel prices on the economical feasibility of PV-RO plants was investigated. It was found that with a 13% nominal interest rate and with the

PV system costs used in this study, i.e. base case (*Table 4-7*), a minimum of 45% increase in the unsubsidized diesel prices, i.e. 1.35 USD/l, is necessary for a PV-RO plant to be more economical than a similar plant driven by a DG (*Figure 4-16*).

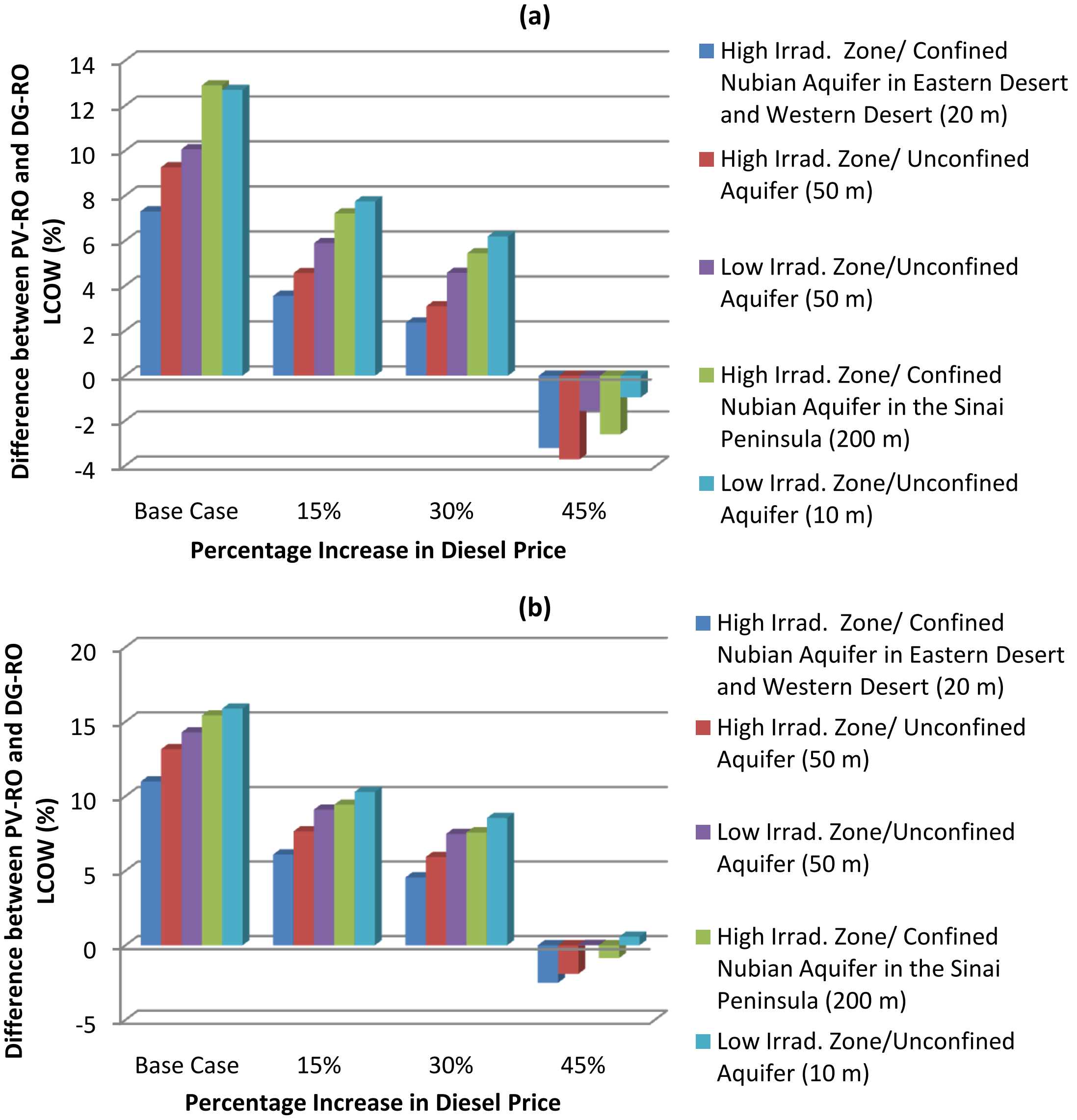

Figure 4-16: Effect of the price of unsubsidized diesel on the percentage increase of the LCOW of a PV-RO over that of a DG-RO plant when the GW salinity is (a) 2,000 mg/l and (b) 10,000 mg/l

4.3 Conclusion

In this chapter, it was shown that with the typical GW compositions found in Egypt, RR's ranging from 75% to 90% for feed water salinities ranging from 2,000 to 10,000 mg/l could be attained without extensive pre-treatment requirements. The corresponding SEC of the RO plant, i.e. excluding the additional energy requirements associated with GW extraction, ranged from 0.65 to 1.55 kWh/m^3 with 2,000 and 10,000 mg/l GW salinity, respectively. The SEC values drop to 0.5 to 1.5 kWh/m^3 after accounting for the increase in the produced water by blending the GW with the RO permeate. The GW temperature variation from one location to another was also found to have negligible effect on the RO plant power consumption.

For a PV-RO plant operating 24 hours and with the typical GW composition found in Egypt, the LCOW ranged from approximately 0.7 USD/m^3 to 1.65 USD/m^3 when GW with salinities ranging from 2,000 to 10,000 mg/l is extracted and treated from most aquifers in Egypt. Higher LCOW ranging from approximately 1.3 to 2.2 USD/m^3 are, however, expected if the plant treats GW extracted from the Nubian aquifer in the Sinai Peninsula due to the high costs associated with GW extraction and well construction. In contrast, the lowest LCOW, i.e. 0.7 USD/m^3, is obtained when GW is extracted from the coastal aquifer along the north western Mediterranean coast and the delta area due to the low cost of well construction and the low depth to water table.

Studying the feasibility of replacing DG’s with a PV energy system showed that if the current subsidies on diesel are removed, a PV-RO plant can be described as cost competitive. In particular, the LCOW of a PV-RO plant operating for 24 hours was estimated to be from approximately 7 to 16% higher than that of a similar plant driven by a DG when brackish GW is desalinated and with the expected range of GW depths and solar irradiances found in Egypt.

A sensitivity analysis also showed that the battery bank specific costs and the interest rate have a significant impact on the LCOW of the RO plant. It was particularly found that a PV-RO plant becomes clearly more economical than a similar plant driven by a DG if the batter bank specific costs dropped from 200 to 100 USD/kWh. Moreover, any reduction in the interest rate will work in favour of a PV-RO plant although will still not result in making a PV-RO plant more economical.

Furthermore, it was found that the SEC and the estimated LCOW range for extracting and desalinating BW using PV driven RO plants are lower than those of PV driven SW RO plants even without considering the additional energy and costs associated with conveying the treated SW to inland areas.

Finally, the analysis considered the effect of the RO plant operating hours on its LCOW. It was found that a PV-RO plant is more economical than a plant driven by a DG when the operation is only during daytime. Nevertheless, the low capacity factor of the RO plant in this case and its higher LCC with respect to that of the PV energy supply caused the LCOW to be from 7 to 36% higher than that for a PV-RO plant operating for 24 hours when BW is desalinated.

5. Feasibility Study of PVT Driven RO Plants

As discussed in Chapter 2, using PVT collectors has the potential to reduce the LCOW of a solar driven RO plant by: reducing the energy consumption of the RO plant through heating the feed water; and by increasing the PV cell energy yield through the extra cooling provided by the feed water flowing through the back of the collectors. Accordingly, in this chapter the feasibility of replacing the standard PV modules by PVT collectors to drive the RO plant, is investigated.

Firstly the methodology used for designing and modelling the PVT collectors and determining their LCC's is presented. Secondly, the condition under which the PVT collectors may reduce the energy consumption of the RO plant is discussed, followed by the energy performance and economic feasibility of PVT-RO plants.

5.1 Methodology

5.1.1 PVT-RO plant configuration

In the PVT-RO plant, GW is pumped through the back of the PVT modules before going to the RO plant (*Figure 5-1*). Flow diverters are used to control the portion of feed flow going through the PVT collectors to control the RO feed water temperature which is discussed in more details in section *5.1.2*.

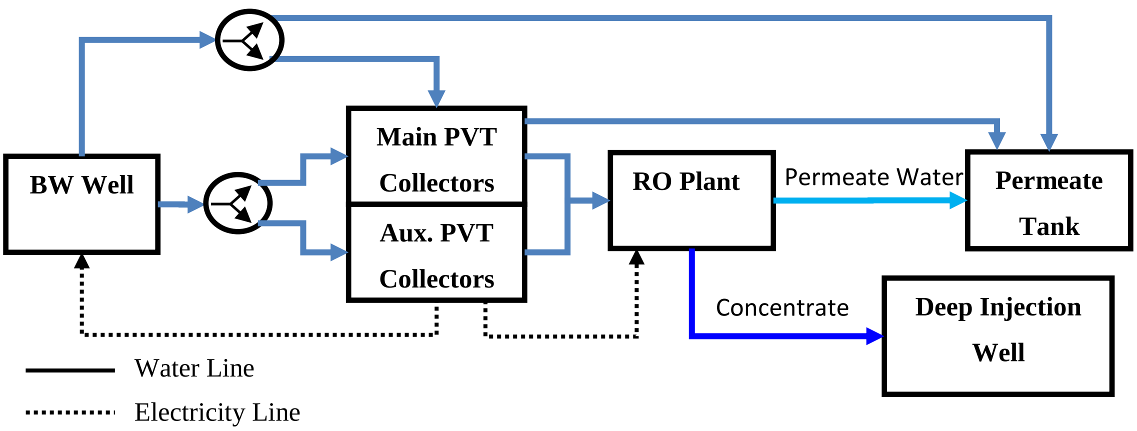

Figure 5-1: Schematic diagram of a PVT driven RO plant

5.1.2 RO plant design

The RO plant design methodology is exactly the same as that discussed in Chapter 4. The RO plant is also designed to operate at the maximum attainable RR estimated from Chapter 4 which depends on the GW composition. In other words, the same RO designs used in Chapter 4, shown in Appendix G, are used in the analysis carried out in this chapter.

To estimate the RO plant power consumption at the varying water temperatures exiting the PVT collectors, polynomial equations for each RO plant design are built based on the power consumption estimated at the expected RO plant feed water temperature range, i.e. 20 to 43.5°C and 30°C to 43.5°C for the LSI and HSI zones respectively. The 43.5°C figure is taken to be the maximum water temperature that can be treated by the RO plant without damaging the RO membranes[146].

It is also assumed that for the 24 hours plant operation case, the feed water is diverted during night operation from the PVT collectors to a separate pipe such that the effect of sky cooling can be neglected and the minimum water temperature can be assumed to equal that of the GW. The PVT collectors are also assumed to be corrosion resistant instead of using additional heat exchangers.

To ensure that the water temperature exiting the PVT collectors will not damage the RO modules when the incident solar irradiance is high, the following measures are taken when the temperature exceeds 43.5°C[147]: the feed flow going through the PVT collectors is increased by diverting the blended GW to go through the collectors; and if the previous measure is not sufficient, the entire extracted GW is diverted to flow through a portion of the PVT collector area, i.e. main PVT collectors (*Figure 5-1*). Accordingly, the PVT collector area heating the water is reduced, in the mean time the flow rate going through it increases, resulting in a reduction in the output water temperature. The size of the auxiliary PVT collector area is determined through a trial and error process such that the water temperature will never exceed 43.5°C at any time of the year.

[146] The maximum operating temperature for the RO module is 45°C (Cotruvo et al., 2010) but for safety a threshold of 43.5°C is used.
[147] A temperature controller with a dead band from 36 to 43.5°C is used in the model.

It should be noted, however, that in this case the remaining PVT collectors, i.e. auxiliary PVT collectors, will operate at high temperatures, i.e. stagnant condition, which is expected to reduce their electrical output. For this reason, the auxiliary PVT collector area is minimized as much as possible as long as the maximum water temperature does not exceed the threshold value at any day of the year.

Finally, it should be noted that for GW extracted from the Nubian aquifer in the Sinai Peninsula, while it may reach 40°C when extracted from larger depths as discussed in Chapter 4, this value is not considered in this analysis. This is because the GW temperature is already near the maximum design temperature of the RO module hence the PVT collectors can only contribute to a negligible water temperature rise.

5.1.3 PVT system modelling and design

The PVT collectors are modelled using TRNSYS simulation tool which allows performing yearly simulations using hourly weather data that in addition to its flexibility to perform any desired calculations other than those available in the software’s model library.

While TRNSYS has its own PVT collector model, i.e. Type50, the model does not account for the effect of sky temperature and also assumes a constant collector efficiency factor[148]. This simplification was found by Bilbao and Sproul (2012a) to considerably overestimate the thermal output of an unglazed PVT collector, hence underestimating the electrical output[149] especially at clear sky conditions, an expected case in Egypt. For this reason, Bilbao and Sproul (2012a) developed a new TRNSYS model, i.e. Type850, which accounts for the effect of sky temperature and calculates the collector efficiency factor giving more accurate estimation of the radiation losses hence the heat and electrical power output.

To provide a common comparison basis with the PV modules used in the PV-RO configuration discussed in Chapter 4, the PVT collector is assumed to have exactly the same electrical characteristics of the PV module used in this study including the temperature dependence of the PV cells (Bakker et al., 2005). Other thermal and optical

[148] The collector efficiency factor is a function of the overall heat loss coefficient of the panel which varies with the wind velocity and the ambient and water temperatures (Bilbao and Sproul, 2012a)
[149] Due to higher estimation of the temperature of the PV cells

characteristics of the PVT collector are based on the values used by Bilbao and Sproul (2012a) and are shown in *Table 5-1*.

Table 5-1: Thermal and optical characteristics of the PVT collector modelled in this study

	Value	Reference
PVT Extra Cover Transmittance	0.85	(Bilbao and Sproul, 2012a)
Collector Absorption Coefficient	0.9	
Collector Plate Emissivity	0.85	
Glass Cover Transmittance	0.92[150]	
Bottom and Edges Heat Loss Coefficient	0.82 $W/m^2.K$	
Absorber- Fluid Heat Transfer Coefficient	56.923 $W/m^2.K$ (unglazed collector) 43.258 $W/m^2.K$ (glazed collector)	
Air gap between absorber and cover	0.025 m	(J. Bilbao, 2013, pers. Comm., 16 Sep)
Glass Cover Thickness	0.002 m	
b_0 [151]	0.06	(Bilbao and Sproul, 2012b)

Both glazed and unglazed PVT collectors are examined in this study. The former have lower overall panel heat loss coefficient hence increasing its thermal output. However, this comes on the expense of reducing the electrical output due to the higher operating temperature of the PV cells and the additional optical losses of the extra cover expected in this case. Conversely, the unglazed PVT collector increases the thermal losses providing more cooling to the PV cells hence boosting their electrical output on the expense of having lower thermal output (Tripanagnostopoulos et al., 2004).

The RO plant operating hours and module orientation, and the array and battery sizing methodology are the same as those used in Chapter 4. However, to estimate the PVT collector size and the battery bank capacity after considering the expected increase in the annual energy yield by cooling the PV cells and the reduction in the RO annual energy requirements, an iterative process is required as follows: the PVT collector area and battery bank size are initially designed exactly the same as a PV-RO plant to initially estimate the percentage increase in the PV annual yield and reduction the annual energy consumption of the RO plant; the PVT collector size is then reduced by

[150] The total transmittance of a glazed collector is 0.92*0.92≈0.85

[151] First order coefficient of the curve fit equation used to calculate the incidence angle modifier

the same percentage increase in the PV annual energy yield; afterwards the TRNSYS PVT model is simulated with the new PVT collector area to estimate the effect of this reduction on the RO plant annual energy requirements; then the RO power consumption data and the array cell temperature are exported to PVSYST to verify whether the new array size covers the load requirements and achieve the minimum required battery SOC. If it does not then the new array size estimated by PVSYST is applied again in TRNSYS and the whole process is repeated.

Finally, the analysis will be mainly based on an RO plant operating for 24 hours as it was shown in Chapter 4 that it is more economical when BW is treated, but day only operation will be also briefly discussed.

5.1.4 PVT system costs

The PVT collector system cost is estimated the same way as the PV system. There is also no change in the inverter costs as it has to be sized to meet the highest load which in this case is the same as that with the PV-RO plant. The only difference is the need to estimate the additional costs of the PVT collector over a standard PV module.

Little data was found in the literature regarding the PVT collector costs. According to Ricaud and Roubeau (1994), an air heating PVT module adds from 60 USD/m^2 to 120 USD/m^2 to the PV module cost, depending on the quality. An additional cost of 326 USD/m^2 for PVT modules increasing to 343 USD/m^2 when the BOS is included was used by Elswijk et al. (2004) for a water heating PVT modules. The latter value is higher than the cost of FPC's which range from 80 USD/m^2 to 287 USD/m^2 (Chapter 7 *Table 7-3*). Tripanagnostopoulos et al. (2004) also indicated that PVT modules are more expensive than a separate PV module and FPC which they attributed to the early development stage of the technology at that time. Elswijk et al. (2004) also stated that the costs they used are based on batch rather than mass production which explains the high additional specific costs they used. In contrast, Bakker et al. (2005) used a very low value of 20 USD/m^2 to estimate the additional costs of using the PV modules for water heating.

In this study, given that PVT modules are already commercialized, an additional specific cost of 150 and 250 USD/m^2 is used for an unglazed and glazed[152] PVT collector respectively including the additional costs for the BOS. However, the assigned specific cost values are very conservative given that corrosion resistant PVT collectors are more expensive than typical PVT collectors. The lifetime of the PVT collectors is also assumed to be similar to that of a PV module and a FPC i.e. 20 years.

5.2 Results and Discussion

5.2.1 Conditions for coupling PVT collectors with RO plants

When coupling PVT collectors with an RO plant, a proper design necessitates that the RO modules operate within their recommended limits over the expected feed water temperature range which in this case ranges from that of the GW to the expected maximum water temperature exiting the PVT collectors.

Nevertheless, it was concluded in Chapter 4 that when the RO plant is designed to operate within the recommended limits at the expected feed water temperatures, no reduction in the energy consumption is attained. This was attributed to the need of higher salt rejection RO modules when the plant is designed to operate with higher temperatures which increased the osmotic pressure hence the energy requirements of the plant offsetting any reduction obtained by decreasing the water viscosity. In this case, using PVT collectors will only show the benefit of increasing the annual yield of the PV system.

A reduction in the RO plant power consumption ranging from approximately 11 to 35.5% is, however, obtained when the same designs for a 20 and 30°C GW are used with higher water temperatures i.e. 40 °C, for water salinities less than 10,000 mg/l (*Figure 5-2*)[153].

Moreover, as shown in *Figure 5-2*, the percentage reduction in power requirements by the RO plant tends to become more significant at lower feed water salinities. This could be attributed to the use of more low salt rejection modules, e.g. BW type modules which

---

[152] The difference between glazed and unglazed PVT collector specific costs is based on the cost data used by Tripanagnostopoulos et al. (2004)

[153] More details on the RO plant SEC and power when the same designs for a 20 and 30°C GW are used with higher water temperatures i.e. 40 °C are shown in Appendix G

resulted in a higher reduction in power requirements at high water temperatures on the expense of a further increase in the permeate water salinity. The increase in water viscosity with the increase in its salinity could be also another reason that makes the percentage reduction in power requirements less significant at high feed water salinities.

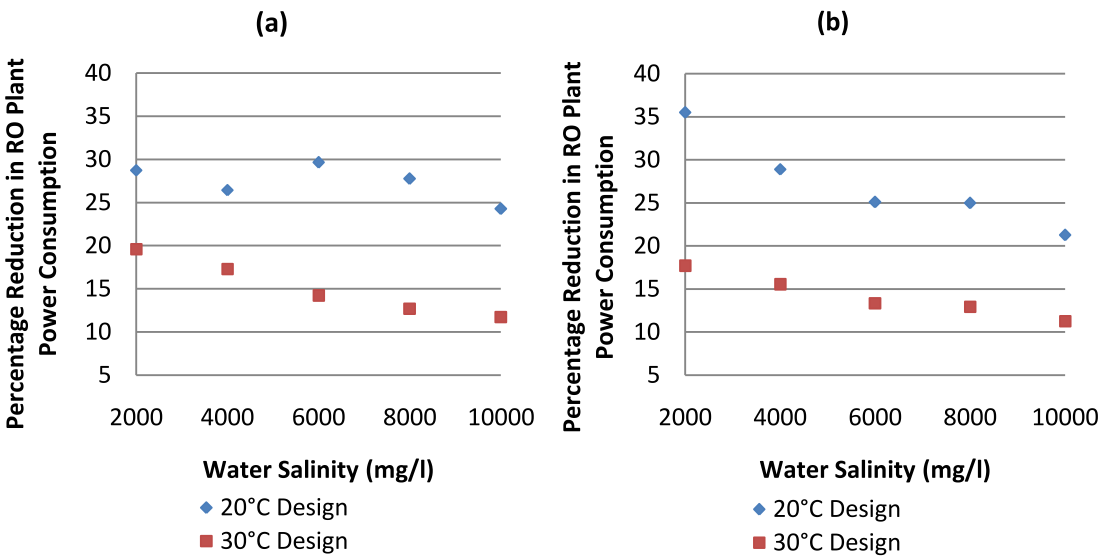

Figure 5-2: Percentage reduction in the RO plant power consumption after increasing the feed water temperature to 40°C for the cases where (a) typical composition GW and (b) low scaling potential GW are desalinated

Using more low salt rejection modules also resulted in a higher percentage reduction in power requirements in most cases with designs for typical composition GW over those for low scaling potential GW. The only exception is when the designs are for a feed water salinity of 2,000 mg/l and 4,000 mg/l with RO plants designed to treat GW with a temperature of 20 °C. This could be explained by the highly unbalanced distribution in the hydraulic load over the modules with typical composition GW designs at the aforementioned water salinities where one of the modules is overloaded by 29.75%[154] (*Table 5-2*) over the recommended permeate flow value. Conversely, with low scaling potential GW the module with the highest hydraulic load is overloaded by only 10.75%[154]. In this case the power consumption increases because the overloaded modules are operating at higher RR's than the other modules which increases the required feed pressure[155].

[154] Flow factor = 0.75

[155] For example, when the boost pressure between stages is varied to balance the hydraulic load, the power consumption for the 2,000 mg/l typical composition GW design at 40°C was reduced by 8%.

It should be noted that despite the reduction in the RO modules salt rejection by increasing the feed water temperatures to 40°C, the maximum overall salinity of the produced water after GW blending did not exceed 660 mg/l (Appendix G) which is still within the range considered by the WHO (2011) to have a good palatability.

Table 5-2: Deviation from the recommended RO module operating limits when 40°C typical composition GW is treated with RO plants designed to operate with feed water temperatures of 20 and 30°C

Feed Water Salinity (mg/l)	Total Number of RO Modules	Percentage by which the recommended Permeate flow rate/RR is exceeded at FF=1 and FF=0.75[156]	
		20°C RO Design Operating at 40°C	30°C RO Design Operating at 40°C
2,000	40	2-1[157]: 11.4% (2.5%) 3-1: 57.6% (29.75%) 3-2: 38.6% (16.45%) 3-3:19% (2.5%)	1-1: 1.25% 2-1: 3.16% 3-1: 5.7%
4,000	46	2-1: 3.8% 3-1: 38% (19.6%) 3-2: 9.5%	1-1: 4.4%
6,000	48	1-1: 21.5% (8.2%) 1-2: 3.2% 2-1: 6.3% (1.9%)	1-1: 1.25%
8,000	48	1-1: 12% (4.4%) 2-1:7% (1.25%) 3-1: 8.2% (0.6%)	1-1: 1.9%
10,000	50	1-1: 23.4% (10.75%) 1-2: 1.9% 2-1: 6.95% (1.9%)	1-1: 2.5%

The reduction in SEC of the RO plant comes however on the expense of allowing a small number of the RO modules to operate outside the recommended operating limits (*Table 5-2*), particularly the first modules in each stage as they experience the highest hydraulic load.

5.2.2 Glazed versus unglazed PVT collectors

As discussed in section *5.1.3*, glazed PVT collectors provide more thermal output, i.e. higher water temperatures, on the expense of a reduction in the electrical output of the PV system. Nevertheless, it was found that for all feed water salinities and GW depths

[156] Values between brackets are at a FF of 0.75. If no value is shown between brackets then the plant is operating within the recommended limits

[157] The first number is the number of stage and the second number is the number of the RO module in that stage. For example 2-1 means the first module in the second stage.

considered in this study in the LSI and HSI zones and with the typical GW compositions found in Egypt, the reduction in the electrical output of the PV system outweighed the reduction in the RO annual energy requirements such that the net energy saving was negative (*Figure 5-3*).

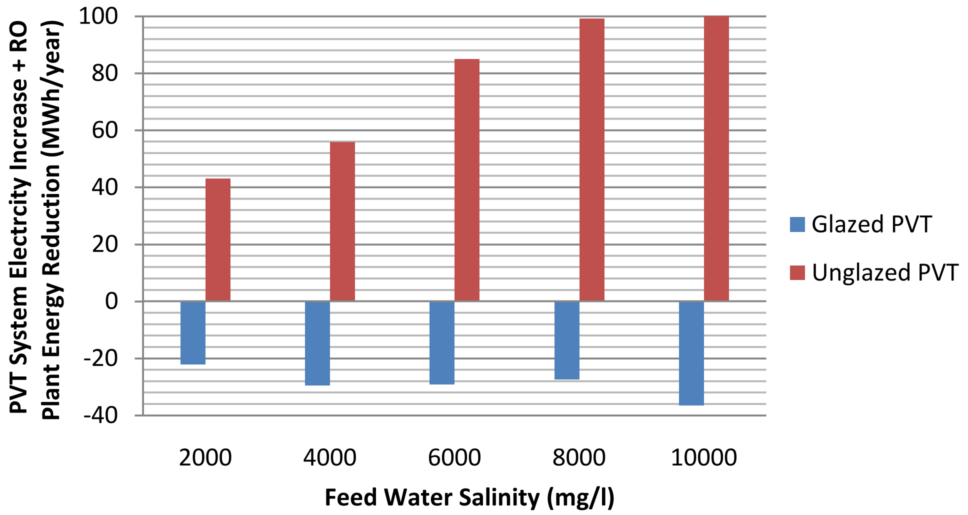

Figure 5-3: Annual net energy saving by replacing standard PV modules with PVT collectors to drive an RO plant located in the LSI zone and desalinating GW extracted from an unconfined aquifer with 50 m depth to water table[158]

In contrast, while the reduction in the annual RO plant energy consumption is slightly lower than that obtained by using glazed PVT collectors, a considerable improvement in the annual electricity yield of the PV system was achieved when unglazed PVT collectors are used (*Figure 5-4*).

It should be noted that for glazed PVT collectors, it is found that a larger annual net energy saving is obtained when only a portion of the PV modules is converted to PVT collectors to prevent the water temperature from exceeding the threshold value (section *5.1.2*). This is instead of converting all the modules to PVT collectors and dividing the system into main and auxiliary units. This is mainly due to the reduction in the optical losses by only converting a portion of the PV modules to PVT collectors. In addition, when glazed PVT collectors are used the number of hours per year where the threshold temperature is exceeded was significant; therefore dividing the system into main and

[158] The same pattern in the net annual energy savings apply for all other cases in the HSI and LSI zones but this particular case is chosen as exemplary case

auxiliary collectors caused the latter to operate most of the time at stagnant conditions considerably reducing the annual yield of the PV system.

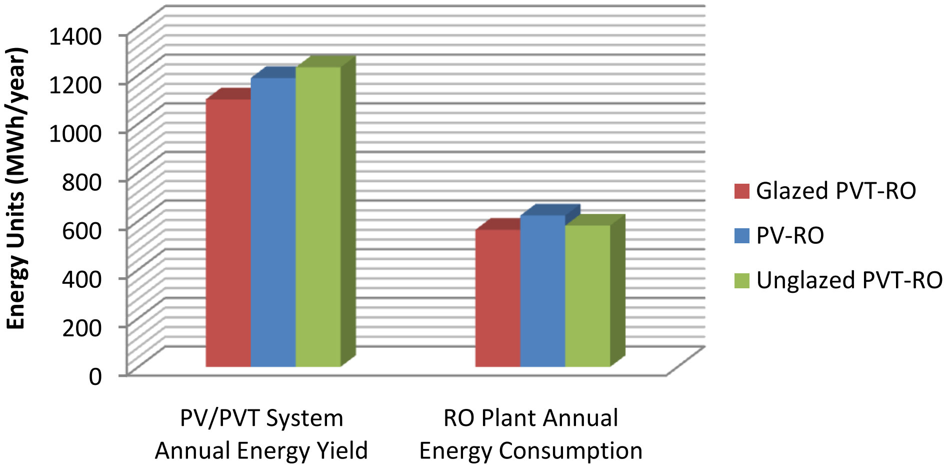

Figure 5-4: Energy performance comparison between PV-RO, glazed PVT-RO and unglazed PVT-RO Plants

Conversely, the number of hours where the threshold temperature is exceeded is small when unglazed PVT collectors are used; and given that in this case there are no extra optical losses, it was better to convert all the PV modules to PVT collectors and divide them into main and auxiliary collectors (*Figure 5-5*).

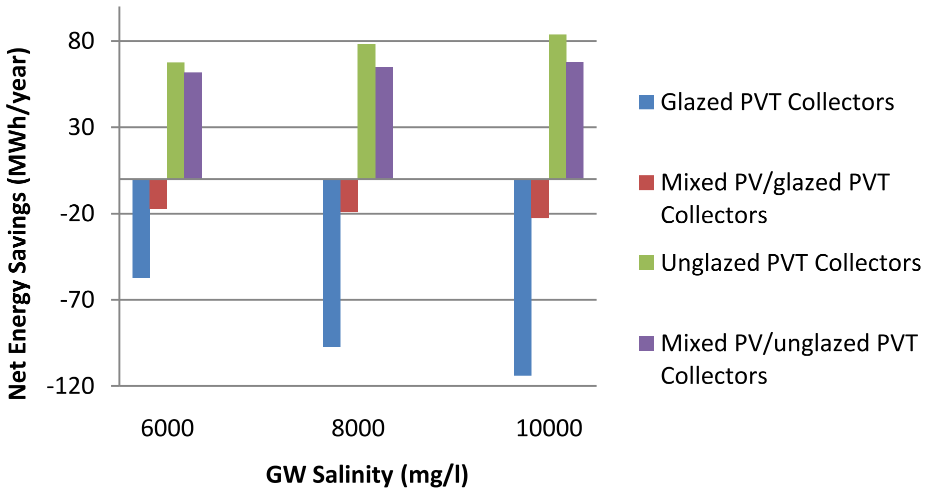

Figure 5-5: Net annual energy saving by partially and fully replacing PV modules by glazed PVT collectors in the HSI zone when the GW is extracted from the confined Nubian aquifer with 20 m depth to water table[159]

[159] The same pattern in the net annual energy savings apply for all other cases in the HSI and LSI zones but this particular case is chosen as exemplary case. It should be also noted that for lower GW salinity there was no need to divert the flow to only a portion of the PVT collectors or to only convert a portion of the PV modules to PVT collectors as the maximum temperature was not exceeded.

5.2.3 Energy performance of unglazed PVT-RO plant

A detailed energy performance analysis is carried out for the case where the RO plant is driven by unglazed PVT collectors which as discussed in the previous section gave a positive annual net energy saving.

5.2.3.1 PVT system annual energy yield

As shown in *Figure 5-6*, a modest increase in the annual energy yield by cooling the PV cells is achieved ranging from approximately 3.6% to 6.7%.

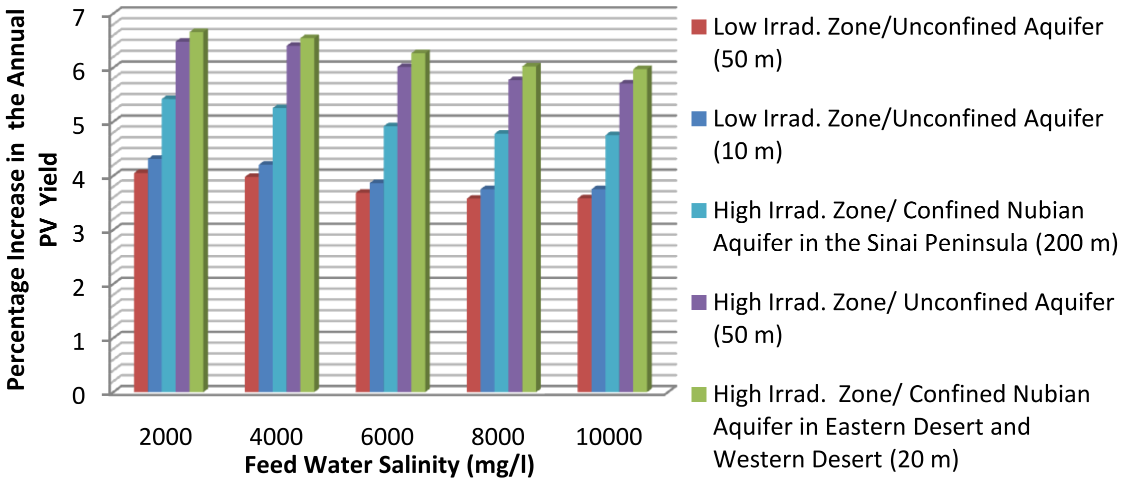

Figure 5-6: Percentage increase in the annual energy yield by replacing the standard PV modules by unglazed PVT collectors

Despite the higher GW temperature, the increase in the annual energy yield by replacing the standard PV modules by unglazed PVT collectors is found to be higher in the HSI zone. This could be attributed to the relatively smaller array size required in the HSI zone which resulted in a low array size to feed flow rate ratio hence a more effective cooling of the PV cells. The other reason is the high ambient temperature in the HSI zone whose effect can be clearly seen from the array temperature losses which were almost double those experienced in the LSI zone[160]. This high ambient temperature decreases the overall heat loss coefficient of the collector and therefore the flowing water becomes more effective in removing the heat from the panels. This, for example, can be observed from *Figure 5-7* where the difference between the temperature of the PV cells in the standard array and that in the PVT collectors is the largest in the HSI zone in summer.

[160] The temperature losses in the HSI zone with respect to the array ideal energy yield is approximately 12% compared to 6.7% in the LSI zone

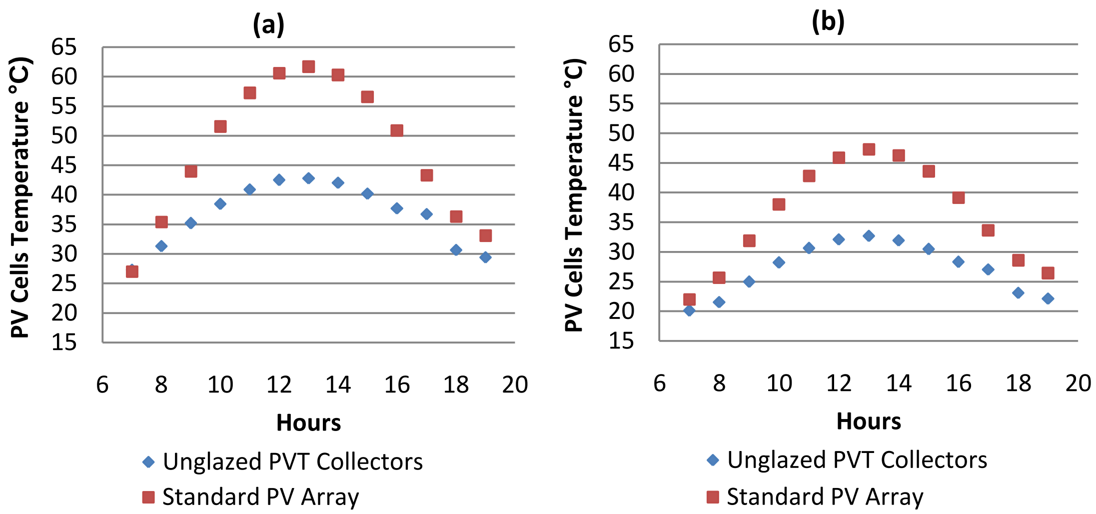

Figure 5-7: PV cell temperature profile in a PV-RO and a PVT-RO plant treating 2,000 mg/l GW extracted from an unconfined aquifer in the (a) HSI zone and (b) LSI zone on a typical summer day

The low array size to feed flow rate ratio also explains the higher percentage increase in the annual electricity yield of the PV system when the depth to water table and the feed water salinity are lower whether in the LSI and HSI zones as a smaller collector area was needed in these cases. In contrast, when GW is extracted from the confined Nubian aquifer in the Sinai Peninsula where the depth to water table is the highest, the large PVT collector area caused the feed flow rate to be diverted during more than half of the year to approximately 50% of the collector area to prevent the water from reaching the threshold temperature. The other 50% of the collector area was therefore operating at stagnant conditions where the PV cell temperatures were slightly higher than that of the standard PV array due to the PVT collector low thermal loss coefficient (*Figure 5-8*).

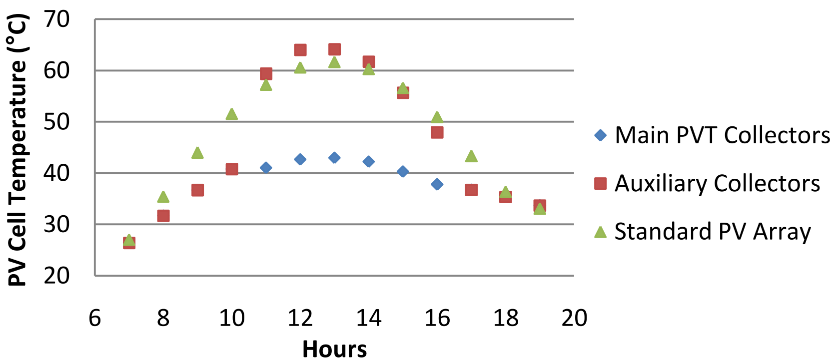

Figure 5-8: PV cell temperature profile in a PVT-RO and a PV-RO plant treating 2,000 mg/l GW extracted from the Nubian aquifer in the Sinai Peninsula on a typical summer day[161]

[161] It should be noted that the TRNSYS model for the PVT collectors used in this study considers the effect of wind velocity[161] when calculating the thermal loss coefficient of the collectors while, as discussed in Chapter 4, the PV array is modelled in PVSYST based on a constant thermal loss coefficient

Finally, if PVT collectors are used with a SW RO plant with the same capacity as the BW RO plants modelled in this study (i.e. 62.5 m^3/h of permeate), and with a typical SEC of 3 kWh/m^3 (Chapter 2 *Table 2-2*) and operating at a RR of 40%[162], the expected array size[163] to feed flow rate ratio is approximately 7.6 and 6.15 for a plant located in the LSI and HSI zone respectively. The aforementioned ratios falls between those of a BW RO plant treating 6,000 and 8,000 mg/l GW extracted from a shallow unconfined aquifer in the LSI zone, and from the confined Nubian aquifer in the eastern and western deserts respectively. Accordingly, the average percentage increase in the annual PV yield is expected to be less than 4% and 6% for a SW RO plant located in the LSI and HSI zone respectively.

5.2.3.2 RO plant energy consumption

A modest reduction in the RO plant annual energy requirements ranging from approximately 3.4% to 6.6%, was also obtained by heating the feed water (*Figure 5-9*).

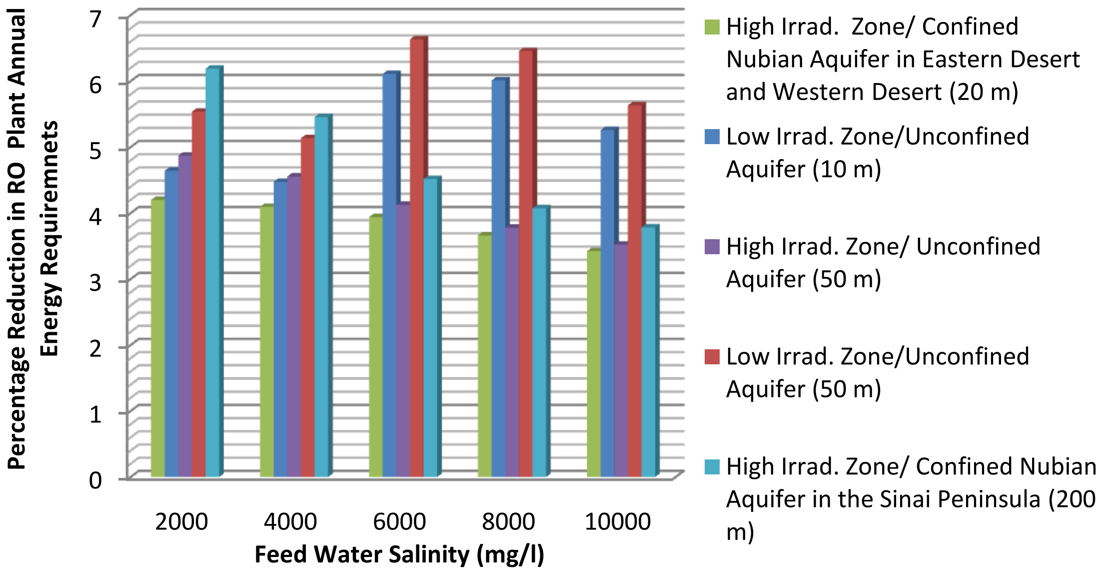

Figure 5-9: Percentage reduction in the RO plant annual energy consumption by replacing the PV modules by unglazed PVT collectors

of 29 W/m^2.K. Accordingly, it is found that the PVT collector TRNSYS model gives higher estimation of the wind thermal losses. For this reason, *Figure 5-8* shows only a small PV cells temperature difference between the unglazed PVT collectors at stagnant conditions and the standard PV array.

[162] Calculated based on the maximum recommended concentrate water salinity, i.e. 70 g/l, as discussed in Chapter 5, and assuming that the SW has a salinity of 40,000 mg/l.

[163] Estimated based on the array size data of the BW RO plants modelled in this study assuming a linear variation of the array size with the daily energy requirements of the RO plant

As shown in *Figure 5-9*, the percentage reduction follows a similar pattern shown in *Figure 5-2* where the highest percentage reduction in the RO plant annual energy requirements is mainly achieved at feed water salinities from 6,000 to 8,000 mg/l in the LSI zone as the plant uses more low salt rejection RO modules.

It is also observed that, as expected, the larger the depth to water table, the higher is the percentage reduction in the RO annual energy requirements. This is simply because a larger collector area increases the annual average feed water temperature going to the RO plant. For example as observed from *Figure 5-10*, the large collector area required when the RO plant is located in the Sinai Peninsula when GW is extracted from the Nubian aquifer (200 m depth to water table) heats the water to higher temperature than a plant located in the eastern and western deserts where the depth to water table is much smaller.

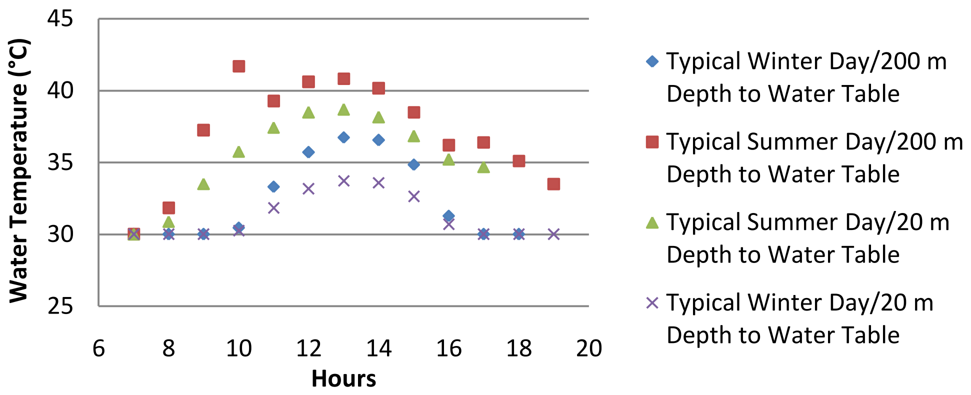

Figure 5-10: Comparison of the temperature profiles of the water exiting the PVT collectors for PVT-RO plants treating 2,000 mg/l GW

Note: the sharp decrease in the water temperature at 10 AM is because the feed flow is diverted to the main PVT collector area to keep the temperature from exceeding the threshold value.

It is therefore observed that while the percentage reduction in the RO plant power consumption by heating the water to 40°C reached up to approximately 30% as discussed in section *5.2.1* (*Figure 5-2*), when PVT collectors were used the maximum percentage reduction in the RO plant annual energy requirements did not exceed 6.6%. This is simply due to the low capacity factor of the PVT collectors, i.e. sun does not shine at night, and that even during the day, it is impossible to keep the water temperature at 40°C (for example see *Figure 5-10*).

It should be also noted that the previous analysis was conducted for an RO plant operating for 24 hours given that, as concluded from Chapter 4, running the RO plant during daytime only was less economical. In the latter case, however, one may expect a much higher percentage reduction in the annual RO plant energy requirements than those shown in *Figure 5-9* if PVT collectors were used; which is simply because the RO plant is mostly operating at the time where the PVT collectors are heating the water. Nevertheless, it was found that the small collector area required in this case did not supply enough heat to the water and the percentage reduction in the annual energy requirements of the plant did not exceed 9.5%.

Finally, if PVT collectors are used with a SW RO plant, an insignificant reduction in the RO plant energy requirements is expected due to the need of using high salt rejection RO modules which, as discussed in section *5.2.1*, results in low energy reduction by heating the feed water.

5.2.4 PVT driven RO plant economic analysis

Given the very modest improvement in the energy yield and reduction in the RO energy consumption, the cost analysis is carried out for only the best case scenarios which are: the case where the percentage increase of the annual electricity yield of the PV system is the highest which applies for the case when 2,000 mg/l GW is extracted from the confined Nubian aquifer in the eastern and western deserts; the case where the reduction in the annual energy requirements of the RO plant is the highest which applies for the case when 6,000 mg/l GW is extracted from an unconfined aquifer with 50 m depth to water table in the LSI zone; and the case where the net annual energy saving is the highest which applies for the case when 2,000 mg/l GW is extracted from the confined Nubian aquifer in the Sinai Peninsula.

As shown in *Figure 5-11*, even with the likely low cost of the PVT collectors used in this study especially (section *5.1.4*), the LCOW for a PVT driven RO plant was found to be higher than that of a PV-RO plant even for the best possible cases.

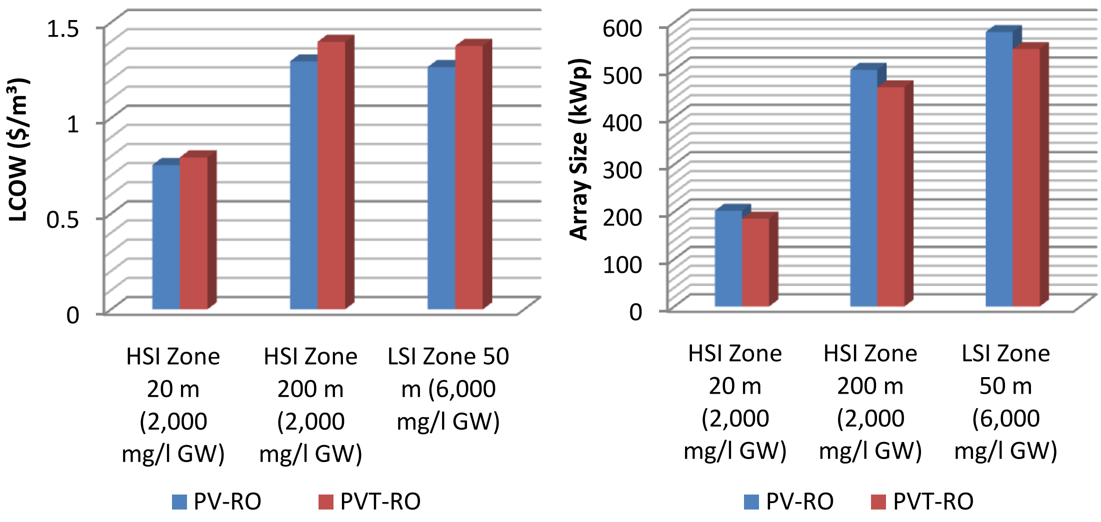

Figure 5-11: Comparison of the array size and LCOW between a PV and a PVT driven RO plant

The LCOW figures shown in *Figure 5-11* do not also include the expected extra costs associated with the expected lower lifetime of the RO modules where, as discussed in section *5.2.1*, some of them are operating outside the manufacture's recommended operating limits.

Moreover, as discussed in section *5.2.3.1*, given that the PVT collector model used in this study gives higher estimates of the wind thermal losses than the standard PV modules modelled in this study, a lower increase in the annual electricity yield of the PV system is expected by replacing the standard PV modules with PVT collectors.

The unfeasibility of replacing standard PV modules with PVT collectors to drive the RO plant is attributed to several factors. The main factor is, as discussed in section *5.2.3.2*, given that it is impossible to keep the water temperature at 40°C the whole day due to the low capacity factor of the PVT collectors and the variability of solar irradiance, much lower percentage reduction in the RO plant annual energy consumption was achieved which did not exceed 6.6% in comparison to values up to approximately 30% if the water was continuously heated to 40°C.

Secondly, it is concluded from section *5.2.3.2* that due to the operating temperature limitation of the RO membranes, increasing the PVT collector area to increase the average yearly water temperature will eventually result in a lower percentage decrease in the RO plant annual energy consumption as a portion of the PVT collectors will be more frequently operating at stagnant conditions.

Thirdly, this modest reduction and increase in the annual energy consumption of the RO plant and in the annual electricity yield of the PV system, respectively, mainly reduced the required PV cell area while had a negligible impact on the battery bank capacity required where a maximum percentage reduction of only 3% was achieved. Now as concluded from the sensitivity analysis carried out in Chapter 4, the PV module costs had a much lower impact on the LCOW in comparison with those of the battery bank. For this reason, even after assuming that replacing the PV modules with PVT collectors will incur no additional costs, the decrease in the LCOW did not exceed 2%.

For the aforementioned reasons, it can be safely concluded that despite the energy gains achieved, using PVT collectors instead of standard PV modules to drive an RO plant is not economical. It can be argued, however, that higher percentage reduction might be achieved if the PVT-RO plant is designed to operate only during day time as a higher reduction in the battery bank size could be achieved[164]. Nevertheless, as concluded in Chapter 4, it is more economical to design the PV-RO plant to operate for 24 hours; and even if at higher salinity the LCOW was found to be similar for both cases, it was previously shown in section *5.2.1* that heating the water in this case is less effective in reducing the annual energy requirements of the RO plant.

5.3 Conclusion

In this chapter, the feasibility of replacing the standard PV modules by PVT collectors to drive a BW RO plant was investigated. It is found that a net energy saving is only achieved using unglazed PVT collectors. Conversely, the high optical losses in glazed collectors outweighed the annual energy reduction by heating the feed water before going to the RO plant for all locations in Egypt and at different feed water salinities.

However, only a modest increase in the annual electricity yield by cooling the PV cells and reduction in the RO plant annual energy requirements by heating the feed water, ranging from approximately 3.5% to less than 7% for both, was achieved using

[164] This is in contrast with the case where the RO plant is operating for 24 hours where the battery storage is mainly required to run the plant during night time when the PVT collectors have no contribution.

unglazed PVT collectors. It was particularly found that while up to approximately 30% reduction in the energy requirements of the RO plant could be achieved by continuously heating the water to 40°C, the low capacity factor of the PVT collectors and the variability of solar irradiance in addition to the operating temperature limitation of the RO membranes resulted in a much lower percentage reduction that did not exceed 6.6%.

For this reason, a PVT-RO plant operating for 24 hours was found to have a higher LCOW than that of a PV-RO plant; and even when the additional costs of using PVT collectors were set to be zero, no more than 2% reduction in the LCOW was achieved. Therefore, it is concluded that using PVT collectors has no economic advantage over standard PV modules when coupled with an RO plant.

Finally, it was also concluded that even with brackish/saline or saline water, the reduction in the RO plant power consumption by increasing the feed water temperature, and the increase in the annual electricity yield by cooling the PV cells are also expected to be insignificant.

6. Membrane Distillation Process Modelling

In Chapter 2, it was shown that all studies on the feasibility of RO/MD plants were based on the performance of laboratory scale modules which have high fluxes that cannot be achieved with full scale modules. Accordingly, the hybrid plant analysis carried out in this thesis will be based on a full scale MD module to guarantee more realistic results. Moreover, it was discussed that there is no available commercial simulation tools for the MD process and the modelling work available in the literature is only for laboratory scale modules.

Accordingly, in this chapter a mathematical model is built to simulate the performance of a commercial full scale spiral wound PGMD module. The results of the model will be used in the analysis on solar driven hybrid RO/MD plants carried out in Chapter 7.

Firstly, this chapter presents the methodology used to model the PGMD module. Secondly, the results of the model are discussed and its validity is verified through a comparison with experimental values obtained from the literature.

6.1 MD Module Description

The PGMD module modelled in this study is a spiral wound module (*Figure 6-1*) where the hot and cold feed water circulate tangentially to the membrane surface and in counter flow direction in alternate evaporator and cooling channels (*Figure 6-2*). This setting maintains a high temperature difference between both channels (Çengel, 2003) over the length of the MD membrane which increases the pressure gradient hence the permeate water production. The permeate water outlet is located at the top of the module to ensure that the permeate channel is completely filled with water (Winter et al., 2012) purging the air outside the membrane such that there will be no additional resistance to vapour mass transfer.

The PGMD module dimensions and other characteristics are obtained from Winter et al. (2011) and are shown in *Table 6-1*.

Figure 6-1: PGMD spiral wound module manufactured by SolarSpring

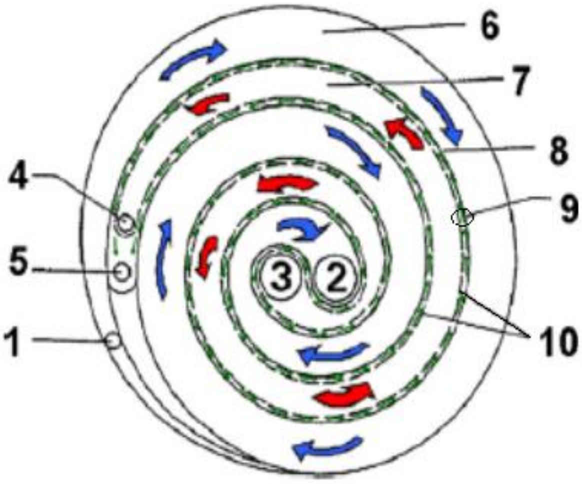

Figure 6-2: A schematic plan view of the PGMD spiral wound module
Source: (Winter et al., 2011)

1] Cooling Channel Inlet 2] Cooling Channel Outlet 3] Evaporator Channel Inlet 4] Evaporator Channel Outlet 5] Permeate Channel Outlet 6] Cooling Channel 7] Evaporator Channel 8] Impermeable Condenser Foil 9] Permeate Channel 10] Porous Membrane

Table 6-1: Properties of the PGMD spiral wound module

Membrane Pore Radius (r_m)	0.1 um	**Channel Length** (L_{ch})	7 m
Membrane Thickness (δ_m)	70 um	**Evaporator/Cooling Channel Thickness** (δ_{ch})	3.2 mm
Membrane Porosity (ε_m)	80%	**Membrane Area** (A)	9.8 m^2
Membrane Material	PTFE	**Permeate Channel Thickness**[165] (δ_p)	0.5 mm
Channel Height (b_{ch})	0.7 m	**Condenser Foil Thickness**[165] (δ_{cf})	127 um
Spiral Coil Diameter	0.28 m	**Condenser Foil Material**	ETFE

[165] (D Winter 2013, pers. Comm., 23 Jan.)

6.2 Methodology

The PGMD spiral wound module is modelled through dividing the membrane into differential elements (DE's) on which mass and heat transfer equations are applied. The overall heat transfer and water permeate flow rate is then obtained through integration over the length of the membrane. Therefore, a mathematical representation of the module geometry is firstly required.

6.2.1 PGMD module mathematical representation

As shown in *Figure 6-2*, the membrane unit, which includes the condenser foil, the porous membrane and the permeate channel in between, is in a loop shape wrapped around the cooling and evaporator channels inlet and exit tubes and laid out in a spiral pattern throughout the module. Given that the thickness of the evaporator and cooling channels is constant throughout the membrane due to the presence of spacers, both channels could be represented by two Archimedean spirals along their axes. Such spirals have a constant rate of change of the radius of the spiral with the angle ($dr/d\phi$) which is calculated using equation *(6-1)*.

$$\frac{dr}{d\phi} = \frac{Sp}{2\pi} \quad \textbf{(6-1)}$$

where Sp is the spacing between two consecutive membrane unit layers in the same spiral

By determining the radius (r) from equation *(6-2)* obtained from Weisstein (2013), the spiral could be then graphically represented as shown in *Figure 6-3*.

$$r = r_0 + \frac{dr}{d\phi}\,\phi \qquad \textbf{(6-2)}$$

where r_0 is the initial radius of the spiral and determines the distance from the origin of the spiral (i.e. the point at which $r = 0$), which is taken to be the centre point of the module, to its actual starting point, i.e. the point at which ϕ is taken to be zero.

The starting point of the spirals representing the evaporator and the cooling channels is the point at which the hot water leaves the evaporator channel inlet tube and enters the hot channel, and the point at which the cooling water enters cooling channel tube and exits the channel respectively. However, given that the modules are not at hand, the initial radius could not be directly determined. Accordingly, the starting points of the spirals representing the evaporator and the cooling channels are initially taken to be the centre of their corresponding tubes where in this case the initial radius is simply the radius of the tube (*Figure 6-3*).

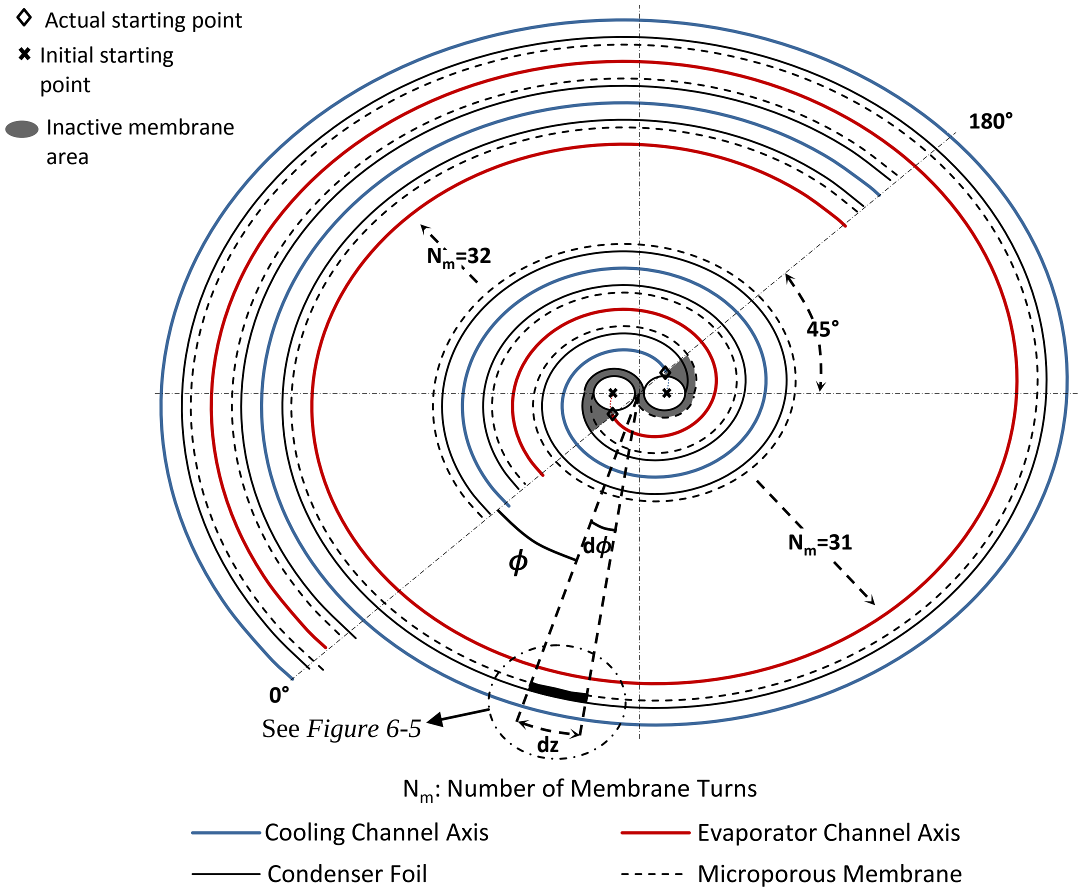

Figure 6-3: Approximated shape of the modelled PGMD spiral wound module

The actual starting points of the evaporator and the cooling channels, assumed to be located at the start of the fourth and second quadrant of their corresponding inlet and outlet tubes respectively, are therefore shifted by 45° from the start of the spiral and the horizontal axis of the module. Therefore, to set the actual starting point of the channel to be the new starting point of the spiral, the initial radius should be equal to:

$$r_{0_{ch}} = 0.5\,(\delta_{\mathrm{ch}} + \delta_{\mathrm{cf}} + \delta_{\mathrm{m}} + \delta_{\mathrm{p}}) + \frac{dr}{d\phi}\frac{\pi}{4} \qquad \textbf{(6-3)}$$

where the second part of equation *(6-3)* accounts for the extra length due to the 45° offset.

As the module channel length is known, i.e. 7 m, using the arc length equation *(6-4)*, obtained from Weisstein (2013), the number of spiral turns (N), hence the number of layers[166], of the evaporator and cooling channels could be calculated.

$$L_{arc} = \int_0^{2\pi N} \sqrt{\left(\frac{dr}{d\phi}\right)^2 + \left(\frac{dr}{d\phi}\phi + r_0\right)^2}\ d\phi \qquad \textbf{(6-4)}$$

where the spacing between two consecutive spirals in the same channel (Sp_{ch}), needed to calculate the rate of change of the radius of the spiral with the angle, is equal to:

$$Sp_{ch} = 2\left(\delta_{ch} + \delta_{cf} + \delta_{m} + \delta_{p}\right) \qquad \textbf{(6-5)}$$

The number of turns is then found to be 16.534 and for simplicity is approximated to be 16.5. It should be noted, however, that Winter al. (2011) did not specify which channel, i.e. the evaporator or the cooling channel, has 7 m length. Accordingly, in this model this length is associated with the cooling channel because the schematic diagram in *Figure 6-2* shows that the cooling channel ends somewhere in the third quadrant of the module plan view area which can only occur if its length is 7 m; otherwise, if the reported length is associated with the evaporator channel, the cooling channel end will be offset by 180°, i.e. in the first quadrant.

Taking the start of the evaporator channel as the reference point (i.e. $\phi = 0$), the starting point of the cooling channel is therefore lagging that of the evaporator channel by a half turn, i.e. 180°. Accordingly the number of turns of the latter is only 16 such that both channels end at the same point. Accordingly, the length of the evaporator channel is about 43 cm shorter (≈6.56 m) than the cooling channel.

As the number of turns of the cooling and evaporator channels is known, the number of the membrane unit turns and their lengths could be determined. To represent the membrane unit by an Archimedean spiral, the membrane unit loop is broken into two separate units after ignoring the membrane sections covering the outlet and inlet tubes of the cooling and the evaporator channels respectively. This assumption should not affect the results because the membrane section covering the outlet tube of the cooling channel is likely to have a small contribution to the permeate production as it has no access to the cooling channel and that covering the inlet tube of the evaporator channel

[166] The terms layers and turn will be used interchangeably in this chapter

does not contribute to the permeate production as it has no access to the evaporator channel.

In this case, the starting point of each membrane unit lies on the same axis at which the starting points of the channels are located (*Figure 6-3*). Accordingly, the number of turns of the membrane unit overlying the evaporator channel is the same as that of the evaporator channel, i.e. 16. However, for the membrane unit overlying the cooling channel, the number of turns is 1 turn less than that of the cooling channel, i.e. 15.5[167], because there is no membrane unit layer overlying the outer layer of the latter (*Figure 6-2*).

After determining the number of turns of the membrane unit, the length of each membrane unit DE with an inscribed angle $d\phi$ could be determined. It should be noted that the lengths of the membrane and the condenser foil, as well as the distillate channel, are assumed to be equal given that their thicknesses are very small (*Table 6-1*). The length of the DE varies according to its position with the respect to the starting point of the spiral and is calculated as follows:

$$\mathrm{dz}\ (n_i, N_{m,i})=\int_a^{a+d\phi} \sqrt{\left(\frac{dr}{d\phi}\right)^2 + \left(\frac{dr}{d\phi}\phi + r_{0_m}\right)^2}\, d\phi \quad \textbf{(6-6)}$$

$$a = \left(N_{m,i} - 1\right)\pi + (n_i\text{-}1)\ d\phi$$

where ϕ is the angle with respect to the starting point of the evaporator channel (*Figure 6-3*), $N_{m,i}$ is the number of the membrane turn and ranges from 1 to 31 for the lower half of the module (i.e. ϕ= 0 to 180°) and 1 to 32 for the upper half (i.e. ϕ= 180 to 360°)[168] where the latter is the maximum number of turns in the module ($N_{m,max}$), and n_i is the number of the DE's in one turn and it ranges from 1 to n_{max}, where n_{max} is the total number of DE's in one turn and determines the accuracy of the model such that:

$$d\phi = \frac{360°}{n_{max}} \quad \textbf{(6-7)}$$

[167] 15.5 turns means that there are 15 layers in the bottom half of the membrane (ϕ=0 to 180°) and 16 in the upper half.

[168] The membrane sections overlying the evaporator and the cooling channels respectively have 16 and 15.5 turns therefore in the module lower half there is a total of 16+15 layers while at the upper half there is 16+16 layers

6.2.2 Mass transfer

There are several models discussed in the literature that describe the mass transfer in an MD process (Lawson, 1995). The Dusty Gas Model (DGM) is the main model used in MD modelling studies (El-Bourawi et al., 2006) and it generally describes diffusion of molecules through a porous media. In the DGM, the porous medium is imagined to behave similarly to stationary uniformly distributed large particles, i.e. dust, that block the moving gas particles. Both particles are then treated as one mixture and the mass transfer equations are derived using the kinetic theory of gases (Schofield et al., 1990a, Lawson, 1995). The DGM model includes the following transport mechanisms (Lawson and Lloyd, 1997, Martínez et al., 2002, Khayet and Matsuura, 2011d):

1- Knudsen diffusion flow where the mass transfer across the membrane is limited by the direct transfer of momentum of the water vapour[169] molecules to the membrane pore wall as they collide with it.
2- Ordinary molecular diffusion flow where the mass transfer across the membrane is limited by the transfer of momentum of the water vapour molecules to that of the air trapped inside the pores as they collide with each other.
3- The viscous or Poiseuille convective flow where the mass transfer across the membrane is limited by the indirect transfer of momentum to the pore wall as the water vapour molecules collide with each other before eventually colliding with the membrane pore wall.
4- The surface diffusion flow where water vapour molecules adsorb on the membrane walls then diffuse under a pressure gradient.

In the DGM model the aforementioned mass transfer resistances are arranged as shown in *Figure 6-4*.

[169] Gas in general but water vapour is used because the main focus of this study is water desalination

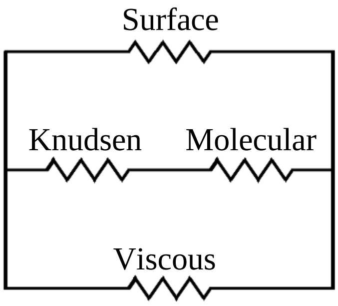

Figure 6-4: Electrical analogy of mass transfer resistances in the DGM model

According to Lawson and Lloyd (1997), the Knudsen and the ordinary molecular diffusion resistances to mass transfer have to be considered for membranes with pore sizes less than 0.5 um as the effect of both resistances become equally important. Moreover, calculating the mean free path[170] of water vapour in air for the expected module operating temperatures, using equation *(6-8)* obtained from Curcio and Drioli (2005), shows that the membrane pore size (0.2 μm) falls within the transition region window, i.e. 0.1 to 100 times[171] the mean free path of the water vapour, at which the combined Knudsen-molecular diffusion mechanism should be considered (Khayet and Matsuura, 2011d).

$$\lambda_{w/a} = \frac{\kappa_B \bar{T}_m}{\pi \left(\frac{\sigma_w + \sigma_a}{2}\right)^2 P \sqrt{1 + \left(\frac{M_w}{M_a}\right)}} \qquad \textbf{(6-8)}$$

where κ_B is the Boltzmann constant, σ_w and σ_a are the collision diameter of water vapour and air molecules respectively (2.7 and 3.7 A° respectively), $\bar{T}_m$ is the membrane mean temperature, P is the total pressure, and M_w and M_a are the molar masses of water and air respectively[172].

[170] Approximately 0.1 to 0.12 μm
[171] The transition region between a dominant Knudsen diffusion and a dominant molecular diffusion mass transfer
[172] It should be noted that there are discrepancies in the literature in calculating the mean free path. Some studies such as (Fernández-Pineda et al., 2002, Khayet and Matsuura, 2011d) used the total pressure, i.e. the atmospheric pressure, to calculate the mean free path and then compared it with the membrane pore size to determine the suitable mass transfer mechanism in the membrane. Other studies such as (Schofield et al., 1987, Lawson and Lloyd, 1997) estimated the mean free path using the water vapour saturation pressure ignoring the presence of air in the pores which increases the mean free path to be larger than the membrane pore size hence the Poiseuille flow contribution is ignored. All the above mentioned studies also calculated the mean free path for a single component, i.e. water, neglecting the effect of air molecules.

The viscous flow is generally negligible in DCMD, which is also applies for PGMD, as the water at the membrane surface in the evaporator and the permeate sides is under a constant total pressure approximately equal to the atmospheric pressure due to the presence of air inside the pores, and therefore there is no trans-membrane hydrostatic pressure difference to initiate the viscous flow (Laganà et al., 2000, Khayet et al., 2001, Yun et al., 2006, Qtaishat et al., 2008).

The surface diffusion flow is generally insignificant in an MD process as the hydrophobic nature of the membrane limit any interaction between the vapour molecules and the membrane (Schofield et al., 1990a, Lawson and Lloyd, 1997).

For the aforementioned reasons, it has been concluded that the mass transfer in the PGMD module analysed in this study could be represented by a combined Knudsen-molecular diffusion mechanism. Accordingly the membrane flux could be estimated using the following equation obtained from Lawson and Lloyd (1997) which is based on the DGM model :

$$J_w = K_M \, \nabla p^{-1} \qquad \textbf{(6-9)}$$

where K_M is the mass transfer coefficient:

$$K_M = -\frac{M_w}{RT}\left[\frac{1}{K_0\sqrt{\frac{8\,RT}{\pi\,M_w}}} + \frac{p_a}{K_1\,PD_{w/a}}\right]^{-1} \qquad \textbf{(6-10)}$$

Where K_0 and K_1 are constants that depend on the membrane geometry and its interaction with vapour molecules and could be related to the membrane structural parameters by assuming that its pores are not interconnected and have cylindrical shape as follows (Lawson and Lloyd, 1997):

$$K_0 = \frac{2\,r_m\,\varepsilon_m}{3\,\chi}$$

$$K_1 = \varepsilon_m/\chi$$

Accordingly equation *(6-9)* and *(6-10)* become:

$$J_w = -\frac{M_w}{RT}\left[\frac{1}{\frac{2\, r_m\, \varepsilon_m}{3\,\chi}\sqrt{\frac{8\,RT}{\pi\, M_w}}} + \frac{p_a}{\frac{\varepsilon_m\, PD_{w/a}}{\chi}}\right]^{-1} \nabla p^{-1} \quad \textbf{(6-11)}$$

Equation *(6-11)* was integrated[173] by Lawson and Lloyd (1996) such that:

$$J_w = \frac{\varepsilon_m\, PD_{w/a} M_w}{\chi \delta_m\, R\overline{T}_m}\ \ln\left[\frac{p_{a,p}\ \frac{2\varepsilon_m r_m}{3\chi}\sqrt{\frac{8\,R\overline{T}_m}{\pi\, M_w}} + \frac{\varepsilon_m PD_{w/a}}{\chi}}{p_{a,e}\ \frac{2\varepsilon_m r_m}{3\chi}\sqrt{\frac{8\,R\overline{T}_m}{\pi\, M_w}} + \frac{\varepsilon_m PD_{w/a}}{\chi}}\right] \quad \textbf{(6-12)}$$

The diffusion coefficient of water vapour in air ($D_{w/a}$) is estimated using the following correlation obtained from Nellis and Klein (2009):

$$D = -2.775 \times 10^{-6} + 4.479 \times 10^{-8}\, \overline{T}_m + 1.656 \times 10^{-10}\, \overline{T}_m{}^{2} \quad \textbf{(6-13)}$$

It should be noted that because the temperature within the membrane pores is not constant (see section *6.2.3.2*), for simplicity all the water and air properties within the membrane are calculated using the arithmetic mean of the membrane surface temperatures such that:

$$\overline{T}_m = 0.5\ (T_{m,e} + T_{m,p}) \quad \textbf{(6-14)}$$

where $T_{m,e}$ and $T_{m,p}$ are membrane surface temperatures at the evaporator and the permeate channel sides respectively.

The partial pressure of air (p_a) on each side of the membrane is calculated by deducting the total pressure at the membrane surface from the water vapour partial pressure on the corresponding side, based on Dalton's law of partial pressure (Winter et al., 2012, Martínez et al., 2002). The total pressure (P) is assumed to be constant and almost equal to the atmospheric pressure (Kimura et al., 1987, Martínez et al., 2002, Qtaishat et al., 2008).

$$p_a = P - p_w \quad \textbf{(6-15)}$$

---

[173] Equation *(6-11)* could be also used without integration by replacing ∇p by its finite value $\Delta p_w / \delta_m$ assuming a linear distribution of pressure across the membrane with a negligible effect on the results

$$P \approx 1 \text{ atm}$$

The correlations used to calculate the water vapour pressure and other water properties at different water temperatures and salinity are shown in Appendix H.

The membrane tortuosity (χ) in equation *(6-12)*, a factor that accounts for the fact that the membrane pore is not a straight cylinder but has a tortuous nature which increases the path through which the vapour molecules need to go through within the membrane (Burgoyne and Vahdati, 2000),is not known and is usually not reported by the manufacturers (Khayet et al., 2001). In this model, the membrane tortuosity is used as an adjustable parameter to obtain the best fit to the experimental data shown in Winter et al. (2011), which is a common practice in MD modelling studies (El-Bourawi et al., 2006, Khayet and Matsuura, 2011d).

It should be noted that the effect of CP on the vapour pressure, hence the flux, is ignored in this model. Concentration polarization is the accumulation of salts at the membrane surface as the water vapour molecules leave the feed solution and cross the membrane resulting in a higher water salinity than that of the bulk solution (Martínez-Díez and Vázquez-González, 1999, Curcio and Drioli, 2005). The high water salinity reduces the water vapour pressure and therefore the flux. However, the effect of CP is insignificant on mass transfer (Schofield et al., 1990b, Martínez-Díez and Vázquez-Gonzàlez, 1999, Curcio and Drioli, 2005). Martínez-Díez and Vázquez-Gonzàlez (1999) in particular showed that the concentration of sodium chloride in water at the membrane surface when the bulk feed water concentration was up to approximately 100 g/l was found to be not more than 4% of that of the bulk solution and therefore has a negligible effect on water vapour pressure.

6.2.3 Heat transfer

6.2.3.1 Heat transfer in the evaporator channel

As the hot feed water flows in the evaporator channel, heat is transferred by convection from the bulk water to the membrane surface across the thermal boundary layer (Lawson and Lloyd, 1997, Ding et al., 2003). Boundary layer heat transfer resistance is a main limitation to mass transfer in the MD process as it causes the temperature at the membrane surface to be less than that of the bulk water in the evaporator channel (and higher than the bulk water temperature in the cooling channel), a phenomenon referred to as temperature polarization. In this case, the lower trans-membrane temperature difference results in a lower vapour pressure gradient reducing the driving force for mass transfer hence the flux. (Fane et al., 1987, Schofield et al., 1987, Martínez-Díez and Vázquez-González, 1999)

Additional heat is also transferred to the membrane surface by the mass transfer of water molecules (Banat and Simandl, 1998). While the heat transfer by mass transfer is usually ignored in most MD modelling studies in the literature, for more accuracy it is considered in this study as its effect could be significant at high temperatures (Phattaranawik and Jiraratananon, 2001).

$$\dot{q_e} = \dot{q}_{e,conv} + \dot{q}_{e,J} = h_e\left(T_{b,e} - T_{m,e}\right) + J_w Cp_{l,e}\left(T_{b,e} - T_{m,e}\right) \quad \textbf{(6-16)}$$

Where $\dot{q_e}$ is the overall heat transfer rate from the bulk water in the evaporator channel to the membrane surface, $\dot{q}_{e,conv}$ is the convective heat transfer rate, $\dot{q}_{e,J}$ is the heat transfer rate by mass transfer, $T_{b,e}$, h_e and $Cp_{l,e}$ are the bulk water temperature, the convective heat transfer coefficient and the specific heat capacity of water in liquid phase of the evaporator channel respectively.

The convective heat transfer coefficient is estimated through semi-empirical equations which are discussed in section *6.2.6*.

6.2.3.2 Heat transfer within the membrane

Within the membrane, heat transfer occurs simultaneously with mass transfer as a result of the latent heat stored in the diffusing water vapour. Heat is also transferred by conduction through the membrane material and the air trapped within the pores (Fane et al., 1987, Schofield et al., 1987, Ding et al., 2003) such that:

$$\dot{q_m} = \dot{q_v} + \dot{q}_{cond} \quad \textbf{(6-17)}$$

$$\dot{q}_{cond} = -k_m \frac{dT_m}{dx} \quad \textbf{(6-18)}$$

$$\dot{q_v} = J_w\left(H_v\{T_{m,x}\} - H_l\{T_{m,p}\}\right) \quad \textbf{(6-19)}$$

where $\dot{q_m}$ is the overall heat transfer rate through the membrane, $\dot{q_v}$ is the heat transfer rate by the vapour mass transfer, $\dot{q}_{cond}$ is the conductive heat transfer rate, k_m is the overall membrane thermal conductivity, $H_v\{T_{m,x}\}$ is the water vapour specific enthalpy at a point within the membrane located at x distance from the evaporator side of the membrane surface, and $H_l\{T_{m,p}\}$ is the liquid water specific enthalpy at the permeate side of the membrane surface.

Taking the reference temperature to be that of the permeate side of the membrane surface, the vapour specific enthalpy at a point x within the membrane is equal to:

$$H_v\{T_{m,x}\} = H_v\{T_{m,p}\} + \int_{T_{m,p}}^{T_{m,x}} Cp_v \, dT \quad \textbf{(6-20)}$$

At the expected temperature differences between the membrane surfaces, the value of the vapour specific heat capacity (Cp_v) could be assumed constant and therefore equation *(6-20)* becomes:

$$H_v\{T_{m,x}\} = H_v\{T_{m,p}\} + Cp_v(T_{m,x} - T_{m,p}) \quad \textbf{(6-21)}$$

It should be noted that while some studies, such as (Gryta and Tomaszewska, 1998, Phattaranawik et al., 2003, Qtaishat et al., 2008), only include the vapour specific enthalpy in estimating the heat transfer by mass transfer within the membrane, it is more accurate to deduct the sensible heat content of the permeate water in equation *(6-19)*.This is because the specific enthalpy values[174] in the saturated water properties tables in the literature (Çengel and Cimbala, 2006) at different temperatures are with respect to a reference temperature of 0°C, while the heat at the evaporator side of the membrane surface is transferred to the permeate side whose temperature is larger than 0°C.

By substituting equation *(6-21)* in equation *(6-19)*, the heat transfer by mass transfer through the membrane is equal to:

$$q_{\dot{v}} = J_w\left(\Delta H_w\{T_{m,p}\} + Cp_v(T_{m,x} - T_{m,p})\right) \quad \textbf{(6-22)}$$

where ΔH_w is the latent heat of vaporization of water

---

[174] The liquid water enthalpy in particular is referenced to 0°C based on which the vapour enthalpy values are estimated

From equation *(6-22)*, it can be observed that the heat transferred by mass transfer ($\dot{q_v}$) is simply the summation of the latent heat of vaporization and the sensible heat transfer[175] through the vapour which is directly stated in some studies such as (Kimura et al., 1987, Kurokawa et al., 1990, Banat and Simandl, 1998, Chang et al., 2010). Nevertheless, the steps leading to equation *(6-22)* were discussed to avoid any ambiguity especially that the aforementioned studies do not specify the temperature at which the latent heat is estimated. Conversely, following the aforementioned steps it is clear that the latent heat should be estimated at the temperature of the permeate side of the membrane surface.

Following the same procedure by Gryta and Tomaszewska (1998), the value of $\dot{q_m}$ is estimated by substituting equation *(6-22)* and *(6-18)* in equation *(6-17)* such that:

$$\int_{T_{m,e}}^{T_{m,p}} \frac{dT}{\left(J_w \Delta H_w\{T_{m,p}\} + J_w Cp_v\left(T_{m,x} - T_{m,p}\right) - \dot{q_m}\right)} = \int_0^{\delta_m} \frac{1}{k_m} dx \quad \textbf{(6-23)}$$

After integrating[176] equation *(6-23)*, the heat transfer across the membrane is calculated as follows:

$$\dot{q_m} = \frac{J_w Cp_v\left(T_{m,e} - T_{m,p}\right)}{1 - e^{-\frac{J_w Cp_v \delta_m}{k_m}}} + J_w \Delta H_w\{T_{m,p}\} \quad \textbf{(6-24)}$$

The overall thermal conductivity of the membrane k_m includes the conductivity of the membrane material and that of the air trapped inside the pores[177]. Different models are available in the literature to determine the combined effect of both conductivities:

a- Isostrain Model (Series Model)

$$k_m = (1 - \varepsilon_m)k_s + \varepsilon_m k_a \quad \textbf{(6-25)}$$

---

[175] The sensible heat transfer may be ignored as it is much smaller than the latent heat of vaporization and this could be the reason that many MD modelling studies, such as Fane et al. (1987), Schofield et al. (1990b), Lawson and Lloyd (1997), Martínez-Díez and Vázquez-Gonzàlez (1999), El-Bourawi et al. (2006), Yun et al. (2006), and Cheng et al. (2008), do not include the sensible heat transfer.

[176] It should be noted that because the temperature distribution is usually nearly linear within the membrane (Phattaranawik et al., 2003) integrating equation *(6-23)* may not be necessary

[177] While the membrane pores contain a mixture of air and water vapour, the thermal conductivity of air was used as it is similar to that of water and therefore the mixture could be treated as one component (Phattaranawik et al., 2003)

b- Isostress Model (Parallel Model)

$$k_m = \left(\frac{\varepsilon_m}{k_a} + \frac{1-\varepsilon_m}{k_s}\right)^{-1} \quad \textbf{(6-26)}$$

c- Maxwell Model

$$k_m = k_a\left(\frac{1+2\beta(1-\varepsilon_m)}{1-(1-\varepsilon_m)\beta}\right) \quad \textbf{(6-27)}$$

$$\beta = \frac{(k_s - k_a)}{(k_s + 2k_a)}$$

where k_s is the thermal conductivity of the membrane material, i.e. PTFE, and is approximately 0.28 W/m^2.K based on the values reported in Phattaranawik et al. (2003), k_a is the thermal conductivity of air and is estimated using the following correlation obtained from Lawson and Lloyd (1997):

$$k_a = 2.72\ 10^{-3} + 7.77\ 10^{-5}\ \bar{T}_m \quad \textbf{(6-28)}$$

The Isostrain model is used in most MD modelling studies in the literature, such as Fane et al. (1987), Schofield et al. (1987), Lawson and Lloyd (1997), and Martínez-Díez and Vázquez-Gonzàlez (1999). Nevertheless, this commonly used model has been reported in several studies, such as Phattaranwik et al. (2003), Guijt et al. (2005) and García-Payo and Izquierdo-Gil (2004), to overestimate the overall membrane thermal conductivity. This overestimation of the conduction heat losses will significantly affect the results especially at higher temperatures as it makes the flux less sensitive to the membrane surface temperatures. Conversely, the Isostress model is rarely used in MD modelling studies and is only mentioned in Phattaranawik et al. (2003) as the study examined the validity of different models to estimate the overall thermal conductivity of several MD membranes. The Isostress model also tends to underestimate the thermal conductivity values (García-Payo and Izquierdo-Gil, 2004). Finally, the Maxwell model is also rarely used in MD modelling studies but is recommended by Garcia-Payo and Izquierdo-Gil (2004) to estimate the thermal conductivities of membranes with porosities higher than 60%.

Accordingly, given that membrane used in the PGMD module has a high porosity of 80%, the Maxwell model shall be used. Nevertheless, the validity of the commonly applied Isostrain model will be also tested.

6.2.3.3 Heat transfer in the permeate channel

The water vapour crossing the membrane pores condenses in the permeate channel after losing its heat to the cooling channel. As the permeate water flows inside the channel towards the channel outlet at the top of the module, convective heat transfer between the membrane surface and the condenser foil is expected to occur. In this case the rate of heat transfer across the permeate channel is:

$$\dot{q_p} = h_p \left(T_{m,p} - T_{cf}\right) \quad \textbf{(6-29)}$$

where T_{cf} is the condenser foil temperature and h_p is the convective heat transfer of the permeate channel.

It could be argued, however, that because the flow rate within the permeate channel is expected to be very small, the heat transfer could be assumed to occur only by conduction (i.e. assuming a Nusselt number of 1). In this case, the rate of heat transfer across the permeate channel can be estimated as follows:

$$\dot{q_p} = \frac{k_p}{\delta_p} \left(T_{m,p} - T_{cf}\right) \quad \textbf{(6-30)}$$

where k_p is the thermal conductivity of the permeate channel which is calculated using equation *(6-27)*, after replacing the thermal conductivity of air (k_a) by that of water (k_w), to account for both the thermal conductivity of water and the spacer material.

6.2.3.4 Heat transfer from the permeate channel to the cooling channel

Finally, heat is transferred from the permeate channel to the cooling channel by conduction through the condenser foil then through the thermal boundary layer of the cooling channel by convection.

$$\dot{q}_{cf/c} = \left(\frac{1}{h_c} + \frac{\delta_{cf}}{k_{cf}}\right)^{-1} \left(T_{cf} - T_{b,c}\right) \quad \textbf{(6-31)}$$

where $q_{cf/c}^{\cdot}$ is rate of heat transfer from the permeate channel to the cooling channel, h_c is the convective heat transfer of the cooling channel and k_{cf} is thermal conductivity of the condenser foil.

6.2.4 Mass and energy balance equations

At steady state, the heat transfer rates across the evaporator channel, the membrane, the permeate channel, the condenser foil and the cooling channel are all equal:

$$q_e^{\cdot} = q_m^{\cdot} = q_p^{\cdot} = q_{cf-c}^{\cdot} = q^{\cdot} \qquad \textbf{(6-32)}$$

Substituting each heat transfer rate in equation *(6-32)* by its corresponding equation, i.e. equations *(6-16), (6-24), (6-29)/(6-30), and (6-31)* respectively, the system of non-linear equations, including the mass transfer equation, i.e. equation *(6-12)*, is solved numerically using MATLAB® for each DE (*Figure* 6-5).

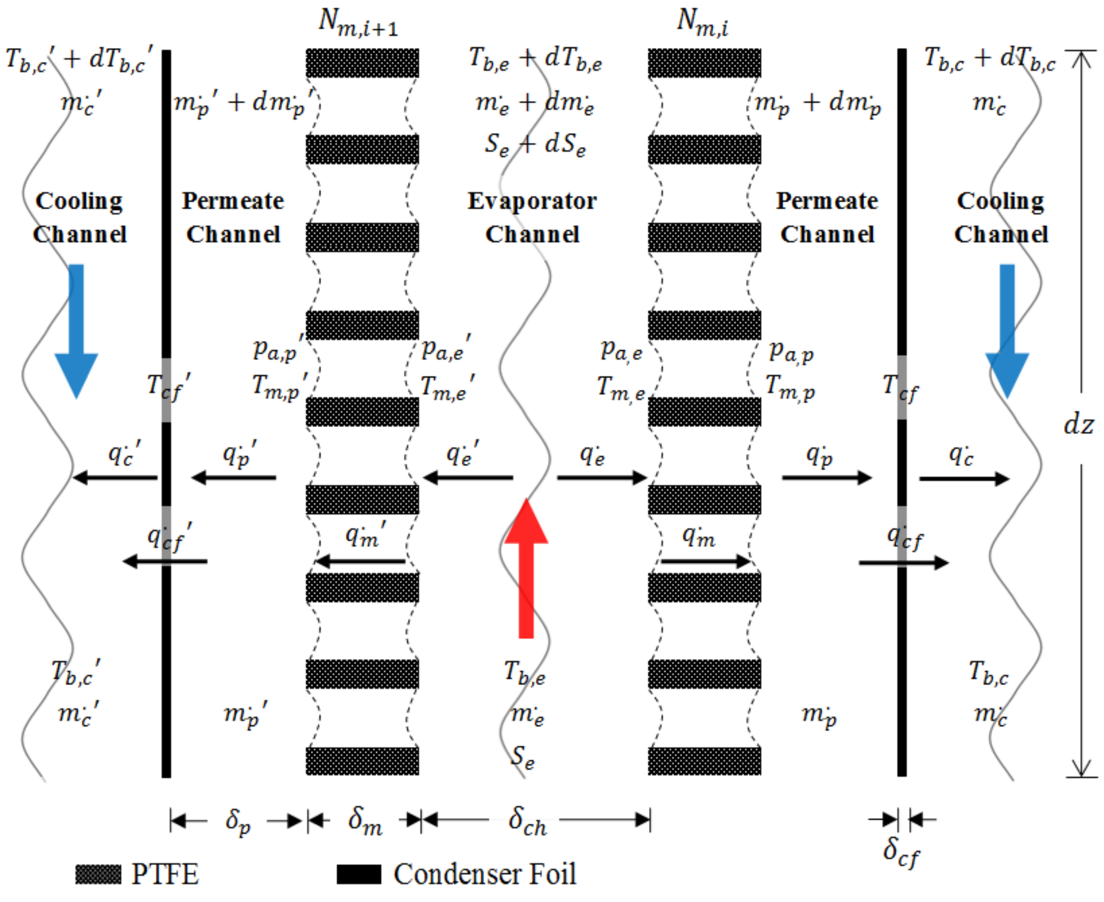

Figure 6-5: Heat and mass transfer through a differential element of the MD membrane unit

Accordingly, the flux (J_w), the heat transfer rate ($q^{\cdot}$), the membrane surfaces and condenser foil temperatures $T_{m,e}$,$T_{m,p}$, and T_{cf} are calculated for each DE. Accordingly, the bulk water temperatures in the evaporator and the cooling channels in addition to the mass flow rate and the water salinity in the former associated with the next DE could be determined through mass and energy balance equations.

In the evaporator channel, the change in the mass flow rate ($\dot{m_e}$) along the length of a DE (dz) is equal to the amount of water vapour crossing the membrane such that:

$$d\dot{m_e} = -J_w b_{ch} dz \quad \textbf{(6-33)}$$

Assuming 100% salt rejection, the salt mass is constant, i.e. $d\dot{m_e} S_e = 0$, the change in the water salinity in the evaporator channel along the length of a DE, hence the water salinity (S_e) of the evaporator channel partition associated with the next DE, is calculated as follows:

$$dS_e = \frac{J_w S_e b_{ch} dz}{\dot{m_e} - J_w b_{ch} dz} \quad \textbf{(6-34)}$$

The change in the bulk water temperature in the evaporator channel is estimated through energy balance equations such that the change in the feed water heat content is equal to the amount of heat transfer rate from the channel to the membrane surface:

$$d\dot{m_e} H_e = (\dot{m_e} + d\dot{m_e}) H_e\{T_{b,e} + dT_{b,e}\} - \dot{m_e} H_e\{T_{b,e}\} = -q^{\cdot} b_{ch} dz \quad \textbf{(6-35)}$$

For the cooling channel, the water salinity (S_c) and the mass flow rate ($\dot{m_c}$) are constant. The water specific heat capacity could be assumed to be constant at the small temperature difference expected between the channel partitions associated with two consecutive DE's and therefore the change in the bulk water temperature is directly calculated as follows:

$$dT_{b,c} = -\frac{q^{\cdot} b_{ch} dz}{\dot{m_c} Cp_l} \quad \textbf{(6-36)}$$

6.2.5 Effect of spacer on convective heat transfer coefficients

In the analysed PGMD module, spacers are used in each channel to separate the membrane layers providing a space for water to flow. The spacers, particularly in the evaporator and the cooling channels, also help to increase the turbulence of the water flow as well as increasing the water flow rate which increases the convective heat transfer rate in both channels hence decreasing the temperature polarization and increasing the water flux (Da Costa et al., 1994, Cipollina et al., 2009).

The presence of a spacer in the channel mainly affects its effective cross sectional area and hydraulic diameter. To calculate the effective cross sectional area of the channel ($CSA_{ch,eff}$), the equations from Schock and Miquel, (1987) are used:

$$CSA_{ch,eff} = \frac{Void\ Volume}{Membrane\ Length} = \delta_{ch} b_{ch} \varepsilon_{sp} \quad \textbf{(6-37)}$$

$$\varepsilon_{sp} = \frac{Void\ Volume}{Channel\ Volume} = 1 - \frac{V_{sp}}{V_{ch}} \quad \textbf{(6-38)}$$

where ε_{sp} is the spacer porosity, V_{sp} is the volume of the spacer and V_{ch} is the volume of the channel where the spacer is present.

The hydraulic diameter is usually determined by dividing four times the cross sectional area by the wetted perimeter of the channel (Çengel and Cimbala, 2006). However, according to Schock and Miquel (1987), because channels containing spacers have periodically variable cross section areas, the hydraulic diameter is estimated by the more general form:

$$d_h = \frac{4\ volume\ of\ flow\ channel}{Wetted\ Surface} = \frac{4(V_{ch} - V_{sp})}{(Sw_{ch} + Sw_{sp})} \quad \textbf{(6-39)}$$

where the volume V_{ch} and the wetted surface Sw_{ch} of the channel are calculated as follows:

$$V_{ch} = \delta_{ch} b_{ch} L_{ch} \quad \textbf{(6-40)}$$

$$Sw_{ch} = 2(\delta_{ch} + b_{ch}) L_{ch} \quad \textbf{(6-41)}$$

Substituting equation *(6-38)*, *(6-40)* and *(6-41)* in *(6-39)*, the hydraulic diameter is calculated as follows:

$$d_h = \frac{4\varepsilon_{sp}}{\frac{2(\delta_{ch} + b_{ch})}{\delta_{ch} b_{ch}} + \left(1 - \varepsilon_{sp}\right) \frac{Sw_{sp}}{V_{sp}}} \quad \textbf{(6-42)}$$

To estimate the volume (V_{sp}) and the wetted surface (Sw_{sp}) of the spacer, the calculation method used by Da Costa et al. (1994) is adopted. Da Costa et al. (1994) calculated the V_{sp} and Sw_{sp} of a unit cell of the spacer consisting of one mesh with half size filaments, as each filament is shared between two unit cells, (*Figure 6-6*) such that:

$$\mathrm{V}_{\mathrm{sp,uc}} = \frac{\pi}{4}\left(L_{ms}\, {d_{fl}}^2 + L_{ml}\, {d_{fs}}^2\right) \tag{6-43}$$

$$\mathrm{Sw}_{\mathrm{sp,uc}} = \pi\left(d_{fs} L_{ml} + d_{fl} L_{ms}\right) \tag{6-44}$$

$$\mathrm{V}_{ch,uc} = \delta_{\mathrm{ch}} A_{msh} = \delta_{\mathrm{ch}} L_{ms} L_{ml} \sin(\theta) \tag{6-45}$$

Equations *(6-43)* and *(6-44)* are simply obtained by adding the volume and the wetted surface of each half filament of the unit cell respectively. However, the previous equations neglect the areas where both filaments are soldered together in the unit cell (*Figure 6-6*).

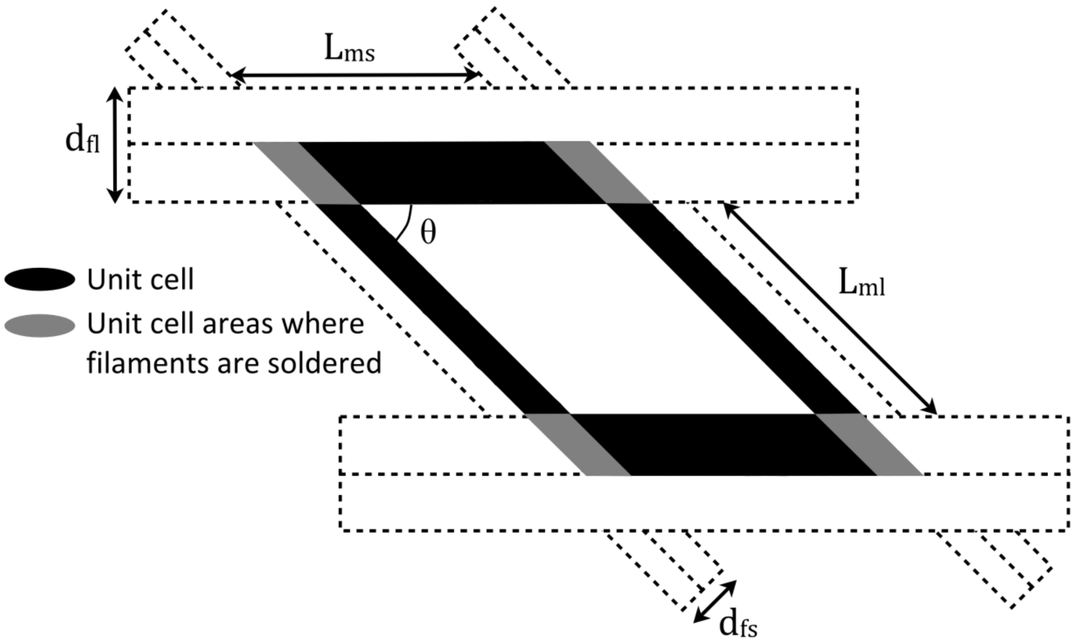

Figure 6-6: Schematic showing a sample of the spacer of the PGMD module and its unit cell

By investigating the effect of neglecting this area, it was found that the porosity and the hydraulic diameter of the spacer used in this study[178] were underestimated by

[178] It should be noted that while the author did not have access to the module, a sample of the spacer used in the module was obtained from the Fraunhofer institute.

approximately 18% and 36.5% respectively. This is because the parts where both filaments are soldered are relatively large in the spacer used in the PGMD module compared to the length of each filament.

Taking into account the extra volume and wetted surface by the areas where the filaments are soldered together, the volume and the wetted surface of the spacer unit cell can be estimated as follows:

$$V_{sp,uc}=\frac{\pi}{4}\left(\left(L_{ms}+\frac{d_{fs}}{\sin(\theta)}\right)d_{fl}^{\ 2}+\left(L_{ml}+\frac{d_{fl}}{\sin(\theta)}\right)d_{fs}^{\ 2}\right) \quad \textbf{(6-46)}$$

$$V_{ch,uc}=\delta_{ch}\left(L_{ms}+\frac{d_{fs}}{\sin(\theta)}\right)\left(L_{ml}+\frac{d_{fl}}{\sin(\theta)}\right)\sin(\theta) \quad \textbf{(6-47)}$$

$$S_{sp,uc}=\pi\left(d_{fs}L_{ml}+d_{fl}L_{ms}+2\,(0.75)\,\frac{d_{fl}d_{fs}}{\sin(\theta)}\right) \quad \textbf{(6-48)}$$

The 0.75 value in the third term in equation *(6-48)* is used as roughly 75% of the surface where both filaments are soldered together is in contact with the water.

Substituting the values from equations *(6-46)*, *(6-47)* and *(6-48)* into equations *(6-37)*, *(6-38)* and *(6-39)*, the porosity of spacer, the effective area of the channel and its hydraulic diameter could be estimated.

Finally, for the permeate channel spacer the equations by Da Costa et al. (1994), i.e. equations *(6-43)*, *(6-44)* and *(6-45)*, are used instead of the modified ones, i.e. equations *(6-46)*, *(6-47)* and *(6-48)*. This is because little data is available on the spacer's dimensions and it is likely that the area where both filaments are soldered to be very small because the spacer has small filament diameters given that the permeate channel's thickness is only 0.5 mm. The porosity of the spacer is in the range of 70% (D Winter, 2013, pers. Comm., 29 JUL.), and it is assumed that both filaments have the same diameter size and equal to half of the thickness of the spacer. Accordingly the mesh size, the hydraulic diameter, and the effective cross section area are determined assuming that the spacer has a rhombus mesh with a hydrodynamic angle of 45°.

6.2.6 Convective heat transfer coefficients

Due to the complexity of the convective heat transfer mechanism, the heat transfer coefficients are usually estimated using semi-empirical correlations based on experimental work (Çengel and Cimbala, 2006). For this reason, existing semi empirical correlations that are originally developed for heat exchangers, which can be mostly found in Gryta et al. (1997) Phattaranawik et al. (2003) and Curcio and Drioli (2005), are used to estimate the convective heat transfer in the channels in almost all of the reviewed MD modelling studies (Kimura et al., 1987, Gostoli and Sarti, 1989, Gryta et al., 1997, Banat and Simandl, 1998, Gryta and Tomaszewska, 1998, Martínez-Díez and Vázquez-Gonzàlez, 1999, Martínez-Díez and Florido-Díaz, 2001, Ding et al., 2003, Yun et al., 2006, Qtaishat et al., 2008). Nevertheless, very few correlations are developed for spacer filled channels and only the following correlations were found in the literature:

$$h = Ksp\ 0.664\ Re^{0.5}\ Pr^{0.33} \left(\frac{2d_h}{L_{ms\,h}}\right)^{0.5} \frac{\kappa_w}{d_h} \qquad \textbf{(6-49)}$$

$$Ksp = 1.654 \frac{d_f}{\delta_{ch}} - 0.039\ \varepsilon_{sp}^{0.75} \left(\sin\left(\frac{\theta}{2}\right)\right)^{0.086}$$

$$h = 0.664\ Re^{0.5}\ Pr^{0.33} \frac{2d_h}{L_{ms\,h}} \frac{\kappa_w}{d_h} \qquad \textbf{(6-50)}$$

$$h = 0.065\ Re^{0.875}\ Pr^{0.25} \frac{\kappa_w}{d_h} \qquad \textbf{(6-51)}$$

where Re is the Reynolds number, Pr is the Prandlt number, $L_{ms\,h}$ is the mesh size[179], and κ_w is the thermal conductivity of water.

The first two correlations were developed by Da Costa (1993) cited in (Da Costa et al., 1994) based on experiments on mass transfer in UF membranes, but the same correlations could be used for heat transfer under the assumed analogy between heat and mass transfer (Phattaranawik et al., 2003). The first correlation is used for spacers that induce directional flow change while the second correlation is used for spacers that do not induce change in flow direction i.e. the water flow is parallel to one set of filament in the spacer mesh. The third correlation is developed by Schock and Miquel (1987) and is independent of the type of spacer.

[179] The correlation is designed for spacers with meshes with filament length while the spacer used in the evaporator and the cooling channel of the module analysed in this study has filaments with different sizes, therefore the average mesh filament length was used instead.

6.2.7 Modelling technique for a spiral wound module

The modelling of the PGMD module is carried out in two steps each with its own model. The aim of the first step, i.e. model “A”, is to determine the proper convective heat transfer coefficient correlation, membrane overall thermal conductivity model, and membrane tortuosity values that give the best fit, i.e. lowest sum of the root mean square error (ΣRMSE), to the experimental values of permeate flow rates and satisfy the entrance conditions in terms of the cooling channel inlet temperature ($T_{c,in}$).

After determining the proper heat transfer coefficient correlation, membrane overall thermal conductivity model, and membrane tortuosity values, the second model step, i.e. model “B”, will be used to estimate the expected deviation from the experimental values as well as calculating the module exit temperatures, permeate flow rates and SHC at different inputs other than those in Winter et. al (2011). The results of Model B are then used to build correlations that can be directly used to estimate the aforementioned parameters without the need to re-run the code to save in computing time. A flowchart of the model corresponding to each step is shown in Appendix I and J.

Given the multi-layer arrangement of the module, an iterative solution is required to consider the interactions between the different layers in terms of heat transfer. The previously discussed heat and mass transfer equations are first applied to the inner most membrane layer associated with the evaporator channel, i.e. $\phi = 0\ to\ 180°$ and $N_m = 1$, (*Figure 6-7*) by initially ignoring the interactions with the outer layers and starting with the first DE ($\phi = 0\ to\ d\phi, N_m = 1$)[180] whose associated evaporator channel partition bulk water temperature is known. However, as the bulk water temperature of the cooling channel associated with the first DE is unknown, for simplicity it is assumed to be always equal to the exit temperature of the cooling channel ($T_{c,o}$) (*Figure 6-7*) given that the length of membrane along this half turn is small (i.e. 2.18 cm) and therefore the bulk water temperature change along this length is expected to be insignificant.

Now the cooling channel exit temperatures were not measured in Winter et. al (2011), however they can be directly calculated using the flux and SHC data reported in the

[180] In the MATLAB code each DE is specified based on its number n_i instead of the angle ϕ

same study[181] and are then used as inputs for model A. As for model B, the cooling channel exit temperature is initially assumed and is then varied until the cooling channel entrance conditions are satisfied.

Using the mass and heat balance equations discussed in section *6.2.4,* the mass flow rate, bulk water salinity and temperatures of the evaporator and cooling channel partitions associated with the next DE can be calculated. After performing the calculations on the last DE of the inner most membrane layer associated with the evaporator channel ($\phi = 180° - \mathrm{d}\phi$ to $180°, \mathrm{Nm} = 1$) the data of the evaporator channel associated with the next DE ($\phi = 180°\ to$ 180°+ dϕ, N_m =1) are known and therefore the calculations could be performed on the inner most membrane layer associated with the cooling channel (N_m =1, $\phi = 180°$ to $360°$).

After reaching the second turn, i.e. N_m =2, the interaction between the evaporator channel and the cooling channel partitions associated with the first DE of the second and first turn respectively ($\phi = 0\ to\ d\phi, \mathrm{Nm} = 2,$ and $\phi = 0\ to\ d\phi, \mathrm{Nm} = 1,$) will vary the parameters of the cooling channel associated with the second DE of the first turn (N_m =1, $\phi = d\phi\ to\ 2\ d\phi$) and therefore the parameters of all evaporator and cooling channel partitions associated with the subsequent DE's in the first turn (N_m =1, $\phi > d\phi\ to\ 360°$) need to be recalculated in an iterative process until no changes occur in the parameters of each partition. This process is repeated such that each time the parameters of a channel partition associated with a certain DE with N_m=i where i>1 and $\phi = j$ change, all the data of the channel partitions associated with the DE's N_m=i-1 and $\phi > j$ need to be recalculated to account for the interactions between the different layers.

To account for the heat transferred from the evaporator channel layers to both the underlying and overlying cooling channel layers the following procedure is carried out. If the mass and heat transfer between the current DE of the evaporator channel and its underlying cooling channel were previously calculated, the mass and heat transferred due the interaction of the current DE of the evaporator channel and its overlying cooling channel is then deducted from the enthalpy and the mass flow rate of the following DE.

---

[181] For more details on the calculations see Appendix K

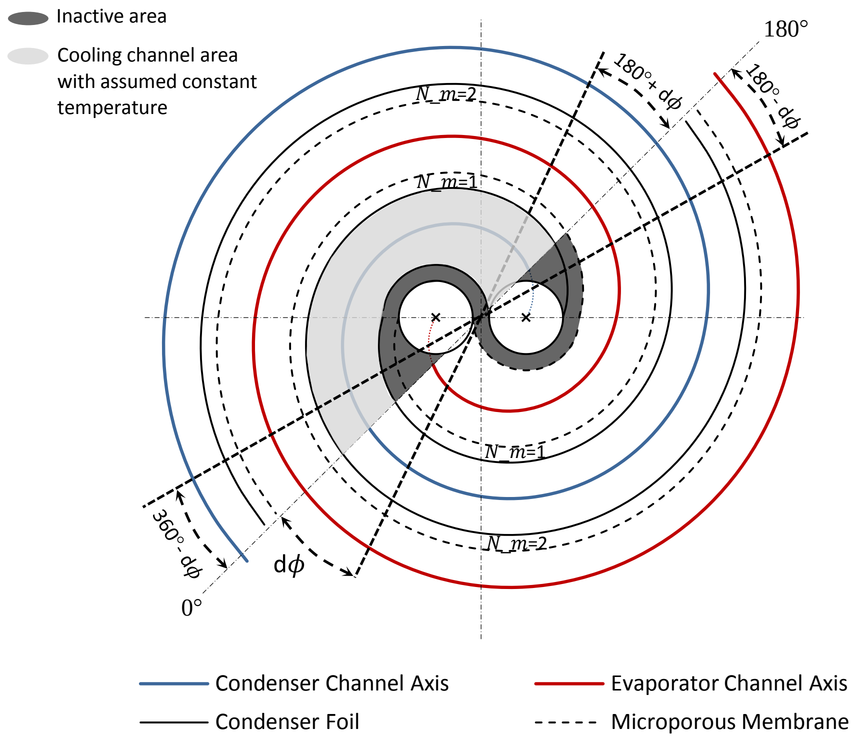

Figure 6-7: Schematic showing the first two turns of the PGMD module membrane unit

This is instead of deducting the enthalpy and the mass flow rate of the current DE as its bulk water properties already include the flux and heat transferred due to the interaction the current DE of the evaporator channel and its underlying cooling channel. This is therefore equivalent to deducting the mass and heat transferred from the interaction of the current DE of the evaporator channel and both its underlying and overlying cooling channel at the same time but greatly simplifies the model.

Finally, the module permeate water mass flow rate production ($\dot{m}_{p,MD}$) and the average temperature of the channel are needed to calculate the convective heat transfer coefficient in the permeate channel. However, because both parameters are initially unknown, an additional iteration loop is used such as their values are initially assumed then are constantly updated after each iteration until the change in their values becomes negligible. It should be noted that because the water completely fills the channel and is moving in a vertical direction against gravity, the water velocity (v_p), needed to calculate the Reynolds number, is assumed to be constant along the channel and is calculated as follows:

$$v_{p,MD,Mod} = \left(\frac{\dot{m}_{p,MD,Mod}}{\rho_{p,MD}}\right) / CSA_{p,eff} \tag{6-52}$$

$$\dot{m}_{p,MD,Mod} = \sum_{n_i=1}^{n_{max}} \sum_{N_{m,i}=1}^{N_{max}} J_w\left(n_i, N_{m,i}\right) b_{ch} dz\left(n_i, N_{m,i}\right) \tag{6-53}$$

where ρ_p is the permeate water density and is estimated at the permeate channel average temperature, i.e. $\frac{(\bar{T}_{m,p}+\bar{T}_{cf})}{2}$.

The aforementioned step is however not required if the heat transfer in the permeate channel is assumed to only occur by conduction.

6.2.8 Effect of salinity and temperature on water properties

The temperature and the salinity of the water have a significant effect on its thermo-physical properties particularly water density, specific heat capacity, specific enthalpy, viscosity, thermal conductivity, vapour pressure and latent heat of vaporization, which needs to be considered to obtain more accurate modelling results.

The effect of temperature and salinity on the thermo-physical properties of water is estimated in the literature using correlations developed from experimental data (Sharqawy et al., 2010). However, the existing correlations are mainly developed for SW thermo-physical properties because of its importance in the science of oceanography and also because SW has a standard composition (Fichtner, 1978) which is shown in *Table 6-2*. Conversely, the GW composition varies from one location to another due to different hydrological conditions, soil type and human activities (Masoud et al., 2003) which is the main barrier for developing similar correlations to that of SW (Pawlowicz and Feistel, 2012). While there are some models to estimate the thermo-physical properties of general multi-component water solutions at lower salinities, there are no readily available models that are suitable for water with high salinities than SW, which is the case in this study, and the existing models need to be altered using available experimental or numerical modelling data which are incomplete and the data from the models are therefore expected to have significant uncertainties (Pawlowicz and Feistel, 2012).

Table 6-2: Comparison of the standard SW composition and the average major ions composition of brackish GW in some wells in Egypt

	Standard SW Composition*	Average Brackish GW Composition of Several Wells in Egypt**
Sodium	30.7%	16.8%
Calcium	1.2%	11.9%
Potassium	1.1%	0.5%
Magnesium	3.7%	5.4%
Chloride	55.1%	38.9%
Sulphate	7.7%	20.1%
Bicarbonate	0.4%	6.5%

*(Fichtner, 1978)
**Based on data from Abdel-Shafy et al. (1992), Abd-El-Samie and Sadek (2001), Masoud et al. (2003), Atta et al. (2005), Sturchio et al. (2005), Sharaky et al. (2007), Abdalla et al. (2009), Elewa and El Nahry (2009), Sultan et al. (2009) and El Alfy (2012)

For this reason SW correlations are used in this study to approximately determine the effect of temperature and salinity on the thermo-physical properties of GW. It should be noted, however, that the different composition of GW from that of SW (*Table 6-2*) will affect the accuracy of the correlations used. For example, Pawlowicz and Feistel (2012) showed that using the solution salinity of limnological surface waters in SW correlations significantly underestimates the density of water when the dominating anion is sulphate which is the case in some of the reviewed BW wells in Egypt. While the study by Pawlowicz and Feistel concluded that for waters where the dominant anions is chloride or bicarbonate, which is the case of most of the reviewed wells in Egypt, the solution salinity could be used in SW correlations to calculate the density with reasonable accuracies, this only applies at low salinities (i.e. <6 g/kg) while higher salinities were not covered in their study.

The type of solute also affects the viscosity of water as discussed in Kwak et al. (2005) where the type of ions affect the structure of the water, i.e. the strength of the bonds. For example, some ions such as nitrate are structure breakers, decreasing the viscosity of water while other ions, e.g. calcium, are structure makers increasing the viscosity of water. The effect of ion type on water structure is determined by the sign of their structural temperature coefficient (Kwak et al., 2005). However, similar to SW, the viscosity of GW is still expected to increase with increasing water salinity because the additional calcium, bicarbonate and sulphate ions are all structure makers. The type of solutes is also expected to affect the specific enthalpy of water where the type of solutes, according to Fichtner (1978), decreases or increases the reference enthalpy, i.e. enthalpy at °0 C, instead of being zero as in pure water depending on whether the dissolution of each solute in the water is endothermic or exothermic.

It should be also noted that the correlations used in this study use different salinity and temperature scales (Sharqawy et al., 2010), however the differences between the water salinity and temperature values based on different scales are insignificant for the purpose of our study[182]. The correlations are mainly developed by Sharqawy et al. (2010) and are discussed in Appendix H.

6.3 Results

As shown in *Figure 6-8* and *Figure 6-9*, a good agreement with the experimental values was achieved at different feed water salinities, cooling channel inlet temperatures and feed flow rates. The average absolute deviation from the experimental cooling channel exit temperature[183], used to calculate the SHC, and permeate flow rates is 0.3% and 3.35% respectively and the maximum deviation ranged from -0.6 to 0.8% and -22.3 to 4.1% respectively.

Using model "A", it was found that the best fit to the experimental permeate flow rate values was obtained at a membrane tortuosity of 3. Regarding heat transfer, using the convective heat transfer correlation developed by Schock and Miquel (1987), i.e. equation *(6-51)*, and assuming that the heat transfer within the permeate channel occurs by conduction gave the best agreement to the experimental values.

---

[182] The correlations used in this model mainly use the reference composition scales and 1990 International Temperature Scale but some correlations use the practical salinity and the 1968 International Practical Temperature scale. The deviation in water salinity and temperature between the aforementioned scales is, however, insignificant with values of only 0.47% and <|0.006|% over the range of 20 to 90°C respectively. For more details see (Sharqawy et al., 2010)

[183] Calculated using model "B" as discussed in section *6.2.7*

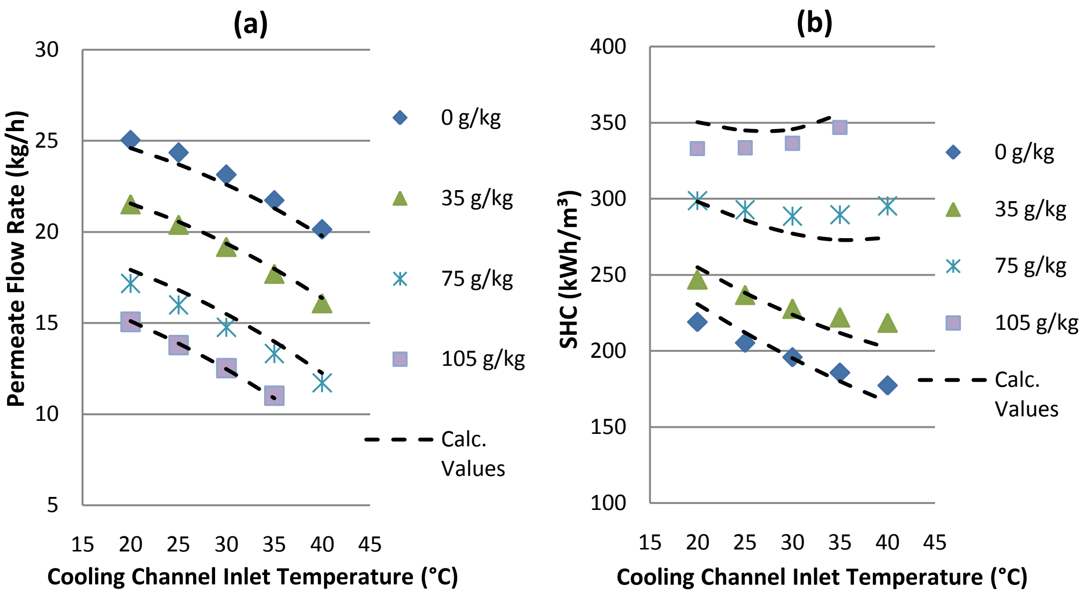

Figure 6-8: Comparison between the experimental and calculated values of (a) the permeate flow rate and (b) the SHC of the PGMD module at different feed water salinities and cooling channel inlet temperatures, and at a constant evaporator channel inlet water temperature of 80°C using equation (6-51) with 0.40 correction factor

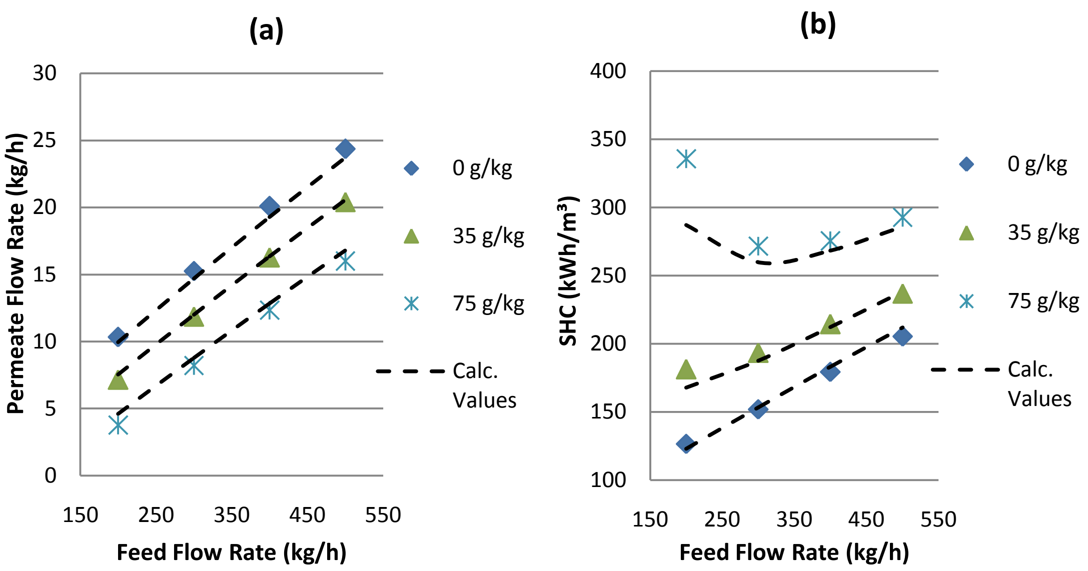

Figure 6-9: Comparison between the experimental and calculated values of the (a) permeate flow rate and (b) the SHC of the PGMD module at different feed water flow rates at constant evaporator and cooling channel inlet water temperatures of 80°C and 25°C respectively using equation (6-51) with 0.40 correction factor

6.4 Discussion

6.4.1 Model accuracy

As discussed in the results section, the model, i.e. model “B”, shows good agreement with experimental values. The largest deviation in the permeate flow rate (i.e. -22.3%) occurred at a feed flow rate of 200 kg/h and salinity of 75 g/kg mainly due to the small value of the permeate flow at this point. Otherwise, the maximum absolute deviation for the other points was below 7%.

The deviation range in the permeate flow rate, i.e. -22.3 to 4.1%, is also well within the values of other MD modelling studies in the literature (*Table 6-3*). As a matter of fact, the model is likely to be considerably more accurate because a similar deviation range in the permeate flow rate to that in the literature which is for laboratory scale modules was obtained for a full scale module where a small deviation in the permeate flow in a single DE would accumulate resulting a larger one for the whole module.

Given that the largest absolute deviation in the condenser exit temperature was only 0.8%, the deviation in the SHC is mainly caused by the deviation in the permeate flow. In all cases, the largest absolute deviation in the SHC, excluding the point at which the feed flow rate of 200 kg/h and salinity of 75 g/kg, was only 7.6%.

Table 6-3: Summary of the modelling studies in the literature and the accuracy of the models

Reference	Module Configuration/ Membrane Type	Max Deviation from experimental flux values[184]	Notes
(Kimura et al., 1987)	AGMD/ Flat Sheet (100 cm^2)	-14.5 to +13.5 % with variable cooling and evaporator channel bulk water temperatures	Convective heat transfer coefficient estimated from semi-empirical equations MTC calculated from theoretical equations
(Fane et al., 1987)	DCMD/Hollow Fibre (1 m^2)	+-10% with variable cooling and evaporator channel bulk water temperatures and flow rates	MTC and convective heat transfer coefficient used as adjustable parameters
(Schofield et al., 1990b)	DCMD/Flat Sheet (28 cm^2)	-11%[185] with variable evaporator channel bulk water temperature and feed water NaCl concentrations	MTC and convective heat transfer coefficient used as adjustable parameters
(Gryta et al., 1997)	DCMD/Flat Sheet (28 cm^2)	-5.5 to +3% with variable evaporator channel bulk water temperature, and evaporator and cooling channels flow rates	Convective heat transfer coefficient estimated from semi-empirical equations MTC calculated from DGM model using membrane properties
(Banat and Simandl, 1998)	AGMD/Flat Sheet (160 cm^2)	• Up to +7%[186] with variable the feed flow rate (laminar flow only) • Up to -19.2%[185] with variable cooling channel bulk water temperature • Up to -23.9%[185] with variable evaporator channel bulk water temperature	Convective heat transfer coefficient estimated from semi-empirical equation. Membrane tortuosity and porosity used as adjustable parameters
(Gryta and Tomaszewska, 1998)	DCMD/ Capillary	2 membranes tested with variable evaporator channel bulk water temperature and flow rate, and feed water NaCl concentration 1st membrane: -20 to +15% 2nd membrane: -11.5% to +10.5%	Convective heat transfer coefficient estimated from semi-empirical equations MTC calculated from DGM model using membrane properties
(Martínez-Díez and Vázquez-Gonzàlez, 1999)	DCMD/Flat Sheet (33.7 cm^2)	Up to -3.5 to +4.5% with variable feed water NaCl concentrations, evaporator channel bulk water temperature, and evaporator and cooling channel flow rates	Convective heat transfer coefficient estimated from semi-empirical equations MTC used as an adjustable parameter.

[184] Approximate values estimated from graphs shown in each study
[185] All values underestimated
[186] All values overestimated

(Martínez-Díez and Florido-Díaz, 2001)	DCMD/ Flat Sheet	-2.5 to 3.5% with variable evaporator and cooling channels temperature and flow rates, feed water NaCl concentration .	Experimental data used to develop a semi-empirical equation to estimate the flux as a function of feed water NaCl concentration and channel water temperatures Convective heat transfer coefficient estimated from semi-empirical equations
(Fernández-Pineda et al., 2002)	DCMD/Flat Sheet ($260\ cm^2$)	-4.5% to +4% with variable average channel bulk water temperatures with fixed bulk water temperature difference between the evaporator and cooling channels	MTC determined from gas permeation tests Convective heat transfer coefficients determined from the DCMD experimental data through linear regression
(Ding et al., 2003)	DCMD/ Flat Sheet ($40\ cm^2$)	Deviation in MTC from up to -12% to 13% depending on the membrane used with variable evaporator channel bulk water temperature	Experimental flux data used to develop a semi-empirical equation to estimate the flux as a function of feed water NaCl concentration and channel water temperatures Convective heat transfer coefficient estimated from semi-empirical equation
(Srisurichan et al., 2006)	DCMD/ Flat Sheet ($47\ cm^2$)	Deviation of up to -14%[185] with variable evaporator channel bulk water temperature	MTC calculated from DGM model using membrane properties with adjustable membrane tortuosity Convective heat transfer coefficient estimated from semi-empirical equation
(Yun et al., 2006)	DCMD/ Flat Sheet ($40\ cm^2$)	1st membrane: • -12 to +7% with pure water as feed and variable evaporator channel bulk water temperature • -10% to +5% with aqueous NaCl solution as feed water and variable evaporator channel bulk water temperature • Up to -5%[185] with aqueous NaCl solution as feed water and variable cooling channel bulk water temperature 2nd membrane: • Up to 25%[186] with aqueous NaCl solution as feed water and variable feed flow rate • Up to -3%[185] with aqueous NaCl solution as feed water and variable cooling channel bulk water temperature	MTC calculated from DGM model using membrane properties Convective heat transfer coefficient estimated from semi-empirical equation
(Qtaishat et al., 2008)	DCMD/Flat Sheet ($236\ cm^2$)	-6 to +30% in MTC with variable evaporator channel bulk water temperature	Membrane overall thermal conductivity and MTC used as adjustable parameters Convective heat transfer coefficient estimated from semi-empirical equation

6.4.2 Optimal value for the membrane tortuosity

As discussed in section *6.3*, the optimal membrane tortuosity that gave the best fit to the experimental data published in Winter et al. (2011) is 3. This value is higher than the typical value of 2 used in the literature (Khayet and Matsuura, 2011d) as well as the value estimated by the correlation, equation *(6-55)*, developed by Mackie and Meares (1955) cited in (Iversen et al., 1997), i.e. 1.8.

$$\chi = \frac{(2-\varepsilon)^2}{\varepsilon} \qquad \textbf{(6-54)}$$

This could be attributed to the questionable accuracy of using the DGM model based equations that incorporate the membrane structural parameters, i.e. using the membrane structural parameters to estimate the constants K_0 and K_1 in equation *(6-10)*, to estimate the MTC.

Several studies such as (Ding et al., 2003, Fernández-Pineda et al., 2002, Lawson and Lloyd, 1997) criticized the use of such equations due to the complexity of the membrane structure which may not be necessarily made of non-interconnected and perfectly cylindrical pores, the main assumption used to estimate K_0 and K_1 from the membrane structural parameters (Lawson and Lloyd, 1997). The questionable accuracy of incorporating the membrane structural parameters in the DGM model based equations could be observed from the study by Schofield et al. (1987) which showed that the values of the MTC calculated using the membrane structural parameters significantly deviated from those determined experimentally from gas permeation tests[187] on three membranes with different structural parameters.

Schofield et al. (1987) particularly showed that the membrane geometry factor, i.e. $\varepsilon/\delta\chi$, calculated using the manufacturer's specified values significantly deviated from that estimated from the gas permeation tests. The authors attributed such discrepancy to the unclear definition of the nominal pore size, which may vary based on the characterization method used (Schofield et al., 1990a, Khayet and Matsuura, 2011c). Such deviation in the membrane parameters estimated from gas permeation tests from those specified by the manufacturer can be also observed in other studies such as

[187] See Martínez et al., (2002,2003) for more information on gas permeation tests

Martínez et al. (2002) and Fernández-Pineda et al. (2002) where the latter estimated the membrane tortuosity to be 3.78 to match the experimental flux values.

The effect of the pore size distribution where the pore size in the membrane is not uniform but varies between a minimum and maximum value, which was ignored in this study, could be also another reason for such discrepancies. However, commercial membranes usually have narrow pore size distribution and therefore using the mean pore size was shown to have a small effect on the membrane MTC (Martínez et al., 2002, Guijt et al., 2005, El-Bourawi et al., 2006, Khayet and Matsuura, 2011d).

Due to the questionable accuracy of using the DGM model based equations that incorporate the membrane structural parameters, in many studies where the MTC was not determined experimentally through gas permeation tests, the whole MTC was used as an adjustable parameter to fit the experimental flux data (Fane et al., 1987, Schofield et al., 1990b, Martínez-Díez and Vázquez-Gonzàlez, 1999, Qtaishat et al., 2008). In other studies, instead of using the DGM model based equations, semi-empirical correlations as a function of temperature and water salinity based on experimental data through curve fitting were developed (Martínez-Díez and Florido-Díaz, 2001, Ding et al., 2003).

It should be noted, however, that the MTC values calculated by the model were in the range of 5×10^{-7} kg/m^2.s.Pa which is well within the typical range reported in the literature, i.e. 3.3 to 13.15×10^{-7} kg/m^2.s.Pa (Fane et al., 1987, Schofield et al., 1987, Ding et al., 2003, Phattaranawik et al., 2003)[188]. Therefore, it is concluded that the optimal tortuosity value obtained is probably compensating for other membrane parameters.

6.4.3 Heat transfer modelling in the permeate channel

The model, i.e. model "A"[189], showed that assuming the heat transfer across the permeate channel to occur only by conduction is valid. This could be attributed to the very low velocities in the permeate channel where the values of the Reynolds number were less than 2.

---

[188] Koschikowski et al. (2009a) reported that the MD MTC could reach 40×10^{-7} kg/m^2.s.Pa but the study where this figure was measured is not indicated

[189] As discussed in section *6.2.7*, model "A" was used here to determine the proper convective heat transfer coefficient correlation in the channels

Moreover, none of the convective heat transfer correlations for spacer filled channel investigated in this study was found to be suitable to describe heat transfer in the permeate channel as they gave heat transfer coefficient values lower than those of the pure conduction case which is invalid.

Furthermore, while the equation developed by Da Costa (1993) for spacers that induce change in flow direction, i.e. equation *(6-49)*, gave higher heat transfer coefficients than those of pure conduction at a feed flow rates larger than 200 kg/h, the estimated heat transfer coefficients in the permeate channel were higher than those of the main channels. Such high values of the heat transfer coefficients are unlikely due to the very low Reynolds number in the permeate channel; that in addition to the high ΣRMSE between the modelled and the experimental values of permeate flow rate and the cooling channel inlet temperature, obtained from Winter et al. (2011), occurring when equation *(6-49)* was used (*Table 6-4*).

Table 6-4: Model deviation from experimental values under different heat transfer mechanisms and thermal conductivity models in the permeate channel, and different convective heat transfer correlations for the main channels

Overall Membrane Conductivity Model	Permeate Flow Heat Transfer Correlation	Evap./Cooling Channel Heat Transfer Correlation	ΣRMSE $\boldsymbol{T}_{c,\mathrm{in}}$	ΣRMSE $\dot{\boldsymbol{m}}_{\boldsymbol{prod}}$	SUM
Maxwell	Pure Conduction	Equ. (*6-50*) with 0.4 CrF*	2.51	0.568	3.07
		Equ. (*6-51*) with 0.4 CrF	1.45	0.504	1.95
Isostrain		Equ. (*6-50*) with 0.35 CrF	2.34	2.71	5.05
		Equ. (*6-51*) with 0.35 CrF	2.33	2.58	4.9
Maxwell	Equ. (6-48)	Equ. (*6-51*) with 0.31 CrF	2.66	0.597	3.26

*Correction factor

The study also showed that the overall thermal conductivity model has a significant impact on the calculated permeate flow rates. The commonly used Isostrain model was particularly found to increase the conductive heat losses[190]. This as expected reduced the value of the optimal tortuosity value to 1.6 which is close to that calculated from

[190] The membrane overall thermal conductivity calculated using the Isostrain model was in the range if 0.079 W/m.K compared to 0.044 when using the Maxwell model

equation *(6-54)*. Nevertheless, the use of this model caused large deviations in the permeate flow rates from the experimental values (*Table 6-4*) particularly at higher feed water salinities where the calculated permeate flow was significantly underestimated which is an indication that the conductive heat losses are likely to be overestimated.

The tendency of the commonly used Isostrain model to overestimate the membrane overall thermal conductivity, was also reported by Phattaranawik et al. (2003). This raises concerns on the accuracy of the models available used in the literature which all used the Isostrain model.

6.4.4 Heat transfer modelling in the evaporator and cooling channels

For the evaporator and cooling channels, the equation developed by Da Costa (1993) for spacers that induce directional flow change, i.e. equation *(6-49)*, significantly overestimated the heat transfer coefficient in the evaporator and the cooling channels. This tendency to overestimate the heat transfer coefficient by this equation was also reported by Phattaranawik et al. (2003).

The equation developed by Da Costa (1993) for spacers that do not induce change in flow direction, i.e. equation *(6-50)*, and the one developed by Schock and Miquel (1987), i.e. equation *(6-51)*, gave better agreement with experimental results. Nevertheless, it was observed that the former significantly overestimated the convective heat transfer coefficient at low feed flow rates and therefore was less able to satisfy the entrance conditions in model "A", i.e. significantly underestimated the cooling channel inlet temperature (*Figure 6-10*).

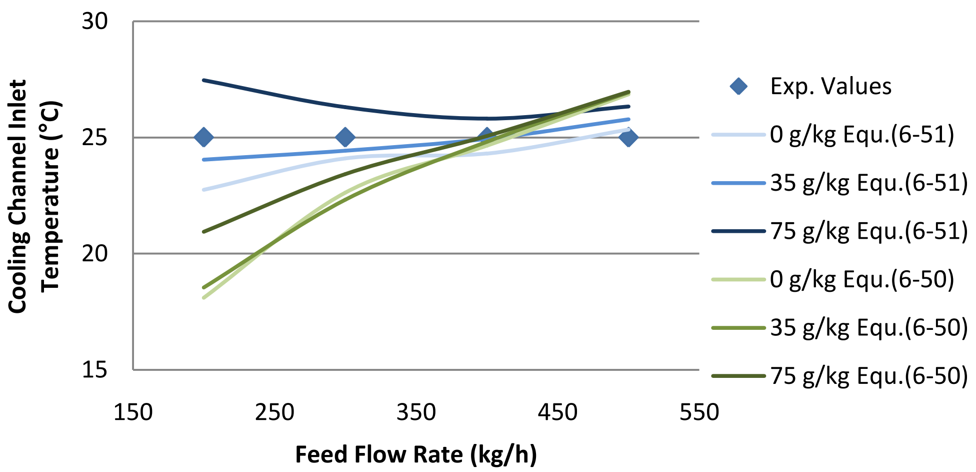

Figure 6-10: Comparison between the calculated cooling channel inlet temperature estimated using equations 6-50 and 6-51 in model "A" at different PGMD feed flow rates and water salinities

This is due to the low power of the Reynolds number which decreases the sensitivity of the correlation to the flow rate. Accordingly, it is concluded that the correlation developed by Schock and Miquel (1987) best describes the convective heat transfer coefficient in the main channels.

Both equations needed, however, to be corrected by a factor of 0.4 to give a better agreement with the experimental results. This could be because the heat is transferred from the evaporator channel to the overlying and underlying cooling channels and the same applies for the heat transferred to the cooling channel. Accordingly, the main channel is actually composed of two convective heat transfer resistances as shown in *Figure 6-11*.

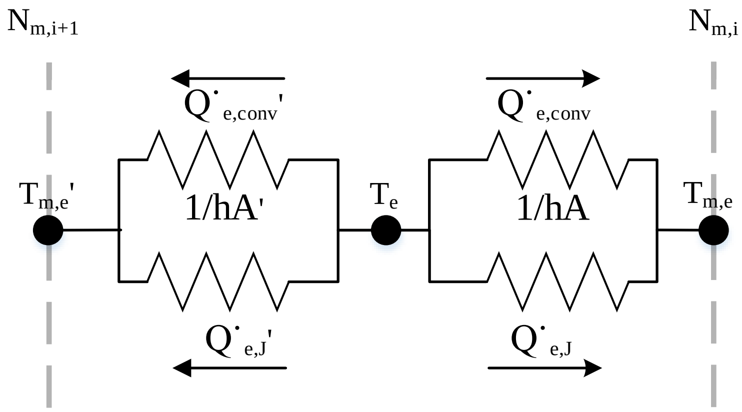

Figure 6-11: Heat transfer resistances within the evaporator channel

In this case, the equivalent convective heat transfer coefficient to transfer the same heat rate through one membrane side is nearly 2 times the value of the convective heat transfer coefficient for one side. However, more investigation is needed to verify this claim.

It should be noted that the need to use a correction factor could be also attributed to the questionable accuracy of the semi-empirical correlations available in the literature in estimating the convective heat transfer in a MD process. For example, the experiments carried out by Gryta and Tomaszewska (1998) showed that a great care should be taken using such correlations as deviations up to 98% from the measured flux were obtained by using the wrong correlation. Moreover, according to Çengel (2003), it is “naïve” to consider these empirical correlations as accurate as two systems cannot be exactly similar and therefore an error of 10% should be normally expected with the use of such correlations in estimating the convective heat transfer rate in heat exchangers which is likely to also apply for an MD module.

Finally, the obtained heat transfer coefficient values in the main channels and the distillate channel could be compensating for other effects. For example, the heat lost by the permeate water transfer out of the module was ignored in this model. This is expected to result in an overestimation of the heat transfer rate from the evaporator to the cooling channel. However, using the experimental data, the heat losses were roughly[191] estimated to be less than 5% for the different cooling channel inlet temperatures, feed flow rates and feed water salinities tested in Winter et. al (2011). Heat losses to the ambient were also neglected which is commonly assumed in MD modelling studies such as (Lawson, 1995, Laganà et al., 2000, Cheng et al., 2008). However, this assumption should not significantly affect the results as the membrane outer layer contains a cooling channel layer therefore heat lost to the ambient is minimized (Winter et al., 2011).

6.5 Further Notes

In this study, as the author did not have access to the PGMD module, it was assumed that the evaporator channel inlet and cooling channel outlet tubes have the same thickness, i.e. diameter, of their corresponding channels, i.e. 3.2 mm. However, after submitting this thesis, it was known through one of the examiners that the core diameter of the module is approximately 10 cm which means that the tubes have a much larger diameter than the previously assumed value.

After adjusting the diameter of each tube to be 4 cm, the number of membrane/ condenser foil layers in the lower and upper half of the module, as expected, dropped from 31 and 32, respectively (*Figure 6-3*), to 23 and 24 (*Figure 6-12*). It should be noted that for simplicity, it was assumed that the first turn takes the shape of an Archimedean spiral although it will likely have an erratic shape which will slightly affect the length of the first few spiral turns.

[191] It was assumed that the permeate water at the entrance and the exit of the channel have temperatures close to that of the average channel bulk water temperatures between the evaporator and the cooling channels at the inlet of the evaporator channel and its exit respectively,

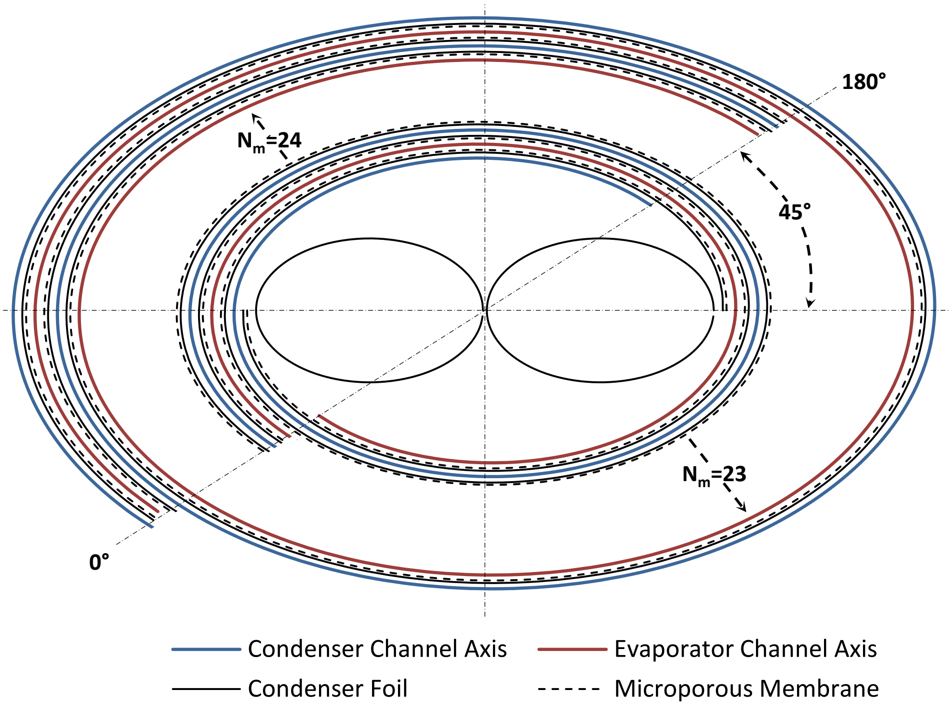

Figure 6-12: Approximated shape of the modelled PGMD module after adjusting the diameter of the inner tubes

To investigate the effect of the change in the module geometry, model "B" was re-run using the new dimensions and tested at different cooling channel inlet temperatures, water salinities and feed flow rates.

It was observed that the change in the geometry had an insignificant effect on the permeate flow rate which did not vary by more than 0.5% than the values obtained with the previous module geometry. However, a more considerable effect on the cooling channel exit temperature and therefore the SHC was observed. Nevertheless, the change was still small, i.e. < 6%, at different cooling channel inlet temperatures and water salinities as shown in *Figure 6-13*. Accordingly, this change in the geometry would have an insignificant effect on the analysis carried out in chapter 7 on the feasibility of solar driven RO/MD plants. It should be also noted that the percentage variation in the SHC after adjusting the module geometry was slightly higher at lower feed flow rates reaching up 8.4% at 300 kg/h feed flow rate; however, the analysis in Chapter 7 was carried out at 500 kg/h as it was observed that it is less economical to operate at lower feed flow rates.

Such change in the geometry is also not expected to affect the estimated optimal tortuosity value, the proper heat transfer mechanism in the permeate channel, or the correlation that was found to better represent the convective heat transfer in the main channels discussed in sections *6.4.2*, *6.4.3* and *6.4.4*, respectively. However, as the change in the geometry resulted in an increase in the SHC for all of the tested operating conditions, it is expected that a slightly higher correction factor, which was used with the heat transfer correlation developed by Schock and Miquel (1987), will give better agreement with the experimental results shown in Winter et al. (2011).

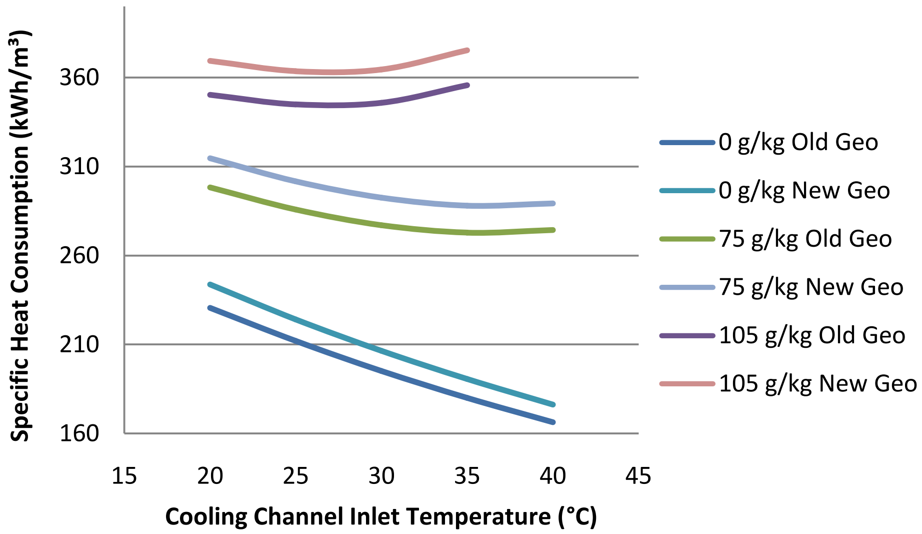

Figure 6-13: Comparison between the calculated SHC of the PGMD module at different cooling channel inlet temperatures and feed water salinities, and a feed flow rate of 500 kg/h before and after the modification in the geometry of the module

6.6 Summary

In this chapter, the methodology used to model a commercial PGMD module and the validity of the model was discussed. The model gave good agreement with the experimental results with a mean deviation of 0.3% and 3.35% from the experimental cooling channel exit temperature and permeate flow rate, respectively. It was also shown that the commonly used Isostrain model tends to overestimate the MD membrane overall thermal conductivity resulting in high deviation in the MD flux from the experimental values particularly at higher feed water salinities.

7. Feasibility Study of Solar Driven Hybrid RO/MD Plants

As discussed in chapter 1, due to the limited GW resources in Egypt, high RR operation of the desalination plant is a necessity; that in addition to reducing the environmental impact and the additional costs associated with brine disposal in inland areas. For this reason the use of a thermal desalination process was suggested to treat the RO plant brine to further increase the RR as it can desalinate water with high salinities in contrast with the RO process where the RR is limited by the osmotic pressure. The MD process is particularly investigated for such use as it is a promising desalination process that is suitable for decentralized applications due to its simplicity and modularity.

In chapter 2, it was shown that studies on the feasibility of hybrid RO/MD plants were not reliable as the SHC of the MD plant was significantly underestimated, and because they were based on high flux values particularly at high water salinity which are likely to be unsustainable due to the effect of scaling. The studies were also based on fluxes obtained from lab scale modules which may not be achieved with full scale modules under the same operating conditions. Moreover, the studies ignored the effect of the operating conditions on the MD process performance where the same flux values reported in Drioli et al. (1999) were used with a different feed water temperature which raises questions on the accuracy of these analyses.

Furthermore, none of these studies were used with BW applications except that of Marinetti et al. (2009) which only focused on investigating the limiting effect of scaling on the hybrid RO/MD plant RR rather than the plant energy performance and economic feasibility. Finally, none of the reviewed studies analysed the performance of a hybrid RO/MD plant driven by solar energy.

For this reason, in this chapter the feasibility of solar driven hybrid RO/MD plants, using a full scale commercial MD module, for brackish GW desalination is investigated. The chapter first shows the methodology used for modelling and designing the hybrid plant. The conditions /limitations for a brackish GW hybrid RO/MD desalination plant to operate at RR's higher than the maximum attainable RR's of the RO plant, estimated from chapter 4, are then discussed. This is followed by an analysis of the performance of the FPC-MD plant and an investigation of the economic feasibility of the solar driven hybrid RO/MD plant.

7.1 Methodology

7.1.1 Hybrid plant configuration

The solar driven hybrid plant consists of a PV driven RO plant and a FPC driven MD plant. The same RO plant designs discussed in chapter 4 are used in the analysis of hybrid RO/MD plants. In other words, the RO plants will be operating at the same operating conditions[192] discussed in chapter 4; and the MD plant is used to desalinate part the RO brine which was otherwise discharged to the deep injection well.

In this case, the brine of the RO plant is first stored in a tank (*Figure 7-1*). A portion of the brine is then circulated through the MD plant where part of it is desalinated while the rest goes back to the tank.

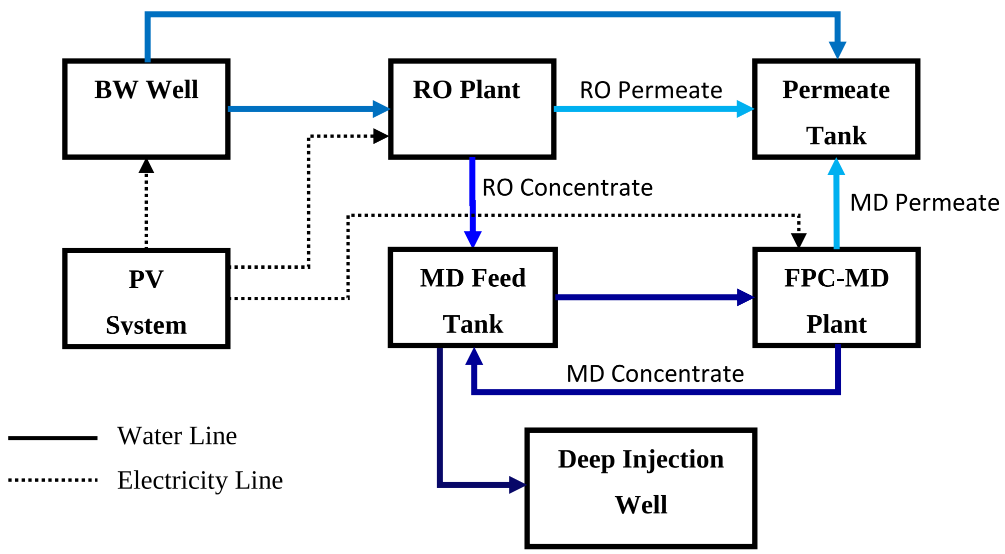

Figure 7-1: Schematic diagram of a PV-RO/FPC-MD hybrid desalination plant

[192] I.e. Same amount of extracted GW, blended GW and RO feed water. It should be noted, however, that while the almost pure permeate produced by the MD plant allows increasing the amount of blended GW, it is found that the increase is too small which resulted in an insignificant reduction in the RO plant SEC.

At the end of the day the remaining brine in the tank is discharged to the deep injection well. The solar driven MD plant configuration and design are discussed in more details in section *7.1.5*.

7.1.2 MD plant capacity

The required number of the MD modules (NMD), hence the MD plant capacity, is determined based on the daily maximum attainable batch RR ($RR_{Hyb,day,batch}$) such that:

$$RR_{Hyb,day,batch} = \frac{\dot{m}_{feed,RO} * RR_{RO} * t_{RO} + NMD * m_{p,MD,Mod,day}}{\dot{m}_{feed,RO} * t_{RO}} \quad \textbf{(7-1)}$$

where $\dot{m}_{feed,RO}$ is the RO plant feed water mass flow rate; $m_{p,MD,Mod,day}$ is the daily permeate water mass produced by one module; and t_{RO} is the daily operating time of the RO plant.

The daily maximum attainable batch RR of the hybrid RO/MD plant is expected to be limited by scaling (Martinetti et al., 2009) and is initially determined based on the results obtained from the chemical simulation software used in this study, after reducing the pH to 6 using sulphuric acid and adding scale inhibitors, at the considered GW compositions discussed in chapter 4 (*Table 4-3*) and the expected operating temperature of the MD process.

It should be noted that with the hybrid plant, the batch RR, which takes into account the operating time of each plant, is used instead of the instantaneous RR. This is because the MD plant is designed to operate the whole day, while the RO plant in this study is designed to operate either only during daytime or for 24 hours. Now when the RO plant operates for fewer hours than the MD plant, the RO brine is recirculated several times through the MD modules and the desired RR is reached at the end of each day. The overall daily produced permeate water ($m_{p,tot,day}$) is then calculated as follows:

$$m_{p,tot,day} = \dot{m}_{blend} * t_{RO} + \dot{m}_{feed,RO} * RR_{RO} * t_{RO} + NMD * m_{p,MD,Mod,day} \quad \textbf{(7-2)}$$

Due to the intermittent nature of solar irradiance, the evaporator inlet temperature hence the module permeate water mass flow rate ($\dot{m}_{p,MD,Mod}$) will vary throughout the day. Accordingly, the required number of MD modules is initially estimated assuming a constant module permeate flow rate ($\dot{m}_{p,MD,Mod,design}$) estimated at the desired evaporator inlet temperature, i.e. 80°C (section *7.1.4*), at a constant operating hours of 22[193]. In this case, the MD module daily permeate water mass is calculated as follows:

$$m_{p,MD,Mod,day} = \int_0^{t_{MD}} \dot{m}_{p,MD,Mod}(t)dt \cong \dot{m}_{p,MD,Mod,design} * t_{MD} \quad \textbf{(7-3)}$$

where t_{MD} is the daily operating hours of the MD plant and water salinity, which will increase as more brine is recovered.

Furthermore, as the MD brine is recirculated, the brine salinity will gradually increase in the tank as more water is removed by the MD process which will result in a gradual reduction in the permeate flow rate of the MD module. For this reason, the required number of MD modules is also estimated at the expected average water salinity in the brine tank which is estimated by calculating the expected salinity of the brine in the tank at each time step as follows:

at $t \leq t_{RO}$:

$$S_{brine,tank}(t) = \frac{\int_0^t S_{brine,RO}\ \dot{m}_{brine,RO}(t) * dt}{m_{brine,Tank}(t)} = \frac{S_{brine,RO} * \dot{m}_{brine,RO} * t}{m_{brine,Tank}(t)} \quad \textbf{(7-4)}$$

$$m_{brine,Tank}(t) = \int_0^t \dot{m}_{brine,RO} * dt - \int_1^t NMD * \dot{m}_{p,MD,Mod}(t) * dt \quad \textbf{(7-5)}$$
$$= \dot{m}_{brine,RO} * t - NMD * \dot{m}_{p,MD,Mod,design} * (t-1)$$

at t > t_{RO}:

$$S_{brine,tank}(t) = \frac{S_{brine,RO} * \dot{m}_{brine,RO} * t_{RO}}{m_{brine,Tank}(t)} \quad \textbf{(7-6)}$$

$$m_{brine,Tank}(t) = m_{brine,Tank}(t_{RO}) - \dot{m}_{p,MD,Mod,design} * NMD * (t - t_{RO}) \quad \textbf{(7-7)}$$

Equations *(7-1)* to *(7-7)* are then applied in MATLAB to estimate the MD plant capacity. It should be noted that an iterative solution is required because the module

[193] The MD plant is designed to operate 1 hour after the RO plant start up to ensure that there is enough brine to fill the MD modules and the pipes, and to shut down 1 hour before the end of the day to dispose the remaining brine to the deep injection well and empty the tank for next day's operation

permeate flow rate is a function of the average water salinity which in turn depends on the module permeate flow rate.

7.1.3 MD module performance

To estimate the module permeate flow rate and exit temperatures at different operating conditions, the mathematical model discussed in chapter 6 is used. Now instead of re-running the model for each variation in the operating conditions which is time consuming, polynomial fit correlations are built after running the model at cooling channel inlet temperatures and feed flow rates ranging from 20 to 40°C with 5°C steps and 300 to 500 kg/h with 50 kg/h steps respectively.

Each correlation calculates the permeate water production and exit temperatures of the MD module as a function of the evaporator inlet temperature and water salinity which are varied from 60 to 85°C and 10 to 120 g/kg at steps of 5°C and 10 g/kg respectively.

For cooling channel inlet temperatures falling between those at which the correlations are built, the corresponding module permeate water production and exit temperatures are assumed to vary linearly between those calculated from the correlations built at the nearest cooling channel inlet temperature range[194].

It should be noted that the correlations show deviations in the permeate flow production, cooling and evaporator channels exit temperatures from the actual modelled values by no more than 0.3%[195], 0.08% and 0.1% respectively.

7.1.4 MD module operating conditions

The MD plant is designed to operate at an evaporator inlet temperature of 80°C which is near the maximum operating temperature of the MD module used in this study, i.e. 85°C (Koschikowski et al., 2003). This is because the higher the operating temperature, the higher is the module productivity and the lower is the SHC. Therefore, running the MD process at high feed water temperatures is more economical (Fane et al., 1987).

---

[194] For example, if the cooling channel inlet temperatures is 23°C, the corresponding permeate water production and exit temperatures of the module are calculated assuming a linear variation between those calculated at a cooling channel inlet temperature of 20 and 25°C.

[195] Higher deviations in the module permeate flow rate occurred at low evaporator channel inlet temperatures (i.e. 65 and 60°C) and high water salinities as the permeate flow rates are very small i.e. <1 kg/h. Such high deviations at the aforementioned operating conditions should not affect the results as the MD permeate flow contribution is negligible in this case.

Regarding the feed flow rate going through the module, higher values result in an increase in the permeate flow rate due to the increase in the heat capacity of the feed water allowing a higher bulk temperature difference across the membrane (Winter et al., 2011); that in addition to the resulting increase in the convective heat transfer coefficient which reduces the effect of temperature polarization (Hogan et al., 1991). However, this comes on the expense of increasing the external heat required as more energy is needed to heat a larger mass of water to the same temperature and therefore the higher the feed flow rate the higher is the SHC as shown in *Figure 7-2*.

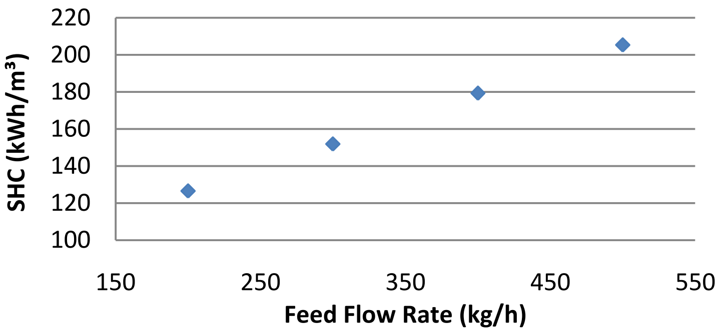

Figure 7-2: The variation of the SHC of the PGMD module with the feed flow rate at an evaporator channel and cooling inlet temperatures of 80°C and 25°C respectively with pure water as the feed water

Moreover, when salty water is used, increasing the feed flow rate does not necessarily increase the SHC and there is an optimal value at which the SHC is minimized depending on the feed water salinity as discussed in Winter et al. (2011). Based on the results of the mathematical model discussed in chapter 6, it is observed that operating at low feed flow rates, e.g. 200 to 300 kg/h, when the feed water salinity is low, i.e. less than 60 g/kg, shows a significant reduction in the SHC as shown in *Figure 7-3*. Conversely, at high feed water salinities, the SHC is minimized at the higher feed flow rates, e.g. 500 kg/h.

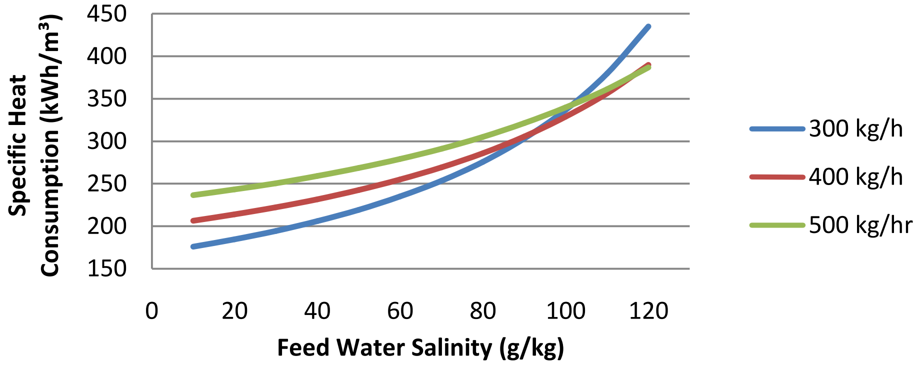

Figure 7-3: The effect of water salinity and feed flow rate on the SHC of the PGMD module at an evaporator and a cooling channel inlet temperatures of 80°C and 20°C respectively

Nevertheless, in selecting the optimal feed flow rate, costs should be the main consideration. In other words, the reduction in the SHC through decreasing the feed flow rate may not be substantial enough to cover the costs of the higher number of modules required in this case to obtain the same permeate water production.

Therefore, the feasibility of the MD plant will be assessed for two cases. First, the MD plant is designed to operate at the maximum feed flow rate, i.e. 500 kg/h, such that the number of modules is minimized; then the design is carried out at the feed flow rate which minimizes the SHC[196].

7.1.5 Solar heat supply system

In this study, the solar water heating system driving the MD Plant is designed similar to the plants discussed in Koschikowski et al. (2009b) and Schwantes et al. (2013) with some modifications in the operation algorithm which is discussed in the next section. The plant performance over the year is modelled using TRNSYS simulation tool using Aswan weather data where the amount of solar irradiance is the highest and therefore the minimum LCOW can be estimated. The plant consists of three main loops: the solar FPC loop, the heat storage loop and the MD plant loop as shown in *Figure 7-4*.

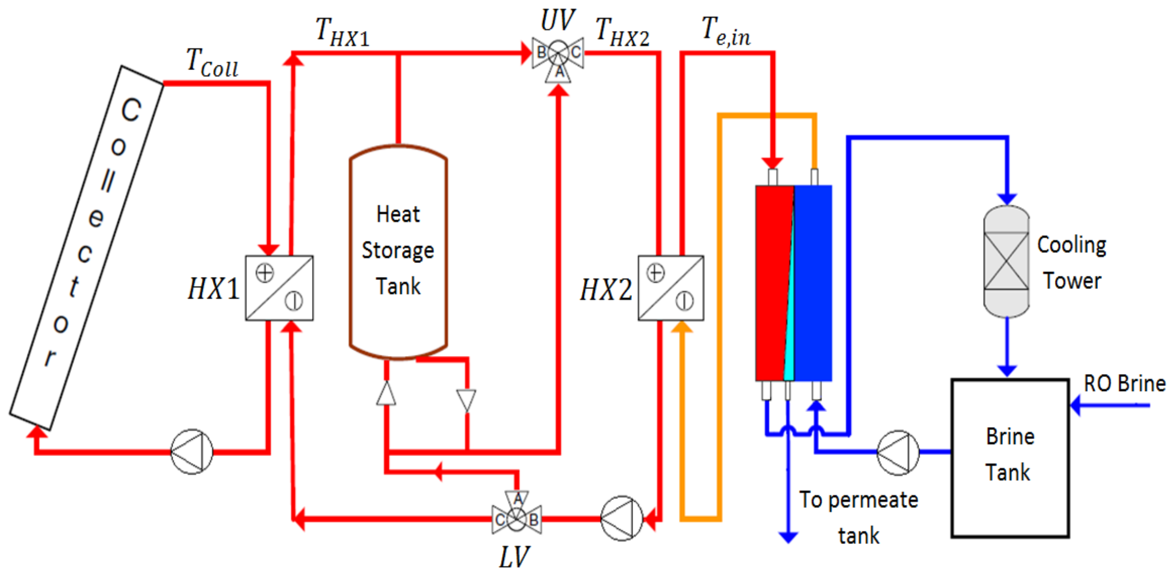

Figure 7-4: Schematic diagram of the solar driven MD Plant
Modified after (Schwantes et al., 2013)

[196] It should be noted that while the SHC of the module is the lowest when the feed flow rates are less than 300 kg/h at low feed water salinities, it is observed that the permeate flow rates in this case are extremely low while the SHC reduction is not significant. In other words, the ratio between the SHC and the permeate flow rate at 200 kg/h is substantially higher than that at 300 kg/h. For this reason, feed flow rates lower than 300 kg/h are not considered in this study.

7.1.5.1 Solar driven MD plant operation description

The solar FPC loop pump is set to operate when the water temperature in the loop (T_{Coll}) exceeds a pre-set value. However, to avoid excessive starting and stopping in the morning[197], the pump is forced to start from 07:30 to 14:00.

Once the FPC loop pump starts, the heat storage loop pump is activated allowing the heat supplied by the collectors to be transferred to the heat storage loop through the heat exchanger HX1. The upper 3 way valve (UV) is set to the B-C position such that the heat is initially transferred directly to the MD plant through the heat exchanger HX2. During noon time, the temperature of the water exiting HX1 significantly increases and as it exceeds 83°C, the UV position is varied such that the excess heat is used to charge the heat storage tank. In this case, portion of the hot water enters through the top of the tank which is replaced by cold water from the bottom of the tank such that the flow rate entering HX2 is constant and T_{HX2} is fixed at 83°C. A set point of 83°C is particularly chosen such that the MD plant will be operating at a temperature close to 80°C (section *7.1.4*). The position of the UV, and therefore the portion of the water flow rate going to the tank, is determined based on the water temperature at the bottom of the tank (T_{cold}) and T_{HX1} such that:

$$UV\ position = \frac{83 - T_{cold}}{T_{HX1} - T_{cold}} \qquad \textbf{(7-8)}$$

A condition is also added to switch back the UV to the B-C position when the tank bottom temperature is higher than 83°C, as in this case the cold water of the tank cannot be used to cool down the water coming from HX1.

Near sunset as the available solar irradiance is low and the heat supplied from the FPC loop is not enough to operate the MD plant at the design temperature, i.e. low T_{Coll}, the collector loop pump is stopped. Now if the heat storage tank has enough heat to run the MD plant, the position of the lower valve LV is switched from B-C to B-A such that the hot water is supplied from the heat storage tank. When the heat in the storage tank is exhausted, i.e. low T_{HX2}, then the whole plant is shut down.

---

[197] Excessive starting and stopping occurs because once the pump starts the water temperature in the collector loop suddenly drops causing the pump to stop which in turn causes a sharp increase in the water temperature.

To protect the MD modules from being damaged, the MD plant is shut down when the operating temperature exceeds the module maximum operating value, i.e. 85°C. It should be noted that while in an actual plant the evaporator inlet temperature should be directly monitored to make sure than the MD maximum operating temperature is not exceeded, in the TRNSYS model $T_{HX2}$is monitored instead as the model is found to work less consistently[198] when the control signal is taken from the same loop.

Furthermore, to prevent the MD plant from experiencing scaling, the whole plant is shut down once the brine salinity associated with the scaling limited maximum attainable RR is exceeded.

A summary of the different control signals used in the model is shown in table below.

Table 7-1: Summary of the solar driven MD plant control algorithm

Collector Loop Pump	**Lower valve Control**	**Heat Storage Loop Pump**	**MD Loop Pump**
Pump is activated when: Time from 7:30 to 14:00 Or T_{Coll} > Pre-set value 1	LV in on the B-C setting when: $T_{Tank,Top}$ < Pre-set value 2 Or T_{HX1}-$T_{Tank,Top}$ > 2°C (Dead Band 0-2°C) Or T_{Coll} > Pre-set value 1	Pump is activated when: T_{HX2}> Pre-set value 4 Or The collector loop pump is on Or $T_{Tank,Top}$ > Pre-set value 2 And $S_{brine} < \frac{S_{RO,brine}}{1-R_{hyb,max}}$	Pump is stopped when: T_{HX2}> Pre-set value 6 (High Temperature Protection) Or Heat storage loop pump is off Or T_{HX2}< Pre-set value 7 (Inefficient MD Operation at low temperatures) Or $S_{brine} > \frac{S_{RO,brine}}{1-R_{hyb,max}}$

The pre-set values for controlling the operation, shown in *Table 7-1*, are selected such that the MD plant operates most of the time at/near 80°C which, as discussed in section *7.1.4*, guarantees the most energy efficient operation of the plant.

Finally, it should be noted that because the brine is recirculated through the MD plant, a cooling tower is required to keep the brine temperature from increasing with each recirculation cycle.

---

[198] Excessive MD plant starts and stops

7.1.5.2 Equipment sizing and specifications

A) FPC design

The FPC specifications used in the TRNSYS model are based on those of the EURO C20 AR-M commercial collector, obtained directly from the collector certification sheet and are shown in table below.

Table 7-2: EURO C20 AR-M FPC specifications

Parameter	Value
Collector Gross Area	2.61 m^2
Collector Aperture Area	2.36 m^2
Intercept Efficiency (a_0)	0.741
Slope of the collector efficiency equation (a_1)	10.8684
Curvature of the collector efficiency equation (a_2)	0.031356
First order coefficient of the IAM[199] curve fit equation (b_0)	0.1089[200]
First order coefficient of the IAM curve fit equation (b_1)	0.00019[200]

The required FPC area is initially estimated based on the calculated heat rate requirements of the MD plant when operating at the design temperature, i.e. 80°C, at an assumed collector efficiency of 50% and the annual average daily solar irradiation in Aswan. The MD plant heat rate requirement ($\dot{Q}_{MD}$)is calculated as follows:

$$\dot{Q}_{MD} = SHC * NMD * \frac{\dot{m}_{p,MD,Mod,design}}{\rho_p} \quad \textbf{(7-9)}$$

The flow rate in the collector loop is kept as small as possible to reduce the electricity requirements hence the PV system cost. The minimum flow rate is determined based on a specific flow rate of 30 kg/m^2/h which maximizes the temperature rise on the expense of slightly reducing the collector efficiency (Reysa, 2012).

The collector orientation is selected such that the incident irradiation is as much as possible uniformly distributed over the year to maximize the annual production. A uniform distribution of the solar irradiation over the year let the MD plant operate at high temperatures during periods of low solar irradiance and prevent it from exceeding its maximum operating temperature during periods of high solar irradiance which would

---

[199] Incidence Angle Modifier

[200] The values are calculated based on the IAM values at different incident angles shown in the certification sheet

otherwise lower the MD plant operating time, i.e. lower capacity factor, as it will be shut down during these periods.

B) Heat storage tank and piping design

The heat storage tank volume (V_{Tank}) is calculated based on the MD plant heat requirements such that:

$$V_{Tank} = \frac{Q_{MD}}{Cp * (100 - T_{co}) * \rho_p} \quad \textbf{(7-10)}$$

where the MD plant heat requirement is calculated as follows:

$$Q_{MD} = \dot{Q_{MD}} * t_{MD} * 3.6 \times 10^6 \quad \textbf{(7-11)}$$

The $(100 - T_{co})$ term is the assumed temperature difference at which heat is transferred between the heat storage tank loop and the MD plant.

Regarding the heat losses from the heat storage tank, the measured overall heat losses coefficients of typical solar domestic hot water storage tanks reported in the literature ranged from 1.2 to 2.5 W/m^2.K (Suter, 2001, Cruickshank and Harrison, 2010). In this study a value of 1.2 W/m^2.K is used assuming that measures such as filling the gaps between the tank wall and the insulation cover, and insulating the areas where the pipes are connected to the tank to stop the air flow between the tank wall and the insulation cover are taken; which were found by Suter (2001) to significantly reduce the heat losses.

The pipes in the system are also insulated and are assumed to have the same U value as that of the heat storage tank.

C) Heat exchanger design

The Heat exchanger is designed based on a number of transfer units (NTU), a measure of the heat exchanger surface area, of 3 and its area is then calculated using equations *(7-12)* and *(7-13)*. It should be noted that higher NTU values show little improvement in the HE effectiveness[201] and therefore the extra costs of using a heat exchanger with a larger area cannot be justified (Çengel, 2003).

$$A_{HX} = \frac{C_{min}}{U_{HX} * NTU} \qquad \textbf{(7-12)}$$

$$C_{min} = minimum(\dot{m}_{hot} * Cp_{hot}, \dot{m}_{cold} * Cp_{cold}) \qquad \textbf{(7-13)}$$

where C_{min} is the minimum heat capacity rate, $\dot{m}_{hot}$ and Cp_{hot} are the water mass flow rate and the specific heat capacity on the hot side of the heat exchanger respectively while $\dot{m}_{cold}$ and Cp_{cold} are those for the cold side.

The U value of the heat exchanger (U_{HX}) is chosen to be 1300 W/m^2.K, an average value for typical water to water heat exchangers[202] (Çengel, 2003).

D) Cooling tower design

The cooling tower size and power requirements are determined using commercial design tools (GEA, 2010)[203] at the corresponding average dry and wet bulb temperatures in Aswan. The cooling tower is particularly designed to restore the temperature of the recirculated brine back to its initial value before entering the MD plant, i.e. 30°C. Therefore, the cooling tower is sized to reduce the water temperature by approximately 10°C. It should be noted that the cooling tower is not considered in the TRNSYS model, and for simplicity it is assumed that the temperature of the brine exiting the cooling tower is constant at 30°C throughout the year regardless of the ambient conditions.

With cooling towers, some of the brine flowing through the cooling tower is lost mainly due to evaporation in addition to other mechanisms discussed in Mulyandasari (2011). Evaporation losses alone are expected to typically range from 2.2%[204] for a 10°C reduction in the water temperature (Yarra Valley Water, n.d.). The significance of such water losses from the cooling tower is investigated in this study using the aforementioned percentage losses.

[201] The ratio between the actual heat transfer rate and the maximum possible heat transfer rate
[202] Typical U values for water to water heat exchangers range from 850 to 1700 W/m^2.K (Çengel, 2003)
[203] Using the GEA design tool, a splash packing type is selected as it can be used with saline water and the power requirements are estimated assuming a motor efficiency of 60%.
[204] 720 l/h for a 352 kW cooling load

E) PV system sizing

The power requirements of the solar driven plant, needed to size the PV system, are those needed by the circulation pumps in the collector, heat storage tank and the MD plant loops. The pipe lengths are roughly assumed based on the plant size and their diameters are then chosen such that the pressure drop in each loop does not exceed 0.5 bar. The pressure drop in the MD modules at different flow rates is obtained directly from Winter et al. (2011).

For simplicity, it is assumed that the circulation pumps in the collector and the heat storage tank loops are only operating 8 hours a day; conversely, the pump in the MD loop is assumed to operate for 22 hours a day (section *7.1.2*). The latter assumption is expected to slightly overestimate the PV system size because the MD plant is not expected to operate for 22 hours every day particularly during periods of low solar irradiance.

To avoid the need to redesign the PV plant size, its LCC is directly calculated as a function of the daily electricity consumption using polynomial fit equations constructed based on the PV-RO plant designs carried out in Chapter 4. In this case, the data of the PV-RO plants operating for 24 hours and during daytime only are used to estimate the LCC cost of the PV system supplying the circulation pumps in the MD loop, and in the collector and heat storage tank loops, respectively, as they have a similar load profile.

7.1.5.3 Solar driven MD plant design methodology

The heat exchanger area and the heat storage tank volume and the initial number of modules and FPC's area are applied in the TRNSYS model.

Now after reviewing some of the available commercial heat storage tanks, it is found that the largest capacity available[205] is 100 m^3 which is much smaller than the sizes required for the MD plant capacities considered in this study. For this reason, the MD plant is divided into several smaller plants where the size of the heat storage tank of each sub-plant does not exceed 25 m^3.

[205] Solar Panels Plus (http://www.solarpanelsplus.com/products/solar-storage-tanks/); Automatic Heating (http://www.automaticheating.com.au/product_category/thermal-storage/); and SunMaxxSolar (http://www.sunmaxxsolar.com/storage-tanks.php)

The pre-set values for controlling the operation, shown in *Table 7-1*, are then varied such that the annual permeate water produced by the sub-plant is maximized. Moreover, given that a too small FPC area will result in a low temperature, i.e. inefficient, MD plant operation, while a too large area may cause the MD plant to be shut down for long periods due to high operating temperatures, the FPC area is varied from the initially calculated value to see if it will result in a significant increase the annual permeate water production. The flow rate in the FPC and the heat storage tank loops, and the Heat exchanger HX1 area are then adjusted to match the new FPC area.

It should be noted that as it is hard to ensure that the desired RR by the MD plant is obtained each day due to the variation of available solar energy, the plant will be designed such that the desired RR is obtained annually such that:

$$RR_{Hyb.year.batch} = \frac{\dot{m}_{feed,RO} * RR_{RO} * t_{RO,year} + NMD * m_{p,MD,Mod,year}}{\dot{m}_{feed,RO} * t_{RO,year}} \quad \textbf{(7-14)}$$

Finally, if the desired annual permeate flow rate is still not reached, the number of MD modules, is increased and the aforementioned steps are repeated.

7.1.5.4 Design assumptions

The effect of wind on the heat losses from the FPC is not considered in this study which will result in an over estimation of the collector efficiency. According to Schwantes et al. (2013), in a solar driven MD plant installed in Gran canary, the efficiency of the collector dropped by 10% in a windy day, i.e. 7.5 m/s wind velocity. In this study, as the average wind velocity in Marsa-Matruh and Aswan in less than 5 m/s, the collector area will be simply oversized by 5%.

The heat losses from the heat exchangers to the ambient are not considered in this study. These losses are expected to be insignificant given that in the solar driven MD plants discussed in Schwantes et al. (2013), which were installed at several locations, the heat losses from both the heat exchangers and the pipes to the environment were less than 5%.

The heat losses from the MD module to the environment either through the module walls or through the heat leaving the modules with the permeate flow are assumed to be constant and were already accounted for in the mathematical model discussed in

Chapter 6. This is expected to slightly underestimate the heat losses from the module walls especially in winter where the ambient temperatures are likely to be lower than those experienced in the location were the modules were tested in Winter et al. (2011).

7.1.6 Cost analysis

As discussed in section *7.1.5*, the MD system modelled in this study is composed of the MD modules, the solar FPC's, two heat exchangers, and a heat storage tank, that in addition to pumps, pipes, feed tank, wiring, and instrumentation and control equipment.

As MD is a relatively new technology, little data on the costs are found in the literature. Therefore, when costs for a specific category are not found, RO plant cost data discussed in Chapter 4 (section *4.1.5.3*) is used.

The price of the MD modules modelled in this study is directly obtained from the seller, i.e. SolarSpring. It should be noted that the specific cost of the module per unit area is significantly higher than the values used in other MD cost analysis studies (*Table 7-3*).

For the FPC's, the specific cost used in the literature (*Table 7-3*) shows wide variation from as low as 80 USD/m^2 and reaching up to 287 USD/m^2. Given that the cheaper prices could be for lower quality solar panels compared to the commercial FPC modelled in this study, the price of the latter is used after reducing it by 20% assuming that the FPC could be obtained at lower prices with the large systems expected in this study.

For heat exchanger costs, little data is also found in the literature. The cost data found in the literature, e.g. (Fane et al., 1987, Banat and Jwaied, 2008), are shown without indicating the area of the heat exchanger such that the specific cost could be estimated. However, in their analysis for a hybrid RO/MD plant, Drioli et al. (2006) and Macedonio et al. (2007) used a correlation developed by Peters et al. (2002) which estimates the heat exchanger cost as function of its area which is used in this study.

The pre-treatment and post-treatment equipment costs in addition to the labour costs are estimated with respect to the overall hybrid system feed and product flow rate using the specific costs discussed in Chapter 4 (section *4.1.5.3*).

Regarding the construction costs, data is only available for conventional RO plants and range from 15 to 30% of the equipment costs (Wade, 2001, Miller, 2003, Banat and Jwaied, 2008). However, Ghaffour et al. (2013) reported higher costs ranging from 50 to 85% of the total capital cost which seems to be more consistent with the construction costs indicated in Hafez and El-Manharawy (2003) for several SW RO plants in Egypt. In this study, the construction costs of the solar driven MD plant are assumed to be only 15% of the total equipment capital costs excluding the instrumentation and control equipment cost for the following reasons: part of the infrastructure, e.g. construction costs related to the pre-treatment and post-treatment equipment, is already accounted for when estimating the RO plant costs; and the MD module cost is nearly 3.5 times that of an RO plant and therefore using the same percentages typically used for RO plants is expected to exaggerate the construction costs.

While Banat and Jwaied (2008) assumed that the instrumentation and control costs of a solar driven MD plant to be 25% of the total purchased equipment costs, in this study a figure of 10% is used because in their study a much lower module cost than that used in this study was assumed[206].

Finally, the cost of cooling towers is assumed to be included with the construction cost as it was hard to get cost data. It should be noted that by contacting one of the manufactures, a cooling tower used to reduce the temperature of saline water by 10°C and having a capacity similar to those used in this study would cost approximately 55,000 USD (Baltimore Aircoil 2014, pers. Comm., 31 Jul.) which is insignificant with respect to the other equipment costs.

Other equipment capital and operating costs and lifetime are shown in *Table 7-3*.

Table 7-3: Solar driven MD plant capital and operating costs available in the literature and the actual values selected for the cost estimation

	Cost/Lifetime	Reference	Value Used
	Capital Costs		
MD Module	36 USD/m^2 of membrane area (AGMD)	(Liu and Martin, 2006, Banat and Jwaied, 2008)	350 USD/m^2
	90 USD/m^2 of membrane area (DCMD)	(Ettouney et al. 2002) cited in (Macedonio et al., 2007) and (Drioli et al., 2006)	

[206] approximately 11 times lower

	350 USD/m^2 of membrane area (PGMD)	(Schwantes, R from Fraunhofer ISE 2014, pers. Comm., 6 May)	
Module Housing	72 USD/m^2 of module area	(Banat and Jwaied, 2008)	10% of MD module cost
FPC	80 to 250 USD/m^2	(Belessiotis and Delyannis, 2001) **c**ited in (Al-Hallaj et al., 2006)	230 USD/m^2
	100 USD/m^2	(Banat and Jwaied, 2008)	
	250 USD/m^2 and 150 USD/m^2 for 10,000 m^2 and 100,000 m^2 collector area respectively	(Fiorenza et al., 2003)	
	750 USD/unit or 287 USD/m^2 (actual commercial FPC modelled in this study)	(Wagner Solar Inc. 2013, pers. Comm., 12 Aug.)	
Module Racking	21 USD/m^2 of solar collector area[207] for a collector area of 72 m^2	(Banat and Jwaied, 2008)	21 USD/m^2 of solar collector area with an assumed 0.9 scaling (Base area=72 m^2)
Heat Exchangers	$[(1102.5)/280]*101.3*3.29*(10.7639*\text{Area})^{0.65}$	(Peters et al., 2002) cited in (Drioli et al., 2006)	-
Piping and tanks (not including storage tank)	1 USD/l/d for an MD system with 500 l/d capacity	(Banat and Jwaied, 2008)	1 USD/l/d with an assumed 0.9 scaling factor (base capacity= 500 l/d)
Instrumentation and control	25 % of total equipment cost (applied for a solar driven MD plant)	(Banat and Jwaied, 2008)	10 % of total purchased equipment cost
Thermal Storage Tank Cost	1250 USD/m^3 for tank with 6 m^3 capacity	(Müller-Holst et al., 1998)	1250 USD/m^3 with an assumed scaling factor of 0.9 (base capacity=6 m^3)
Installation Costs	15 % of the total plant equipment cost (applied for an SW RO plant)	(Wade, 2001)	15% of the total purchased equipment cost excluding instrumentation and control
	25% of the total equipment costs excluding instrumentation and control (applied for a solar driven MD plant)	(Banat and Jwaied, 2008)	
	30 % of the total equipment costs (applied for a BW RO plant)	(Pittner et al., 1993) cited in (Miller, 2003)	
	50 to 85% of the total plant capital cost (applied for an SW RO plant)	(Ghaffour et al., 2013)	

[207] Value calculated based on the collector area and the heat exchanger capital costs indicted by Banat and Jwaied (2008)

Operating Costs			
Maintenance & Spare parts (not including MD module replacement	2% of the total plant capital cost (applied for an SW RO plant)	(El-Dessouky and Ettouney, 2002, Fiorenza et al., 2003)	2% of the total solar driven MD plant capital cost
Insurance Annual Costs	0.5 % of the total capital cost	(Drioli et al., 2006)	-
Equipment Lifetime			
FPC Lifetime	10 to 25 years	(Guyer, 2012)	20 years
	Excess of 15 years with minimum maintenance	(Rudnick et al., 1986)	
	15 to 20 years	(Kumar, 2013)	
	18 years[208]	(Fan et al., 2009)	
	25 years on average	(SolarContact, 2014)	
MD Module Lifetime	5 years	(Wieghaus et al., 2008)	5 years
Pump Lifetime	20 years	(Richards and Schafer, 2003)	20 years
Thermal Storage Tank lifetime	25 years	(Müller-Holst et al., 1998)	25 years

7.2 Results and Discussion

7.2.1 Scaling effect on the RO/MD plant maximum recovery rate

In chapter 4, it was shown that for the typical GW composition found in Egypt, the scaling limited maximum attainable RR's were nearly the same at those limited by the RO plant design. For the same reason, as shown in *Figure 7-5*, it is clear that unless GW has low scaling potential, using MD to enhance the RO plant RR is not possible even when using scale inhibitors and acid dosing.

The use of MD to enhance the RO RR is however feasible with additional pre-treatment steps such as the use of an ion-exchange process and lime softening. For example, with an RO brine with 7,500 mg/l salinity and a chemical composition with similar calcium and sulphate concentrations as those of the typical GW composition in Egypt but with much higher silica concentrations, i.e. 116 mg/l, Martinetti et al. (2009) showed that with chemical softening and the use of clarification and dual media filters to remove the

[208] The value is the lifetime of an actual 4000 m^2 flat plate collector field installed in Sweden in 1982 and shut down in 2000

precipitated solids, that in addition to the use of sulphuric acid and scale inhibitors, a RR of up to 98% could be obtained using a hybrid RO/MD plant.

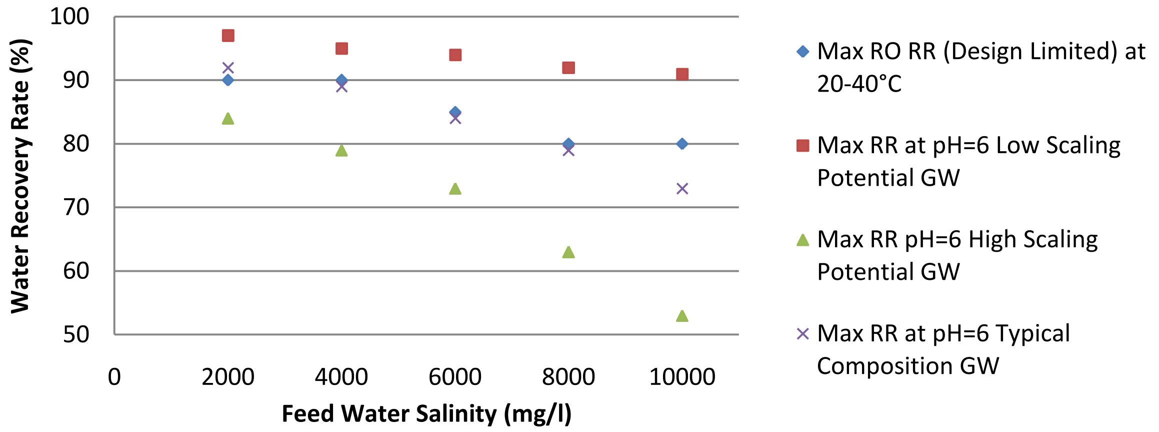

Figure 7-5: Comparison between the maximum scaling limited RR's that can be attained with simple pre-treatment with different GW compositions at the expected operating temperatures of the MD process[209] and those limited by the RO plant design

However, as discussed in chapter 2, ion exchange is an expensive process, and lime softening will also increase the costs, complexity and maintenance requirements of the desalination plant. Accordingly, these pre-treatment processes may not be suitable for decentralized applications in remote/rural areas in Egypt.

7.2.2 Effect of cooling tower water losses on the RO/MD plant maximum recovery rate

After considering the evaporation losses in the cooling tower, it was observed that the annual permeate production estimated from the TRNSYS model dramatically decreased. Therefore, the maximum attainable RR after considering the evaporation losses was preliminary estimated after assuming a constant MD permeate flow rate estimated at the average expected salinity, 80°C evaporator inlet temperature and 22 hours operation to calculate the initial number of MD modules required as discussed in section *7.1.2*. The MATLAB code was then used to estimate the maximum attainable RR and the corresponding initial number of modules required after applying the following modifications:

A) Equations *(7-4)* to *(7-7)* were modified to account for the evaporation losses in the cooling tower as follows:

[209] 60-85°C

at $t \leq t_{RO}$:

$$m_{brine,Tank}(t) = \dot{m}_{brine,RO} * t + NMD * \left[(1 - Loss) * \dot{m}_{e,o} - \dot{m}_{c,i}\right] * (t-1) \quad \textbf{(7-15)}$$

$$\dot{m}_{e,o} = \dot{m}_{e,i} - \dot{m}_{p,MD,Mod,design} \quad \textbf{(7-16)}$$

$$\dot{m}_{e,i} = \dot{m}_{c,i} \quad \textbf{(7-17)}$$

at t>t_{RO}:

$$m_{brine,Tank}(t) = m_{brine,Tank}(t_{RO}) + NMD * \left[(1 - Loss) * m_{e,o} - m_{c,i}\right] * (t - t_{RO}) \quad \textbf{(7-18)}$$

where $\dot{m}_{e,o}$, $\dot{m}_{e,i}$, and $\dot{m}_{c,i}$ are the evaporator channel outlet and inlet mass flow rate and the cooling channel inlet mass flow rate respectively and $Loss$ is the evaporation losses from the cooling tower.

B) A condition was added to ensure that the brine salinity in the tank at any time step during the day does not exceed the maximum allowable salinity associated with the hybrid plant maximum scaling limited RR when GW with low scaling potential is used. In this case, starting from the maximum scaling limited RR, the hybrid RO/MD plant RR is reduced until the condition below is satisfied:

$$S_{brine,tank}(t) \leq \frac{S_{feed}}{1 - R_{hyb,max}} \quad \textbf{(7-19)}$$

As shown in *Figure 7-6*, it is found that the water losses from the cooling tower, while small, greatly limited the maximum attainable RR by the hybrid RO/MD plant. The evaporation losses from the cooling tower were actually the main RR limiting factor. The maximum attainable RR's at different feed water salinities were even lower than those obtained when simple pre-treatment is used with low scaling potential GW. Furthermore, even after assuming that pre-treatment measures such as those discussed in Martinetti et al.(2009) are taken and that the brine salinity in this case can reach a salinity of 250 g/kg[210] without scaling issues, the maximum attainable RR was still lower than the scaling limited RR.

[210] It is assumed that the brine is mainly a sodium chloride solution. The 250 g/kg value is in this case slightly below the value at which Yun et al. (2006) observed a sharp decline in MD flux due to the precipitation of sodium chloride on the MD membrane surface due to the effect of concentration polarization.

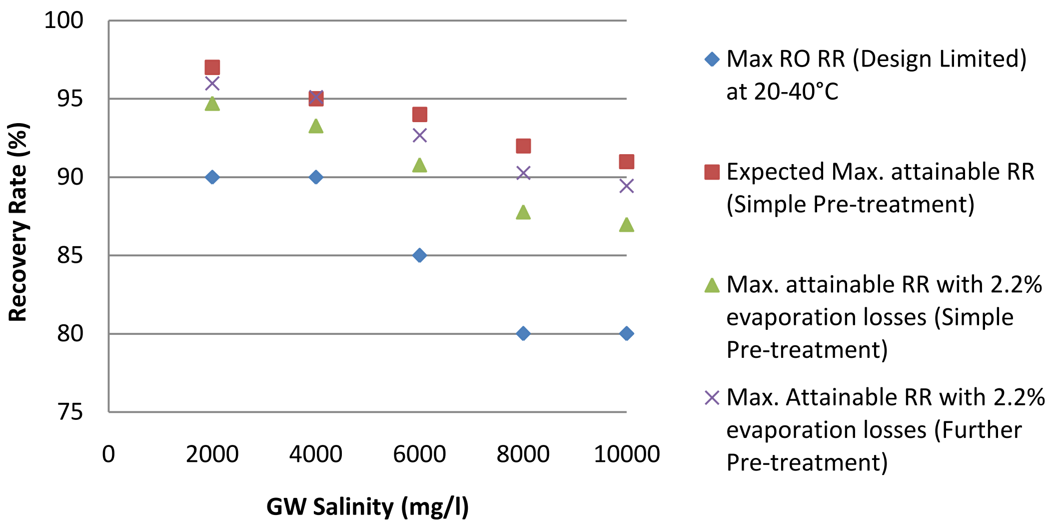

Figure 7-6: Comparison of the maximum attainable RR of the hybrid RO/MD plant before and after accounting for the effect of 2.2% evaporation losses from the cooling tower when the RO plant is designed to operate only during daytime and when the PGMD module is operating at 20°C cooling channel inlet temperature and 500 kg/h feed flow rate

The increase in water salinity due to the evaporation losses in the cooling tower can be observed from *Figure 7-7*, which shows the change in the water salinity and the available brine mass in the tank for a hybrid RO/MD plant desalinating 20,000 mg/l water with an overall RR of 82%.

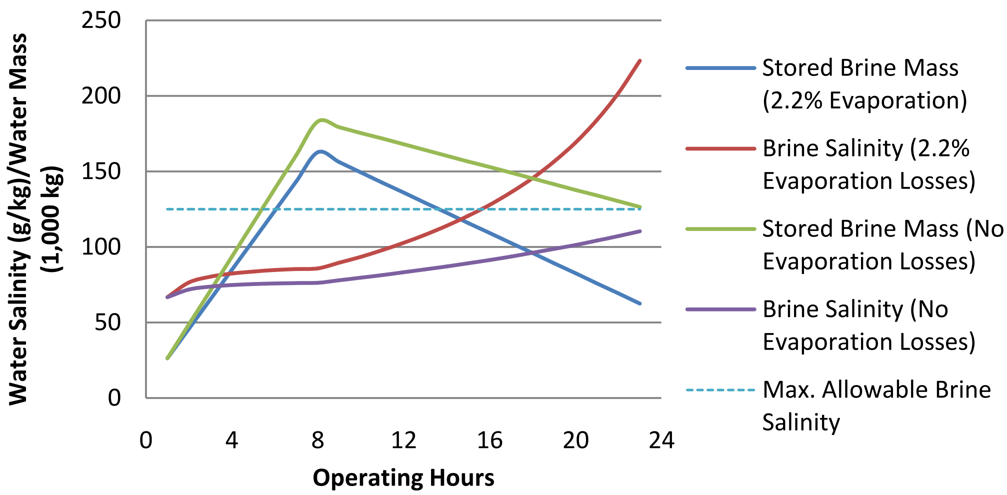

Figure 7-7: Effect of cooling tower evaporation losses on the available brine mass and salinity at an overall hybrid RO/MD plant RR of 82%, when the PGMD module is operating at 20°C cooling channel inlet temperature and 500 kg/h feed flow rate and when the RO plant is designed to operate only during daytime with 20,000 mg/l GW salinity

In this example, without the evaporation losses, the targeted 82% hybrid plant RR is attained without the brine salinity exceeding the maximum value at which scaling would occur when GW with low scaling potential is used[211]. In contrast, with the evaporation losses the maximum brine salinity is exceeded at approximately the 16th hour at which the hybrid plant RR is only 78.2%.

It should be also noted that when the RO plant is operating for 24 hours, the maximum attainable RR is even lower than the case where the RO plant is only operating during daytime (*Figure 7-8*). This is mainly due to the different salinity profiles such that when the RO plant is only operating during daytime, the brine salinity in the tank slightly increases until the RO plant stops, after which it exponentially increases as shown in *Figure 7-9*. In contrast, when the RO plant is operating for 24 hours, the large number of modules required in this case[212] causes a logarithmic increase in the salinity at the beginning of the day where large amount of water is recovered. Afterward, the high brine salinity at the end of the day reduces the permeate flow rate hence slowing down the increase in the brine salinity. Accordingly, the MD modules operate at higher average salinity than the case where the RO plant is operating during daytime only. For this reason, while the amount of permeate that needs to be produced by the MD plant is tripled[213], the required number of MD modules increased 4.4 times which resulted in an increase in the water losses.

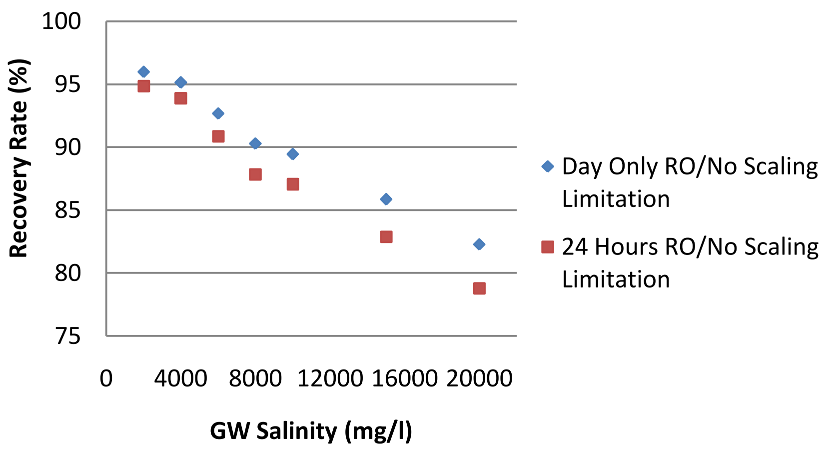

Figure 7-8: Comparison between the maximum attainable RR by the hybrid RO/MD plant when the PGMD module is operating at 20°C cooling channel inlet temperature and 500 kg/h feed flow rate and under the assumption that the brine can be concentrated to 250 g/kg

[211] The scaling limited RR is 84% at which the maximum brine salinity is 125 g/kg

[212] Larger number of modules required as larger amount of brine needs to be desalinated by the MD plant

[213] RO plant operating hours increased from 8 to 24 hours

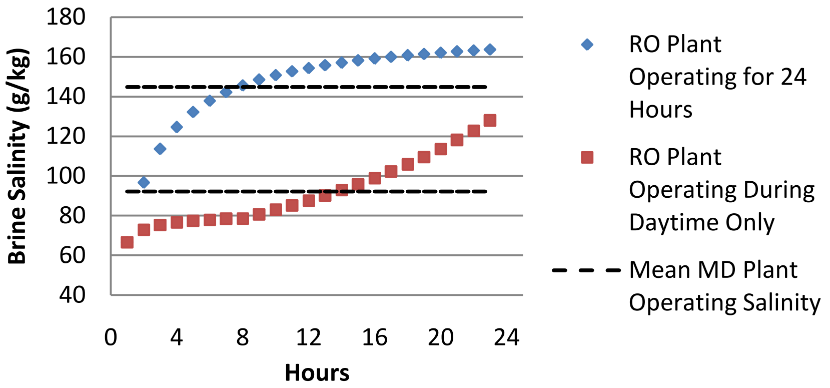

Figure 7-9: MD brine tank salinity profile comparison when the RO plant is designed to operate during daytime only and for 24 hours at 79% hybrid plant RR, 20,000 GW salinity and 20°C MD cooling channel inlet temperature

It is also worth mentioning that the high RR's reported in other studies in the literature concerning the feasibility of hybrid RO/MD plants such as those of Drioli et al. (1999), Criscuoli and Drioli (1999) Drioli et al. (2006) and Macedonio et al. (2007) is found to be not feasible if a cooling tower is used. In their studies, an overall RR of 86% was achieved by desalinating the brine of a SW RO plant using a DCMD process whose performance was based on the experimental work of Drioli et al. (1999). Drioli et al. (1999) performed their experiment on a lab scale DCMD module which operated at fluxes ranging from 2.4 to 1.4 kg/m^2/h at feed water salinities of 75 (start salinity) and 320 g/l (final salinity) respectively, an evaporator inlet temperature of 35°C and feed flow rate of 300 l/h. While the flux at 75 g/l is 3 times higher than that obtained from the full scale module used in this study even when the latter is operating at 80°C evaporator inlet temperature, if a cooling tower with 2.2% evaporation losses is used, the membrane area of each MD module would need to be at least 90 m^2 such that the overall RR of the hybrid plant exceeds 85% when the RO plant is operating during daytime only. Such large area is required to increase the RR of the MD module's to reduce the required number of modules hence the amount of brine that needs to be recirculated. However, as discussed in Chapter 2 (section *2.5.3*), it is not possible to obtain the same flux of a lab scale module with a full scale module especially if the membrane area is a large as 90 m^2. The reported high RR could be however attained if additional SW is used to cool the brine through a heat exchanger, as in the MD system discussed in Zhao et al. (2013), instead of using a cooling tower.

7.2.3 Enhanced MD configurations for higher RO/MD plant recovery rates

As discussed in the previous section, the low RR of the PGMD module used in this study greatly limited the maximum attainable RR of a hybrid plant as it resulted in increasing the water losses in the cooling tower.

In this case, enhanced MD configurations such as VMD might be a better alternative for a hybrid RO/MD plant. The VMD configuration has much higher fluxes than DCMD and AGMD as could be clearly observed from the experimental work of Cerneaux et al. (2009) which compared the performance of different MD configurations. The other advantage of VMD modules is that high fluxes can be attained at low feed water temperatures which helps in limiting calcium sulphate scaling due to its higher solubility at lower temperatures (Martinetti et al., 2009).

An example of a commercially available full scale VMD module is the vacuum multi-effect MD produced by memsys in partnership with GE (memsys, 2014). Similar to MSF and MED, the module consists of several stages, each containing a flat sheet hydrophobic membrane, where the latent heat of the water vapour produced in one stage is used to heat the brine in the following stage to increase the thermal efficiency of the process by reusing the latent heat several times. But most importantly, the MD flux of the module is enhanced by applying vacuum to the permeate channel of each stage which increases the pressure gradient across the membrane and makes the conductive heat losses negligible as discussed in Chapter 2 (section *2.4.2*). Based on the manufacture's data sheet (memsys, 2015), a RR of up to approximately 39% is obtained from a memsys module consisting of 6 effects with a total membrane area of 52 m^2 and at a heating water temperature of 75-80°C using tap water as the feed and at a coolant water temperature of 30-35°C. This RR is approximately 9 times higher than that obtained from the PGMD module at similar operating conditions[214].

However, such module requires a large cooling flow rate in the condenser chamber which is up to 9 times the feed flow rate (memsys, 2015). Accordingly, the increase in the MD module RR was totally offset by the large cooling flow rate which increased the

[214] The PGMD RR is approximately 4.4% at an evaporator channel and cooling channel temperatures of 80 and 30-35°C respectively and a feed flow rate of 500 kg/h

evaporation losses in the cooling tower. A preliminary investigation[215] showed that nearly the same hybrid plant RR's obtained using the PGMD module was achieved by the memsys module in spite of its much larger RR (*Figure 7-10*).

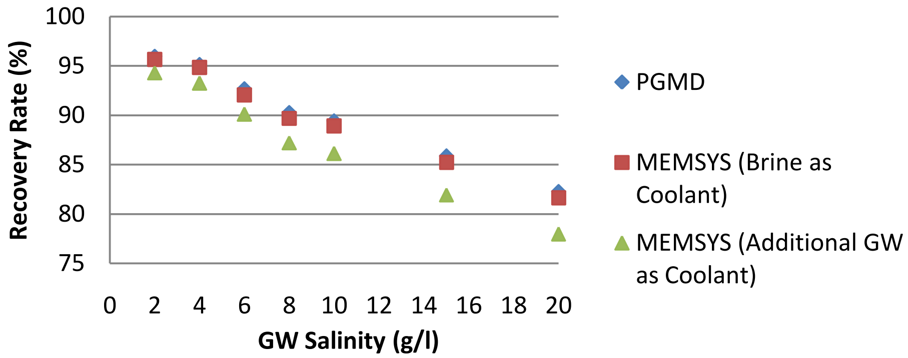

Figure 7-10: Comparison of the maximum attainable RR between a hybrid RO/MD plant using the PGMD module and another using the memsys module with 2.2% water losses from the cooling tower, 20°C MD cooling channel inlet temperature, 500 kg/h feed flow rate and when the RO plant is designed to operate only during daytime

It is also worthwhile mentioning that with the memsys module and any other MD module configurations using a separate condenser channel, there is the option of pumping additional amount of GW to act as the coolant. In this case, the maximum attainable RR will be also limited by the evaporation losses in the cooling tower. However, the RR limitation is caused by the additional GW that needs to be pumped rather than scaling issues. In this case, a preliminary analysis shows that using additional GW to act as a coolant will significantly limit the hybrid plant RR[216] and it is better to use the brine from the tank instead (*Figure 7-10*).

7.2.4 Solar driven MD plant performance

In the previous section, it was concluded that in spite of its very low RR, the PGMD module used in this study could still be used to desalinate the brine of a BW RO plant operating during daytime only and in inland areas, where a cooling tower is needed, as in this case RR's of at least 90% could be achieved. Accordingly the performance of a

---

[215] In the analysis, it was assumed that the memsys module has a RR that is always 9 times that of the PGMD module at similar operating conditions. Moreover, as the memsys module has a separate condenser channel, it was assumed that the brine from the tank flows through the condenser channel acting as the coolant similar to the PGMD module. The brine exiting the condenser channel and that exiting the MD module then go through the cooling tower before being recirculated back to the brine tank.

[216] The maximum attainable RR was calculated using equations (*7-4*) to (*7-7*) and then the denominator of equation (*7-1*) was modified to account for the additionally pumped GW which is equal to $10 * NMD * Loss * m_{c,i}$ where the 10 factor accounts for the additional 9 folds of the flow rate circulated in the memsys module, that needs to flow in the condenser chamber

solar driven hybrid RO/MD plant was investigated for the aforementioned case after assuming that additional pre-treatment measures like water softening and clarification are taken.

7.2.4.1 TRNSYS model validity

Figure 7-11 shows the performance of a solar driven MD plant during a sunny day where the plant is used to desalinate the brine from an RO plant desalinating 2,000 mg/l GW. The plant operates exactly as described in section *7.1.5.1*.

The FPC loop pump starts at 8:30 (A) followed by the heat storage loop pump. T_{Coll} and T_{HX2} then keep increasing with the increase in the incident solar irradiance. At 10:30 (B), T_{HX2} exceeds pre-set value 7 (*Table 7-1*) and therefore the MD plant starts to operate. At 11:30 (C), as the sun irradiance is about to reach its peak, the water temperature exiting HX1 exceeds 83°C and therefore the additional heat is used to charge the storage tank such that T_{HX2} remains at 83°C. At 16:40, the tank bottom temperature approaches 83°C and therefore the UV valve is switched back to the B-C position which explains the sudden increase in T_{HX2} and $T_{e,in}$ from 16:40 to 18:20 (D to E)[217].

Near sunset, i.e. 18:20 (E), T_{Coll} is below pre-set value 1 and therefore the FPC loop pump is switched off and LV is switched to the B-A position such that the heat is supplied from the storage tank. However, as the tank top temperature is initially very high, the MD plant is shut down until T_{HX2} is below pre-set value 6. The MD plant then keeps operating until the heat in the storage tank is exhausted, i.e. top tank temperature is less than Pre-set value 2, at which the LV position is reset to the B-C position. Finally the MD plant operates for a short time due to the residual heat in the pipes before eventually shutting down when T_{HX2} goes below pre-set value 7.

[217] This case occurred in this day in particular where the solar irradiance is one of the highest in the whole year.

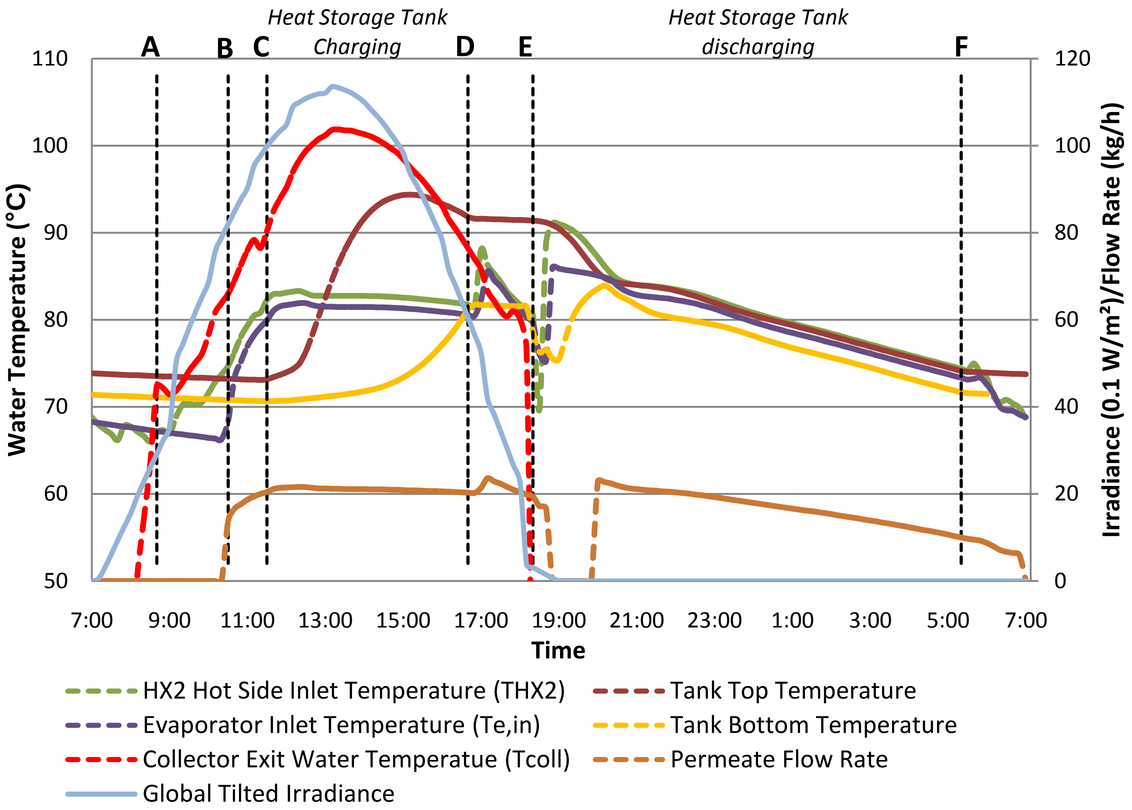

Figure 7-11: The performance of the MD plant during a sunny day

7.2.4.2 Design optimization

A) Effect of FPC area on the MD plant performance

Figure 7-12 shows the effect of the FPC area on the MD plant annual permeate production and LCOW. As expected, increasing the FPC area allowed the MD plant to operate for longer time higher evaporator inlet temperatures which resulted in an increase in the annual permeate production.

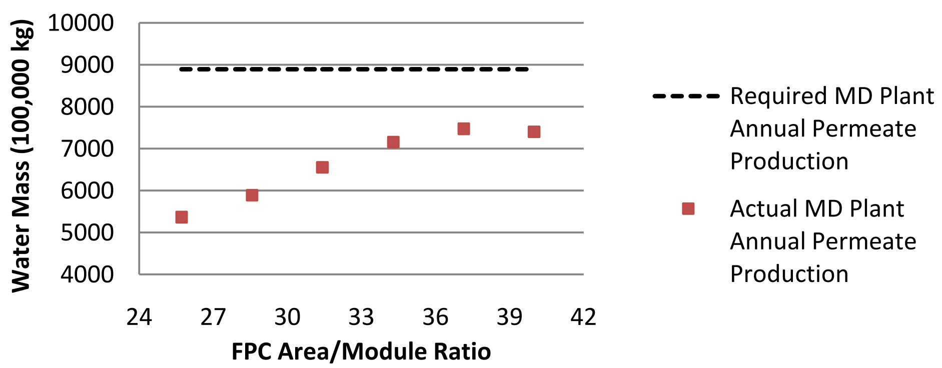

Figure 7-12: Effect of the FPC area on the annual permeate production and LCOW of the MD plant with the initially estimated number of modules (NMD=63) and when GW with 2,000 mg/l salinity is desalinated by the hybrid plant

However, at some point increasing the FPC area resulted in a significant increase in the duration at which the MD plant is shut down to protect the modules from high temperature operation particularly during periods of high solar irradiance increasing the duration at which the plant is shut down to protect the modules. Accordingly, in spite of the increase in the plant annual average operating temperature, the increase in the FPC area resulted in a limited increase in the annual permeate production and eventually a reduction in the production at very large FPC areas[218].

For this reason the LCOW of the MD plant is the lowest when the FPC area is just enough for the MD plant to operate as long as possible near 80°C while minimizing the shutdown period due to high temperature operation. It is important to note, however, that the FPC area/module ratio at which the LCOW is the lowest is not necessarily the optimal case as the increase in the LCOW at higher FPC area/module ratios is also due to the increase in the RR, and therefore the operating salinity.

B) Effect of number of MD modules on the annual permeate production

It is also observed from *Figure 7-12* that the annual MD plant production required to reach the maximum attainable hybrid plant RR was not reached with the initially estimated number of modules[219]. This is expected because the initial number of modules was estimated under the assumption that the MD plant can constantly operate at 80°C for 22 hours every day of the year, i.e. approximately 92% of the year. However, this is not the case with a solar driven plant due to the intermittent nature of solar energy. For example, the actual MD plant annual average operating temperature at the optimal FPC area was 78.4°C and only operated for approximately 76% of the year when 2,000 mg/l GW is desalinated by the hybrid plant.

For this reason, the number of modules was gradually increased to reach the required annual permeate production. *Figure 7-13* shows the effect of increasing the number of MD modules on the annual permeate production. It is observed that while as expected higher annual permeate production was obtained with larger number of modules, at the same FPC area/module ratio the more modules added the less significant was the

[218] It should be noted that during the optimization process, the annual permeate production at very large FPC areas was maximized when the FPC and heat storage loops operating temperature window was increased. In other words, both loops were set to also operate at low temperatures where the operation is less thermally efficient to consume the excess heat available hence reducing the duration at which the plant is shut down.
[219] E.g. approximately 16% and 14% shortage from the required annual permeate production when 2,000 and 10,000 mg/l GW, respectively, is desalinated by the hybrid plant

increase in the permeate production. This is attributed to the increase in the MD plant operating salinity mainly as a result of the increase in the evaporation losses as more modules are used; that in addition to the increase in the RR which increases the operating salinity.

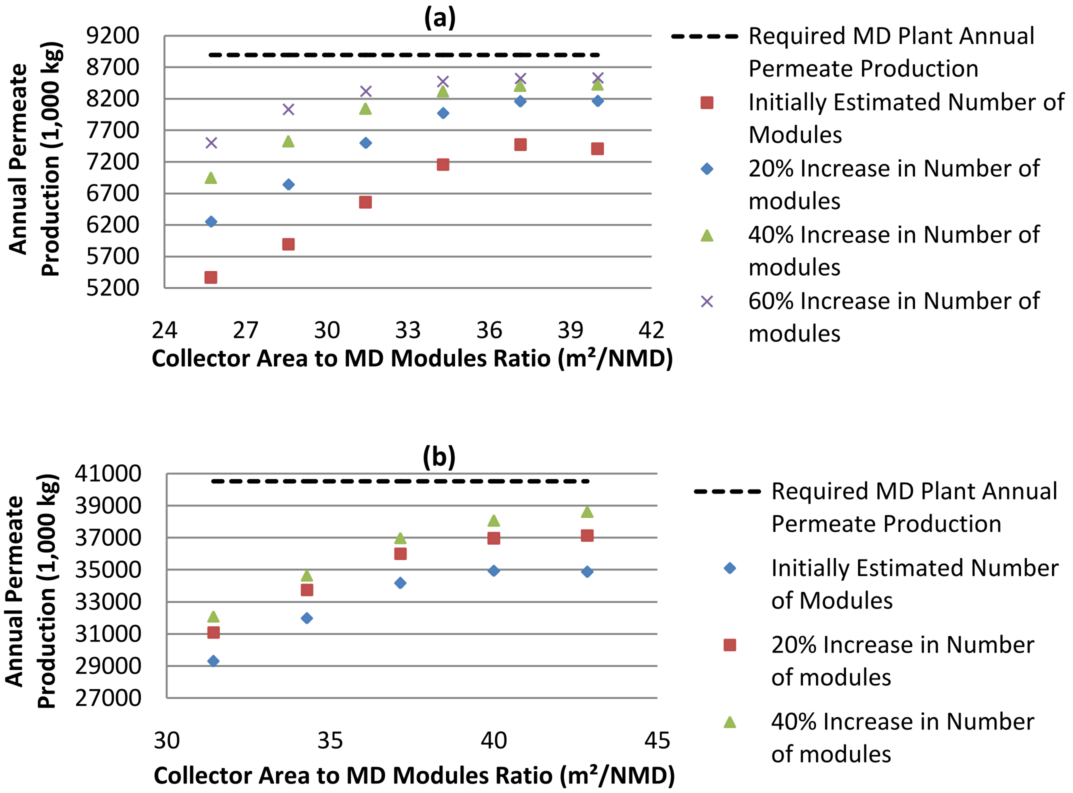

Figure 7-13: Effect of increasing the number of PGMD modules on the annual permeate production of the MD plant when GW with 2,000 mg/l salinity is desalinated by the hybrid plant and when the RO plant is designed to operate during daytime only and (b) when GW with 10,000 mg/l salinity is desalinated by the hybrid plant and when the RO plant is designed to operate 24 hours

It is also observed that increasing the FPC area/module ratio was less effective in increasing the annual permeate production when the RO plant is operating during daytime only especially with more modules added. It was particularly observed that the percentage increase in the average operating salinity, associated with the increase in the annual permeate production with higher FPC area/module ratios, was much higher when the RO plant is operating during daytime only. Therefore, it is concluded that this behaviour is likely due to the different salinity profiles as discussed in section *7.2.2*. In particular, increasing the FPC area/module ratio extends the operating time of the MD plant, i.e. operate more time during evening and night time. Therefore, when the RO plant is operating during daytime, the extended operating time is after the RO plant is shut down where the brine salinity starts to increase exponentially lowering the MD module permeate production. In contrast, when the RO plant is operating 24 hours, the operating salinity during evening and night time does not increase by much from its value during daytime.

For the same reason, at larger number of MD modules, it was more economical to design the plant to operate at low FPC area/Module ratios when the RO plant operates during daytime only as shown in *Figure 7-14*. In this case, as less heat is available the annual permeate production decreased and therefore resulting in a reduction in the average operating salinity. However, reducing the FPC area defeats the purpose of increasing the number of modules to increase the annual permeate production. It is therefore more economical to operate at high FPC/module ratio with lower number of modules as the MD plant operates at higher evaporator inlet temperatures hence more efficiently. For example, as shown in *Figure 7-13a* and *Figure 7-14a*, for the case where the RO plant is operating during daytime only, the annual permeate flow rate when the number of modules is increased by 40% and 60% over the initially estimated value and at an FPC area/module ratio of 28.6 and 25.7 respectively was the nearly the same, however the LCOW of the former was approximately 8% lower.

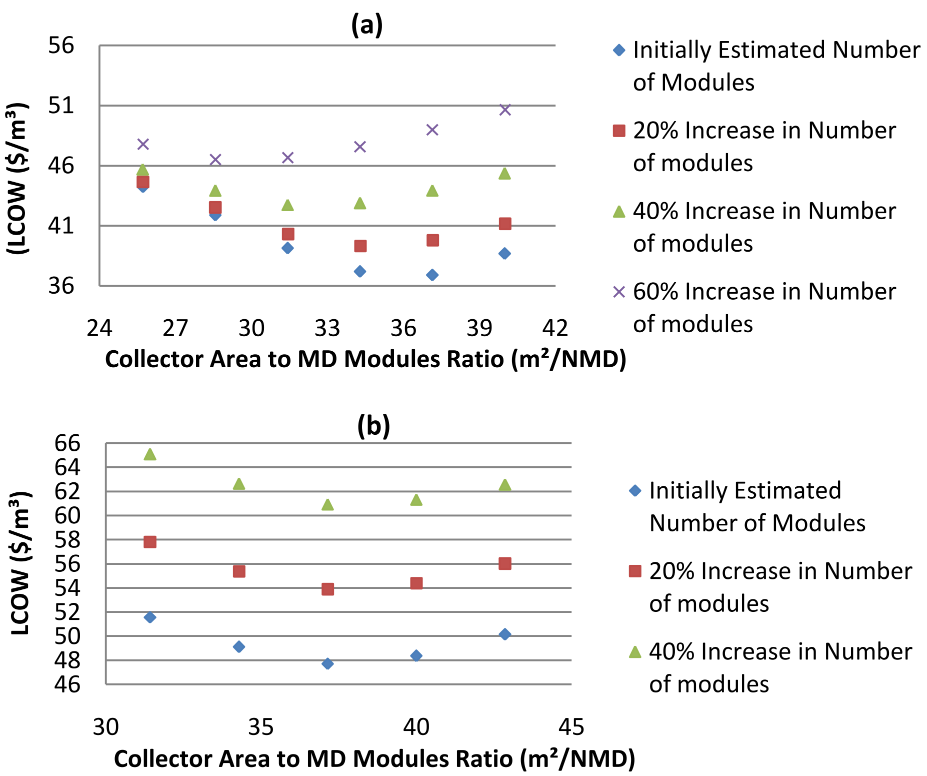

Figure 7-14: Effect of increasing the number of PGMD modules on the LCOW of the MD plant when GW with 2,000 mg/l salinity is desalinated by the hybrid plant and when the RO plant is designed to operate during daytime only and (b) when GW with 10,000 mg/l salinity is desalinated by the hybrid plant and when the RO plant is designed to operate 24 hours

7.2.4.3 Economic feasibility of PV-RO/FPC-MD hybrid plant

As discussed in section *7.2.4.2*, the annual permeate production, hence the hybrid plant annual RR, depends on the FPC collector area and number of MD modules used. It was particularly shown that increasing the number of MD modules, while increased the annual permeate production, resulted in a significant increase in the LCOW due to the increase in the operating salinity especially when the RO plant operates during daytime only.

For this reason, in this study the MD plant design at which at least 90% of the required annual permeate production is obtained will be used to determine the LCOW of the hybrid plant. In other words, increasing the number of modules to increase the annual permeate production beyond the 90% of the required value will be considered as uneconomical.

Figure 7-15 shows an estimation of the LCOW of the hybrid plant when brackish GW is desalinated and with the typical GW depths found in Egypt. It is clear that desalinating the RO brine by an MD process using PGMD modules will significantly increase the LCOW. The LCOW of the hybrid plant ranged from 2.65 to 6.8 USD/m^3 with 2, 000 and 10,000 mg/l GW, respectively, when the RO plant is operating during daytime only, and 2.3 to 5.7 USD/m^3 when it is operating for 24 hours. In other words, the small percentage increase in the RR over that the RO only plant achieved using a hybrid plant increased the LCOW by approximately 1.9 to 3.6 folds. The LCOW of the hybrid plant did not also include the additional cost of pre-treatment that can allow such high RR's to be attained as discussed in section *7.2.1* which will result in a further increase in the costs.

Moreover, as expected, using a hybrid plants becomes more economical when the GW is extracted from the Nubian aquifer in the Sinai Peninsula where high RR's are needed the most due to the high costs associated with GW extraction. The LCOW of the hybrid plant, in this case, was 1.9 to 2.6 times higher than that of the RO only plant (*Figure 7-16*).

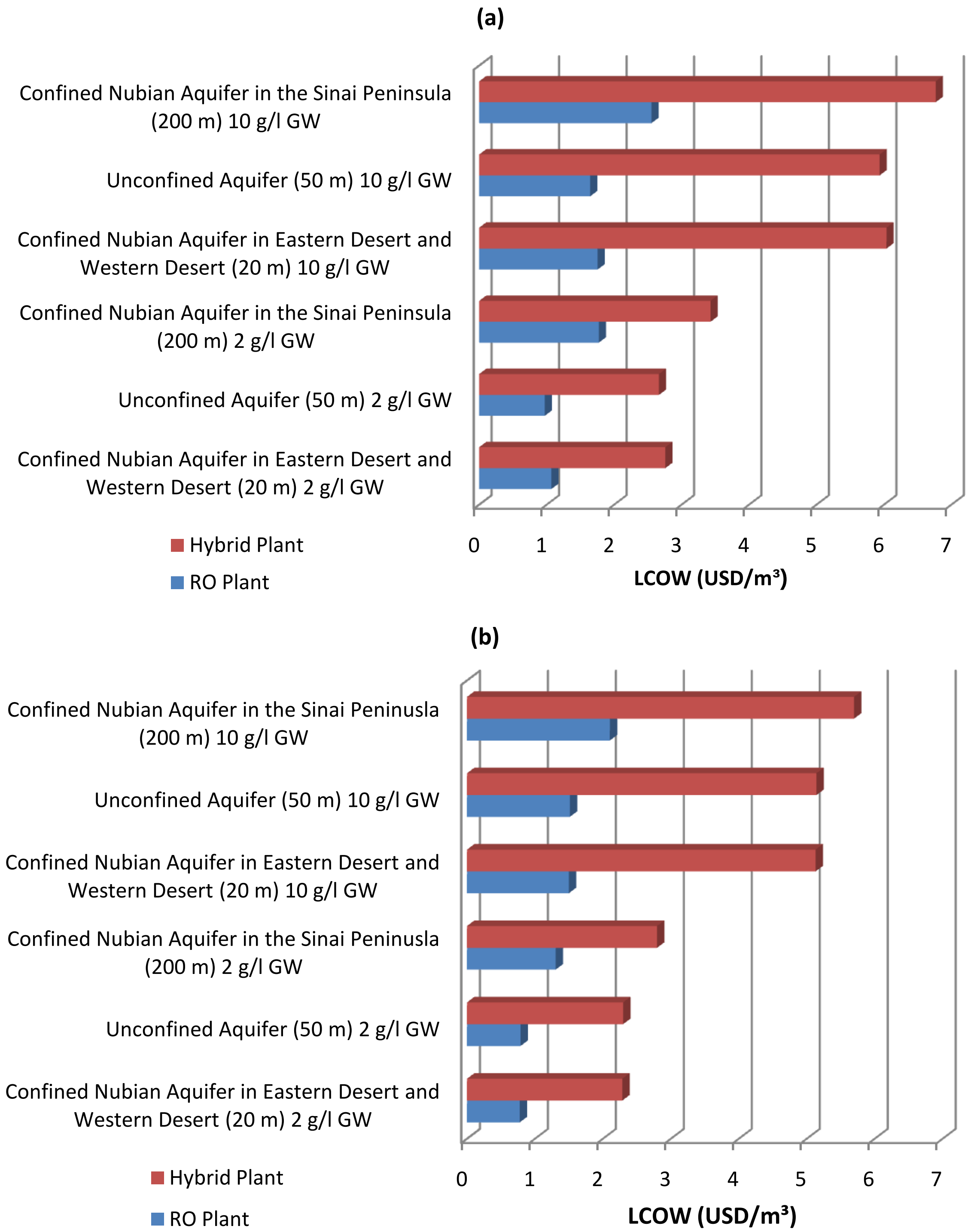

Figure 7-15: LCOW of the solar driven hybrid RO/MD plant with the typical GW depths in the HSI zone when the RO plant is designed to operate (a) during daytime only and (b) for 24 hours

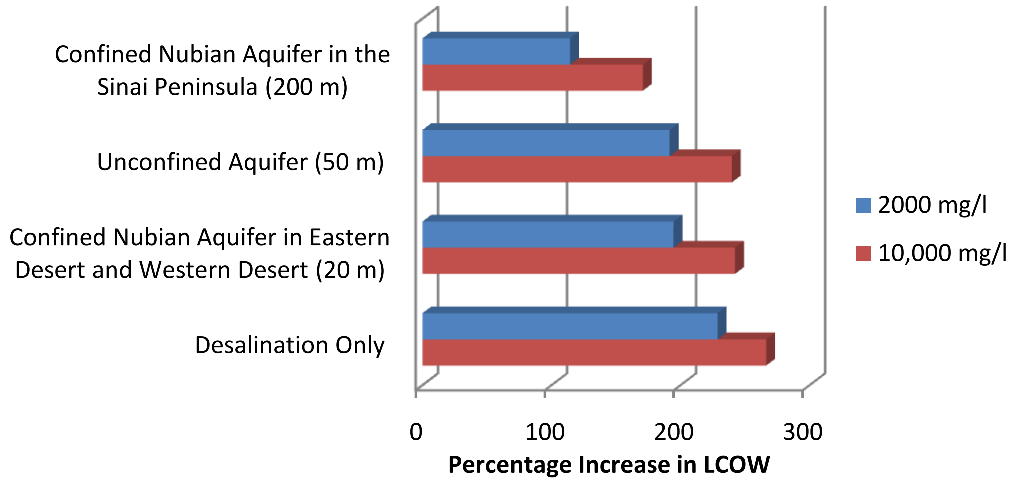

Figure 7-16: Percentage increase in the LCOW after using an MD process to enhance the RR above the design limited values of the RO plant with the typical GW depths in the HSI zone and when the RO plant is designed to operate for 24 hours

The LCOW of the MD plant alone ranged from approximately 40.5 to 50.5 USD/m^3 which is extremely high especially when compared to that of the RO plant. Moreover, as expected the LCOW of the MD plant was slightly higher, i.e. 6.2 to 7.7%, when the RO plant is operating for 24 hours than in the case where it is only operating during daytime due to the higher average operating salinity of the MD plant in the former, as discussed in section *7.2.2*, which increased the number of modules required as well as the SHC. Nevertheless, the LCOW of the hybrid plant was lower in the former case simply because the LCOW of the RO plant, which desalinates most of the water, was lower as discussed in Chapter 4 (section *4.2.3.1*).

It should be noted that the estimated LCOW of the MD plant in this study is higher than that reported in Banat and Jwaied (2008) for a similar solar driven plant which was estimated to be 36 USD/m^3. This is due to the low MD module specific cost used in their study which was approximately 10 times lower than that used in this study. The study also assigned a specific cost to the FPC's that is nearly half that used in this study. Moreover, the MD plant in Banat and Jwaied (2008) was used to desalinate SW and therefore the operating salinity is lower than the annual average operating salinity of the MD plant discussed in this study which ranged from approximately 55 to 100 g/kg. This could be observed from the ratio between the FPC area and the MD membrane area which in Banat and Jwaied (2008) was less than half that of the plant analysed in this study. Finally, it should be noted that for the same plant, Banat and Jwaied (2008) reported that the unit water costs can drop to 18 USD/m^3 under the assumption that the permeate water of the MD plant can be mixed with the feed water with 1:1 mixing ratio. However, this assumption is not adequate given that 1:1 mixing ratio would result in a permeate water salinity of at least 17.5 g/l[220] which is not suitable for drinking or irrigation.

7.2.4.4 Effect of the feed flow rate on the LCOW of the MD plant

The previous analysis was carried out with the case where the MD module is operating at 500 kg/h feed flow rate to reduce the number of MD modules required. However, as discussed in section *7.1.4*, operating a lower feed flow rates can reduce the SHC of the MD process.

However, it was found that while the SHC was indeed reduced, reducing the feed flow rate did not result in a reduction in the LCOW. As shown in *Figure 7-17*, even in the best case where the MD plant is operating at the lowest average salinity, which occurs when 2,000 mg/l GW is desalinated by the hybrid plant, and therefore lowering the feed flow rate would result in the highest reduction in the SHC (section *7.1.4*), the LCOW increased by 6.7%. While the MD plant indeed operated more efficiently by lowering the feed flow rate with an increase of 15% in the annual permeate produced per 1 m^2 of FPC area, the reduction in the FPC area was outweighed by the increase in the number of modules required, where 46% more modules were needed to produce the same amount of annual permeate production.

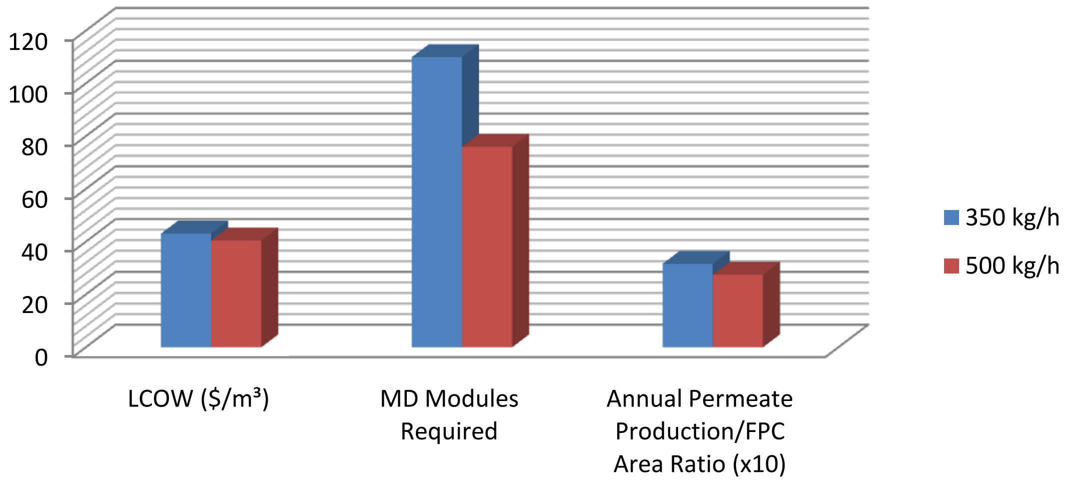

Figure 7-17: Effect of the feed flow rate of the PGMD module on the LCOW of the solar driven MD plant, the required number of modules, and its thermal efficiency when 2,000 GW is desalinated by the hybrid plant

[220] Red Sea water salinity, desalinated by the plant discussed in Banat and Jwaied (2008), is assumed to be approximately 35 g/l

7.2.5 Sensitivity analysis

A sensitivity analysis was carried out to assess the impact of the different components of the MD plant on its LCOW.

Similar to the sensitivity analysis carried out in Chapter 4, the cost of each component of the MD plant was reduced by 20% and the corresponding percentage decrease in the LCOW of the plant was examined.

It is clear from *Figure 7-18* that the costs associated with the MD modules, the FPC's and the heat exchangers in addition to the indirect costs, which are a function of MD plant direct cost, have the biggest impact o the LCOW of the MD plant; which can be also observed from *Figure 7-19.*

The high cost associated with the MD modules is mainly due to the low flux of the PGMD module which required the use of a large number of modules; that in addition to their current high costs which is at least 3.5 fold higher than that of an RO module. Conversely, the very high SHC of the module required the use of a very large FPC and heat exchanger areas.

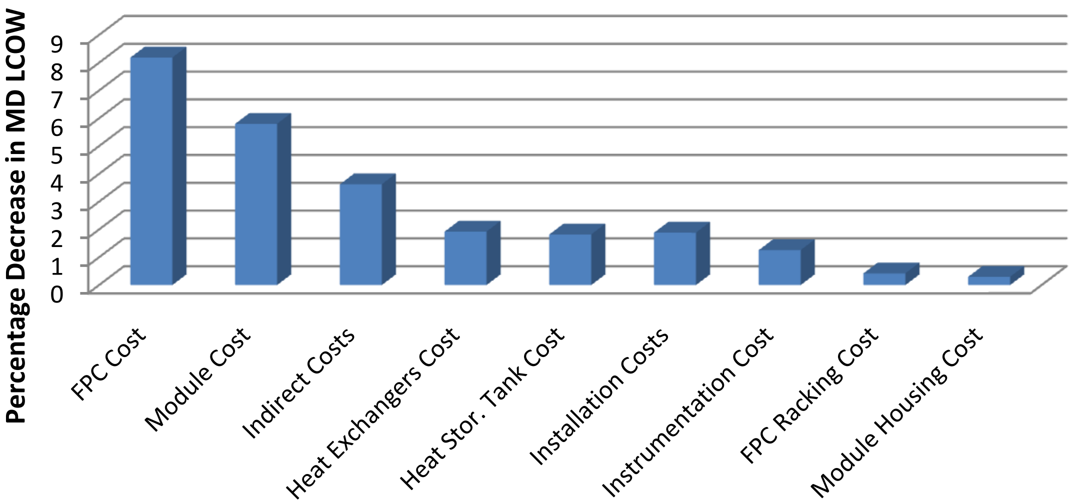

Figure 7-18: Impact of a 20% reduction in the equipment and indirect costs of the solar driven MD plant on its LCOW when the plant is used to desalinate the brine of an RO plant designed to operate for 24 hours and desalinating 10,000 mg/l GW

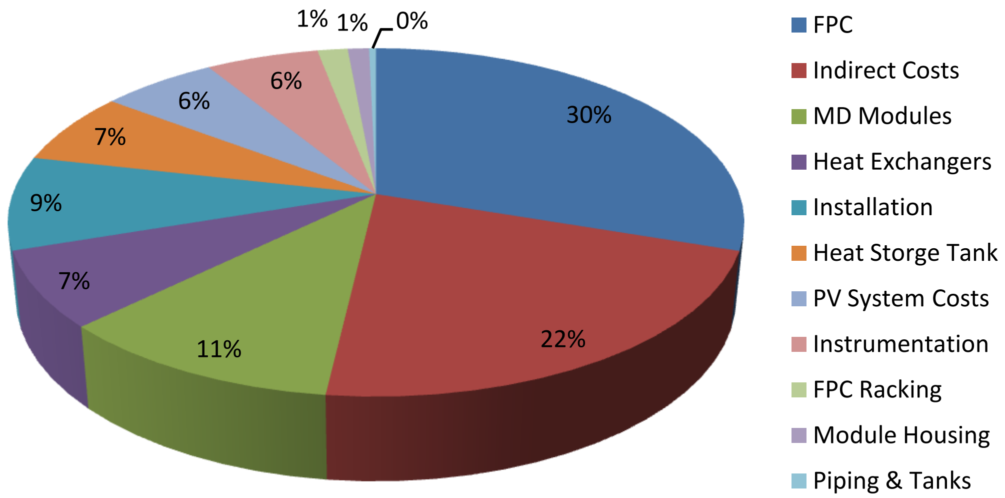

Figure 7-19: Capital cost breakdown of a solar driven MD plant used to desalinate the brine of an RO plant designed to operate for 24 hours and desalinating 10,000 mg/l GW

7.2.6 Possibilities to reduce the LCOW of the MD plant

Based on the sensitivity analysis carried out in section *7.2.5*, it is concluded that in order to reduce the LCOW of the MD plant, hence that of the hybrid plant, it is necessary to reduce the cost associated with the MD modules and FPC's or increase the productivity of the MD module and decrease its SHC.

Several scenarios were investigated and their effect on the LCOW was examined which are summarized in *Table 7-4*. It was already discussed in the previous section that the current module price is very high and at least 3.5 time that of the RO plant. Accordingly, the scenario where the MD module price would be similar to that of the RO was also investigated.

It was also discussed that the flux and the SHC of the PGMD module used in the analysis were very low and high, respectively. Accordingly, the following scenarios are also investigated: a scenario where under the same operating conditions and with the same heat consumption of the PGMD module, the flux of the PGMD is quadrupled while the heat consumption remains unchanged; a scenario where the same flux of the PGMD module could be obtained at only quarter of the heat energy consumption under the same operating conditions; and a scenario where the flux and the heat consumption of the PGMD module are doubles and halved, respectively, under the same operating conditions. These particular ratios were chosen because the lowest SHC reported so far for a commercial MD module was 55.5 kWh/m^3 obtained from the memstill module

(Chapter 2 section *2.5.3*) when SW is desalinated. This value is approximately 4 times lower than that of the PGMD module at the same feed water salinity. Accordingly, a 4 times reduction in the SHC could be either achieved by a 4 fold increase in the flux, 4 fold reduction in the heat consumption, or 2 fold increase in the flux and 2 fold reduction in the heat consumption.

Table 7-4: Suggested scenarios to reduce the LCOW of the solar driven hybrid RO/MD plant

Case	Conditions
A	100 USD/m² Module Cost
B	4x MD Module Flux Increase
C	4x MD Module Flux Increase + 100 USD/m² Module Cost
D	4x MD Module Heat Energy Reduction
E	4x MD Module Heat Energy Reduction + 100 USD/m² Module Cost
F	2x MD Module Heat Energy Reduction + 2x MD Module Flux Increase
G	2x MD Module Heat Energy Reduction + 2x MD Module Flux Increase + 100 USD/m² Module Cost
H	Solar Waste Heat Available
I	Solar Waste Heat Available + 100 USD/m² Module Cost
J	Solar Waste Heat Available + 4x MD Module Flux Increase
K	Solar Waste Heat Available + 4x MD Module Flux Increase +100 USD/m² Module Cost
L	Solar Waste Heat Available + 4x MD Module Heat Energy Reduction
M	Solar Waste Heat Available + 4x MD Module Heat Energy Reduction + 100 USD/m² Module Cost
N	Solar Waste Heat Available + 2x MD Module Heat Energy Reduction + 2x MD Module Flux Increase
O	Solar Waste Heat Available + 2x MD Module Heat Energy Reduction + 2x MD Module Flux Increase + 100 USD/m² Module Cost

It should be noted that with the scenarios involving a reduction in the heat consumption, for simplicity, it is assumed that the area of the FPC and the heat exchangers, the volume of the heat storage tank, and the flow rates in the collector and heat storage tank loops are directly proportional to the heat consumption.

Finally, the case where the heat required by the MD plant can be obtained from the waste heart of an electricity generating solar plant such as a CPV or CSP plant. A discussed in Chapter 2 (section *2.2.1*), the excess heat from both technologies could be used to drive a thermal desalination process which would increase the overall utilization of solar energy. In this case, for simplicity, it is assumed that the same heat supplied by the FPC's can be supplied by excess heat such that the costs associated with the collectors and their racks are completely offset. In other words, the performance of MD plant is assumed to be unchanged and therefore the area of the heat exchangers, the volume of the heat storage tank and the flow rates in the collector and heat storage tank loops, hence the PV system size, are kept unchanged.

Figure 7-20 shows several scenarios and their effect on the LCOW of the MD plant. It is clear the scenarios where a source of waste heat is available show the greatest reduction in the LCOW of the MD plant. The availability of a waste heat was more effective in reducing the LCOW of the MD plant than the scenario where the MD plant heat consumption is reduced by 4 folds, although the latter case involves a reduction in the costs associated with the heat storage tank, PV system and heat exchangers. This emphasizes that, as discussed in section *7.2.5*, the costs associated with the FPC's is the main factor affecting the LCOW of the MD plant.

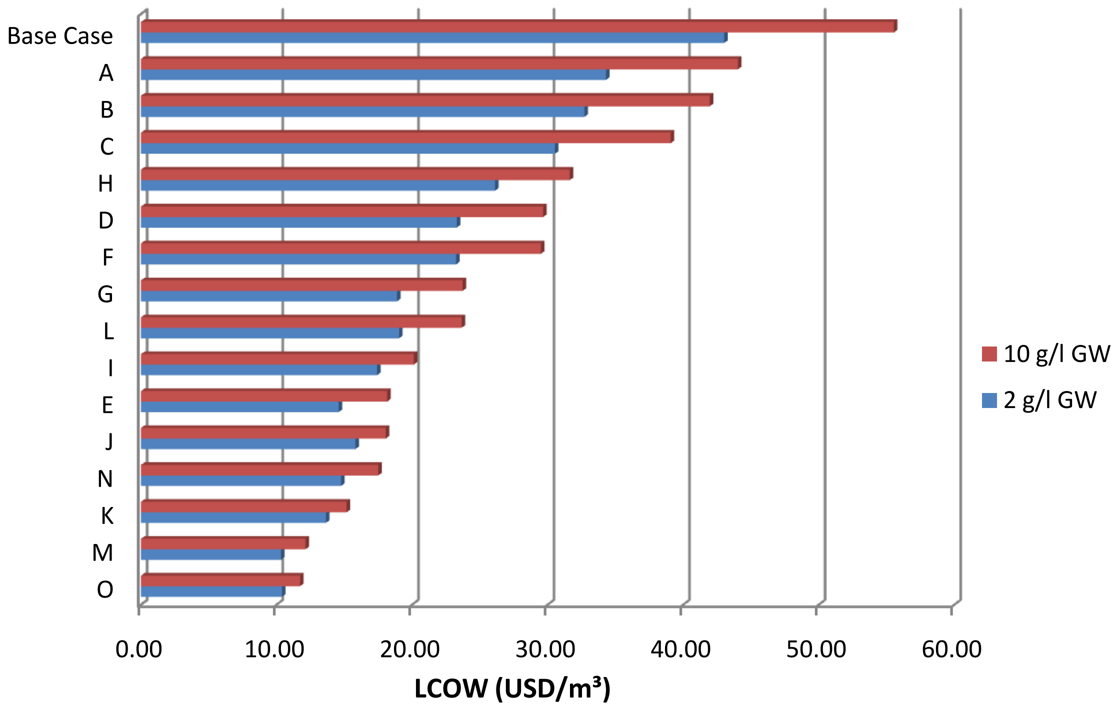

Figure 7-20: LCOW of the hybrid RO/MD plant under different scenarios when the RO plant is designed to operate for 24 hours

The lowest LCOW is achieved with the cases where a source of waste heat is available and the MD module experiences either a 4 folds decrease in the heat consumption, or a 2 fold increase in the flux and 2 fold reduction in the heat consumption; and in both scenarios the MD module specific costs had to be reduced to 100 USD/m^2. Under these scenarios, the increase in the RR over that the RO only plant achieved using a solar driven hybrid plant will result in a percentage increase in the LCOW ranging from 26 to

47% depending on the GW depths (*Figure 7-21*) i.e. the LCOW of the hybrid plant ranged from 1 to 2.8 USD/m³.

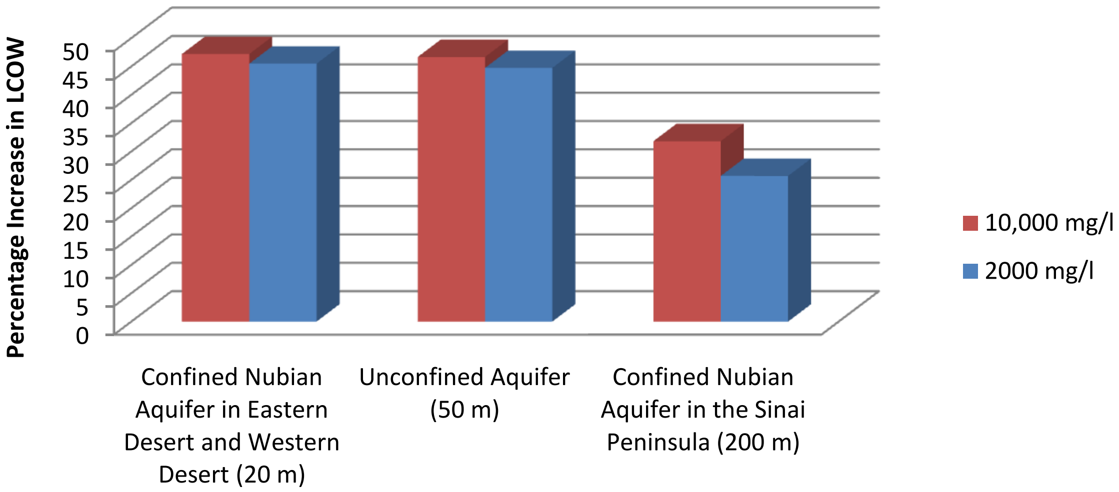

Figure 7-21: Percentage increase in the LCOW after using an MD process under the "O" scenario to enhance the RR above the design limited values of the RO plant with the typical GW depths in the HSI zone and when the RO plant is designed to operate for 24 hours

7.3 Conclusion

In this chapter, a feasibility study of using an MD process to enhance the RR of the RO plant was carried out. It was found that an enhancement in the RR is only feasible with additional pre-treatment steps such as chemical softening, clarification and media filtration which will increase the complexity and cost of the plant.

Most importantly it was found that the evaporation losses from the cooling tower have a significant impact on the maximum attainable RR from a hybrid RO/MD plant. For the PGMD module used in this study, such losses were the main RR limiting factor for a hybrid RO/MD plant where no more than 10% enhancement in the RO RR was obtained with brackish GW even after assuming that the brine can be concentrated to 250 g/kg without scaling issues. Moreover, even with enhanced MD process configurations such as the memsys module, which is based on a VMD process, the large cooling requirements resulted in an increase in the evaporation losses which limited the maximum attainable RR of the hybrid plant to values similar to those obtained with the PGMD module although the RR of the former was up to 9 times higher. Accordingly, it is concluded that higher RR's are only possible with high RR modules that have low cooling requirements.

Moreover, the small percentage increase in the RR over that the RO only plant achieved using a hybrid plant, resulted in an increase in the LCOW by approximately 1.9 to 3.6 folds for the typical GW depths found in Egypt. Furthermore, as expected, using a hybrid plant was more economical in areas where the GW is found at large depths where high RR's are needed the most due to the high costs associated with GW extraction.

Based on the results of the sensitivity analysis carried out on the solar driven MD plant, it was particularly found that the low flux and the high SHC of the PGMD module in addition to its current high costs are the main contributors to the very high LCOW of the MD plant. It is, therefore, concluded that hybrid RO/MD plants are likely to be only economically feasible if a source of a waste heat is available from a CPV or a CSP plant, the SHC of the process is reduced by 4 folds and the MD module costs become similar to that of an RO module. In this case, the LCOW of the MD plant is reduced to values ranging from 10.4 to 11.7 USD/m^3 which resulted in a more reasonable percentage increase in the LCOW of the hybrid plant over that of the RO only plant ranging from 26 to 47% for the range of GW depths found in Egypt.

8. Conclusion

The aim of this thesis is to investigate the feasibility of using solar driven plants for brackish GW extraction and desalination. Such plants were suggested to help establishing autonomous decentralized agricultural communities in Egypt away from the heavily populated Nile valley and delta.

Reviewing water resources in Egypt showed that the Nile water, the main source of fresh water, is almost fully exploited and that SW desalination and GW extraction will be the best options to increase Egypt's water supply. The latter option, however, was shown to suit decentralized applications and could potentially be more economical than SW desalination.

Accordingly, GW properties in the seven main hydro-geological systems across six regions in Egypt as well as its potential for sustainable development were investigated. It was found that approximately 55% of Egypt's area has access to brackish GW, with whole regions such as the Eastern Desert and the Sinai Peninsula mostly having access to only BW. Conversely, fresh GW was found to be only confined to the overpopulated Nile delta and valley area in addition to the western and south western parts of the Western Desert which are found to be exposed to sand drift hazards and are not attractive to establish decentralized communities due to their remoteness. The study also showed that 47% of BW aquifers have moderate to high potential for sustainable extraction. Five main areas were particularly identified to have priority for establishing decentralized agricultural communities based on brackish GW extraction and desalination: areas along the Nile River in the Western Desert and the Eastern Desert having access to the Nubian aquifer and the shallow Quaternary aquifer; the central parts of the Sinai peninsula tapping the Quaternary and the Nubian aquifer; the coastal area along both shores of the Suez gulf; and the Mediterranean North West coastal area.

Due to the limited GW resources in Egypt and the need to desalinate brackish GW to be suitable for drinking and irrigation use, the study mainly focused on investigating the feasibility of high RR PV driven RO desalination plants. It was found that the RO plants can operate at RR's ranging from 75 to 90% with a SEC ranging from 0.65 to 1.55

kWh/m^3 at 2,000 and 10,000 mg/l salinity, respectively, with the typical brackish GW composition found in Egypt excluding the additional energy requirements associated with GW extraction. The SEC values drop to 0.5 to 1.5 kWh/m^3 after accounting for the increase in the produced water by blending the GW with the RO permeate.

The LCOW of the PV-RO plant was investigated for an RO plant designed to operate only during daytime, and another designed to operate for 24 hours. It was found that the GW salinity and depth, hence the size of the PV system, play a major role in determining which case is more economical. In particular, it was found that due to the dominating LCC of the RO plant, it is more economical to design the PV-RO plant to operate for 24 hours. In this case its LCOW was 7 to 36% lower than that of a plant operating only during daytime when BW is desalinated.

For a PV-RO plant operating 24 hours and with the typical GW composition found in Egypt, the LCOW ranged from approximately 0.7 USD/m^3 to 1.65 USD/m^3 when GW with salinity ranging from 2,000 to 10,000 mg/l is extracted and treated from most aquifers in Egypt. Higher LCOW ranging from approximately 1.3 to 2.2 USD/m^3 are however expected if the plant desalinates GW extracted from the Nubian aquifer in the Sinai Peninsula due to the high costs associated with GW extraction and well construction. In contrast, the lowest LCOW, i.e. 0.7 USD/m^3, is obtained when GW is extracted from the coastal aquifer along the north western Mediterranean coast and the delta area as the GW exists at shallow depths. The variation in solar resources between the northern coastal areas and the rest of Egypt was also found to have an insignificant effect on the LCOW of a PV-RO plant.

Furthermore, it was found that a PV driven RO plant operating for 24 hours could be described as cost competitive with a similar plant driven by a diesel generator if the current subsidies on diesel are removed. The LCOW of the former was approximately 7 to 16% higher than that of a DG-RO plant when brackish GW is desalinated and for the expected range of GW depths and solar irradiances in Egypt.

A sensitivity analysis also showed that the battery bank specific costs and the interest rate have a significant impact on the LCOW of the PV-RO plant. It was particularly found that a PV-RO plant operating for 24 hours becomes clearly more economical than a similar plant driven by a DG if the batter bank specific costs dropped from 200 to 100

USD/kWh. Moreover, any reduction in the interest rate will work in favour of a PV-RO plant but will still not result in making a PV-RO plant more economical.

It was also found that the SEC and the estimated LCOW range for extracting and desalinating BW using PV driven RO plants are lower than those of PV driven SW RO plants even without considering the additional energy and costs associated with conveying the treated SW to inland areas.

The feasibility of replacing standard PV modules with PVT collectors to drive the RO plant was also investigated. In particular, the potential reduction and increase in the RO plant energy consumption by heating the water and in the PV system electricity yield by cooling the PV cells, respectively, was explored. It was found that a net energy saving is only achieved using unglazed PVT collectors given the high optical losses of glazed collectors which for all locations in Egypt and at different feed water salinities outweighed the annual energy reduction achieved by heating the feed water going to the RO plant. However, only a modest increase in the annual electricity yield by cooling the PV cells and reduction in the RO plant annual energy requirements by heating the feed water, ranging from approximately 3.5% to less than 7% for both, was achieved using unglazed PVT collectors. It was particularly found that the low capacity factor of the PVT collectors and the variability of solar irradiance in addition to the operating temperature limitation of the RO membranes are the main limitations for the PVT collectors to have any economic advantage over standard PV modules when coupled with an RO plant regardless of the feed water salinity.

This thesis also explored the feasibility of using an MD process to enhance the RR of the RO plant. Due to the lack of commercially available MD process simulation tools, a mathematical model for a full scale spiral wound PGMD module was built. The mathematical model gave good agreement with experimental results available in the literature with a mean deviation of 0.3% and 3.35% from the experimental cooling channel exit temperatures and permeates flow rates, respectively. An important finding by building this model was that the commonly used Isostrain model tend to overestimate the MD membrane overall thermal conductivity resulting in high deviation in the MD flux from the experimental values particularly at higher feed water salinities.

This raises concerns on the accuracy of the models available in the literature which all used the Isostrain model.

It was then found that an enhancement in the RR is only feasible with additional pre-treatment steps such as chemical softening, clarification and media filtration which will increase the complexity and cost of the plant. Furthermore, even with such pre-treatment, it was found that the evaporation losses from the cooling tower have a significant impact on the maximum attainable RR from a hybrid RO/MD plant. In particular, it was found that with the PGMD module used in this study, such losses were the main RR limiting factor for a hybrid RO/MD plant where no more than 10% enhancement in the RR was possible with brackish GW even after assuming that the brine can be concentrated to 250 g/kg without scaling issues. Such evaporation losses were also found to limit the RR of the hybrid plant even with enhanced MD process configurations such as those using vacuum to enhance the flux, due to the large coolant flow rates required. Accordingly, it is concluded that higher RR's are only possible with high RR MD modules with low cooling requirements.

The economic analysis of the hybrid RO/MD plant also showed that the small enhancement in the RR by using a solar driven hybrid plant resulted in a 1.9 to 3.6 times increase in the LCOW over that of the RO only plant when brackish GW is desalinated and for the typical GW depths found in Egypt. It was particularly found that the low flux and the high SHC of the PGMD module in addition to its current high costs are the main contributors to the high LCOW of the hybrid plant.

It was therefore concluded that hybrid RO/MD plants are likely to be only feasible if a source of a waste heat is available from a renewable energy source such as a CPV or a CSP plant, the SHC of the process is reduced by 4 folds, and the MD module costs become similar to that of an RO module. In this case, the LCOW of the MD plant is reduced to values ranging from 10.4 to 11.7 USD/m^3 which resulted in a more reasonable percentage increase in the LCOW of the hybrid plant over that of the RO only plant ranging from 26 to 47% for the typical GW depths found in most of Egypt.

The main implication of this thesis is to provide evidence for decision makers in Egypt regarding the potential for developing brackish GW resources to start establishing decentralized communities with safe access to water and energy supplies which could assist in alleviating rural poverty levels. For this reason, a feasibility study of high RR PV-RO desalination plants to provide a sustainable access of water was carried out. With the results obtained which showed that a PV-RO plant is only slightly more expensive than a similar plant driven by DG's operating with unsubsidized diesel, the GOE can consider the application of such plants especially that the government is planning to gradually remove the subsidies on diesel. Using solar energy instead of fossil fuels is a necessity due to lack of fossil fuel resources in Egypt. Moreover, the estimated LCOW of the PV-RO plant, which also includes the costs associated with GW extraction, in addition to the brackish GW potential study carried out in this thesis, will certainly help with studies concerning the feasibility of establishing decentralized communities in Egypt. The study also gives important insight on the conditions at which a solar driven hybrid RO/MD plant will be worth using to further increase the RR of the RO plant. The results can particularly motivate other researchers and manufacturers to help improve the performance of the MD process as well as examining potential sources of renewable waste heat, such as that generated from a CSP or CPV plant, to run the process.

8.1 Original Contributions

In this thesis, brackish GW potential in Egypt was investigated. While there are other studies that discussed brackish GW availability in Egypt, the long term potential for brackish GW extraction was not considered in these studies. In particular, the previous studies only focused on reporting the GW properties such as salinity and depth while in this study the aquifer productivity and recharge potential were also included in the multi-criteria analysis used to determining the potential for brackish GW extraction in different areas in Egypt.

Furthermore, while there are numerous studies on the feasibility of PV driven RO plants in the literature, it was found that most of the designs were carried out in an ad-hoc manner where the RO modules are operating in non-optimal conditions which will compromise their lifetime and increase the risk of fouling. In addition, almost all of the reviewed plants were operating at low RR's which is not suitable for water scarce countries like Egypt and also resulted in a significant increase in the SEC. Moreover, the methodology for cost analysis in general and for those carried out for plants applied in Egypt were either not discussed or were based on simplified designs of the PV system. In this thesis the RO plants were designed to operate at high RR’s and within the recommended operating parameters of the manufacturer which guarantees realistic energy consumption values and that the RO modules will operate within their typical reported lifetime. The PV system was also properly designed using hourly weather data using PVSYST which also ensured a more accurate battery bank sizing.

This thesis also explored the feasibility of replacing standard PV modules with PVT collectors which, to the author’s knowledge, was not studied before. It was concluded that it is unlikely that PVT collectors will be able to make a significant contribution to solar driven desalination.

Moreover, in this thesis a mathematical model for a full scale commercial PGMD module was built. While this module has been previously modelled in the literature, the model assumed a simplified flat geometry for the module ignoring the complex heat interactions between its different layers. Conversely, in this thesis, the model accounted for the actual spiral wound geometry which, to the author’s knowledge, has not been carried out before.

Finally, the feasibility of a solar driven hybrid RO/MD was investigated with a full scale commercial MD module. Other studies in the literature on hybrid RO/MD plants were found to be unreliable and also based their analysis on lab scale MD modules which may have high fluxes that cannot be achieved with full scale modules under the same operating conditions. For this reason, the study carried out in this thesis gives a more realistic assessment of the feasibility of hybrid RO/MD plants. The study also considered the effect of the evaporation losses in the cooling tower on the maximum attainable RR of a hybrid plant which was not considered in any of the previous studies, and was found to be a major limiting factor of the use of an MD process to enhance the RR of an RO plant in inland areas. The performance of a hybrid plant driven by solar energy was also investigated which, to the author’s knowledge, has not been carried out before.

8.2 Future Work Recommendations

While reviewing the literature on the availability of brackish GW in Egypt, it was observed that there are very few studies on estimating the amount of GW that could be economically and sustainably extracted from different aquifers in Egypt in different areas. Such data was only found for fresh GW extracted from the Nubian aquifer in the New Valley Oases and East Oweinat area and is based on old studies carried out in the 1980's. Moreover, while they cover a large area of Egypt, the fissured carbonate and Al-Moghra aquifers were particularly found to be not well studied in terms of their GW reserves and the amount of GW recharge from rainfall and other aquifers. Such studies on the aquifer's GW reserves and the amount that could be economically extracted are essential to determine the feasibility of establishing decentralized communities or any economic activity based on GW extraction.

It was also discussed that the RO plant energy consumption has a significant impact on determining whether it is more economical to run design the PV-RO plant to operate during the daytime only or for 24 hours. This result is very important in the context of the different studies concerning battery-less PV-RO plants where, to the author's knowledge, none of them discussed the effect of operating the plant only during the day on the LCOW. It is therefore worth investigating whether the cost saving by not using a battery bank could offset the LCOW increase caused by operating the RO plant at low capacity factor especially with BW applications.

In the mathematical model of the full scale PGMD module, the heat transfer coefficients in each channel were determined by varying their values until the best fit to the experimental data is achieved. The values of the heat transfer coefficient were found to be 40% that estimated by existing correlations for spacer filled channels. For this reason, it is recommended to verify the estimated values through independent experiments such as those carried out by Phattaranawik et al. (2003). In their study, the membrane in a DCMD module was replaced by an Aluminium foil to eliminate the effect of mass transfer on heat transfer and therefore the module was basically treated as a heat exchanger. Such experiment would be however more challenging with a PGMD due to the existence of the additional permeate channel. It is also recommended to conduct gas permeation tests on the PGMD module to verify the MTC value estimated in this study. This is because the MTC was estimated using the DGM model based equations that incorporate the membrane structural parameters whose accuracy was criticized in many MD modelling studies and resulted in a high tortuosity value of 3 which could be compensating for other membrane parameters. It will be also interesting to modify the model to properly calculate the heat losses from the walls of the MD module and by the removed permeate flow especially which could be significant if the MD module is operating in a cold climate. Furthermore, it will be interesting to compare the results of the model built in this study which accounted for the actual spiral geometry of the PGMD module with the model where a simplified flat geometry was assumed.

It was also discussed that there are currently no models available to estimate the thermo-physical properties of general multi-component water solutions at high salinities. Moreover, using the existing models will require some modifications using available experimental or numerical modelling data which are incomplete and the data from the models are therefore expected to have significant uncertainties (Pawlowicz and Feistel, 2012). For this reason, in this thesis existing correlations developed for SW was used to estimate the thermo-physical of the brine desalinated by the MD process although its composition is different than that of SW. Therefore, it is recommended to test the accuracy of using existing models developed for SW with high salinity water that has different chemical composition than that of SW.

Further research is also needed to develop more thermally efficient full scale commercial MD modules with enhanced RR’s that do not require large coolant flow rates. As concluded in this thesis, this kind of modules will be more suitable to be coupled with an RO plant to enhance the RR particularly in inland areas where cooling towers are needed.

Finally, CPV is a very promising technology with generally lower LCOW then CSP’s and are also expected to be competitive with standards non-concentrating PV in the near future as was shown in this study. Therefore, it is recommended to investigate the dual use of CPV to generate both heat and electricity similar to PVT modules. The excess heat of the CPV is recommended to drive a low temperature thermal desalination process such as MD. It was shown that such measure will significantly lower the

LCOW of the hybrid plant. This investigation is particularly recommended to be carried out with CPV technologies using Fresnel lenses to refract sun radiation where it is likely to be less challenging to extract the heat from the panels compared to configurations using parabolic dishes.

9. Bibliography

AB KADIR, M. Z. A., RAFEEU, Y. & ADAM, N. M. 2010 Prospective scenarios for the full solar energy development in Malaysia, *Renewable and Sustainable Energy Reviews* 14**,** 3023-3031.

ABD-ALLAH, A. 2012 'Urgent statement on the crisis of drinking water in Matruh', *AlMasryAlYoum*, 15 June, accessed 14 November 2012, http://today.almasryalyoum.com/article2.aspx?ArticleID=342733.

ABD-ALLAH, A. 2015 '40% Increase in Drinking Water Prices in Matruh', *Journal Masr*, 15 January 2015, accessed 19 February 2015, http://www.misrjournal.com/40-%D8%B2%D9%8A%D8%A7%D8%AF%D8%A9-%D9%81%D9%8A-%D8%A3%D8%B3%D8%B9%D8%A7%D8%B1-%D9%85%D9%8A%D8%A7%D9%87-%D8%A7%D9%84%D8%B4%D8%B1%D8%A8-%D8%A8%D9%85%D8%B7%D8%B1%D9%88%D8%AD/.

ABD-EL-RAHMAN, H. 2001 Evaluation of Groundwater Resources in Lower Cretaceous Aquifer System in Sinai, *Water Resources Management* 15**,** 187-202.

ABD-EL-SAMIE, S. & SADEK, M. 2001 Groundwater recharge and flow in the Lower Cretaceous Nubian Sandstone aquifer in the Sinai Peninsula, using isotopic techniques and hydrochemistry, *Hydrogeology Journal* 9**,** 378-389.

ABD EL SAMIE, S. & SADEK, M. 2001 Groundwater recharge and flow in the Lower Cretaceous Nubian Sandstone aquifer in the Sinai Peninsula, using isotopic techniques and hydrochemistry, *Hydrogeology Journal* 9**,** 378-389.

ABDALLA, F. A., AHMED, A. A. & OMER, A. A. 2009 Degradation of groundwater quality of Quaternary aquifer at Qena, Egypt, *Journal of Environmental Studies* 1**,** 19-32.

ABDALLAH, A. 2012 El Salam Canal: failed development and tragic planning, EGYPT VOTES.ORG, accessed 8 March 2012, www.egyptvotes.org/en/politics/item/443-el-salam-canal-failed-development-and-tragic-planning.html.

ABDALLAH, G. 2006 Management of Groundwater Aquifers along the Mediterranean Sea in Sinai Peninsula, *The 2nd International Conference on Water Resources and Arid Environment* King Saud University Riyadh.

ABDEL-AZIM, R. & ALLAM, M. N. 2004 Agricultural Drainage Water Reuse in Egypt: Strategic Issues and Mitigation Measures, The International Centre for Advanced Mediterranean Agronomic Studies (CIHEAM), accessed 21 August 2012, http://ressources.ciheam.org/om/pdf/b53/00800755.pdf.

ABDEL-KADER, F. H. & YACOUB, R. K. 2005, Land resources assessment of landmine-affected areas, northwest of Egypt, *SUITMA Symposium*, Cairo.

ABDEL-LAH, A. K. & SHAMRUKH, M. 2001 Impact of Septic System on Ground Water Quality in a Nile Valley Village, Egypt, *Sixth International Water Technology Conference*, Alexandria, Egypt.

ABDEL-LATIF, A. & EL-KASHOUTY, M. 2010 Groundwater Investigation in Awlad Salameh, Southern Sohag, Upper Egypt, *Earth Sciences* 14**,** 63-75.

ABDEL-MOHSEN, A. 2012 'Army: Egypt clears 23 million landmines', *Egypt Independent*, 19 February, accessed 18 August 2012, http://www.egyptindependent.com/news/army-egypt-clears-23-million-landmines.

ABDEL-MONEIM, A. A. 2005 Overview of the geomorphological and hydrogeological characteristics of the Eastern Desert of Egypt, *Hydrogeology Journal* 13**,** 416-425.

ABDEL-REHIM, Z. S. & LASHEEN, A. 2007 Experimental and theoretical study of a solar desalination system located in Cairo, Egypt, *Desalination* 217**,** 52-64.

ABDEL-SHAFY, H. & ALY, R. 2007, 'Wastewater Management in Egypt, Wastewater Reuse–Risk Assessment, Decision-Making and Environmental Security', Springer Netherlands,

ABDEL-SHAFY, H. I., EL-GAMAL, I. M. & ABDEL-HAMID, M. M. 1992 Studies of Characteristics of Water, Soil and Plants of the Siwa Oasis, Egypt, *International Journal of Environmental Studies* 40**,** 299-309.

ABDEL-WAHAAB, R. 2012 Wastewater Reuse in Egypt: Opportunities and Challenges, *The International Trade Fair for Environment, Waste Water and Waste Disposal*, Munich, Germany.

ABDELRASSOUL, R. A. 1998 Potential for economic solar desalination in the Middle East, *Renewable Energy* 14**,** 345-349.

ABDIN, A. E. & GAAFAR, I. 2009, Rational water use in Egypt, CIHEAM,

ABO ALABASS, B. 2012 'Egypt's butane crisis still cooking', *ahramonline*, 16 March 2012, accessed 29 August 2012, http://english.ahram.org.eg/News/36786.aspx.

ABU-ARABI, M. 2007, 'Status and prospects for solar desalination in the MENA region', *Solar Desalination for the 21st Century*, Springer Netherlands,

ABU ZEID, M. 1992 Water resources assessment for Egypt, *International Journal of Water Resources Development* 8**,** 76-86.

AHMAD, G. E. & SCHMID, J. 2002 Feasibility study of brackish water desalination in the Egyptian deserts and rural regions using PV systems, *Energy Conversion and Management* 43**,** 2641-2649.

AHMED, A. & ALI, M. 2011 Hydrochemical evolution and variation of groundwater and its environmental impact at Sohag, Egypt, *Arabian Journal of Geosciences* 4**,** 339-352.

AHRAM ONLINE 2013 'Egypt sets LE1200 as minimum wage for government workers', 18 September, accessed 18 December 2013, http://english.ahram.org.eg/News/81942.aspx.

AHRAM ONLINE 2014 'First price hike on water bills for Egyptian households in nearly a decade', *Ahram Online*, 1 May 2014, accessed 19 February 2015, http://english.ahram.org.eg/News/100283.aspx.

AL-HALLAJ, S., FARID, M. M. & RAHMAN TAMIMI, A. 1998 Solar desalination with a humidification-dehumidification cycle: performance of the unit, *Desalination* 120**,** 273-280.

AL-HALLAJ, S., PAREKH, S., FARID, M. M. & SELMAN, J. R. 2006 Solar desalination with humidification–dehumidification cycle: Review of economics, *Desalination* 195**,** 169-186.

AL-KARAGHOULI, A. & KAZMERSKI, L. L. 2013 Energy consumption and water production cost of conventional and renewable-energy-powered desalination processes, *Renewable and Sustainable Energy Reviews* 24**,** 343-356.

AL-KARAGHOULI, A., RENNE, D. & KAZMERSKI, L. L. 2010 Technical and economic assessment of photovoltaic-driven desalination systems, *Renewable Energy* 35**,** 323-328.

AL-SAYED, M. A., MAHMOUD, M. K., HAMDY, A., KHALED, Z. M. & ABBAS, M. A. 2012 Reverse Osmosis Pretreatment: Removal of Iron in Groundwater Desalination Plant in Shupramant-Giza - A Case Study, *Curr World Environ* 7**,** 23-32.

AL SULEIMANI, Z. & NAIR, V. R. 2000 Desalination by solar-powered reverse osmosis in a remote area of the Sultanate of Oman, *Applied Energy* 65**,** 367-380.

ALAWAJI, S., SMIAI, M. S., RAFIQUE, S. & STAFFORD, B. 1995 PV-powered water pumping and desalination plant for remote areas in Saudi Arabia, *Applied Energy* 52**,** 283-289.

ALI, M. T., FATH, H. E. S. & ARMSTRONG, P. R. 2011 A comprehensive techno-economical review of indirect solar desalination, *Renewable and Sustainable Energy Reviews* 15**,** 4187-4199.

ALLAM, A. R., SAAF, E.-J. & DAWOUD, M. A. 2003 Desalination of brackish groundwater in Egypt, *Desalination* 152**,** 19-26.

ALLAM, M. N. & ALLAM, G. I. 2007 Water Resources In Egypt: Future Challenges and Opportunities, *Water International* 32**,** 205-218.

ALLAM, M. N., ELASSIOUTI, I. M. & RILEY, P. 1994 Irrigation Water Cost in Egypt, *Water International* 19**,** 145-151.

AMIN, S. 2010 'Egypt's farmers desperate for clean water', *CNN*, 10 November, accessed 23 November 2012, http://edition.cnn.com/2010/WORLD/africa/11/09/egypt.water.shortage/index.html.

AMMAR, A. I. 2010 Estimating the Groundwater Storage from the Electrical Resistivity Measurements in Wadi El-Natrun Area, Western Desert, Egypt, *Journal of American Science* 6**,** 492-502

AMONIX 2012a, Coming Soon : The Amonix 8700, accessed 4 November 2013, http://amonix.com/content/cpv-technology.

AMONIX 2012b CPV Technology: Concentrated Solar Power, AMONIX, accessed 4 November 2013, http://amonix.com/content/concentrator-optics.

AQUAVER 2015 Aquaver Datasheet, Aquaver, accessed 1 February 2015, http://www.aquaver.com/wp-content/themes/aquaver/assets/othermedia/Aquaver_MDS_Datasheet.pdf.

ARNOUS, M. O. & HASSAN, M. A. A. 2006 Image Processing and Land Information System for Soil Assessment of El-Maghara Area, North Sinai, Egypt, *The 2nd International Conference on Water Resources & Arid Environment*, Riyadh, Saudi Arabia.

ARUN, P., BANERJEE, R. & BANDYOPADHYAY, S. 2008 Optimum sizing of battery-integrated diesel generator for remote electrification through design-space approach, *Energy* 33**,** 1155-1168.

ASSIMACOPOULOS, D. 2001 Water water everywhere... : Desalination powered by renewable energy sources, *Refocus* 2**,** 38-40.

ATTA, S. A., SHARAKY, A. M., EL HASSANEIN, A. S. & KHALLAF, K. 2005 Salinization of the Groundwater in the Coastal Shallow Aquifer, Northwestern Nile Delta, Egypt, *First International Conference on the Geology of Tethys*, Cairo, Egypt.

AWAD, M. A., EL ARABI, N. E. & HAMZA, M. S. 1997 Use of Solute Chemistry and Isotopes to Identify Sources of Ground-Water Recharge in the Nile Aquifer System, Upper Egypt, *Ground Water* 35**,** 223-228.

AWAD, M. A., HAMZA, M. S., ATWA, S. M. & SALLOUMA, M. K. 1996 Isotopic and hydrogeochemical evaluation of groundwater at Qusier-Safaga area, eastern desert, Egypt, *Environmental Geochemistry and Health* 18**,** 47-54.

AWWA RESEARCH FOUNDATION STAFF, LYONNAISE DES EAUX-DUMEZ & WATER RESEARCH COMMISSION OF SOUTH AFRICA 1996 *Water treatment membrane processes,* McGraw-Hill New York.

AYBAR, H. 2007, 'A REVIEW OF DESALINATION BY SOLAR STILL', *Solar Desalination for the 21st Century,* Springer Netherlands,

AYERS, R. S. & WESTCOT, D. W. 1994 *Water Quality for Agriculture*, e-book, accessed 12 July 2012, http://www.fao.org/docrep/003/T0234E/T0234E00.htm.

BACHA, H., MAALEJ, A. Y. & DHIA, H. B. 2007, 'A METHODOLOGY TO PREDICT OPERATION OF A SOLAR POWERED DESALINATION UNIT', *Solar Desalination for the 21st Century,* Springer Netherlands,

BAKKER, M., ZONDAG, H. A., ELSWIJK, M. J., STROOTMAN, K. J. & JONG, M. J. M. 2005 Performance and costs of a roof-sized PV/thermal array combined with a ground coupled heat pump, *Solar Energy* 78**,** 331-339.

BAMBROOK, S. 2011, 'Investigation of Photovoltaic/Thermal Air Systems to Create a Zero Energy House in Sydney', Doctor of Philosophy, University of New South Wales.

BANAT, F. & JWAIED, N. 2008 Economic evaluation of desalination by small-scale autonomous solar-powered membrane distillation units, *Desalination* 220**,** 566-573.

BANAT, F. & QIBLAWEY, H. 2007, 'Membrane Desalination Driven by Solar Energy', *Solar Desalination for the 21st Century*, Springer Netherlands,

BANAT, F. A. & SIMANDL, J. 1998 Desalination by Membrane Distillation: A Parametric Study, *Separation Science and Technology* 33**,** 201-226.

BCC RESEARCH 2009, Major Reverse Osmosis System Components for Water Treatment: The Global Market, BCC Research,

BECCALI, M., SORCE, M. & GALLETTO, J. 2007, 'The potential of renewable energies in sicily for water desalination applications', *Solar Desalination for the 21st Century*, Springer Netherlands,

BELESSIOTIS, V. & DELYANNIS, E. 2001 Water shortage and renewable energies (RE) desalination — possible technological applications, *Desalination* 139**,** 133-138.

BHUIYAN, M. M. H., ASGAR, M. A., MAZUMDER, R. K. & HUSSAIN, M. 2000 Economic evaluation of a stand-alone residential photovoltaic power system in Bangladesh, *Renewable Energy* 21**,** 403-410.

BILBAO, J. & SPROUL, A. B. 2012a, Analysis of Flat Plate Photovoltaic-Thermal (PVT) Models, *World Renewable Energy Forum (WREF) Including World Renewable Energy Congress XII and Colorado Renewable Energy Society (CRES) Annual Conference*, Denver, Colorado, USA.

BILBAO, J. & SPROUL, A. B. 2012b, 'Photovoltaic thermal water Systems - modelling and design considerations for residential applications in different climates and demand conditions', Doctor of Philosiphy, University of New South Wales.

BORSANI, R. & REBAGLIATI, S. 2005 Fundamentals and costing of MSF desalination plants and comparison with other technologies, *Desalination* 182**,** 29-37.

BRADLEY, M. 2012 'Egypt's Brewing Crisis: Subsidies', *The Wall Street Journal*, 27 August, accessed 29 November 2012, http://online.wsj.com/article/SB1000142405297020405980457722898428591O816.html.

BRANKER, K., PATHAK, M. J. M. & PEARCE, J. M. 2011 A review of solar photovoltaic levelized cost of electricity, *Renewable and Sustainable Energy Reviews* 15**,** 4470-4482.

BROUWER, C., HOEVENAARS, J. P. M., VAN BOSCH, B. E., HATCHO, N. & HEIBLOEM, M. 1992 Irrigation Water Management: Training Manual No. 6 - Scheme Irrigation Water Needs and Supply, FAO, accessed 27 November 2013, http://www.fao.org/docrep/u5835e/u5835e00.htm#Contents.

BROUWER, C., PRINS, K. & HEIBLOEM, M. 1989 Irrigation Water Management: Irrigation Scheduling, FAO, accessed 12 March 2011, http://www.fao.org/docrep/t7202e/t7202e00.htm.

BROUWER, C., PRINS, K., KAY, M. & HEIBLOEM, M. 1988 *Irrigation Water Managment: irrigation Methods*, e-book, accessed 13 July 2012, www.fao.org/docrep/s8684E/s8684E00.htm.

BURGOYNE, A. & VAHDATI, M. M. 2000 Direct Contact Membrane Distillation, *Separation Science and Technology* 35**,** 1257 - 1284.

BUROS, O. K. 2000 *The ABCs of Desalting,* International Desalination Association.

CARTER, J. M., DRISCOLL, D. G. & WILLIAMSON, J. E. 2005, Atlas of Water Resources in the Black Hills Area, South Dakota: Definition of Terms, U.S. Geological Survey, accessed 20 June 2012, http://pubs.usgs.gov/ha/ha747/pdf/definition.pdf.

CATH, T. Y., CHILDRESS, A. E. & ELIMELECH, M. 2006 Forward osmosis: Principles, applications, and recent developments, *Journal of Membrane Science* 281**,** 70-87.

ÇENGEL, A. Y. 2003 *Heat Transfer: A Practical Approach,* Jones, E.A.

ÇENGEL, Y. & CIMBALA, J. 2006 *Fluid Mechanics: Fundamentals and Applications,* McGraw-Hill.

CENTRAL AGENCY FOR PUBLIC MOBILIZATION & STATISTICS 2010 Self-Sufficiency Percentage For Some Alimentary Commodities, CAPMAS, accessed 23 February 2011, http://www.capmas.gov.eg/pdf/egypt/agre/40.pdf.

CENTRAL AGENCY FOR PUBLIC MOBILIZATION & STATISTICS 2011 Indicators of poverty, according to data from income and expenditure and consumption, CAPMAS, accessed 28 August 2012, http://capmas.gov.eg/pdf/studies/pdf/enf1.pdf.

CENTRAL AGENCY FOR PUBLIC MOBILIZATION & STATISTICS 2013, Arab Republic of Egypt: Central Agency for Public Mobilization & Statistics, CAPMAS, accessed 11 December 2013, http://capmas.gov.eg/?lang=2.

CERNEAUX, S., STRUŻYŃSKA, I., KUJAWSKI, W. M., PERSIN, M. & LARBOT, A. 2009 Comparison of various membrane distillation methods for desalination using hydrophobic ceramic membranes, *Journal of Membrane Science* 337**,** 55-60.

CHANG, H., WANG, G.-B., CHEN, Y.-H., LI, C.-C. & CHANG, C.-L. 2010 Modeling and optimization of a solar driven membrane distillation desalination system, *Renewable Energy* 35**,** 2714-2722.

CHENG, L., WU, P. & CHEN, J. 2008 Modeling and optimization of hollow fiber DCMD module for desalination, *Journal of Membrane Science* 318**,** 154-166.

CHOI, J.-S., CHO, J.-S., LEE, S., HWANG, T.-M., OH, H., YANG, D. R. & KIM, J. H. 2010 Understanding boron rejection by reverse osmosis membranes, *Desalination and Water Treatment* 15**,** 129-133.

CHUNG, T.-S., ZHANG, S., WANG, K. Y., SU, J. & LING, M. M. 2012 Forward osmosis processes: Yesterday, today and tomorrow, *Desalination* 287**,** 78-81.

CIPOLLINA, A., DI MICELI, A., KOSCHIKOWSKI, J., MICALE, G. & RIZZUTI, L. 2009 CFD simulation of a membrane distillation module channel, *Desalination and Water Treatment* 6**,** 177-183.

CIPOLLINA, A., DI SPARTI, M. G., TAMBURINI, A. & MICALE, G. 2012 Development of a Membrane Distillation module for solar energy seawater desalination, *Chemical Engineering Research and Design* 90**,** 2101-2121.

COLEMAN, I. 2012 Reforming Egypt's Untenable Subsidies Council on Foreign Relations (CFR), accessed 27 August 2012, http://www.cfr.org/egypt/reforming-egypts-untenable-subsidies/p27885.

COLTER, A. & MAHLER, R. L. 2006 Iron in Drinking Water, University of Idaho, accessed 24 July 2012, http://www.cals.uidaho.edu/edComm/pdf/pnw/pnw589.pdf.

COMMITTEE EL-042 2010, AS/NZS 4509.2 Stand-alone power systems Part 2: System design, SAI Global Limited,

COTRUVO, J., VOUTCHKOV, N., FAWELL, J., PAYMENT, P., CUNLIFFE, D. & LATTEMANN, S. 2010 *Desalination Technology: Health and Environmental Impacts*, IWA.

CRISCUOLI, A. & DRIOLI, E. 1999 Energetic and exergetic analysis of an integrated membrane desalination system, *Desalination* 124**,** 243-249.

CRITTENDEN, J. C., TRUSSELL, R. R., HAND, D. W., HOWE, K. J. & TCHOBANOGLOUS, G. 2012a, 'Chemical Oxidation and Reduction', *MWH's Water Treatment : Principles and Design*, Wiley,

CRITTENDEN, J. C., TRUSSELL, R. R., HAND, D. W., HOWE, K. J. & TCHOBANOGLOUS, G. 2012b, 'Gravity Separation', *MWH's Water Treatment : Principles and Design*, Wiley,

CRITTENDEN, J. C., TRUSSELL, R. R., HAND, D. W., HOWE, K. J. & TCHOBANOGLOUS, G. 2012c, 'Membrane Filtration', *MWH's Water Treatment : Principles and Design*, Wiley,

CRITTENDEN, J. C., TRUSSELL, R. R., HAND, D. W., HOWE, K. J. & TCHOBANOGLOUS, G. 2012d, 'Removal of Selected Constituents', *MWH's Water Treatment : Principles and Design*, Wiley,

CRITTENDEN, J. C., TRUSSELL, R. R., HAND, D. W., HOWE, K. J. & TCHOBANOGLOUS, G. 2012e, 'Reverse Osmosis', *MWH's Water Treatment : Principles and Design*, Wiley,

CRITTENDEN, J. C., TRUSSELL, R. R., HAND, D. W., HOWE, K. J. & TCHOBANOGLOUS, G. 2012f, 'Water Quality Management Strategies', *MWH's Water Treatment : Principles and Design*, Wiley,

CRUICKSHANK, C. A. & HARRISON, S. J. 2010 Heat loss characteristics for a typical solar domestic hot water storage, *Energy and Buildings* 42**,** 1703-1710.

CURCIO, E., CRISCUOLI, A. & DRIOLI, E. 2001 Membrane crystallizers, *Industrial and Engineering Chemistry Research* 40**,** 2679-2684.

CURCIO, E. & DRIOLI, E. 2005 Membrane Distillation and Related Operations—A Review, *Separation & Purification Reviews* 34**,** 35-86.

DA COSTA, A. R., FANE, A. G. & WILEY, D. E. 1994 Spacer characterization and pressure drop modelling in spacer-filled channels for ultrafiltration, *Journal of Membrane Science* 87**,** 79-98.

DANFOSS 2014 Data sheet APP 21-43, Danfoss, accessed 1 April 2014, http://www.danfoss.com/NR/rdonlyres/5BC2A79A-6902-4672-A6BF-9572B3A47E00/0/521B0852_DataSheetAPP2143_UK.pdf.

DARWISH, M. A. & AL-NAJEM, N. M. 1987 Energy consumptions and costs of different desalting systems, *Desalination* 64**,** 83-96.

DAVISON, W. 2013 Egypt, Ethiopia and Sudan Mull New Probe Nile Dam Impact, Bloomberg, accessed 28 November 2013, http://www.bloomberg.com/news/2013-10-21/egypt-ethiopia-and-sudan-mull-new-probe-nile-dam-impact.html.

DAWOUD, M., DARWISH, M. & EL-KADY, M. 2005 GIS-Based Groundwater Management Model for Western Nile Delta, *Water Resources Management* 19**,** 585-604.

DAWOUD, M. A. 2004 Design of National Groundwater Quality Monitoring Network in Egypt, *Environmental Monitoring and Assessment* 96**,** 99-118.

DE CARVALHO, P. C. M., RIFFEL, D. B., FREIRE, C. & MONTENEGRO, F. F. D. 2004 The Brazilian experience with a photovoltaic powered reverse osmosis plant, *Progress in Photovoltaics: Research and Applications* 12**,** 373-385.

DE MUNARI, A., CAPAO, D. P. S., RICHARDS, B. S. & SCHAFER, A. I. 2009 Application of solar-powered desalination in a remote town in South Australia, *Desalination* 248**,** 72-82.

DESALINATION.COM 2008, Low energy desal study funded, Desalination.com, accessed 13 October 2013, http://www.desalination.com/wdr/44/24/low-energy-desal-study-funded.

DING, Z., MA, R. & FANE, A. G. 2003 A new model for mass transfer in direct contact membrane distillation, *Desalination* 151**,** 217-227.

DOTREMONT, C., KREGERSMAN, B., SIH, R., LAI, K. C., KOH, K. & SEAH, H. 2010 Seawater desalination with memstill technology - a sustainable solution for the industry, *Water Practice & Technology* 5.

DOW CHEMICAL COMPANY 2011, FILMTEC Membranes - Concentration of Salt Solutions,, DOW Chemical Company, accessed 31 July 2013, http://dowwater.custhelp.com/app/answers/detail/a_id/677/kw/pressure.

DOW CHEMICAL COMPANY 2012 Flow Factor for RO System Design, DOW Chemical Company, accessed 15 February 2014, http://msdssearch.dow.com/PublishedLiteratureDOWCOM/dh_057a/0901b8038057a939.pdf?filepath=liquidseps/pdfs/noreg/609-02208.pdf&fromPage=GetDoc.

DOW CHEMICAL COMPANY 2013a, Electrodeionization, DOW Chemical Company, accessed 24 October 2013, http://www.dowwaterandprocess.com/en/industries-and-applications/industrial_water/boiler_feed_and_process_water/polishing/electrodeionization.

DOW CHEMICAL COMPANY 2013b FILMTEC Membranes: Water Chemistry and Pretreatment, DOW Chemical Company, accessed 1 May 2012, http://msdssearch.dow.com/PublishedLiteratureDOWCOM/dh_003b/0901b8038003b48d.pdf?filepath=/609-02009.pdf&fromPage=GetDoc.

DOW CHEMICAL COMPANY 2013c FILMTEC™ Membranes System Design: Membrane System Design Guidelines for Commercial Elements, DOW Chemical Company, accessed 19 October 2013, http://msdssearch.dow.com/PublishedLiteratureDOWCOM/dh_08ca/0901b803808caf76.pdf?filepath=liquidseps/pdfs/noreg/609-02054.pdf&fromPage=GetDoc.

DOW CHEMICAL COMPANY 2013d Membrane System Design Guidelines for 8-Inch FILMTEC™ Elements, DOW Chemical Company, accessed 28 December 2013, http://msdssearch.dow.com/PublishedLiteratureDOWCOM/dh_084f/0901b8038084f998.pdf?filepath=liquidseps/pdfs/noreg/609-21010.pdf&fromPage=GetDoc.

DOW CHEMICAL COMPANY 2013e, Reverse Osmosis System Analysis (ROSA), DOW Chemical Company, http://www.dowwaterandprocess.com/support_training/design_tools/rosa.htm.

DOW CHEMICAL COMPANY 2013f, Steps to Design an RO / NF Membrane System, DOW Chemical Company, accessed 5 August 2013, http://www.dowwaterandprocess.com/en/resources/steps_to_design_an_ro_nf_membrane_system.

DOW CHEMICAL COMPANY 2013g Water Chemistry and Pretreatment: Scale Control, DOW Chemical Company, accessed 31 July 2013, http://msdssearch.dow.com/PublishedLiteratureDOWCOM/dh_01da/0901b803801da36c.pdf?filepath=liquidseps/pdfs/noreg/609-02013.pdf&fromPage=GetDoc.

DOW CHEMICAL COMPANY 2014a FILMTEC™ Membranes: Water Chemistry and Pretreatment: Biological Fouling Prevention, DOW Chemical Company, accessed 24 January 2014, http://msdssearch.dow.com/PublishedLiteratureDOWCOM/dh_0039/0901b80380039060.pdf?filepath=liquidseps/pdfs/noreg/609-02034.pdf&fromPage=GetDoc.

DOW CHEMICAL COMPANY 2014b Water Chemistry and Pretreatment: Barium Sulphate Scale Prevention, DOW Chemical Company, accessed 4 February 2014, http://msdssearch.dow.com/PublishedLiteratureDOWCOM/dh_003e/0901b8038003e65d.pdf?filepath=liquidseps/pdfs/noreg/609-02019.pdf&fromPage=GetDoc.

DOW CHEMICAL COMPANY 2014c Water Chemistry and Pretreatment: Colloidal and Particulate Fouling Prevention, DOW Chemical Company, accessed 25 March 2014, http://msdssearch.dow.com/PublishedLiteratureDOWCOM/dh_003c/0901b8038003c077.pdf?filepath=liquidseps/pdfs/noreg/609-02030.pdf&fromPage=GetDoc.

DOW CHEMICAL COMPANY 2014d Water Chemistry and Pretreatment: Guidelines for Feedwater Quality, DOW Chemical Company, accessed 22 March 2014, http://msdssearch.dow.com/PublishedLiteratureDOWCOM/dh_0043/0901b803800435ac.pdf?filepath=liquidseps/pdfs/noreg/609-02043.pdf&fromPage=GetDoc.

DRIOLI, E., CRISCUOLI, A. & CURCIO, E. 2002 Integrated membrane operations for seawater desalination, *Desalination* 147**,** 77-81.

DRIOLI, E., CURCIO, E., DI PROFIO, G., MACEDONIO, F. & CRISCUOLI, A. 2006 Integrating Membrane Contactors Technology and Pressure-Driven Membrane Operations for Seawater Desalination: Energy, Exergy and Costs Analysis, *Chemical Engineering Research and Design* 84**,** 209-220.

DRIOLI, E., LAGANÀ, F., CRISCUOLI, A. & BARBIERI, G. 1999 Integrated membrane operations in desalination processes, *Desalination* 122**,** 141-145.

DUFFIE, J. A. & BECKMAN, W. A. 2006 *Solar Engineering of Thermal Processes*, John Wiley & Sons Inc.

DUFO-LÓPEZ, R. & BERNAL-AGUSTÍN, J. L. 2005 Design and control strategies of PV-Diesel systems using genetic algorithms, *Solar Energy* 79**,** 33-46.

EBRAHEEM, A. M., SENOSY, M. M. & DAHAB, K. A. 1997 Geoelectrical and Hydrogeochemical Studies for Delineating Ground-Water Contamination Due to Salt-Water Intrusion in the Northern Part of the Nile Delta, Egypt, *Ground Water* 35**,** 216-222.

EGYPT STATE INFORMATION SERVICE 2011 Landmines in Egypt, Egypt State Information Service, accessed 8 December 2011, http://www.sis.gov.eg/En/LastPage.aspx?Category_ID=61.

EGYPT STATE INFORMATION SERVICE n.d. Water resources, Egypt State Information Service, accessed 15 August 2012, http://www.sis.gov.eg/En/Story.aspx?sid=177.

EI-NAGGAR, H. M. 2010 Environmental Engineering Interventions To Control The Expansion Of Salty Lakes And Marshes In Siwa Oasis, *Journal of The Egyptian Public Health Association* 85.

EL-BEHARY, H. 2012 'Continuous blackouts hit Egypt metal industries hard', *Ahram Online* 23 August 2012, accessed 27 August 2012, http://english.ahram.org.eg/News/51009.aspx.

EL-BOURAWI, M. S., DING, Z., MA, R. & KHAYET, M. 2006 A framework for better understanding membrane distillation separation process, *Journal of Membrane Science* 285**,** 4-29.

EL-DESSOUKY, H. T. & ETTOUNEY, H. M. 2002, 'Chapter 10 - Economic Analysis of Desalination Processes', *Fundamentals of Salt Water Desalination*, Elsevier Science B.V., Amsterdam.

EL-FIKY, A. A. 2010 Hydrogeochemical Characteristics and Evolution of Groundwater at the Ras Sudr-Abu Zenima Area, Southwest Sinai, Egypt *Earth Sciences* 21**,** 79 -109

EL-GAMMAL, S. & EL-GAMMAL, A. 2010 Hazard impact and genetic development of sand dunes west of Samalut, Egypt, *The Egyptian Journal of Remote Sensing and Space Science* 13**,** 137-151.

EL-KADY, M. & EL-SHIBINI, F. 2001 Desalination in Egypt and the future application in supplementary irrigation, *Desalination* 136**,** 63-72.

EL-KASHOUTY, M. & EL-SABBAGH, A. 2011 Distribution and immobilization of heavy metals in Pliocene aquifer sediments in Wadi El Natrun depression, Western Desert, *Arabian Journal of Geosciences* 4**,** 1019-1039.

EL-SADEK, A. 2010 Water desalination: An imperative measure for water security in Egypt, *Desalination* 250**,** 876-884.

EL-SHERIF, M. 1997, Egypt, FAO, http://www.fao.org/docrep/v9978e/v9978e0e.htm#egypt.

EL ALFY, M. 2012 Integrated geostatistics and GIS techniques for assessing groundwater contamination in Al Arish area, Sinai, Egypt, *Arabian Journal of Geosciences* 5**,** 197-215.

EL SAMANOUDI, M. A., EBID, G. S., ROFAIL, N. N., ISMAIL, Y. L. & HAWASH, S. A. F. 2011 Assessment of Groundwater Resources in North Eastern Sinai Peninsula Constrained By Mathematical Modeling Techniques, *Fifteenth International Water Technology Conference*, Alexandria, Egypt.

EL TAHLAWI, M., FARRAG, A. & AHMED, S. 2008 Groundwater of Egypt: “an environmental overview”, *Environmental Geology* 55**,** 639-652.

ELEWA, H. & QADDAH, A. 2011 Groundwater potentiality mapping in the Sinai Peninsula, Egypt, using remote sensing and GIS-watershed-based modeling, *Hydrogeology Journal* 19**,** 613-628.

ELEWA, H. H. & EL NAHRY, A. H. 2009 Hydro-environmental status and soil management of the River Nile Delta, Egypt, *Environmental Geology* 57**,** 759-774.

ELIMELECH, M. & PHILLIP, W. A. 2011 The Future of Seawater Desalination: Energy, Technology, and the Environment, *Science* 333**,** 712-717.

ELSOBKI, M., WOODERS, P. & SHERIF, Y. 2009 Clean Energy Investment in Developing Countries: Wind power in Egypt, International Institute for Sustainable Development, accessed 30 January 2014, http://www.iisd.org/pdf/2009/bali_2_copenhagen_egypt_wind.pdf.

ELSWIJK, M. J., JONG, M. J. M., STROOTMAN, K. J., BRAAKMAN, J. N. C., DE LANGE, E. T. N. & SMIT, W. F. 2004 Photovoltaic/Thermal Collectors in Large Solar Thermal Systems, *19th European PV Solar Energy Conference and Exhibition*, Paris, France.

ELTAWIL, M. A., ZHENGMING, Z. & YUAN, L. 2009 A review of renewable energy technologies integrated with desalination systems, *Renewable and Sustainable Energy Reviews* 13**,** 2245-2262.

EMERSON, W. H. & JAMIESON, D. T. 1967 Some physical properties of sea water in various concentrations, *Desalination* 3**,** 213-224.

ENERGYBAY 2014a, EnergyBay, accessed 7 May 2014, http://www.energybay.org/sma-sunny-central-sc250u-commercial-grid-tie-inverter.

ENERGYBAY 2014b, SMA SUNNY ISLAND SI5048 50HZ EXPORT INVE, EnergyBay, accessed 7 May 2014, http://www.energybay.org/sma-sunny-island-si5048-50hz-export-inve-1#.U2w8D_mSzDw.

ENERGYTREND 2013, Price Trend: PV Spot Price, EnergyTrend, accessed 4 November 2013, http://pv.energytrend.com/pricequotes.html.

ETHIOPIAN ELECTRIC POWER CORPORATION 2013, About Grand Ethiopian Renaissance Dam, Ethiopian Electric Power Corporation, accessed 28 November 2013, http://www.eepco.gov.et/abouttheproject.php?pid=1&pcatid=2.

EXTANCE, A. 2010 The Concentrated Photovoltaics Industry Report 2010, FC Business Intelligence Limited, accessed 6 November 2013.

FAHIM, W., SALLAM, W., SIDDIK, I., BEHERY, A. & ABD EL-WAHAB, M. 2011 Integrated Water Resource Management: Introducing High Value/Low Water Consumption Crops to East Delta Farmers, accessed 1 January 2014, http://www.iwrm2eg.org/report/IWRMII/Report23INTRODUCING_HIGH_VALUE.pdf.

FAN, J., CHEN, Z., FURBO, S., PERES, B. & KARLSSON, B. 2009, Efficiency and Lifetime of Solar Collectors for Solar Heating Plants, *ISES Solar World Congress*, Johannesburg, South Africa.

FANE, A. G., SCHOFIELD, R. W. & FELL, C. J. D. 1987 The efficient use of energy in membrane distillation, *Desalination* 64**,** 231-243.

FAO AQUASTAT 2005 Egypt profile, FAO, accessed 5 September 2010, http://www.fao.org/nr/water/aquastat/countries_regions/EGY/index.stm.

FATH, H. E. S. 1998 Solar distillation: a promising alternative for water provision with free energy, simple technology and a clean environment, *Desalination* 116**,** 45-56.

FATH, H. E. S., ELSHERBINY, S. M., HASSAN, A. A., ROMMEL, M., WIEGHAUS, M., KOSCHIKOWSKI, J. & VATANSEVER, M. 2006 PV and thermally driven small-scale, stand-alone solar desalination systems with very low maintenance needs, *Tenth International Water Technology Conference*, Alexandria, Egypt.

FELDMAN, D., BARBOSE, G., MARGOLIS, R., WISER, R., DARGHOUTH, N. & GOODRICH, A. 2012 Photovoltaic (PV) Pricing Trends: Historical, Recent, and Near-Term Projections, NREL, accessed 5 December 2013, http://www.nrel.gov/docs/fy13osti/56776.pdf.

FERNÁNDEZ-PINEDA, C., IZQUIERDO-GIL, M. A. & GARCíA-PAYO, M. C. 2002 Gas permeation and direct contact membrane distillation experiments and their analysis using different models, *Journal of Membrane Science* 198**,** 33-49.

FICHTNER, W. 1978 *Seawater and Seawater Distillation*, e-book, accessed 16 May 2012.

FIORENZA, G., SHARMA, V. K. & BRACCIO, G. 2003 Techno-economic evaluation of a solar powered water desalination plant, *Energy Conversion and Management* 44**,** 2217-2240.

FORSTMEIER, M., FEICHTER, W. & MAYER, O. 2008 Photovoltaic powered water purification - challenges and opportunities, *Desalination* 221**,** 23-28.

FRAENKEL, P. & THAKE, J. 2006 *Water lifting devices: a handbook for users and choosers*, Practical Action Publishing.

FRANKEN, K. 2005 Irrigation in Africa in figures: AQUASTAT Survey – 2005, FAO, accessed 22 January 2012, ftp://ftp.fao.org/agl/aglw/docs/wr29_eng.pdf.

GABELICH, C. J., WILLIAMS, M. D., RAHARDIANTO, A., FRANKLIN, J. C. & COHEN, Y. 2007 High-recovery reverse osmosis desalination using intermediate chemical demineralization, *Journal of Membrane Science* 301**,** 131-141.

GAD, A. 2009 Assessment and mapping of desertification sensitivity in some of the western desert oases, Egypt, based on Remote Sensing and GIS, *The Fourth National GIS Symposium*, Eastern Province, Saudi Arabia.

GAD, A. & RAMADAN ALI, R. 2009, 'Water rationalization in Egypt from the perspective of the virtual water concept', *Technological perspectives for rational use of water resources in the Mediterranean region,* CIHEAM, Bari, accessed 1 January 2014, http://om.ciheam.org/article.php?IDPDF=801205.

GARCÍA-PAYO, M. C. & IZQUIERDO-GIL, M. A. 2004 Thermal resistance technique for measuring the thermal conductivity of thin microporous membranes, *Journal of Physics D: Applied Physics* 37**,** 3008.

GARCIA-RODRIGUEZ, L. 2003 Renewable energy applications in desalination: state of the art, *Solar Energy* 75**,** 381-393.

GARCÍA-RODRÍGUEZ, L. 2002 Seawater desalination driven by renewable energies: a review, *Desalination* 143**,** 103-113.

GARCÍA-RODRÍGUEZ, L., PALMERO-MARRERO, A. I. & GÓMEZ-CAMACHO, C. 2002 Comparison of solar thermal technologies for applications in seawater desalination, *Desalination* 142**,** 135-142.

GEA 2010, Cooling Tower Calculator, GEA, accessed 2 August 2014, www.gea-energytechnology.com.

GEIRNAERT, W. & LAEVEN, M. P. 1992 Composition and history of ground water in the western Nile Delta, *Journal of Hydrology* 138**,** 169-189.

GERSFELT, B. 2007 Allocating Irrigation Water in Egypt, Cornell University Division of Nutritional Sciences, accessed 19 February 2015, http://cip.cornell.edu/dns.gfs/1200428192.

GHAFFOUR, N., MISSIMER, T. M. & AMY, G. L. 2013 Technical review and evaluation of the economics of water desalination: Current and future challenges for better water supply sustainability, *Desalination* 309**,** 197-207.

GHEITH, H. & SULTAN, M. 2002 Construction of a hydrologic model for estimating Wadi runoff and groundwater recharge in the Eastern Desert, Egypt, *Journal of Hydrology* 263**,** 36-55.

GHEITH, H. & SULTAN, M. I. 2001 *Assessment of the renewable groundwater resources of Wadi El-Arish, Sinai, Egypt: modelling, remote sensing and GIS applications,* International Association of Hydrological Sciences, Wallingford, ROYAUME-UNI.

GHOSH, P. C., EMONTS, B. & STOLTEN, D. 2003 Comparison of hydrogen storage with diesel-generator system in a PV–WEC hybrid system, *Solar Energy* 75**,** 187-198.

GLEICK, P. 2013 The Promise and Threat of Ethiopia's Dam on the Nile: 21st century Water Conflicts, ScienceBlogs, accessed 7 June 2013, http://scienceblogs.com/significantfigures/index.php/2013/06/02/the-promise-and-threat-of-ethiopias-dam-on-the-nile-21st-century-water-conflicts/.

GOOSEN, M. F. A., SABLANI, S. S., SHAYYA, W. H., PATON, C. & AL-HINAI, H. 2000 Thermodynamic and economic considerations in solar desalination, *Desalination* 129**,** 63-89.

GORMLEY, M. 2013 Amonix Achieves World Record 35.9% Module Efficiency Rating at NREL, AMONIX, accessed 4 November 2013, http://amonix.com/pressreleases/amonix-achieves-world-record-359-module-efficiency-rating-nrel-4.

GOSSEL, W., SEFELNASR, A., WEISE, S. M., FRIESE, K., STEFANOVA, A. & WYCISK, P. 2010, Hydrochemical and isotope analysis of deep groundwater from the Nubian Aquifer system in the Egyptian Oases, *The 38th International Association of Hydrogeologists Congress*, Krakow.

GOSTOLI, C. & SARTI, G. C. 1989 Separation of liquid mixtures by membrane distillation, *Journal of Membrane Science* 41**,** 211-224.

GOSTOLI, C., SARTI, G. C. & MATULLI, S. 1987 Low Temperature Distillation Through Hydrophobic Membranes, *Separation Science and Technology* 22**,** 855-872.

GRYTA, M. & TOMASZEWSKA, M. 1998 Heat transport in the membrane distillation process, *Journal of Membrane Science* 144**,** 211-222.

GRYTA, M., TOMASZEWSKA, M. & MORAWSKI, A. W. 1997 Membrane distillation with laminar flow, *Separation and Purification Technology* 11**,** 93-101.

GSES 2009 *Stand Alone Power Supply Systems: Design and Installation*, Global Sustainable Energy Solutions Pty Ltd.

GUIJT, C. M., MEINDERSMA, G. W., REITH, T. & DE HAAN, A. B. 2005 Air gap membrane distillation: 1. Modelling and mass transport properties for hollow fibre membranes, *Separation and Purification Technology* 43**,** 233-244.

GUYER, J. P. 2012 Introduction to Solar Collectors for Heating & Cooling Buildings and Domestic Hot Water, CEDengineering.com accessed 25 May 2014, http://www.cedengineering.com/upload/Intro%20to%20Solar%20Collectors.pdf.

HAFEZ, A. & EL-MANHARAWY, S. 2003 Economics of seawater RO desalination in the Red Sea region, Egypt. Part 1. A case study, *Desalination* 153**,** 335-347.

HAMZA, M. S., ALY, A. I. M. & SWAILEM, F. M. 1984 Groundwater recharge and pollution in Wadi El-natrun, Egypt, *International Journal of Water Resources Development* 2**,** 39-44.

HAMZA, M. S., AWAD, M. A., EL-GAMAL, S. A. & SADEK, M. A. 2000 Geochemical Characteristics and Environmental Isotopes of Groundwater Resources in some Oases in the Western Desert, Egypt, *Seventh Conference of Nuclear Sciences & Applications*, Cairo, Egypt.

HAMZA, W. & MASON, S. 2004 Water availability and food security challenges in Egypt, *International Forum on Food Security Under Water Scarcity in the Middle East: Problems and Solutions*, Como, Italy.

HANSON, B. & MAY, D. 2011 Drip Irrigation Salinity Management for Row Crops, accessed 26 September 2012, http://anrcatalog.ucdavis.edu/pdf/8447.pdf.

HARRISON, D. G., HO, G. E. & MATHEW, K. 1996 Desalination using renewable energy in Australia, *Renewable Energy* 8**,** 509-513.

HASSAN, T. H., ATTIA, F. A. & EL-ATTFY, H. A. 2004 Groundwater Potentiality Map of The Nile Basin Countries - a Step Towards Integrated Water Management, *International Conference and Exhibition on Groundwater in Ethiopia: Providing Water for Millions*, Addis Ababa, Ethiopia.

HEFNY, K., FARID, M. S. & HUSSEIN, M. 1992 Groundwater assessment in Egypt, *International Journal of Water Resources Development* 8**,** 126 - 134.

HEFNY, K. & SHATA, A. 2004 *Groundwater in Egypt*, Ministry of Water Supplies and Irrigation, Cairo.

HEREHER, M. 2010 Sand movement patterns in the Western Desert of Egypt: an environmental concern, *Environmental Earth Sciences* 59**,** 1119-1127.

HEROLD, D., HORSTMANN, V., NESKAKIS, A., PLETTNER-MARLIANI, J., PIERNAVIEJA, G. & CALERO, R. 1998 Small scale photovoltaic desalination for rural water supply - demonstration plant in Gran Canaria, *Renewable Energy* 14**,** 293-298.

HOELZGEN, J. 2008 Landmines in the Desert Sand: Nazi Landmines Block Egypt's Access to Oil and Gas, SPIEGEL ONLINE INTERNATIONAL, accessed 5 December 2011, http://www.spiegel.de/international/world/0,1518,540756,00.html.

HOGAN, P. A., SUDJITO, FANE, A. G. & MORRISON, G. L. 1991 Desalination by solar heated membrane distillation, *Desalination* 81**,** 81-90.

HÖMIG, H. E. 1978 *Seawater And Seawater Distillation*, Vulkan-Verlag.

HONSBERG, C. & BOWDEN, S. 2013, PVCDROM, pveducation.org, accessed 29 October 2013, www.pveducation.org/pvcdrom.

HOWE, E. D. 1974 *Fundamentals of Water Desalination*, MARCEL DEKKER, INC., New York.

HRAYSHAT, E. S. 2008 Brackish water desalination by a stand alone reverse osmosis desalination unit powered by photovoltaic solar energy, *Renewable Energy* 33**,** 1784-1790.

HUSSEIN, M. 2013 'Egypt govt struggles with ongoing diesel fuel shortages', *Ahramonline*, 12 February accessed 18 December 2013, http://english.ahram.org.eg/NewsContent/3/12/64625/Business/Economy/Egypt-govt-struggles-with-ongoing-diesel-fuel-shor.aspx.

HYDRAULIC INSTITUTE, EUROPUMP & U.S. DEPARTMENT OF ENERGY’S OFFICE OF INDUSTRIAL TECHNOLOGIES 2001 Pump Life Cycle Costs: A Guide to LCC Analysis for Pumping Systems, The Office of Energy Efficiency and Renewable Energy (EERE) accessed 21 May 2014, http://energy.gov/eere/about-us.

IDA 2013, IDA Desalination Plants Inventory, Global Water Intelligence and Water Desalination Report, accessed 8 November 2012, http://www.desaldata.com/.

IDRIS, H. & NOUR, S. 1990 Present groundwater status in Egypt and the environmental impacts, *Environmental Geology* 16**,** 171-177.

IMDAKM, A. O. & MATSUURA, T. 2004 A Monte Carlo simulation model for membrane distillation processes: direct contact (MD), *Journal of Membrane Science* 237**,** 51-59.

INTERNATIONAL CAMPAIGN TO BAN LANDMINES 2010 Landmine Monitor Report Egypt, accessed 5 December 2011, www.the-monitor.org

INTERNATIONAL FEDERATION OF RED CROSS AND RED CRESCENT SOCIETIES 2010 Egypt: Flash Floods, International Federation of Red Cross and Red Crescent Societies (IFRC), accessed 17 january 2012, http://www.ifrc.org/docs/appeals/10/MDREG009do.pdf.

INTERNATIONAL FUND FOR AGRICULTURAL DEVELOPMENT 2008 The role of high-value crops in rural poverty reduction in the Near East and North Africa Enabling poor, International Fund for Agricultural Development (IFAD), accessed 1 January 2014, http://www.ifad.org/pub/pn/crop.pdf.

INTERNATIONAL FUND FOR AGRICULTURAL DEVELOPMENT 2009 Egypt: Smallholder contract farming for high-value and organic agricultural exports, International Fund for Agricultural Development (IFAD), accessed 1 January 2014, http://www.ifad.org/pub/pn/egypt.pdf.

INTERNATIONAL RENEWABLE ENERGY AGENCY 2012 Solar Photovoltaics, International Renewable Energy Agency, accessed 15 FEB 2013, http://www.irena.org/DocumentDownloads/Publications/RE_Technologies_Cost_Analysis-SOLAR_PV.pdf.

IRRIGATION SUPPORT PROJECT FOR ASIA AND THE NEAR EAST 1993 Irrigation Water Cost Recovery In Egypt: Determination of Water Costs, USAID, accessed 19 February 2015, http://pdf.usaid.gov/pdf_docs/PNABR870.pdf.

IVERSEN, S. B., BHATIA, V. K., DAM-JOHANSEN, K. & JONSSON, G. 1997 Characterization of microporous membranes for use in membrane contactors, *Journal of Membrane Science* 130**,** 205-217.

JACOBSON, N., WYDER, J., FRANKLIN, S. & MCCRACKEN, P. 2013 Data Collection of Diesel Generators in South Australia, Government of South Australia, accessed 7 May 2014, http://www.renewablessa.sa.gov.au/files/130924-sa-diesel-assess-24sept2013-(2).pdf.

JAMIESON, D. T. & TUDHOPE, J. S. 1970 Physical properties of sea water solutions: thermal conductivity, *Desalination* 8**,** 393-401.

JAMIESON, D. T., TUDHOPE, J. S., MORRIS, R. & CARTWRIGHT, G. 1969 Physical properties of sea water solutions: heat capacity, *Desalination* 7**,** 23-30.

JANSEN, A., HANEMAAIJER, J. H., ASSINK, J. W., SONSBEEK, E. V., DOTREMONT, C. & MEDEVOORT, J. V. 2010 Pilot plants prove feasibility of a new desalination technique, EARTO, accessed 10 February 2015, http://www.earto.eu/fileadmin/content/10_Hidden_Pages/Case_Studies_2011/TNO-Memstill_Asian_Water_pub.pdf.

JOYCE, A., LOUREIRO, D., RODRIGUES, C. & CASTRO, S. 2001 Small reverse osmosis units using PV systems for water purification in rural places, *Desalination* 137**,** 39-44.

KAISER, M. F. & GERIESH, M. H. 2007, Water resources assessment at El-Arish area, using remote sensing and GIS, North Sinai, Egypt, *Geoscience and Remote Sensing Symposium, 2007. IGARSS 2007. IEEE International*,

KALOGIROU, S. A. 2004 Solar thermal collectors and applications, *Progress in Energy and Combustion Science* 30**,** 231-295.

KALOGIROU, S. A. 2005 Seawater desalination using renewable energy sources, *Progress in Energy and Combustion Science* 31**,** 242-281.

KARAGIANNIS, I. C. & SOLDATOS, P. G. 2008 Water desalination cost literature: review and assessment, *Desalination* 223**,** 448-456.

KARAKULSKI, K., GRYTA, M. & MORAWSKI, A. 2002 Membrane processes used for potable water quality improvement, *Desalination* 145**,** 315-319.

KASENOW, M. 2001 *Applied Ground-Water Hydrology and Well Hydraulics,* Water Resources Publications.

KERSHMAN, S. A., RHEINLÄNDER, J., NEUMANN, T. & GOEBEL, O. 2005 Hybrid wind/PV and conventional power for desalination in Libya—GECOL's facility for medium and small scale research at Ras Ejder, *Desalination* 183**,** 1-12.

KHALIFA, E. 2011a Municipal Wastewater Production, Collection and Treatment & Direct Municipal Wastewater Use/Discharge, The UN-Water Activity Information System (UNW-AIS), accessed 21 August 2012, http://www.ais.unwater.org/ais/pluginfile.php/356/mod_page/content/111/EGYPT_FAO.pdf.

KHALIFA, E. 2011b Safe wastewater use in agriculture in Egypt: Case study, The UN-Water Activity Information System (UNW-AIS), accessed 23 August 2012, http://www.ais.unwater.org/ais/pluginfile.php/356/mod_page/content/111/Egypt%20FAO-Essam_3.pdf.

KHAYDARO, R., KHAYDAROV, R., GAPUROVA, O. & YULDASHEV, B. 2007, 'Solar Water Desalination in The Aral Sea Region', *Solar Desalination for the 21st Century*, Springer Netherlands,

KHAYET, M., GODINO, M. P. & MENGUAL, J. I. 2001 Modelling Transport Mechanism Through a Porous Partition, *Journal of Non-Equilibrium Thermodynamics* 26**,** 1-14.

KHAYET, M. & MATSUURA, T. 2011a, 'Chapter 1 - Introduction to Membrane Distillation', *Membrane Distillation,* Elsevier, Amsterdam.

KHAYET, M. & MATSUURA, T. 2011b, 'Chapter 2 - Membranes Used in MD and Design', *Membrane Distillation*, Elsevier, Amsterdam.

KHAYET, M. & MATSUURA, T. 2011c, 'Chapter 8 - MD Membrane Characterization', *Membrane Distillation*, Elsevier, Amsterdam.

KHAYET, M. & MATSUURA, T. 2011d, 'Chapter 10 - Direct Contact Membrane Distillation', *Membrane Distillation*, Elsevier, Amsterdam.

KHAYET, M. & MATSUURA, T. 2011e, 'Chapter 12 - Vacuum Membrane Distillation', *Membrane Distillation*, Elsevier, Amsterdam.

KHAYET, M. & MATSUURA, T. 2011f *Membrane Distillation: Principles and Applications*, Elsevier.

KIMURA, S., NAKAO, S.-I. & SHIMATANI, S.-I. 1987 Transport phenomena in membrane distillation, *Journal of Membrane Science* 33**,** 285-298.

KOLHE, M., KOLHE, S. & JOSHI, J. C. 2002 Economic viability of stand-alone solar photovoltaic system in comparison with diesel-powered system for India, *Energy Economics* 24**,** 155-165.

KONER, P. K., DUTTA, V. & CHOPRA, K. L. 2000 A comparative life cycle energy cost analysis of photovoltaic and fuel generator for load shedding application, *Solar Energy Materials and Solar Cells* 60**,** 309-322.

KOSCHIKOWSKI, J. 2011, 'Entwicklung von energieautark arbeitenden Wasserentsalzungsanlagen auf Basis der Membrandestillation', Doctoral Thesis, University of Kassel/Fraunhofer ISE.

KOSCHIKOWSKI, J., WIEGHAUS, M. & ROMMEL, M. 2003 Solar thermal-driven desalination plants based on membrane distillation, *Desalination* 156**,** 295-304.

KOSCHIKOWSKI, J., WIEGHAUS, M. & ROMMEL, M. 2009a, 'Membrane Distillation for Solar Desalination', *Seawater Desalination*, Springer Berlin Heidelberg,

KOSCHIKOWSKI, J., WIEGHAUS, M., ROMMEL, M., ORTIN, V. S., SUAREZ, B. P. & BETANCORT RODRÍGUEZ, J. R. 2009b Experimental investigations on solar driven stand-alone membrane distillation systems for remote areas, *Desalination* 248**,** 125-131.

KOST, C., MAYER, J., THOMSEN, J., HARTMANN, N. M., SENKPIEL, C., PHILIPPS, S., NOLD, S., LUDE, S., SAAD, N. & SCHLEGL, T. 2013 Levelized Cost of Electricity Renewable Energy Technologies, Fraunhofer ISE, accessed 12 May 2014, http://www.ise.fraunhofer.de/en/publications/veroeffentlichungen-pdf-dateien-en/studien-und-konzeptpapiere/study-levelized-cost-of-electricity-renewable-energies.pdf.

KOST, C., SCHLEGL, T., THOMSEN, J., NOLD, S. & MAYER, J. 2012 Study Levelized Cost of Electricity Renewable Energies, Fraunhofer ISE, accessed 4 November 2013, http://www.ise.fraunhofer.de/en/publications/veroeffentlichungen-pdf-dateien-en/studien-und-konzeptpapiere/study-levelized-cost-of-electricity-renewable-energies.pdf.

KUCERA, J. 2010a, 'Basic Terms and Definitions', *Reverse Osmosis - Design, Processes, and Applications for Engineers,* Wiley - Scrivener,

KUCERA, J. 2010b, 'Design Considerations', *Reverse Osmosis - Design, Processes, and Applications for Engineers,* Wiley - Scrivener,

KUCERA, J. 2010c, 'Issues Concerning System Engineering', *Reverse Osmosis - Design, Processes, and Applications for Engineers,* Wiley - Scrivener,

KUCERA, J. 2010d, 'Techniaues and Technologies ', *Reverse Osmosis - Design, Processes, and Applications for Engineers,* Wiley - Scrivener,

KUCERA, J. 2010e, 'Water Quality Guidelines', *Reverse Osmosis - Design, Processes, and Applications for Engineers,* Wiley - Scrivener,

KUMAR, S. 2013 Thermal–economic analysis of a hybrid photovoltaic thermal (PVT) active solar distillation system: Role of carbon credit, *Urban Climate* 5**,** 112-124.

KUROKAWA, H., KURODA, O., TAKAHASHI, S. & EBARA, K. 1990 Vapor Permeate Characteristics of Membrane Distillation, *Separation Science and Technology* 25**,** 1349-1359.

KWAK, H. T., ZHANG, G. & CHEN, S. 2005 The Effects of Salt Type and Salinity on Formation Water Viscosity and NMR Responses, *International Symposium of the Society of Core Analysts*, Toronto, Canada.

LABORDE, H. M., FRANCA, K. B., NEFF, H. & LIMA, A. M. N. 2001 Optimization strategy for a small-scale reverse osmosis water desalination system based on solar energy, *Desalination* 133**,** 1-12.

LAGANÀ, F., BARBIERI, G. & DRIOLI, E. 2000 Direct contact membrane distillation: modelling and concentration experiments, *Journal of Membrane Science* 166**,** 1-11.

LAMEI, A., VAN DER ZAAG, P. & VON MUNCH, E. 2008 Impact of solar energy cost on water production cost of seawater desalination plants in Egypt, *Energy Policy* 36**,** 1748-56.

LAMOREAUX, P., MEMON, B. & IDRIS, H. 1985 Groundwater development, Kharga Oases, Western Desert of Egypt: A long-term environmental concern, *Environmental Geology* 7**,** 129-149.

LATTEMANN, S. & HÖPNER, T. 2008 Environmental impact and impact assessment of seawater desalination, *Desalination* 220**,** 1-15.

LAU, K. Y., YOUSOF, M. F. M., ARSHAD, S. N. M., ANWARI, M. & YATIM, A. H. M. 2010 Performance analysis of hybrid photovoltaic/diesel energy system under Malaysian conditions, *Energy* 35**,** 3245-3255.

LAWSON, K. W. 1995, 'Membrane Distillation', Doctor of Philosiphy, The University of Texas.

LAWSON, K. W. & LLOYD, D. R. 1996 Membrane distillation. II. Direct contact MD, *Journal of Membrane Science* 120**,** 123-133.

LAWSON, K. W. & LLOYD, D. R. 1997 Membrane distillation, *Journal of Membrane Science* 124**,** 1-25.

LEACH, G. 1975 Energy and food production, *Food Policy* 1**,** 62-73.

LEILA, R. 2012 'Power to the people?', *Al-Ahram Weekly*, 25 - 31 July, accessed 27 August 2012, http://weekly.ahram.org.eg/2012/1108/eg5.htm.

LENNEY, M. P., WOODCOCK, C. E., COLLINS, J. B. & HAMDI, H. 1996 The status of agricultural lands in Egypt: The use of multitemporal NDVI features derived from landsat TM, *Remote Sensing of Environment* 56**,** 8-20.

LI, C., GOSWAMI, Y. & STEFANAKOS, E. 2013 Solar assisted sea water desalination: A review, *Renewable and Sustainable Energy Reviews* 19**,** 136-163.

LIBERT, J. J. & MAUREL, A. 1981 Desalination and renewable energies-a few recent developments, *Desalination* 39**,** 363-372.

LINACRE, E. T. 1977 A simple formula for estimating evaporation rates in various climates, using temperature data alone, *Agricultural Meteorology* 18**,** 409-424.

LIU, C., CAOTHIEN, S., HAYES, J. & CAOTHUY, T. 2001, Membrane Chemical Cleaning: From Art to Science, *Water Quality Technology Conference*, Denver, Colorado.

LIU, C. & MARTIN, A. 2006 Applying Membrane Distillation in High-Purity Water Production for Semiconductor Industry, *Ultrapure Water: the definitive journal of high-purity water*.

LONERGAN, S. & WOLF, A. T. 2001 Moving Water to Move People The Toshka Project in Egypt A Water Forum Contribution, *Water International* 26**,** 589-596.

MACEDONIO, F., CURCIO, E. & DRIOLI, E. 2007 Integrated membrane systems for seawater desalination: energetic and exergetic analysis, economic evaluation, experimental study, *Desalination* 203**,** 260-276.

MACEDONIO, F. & DRIOLI, E. 2008 Pressure-driven membrane operations and membrane distillation technology integration for water purification, *Desalination* 223**,** 396-409.

MAHMOUD, M. M. & IBRIK, I. H. 2006 Techno-economic feasibility of energy supply of remote villages in Palestine by PV-systems, diesel generators and electric grid, *Renewable and Sustainable Energy Reviews* 10**,** 128-138.

MARTINETTI, C. R., CHILDRESS, A. E. & CATH, T. Y. 2009 High recovery of concentrated RO brines using forward osmosis and membrane distillation, *Journal of Membrane Science* 331**,** 31-39.

MARTÍNEZ-DÍEZ, L. & FLORIDO-DÍAZ, F. J. 2001 Desalination of brines by membrane distillation, *Desalination* 137**,** 267-273.

MARTÍNEZ-DÍEZ, L. & VÁZQUEZ-GONZÀLEZ, M. I. 1999 Temperature and concentration polarization in membrane distillation of aqueous salt solutions, *Membrane Science* 156**,** 265-273.

MARTíNEZ-DíEZ, L. & VÁZQUEZ-GONZÁLEZ, M. I. 1999 Temperature and concentration polarization in membrane distillation of aqueous salt solutions, *Journal of Membrane Science* 156**,** 265-273.

MARTíNEZ, L., FLORIDO-DíAZ, F. J., HERNÁNDEZ, A. & PRÁDANOS, P. 2002 Characterisation of three hydrophobic porous membranes used in membrane distillation: Modelling and evaluation of their water vapour permeabilities, *Journal of Membrane Science* 203**,** 15-27.

MASHALY, H. 2012 'The armed forces and Matruh water company succeeded in ending the drinking water crisis', *Youm7*, 15 June, accessed 14 November 2012, http://www1.youm7.com/News.asp?NewsID=706376&SecID=296&IssueID=144.

MASON, S. A. 2004, 'From Conflict to Cooperation in the Nile Basin', Doctoral Thesis, Swiss Federal Institute of Technology Zurich.

MASOUD, A. 2011 Runoff modeling of the wadi systems for estimating flash flood and groundwater recharge potential in Southern Sinai, Egypt, *Arabian Journal of Geosciences* 4**,** 785-801.

MASOUD, A. & KOIKE, K. 2006 Arid land salinization detected by remotely-sensed landcover changes: A case study in the Siwa region, NW Egypt, *Journal of Arid Environments* 66**,** 151-167.

MASOUD, M. S., ZAID, M. & ABDOU, A. M. 2003 Study of ground water quality in kom hamada area, Beheira governorate, Egypt, *Bulletin of the Chemists and Technologists of Macedonia* 22**,** 143-154.

MCDOUGALL, T. J., FEISTEL, R., WRIGHT, D. G., PAWLOWICZ, R., MILLERO, F. J., JACKETT, D. R., KING, B. A., MARION, G. M., SEITZ, S., SPITZER, P. & CHEN, C. 2010, The International Thermodynamic Equation Of Seawater - 2010 (TEOS-10), accessed 21 May 2013, www.teos-10.org/.

MEGAHED, S. M., ALI, H. F. M. & HUSSEIN, A. H. 2010, Egypt Landmine Problem: History, Facts, Difficulties and Clearance Efforts, *International Symposium "Humanitarian Demining 2010"*, Šibenik, Croatia.

MEMSYS 2014, Technology of thermal membrane distillation, memsys, accessed 4 July 2014, http://www.memsys.eu/technology.html.

MEMSYS 2015 memDist 6-52: Technical description of process, modules and applications, memsys, accessed 28 January 2015, http://www.memsys.eu/dateien/products/memsys_datasheet_6_52.pdf.

MERKASOL 2014, Enersol OPzS Classic Solar Battery 4600Ah 2V, MERKASOL, accessed 3 May 2014, http://www.merkasol.com/Enersol-OPzS-Classic-Solar-Battery-4600Ah-2V.

MICALE, G., CIPOLLINA, A. & RIZZUTI, L. 2009, 'Seawater Desalination for Freshwater Production', Springer Berlin Heidelberg,

MILEWSKI, A., SULTAN, M., YAN, E., BECKER, R., ABDELDAYEM, A., SOLIMAN, F. & GELIL, K. A. 2009 A remote sensing solution for estimating runoff and recharge in arid environments, *Journal of Hydrology* 373**,** 1-14.

MILLER, J. E. 2003 Review of Water Resources and Desalination Technologies, Sandia National Laboratories, accessed 1 October 2013, http://www.sandia.gov/.

MILLS, A. C. & SHATA, A. 1989 Ground-Water Assessment of Sinai, Egypt, *Ground Water* 27**,** 793-801.

MILOW, B. & ZARZA, E. 1997 Advanced MED solar desalination plants. Configurations, costs, future — seven years of experience at the Plataforma Solar de Almeria (Spain), *Desalination* 108**,** 51-58.

MISAK, R. F. & DRAZ, M. Y. 1997 Sand drift control of selected coastal and desert dunes in Egypt: case studies, *Journal of Arid Environments* 35**,** 17-28.

MOHAMED, E. S. & PAPADAKIS, G. 2004 Design, simulation and economic analysis of a stand-alone reverse osmosis desalination unit powered by wind turbines and photovoltaics, *Desalination* 164**,** 87-97.

MOHAMMAD RUSAN, M. J., HINNAWI, S. & ROUSAN, L. 2007 Long term effect of wastewater irrigation of forage crops on soil and plant quality parameters, *Desalination* 215**,** 143-152.

MORGAN, P. & SWANBERG, C. 1978 Heat flow and the geothermal potential of Egypt, *pure and applied geophysics* 117**,** 213-226.

MORRISON, G. & ROSENGARTEN, G. 2012 *Solar Thermal Energy Design,* School of Mechanical and Manufacturing Engineering, University of New South Wales.

MOSTAFA, H., EL-GAMAL, F. & SHALABY, A. 2004 Reuse of Low Quality Water in Egypt, International Centre for Advanced Mediterranean Argonomic Studies (CIHEAM), accessed 23 january 2012, http://ressources.ciheam.org/om/pdf/b53/00800754.pdf.

MÜLLER-HOLST, H. 2007, 'Solar Thermal Desalination Using the Multiple Effect Humidification (MEH)-Method', *Solar Desalination for the 21st century,* Springer Netherlands,

MÜLLER-HOLST, H., ENGELHARDT, M., HERVE, M. & SCHÖLKOPF, W. 1998 Solarthermal seawater desalination systems for decentralised use, *Renewable Energy* 14**,** 311-318.

MULYANDASARI, V. 2011 Cooling Tower Selection and Sizing, KLM Technology Group, accessed 28 July 2014, http://www.klmtechgroup.com/PDF/EDG/ENGINEERING%20DESIGN%20GUIDELINES%20-%20Cooling%20Towers%20-%20Rev01.pdf.

MURDOCH UNIVERSITY 2013, Concentrated Solar, Murdoch University, accessed 30 October 2013, http://www.see.murdoch.edu.au/resources/info/Tech/hightemp/.

MUSELLI, M., NOTTON, G. & LOUCHE, A. 1999 Design of hybrid-photovoltaic power generator, with optimization of energy management, *Solar Energy* 65**,** 143-157.

MWRI 2010 Water Challenges in Egypt, Ministry of Water Resources and Irrigation, accessed 15 August 2012, http://www.mwri.gov.eg/En/pdf_files%20english/Brochure%20%20Eng.pdf.

NAFEY, A. S., MOHAMAD, M. A., EL-HELABY, S. O. & SHARAF, M. A. 2006 Theoretical and experimental study of a small unit for water desalination using solar energy and flashing process, *Tenth International Water Technology Conference*, Alexandria, Egypt.

NATIONAL DRINKING WATER CLEARINGHOUSE 1998 Iron and Manganese Removal, The National Environmental Services Center, accessed 29 October 2012, http://www.nesc.wvu.edu/pdf/dw/publications/ontap/2009_tb/iron_DWFSOM42.pdf.

NATIONAL ENERGY TECHNOLOGY LABORATORY, RUBIN, E., ELECTRIC POWER RESEARCH INSTITUTE, GLOBAL CCS INSTITUTE, IEA GREENHOUSE GAS R&D PROGRAMME, INTERNATIONAL ENERGY AGENCY & ZERO EMISSIONS PLATFORM 2013 *Toward a common method of cost estimation for CO2 capture and storage at fossil fuel power plants*, e-book, accessed 12 May 2014, http://www.globalccsinstitute.com/publications/toward-common-method-cost-estimation-co2-capture-and-storage-fossil-fuel-power-plant-40.

NATIONAL RESEARCH COUNCIL 2008 Desalination: A National Perspective, The National Academic Press, accessed 15 January 2013, http://waterwebster.org/documents/NRCDesalinationreport_000.pdf.

NELLIS, G. & KLEIN, S. 2009 *Heat Transfer*, Cambridge University Press.

NICOLAISEN, B. 2003 Developments in membrane technology for water treatment, *Desalination* 153**,** 355-360.

NOUR, S. 1996 Groundwater potential for irrigation in the East Oweinat area, Western Desert Egypt, *Environmental Geology* 27**,** 143-154.

NOUR, S. & KHATTAB, A. F. 1998 Hydrogeology of deep aquifers in the western desert and Sinai, Ministry of Public Works and Water Resources, accessed 5 January 2011, http://www.iwrmeg.org/.

NREL 2010, Parabolic Trough Solar Field Technology, NREL, accessed 30 October 2013, http://www.nrel.gov/csp/troughnet/solar_field.html.

NREL 2012, PVWATTS, NREL, accessed 26 December 2013, http://rredc.nrel.gov/solar/calculators/PVWATTS/version1/International/pvwattsv1_intl.cgi.

NREL 2013, Renewable Energy Data Exploration, NREL, http://maps.nrel.gov/SWERA.

OIL&GAS, E. 2012, Concession Map, Egypt Oil&Gas, accessed 3 March 2013, http://www.egyptoil-gas.com/concession_map.php.

OMAR, M. 2010 'Fayoum villagers block road to protest water shortage', *Egypt Independent*, 18 August, accessed 18 August 2010, http://www.egyptindependent.com/news/fayoum-villagers-block-road-protest-water-shortage.

ORON, G., GILLERMAN, L., BICK, A., BURIAKOVSKY, N., MANOR, Y., BEN-YITSHAK, E., KATZ, L. & HAGIN, J. 2006 A two stage membrane treatment of secondary effluent for unrestricted reuse and sustainable agricultural production, *Desalination* 187**,** 335-345.

ORON, G., GILLERMAN, L., BICK, A., MANOR, Y., BURIAKOVSKY, N. & HAGIN, J. 2008 Membrane technology for sustainable treated wastewater reuse:

Agricultural, environmental and hydrological considerations, *Water Science and Technology* 57**,** 1383-1388.

ORON, G., GILLERMAN, L., BICK, A., MNAOR, Y., BURIAKOVSKY, N. & HAGIN, J. 2007 Advanced low quality waters treatment for unrestricted use purposes: imminent challenges, *Desalination* 213**,** 189-198.

PAREKH, S., FARID, M. M., SELMAN, J. R. & AL-HALLAJ, S. 2004 Solar desalination with a humidification-dehumidification technique — a comprehensive technical review, *Desalination* 160**,** 167-186.

PARKINSON, G. 2012 Silex Systems sees CPV costs below 10c/kWh, REneweconomy, accessed 4 November 2013, http://reneweconomy.com.au/2012/silex-systems-sees-cpv-costs-below-10ckwh-86400.

PAWLOWICZ, R. & FEISTEL, R. 2012 Limnological applications of the Thermodynamic Equation of Seawater 2010 (TEOS-10), *Limnology and Oceanography: Methods***,** 853-867.

PEARSON, K. E. 2009 The Basics of Salinity and Sodicity Effects on Soil Physical Properties Montana State University, accessed 15 January 2011, http://waterquality.montana.edu/docs/methane/basics_highlight.shtml.

PHATTARANAWIK, J. & JIRARATANANON, R. 2001 Direct contact membrane distillation: effect of mass transfer on heat transfer, *Journal of Membrane Science* 188**,** 137-143.

PHATTARANAWIK, J., JIRARATANANON, R. & FANE, A. G. 2003 Heat transport and membrane distillation coefficients in direct contact membrane distillation, *Journal of Membrane Science* 212**,** 177-193.

PHILIP, G., ATTIA, O. E. A., DRAZ, M. Y. & EL BANNA, M. S. 2004, Dynamics of Sand Dunes Movement and their Environmental Impacts on the Reclamation Area in North West Sinai, Egypt, *The 7th Conf. Geology of Sinai for Development* Ismailia, Egypt.

PINNEKAMP, J. & FRIEDRICH, H. 2006 *Membrane technology for waste water treatment*, FiW-Verlag.

POPIEL, C. O., WOJTKOWIAK, J. & BIERNACKA, B. 2001 Measurements of temperature distribution in ground, *Experimental Thermal and Fluid Science* 25**,** 301-309.

PORTEOUS, A. 1975 *Saline Water Distillation Processes*, Prentice Hall Press.

PORTEOUS, A. 1984 *Desalination Technology Developments and Practice*, Applied Science Publishers.

PRIHASTO, N., LIU, Q.-F. & KIM, S.-H. 2009 Pre-treatment strategies for seawater desalination by reverse osmosis system, *Desalination* 249**,** 308-316.

PV INSIGHTS 2013, Solar PV Module Weekly Spot Price, accessed 5 August 2013, http://pvinsights.com/.

PVSYST 2013a PVsyst 6 Help: Array Thermal Losses, PVSYST, accessed 19 April 2014, http://files.pvsyst.com/help/.

PVSYST 2013b PVsyst 6 Help: Batteries - Model Description, PVSYST, accessed 19 April 2014, http://files.pvsyst.com/help/.

PVXCHANGE 2013, PRICE INDEX, pvXchange, accessed 22 November 2013, http://www.pvxchange.com/priceindex/Default.aspx?langTag=en-GB.

QTAISHAT, M., MATSUURA, T., KRUCZEK, B. & KHAYET, M. 2008 Heat and mass transfer analysis in direct contact membrane distillation, *Desalination* 219**,** 272-292.

RALUY, R. G., SERRA, L. & UCHE, J. 2005 Life cycle assessment of desalination technologies integrated with renewable energies, *Desalination* 183**,** 81-93.

RAYAN, M. A., DJEBEDJIAN, B. & KHALED, I. 2001 Water supply and demand and a desalination option for Sinai, Egypt, *Desalination* 136**,** 73-81.

RAYGEN 2013, RAYGEN Technology, RAYGEN, accessed 4 November 2013, http://www.raygen.com/live/technology.html.

REAHL, E. R. 2006 Half A Century of Desalination With Electrodialysis, The McIlvaine Company accessed 9 October 2013, http://www.mcilvainecompany.com/Decision_Tree/subscriber/articles/GE_Desalination_Electrodialysis.pdf.

REDDY, K. V. & GHAFFOUR, N. 2007 Overview of the cost of desalinated water and costing methodologies, *Desalination* 205**,** 340-353.

REHMAN, S. & AL-HADHRAMI, L. M. 2010 Study of a solar PV–diesel–battery hybrid power system for a remotely located population near Rafha, Saudi Arabia, *Energy* 35**,** 4986-4995.

RETNANESTRI, M. 2007, 'The I3A Framework: enhancing the sustainability of off-grid photovoltaic energy service delivery in Indonesia', Doctor of Philosophy, University of New South Wales.

REYSA, G. 2012, Determining Collector Flow Rate, Build It Solar, accessed 19 August 2013, http://www.builditsolar.com/References/ColFlowRate.htm.

RHEINLÄNDER, J. 2007, 'De-central Water and Power Supply Integrating Renewable Energy – Technical and Economic Performance Prediction', *Solar Desalination for the 21st Century*, Springer Netherlands,

RHOADES, J. D., KANDIAH, A. & MASHALI, A. M. 1992 The use of saline waters for crop production - FAO irrigation and drainage paper 48, FOOD AND AGRICULTURE ORGANIZATION accessed 29 December 2013, http://www.fao.org/docrep/t0667e/t0667e00.htm#Contents.

RICAUD, A. & ROUBEAU, P. 1994, "CAPTHEL", A 66% efficient hybrid solar module and the "ECOTHEL" co-generation solar system, *Photovoltaic Energy Conversion*, Waikoloa, HI.

RICHARDS, B. S., CAPAO, D. P. S. & SCHAFER, A. I. 2008 Renewable energy powered membrane technology. 2. The effect of energy fluctuations on performance of a photovoltaic hybrid membrane system, *Environmental Science and Technology* 42**,** 4563-4569.

RICHARDS, B. S. & SCHAFER, A. I. 2002 Design considerations for a solar-powered desalination system for remote communities in Australia, *Desalination* 144**,** 193-199.

RICHARDS, B. S. & SCHAFER, A. I. 2003 Photovoltaic-powered desalination system for remote Australian communities, *Renewable Energy* 28**,** 2013-2022.

RIFFEL, D. B. & CARVALHO, P. C. M. 2009 Small-scale photovoltaic-powered reverse osmosis plant without batteries: Design and simulation, *Desalination* 247**,** 378-389.

RIGW 1988 *Hydrogeological map of Egypt*, Research Institute for Groundwater, Water research Center, Ministry of Public Works and Water Resources.

RIZK, Z. S. & DAVIS, A. D. 1991 Impact of the Proposed Qattara Reservoir on the Moghra Aquifer of Northwestern Egypt, *Ground Water* 29**,** 232-238.

ROMMEL, M., KOSCHIKOWSKI, J. & WIEGHAUS, M. 2007, 'Solar driven desalination systems based on membrane distillation', *Solar Desalination for the 21st Century,* Springer Netherlands,

RUDNICK, A., KAPLAN, Y., KUDISH, A. I. & WOLF, D. 1986 A study of solar collector aging, installation and materials problems, *Solar Energy* 36**,** 227-240.

RURAL POVERTY PORTAL 2010 Egypt Statistics, The International Fund For Agricultural Development (IFAD), accessed 6 December 2010, http://www.ruralpovertyportal.org/web/guest/country/statistics/tags/egypt.

SABRY, B. 2012 'A Guide to Egypt's Challenges: Fuel & Electricity Shortages', 16 August, accessed 27 August 2012, http://english.ahram.org.eg/News/49603.aspx.

SAENGPRAJAK, A. 2007, 'Efficiency of Demand Side Management Measures in Small Village Electrification Systems*'*, Doctor of Philosophy, kassel university.

SAGIE, D., FEINERMAN, E. & AHARONI, E. 2001 Potential of solar desalination in Israel and in its close vicinity, *Desalination* 139**,** 21-33.

SAID, M. K. 2003, 'Landmines from External Powers in World War II at El-Alamein in Egypt', *Security and environment in the Mediterranean: conceptualising security and environmental conflicts,* Springer,

SALEH, A. 2012 'Marsa Matruh exposed to severe water shortage crisis', *Almesryoon*, 14 June, accessed 14 November 2012, http://www.almesryoon.com/permalink/12658.html.

SALIM, M. G. 2011 Selection of groundwater sites in Egypt, using geographic information systems, for desalination by solar energy in order to reduce greenhouse gases, *Journal of Advanced Research* 3**,** 11-19.

SANDIA NATIONAL LABORATORIES 2008, Stirling Energy Systems set new world record for solar-to-grid conversion efficiency, SANDIA, accessed 15 October 2013, https://share.sandia.gov/news/resources/releases/2008/solargrid.html.

SANDIA NATIONAL LABORATORIES n.d. Solar One, solar furnace project, Barstow, California, NREL, accessed 15 October 2013, http://images.nrel.gov/viewphoto.php?imageId=6323048.

SCHAFER, A., BROECKMANN, A. & RICHARDS, B. 2005 Membranes and renewable energy - A new era of sustainable development for developing countries, *Membrane Technology***,** 6-10.

SCHAFER, A. I., BROECKMANN, A. & RICHARDS, B. S. 2007 Renewable energy powered membrane technology. 1. Development and characterization of a photovoltaic hybrid membrane system, *Environmental Science and Technology* 41**,** 998-1003.

SCHAFER, A. I. & RICHARDS, B. S. 2005 Testing of a hybrid membrane system for groundwater desalination in an Australian national park, *Desalination* 183**,** 55-62.

SCHAFER, A. I. & RICHARDS, B. S. 2007 From concept to commercialisation: student learning in a sustainable engineering innovation project, *European Journal of Engineering Education* 32**,** 143-65.

SCHOCK, G. & MIQUEL, A. 1987 Mass transfer and pressure loss in spiral wound modules, *Desalination* 64**,** 339-352.

SCHOFIELD, R. W., FANE, A. G. & FELL, C. J. D. 1987 Heat and mass transfer in membrane distillation, *Journal of Membrane Science* 33**,** 299-313.

SCHOFIELD, R. W., FANE, A. G. & FELL, C. J. D. 1990a Gas and vapour transport through microporous membranes. I. Knudsen-Poiseuille transition, *Journal of Membrane Science* 53**,** 159-171.

SCHOFIELD, R. W., FANE, A. G., FELL, C. J. D. & MACOUN, R. 1990b Factors affecting flux in membrane distillation, *Desalination* 77**,** 279-294.

SCHWANTES, R., CIPOLLINA, A., GROSS, F., KOSCHIKOWSKI, J., PFEIFLE, D., ROLLETSCHEK, M. & SUBIELA, V. 2013 Membrane distillation: Solar and waste heat driven demonstration plants for desalination, *Desalination* 323**,** 93-106.

SHALABY, M. Y., AL-ZAHRANI, K. H., BAIG, M. B., S., S. G. & ALDOSARI, F. 2011 Threats and challenges to sustainable agriculture and rural development in Egypt: Implications for agricultural extension, *Journal of Animal and Plant Sciences* 21**,** 581-588.

SHARAKY, A. M., ATTA, S. A., EL HASSANEIN, A. S. & KHALLAF, K. 2007 Hydrogeochemistry of Groundwater in the Western Nile Delta Aquifers, Egypt, *2nd International Conference on the Geology of Tethys*, Cairo.

SHARQAWY, M. H., LIENHARD, J. H. & ZUBAIR, S. M. 2010 Thermophysical properties of seawater: a review of existing correlations and data, *Desalination and Water Treatment* 16**,** 354-380.

SHATA, A. A. 1982 Hydrogeology of the Great Nubian Sandstone basin, Egypt, *Quarterly Journal of Engineering Geology and Hydrogeology* 15**,** 127-133.

SHAWKI, S. H. 2011 Impact of flash floods on the hydrogeological aquifer system at delta wadi El-Arish (North Sinai), *Fifteenth International Water Technology Conference*, Alexandria, Egypt.

SHERIF, M., SEFELNASR, A. & JAVADI, A. 2012 Incorporating the concept of equivalent freshwater head in successive horizontal simulations of seawater intrusion in the Nile Delta aquifer, Egypt, *Journal of Hydrology* 464–465**,** 186-198.

SHERIF, M. M. & SINGH, V. P. 1996, 'Saltwater Intrusion', *Hydrology of Disasters*, Springer Netherlands,

SHERIF, M. M. & SINGH, V. P. 2002 Effect of Groundwater Pumping on Seawater Intrusion in Coastal Aquifers, *Agricultural Sciences* 7**,** 61-67.

SOBHANI, R., ABAHUSAYN, M., GABELICH, C. J. & ROSSO, D. 2012 Energy Footprint analysis of brackish groundwater desalination with zero liquid discharge in inland areas of the Arabian Peninsula, *Desalination* 291**,** 106-116.

SOITEC 2013, Soitec's high-performance Concentrix™ technology, Soitec, accessed 29 October 2013, http://www.soitec.com/en/technologies/concentrix/components/.

SOLARCONTACT 2014, Flat Plate Collector, SolarContact, accessed 25 May 2014, http://www.solarcontact.com/solar-water/solar-collector/flat-plate.

SOLARSYSTEMS 2011 About Solar Systems, SolarSystems, accessed 4 November 2013, http://solarsystems.com.au/wp-content/uploads/2013/07/About-Solar-Systems-Flyer1.pdf.

SOLTAN, M. E. 1998 Characterisation, classification, and evaluation of some ground water samples in upper Egypt, *Chemosphere* 37**,** 735-745.

SONBOL, M. A. 2009 Sustainable Systems of Water Harvesting in Arid Regions A Case Study:Sinai Peninsula– Egypt, *The 2nd International Conf. on Water Resources & Arid Environment*, Riyadh, Saudi Arabia.

SRISURICHAN, S., JIRARATANANON, R. & FANE, A. G. 2006 Mass transfer mechanisms and transport resistances in direct contact membrane distillation process, *Journal of Membrane Science* 277**,** 186-194.

STAPLETON, G., GARRETT, S. & THORNE, B. 2009 *Grid-Connected PV Systems Design and Installation*, Global Sustainable Energy Solutions Pty Ltd.

STINE, W. B. & GEYER, M. 2001 Flat-Plate Collectors, Power From The SUN.net, accessed 3 November 2013, http://www.powerfromthesun.net/Book/chapter06/chapter06.html.

STURCHIO, N. C., PATTERSON, L. J., WAGDY, A., SULTAN, M. I. & BECKER, R. 2005 Geochemical and Isotopic Constraints on the Origin of the Eastern Desert Groundwaters: A Progress Report, Ministry of Water Resources and Irrigation, accessed 14 June 2012, http://gis.mwri.gov.eg/gis/pdf/geo%20chemical%20final.pdf.

SULTAN, A. S., MOHAMEDEN, M. I. & SANTOS, F. M. 2009 Hydrogeophysical study of the El Qaa Plain, Sinai, Egypt, *Bulletin of Engineering Geology and the Environment* 68**,** 525-537.

SULTAN, M., GHEITH, H., STURCHIO, N. C., EL ALFY, Z. & DANISHWAR, S. 2002 *Origin and recharge rates of alluvial ground waters, Eastern Desert, Egypt*.

SULTAN, M., MANOCHA, N., MILEWSKI, A., BECKER, R., STURCHIO, N., YAN, E. & WAGDY, A. 2008 Developing Renewable Groundwater Resources in Arid Lands: Pilot Case: The Eastern Desert of Egypt, UNDP,Global Environment Facility (GEF), Cairo University, MWRI, accessed 19 March 2012, http://gis.mwri.gov.eg/gis/pdf/Generation%20of%20the%20Arc%20GIS%20Server%20Web%20Application%201.pdf.

SULTAN, M., STURCHIO, N. C., GHEITH, H., HADY, Y. A. & EL ANBEAWY, M. 2000 Chemical and Isotopic Constraints on the Origin of Wadi El-Tarfa Ground Water, Eastern Desert, Egypt, *Ground Water* 38**,** 743-751.

SULTAN, M., YAN, E., STURCHIO, N., WAGDY, A., ABDEL GELIL, K., BECKER, R., MANOCHA, N. & MILEWSKI, A. 2007 Natural discharge: A key to sustainable utilization of fossil groundwater, *Journal of Hydrology* 335**,** 25-36.

SUTER, J. M. 2001 *Heat Losses From Storage Tanks: Up to 5 Times Higher than Calculated!*, Report Task 26, Industry Newsletter no. 2, Danish Technological Institute, accessed 23 June 2014, http://www.solenergi.dk/task26/pdf/heat_losses_from_storage_tanks_by_jm_suter.pdf.

SWAIN, A. 1997 Ethiopia, the Sudan, and Egypt: The Nile River Dispute, *The Journal of Modern African Studies* 35**,** 675-694.

SWANBERG, C. A., MORGAN, P. & BOULOS, F. K. 1983 Geothermal potential of Egypt, *Tectonophysics* 96**,** 77-94.

TALAAT, H. A., SOROUR, M. H., ABULNOUR, A. G. & SHAALAN, H. F. 2003 The potential role of brackish water desalination within the Egyptian water supply matrix, *Desalination* 152**,** 375-382.

TANTAWI, M. A., EL-SAYED, E. & AWAD, M. A. 1998 Hydrochemical and stable isotope study of groundwater in the Saint Catherine-Wadi Feiran area, south Sinai, Egypt, *Journal of African Earth Sciences* 26**,** 277-284.

TARNACKI, K., MENESES, M., MELIN, T., VAN MEDEVOORT, J. & JANSEN, A. 2012 Environmental assessment of desalination processes: Reverse osmosis and Memstill®, *Desalination* 296**,** 69-80.

THE ENCYCLOPEDIA OF DESALINATION AND WATER RESOURCES 2013, Energy requirements of desalination processes, The Encyclopedia of Desalination and Water Resources (DESWARE), accessed 2 October 2013, http://www.desware.net/desa4.aspx.

THE INTERNATIONAL ASSOCIATION FOR THE PROPERTIES OF WATER AND STEAM 2008 Release on the IAPWS Formulation 2008 for the Thermodynamic Properties of Seawater, TEOS-10, accessed 22 May 2013, http://www.teos-10.org/pubs/IAPWS-08.pdf.

THE INTERNATIONAL RENEWABLE ENERGY AGENCY 2012 Renewable Energy Technologies: Cost Analysis Series: Solar Photovoltaics, The International Renewable Energy Agency, accessed 15 April 2014, http://www.irena.org/DocumentDownloads/Publications/RE_Technologies_Cost_Analysis-SOLAR_PV.pdf.

THE NATIONAL RESERACH COUNCIL 2004 Review of the Desalination and Water Purification Technology Roadmap, The National Academy Press, accessed 2 October 2013, http://www.nap.edu/openbook.php?record_id=10912.

THE U.S. NUCLEAR REGULATORY COMMISSION 2014, Capacity factor (net) The U.S. Nuclear Regulatory Commission, accessed 1 June 2014, http://www.nrc.gov/reading-rm/basic-ref/glossary/capacity-factor-net.html.

THE UNIVERSITY OF QUEENSLAND 2013, PV Cell Technology The University of Queensland, accessed 29 October 2013, http://www.uq.edu.au/solarenergy/pv-array/uq-pv-modules.

THE WORLD FACT BOOK 2014, Egypt Profile, Central Intelligence Agency (CIA), accessed 22 January 2015, https://www.cia.gov/library/publications/the-world-factbook/geos/eg.html.

THIESEN, S. 2007, 'Beyond Pilot Projects: The Feasibility of Immediate Technology Transfer From Tried and Tested Maritime and Offshore Reverse Osmosis Systems to Stationary Solar and Wind Powered Desalination Solutions', *Solar Desalination for the 21st Century*, Springer Netherlands,

THOMSON, J., SLUNJSKI, M., FABIG, M. & CRISP, G. 2009 Potable Water HERO Process at Yalgoo, *Water Practice & Technology* 4.

THOMSON, M. & INFIELD, D. 2003a A photovoltaic-powered seawater reverse-osmosis system without batteries, *Desalination* 153**,** 1-8.

THOMSON, M. & INFIELD, D. 2003b A photovoltaic-powered seawater reverse-osmosis system without batteries, *Desalination* 153**,** 1-8.

TIAN, Y. & ZHAO, C. Y. 2013 A review of solar collectors and thermal energy storage in solar thermal applications, *Applied Energy* 104**,** 538-553.

TREVELYAN, J. 2001 Technology Needs Mine Clearance in Egypt and Jordan, *Journal of ERW and Mine Action* 3.

TRIPANAGNOSTOPOULOS, Y., TSELEPIS, S., SOULIOTIS, M. & TONUI, J. K. 2004 Design Aspects of Hybrid PVT/Water Solar Systems, *19th European Solar Energy Conference and Exhibition* Paris, France

TUN, C. M., FANE, A. G., MATHEICKAL, J. T. & SHEIKHOLESLAMI, R. 2005 Membrane distillation crystallization of concentrated salts—flux and crystal formation, *Journal of Membrane Science* 257**,** 144-155.

TZEN, E. 2005, Desalination units powered by RES: opportunities and challenges, *ADU RES Seminar*, Tunisia, Hammamet.

TZEN, E., PERRAKIS, K. & BALTAS, P. 1998 Design of a stand alone PV - desalination system for rural areas, *Desalination* 119**,** 327-334.

TZEN, E., THEOFILLOYIANAKOS, D. & KOLOGIOS, Z. 2008 Autonomous reverse osmosis units driven by RE sources experiences and lessons learned, *Desalination* 221**,** 29-36.

TZEN, E., THEOFILLOYIANAKOS, D., SIGALAS, M. & KARAMANIS, K. 2004 Design and development of a hybrid autonomous system for seawater desalination, *Desalination* 166**,** 267-274.

U.S. DEPARTMENT OF ENERGY 2011 2010 Solar Technologies Market Report, NREL, accessed 20 October 2013, http://www.nrel.gov/docs/fy12osti/51847.pdf.

U.S. ENERGY INFORMATION ADMINISTRATION 2013, Egypt, EIA, accessed 16 November 2013, http://www.eia.gov/countries/country-data.cfm?fips=EG.

U.S. GEOLOGICAL SURVEY 2014, Water Science Glossary of Terms, U.S. Geological Survey, accessed 14 March 2014, http://water.usgs.gov/edu/dictionary.html.

UNITED NATIONS COUNTRY TEAM 2005 UN Common Country Assessment: Egypt, Moody Graphic Int., accessed 23 December 2011, http://egypt.unfpa.org/pdfs/Country_Profile/CCA_Egypt.pdf.

VERTEX HYDROPORE 2010, WHAT IS ELECTRODEIONISATION or EDI ?, Vertex Hydropore accessed 24 October 2013, http://www.reverseosmosis.com.au/webcontent6.htm.

VETTER, M., SCHIES, A., WACHTEL, J., KOIRALA, B. P., HEILE, I., GOMBERT, A. & ABULFOTUH, F. 2010, The World's First CPV Stand-Alone System – Water Supply in Remote Areas of Egypt, *25th European Photovoltaic Solar Energy Conference and Exhibition (EU PVSEC)*, Valencia, Spain.

VINEY, S. 2012 'Rural irrigation canals are afflicted by water shortages and contaminated water', *Egypt Independent*, 13 August, accessed 23 November 2012, http://www.egyptindependent.com/news/rural-irrigation-canals-are-afflicted-water-shortages-and-contaminated-water.

WADE, N. M. 1993 Technical and economic evaluation of distillation and reverse osmosis desalination processes, *Desalination* 93**,** 343-363.

WADE, N. M. 2001 Distillation plant development and cost update, *Desalination* 136**,** 3-12.

WAHAAB, R. A. & BADAWY, M. I. 2004 Water quality assessment of the River Nile system: an overview, *Biomedical and Environmental Sciences* 17**,** 87-100.

WANG, J., GAO, N., DENG, Y. & LI, Y. 2012 Solar power-driven humidification–dehumidification (HDH) process for desalination of brackish water, *Desalination* 305**,** 17-23.

WANG, L. K., CHEN, J. P., HUNG, Y. & SHAMMAS, N. K. 2010, 'Membrane Systems Planning and Design', *Membrane and Desalination Technologies*, Springer, Dordrecht.

WATER QUALITY ASSOCIATION 2005 Osmosis Process, HM Digital, accessed 11 August 2010, http://www.tdsmeter.com/what-is?id=0013.

WATER QUALITY ASSOCIATION 2012, The WQA Glossary of Terms: Salt Water, Water Quality Association, accessed 9 September 2012, http://www.wqa.org/sitelogic.cfm?varCenterColumn=glossary.cfm&gl=352.

WATSON, I. C., MORIN, O. J. & HENTHOME, L. 2003 Desalting Handbook for Planners, Third Edition, accessed 9 October 2013, http://www.usbr.gov/research/AWT/reportpdfs/report072.pdf.

WEINER, D., FISHER, D., MOSES, E. J., KATZ, B. & MERON, G. 2001 Operation experience of a solar- and wind-powered desalination demonstration plant, *Desalination* 137**,** 7-13.

WEISSTEIN, E. W. 2013, Arc Length, MathWorld--A Wolfram Web Resource., accessed 25 April 2013, http://mathworld.wolfram.com/ArcLength.html

WENHAM, S. R., GREEN, M. A., WATT, M. E. & CORKISH, R. 2006 *Applied Photovoltaics*, Centre for Photovoltaic Engineering, UNSW.

WHITTINGTON, D. & MCCLELLAND, E. 1992 Opportunities for Regional and International Cooperation in the Nile Basin, *Water International* 17**,** 144-154.

WHO 2011 Guidelines for drinking-water quality, World Health Organization, accessed.

WIEGHAUS, M., KOSCHIKOWSKI, J. & ROMMEL, M. 2008 Solar membrane distillation ideal for remote areas *The international desalination & water reuse* 18**,** 37-40.

WILLIS, B. 2012 Report: CPV could be 30% cheaper than PV by 2016, PVTECH, accessed 4 November 2013, http://www.pv-tech.org/news/report_cpv_could_be_30_cheaper_than_pv_by_2016.

WINTER, D., KOSCHIKOWSKI, J. & RIPPERGER, S. 2012 Desalination using membrane distillation: Flux enhancement by feed water deaeration on spiral-wound modules, *Journal of Membrane Science* 423–424**,** 215-224.

WINTER, D., KOSCHIKOWSKI, J. & WIEGHAUS, M. 2011 Desalination using membrane distillation: Experimental studies on full scale spiral wound modules, *Membrane Science* 375**,** 104-112.

YARRA VALLEY WATER n.d. Best Practice Guidelines - Cooling Towers, Yarra Valley Water, accessed 29 July 2014, https://www.yvw.com.au/yvw/groups/public/documents/document/yvw001670.pdf.

YIRGU, B. 2012 Ethiopia's Renaissance Dam: A dam of Mega-Benefits, TIGRAI Online, accessed 4 December 2013, http://www.tigraionline.com/articles/article121230.html.

YOUNOS, T. 2005 The Economics of Desalination, *Journal of Contemporary Water Research & Education* 132**,** 39-45.

YOUNOS, T. & TULOU, K. E. 2005 Overview of Desalination Techniques, *Journal of Contemporary Water Research & Education* 132**,** 3-10.

YOUSIF, H. 2012 'Ethiopia's Renaissance Dam: A Mega-Dam with Potentially Mega-Consequences', *Think Africa Press*, 3 December, accessed 4 December 2013, http://thinkafricapress.com/ethiopia/nile-concerns-over-new-mega-dam-egypt-sudan.

YUN, Y., MA, R., ZHANG, W., FANE, A. G. & LI, J. 2006 Direct contact membrane distillation mechanism for high concentration NaCl solutions, *Desalination* 188**,** 251-262.

ZEJLI, D. & ELMIDAOUI, A. 2007, 'Moroccan Potentialities of Renewable Energy Sources for Water Desalination', *Solar Desalination for the 21st Century,* Springer Netherlands,

ZHAO, K., HEINZL, W., WENZEL, M., BÜTTNER, S., BOLLEN, F., LANGE, G., HEINZL, S. & SARDA, N. 2013 Experimental study of the memsys vacuum-multi-effect-membrane-distillation (V-MEMD) module, *Desalination* 323**,** 150-160.

ZHAO, S., ZOU, L., TANG, C. Y. & MULCAHY, D. 2012 Recent developments in forward osmosis: Opportunities and challenges, *Journal of Membrane Science* 396**,** 1-21.

Appendix A: Groundwater Extraction and Estimated Reserves in Egypt

Location	Aquifer/ Type of Water	GW Extracted (bcm/yr)	Date	GW Reserves (bcm/yr)	Comments on GW Estimated Reserves
New Valley Oases	Nubian/Fresh GW	0.547[a]	2000	1.045[b]	● Amount that could be economically extracted over a period of 100 years
East Oweinat	Nubian/Fresh GW	0.8[b]	2000	2.346[c]	● Amount that could be economically extracted (period unspecified)
Lake Nasser Shores	Nubian (Upper Zone)/ <1,500 mg/l	0.05[a]	-	0.257[d]	● Amount that could be extracted with expected drawdown from 60 to 70 m
Siwa Oasis	Nubian & Fissured Carbonate/ Mainly brackish GW	0.15[a]	2000	0.182[e]	-
Eastern Desert and Red Sea Coast	Unspecified Aquifers/ Mainly brackish GW	0.05[a]	-	0.21[a]	● Available in the Nubian aquifer in the main wadis between the cities of Aswan and Qena ● The amount represents the aquifers' maximum annual recharge rates[221]
				0.031[a]	● Available in the Red Sea coastal aquifer ● 0.03 bcm/year from rainfall + 0.001 bcm/year from the underlying Nubian aquifer
				0.02[a]	● Available in the alluvial deposits aquifers along the coastal zone ● The amount represents the aquifer's maximum annual rainfall recharge rates[221]
Wadi Al Fareigh	Al-Moghra/ Fresh GW	0.0572[f]	-	0.12[f]	● Could be potentially extracted over long term period (period unspecified)

[221] That is if entirely extracted will result in a drop in GW levels beyond economical limits

Sinai Peninsula	Unspecified Aquifers / Fresh & Brackish GW	0.15[a,g]	-	0.03 to 0.04[a]	● The first value range is available in the Suez Gulf coastal aquifer ● The second value range is available in the alluvial deposits aquifer in south east and north of the Sinai Peninsula ● Both amounts represent the aquifers' maximum annual rainfall recharge rates ● Lack of studies regarding GW potential in the Sinai Peninsula especially for the Nubian aquifer
				0.012 to 0.018[a]	
North West Mediterranean Coast	Coastal Aquifer/ Mainly brackish GW	> 0.005[a]	-	>0.05[a]	-
Total		> 1.8		> 4.16 fossil GW + 1.3[h] of renewable GW	

a] (Hefny and Shata, 2004)

b] (Euroconsult/Pacer Consultants, 1983) cited in (Nour and Khattab, 1998)

c] (Salim 1984) cited in (Hefny and Shata, 2004)

d] (Soliman 1987) cited in (Nour and Khattab, 1998)

e] (Cedare, 2000) cited in (Hefny and Shata, 2004)

f] (Nour and Khattab, 1998)

g] (FAO AQUASTAT, 2005)

Appendix B: Review of Solar Energy Systems

B-1: Solar Thermal Collectors

Solar thermal collectors are devices that convert solar radiation into heat energy which is transferred to a working fluid such as air, water or oil. The heat could be used directly in a heating process or could be used to generate electricity via a steam turbine, a Rankine cycle engine or a Stirling heat engine (Morrison and Rosengarten, 2012). Solar thermal collectors are either classified in the literature as stationary and non-stationary[222] collectors (Kalogirou, 2004), or as concentrating and non-concentrating collectors (Duffie and Beckman, 2006). In concentrating collectors mirrors or lenses are used to concentrate solar radiation such that the area receiving sun radiation, i.e. the aperture area, is much larger than the absorber area, while in non-concentrating systems both areas are equal. Stationary and non-stationary collectors are usually non-concentrating and concentrating devices respectively. Solar ponds are also considered in this study as solar thermal collectors and are discussed under a separate heading.

B-1-1: Stationary collectors

This section is based on data obtained from the literature (Stine and Geyer, 2001, Kalogirou, 2004, Duffie and Beckman, 2006, Abu-Arabi, 2007, Morrison and Rosengarten, 2012). Flat plate and evacuated tube collectors are the main types of stationary solar thermal collectors. Flat plate collectors (*Figure B-1*) are the most common type of solar collectors and are used for low temperature water and air heating applications. Flat plate collectors are typically made of a black painted metal surface, referred to as the absorber, which has high absorptivity of sun radiation. The heat energy in the absorber is transferred to a working fluid flowing into tubes bonded to or integrated in the absorber plate. The absorber is covered by a transparent envelop made of glass or plastic to reduce heat losses by convection and radiation. Some FPC's, however, do not use covers, i.e. unglazed FPC's, and are only used for applications

[222] Equipped with single or double axis tracking systems

where the desired fluid temperature is close to ambient (maximum operating temperature < 35°C) such as in swimming pool water heating applications. The back side and the sides of the absorber area are covered by a heat insulating material to reduce conductive heat losses. Flat plate collectors use both direct and diffuse components of solar radiation and therefore do not necessarily need solar tracking devices. Flat plate collectors, however, have high heat losses which limit their operating temperature to less than 60°C unless the collectors are double glazed or have selective coatings where operating temperatures up to 90°C can be obtained. In a double glazed FPC, the air trapped between the two glass covers minimizes convective and conductive heat losses. Selective coatings, e.g. black chrome, are thin layers that have high absorption of short wave length solar radiation, which comprise most of the incident solar radiation, but low emissivity of long wave length radiations, i.e. infrared radiation, which are otherwise re-emitted from the absorber and lost to the surrounding, i.e. heat lost by radiation, resulting in a reduction in the collector efficiency.

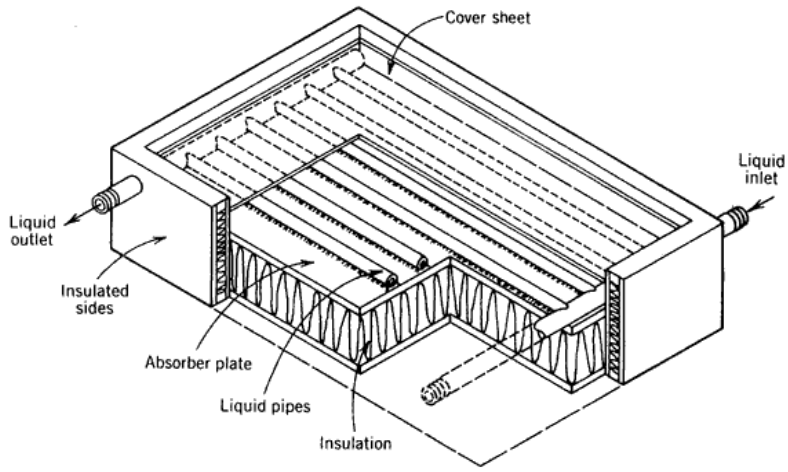

Figure B-1: Typical flat plate collector
Source: (Stine and Geyer, 2001)

Evacuated tube collectors are also non-concentrating solar thermal collectors which can absorb both diffuse and direct solar radiation. However, in these systems the absorber is mounted into vacuum glass tubes to eliminate convective heat losses. For this reason, ETC's have higher efficiency than FPC's and higher working fluid temperatures reaching up to 180°C. The most common type of ETC's use a heat pipe bonded to the absorber plate where the liquid inside, e.g. pure water or methanol, evaporates as the solar radiation is absorbed (*Figure B-2*). A manifold is installed at the top of the evacuated tube where the working fluid is circulated acting as a heat exchanger. The vapour in the heat pipe therefore condenses at the top of the heat pipe while giving its heat to the working fluid through the manifold. However, there are ETC configurations, such as Dewar tubes, where the working fluid is heated directly inside the evacuated tubes. (Kalogirou, 2004, Duffie and Beckman, 2006, Morrison and Rosengarten, 2012)

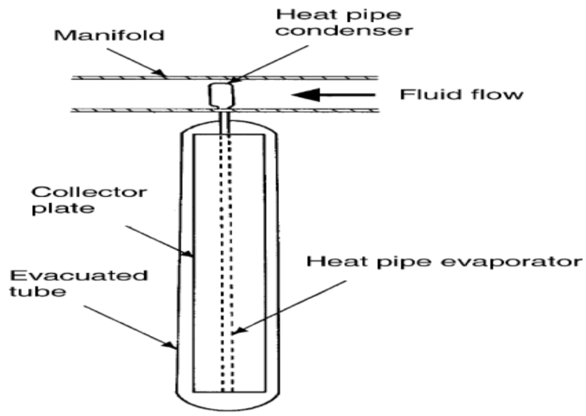

Figure B-2: Schematic showing a heat pipe ETC
Source: (Kalogirou, 2004)

Compound parabolic collectors are a special type of stationary collectors that combine ETC's or simple absorber plates with parabolic reflectors to increase the amount of absorbed incident solar radiation (*Figure B-3*). Accordingly, higher operating temperatures are attained reaching up to 220 °C without the need for solar tracking devices as the reflectors allow the absorber to receive solar radiation at a wider incident angles including diffuse solar radiation. (Kalogirou, 2004, Morrison and Rosengarten, 2012)

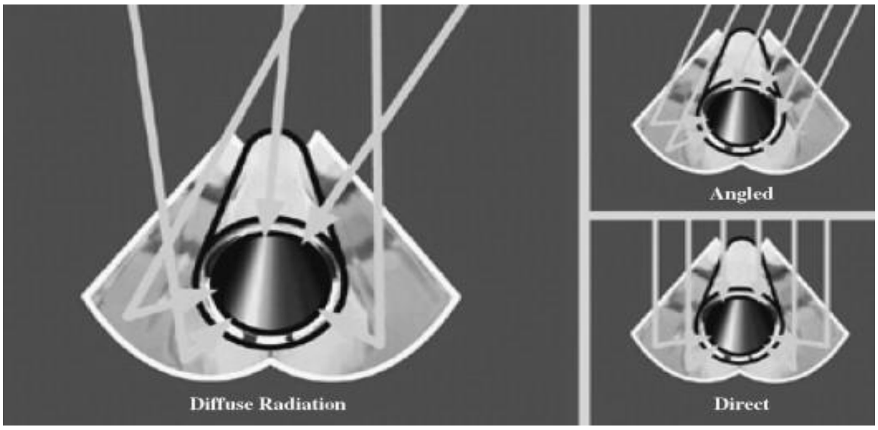

Figure B-3: Schematic showing a compound parabolic ETC
Source: INS-SOLAR (2009) cited in (Ab Kadir et al., 2010)

B-1-2: Non-stationary collectors

This section is based on data obtained from the literature (Kalogirou, 2004, Duffie and Beckman, 2006, U.S. Department of Energy, 2011, Morrison and Rosengarten, 2012). Non-stationary collectors are usually concentrating collectors that use reflective or refractive surfaces, i.e. mirrors or lenses, to focus solar radiation onto a focal line or point receiver to increase the amount of solar radiation energy received per unit area which allows a smaller absorber surface area to be used which also reduces the heat losses. Accordingly, concentrating collectors have high operating temperatures, i.e. up to 1,500 °C, which is not possible with non-concentrating collectors. These high levels of temperature are mainly used for electricity generation and for this reason these systems are usually referred to as concentrated solar power (CSP) systems. Concentrating collectors require single or double axis tracking as they can only use the direct component of solar radiation. Therefore, precise tracking is required to ensure that the solar radiation falls exactly on the absorbing surface. The main types of non-stationary concentrating collectors are PTC's, central receiver power towers, parabolic dishes, and LFR's. Based on a review by Tian and Zhao (2013) of the existing and under construction CSP plants, PTC is the most commonly used CSP technology (71%) followed by power towers (15.7%), LFR's (10.5%) and finally parabolic dishes where only one plant was reported to use this technology.

Parabolic trough collectors (*Figure B-4*) use parabolic trough shaped single axis tracking mirrors which focus direct solar radiation onto a linear receiver carrying the working fluid. The linear receiver is a black tube, usually with selective coating, covered with glass and is placed in the focal zone of the mirrors. Temperatures up to 400°C could be obtained from such systems and are mainly used to produce steam to run conventional turbine generators. Solar to electricity conversion efficiencies as high as 20 to 26% can be obtained from PTC's.

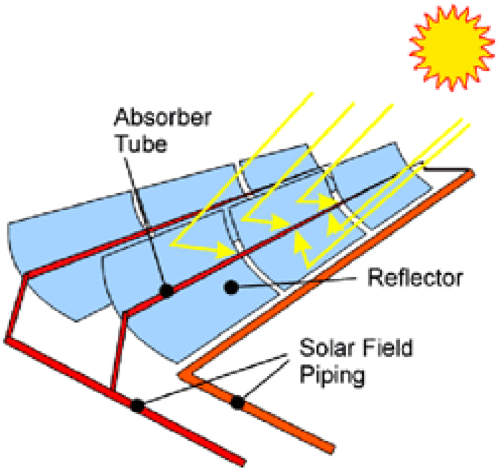

Figure B-4: Schematic showing a PTC
Source: (NREL, 2010)

Central receiver power towers (*Figure B-5*) use an array of heliostats, i.e. two axis tracking individual mirrors, to focus solar radiation onto a receiver located on the top of a tower. The generated heat is absorbed by the working fluid, e.g. molten salt, circulating in the tower. In such systems temperatures up to 1,500 °C could be attained and are used for electricity generation through steam turbines. Central receiver power towers are usually coupled with thermal storage for more flexibility in electricity generation as well as extended operation. These systems are used for large applications where one central receiver system generates more than 10 MW of power. Central receiver power towers have an electricity conversion efficiency of up to 23%.

Figure B-5: A central receiver power tower 10 MW plant installed in California, USA
Source: (Sandia National Laboratories, n.d.)

Parabolic dish collectors (*Figure B-6*) use an array of two axis tracking parabolic mirrors where a receiver is positioned on the focal point of each dish. A Stirling heat engine is usually mounted on the receiver to convert the generated heat energy in the absorber into electrical energy. Accordingly, parabolic dishes are modular and suitable for small scale applications where a single dish can have power capacities ranging from

7 to 25 kW. Such systems have the highest electrical conversion efficiency compared to other CSP's with a record value of 31.4%. In another parabolic dish CSP system configuration, the heat generated from each dish is collected and transferred to a central power generation unit.

Figure B-6: A parabolic dish collectors coupled with Stirling engines
Photo by Randy Montoya (Sandia National Laboratories, 2008)

Linear Fresnel reflectors (*Figure B-7*) are very similar to PTC's where mirrors are used to focus the solar radiation onto a linear receiver. However, instead of using one long mirror, the mirror is segmented into an array of smaller individual mirrors. Therefore, in such systems the mirrors do not have to be parabolic and cheaper flat mirrors are used. The absorber in these systems is separated from the mirrors and therefore is stationary which allows larger absorbers to be used. Furthermore, as small mirrors could be used the structural complexity of the system is reduced and it is also easier to clean the mirrors than in PTC's. Linear Fresnel reflectors are also more able to handle wind loading problems. However, LFR CSP systems have a lower solar to electricity conversion efficiency than systems using PFC's with values ranging from 15 to 25%.

Figure B-7: A linear receiver Fresnel concentrator from a plant installed in New South Wales, Australia
Source: Solar Paces (n.d.) cited in (Murdoch University, 2013)

Table B-1: Summary of main properties of different solar thermal collectors

Collector type	Sun tracking	Maximum useful operating temperature[223]	Solar to electricity conversion efficiency
Flat Plate Collector	Stationary/Non-Tracking	90°C	-
Evacuated Tube Collector	Stationary/Non-Tracking	180°C	-
Compound Parabolic Collector	Stationary/Non-Tracking	220°C	-
Linear Fresnel Reflectors	Single axis tracking	300 °C	15 to 25%
Parabolic Troughs	Single axis tracking	400°C	20 to 26%
Parabolic Dishes	Double axis tracking	1,000 °C	Up to 31.4% for a system using Stirling Engines
Power Towers	Double axis tracking	1,500 °C	20 to 23%

Source: (U.S. Department of Energy, 2011, Morrison and Rosengarten, 2012)

B-1-3: Solar ponds

This section is based on data obtained from the literature (Kalogirou, 2005, Duffie and Beckman, 2006, Morrison and Rosengarten, 2012). Solar ponds are large shallow, i.e. 1 to 6 m deep, mass of water that work similarly to a large horizontal thermal collector where solar radiation is converted to heat raising the temperature of a working fluid. The solar pond is characterized by three main zones. The bottom layers, referred to as the lower convective zone, are where the solar radiation is mainly absorbed. Water in this zone has a constant and a near saturation salinity, typically about 6 times of that of seawater, and its temperature is also constant. The middle layers, referred to as the non-convective zone, which have a thickness from 0.5 to 1.5 m. The water salinity and temperature in this zone increase with depth and this salinity gradient stops natural convection from occurring between the high temperature lower zone and the lower temperature upper zone as the salinity increase offsets the reduction in water density caused by the temperature gradient between both zones. For this reason, the heat absorbed in the lower zone is not transferred to the upper zone, where it would be otherwise lost to the environment by convection and radiation, and is stored in the lower zone which acts as a thermal storage while the middle zone acts as a thermal insulator.

[223] The word useful is used to distinguish the maximum operating temperature from stagnation temperatures which are equivalent to no-load /zero flow temperatures and are higher than the values shown in the table

The top layers are referred to as the upper convective zone and it is a thin zone, i.e. 0.3 m, whose salinity and temperature are almost constant and the latter is close to that of ambient temperature. Mixing and convection occur in this zone due to the effect of wind. For this reason, wind breakers and wave suppressors are required to keep the wind from increasing the upper convective zone's thickness on the expense of the insulating middle zone, which would otherwise reduce the performance of the solar pond. The salinity gradient in the pond also needs to be continuously maintained due to the diffusion of salts from the high salinity to the lower salinity zones which disturbs the salinity gradient in the pond and also reduces its performance. Accordingly, salts need to be continuously added to the bottom layers, while removed from the top layers i.e. adding a concentrated water solution to the pond and removing the dilute solution respectively. Solar ponds also need to have a lined bottom to prevent the high salinity water from seeping into underground aquifers polluting them, as well as preventing heat losses through the seeping water. Temperatures up to 90°C could be obtained from solar ponds which could be used to generate electricity through a Rankine cycle engine, or to drive a desalination process. (Kalogirou, 2005, Duffie and Beckman, 2006, Morrison and Rosengarten, 2012)

B-2: Photovoltaic Systems

Photovoltaic (PV) cells are devices used to directly convert solar radiation into electrical energy. They are made of semi-conductor materials where silicon is the most widely used material but other semi-conductor materials such as gallium arsenide, copper indium-gallium diselenide and cadmium telluride are also used. A typical silicon based PV cell has two layers: a very thin top layer, in order of 1 um thick, which is doped with phosphorous atoms and is referred to as the N- junction or the emitter; and a thick layer, in order of 300 um thick, which is doped with boron atoms and is referred to as the P-junction or the base. Phosphorous atoms in the N-junction make covalent bonds with silicon atoms and because they have 5 electrons in their valence band compared to 4 for the silicon atoms, the extra electron easily breaks free, i.e. move to the conduction band, at room temperature. Therefore, the N-junction is dominated by free electrons. Conversely, the boron atoms in the P-junction have only 3 electrons in the valence band and therefore after bonding with silicon atoms, an empty space is created. This empty space is waiting to receive an electron to complete the covalent bond and is thus considered to be positively charged and referred to as a hole. The P-Junction is therefore dominated by positively charged holes. When both junctions are connected, the electrons in the N-junction diffuse to the P-Junction and the holes in the latter diffuse to the former. Both electrons and holes therefore move leaving behind exposed ions which are fixed to the lattice structure. These oppositely charged ions create an electrical field which opposes the diffusion of electrons and holes between the junctions and creates a charge free region referred to as the depletion region[224]. When solar radiation falls on the surface of the PV cell, some of the incident photons which have energy higher than the band gap energy[225] of silicon will be absorbed generating electrons in the conduction band and a corresponding hole in the valence band. If the generated electron-hole pairs are within the depletion region or close to it, the electrical field will swipe these charges and therefore the electrons could reach the metal contact on the top of the cell then move to the external circuit generating current while the holes move towards the cell's rear metal contact waiting to recombine from the electrons coming from the external circuit. (Honsberg and Bowden, 2013)

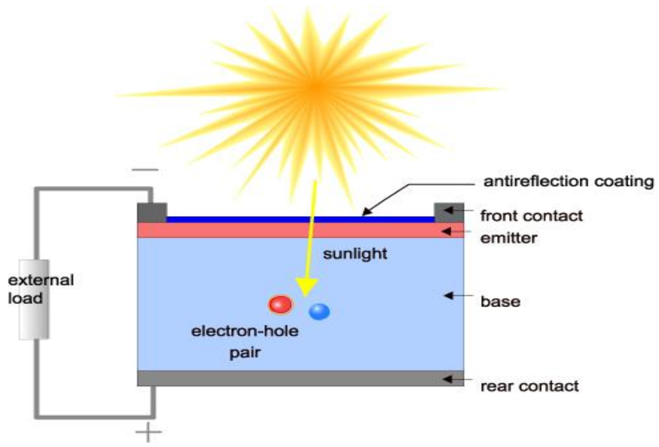

Figure B-8: Schematic showing the basic operation of a photovoltaic cell
Source: (Honsberg and Bowden, 2013)

Several PV cells are connected together, e.g. 36 or 72 cells connected in series, and are typically encapsulated between two Ethyl Vinyl Acetate (EVA) layers, a Tedlar layer at the bottom and a glass cover at the top to provide electrical isolation as well as mechanical and corrosion protection. This whole set is referred to as a PV module.

Photovoltaic based technology comprises non-concentrating PV, PVT, and CPV systems.

[224] Region depleted of electrons
[225] Energy level required to excite the electrons

B-2-1: Non-concentrating PV systems

Non-concentrating PV systems are typically used for roof mounted residential grid connected systems, standalone systems in remote areas, and utility scale power plants. In such systems, the PV modules are usually stationary but some systems use tracking devices to enhance electricity production. There are three main types of PV cells used in commercial modules in non-concentrating PV systems: mono-crystalline cells, poly-crystalline cells and amorphous silicon cells.

Mono-crystalline cells have the highest conversion efficiency due to their highly ordered crystal structure, but are the most expensive as they are slow to manufacturer. Poly-crystalline cells are the most widely used type and they are cheaper than mono-crystalline cells as they are easier to manufacture. However, they have less ordered lattice structure than mono-crystalline cells as they are made of many small crystals attached together instead of one single crystal as in the latter. Therefore, poly-crystalline cells have more defects because of the boundaries between the crystals, referred to as grain boundaries, decreasing the amount of light generated electron-hole pair that can be effectively used. The typical efficiency of mono-crystalline commercial modules[226] range from 13.3 to 15.9% compared to 9.5 to 15.3% for poly-crystalline modules, obtained from The University of Queensland website (2013), but some commercial mono-crystalline and poly-crystalline modules have efficiencies reaching up to 21.5%[227] and 16.3% respectively[228]. Amorphous silicon cells are very thin PV cells, i.e.1 to 50 um thick, and therefore are classified as thin film cells. These cells have a better photon absorption capability and for this reason can be made thinner thus using less material. Amorphous silicon cells are therefore cheap, and easier and faster to manufacture. However, such cells have no long range order in the lattice structure where the silicon atoms are randomly arranged creating dangling, i.e. incomplete, bonds which reduce the collection efficiency of the light generated electron-holes. Therefore the amorphous silicon modules have low efficiency in the range of 6% obtained from The University of Queensland website (2013). Other thin film modules using CIS or CdTe as semi-conductor material have better efficiencies than amorphous silicon modules with values

---

[226] Module efficiency is lower than cell efficiency mainly because not all the module area is covered with PV cells and due to losses in metal contacts connecting the cells

[227] E.g. SUNPOWER X Series Modules. Datasheet: http://us.sunpowercorp.com/support/datasheets/

[228] E.g. Phono Solar Diamond Series. Datasheet: http://www.phonosolar.com/uploadfiles/solar/235-265_131023080637.pdf

in the range of 11% (U.S. Department of Energy, 2011), and values as high as 13.8% are obtained such as that of the STION STN 150 model[229] which is a CIGS thin film module. For more details in each type of silicon based solar cells please see Wenham et al. (2006) and Stapleton et al. (2009).

B-2-2: Photovoltaic thermal collectors

Photovoltaic thermal collectors are a special configuration of PV modules which make use of the extra heat generated by the modules. Not all of the incident solar radiation on the PV module generates electricity but the majority is absorbed by the module material generating unwanted heat. This heat raises the temperature of the PV module and lowers its conversion efficiency. For example, typical poly-crystalline modules have 0.5% power reduction for every 1°C increase above 25°C, the standard test condition[230] temperature (Stapleton et al., 2009). Therefore, in PVT systems air or water are used to absorb this extra heat reducing the module's operating temperature thus increasing its efficiency. In the meantime, the air or water gets pre-heated before being used in another process. In this case, a larger fraction of the incident solar energy is converted into useful energy increasing the overall conversion efficiency per unit area compared to a system using separate PV modules and FPC's to generate electricity and heat respectively (Bambrook, 2011) which saves in the amount of material used and potentially the costs.

Photovoltaic/thermal collectors generate more solar energy per unit surface area than a combination of separate photovoltaic panels and solar thermal collectors.(Elswijk et al., 2004)

The additional thermal output that is provided from the PVT systems makes them cost effective compared to separate PV and thermal units of same total used aperture surface area (Tripanagnostopoulos et al., 2004)

B-2-3: Concentrating PV systems

In concentrating Photovoltaic systems solar radiation is concentrated using mirrors or lenses on a focal zone where PV cells are located. Therefore the amount of incident

---

[229] Datasheet: http://www.stion.com/wp-content/uploads/2013/03/Stion-Product-Data-Sheet-STN-Module-135-150.pdf

[230] 1000 W/m^2 of incident radiation, 25°C cell temperature, and air mass of 1.5

solar radiation per unit area is significantly increased allowing the use of a much smaller area of PV cells. In this case, high efficiency and more expensive PV cells such as tandem solar cells, also called multi-junction cells, could be used. Tandem cells are PV cells made of different materials attached together where each cell has a different band gap. In this case, the tandem cells allow a more efficient absorption of solar radiation compared to typical solar cell which has only one band gap allowing a limited portion of the light spectrum to be absorbed. Accordingly, a CPV module has much higher efficiencies than typical PV modules with a commercial world record efficiency of 35.9% at standard test conditions (Gormley, 2013).

There are three main configurations of CPV systems. Some systems use parabolic dishes with tandem PV cells located at the focal point of each dish such as the systems manufactured by SolarSystems (SolarSystems, 2011). Another configuration is similar to the central receiver power tower where the PV cells are located at the top of the tower, such as the systems manufactured by RAYGEN (RAYGEN, 2013). In the last configuration, instead of reflecting sun radiation onto the PV cells which are installed in front of the reflectors, Fresnel lenses are used to refract sun radiation onto the PV cells installed behind each of the lenses, such as the systems manufactured by Soitec (Soitec, 2013) and AMONIX (AMONIX, 2012b).

Figure B-9: The CS500 CPV System manufactured by SolarSystems
Source: (SolarSystems, 2011)

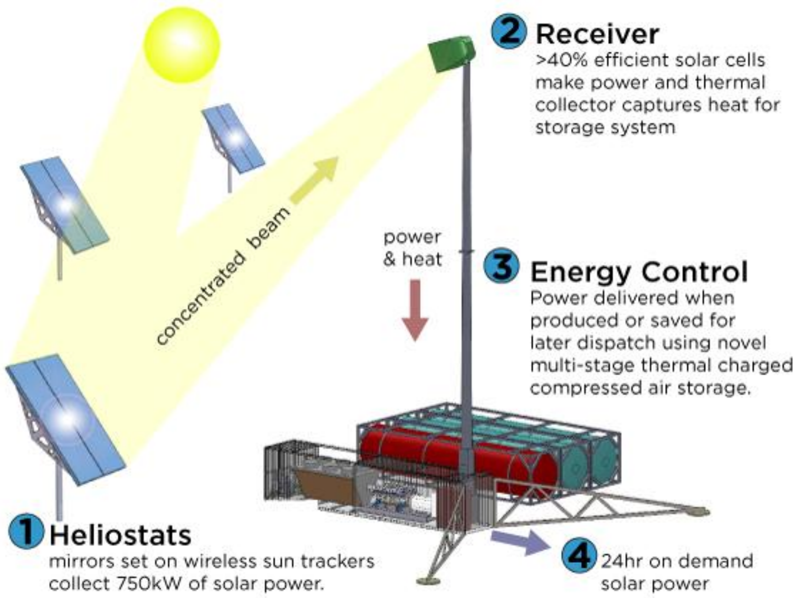

Figure B-10: Schematic showing a central receiver CPV type manufactured by RAYGEN
source: (RAYGEN, 2013)

Figure B-11: A CPV System using refractor Fresnel Lenses
Source: (AMONIX, 2012a)

Appendix C: Review of Desalination Processes

C-1: Major Desalination Processes

C-1-1: Multi-stage flash distillation

Multi-stage flash distillation is one of the most widely used desalination processes producing approximately one quarter of the worldwide desalinated water (IDA, 2013). The MSF process is typically used for medium and large scale applications (Buros, 2000). Nevertheless, the process seems to be gaining more market in small scale applications where approximately 21% of the MSF plants reported in the International Desalination Association (IDA) (2013) inventory are small scale plants with capacities ranging from 96 to 1,000 m^3 per day.

The following information on the MSF process is obtained from the literature (Howe, 1974, Porteous, 1975, Buros, 2000, Wade, 2001, The National Reserach Council, 2004, Eltawil et al., 2009, Cotruvo et al., 2010, Al-Karaghouli and Kazmerski, 2013). The MSF desalination plant consists of up to 40 vessels referred to as stages, each operating at progressively lower pressure. Each vessel comprises two chambers: the evaporator/flash chamber located at the bottom of the vessel and it is where the feed water evaporates; and the condenser chamber located at the top of the vessel and it is where the produced steam condenses. The feed water, usually seawater, enters into the condenser chamber of the last stage then flows through the condenser chambers of the other stages acting as the coolant liquid. In the meantime, the feed water is preheated by recovering the heat of condensation in each stage reducing the external thermal energy required to heat the feed water. The feed water exiting the condenser chamber of the first stage enters the brine heater vessel. This vessel contains a heat exchanger where the feed water is heated under pressure to a near saturation temperature, referred to as the top brine temperature and ranges from 90 to 110 °C, by using an external steam supply. The feed water then enters into the first stage through an orifice in a throttling process which causes a sudden drop in pressure. The pressure therefore becomes less than the saturation pressure of the water at the corresponding top brine temperature hence a small part of the bulk feed water suddenly evaporates, i.e. flash evaporates, to reduce the water's temperature to match the new saturation conditions at the lower pressure. The brine in the first stage, now at lower temperature, enters the next stage through an orifice undergoing a further reduction in pressure and the same process is repeated. In each stage the generated steam condenses on the surface of the heat exchanger tubes in the condenser chamber and the distilled water is collected from trays located beneath the heat exchanger tubes in each stage.

The thermal efficiency of MSF plants increases with higher top brine temperatures, however the maximum temperature is limited by scale formation particularly calcium sulphate scaling. Increasing the number of stages in the MSF process increases its performance ratio (PR) which means that less external heat will be required to produce the same amount of distilled water. Nevertheless, increasing the number of stages increases the capital cost to the point where a further increase in the number of stages becomes uneconomical and for this reasons MSF desalination plants typically consist of 15 to 25 stages.

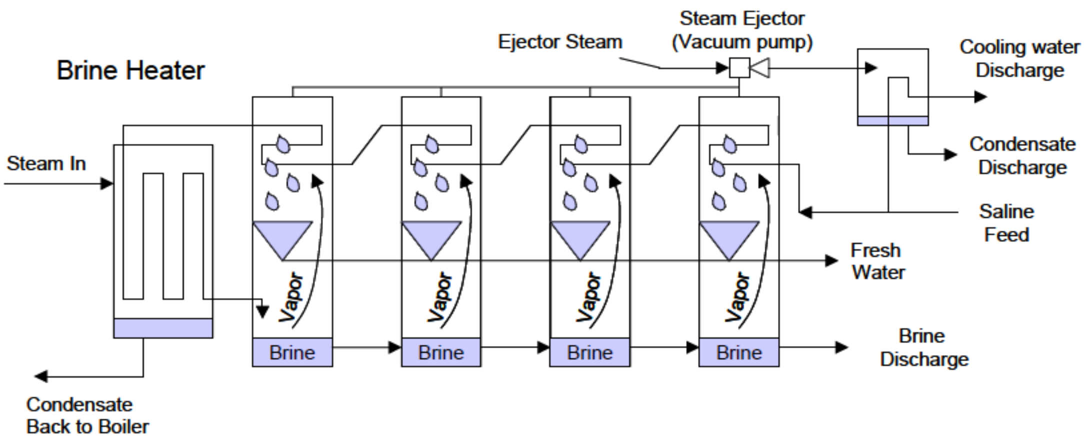

Figure C-1: Schematic showing a typical MSF process
Source: (Miller, 2003)

C-1-2: Multi-Effect distillation

Multi-Effect distillation is one of the oldest desalination processes that has been used since 1900 mainly in chemical industry then in naval vessels (Reddy and Ghaffour, 2007). However, at that time MSF gained more popularity than the MED process as it was less prone to scaling problems. The interest in the MED process was then renewed since the 1980's due to improved designs that allowed the operation at lower temperatures minimizing scaling problems (Buros, 2000). Nevertheless, the technology still has a small market share in the desalination industry where based on the IDA inventory (2013), the process's share of overall worldwide desalinated water is only 8%. The MED process is typically used for small to medium scale applications consisting 48% and 43% respectively of the plants reported in the IDA inventory. The following information on the MED process is obtained from the literature (Howe, 1974, Wade, 1993, Buros, 2000, Wade, 2001, Watson et al., 2003, Reddy and Ghaffour, 2007, Eltawil et al., 2009). Multi-Effect Distillation plants work similarly to MSF plants where evaporation and condensation occur in successive vessels, referred to as effects, progressively kept at lower pressure. The heat required for evaporation is also supplied by an external steam supply. However, in an MED plant the steam generated in each vessel is used to evaporate the feed water in the following vessel instead of condensing in the same vessel as in MSF. The steam of the previous effect enters the condensing side of the heat exchange tubes of the next effect and loses its latent heat to the feed water sprayed over the surface of the heat exchanger tubes. The effect is kept at lower pressure than the previous one such that the latent heat transferred to the sprayed feed water is enough to raise the water's temperature beyond the saturation point and evaporate. The same process is repeated in each effect except the first one where the feed water is heated through the external steam supply. In the last effect, the generated steam is condensed in a separate heat exchanger, referred to as the main condenser, where the feed water is used as the coolant. The distilled water is then collected from each effect and the main condenser.

The top brine temperature of the MED process is usually less than MSF to prevent scaling problems and it ranges from 60 to 70 °C but some designs can operate at temperatures up to 110 °C. While, the MED process needs to operate at low temperatures, it still has a high PR as spraying the feed water over the surface of the heat transfer tubes increases the heat transfer rate. The PR of the MED process is also proportional to the number of effects but is limited by the costs and therefore an MED plant will typically consist of 8 to 16 effects.

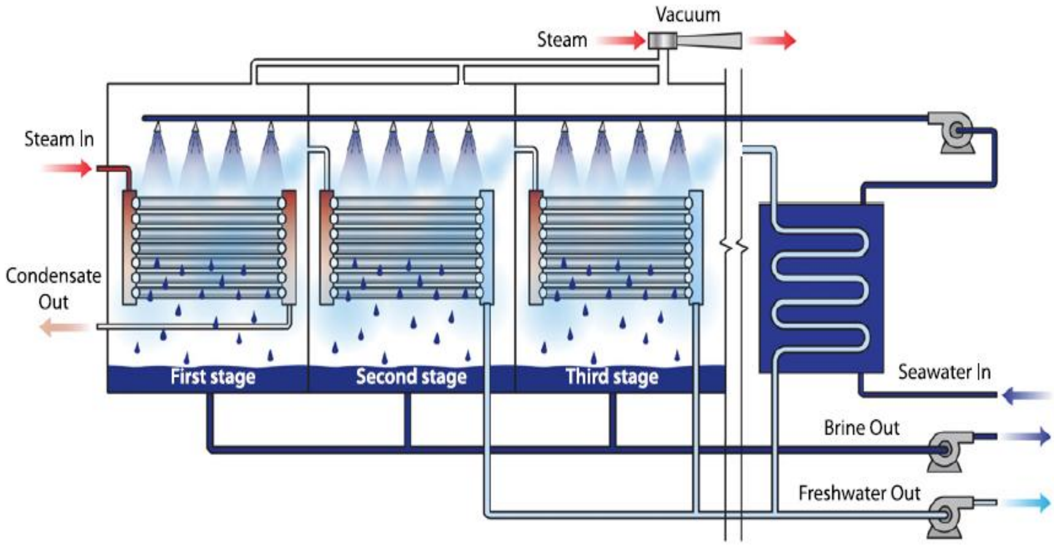

Figure C-2: Schematic showing a typical MED process
Source: (Al-Karaghouli and Kazmerski, 2013)

C-1-3: Vapour compression

Vapour compression is also a distillation process and is usually combined with MED plants to increase the latter's PR. Approximately 60% of the reported MED plants in the IDA inventory (2013) are combined with a VC process. Conversely, desalination plants using only a VC process are rarely used, with only 3 plants using this process out of approximately 13,000 desalination plants currently operating worldwide.

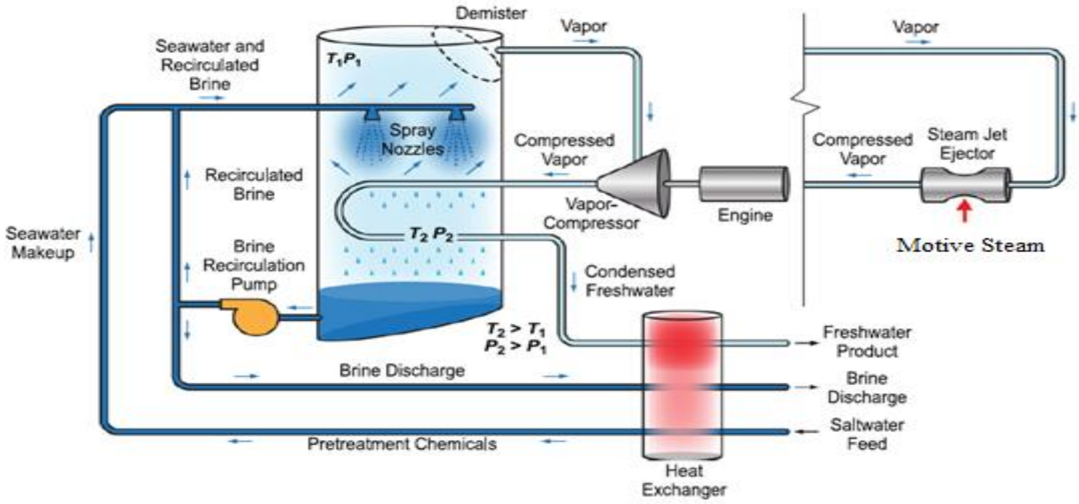

Figure C-3: Schematic showing a typical VC process driven by either a mechanical or a thermal compressor
Source: modified after (Al-Karaghouli and Kazmerski, 2013)[231]

[231] Al-Karaghouli and Kazmerski (2013) indicated that a high pressure steam is used in the ejector while usually a low to medium pressure steam is used and therefore the high pressure steam indicated in the original figure was replaced with motive steam

The following information on the VC process is obtained from the literature (Howe, 1974, Darwish and Al-Najem, 1987, Buros, 2000, Miller, 2003, Watson et al., 2003, Kalogirou, 2005). The VC plant, similar to an MED plant, consists of one or more vessels kept at progressively lower pressures. The feed water enters into the vessels and is sprayed over the surface of the heat exchanger tubes inside which steam is flowing. The steam loses its heat to the feedwater and condenses while part of the feedwater evaporates such that the water saturation pressure matches the low pressure inside the vessel. The process also operates at low temperatures similar to MED. In the VC process, however, the main heat of evaporation is obtained by compressing the steam generated in the last effect then reintroducing it into the first effect, instead of using a heat exchanger to supply the heat required for the first effect from the external steam supply. The VC process is carried out either through mechanical compression, i.e. MVC process, or through thermal compression, i.e. TVC process.

The MVC process usually consists of one effect as adding more effects does not increase the PR. In this case, the steam generated in the effect is compressed through a mechanical compressor and reintroduced inside the tubes of the heat exchanger of the same effect to evaporate more feed water. This recycled steam then condenses and becomes a part of the distilled water. It should be noted that an external steam supply is initially required to start the MVC process. Conversely, the TVC process can have more than one effect as its PR increases with the number of effects. In the TVC process, steam ejectors use a low to medium pressure motive steam, supplied by a boiler or a cogeneration turbine, to remove and compress part of the steam generated in the last effect, as it mixes with the motive steam, before reintroducing it in the first effect. The TVC process is usually combined with MED and is used for medium to large scale applications with capacities ranging from 10,000 to 30,000 m^3 per day; while the MVC process is mainly used by itself for small and medium scale applications with typical plant sizes up to 3,000 m^3 per day because of compressor capacity limitations. In a hybrid MED/TVC system, the TVC process is used to recover the low temperature steam in the last MED effect to increase the overall system efficiency. It should be noted that some authors such as Li et al. (2013), considered the MVC and TVC processes as heat pump processes and discussed other methods such as absorption heat pump and adsorption heat pumps that could be also used to recycle the steam in the last effect of the MED process.

C-1-4: Electro-dialysis

Electro-dialysis is a membrane desalination process mainly used for BW desalination (Abu-Arabi, 2007, Eltawil et al., 2009). While it is a promising technology that was commercialized a decade before the RO process and used to compete with the latter in 1970's (Reahl, 2006), it currently has a low share of the desalination market producing only 3% of the worldwide desalinated water (IDA, 2013). The ED process is mostly, i.e. 94.5% of the plants, used for small and medium scale applications.

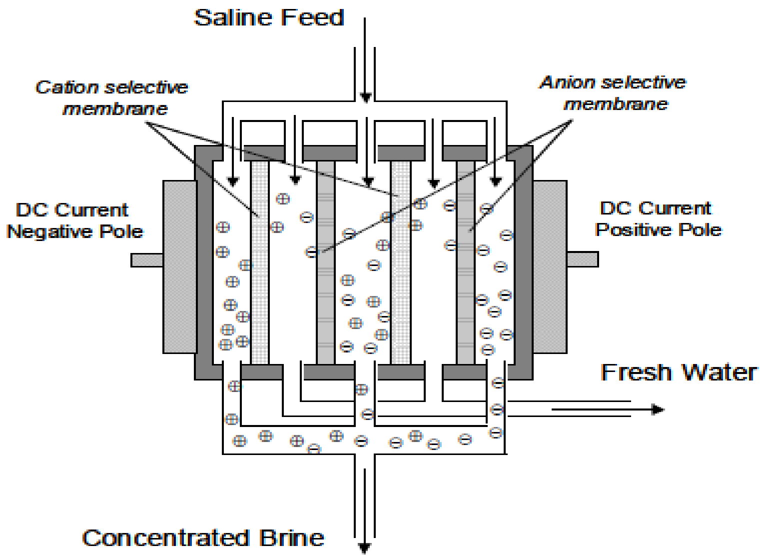

Figure C-4: Schematic showing a typical ED process
Source: (Miller, 2003)

The ED unit consists of two electrodes and several hundred pairs of closely spaced anion and cation selective membranes between which the feed water flows. A potential difference is applied across the membrane pairs such that the generated electrical field moves the anions and the cations in the feed water towards the positive and the negative electrodes, respectively. Due to the presence of successive anion and cation selective membranes, as the ions move they eventually become trapped in one channel, i.e. the brine, while the adjacent channel is mostly depleted of ions, i.e. the desalinated water. The process is therefore referred to as electro-dialysis as the diffusion of salts through a membrane, i.e. the dialysis process, is forced by an electrical field. (Howe, 1974, Porteous, 1975, Buros, 2000)

Electro-dialysis Reversal (EDR) is another configuration of ED where the polarity of the applied voltage is regularly reversed, i.e. several times an hour, such that the desalinated water channel becomes a brine channel and vice versa. In this case, the ions are kept from accumulating on the membrane surface limiting inorganic scaling and fouling occurrences which increases the lifetime of the membrane as well as minimizing pre-treatment requirements. (Buros, 2000, Miller, 2003).

C-2: Minor Desalination Processes

C-2-1: Freezing

Freezing is a desalination process that is based on phase change by freezing the salty water using a typical refrigeration cycle driven by compressors. In this case, ice crystals form and the salts are naturally excluded. The salts are then removed from the frozen mixture and the ice is melted to obtain fresh water. (Buros, 2000, Miller, 2003)

C-2-2: Humidification-dehumidification

Humidification-dehumidification is a thermal desalination process that involves water evaporation and condensation similar to MSF and MED. However, in an HDH process surface evaporation at atmospheric pressure occurs instead of water boiling. Therefore, the process operates at low temperatures requiring a low grade source of heat and for this reason HDH processes are usually driven by solar energy. The second factor that characterizes the HDH process from MSF and MED, is that air is the medium used to carry the water vapour from the evaporation zone, i.e. humidification, to the condensation zone where the air is cooled to extract the water vapour i.e. air dehumidification.

Single effect solar stills use an HDH process and they are the simplest method of desalination. A Single effect solar still consists of a basin with sloping transparent glass or plastic cover and a black lined bottom. The solar radiation falling on the basin is absorbed by the feed water and the bottom of the basin, increasing the temperature of the former hence its vapour pressure. Accordingly, the feed water surface evaporation is significantly enhanced and the air between the feed water and the glass cover becomes humidified and warmed. The warmed air then starts to circulate by natural convection towards the inner side of the relatively cool glass cover and part of its water vapour content condenses. The produced water is then collected from the base of the cover. (Howe, 1974, Miller, 2003)

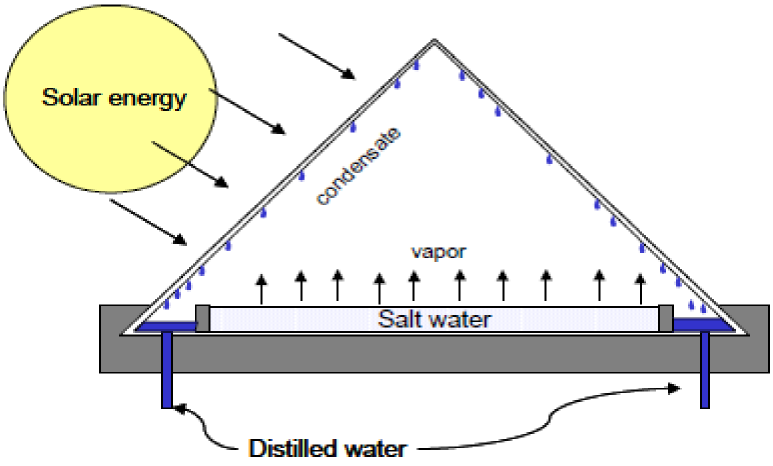

Figure C-5: Schematic showing a typical single basin solar still process
Source: (Miller, 2003)

A single effect solar still has a low efficiency ranging from 30 to 45%[232] with productivities of less than 5 $l/d/m^2$ of still area (Al-Hallaj et al., 1998, Abu-Arabi, 2007, Zejli and Elmidaoui, 2007) with a large SHC of about 1,950 kWh/m^3 (Joyce et al., 2001). The low efficiency of single basin solar stills is mainly due to the high heat losses from the glass cover and because the latent heat of condensation could not be recovered (Parekh et al., 2004). Some single effect solar stills are coupled with solar thermal collectors, referred to as active solar stills, to increase the amount of heat transferred to the feed water. The feed water could therefore be heated to higher temperatures increasing the productivity of the solar still with values that could be 24% higher than that of passive solar stills (Fath, 1998).

The low thermal efficiency of single effect solar stills led to the development of multi-effect solar stills. Multi-effect solar stills allow the reuse of the latent heat several times. In these systems, the latent heat of condensation of one effect is used to evaporate the feed water in the following effect similar to an MED process. The multi effect solar stills are therefore more thermally efficient than single effect stills (Goosen et al., 2000) with PR's[233] of up to 80% higher (Parekh et al., 2004). For a review on different configurations of multi effect solar stills see (Fath, 1998).

---

[232] The authors did not define the efficiency represented by those values but it is normally the ratio between the actual water produced and the amount of fresh water that could be produced if all the energy of the incident solar radiation contributed to evaporation as defined by Goosen et al. (2000)

[233] Defined here as the ratio between the energy used during distillate production and the total energy input

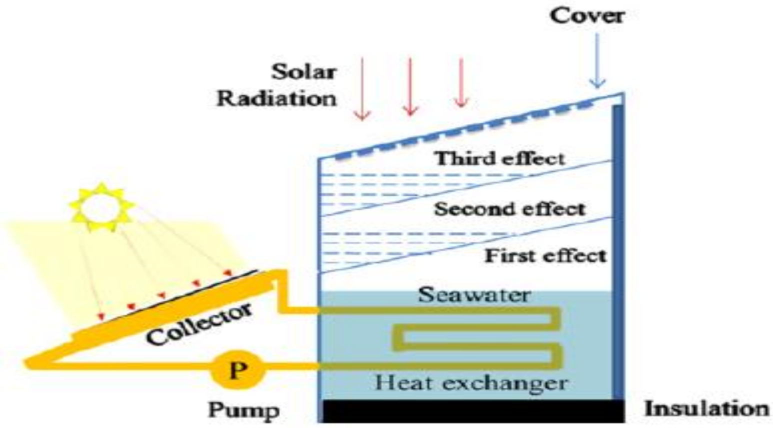

Figure C-6: Schematic showing a multi-effect solar still process
Source: (Li et al., 2013)

Multi-effect humidification[234] is another configuration of the HDH process and is sometimes directly referred to as an HDH process. The MEH process is different than solar stills in that it uses separate sections for evaporation and condensation. Accordingly, MEH plants can have higher capacities than solar stills whose capacity is limited as both the evaporator and the condenser are integrated together in one unit (Al-Hallaj et al., 1998).In typical solar driven MEH systems, such as the ones discussed in Müller-Holst et al. (1998), Al-Hallaj et al. (1998) and Bacha et al. (2007), the feed water passes through a heat exchanger in the condensation chamber to recuperate the latent heat of the condensing vapour. The warmed feed water is then heated by solar collectors before entering the evaporation chamber where a circulating air flow carries the water vapour to the condensing chamber. The humidified air is circulated to the condenser chamber either through natural convection or fan forced convection. The water vapour in the air then cools down in the condenser chamber and part of it condenses producing fresh water. The MEH process has two main configurations: the open-water/closed-air cycle and the open-air/closed-water cycle. In the first, a continuous flow of feed water enters the condenser chamber while the air keeps recirculating in a closed cycle carrying the water vapour from the evaporation to the condensation chamber in a repeating process of humidification and de-humidification. The second MEH configuration is a batch process used to obtain higher RR's, where the feed water keeps recirculating between the evaporation and condensation chambers. Meanwhile, a continuous flow of air enters the evaporator chamber to cool the water exiting the chamber so it will still be

[234] Although there is only one stage in this system, the term "multi effect' is used to denote that the process has a gain output ratio, i.e. the ratio between the heat required by the process to the heat used in distillate production, larger than 1 (Parekh et al., 2004)

able to condensate the water vapour in the condensation channel. The dehumidified air is then discharged outside the unit instead of being recirculated as in the open-water/closed-air configuration.

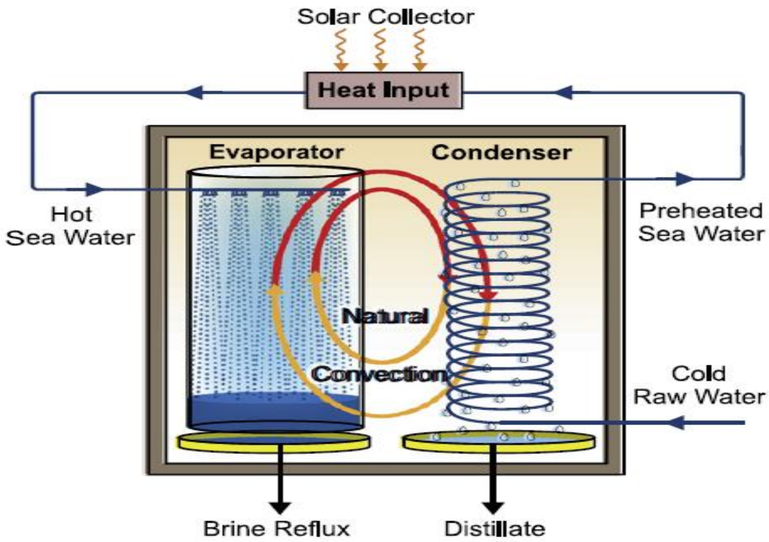

Figure C-7: Schematic showing an open-water/close air cycle MEH
Source: (Al-Karaghouli and Kazmerski, 2013)

Multi-effect humidification have higher productivities than single effect solar stills where the productivities of several solar MEH plants without thermals storage built in the Canary Islands in Spain were 11.8 l/m^2/d (Parekh et al., 2004). Higher nominal productivity of about 35.7 l/m^2/d were also reported by Müller-Holst (2007) for a demonstration MEH plant with thermal storage that was installed in Jeddah in Saudi Arabia, however its actual productivity was not reported.

A review of other configurations of solar HDH processes and different work carried out to improve the efficiency of different HDH processes can be found in (Fath, 1998), (Goosen et al., 2000), (Miller, 2003), (Parekh et al., 2004), and (Kalogirou, 2005).

C-2-3: Forward osmosis

The FO process is based on the osmotic phenomenon similar to RO. However, instead of pressurizing the feed water to overcome the osmotic pressure, the osmotic phenomenon itself is the driving force for desalinating the water. This is achieved through adding a solute to the pure water, referred to as the draw agent, such that the water concentration becomes higher than that of the feed water. Accordingly, the feed water will cross the semi-permeable membrane to dilute the water on the permeate side and all the contaminants are blocked by the membrane. The remaining draw agent in the filtered water is then removed. The FO process is, however, an emerging technology that is still under research and development and therefore there is still a limited work on using it in desalination. (Cath et al., 2006, Khaydaro et al., 2007, Zhao et al., 2012)

C-2-4: Other processes associated with desalination

There are other novel desalination technologies that were not reviewed in this study. These technologies are briefly reviewed in Miller (2003), Younos and Tulou (2005) and Li et al. (2013) and are mostly still in a research and development stage. There are also other methods that are used to obtain fresh water but they may not be considered as desalination processes such as the processes that extract the humidity in the atmosphere through, among others, cooling the air or using desiccants or adsorption material which are briefly reviewed in Parekh et al. (2004).

Other processes such as ion exchange and electro-deionization are used to partially treat the feed water either as a pre-treatment for desalination processes especially RO or as a post-treatment for water polishing to obtain ultra-pure water (Miller, 2003, Younos and Tulou, 2005, Vertex Hydropore, 2010, DOW Chemical Company, 2013a). However, while in theory such processes could be used for desalination they are not economical for such application.

There are also other pressure driven membrane treatment technologies such as ultra-filtration (UF), pore size ranging from 0.005 to 0.1 μm, and micro-filtration (MF), pore sizes from 0.1 to 5 μm, that are mainly used for pre-treating the feed water, mainly before an RO process. These membranes remove, through a screening separation mechanism, suspended solids, colloids, bacteria, and other organic content which can foul or clog the RO membranes but cannot remove dissolved solids due to the large pore size of the membrane (Pinnekamp and Friedrich, 2006, Crittenden et al., 2012d).

Appendix D: Guidelines for Irrigation Water

While BW is not suitable for drinking without proper treatment, it might be directly used in irrigation. The suitability of water for irrigation purposes depends on its salinity, sodicity and the toxic effect of some chemical substances, which are discussed in this section and are based on the FAO guidelines (Ayers and Westcot, 1994).

D-1: Effect of Water Salinity

The use of high salinity water in irrigation increases the amount of salts accumulating at the plant root zone impeding water absorption by the plant as more energy is required to extract relatively salt free water from the higher salinity water available in the soil. Accordingly, the plant is less able to use the available water which could result in a water stress affecting the plant growth and hence its yield. (Ayers and Westcot, 1994, Pearson, 2009).

Table D-1 shows the effect of water salinity on the yield of some of the suggested HVLWC crops to be cultivated in Egypt. As observed from *Table D-1*, water with salinities less than 450 mg/l (EC<0.7) is generally suitable for all crops while higher water salinities impose restrictions on crop selection depending on the salinity level. For example, salt tolerant crops can tolerate water salinities up to 5,200 mg/l without any reduction in the yield compared to salt sensitive crops which would experience 50% or more yield reduction if irrigated with the same water. Water with salinities higher than 8,000 mg/l (EC>8.7) is expected to cause more than 25% yield losses to all crops and is considered in this study to be unsuitable for irrigation.

Table D-1: FAO irrigation water salinity guidelines for different crops when sprinkler irrigation is used

High value Low water consuming Crops	Salt tolerance	Water Salinity Limits in mg/l (EC in ds/m)[235,*]		
		No Effect	**10% to 25% yield loss**	**> 50% yield loss**
Bean[236], Onions, Sesame,	Salt Sensitive	450 (<0.7)	770-1,220 (1.2-1.9)	1,920 (>3)
Cucumbers, Broad Bean, Grapes, Maize, Melon, Potatoes, Tomatoes	Moderately Sensitive	1,220 (<1.9)	1,730- 2,500 (2.7-3.9)	4,960 (>6.2)
Cowpeas, Figs, Squash Zucchini,	Moderately Tolerant	2,500 (<3.9)	3,200-5,440 (5.0-6.8)	7,840 (>9.8)
Cotton	Tolerant	5,200 (<6.5)	6,320-8,000 (7.9-10)	10,960 (>13.7)

*The FAO guideline values are based on the study by Maas (1994) cited in (Ayers and Westcot, 1994)

It should be noted that the FAO water salinity guideline values shown in *Table D-1* are not absolute tolerances and will vary based on soil conditions and cultural practices. The guideline values apply for crops irrigated by sprinklers, where water is applied infrequently[237]. This suits the context of this study given that in areas away from the Nile delta and valley the use of the water efficient sprinkler and drip irrigation is mandatory (FAO AQUASTAT, 2005). However, the guideline values might be too restrictive when drip irrigation is used as this method allows the use of higher salinity water than sprinkler irrigation without compromising the crop yield[238] (Brouwer et al., 1988). This is especially true for crops that are sensitive to salt accumulation on the

[235] FAO salinity guideline values are based on the following conditions: 1) 15 to 20% leaching factor 2) good drainage condition with no uncontrolled shallow water table present within 2 metres of the surface such that the salts accumulating in the crop root zone comes only from the irrigation water. 3) Soil textures ranging from sandy-loam to clay-loam 4) Arid and semi-arid climates 5) Crop water uptake profile was based on the average uptake of different crops where 40% of water is absorbed from the upper quarter of root zone, and 30%, 20% and 10% from the other three quarters

[236] Phaseolus vulgaris

[237] Crop gets its water needs between irrigations from the stored water in the soil

[238] The frequent application of water in drip irrigation allows the plant to directly use the readily available applied water instead of the higher salinity soil water that exists deeper in the root zone. Conversely, with infrequent irrigation methods, i.e. sprinkler irirgation, water becomes depleted in the low salinity upper root zone with extended irrigation intervals and therefore the plant is forced to use the more saline water in the soil. Moreover, as less amounts of irrigation water is applied in drip irigation, less salts accumlate in the soil and therefore higher salinity water could be used. (Ayers and Westcot,1994, Alam et al., 2007)

leaves (section *D-3*); otherwise not much variation in the salinity limits is expected with salt tolerant crops (Hanson and May, 2011). The guideline values also apply for arid and semi-arid climates, which is the case in Egypt. Moreover, the guideline values are based on a 15 to 20% leaching factor, which is the percentage of the applied irrigation water that percolates below the root zone and is directly proportional to the amount of applied irrigation water. However, leaching factors may vary according to the salinity of the water used in irrigation. For example, higher leaching factors allow the use of higher salinity water than the values shown in *Table D-1*, as the additional amount of irrigation water increases the portion of the accumulated salts that leaches deeper into the ground away from the plant roots preventing them from accumulating at the root zone. In contrast, using lower leaching factors makes the crops more sensitive to irrigation water salinity.

Finally, it should be noted that while the crops can handle more saline water when drip irrigation is used, high water salinity cause clogging issues with drip irrigation equipment especially with salinities exceeding 2,000 mg/l where severe clogging issues are expected (Nakayama, 1982 cited in Ayers and Westcot, 1994).

D-2: Effect of Sodium in Irrigation Water

The presence of high sodium concentrations relative to those of calcium and magnesium in irrigation water increases the soil sodicity. An increase in soil sodicity causes soil dispersion which reduces the water infiltration rate in the upper surface of the soil hence reducing the water supply to the crop. Soil dispersion occurs as the large sodium ions disrupt the binding forces between the soil clay particles and disperse them blocking the soil pores and reducing the soil permeability. In contrast, calcium and magnesium ions are smaller in size and tend to from divalent bonds and therefore do not affect the binding forces between the clay particles. The tendency of irrigation water to cause soil dispersion is determined by the Sodium Adsorption Ratio (SAR) which compares sodium ion concentrations to those of calcium and magnesium given that the latter two compete with the sodium ions to occupy spaces between the clay particles. However, as the water salinity helps to aggregate the soil fine particles resulting in an increase in the soil aeration and permeability, the SAR values should be considered in conjunction with the irrigation water salinity (*Table D-2*). It should be also noted that soil infiltration problems also occur when using water with very low salinity (< 350 mg/l) as it is usually highly corrosive and therefore dissolves the soil soluble minerals particularly calcium which causes soil dispersion. (Ayers and Westcot, 1994, Pearson, 2009)

Table D-2: FAO water salinity and SAR guideline values when sprinkler irrigation is used

	Water Salinity Limits in mg/l (EC in ds/m)[235,*]		
SAR	**No effect on infiltration**	**Slight to moderate**	**Severe effect**
0-3	> 450 (> 0.7)	128-450 (0.2-0.7)	< 130 (< 0.2)
3-6	> 770 (>1.2)	190-770 (0.3-1.2)	< 190 (< 0.3)
6-12	> 1,200 (> 1.9)	320-1,200 (0.5-1.9)	< 320 (< 0.5)
12-20	> 1,850 (> 2.9)	830-1,850 (1.3-2.9)	< 830 (< 1.3)
12-40	> 3,200 (> 5.0)	1,850-3,200 (2.9-5.0)	< 1,850 (< 2.9)

***** FAO guidelines used the data from the University Of California Committee Of Consultants (1974)

D-3: Specific Elements Affecting Crops

High levels of chloride, sodium and boron ions in the water have toxic effects on the plant and reduce its yield. Chloride and sodium ions are absorbed directly by the leaves causing leaf burn and defoliation resulting in crop damage when surface irrigation, e.g. sprinkler irrigation, is used. *Table D-3* shows the FAO guideline limits for sodium and chloride concentrations in irrigation water of some of the suggested HVLWC crops investigated in this study when sprinkler irrigation is used.

Table D-3: FAO guideline limits for sodium and chloride concentrations in irrigation water of some of the suggested HVLWC crops when sprinkler irrigation is used

	Crop Category	**Sodium[*,^] (mg/l)**	**Chloride [*,^] (mg/l)**
Grape	Moderately Sensitive	115-230	175-355
Potato			
Tomato			
Corn (Maize)	Moderately Tolerant	230-460	355-710
Cucumber			
Sesame			
Cotton	Tolerant	>460	>710

*FAO guideline values are based on the data from Maas (1984)

^The guideline values are not absolute tolerances and should be only used as a first approximation for potential hazard.

Moreover, while boron is considered an essential element for plant growth, excessive concentrations have toxic effect on the plant leading to yield losses. This is particularly important when GW is used as it is more likely to have high boron concentrations.

Similarly, while nitrogen, mainly existing in the form of nitrate ions, is a good fertilizer, excessive concentrations produce crops of poor quality, cause crop over growth, or delay crop maturity reducing the yields. *Table D-4* shows the FAO guideline limits for boron concentrations in irrigation water of some of the suggested HVLWC crops investigated in this study.

Table D-4: FAO guideline limits for boron concentrations in irrigation water of some of the suggested high value low water consuming crops

	Crop Category	Maximum boron tolerance* (mg/l)
Cowpeas	Sensitive	0.5-0.75
Grape		0.5-0.75
Onion		0.5-0.75
Beans		0.75-1
Sesame		0.75-1
Cucumber	Moderately Sensitive	1-2
Potato		
Corn (Maize)	Moderately Tolerant	2-4
Squash		
Tomato	Tolerant	4-6
Cotton	Very Tolerant	6-15

*FAO guideline values are based on the data from Maas (1984)

Furthermore, high concentrations of bicarbonate in water causes unsightly deposits on leaves and fruits when sprinkler irrigation is used, reducing their marketability. Finally, in spite of their typical low concentrations in water, trace elements accumulate in the soil in an irreversible process and can permanently make the soil unproductive.

FAO guideline limits for other elements in water and their effect on the soil and/or the crops are shown in table below.

Table D-5: FAO guideline limits for some elements in water which affect the soil and/or the crops

<table>
<tr><th rowspan="2">Element</th><th colspan="2">Limits (mg/l)</th><th rowspan="2">Effect</th></tr>
<tr><th>No effect</th><th>Severe restrictions on crop selection[1]</th></tr>
<tr><td>HCO_3[2]</td><td>< 90 (Sprinkler Irrigation)</td><td>520 (Sprinkler Irrigation)</td><td>● Unsightly deposits on leaves and fruits when sprinkler irrigation is used reducing fruit marketability</td></tr>
<tr><td>NO_3[2]</td><td>< 20</td><td>130</td><td>● Excessive vegetative growth, delayed crop maturity</td></tr>
<tr><td>pH[2]</td><td colspan="2">6.5 to 8.4</td><td>● High pH is due to carbonate and bicarbonate content. Carbonate and bicarbonate causes calcium and magnesium ions to form insoluble minerals, which intensifies the soil sodicity problem as sodium ions will dominate in this case.
● Low pH cause equipment corrosion
● pH >8 cause severe clogging issues with drip irrigation equipment [3,4]</td></tr>
<tr><td colspan="4">Trace Elements Recommended Maximum Concentration[5,6] in Irrigation Water</td></tr>
<tr><td>As</td><td colspan="2">0.1 l</td><td>● Toxic Effect</td></tr>
<tr><td>F</td><td colspan="2">1.0</td><td>● N/A</td></tr>
<tr><td>Pb</td><td colspan="2">5</td><td>● Can inhibit plant growth</td></tr>
<tr><td>Mn</td><td colspan="2">0.2</td><td>●Toxic Effect
● >1.5 mg/l will cause severe clogging issues with drip irrigation equipment [3,4]</td></tr>
<tr><td>Se</td><td colspan="2">0.02</td><td>● Toxic effect reducing productivity[7]</td></tr>
<tr><td>Cu</td><td colspan="2">0.2</td><td>● Toxic effect</td></tr>
<tr><td>Cd</td><td colspan="2">0.01</td><td>● Toxic effect
● Can Accumulate in plants and soil affecting human health</td></tr>
<tr><td>Fe</td><td colspan="2">5.0</td><td>● Can contribute to soil acidification and loss of essential phosphorus and molybdenum reducing the crop yield
● Unsightly deposits on leaves and fruits when sprinkler irrigation is used
● >1.5 mg/l cause severe clogging issues with drip irrigation equipment[3,4]</td></tr>
<tr><td>Li</td><td colspan="2">2.5</td><td>● Toxic effect</td></tr>
<tr><td>Zn</td><td colspan="2">2.0</td><td>● Toxic effect</td></tr>
<tr><td>Ni</td><td colspan="2">0.2</td><td>● Toxic effect</td></tr>
<tr><td>Cr</td><td colspan="2">0.1</td><td>● Conservative limits recommended due to lack of knowledge on its toxicity to plants</td></tr>
</table>

[1] Water users should experience soil and cropping problems or reduced yields
[2] FAO guidelines used the data from the University Of California Committee Of Consultants (1974)
[3] Relative value at which clogging may occur based on limited experience and is not a precise value.
[4] FAO guideline values obtained from Nakayama (1982)
[5] The maximum concentration is based on a water application rate consistent with good irrigation practices i.e. 10,000 m^3 per hectare per year. If the water application rate greatly exceeds this value, the maximum concentrations should be adjusted downward accordingly. No adjustment should be made for application rates less than 10,000 m^3 per hectare per year.

[6] The limits include the long term effect of accumulation in soil which can permanently affect its productivity
[7] (Oron et al., 2007)

Source: (Ayers and Westcot, 1994)

D-4: Water Drinking Guidelines for Livestock and Poultry

FAO guidelines recommend[239] water salinities less than 3,200 mg/l (5.0 dS/m) to prevent serious physiological disturbance for livestock[240] and poultry. Otherwise, water salinities of up to 6,400 mg/l (8.0 dS/m) are unfit for poultry use while salinities exceeding 8,800 mg/l (11.0 dS/m) are not recommended for livestock use. The guidelines also recommend maximum magnesium concentrations, which if exceeded would cause diarrhoea to animals, as follows: less than 250 mg/l for poultry, cows and lambs; less than 400 mg/l for beef cattle; and less than 500 mg/l for sheep. The guideline limits for other trace elements that cause toxicity to animals are shown in table below.

Table D-6: FAO guideline limits for some trace elements that cause toxicity to animal

Elements	Upper limit (mg/l)
Al	5.0
As	0.2
B	5.0
F	2.0
Pb	0.1
Mn	0.05
Se	0.05
NO_3	400
Cu	0.5
Cd	0.05
Zn	24
Cr	1.0

FAO guidelines used the data from the National Academy of Sciences (1972)
Source: (Ayers and Westcot, 1994)

[239] Based on the study by the National Academy of Sciences (1972)
[240] Beef cattle, sheep, lambs, cows, swine and horses

Appendix E: Groundwater Depth Data in Several Locations in Egypt

Location	Depth to Water Level (m)	Depth to Top Aquifer (m)	Aquifer Accessed
High Irradiation Zone			
South East WD	30-110	Unconfined	Nubian
Wadi Asyuti	31-65	Unconfined	Quaternary
Qena Area (Inc. Wadi Qena and Wadi Hammamat)	8-46	Unconfined	Quaternary
	0-40	100-500	Nubian
Central Sinai South	300-400	500-900	Nubian
Central Sinai Middle	100-400	500-1000	
Al-Qaa	50-70	50-100	Quaternary
Low Irradiation Zone			
Nile Delta	0-3 (Confined area)	0-30	Nile Delta Aquifer
	35-60 (Unconfined area)	40-80	
Alexandria	3-21	7-32	Coastal Aquifer
Al-Arish Area	<4-85	44 to 95	Coastal Aquifer

Sources: (Nour and Khattab, 1998, Sultan et al., 2007, Hefny and Shata, 2004, RIGW, 1988, Atta et al., 2005, Sharaky et al., 2007, El Alfy, 2012, El Samanoudi et al., 2011)

Appendix F: RO Plant Design Example

With the given feed flow rate and recovery rate shown in table below, the number of RO modules can be determined such that the flux is in the range of 30 $l/m^2/h$ which in this case is 46 modules giving a flux of 29.45 $l/m^2/h$.

Table F-1: Design parameters used in the example

Feed Water Salinity	4,000 mg/l	**Feed Water Temperature**	20°C
RO RR	90%	**RO Feed Flow**	61.5 m^3/h

There are numerous configurations that could be obtained with 46 modules. Nevertheless, based on the DOW Chemical Company guidelines (DOW Chemical Company, 2013f), 18 modules in series are likely to be needed to obtain 90% RR. Accordingly, the configurations with a number of modules in series close to 18 are first considered (*Table F-2*). Moreover, the design should aim to put as much RO modules as possible in the first stage (DOW Chemical Company, 2014, pers. comm., 2 Feb.), which was found to reduce the hydraulic load on the modules in this stage and evenly distribute it over the whole array. In most cases this also resulted in reducing the SEC as the modules in the other stages operated at lower recovery rate.

Regarding the module type, the DOW Chemical Company guidelines recommend using BW modules when water with salinity less than 5,000 mg/l is the feed water. Therefore, as a starting point, the RO plant performance is projected using BW modules in all stages for each configuration shown in column 1 in *Table F-2*. With each design, the pressure of the booster pumps is varied to balance the hydraulic load on the RO modules.

Table F-2: Different RO array configurations considered in the example

RO Array Configurations*	Module Type	Comment
4-4+3-6+2-6 (16)**	BWHR+BWHR+BWHR BW+BWHR+BWHR BW+BW+BWHR BW+BW+BW SWULE+BWHR+BWHR SWULE+BW+BWHR	Permeate Flow Limit Exceeded
5-5+3-5+1-6 (16)	BWHR+BWHR+BWHR	Permeate Flow Limit Exceeded
	BW+BWHR+BWHR	Permeate Flow Limit Exceeded
	BW+BW+BWHR	Permeate Flow Limit Exceeded
	BW+BW+BW	Permeate Flow Limit Exceeded
	SWULE+BWHR+BWHR	Permeate Flow Limit Exceeded
	SWULE+BW+BWHR	***Design Within Limits***
4-6+3-4+2-5 (15)	BWHR+BWHR+BWHR	Permeate Flow and RR Limits Exceeded
5-5+3-6+1-3 (14)	BWHR+BWHR+BWHR	Permeate Flow and RR Limits Exceeded

*A1-B1+A2-B2+A3-B3 where A and B are the number of pressure vessels and RO modules in series in each stage respectively

** Number of RO modules in series

As observed from *Table F-2*, the maximum recommended recovery rate limit of the modules was exceeded when the array consisted of 14 and 15 modules in series. Therefore it is likely that a configuration with at least 16 modules in series would be required. With the 16 series modules configuration, the permeate flow is however exceeded. Therefore, the next step is to gradually use higher salt rejection modules as they help to evenly distribute the hydraulic load within the same stage.

Appendix G: RO Plant Rosa Designs

A) Low Scaling Potential GW

Water Temperature	RO Feed Flow Rate (m3/h)	Direct Feed (m3/h)	Permeate Flow Rate After Blending (m3/h)	Module Type	RO Plant Configuration	Feed Pressure (Bar)	Stage 2 Boost Pressure (bar)	Stage 3 Boost Pressure (bar)	SEC (kWh/m^3)	Power (kW)	Overall Permeate Salinity after blending (mg/l)
Feed Salinity=2,000 mg/l RR=90% Number of Modules=40 Flux=29.39 $l/m^2/h$											
20°C	53.4	14.42		S1*: BW30HR-440i		17.66			0.88	42.25	481
40°C using 20°C Design	53.4	14.42		S2: BW30HR-440i S3: HRLE-440i	4-6+2-5+1-6	9.99	4.5	1.5	0.57	27.25	536
30°C	53.4	14.42	62.5	S1: SW30ULE-440i		16.93			0.82	39.45	488
40°C using 30°C Design	53.4	14.42		S2: BW30HR-440i S3: BW30HR-440i	4-6+2-6+1-4	13.66	0.5	8	0.68	32.45	508
40°C	53.4	14.42		S1: SW30XLE-440i S2: SW30ULE-440i S3: SW30ULE-440i	4-6+2-5+1-6	15.76	2	6.5	0.8	38.3	487
Feed Salinity=4,000 mg/l RR=90% Number of Modules=46 Flux=29.45 $l/m^2/h$											
20°C	61.53	7.12		S1: SW30ULE-440i		25.8			1.32	73.2	490
40°C using 20°C Design	61.53	7.12		S2:BW30-440i S3: BW30HR-440i	5-5+3-5+1-6	17.67	3.5	12.5	0.94	52.05	569
30°C	61.53	7.12		S1: SW30XLE-440i	5-5+3-5+1-6	23.75	6.5	13.5	1.3	72.15	479

40°C using 30°C Design	61.53	7.12	62.5	S2: SW30XLE-440i S3: SW30XLE-440i		19.39			1.1	60.95	495
40°C	61.53	7.12		S1: SW30XHR-440i S2: SW30HRLE-440i S3: SW30HRLE-440i	5-5+3-5+1-6	27.97	1.5	14	1.39	76.75	486
Feed Salinity=6,000 mg/l RR=85% Number of Modules=48 Flux=29.44 l/m²/h											
20°C	67.97	4.73	62.5	S1: SW30ULE-440i	6-4+3-4+2-6	27.88	6.5	6.5	1.57	90.55	484
40°C using 20°C Design	67.97	4.73		S2: SW30ULE-440i S3: BW30HR-440i		20.26			1.17	67.85	541
30°C	67.97	4.73		S1: SW30XLE-440i	6-4+4-4+2-4	25.62	6.5	10	1.49	86.3	494
40°C using 30°C Design	67.97	4.73		S2: SW30XLE-440i S3: SW30ULE-440i		21.63			1.29	74.75	521
40°C	67.97	4.73		S1: SW30HRLE-440i S2: SW30HRLE-440i S3: SW30XLE-440i	6-4+4-4+2-4	24.46	7	10.5	1.46	84.2	500
Feed Salinity=8,000 mg/l RR=80% Number of Modules=48 Flux=30.05 l/m²/h											
20°C	73.7	3.54	62.5	S1: SW30ULE-440i	6-4+3-4+2-6	30.5	7	10	1.9	111.95	492
40°C using 20°C Design	73.7	3.54		S2: SW30ULE-440i S3: SW30ULE-440i		21.3			1.42	84	565
30°C	73.7	3.54		S1: SW30HRLE-440i	6-4+4-4+2-4	32.7	3.5	9	1.87	110.35	497
40°C using 30°C Design	73.7	3.54		S2: SW30XLE-440i S3: SW30ULE-440i		21.63			1.63	96.05	526
40°C	73.7	3.54		S1: SW30XHR-440i S2: SW30HRLE-440i S3: SW30XLE-440i	6-5+4-3+2-3	32.53	6	9	1.9	111.9	500
Feed Salinity=10,000 mg/l RR=80% Number of Modules=50 Flux=29.2 l/m²/h											
20°C	74.59	2.83		S1: SW30ULE-440i	6-4+4-4+2-5	32.33	8.5	14	2.09	124.65	504
40°C using 20°C Design	74.59	2.83		S2: SW30ULE-440i S3: SW30ULE-440i		23.86			1.64	98.15	598
30°C	74.59	2.83		S1: SW30HRLE-440i	6-5+4-3+2-4	35.15	8	9.5	2.1	125.35	508

40°C using 30°C Design	74.59	2.83	62.5	S2: SW30XLE-440i S3: SW30ULE-440i		30.72			1.86	111.2	546
40°C	74.59	2.83		S1: SW30XHR-440i S2: SW30HRLE-440i S3: SW30XLE-440i	6-5+4-3+2-3	34.71	6	9	2.09	124.95	515
Feed Salinity=15,000 mg/l RR=75% Number of Modules=50 Flux=29.66 l/m^2/h											
20°C	80.83	1.88		S1: SW30ULE-440i		38.11			2.76	167.1	521
40°C using 20°C Design	80.83	1.88		S2: SW30ULE-440i S3: SW30ULE-440i	7-3+5-4+3-3	29.72	9.5	20.5	2.29	139	648
30	80.83	1.88		S1: SW30HRLE-440i		41.61			2.81	170.1	526
40°C using 30°C Design	80.83	1.88	62.5	S2: SW30HRLE-440i S3: SW30ULE-440i	7-3+5-4+3-3	36.98	10	12.5	2.54	154	575
40°C	80.83	1.88		S1: SW30XHR-440i S2: SW30XHR-440i S3: SW30XLE-440i	7-3+5-4+3-3	41.41	10.5	14	2.84	172.28	530
Feed Salinity=20,000 mg/l RR=75% Number of Modules=50 Flux=29.89 l/m^2/h											
20°C	87.27	1.41		S1: SW30XLE-440i		49.52			3.57	218	525
40°C using 20°C Design	87.27	1.41		S2: SW30ULE-440i S3: SW30ULE-440i	7-3+5-4+3-3	40.56	6	22	3.03	185.3	660
30°C	87.27	1.41		S1: SW30HRLE-440i		47.69			3.5	213.65	540.
40°C using 30°C Design	87.27	1.41	62.5	S2: SW30HRLE-440i S3: SW30ULE-440i	7-3+5-4+3-3	43.16	12	13.5	3.22	196.6	599
40°C	87.27	1.41		S1: SW30XHR-440i S2: SW30XHR-440i S3: SW30XLE-440i	7-3+5-4+3-3	48.44	12.5	20	3.7	226.3	541

* Stage number
^ Total number of RO modules

B) Typical GW Composition

Water Temperature	RO Feed Flow Rate (m3/h)	Direct Feed (m3/h)	Permeate Flow Rate After Blending (m3/h)	Module Type	RO Plant Configuration	Feed Pressure (Bar)	Stage 2 Boost Pressure (bar)	Stage 3 Boost Pressure (bar)	SEC (kWh/m^3)	Power (kW)	Overall Permeate Salinity after mixing (mg/l)
Feed Salinity=2,000 mg/l RR=90% Number of Modules=40 Flux=29.39 l/m^2/h											
20°C	53.4	14.42	62.5	S1: HRLE-440i		11.78			0.7	33.5	485
40°C using 20°C Design	53.4	14.42		S2: HRLE-440i S3: BW30-440i	4-6+2-5+1-6	6.46	3.5	11.5	0.5	23.85	528
30°C	53.4	14.42		S1: BW30HR-440i		12.06			0.65	31.45	486
40°C using 30°C Design	53.4	14.42		S2: BW30HR-440i S3: BW30HR-440i	4-6+2-6+1-4	9.14	3.5	6.5	0.53	25.3	504
Feed Salinity=4,000 mg/l RR=85% Number of Modules=46 Flux=29.45 l/m^2/h											
20°C	65.15	7.12	62.5	S1: HRLE-440i		13.3			0.86	47.4	498
40°C using 20°C Design	61.53	7.12		S2: HRLE-440i S3: BW30HR-440i	6-4+3-4+2-5	7.95	3.5	10.5	0.63	34.85	588
30°C	65.15	7.12		S1: BW30-440i		14.48			0.84	46.35	511
40°C using 30°C Design	61.53	7.12		S2: BW30HR-440i S3: BW30HR-440i	6-4+3-4+2-5	19.39	3	6	0.69	38.35	553
Feed Salinity=6,000 mg/l RR=85% Number of Modules=48 Flux=29.44 l/m^2/h											
20°C	67.97	4.73	62.5	S1: BW30HR-440i		20.83			1.23	71.05	490
40°C using 20°C Design	67.97	4.73		S2: BW30HR-440i S3: BW30HR-440i	6-4+3-4+2-6	19.72	5	8.5	0.86	49.95	516.4
30°C	67.97	4.73		S1: SW30ULE-440i		19.72			1.16	67.0	516
40°C using 30°C Design	67.97	4.73		S2: SW30ULE-440i S3: BW30-440i	6-4+4-4+2-4	16.26	5.5	7.5	0.99	57.5	560

Feed Salinity=8,000 mg/l RR=80% Number of Modules=48 Flux=30.05 l/m²/h											
20°C	73.7	3.54		S1: BW30HR-440i		22.74			1.46	86.05	494
40°C using 20°C Design	73.7	3.54		S2: BW30HR-440i S3: BW30HR-440i	6-4+4-4+2-4	14.67	6	10	1.05	62.15	579
30°C	73.7	3.54	62.5	S1: SW30ULE-440i		21.81			1.41	82.9	503
40°C using 30°C Design	73.7	3.54		S2: SW30ULE-440i S3: SW30ULE-440i	6-4+4-4+2-4	21.63	6	9.5	1.23	72.4	534
Feed Salinity=10,000 mg/l RR=75% Number of Modules=50 Flux=29.2 l/m²/h											
20°C	79.56	2.83		S1: BW30HR-440i		23.77			1.55	92.65	507
40°C using 20°C Design	74.59	2.83		S2: BW30HR-440i S3: HRLE-440i	6-5+4-3+2-4	17	8.5	2.5	1.18	70.25	623
30°C	79.56	2.83	62.5	S1: SW30ULE-440i		23			1.54	91.7	504
40°C using 30°C Design	74.59	2.83		S2: SW30ULE-440i S3: BW30HR-440i	6-5+4-3+2-4	19.6	8	4.5	1.36	80.95	536

Appendix H: Correlations to Estimate the Effect of Salinity and Temperature on Water Properties

H-1: Density

The correlation shown below is based on experimental measurements in the literature carried out on synthetic seawater, which does not contain calcium which will otherwise cause scaling at higher temperature, and has an accuracy of ± 0.1%. The equation covers a wide range of temperature and salinity ranging from 0 to 180°C and salinities from 0 to 160 g/kg respectively.

$$\rho = (a_1 + a_2T + a_3T^2 + a_4T^3 + a_5T^4) + (b_1S + b_2ST + b_3ST^2 + b_4ST^3 + b_5S^2T^2) \quad \textbf{(H-1)}$$

$a_2 = 9.999 \times 10^2$, $a_2 = 2.034 \times 10^{-2}$, $a_3 = -6.162 \times 10^{-3}$, $a_4 = 2.261 \times 10^{-5}$
$a_5 = -4.657 \times 10^{-8}$, $b_1 = 8.02 \times 10^2$, $b_2 = -2.001$, $b_3 = 1.677 \times 10^{-2}$
$b_4 = -3.06 \times 10^{-5}$, $b_5 = -1.613 \times 10^{-5}$

The water salinity and the temperature in correlation *(H-1)* are in kg_s/kg_{sol} and °C respectively.

H-2: Specific Heat Capacity

The effect of water salinity and temperature on its specific heat capacity is estimated using the correlation developed by Jamieson et al. (1969), cited in Sharqawy et al. (2010), which is based on experimental measurements carried out on synthetic seawater. Sharqawy et al. (2010), concluded that the correlation gives the best match to the values calculated by the International Association for the Properties of Water and Steam (IAWPS) 2008 (The International Association for the Properties of Water and Steam, 2008) formulation compared to other correlations in the literature. The correlation is valid for water temperatures ranging from 0 to 180 °C and salinities from 0 to 180 g/kg and has an accuracy of ± 0.28% compared to experimental data.

$$Cp_l = \mathrm{A} + \mathrm{BT} + \mathrm{CT}^2 + \mathrm{DT}^3 \quad \textbf{(H-2)}$$

$$A = 5.328 - 9.76 \times 10^{-2}\, S + 4.04 \times 10^{-4}\, S^2$$
$$B = -6.913 \times 10^{-3} + 7.351 \times 10^{-4}\, S - 3.15 \times 10^{-6}\, S^2$$
$$C = 9.6 \times 10^{-6} - 1.927 \times 10^{-6}\, S + 8.23 \times 10^{-9}\, S^2$$
$$D = 2.5 \times 10^{-9} + 1.666 \times 10^{-9}\, S - 7.125 \times 10^{-12}\, S^2$$

H-3: Specific Enthalpy

The correlation below is based on the data calculated by IAWPS 2008 formulation. The equation is valid for water temperatures ranging from 0 to 120°C and salinities from 0 to 120 g/kg.

$$h = h_w - S(a_1 + a_2S + a_3S^2 + a_4S^3 + a_5T + a_6T^2 + a_7T^3 + a_8ST + a_9S^2T + a_{10}ST^2) \quad \textbf{(H-3)}$$

$$h_w = 141.355 + 4202.07\, T - 0.535\, T^2 + 0.004\, T^3 \quad \textbf{(H-4)}$$

$$a_1 = -2.348 \times 10^4, a_2 = 3.152 \times 10^5, a_3 = 2.803 \times 10^6, a_4 = -1.446 \times 10^7$$
$$a_5 = 7.826 \times 10^3, a_6 = -44.17, a_7 = 0.2139, a_8 = -1.991 \times 10^4,$$
$$a_9 = 2.778 \times 10^4, a_{10} = 97.28$$

The water salinity and temperature in correlation (*H-3*) and (*H-4*) are in kg_s/kg_{sol} and °C respectively.

H-4: Water Dynamic Viscosity

The equation below is based on experimental data from the literature that were carried out on synthetic seawater and has an accuracy of ± 1.5%. The equation is valid for water temperatures ranging from 0 to 180°C and salinities from 0 to 150 g/kg.

$$\mu = \mu_w\, (1 + a_1\, S + a_2\, S^2) \quad \textbf{(H-5)}$$

$$u_w = 4.2844 \times 10^{-5} + (0.157(T + 64.993)^2 - 91.296)^{-1} \quad \textbf{(H-6)}$$

$$a_1 = 1.541 + 1.998 \times 10^{-2}\, T - 9.52 \times 10^{-5}\, T^2$$

$$a_2 = 7.974 - 7.561 \times 10^{-2}\, T - 4.724 \times 10^{-4}\, T^2$$

The salinity and temperature in correlations *(H-5)* and *(H-6)* are in kg_s/kg_{sol} and °C respectively

H-5: Water Thermal Conductivity

The effect of water salinity and temperature on its thermal conductivity is estimated using the correlation developed by Jamieson and Tudhope (1970) which is based on experimental measurements carried out on synthetic seawater. The correlation gives, according to Sharqawy et al. (2010), the best fit to experimental measurements available in the literature especially at the temperature range between 40°C to 180°C where the equation gives a maximum deviation of ± 1% from experimental measurements within 0 to 160 g/kg salinity range.

$$\log k = \log(240 + 0.0002\, S) + 0.434 \left(2.3 - \frac{343.5 + 0.037\, S}{T}\right) \left(1 - \frac{T}{647 + 0.03\, S}\right)^{0.333} \quad \textbf{(H-7)}$$

H-6: Vapour Pressure

The effect of water salinity on vapour pressure is calculated using the correlation by Emerson and Jamieson (1967), which is based on experimental data carried out on synthetic seawater as it gives the best fit to experimental data (Sharqawy et al., 2010). The correlation, according to Fichtner (1978) could be used for water temperatures ranging from 10 to 200°C and salinities from 0 to 160 g/kg with errors less than 2.5%.

$$\log_{10} \frac{p}{p_w} = -2.1609\ 10^{-4}\ S - 3.5012\ 10^{-7}\ S^2 \quad \textbf{(H-8)}$$

To calculate the pure water vapour pressure (p_w) at different temperatures Antoine equation is used (Lawson and Lloyd, 1997, Phattaranawik et al., 2003, Winter et al., 2012) which has less than 0.44% deviation from the values shown in the steam tables in Çengel and Cimbala (2006) over the expected operating temperature range in this study (i.e. 20 to 85°C).

$$p_w = 133.32 * 10^{\left(\mathrm{A} - \frac{\mathrm{B}}{\mathrm{C+T}}\right)} \quad \textbf{(H-9)}$$

Where the constants A, B and C are 8.07131, 1730.63 and 233.426 respectively for water

The temperature in equation *(H-9)* is in °C

H-7: Latent Heat of Vaporization

The latent heat of vaporization for salty water was shown by Sharqawy et al. (2010), to be the same as that of pure water and could be estimated from the following correlation.

$$\Delta H_w = 2.501 \times 10^6 - 2.369 \times 10^3\, T + 0.2678\, T^2 - 8.103 \times 10^{-3}\, T^3 - 2.079 \times 10^{-5}\, T^4 \quad \textbf{(H-10)}$$

The temperature in the correlation is in °C

It should be noted that while Sharqawy et al. (2010) multiplied equation by $(1 - \frac{S}{1000})$ to consider that the latent heat of vaporization is with respect to 1 kg of seawater solution, I believe that this is inaccurate given that by definition the latent heat of vaporization is the amount of heat released from the condensation of 1 kg of condensed vapour and therefore the mass of the solution is irrelevant in this case. Moreover, the latent heat of vaporization calculated using the 2010 Thermodynamic Equation of Seawater (TEOS-10) (McDougall et al., 2010) do not consider this factor.

H-8: Specific Heat Capacity of Water Vapour

The specific heat capacity of water vapour is estimated using the following polynomial fit correlation developed based on the data in Çengel and Cimbala (2006) with less than 0.05% deviation from the latter within the expected temperature operating range in this study.

$$Cp_v = 0.01775T^2 - 0.2432T + 1867 \quad \textbf{(H-11)}$$

The temperature in the correlation is in °C

Appendix I: Model "A" Flowchart

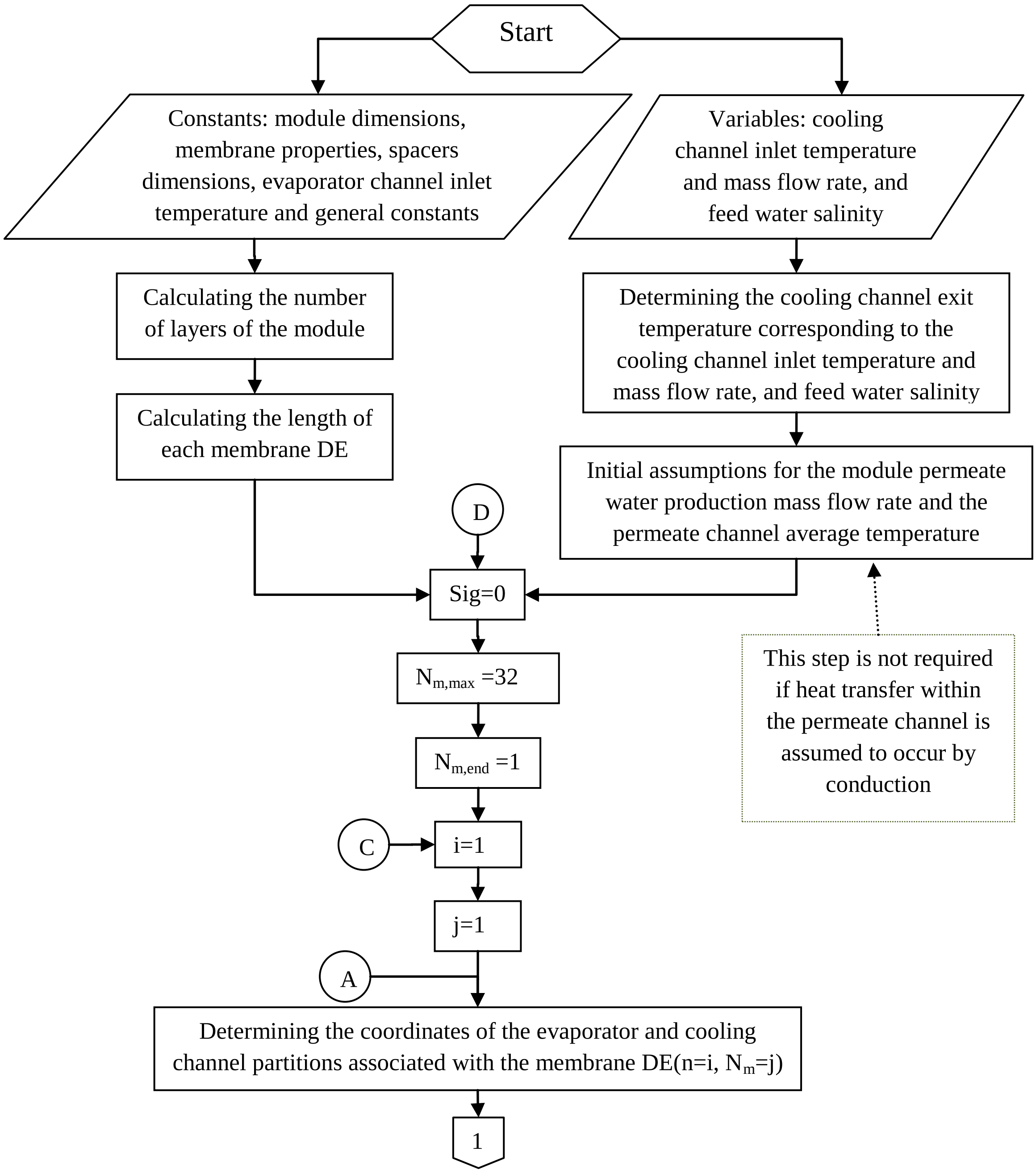

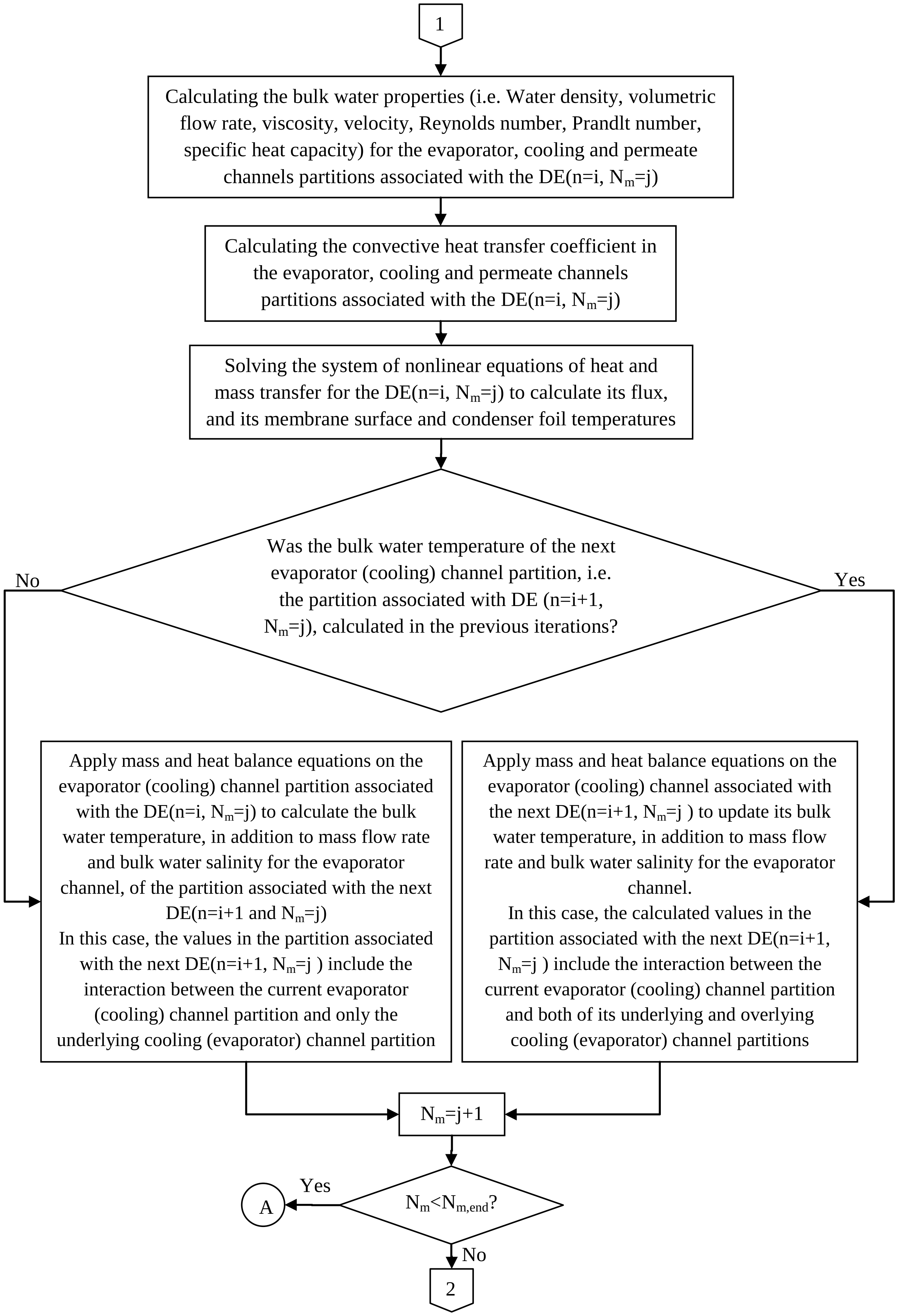
1
Calculating the bulk water properties (i.e. Water density, volumetric flow rate, viscosity, velocity, Reynolds number, Prandlt number, specific heat capacity) for the evaporator, cooling and permeate channels partitions associated with the DE(n=i, N_m=j)
Calculating the convective heat transfer coefficient in the evaporator, cooling and permeate channels partitions associated with the DE(n=i, N_m=j)
Solving the system of nonlinear equations of heat and mass transfer for the DE(n=i, N_m=j) to calculate its flux, and its membrane surface and condenser foil temperatures
Was the bulk water temperature of the next evaporator (cooling) channel partition, i.e. the partition associated with DE (n=i+1, N_m=j), calculated in the previous iterations?
No
Yes
Apply mass and heat balance equations on the evaporator (cooling) channel partition associated with the DE(n=i, N_m=j) to calculate the bulk water temperature, in addition to mass flow rate and bulk water salinity for the evaporator channel, of the partition associated with the next DE(n=i+1 and N_m=j) In this case, the values in the partition associated with the next DE(n=i+1, N_m=j) include the interaction between the current evaporator (cooling) channel partition and only the underlying cooling (evaporator) channel partition
Apply mass and heat balance equations on the evaporator (cooling) channel associated with the next DE(n=i+1, N_m=j) to update its bulk water temperature, in addition to mass flow rate and bulk water salinity for the evaporator channel.
In this case, the calculated values in the partition associated with the next DE(n=i+1, N_m=j) include the interaction between the current evaporator (cooling) channel partition and both of its underlying and overlying cooling (evaporator) channel partitions
N_m=j+1
N_m<$N_{m,end}$?
Yes
A
No
2

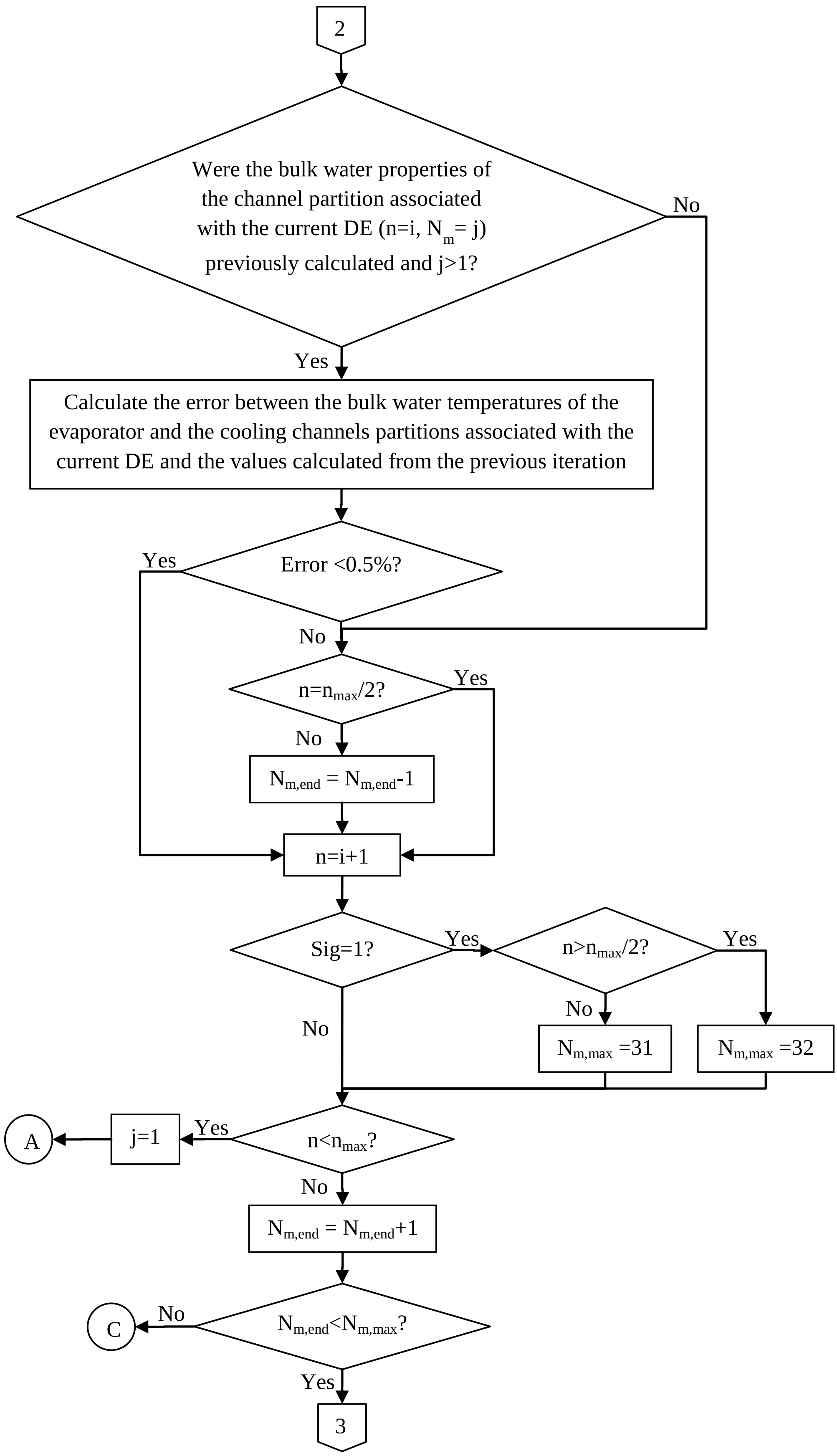

2
Were the bulk water properties of the channel partition associated with the current DE (n=i, N_m = j) previously calculated and j>1?
No
Yes
Calculate the error between the bulk water temperatures of the evaporator and the cooling channels partitions associated with the current DE and the values calculated from the previous iteration
Yes
Error <0.5%?
No
n=n_max/2?
Yes
No
N_m,end = N_m,end-1
n=i+1
Sig=1?
Yes
n>n_max/2?
Yes
No
No
N_m,max =31
N_m,max =32
A
j=1
Yes
n<n_max?
No
N_m,end = N_m,end+1
C
No
N_m,end<N_m,max?
Yes
3

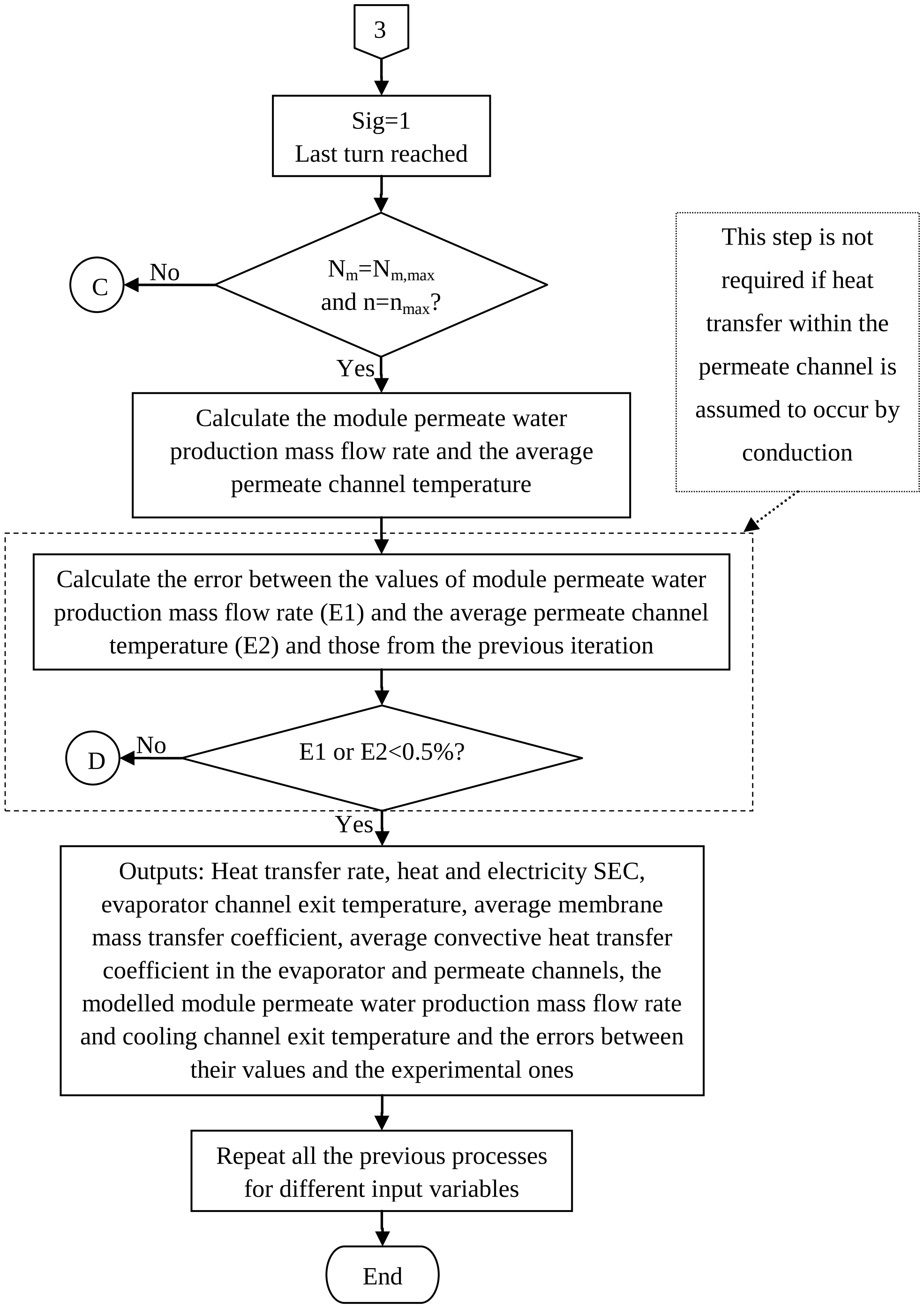
3
Sig=1
Last turn reached
No
C
N_m=$N_{m,max}$
and n=n_{max}?
Yes
This step is not required if heat transfer within the permeate channel is assumed to occur by conduction
Calculate the module permeate water production mass flow rate and the average permeate channel temperature
Calculate the error between the values of module permeate water production mass flow rate (E1) and the average permeate channel temperature (E2) and those from the previous iteration
D
No
E1 or E2<0.5%?
Yes
Outputs: Heat transfer rate, heat and electricity SEC, evaporator channel exit temperature, average membrane mass transfer coefficient, average convective heat transfer coefficient in the evaporator and permeate channels, the modelled module permeate water production mass flow rate and cooling channel exit temperature and the errors between their values and the experimental ones
Repeat all the previous processes for different input variables
End

Appendix J: Model "B" Flowchart

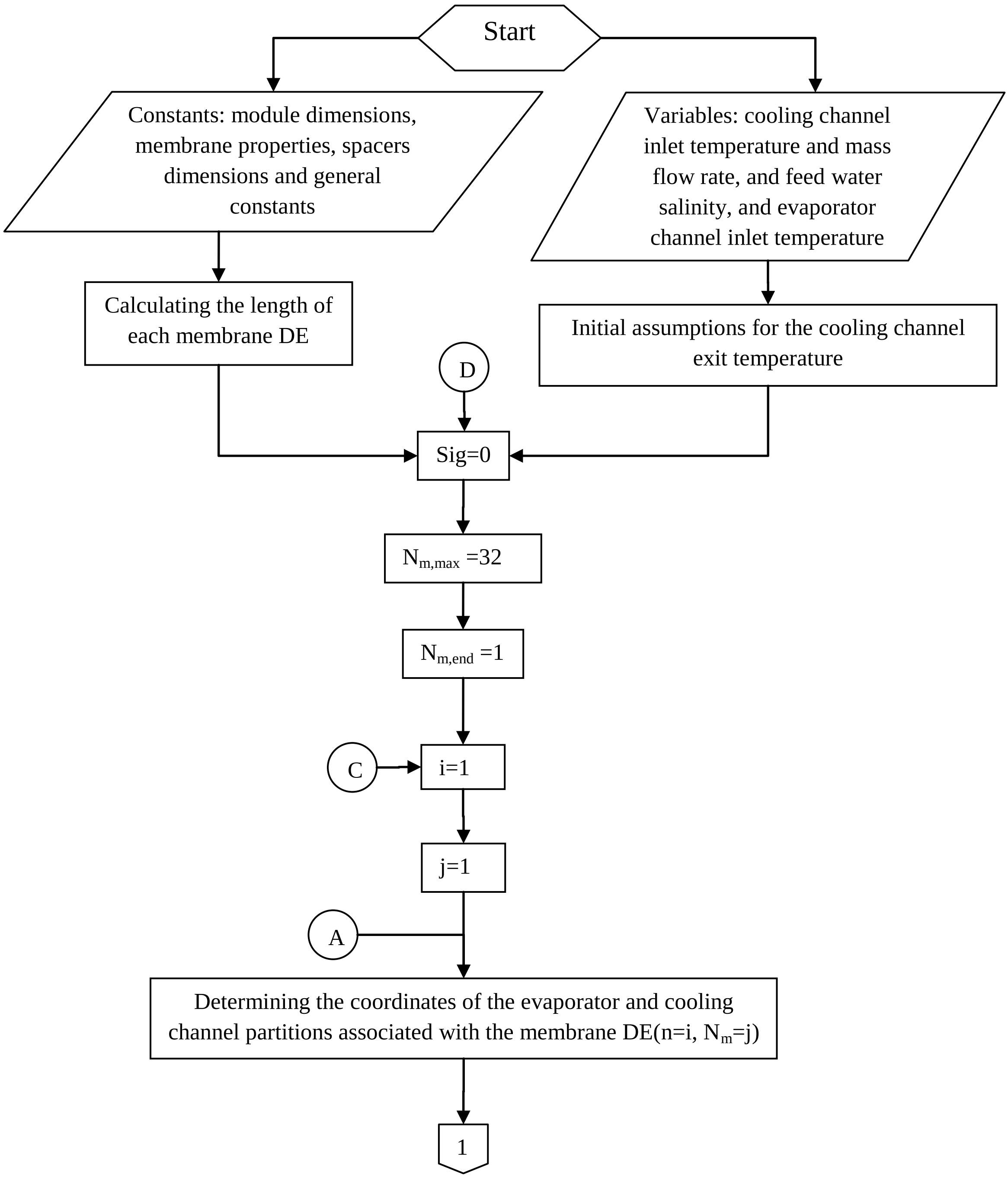

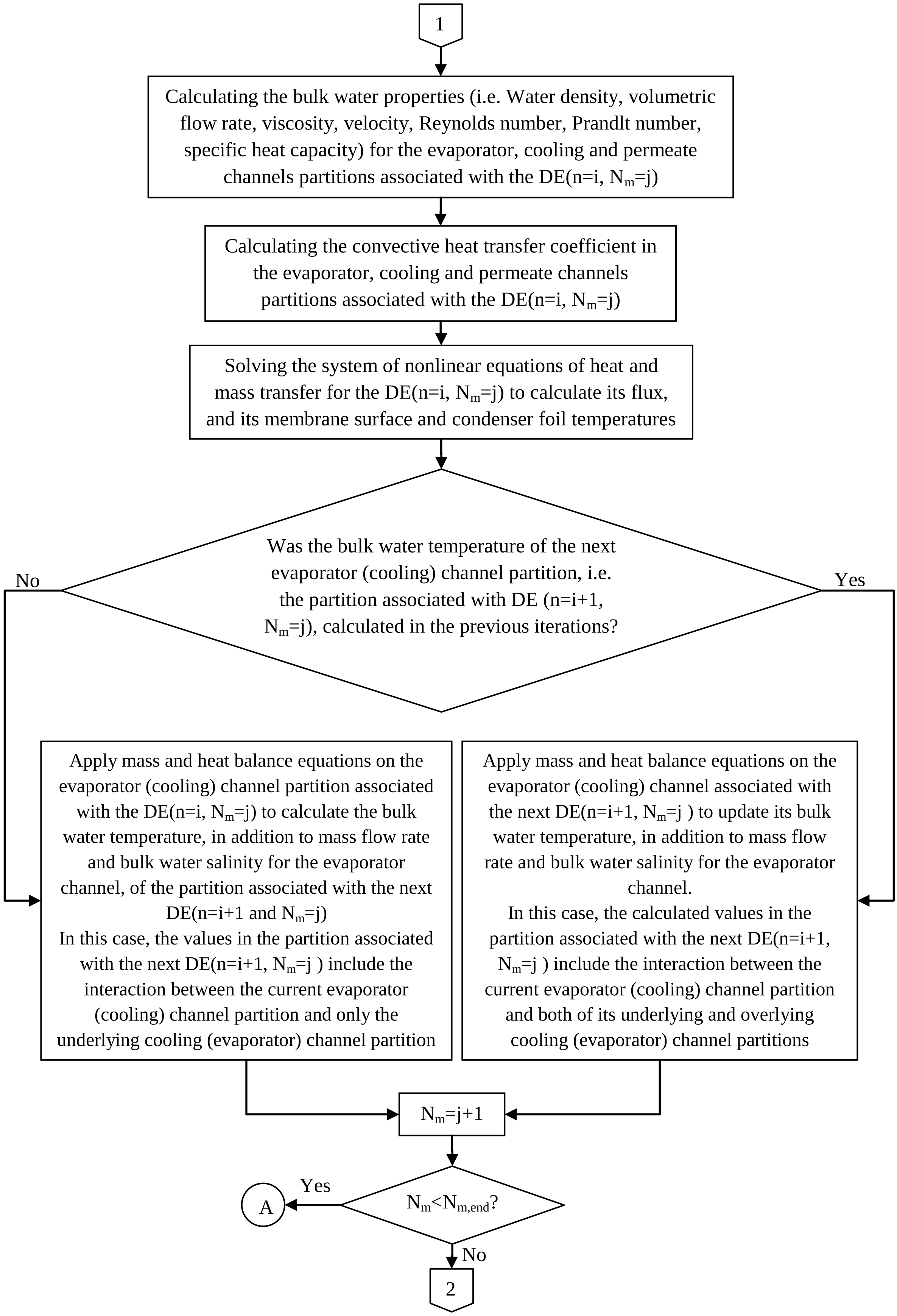
1
Calculating the bulk water properties (i.e. Water density, volumetric flow rate, viscosity, velocity, Reynolds number, Prandlt number, specific heat capacity) for the evaporator, cooling and permeate channels partitions associated with the DE(n=i, N_m=j)
Calculating the convective heat transfer coefficient in the evaporator, cooling and permeate channels partitions associated with the DE(n=i, N_m=j)
Solving the system of nonlinear equations of heat and mass transfer for the DE(n=i, N_m=j) to calculate its flux, and its membrane surface and condenser foil temperatures
Was the bulk water temperature of the next evaporator (cooling) channel partition, i.e. the partition associated with DE (n=i+1, N_m=j), calculated in the previous iterations?
No
Yes
Apply mass and heat balance equations on the evaporator (cooling) channel partition associated with the DE(n=i, N_m=j) to calculate the bulk water temperature, in addition to mass flow rate and bulk water salinity for the evaporator channel, of the partition associated with the next DE(n=i+1 and N_m=j) In this case, the values in the partition associated with the next DE(n=i+1, N_m=j) include the interaction between the current evaporator (cooling) channel partition and only the underlying cooling (evaporator) channel partition
Apply mass and heat balance equations on the evaporator (cooling) channel associated with the next DE(n=i+1, N_m=j) to update its bulk water temperature, in addition to mass flow rate and bulk water salinity for the evaporator channel.
In this case, the calculated values in the partition associated with the next DE(n=i+1, N_m=j) include the interaction between the current evaporator (cooling) channel partition and both of its underlying and overlying cooling (evaporator) channel partitions
N_m=j+1
N_m<$N_{m,end}$?
Yes
A
No
2

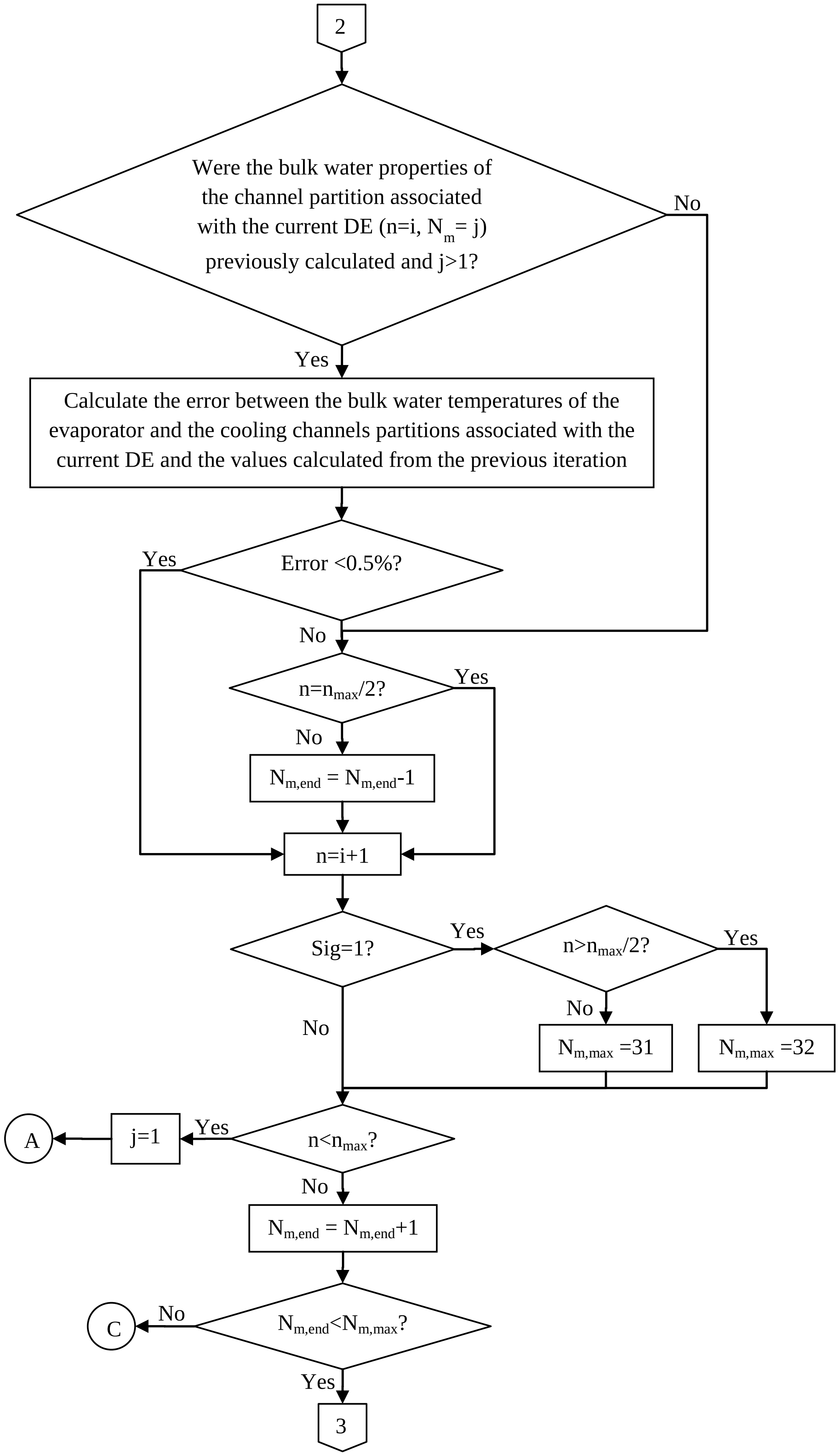

2
Were the bulk water properties of the channel partition associated with the current DE (n=i, N_m = j) previously calculated and j>1?
No
Yes
Calculate the error between the bulk water temperatures of the evaporator and the cooling channels partitions associated with the current DE and the values calculated from the previous iteration
Error <0.5%?
Yes
No
n=n_max/2?
Yes
No
N_m,end = N_m,end-1
n=i+1
Sig=1?
Yes
n>n_max/2?
Yes
No
N_m,max =31
N_m,max =32
No
A
j=1
Yes
n<n_max?
No
N_m,end = N_m,end+1
C
No
N_m,end<N_m,max?
Yes
3

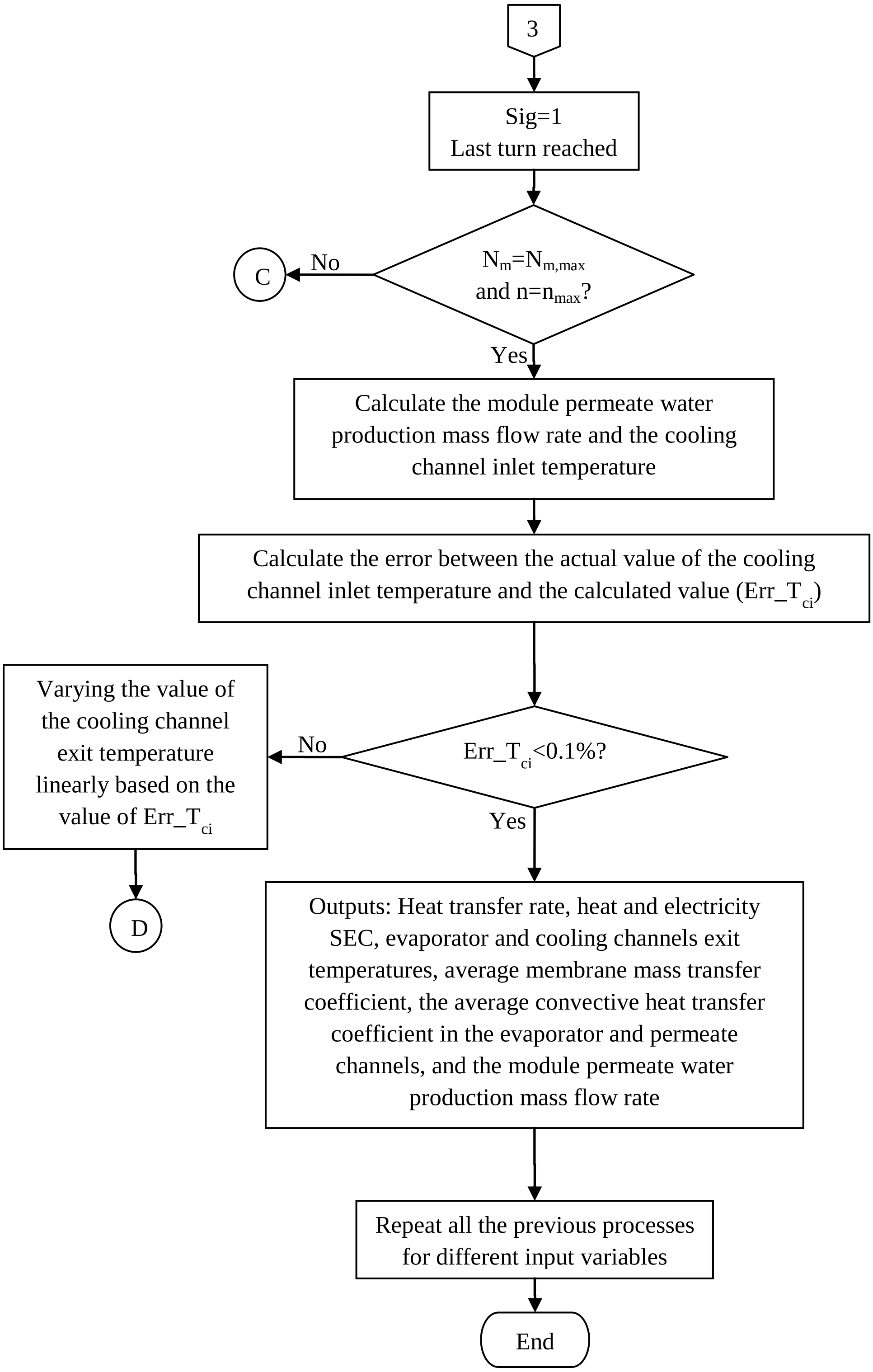

3
Sig=1
Last turn reached
$N_m=N_{m,max}$
and $n=n_{max}$?
No
C
Yes
Calculate the module permeate water production mass flow rate and the cooling channel inlet temperature
Calculate the error between the actual value of the cooling channel inlet temperature and the calculated value (Err_T_{ci})
Err_T_{ci}<0.1%?
No
Varying the value of the cooling channel exit temperature linearly based on the value of Err_T_{ci}
D
Yes
Outputs: Heat transfer rate, heat and electricity SEC, evaporator and cooling channels exit temperatures, average membrane mass transfer coefficient, the average convective heat transfer coefficient in the evaporator and permeate channels, and the module permeate water production mass flow rate
Repeat all the previous processes for different input variables
End

Appendix K: Estimating the Cooling Channel Exit Temperature from Experimental Data

Using the flux and SHC data in Winter et al. (2011), the amount of heat added to the water exiting the cooling channel and entering the evaporator channel can be calculated as follows:

$$\dot{V_{p,MD}}\ (m^3/h) = \frac{3600\ \dot{m_{p,MD}}}{\rho_p} \qquad \textbf{(K-1)}$$

$$Q_{add} = SHC \times \dot{V_{p,MD}} \qquad \textbf{(K-2)}$$

$$Q_{add} = \dot{m_c}\ Cp\ (T_{e,i} - T_{c,o}) \qquad \textbf{(K-3)}$$

where ρ_p is the density of the permeate water and is estimated at the average module temperature, i.e. $\frac{(T_{e,i}+T_{c,i})}{2}$, Q_{add} is the amount of external heat added to the feed flow to increase its temperature to the desired value ($T_{e,i}$) and $\dot{V_{p,MD}}$ is the MD permeate water volumetric flow rate.

In equation *(K-3)*, the specific heat capacity of water is assumed to be constant and is estimated at the evaporator channel inlet temperature.

Accordingly, by knowing the SHC, the feed and permeate flow rates, and the evaporator inlet temperature, the amount of external heat added and the cooling channel exit temperature ($T_{c,o}$) can be calculated.